NASA
Reference
Publication
1157

January 1986

Single Scattering From Nonspherical Chebyshev Particles: A Compendium of Calculations

Warren J. Wiscombe
and Alberto Mugnai

NASA

NASA Reference Publication 1157

1985

Single Scattering From Nonspherical Chebyshev Particles: A Compendium of Calculations

Warren J. Wiscombe
Goddard Space Flight Center
Greenbelt, Maryland

Alberto Mugnai
Colorado State University
Fort Collins, Colorado

National Aeronautics and Space Administration

Scientific and Technical Information Branch

PREFACE

Our interest in scattering by nonspherical particles was originally motivated by a desire to understand the impact of atmospheric aerosols on the Earth's climate. Since such aerosols are routinely assumed to be spheres, yet few except haze drops are spheres, we were naturally interested in what the differences in scattering and absorption might be.

After a time, however, we realized that our study had a considerably wider applicability. Scattering by nonspherical particles is important in practically every field of science and engineering. Biologists study nonspherical cellular structures by light scattering. Medical laboratories analyze blood corpuscles. Astronomers study interstellar grains. Engineers analyze coal slurries. And on and on. What all these enterprises share, is a deep lack of knowledge of nonspherical scattering. Hence we began to see our calculations as of much wider significance. Specialists in all these fields may find them of value.

PRECEDING PAGE BLANK NOT FILMED

TABLE OF CONTENTS

I. INTRODUCTION

When we first embarked on a course of research into the scattering properties of nonspherical particles, our goal was simple: to search for the main differences between spherical and nonsperical particle scattering by examining a number of special cases. By taking such an inductive approach, we essentially cast ourselves in the role of experimenters, with the important distinction that we solved Maxwell's Equations on the computer rather than letting Nature do so in the laboratory. This allowed us to obtain data which is very difficult to measure, and hence rarely measured — for example, the absorption cross-section and the backscattering near 180 degrees.

Our initial motivation was <u>not</u> to examine the scattering features of individual particles, but rather to unearth scattering features common to *all* nonspherical particles. In order to do so, we selected what we considered to be a rather general class of particles which could be continuously deformed from a sphere. These "Chebyshev particles" are obtained by rotating the curve

$$r_s = r_0 [1 + \epsilon T_n(\cos \Theta_s)]$$

$$= r_0 [1 + \epsilon \cos(n \Theta_s)] \qquad (1)$$

about the vertical axis $\Theta_s = 0$ (T_n is then the n-th Chebyshev polynomial and ϵ is the deformation parameter). Various examples of these particles are shown in Figure 1.

Following an extensive literature survey of scattering methods, summarized in Appendix A, we selected the "Extended Boundary Condition Method" (EBCM) invented by Waterman (1965, 1971) and further developed by Barber and Yeh (1975). Prof. Barber of the University of Utah was kind enough to supply us with a copy of his EBCM computer code. After considerable modification to improve its efficiency and speed, and to automate the convergence testing, we ran a large number of cases: 23 different particles in all, with deformation parameters $\epsilon = -0.20$ to 0.20 (in steps of 0.05) and 'equal-volume-sphere' size parameters $x = 1$ to 25 (in steps of 1).

Our initial paper (Mugnai and Wiscombe, 1980) examined only a tiny subset of all this data — just the extinction and absorption cross-sections and the phase function at 180 degrees for size parameters $x \leq 10$. We reserved the study of phase function and degree of polarization to a future paper. As we planned this second paper, however, it became clear that we would still be able to show only the smallest fraction of our data, namely that part which was most indicative of general trends. This, of course, was in line with our original goal.

But the question naturally arose, should we throw out the remainder of our data? Here the analogy between our study and an experimental investigation pressed itself upon us. A good experimenter will publish some of his basic data as well as his interpretation of it. The reason is, that others may be able to use the data, or draw conclusions from it, in ways not envisioned by the experimenter.

The next question was, would our data really be useful to other investigators? Naturally, we could not give a definitive answer, since it is the element of unpredictability in research which makes it essential to publish experimental data. But in several ways it did seem that we had generated a unique resource — "unique", because:

- almost all other published scattering results are for spheroids and infinite cylinders; in particular, there are no published results for concave particles like ours
- the available laboratory data are almost exclusively for scattered intensity in the angular range 10–170 degrees; cross sections and phase functions are rarely measured directly
- most studies are restricted to size parameters below 10
- electrical engineers, though a prolific source of nonspherical scattering calculations (Bowman, et. al., 1969), restrict themselves almost exclusively to metallic (perfectly conducting) particles
- our 'experiments' consumed perhaps 15 hours of CRAY computer time, an investment that few other investigators would be able to make.

We also envisioned at least three good uses to which our data might be put:

(i) testing the "Rayleigh hypothesis" (that outgoing wave expansions are satisfactory even for concave particles; see Millar, 1969, 1973) by comparing our results against microwave-analogue measurements (Zerull, 1976; Zerull, et. al., 1977; Schuerman, et. al., 1981);

(ii) testing semi-empirical theories claiming to give a general account of nonspherical scattering (e.g., Pollack and Cuzzi, 1980); and suggesting new theories of this sort;

(iii) testing the assumptions used in lidar research concerning the extinction-to-backscatter ratio of aerosol particles (see Collis and Russell, 1976).

As a result of the above considerations, we decided to publish the present compendium. A considerable reduction in the volume of data had still to be accomplished, but nothing of importance has been omitted.

The remaining sections discuss the EBCM itself (emphasizing the improvements we made in it, and our numerical experience with it); and the criteria we used in selecting which data to present. Naturally, these selection criteria embodied some preliminary data interpretation, but no further analysis of the results is undertaken here; that is reserved for a forthcoming journal article.

Appendix A, which is condensed from an intended review article, summarizes the entire field of nonspherical scattering. The book edited by Schuerman (1980) and our first paper (Mugnai and Wiscombe, 1980) can also be recommended as surveys of the state-of-the-art.

II. PARTICLE SHAPE

It seems to us that, along with ellipsoids and cylinders, Chebyshev particles constitute the most interesting class of fundamental nonspherical shapes whose scattering properties deserve attention. Among all simple analytical forms which we considered, they seemed the most attractive for several reasons:

- they differ distinctly from other shapes for which extensive calculations have been made (spheroid and cylinder)

- by increasing the magnitude of ϵ, a continuous deformation away from a sphere can be achieved — a property Chebyshev particles shared with spheroids, but not, for example, with cylinders and cubes

- while starting as convex, they quickly develop concavity as the magnitude of ϵ increases

- they exhibit surface roughness in its simplest possible manifestation, namely "waves" of uniform amplitude running completely around the particle; the effect of surface roughness can be studied in a systematic way, by varying ϵ and the waviness parameter 'n'

- the surface of the particle is smooth in the mathematical sense — all its derivatives exist and are bounded; hence highly-efficient Gauss quadrature rules can be employed at key points in the EBCM calculation

- the particles are rotationally symmetric, the only practical case for the EBCM (see Barber, 1973, pp. 43-50; also Mugnai and Wiscombe, 1980)

- The Chebyshev polynomials form a complete set, so that any rotationally-symmetric shape can be represented as a sum of elementary shapes of the form of Eq. (1).

Although we were unaware of their work when we selected Chebyshev particles, Pruppacher and Pitter (1971) assumed the shape of deformed raindrops to be a sum of elementary Chebyshev particles. This is a natural choice, being none other than a Fourier cosine series.

The 23 Chebyshev particles which were used in this investigation are:

for $\epsilon = \pm 0.05$: T_3, T_4, T_6, T_8, T_{20}

for $\epsilon = \pm 0.10$: T_2, T_3, T_4, T_6, T_8

for $\epsilon = \pm 0.15$: T_3, T_4

for $\epsilon = \pm 0.20$: T_2

T_3 particles are the same whatever the sign of ϵ, hence there are only 23 different particles in this seeming list of 26. A 24th 'particle', which we call MIXTURE, is a blend of these 23 in equal proportions. Figure 1 presents 3-D pictures of all these particles except the ones with $\epsilon = \pm 0.05$ (which do not look much different from a sphere).

We shall refer to these particles with the following notations, the first of which was used in Mugnai and Wiscombe (1980):

T_n^+, T_n^-: Chebyshev particle in fixed orientation with waviness parameter 'n' and positive (+) or negative (–) value of deformation parameter ϵ

T_n (+e), T_n (–e): Chebyshev particle in fixed orientation with waviness parameter 'n' and deformation parameter $\epsilon = \pm$ e or $-$e

For Chebyshev particles in <u>random</u> orientation, we use a similar notation, but now between angle brackets, e.g. $<T_n\,(+e)>$.

$T_2(\pm 0.10)$ particles are convex and quasi-spheroidal (prolate for +, oblate for $-$). $T_2(\pm 0.20)$ particles, however, have almost perfectly flat sides (+) or perfectly flat tops and bases ($-$), more resembling cylinders or disks (with rounded edges) than spheroids. For even larger deformations, the T_2 particles become concave, with T_2^+ tending toward dumbbells and T_2^- toward toroids.

T_3 particles are pear shaped, T_3^+ and T_3^- are actually the same particles; this is true for all T_n particles with odd 'n' (but not with even 'n'). They are the only case we study that is not mirror-symmetric in the plane perpendicular to the rotation axis (there are substantial computational savings in the EBCM, and different branches in the code, for particles with such a plane of symmetry). To our knowledge, ours are the first published EBCM results for particles lacking a plane of symmetry since Waterman (1971) studied a cone-sphere combination.

T_4^+ particles have two shallow valleys girdling them at mid-latitudes; T_4^- particles, one girdling valley at the equator, plus two dimples at the top and base. T_6 and T_8 particles are similar, but with more valleys; the only new features are pimples (instead of dimples) at the top and base for the '+' cases. All these particles have either bulges at the waist, or pinched waists.

In spite of their notational similarity, $T_n(+e)$ and $T_n(-e)$ particles look quite different to the eye. They bear a subtle 'conjugacy' to each other, however; for if we imagine the sphere $r_s = r_o$ as a mirror, the two particles are mirror reflections of each other. It is therefore of some interest for the reader to compare scattering quantities for these particle pairs. For that reason, their plots are made nearest neighbors in the various plot groupings to follow.

The particle refractive index was fixed at $\tilde{m} = 1.5 - 0.02\,i$, a value typical of some maritime aerosols in the visible region (Gerber, 1979). In Mugnai and Wiscombe (1980), we explored imaginary indices of 0, 0.05 and 1.0, but for the present study, we felt it was more important to explore as large a range of particle shapes and sizes as possible. We avoided a zero imaginary index because, in that case, the Mie results are full of the worst spikes and "ripple" (see Sec. VIII). This jagged behavior of the Mie quantities is reflected, in somewhat muted form, in the nonspherical quantities, making it more difficult to obtain convergence in the EBCM, with less accurate results. On the other hand, for very large imaginary indices, the spherical-nonspherical differences become very small and therefore less interesting, even though EBCM convergence is excellent.

All our EBCM results for Chebyshev particles are compared to results for an equal-volume sphere. Let $V_n(\epsilon)$ be the volume of a Chebyshev particle as given by Mugnai and Wiscombe (1980) (note that their expression for particle surface area is incorrect; the correct formula is given by Chylek, et. al., 1982). Then the radius of the equal-volume sphere, r_{ev}, is defined by

$$V_n(\epsilon) = 4\pi r_{ev}^3/3 \tag{2}$$

and the equal-volume-sphere size parameter, x, is given by

$$x = 2\pi r_{ev}/\lambda \tag{3}$$

where λ = wavelength. The units of r_{ev} and λ are neither needed nor specified in this study; only the non-dimensional parameter x is used to characterize the size of the scatterer.

In our calculations, we always chose a value of x a priori, then adjusted the r_0 of each Chebyshev particle in order to yield that value of x (actually, it is r_0/λ that is adjusted). Thus, for each fixed x, the 'basal radii' r_0 of the various Chebyshev particles differ slightly. In particular, r_0 will be different for T_n^+ and T_n^- particles having the same size parameter x. Thus, this pair of particles will not be exactly 'conjugate' in the sense discussed above.

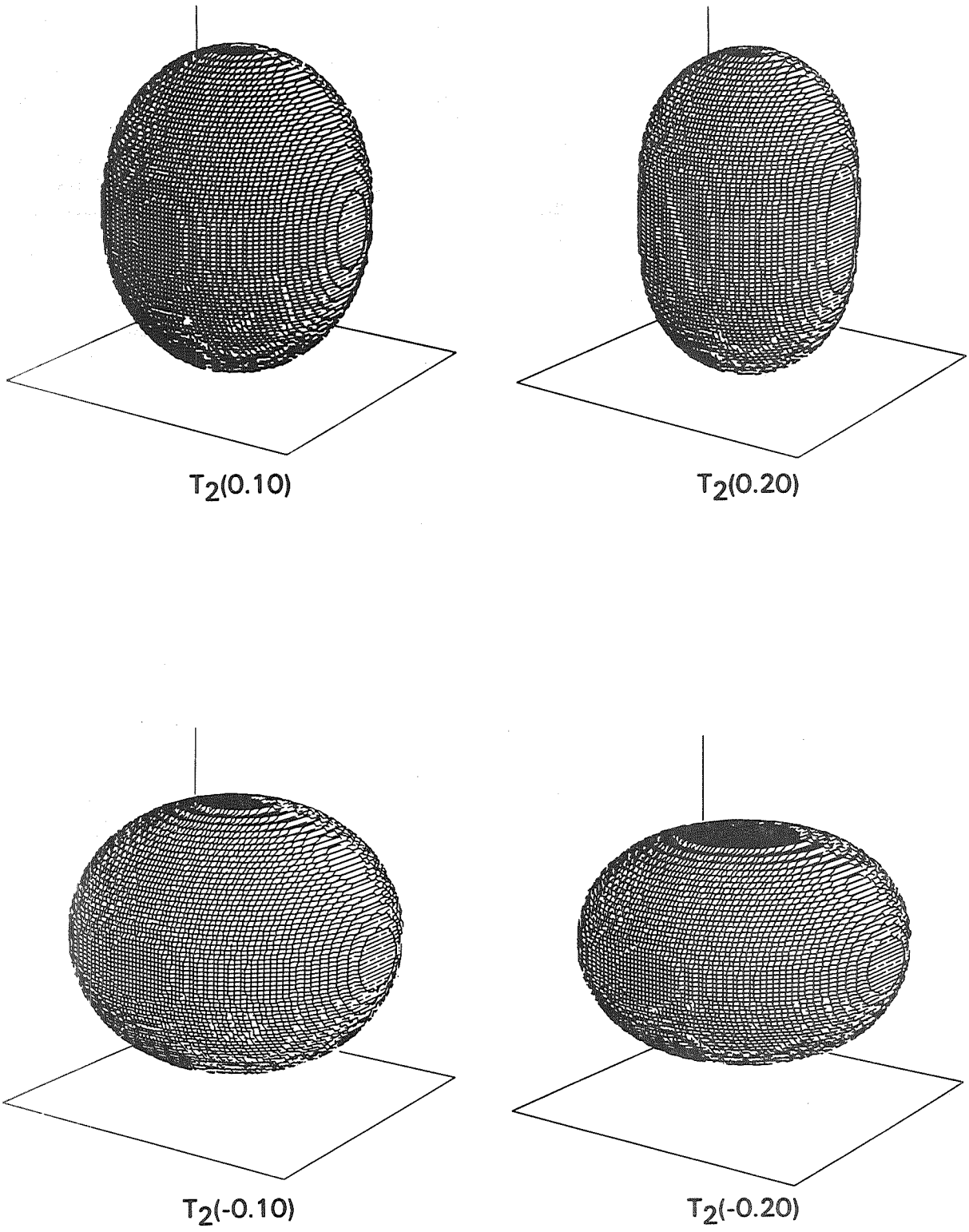

Figure 1. Three-dimensional drawings of 18 of the Chebyshev particles used in this scattering study.

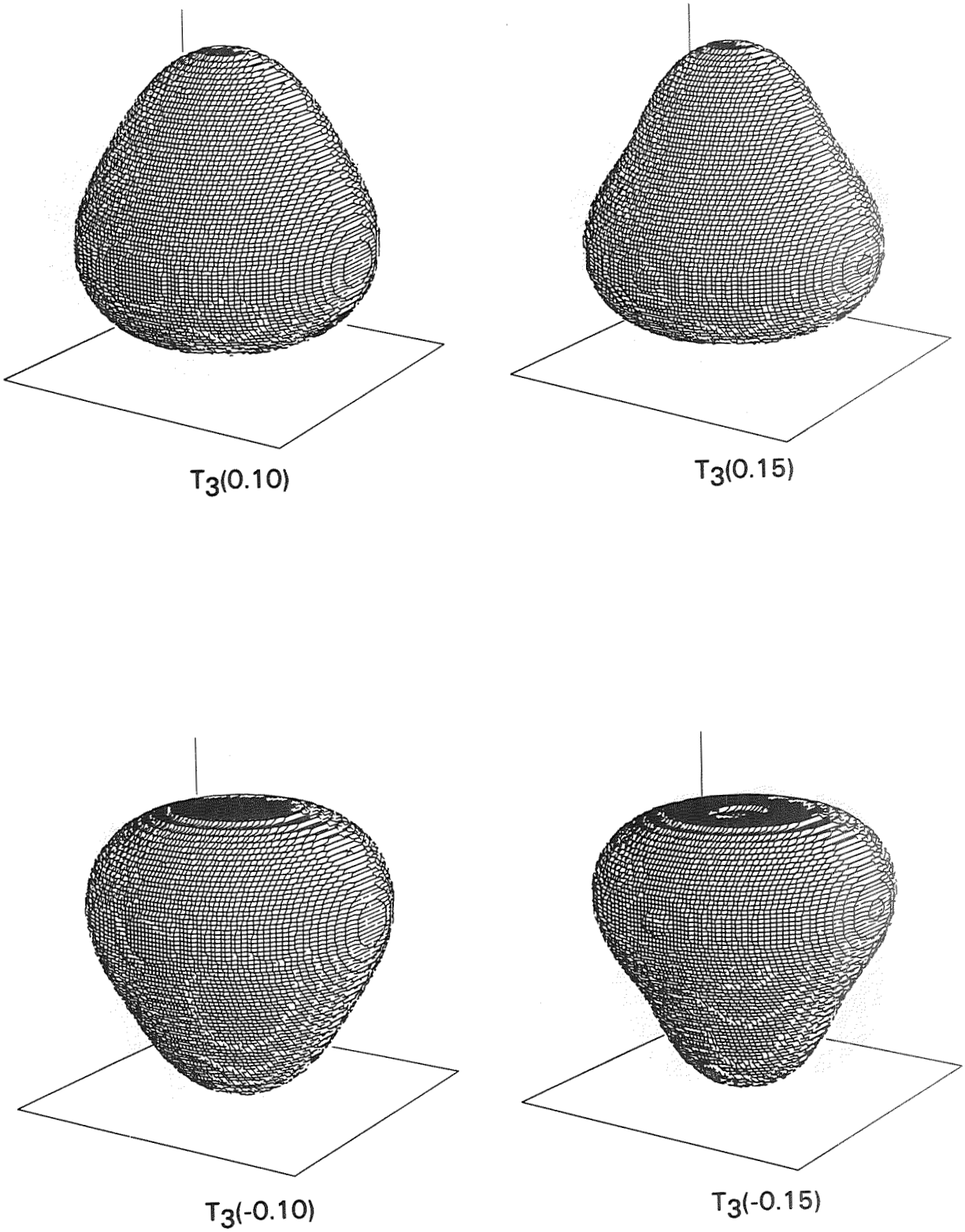

Figure 1 (Continued)

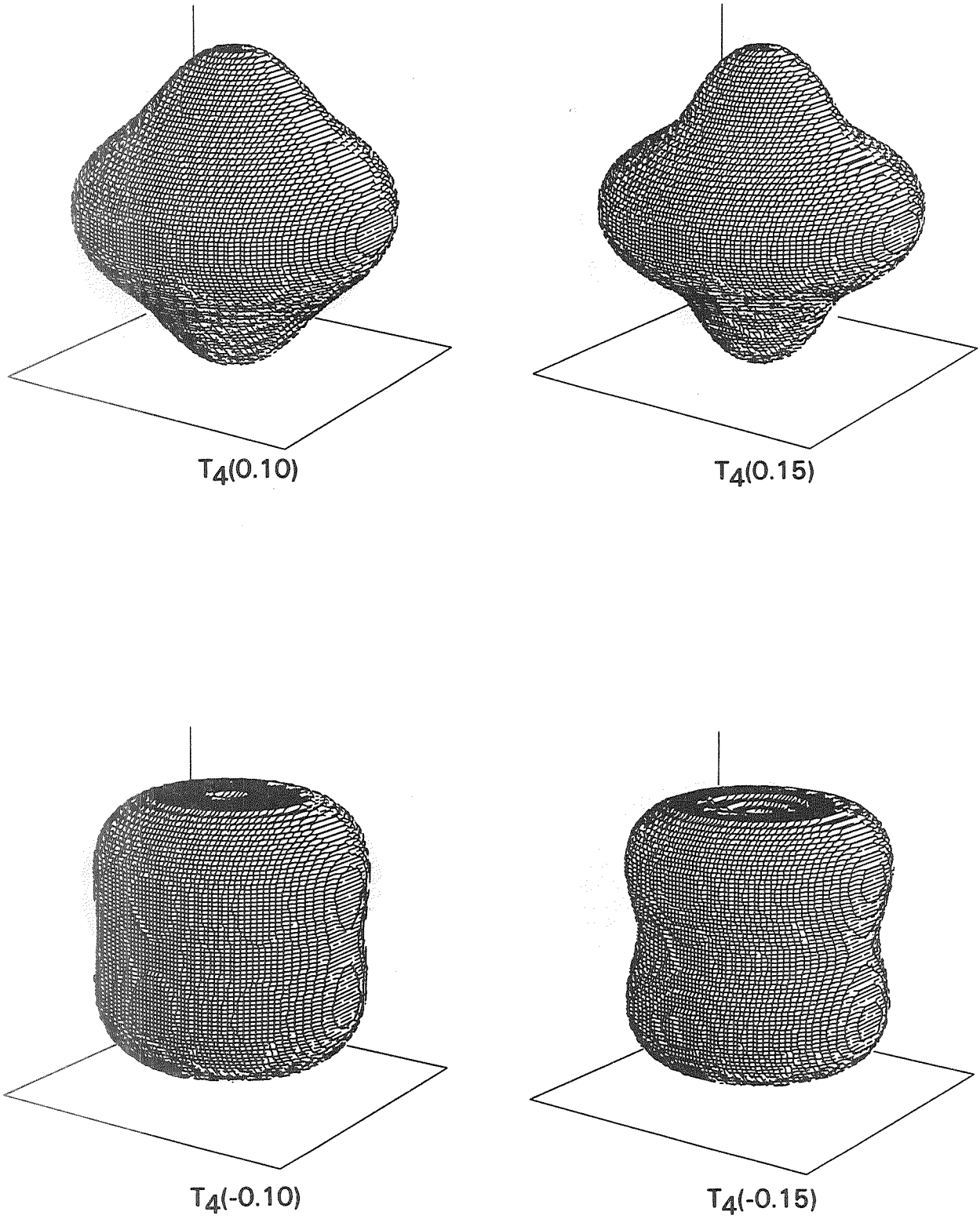

Figure 1 (Continued)

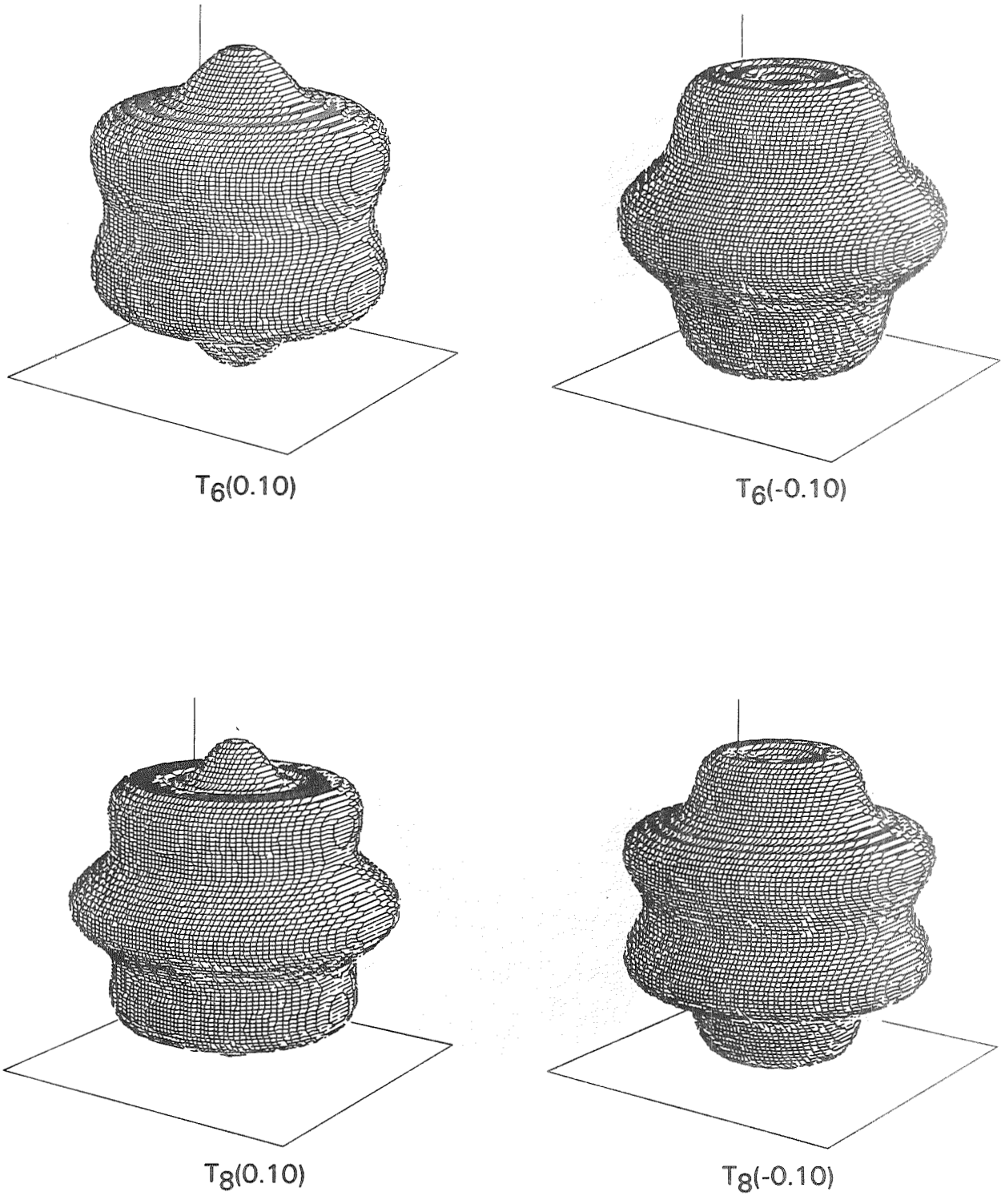

Figure 1 (Continued)

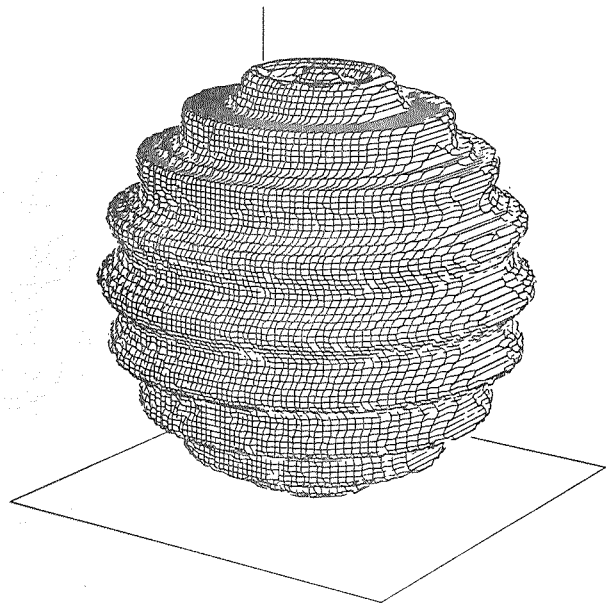

$T_{20}(0.05)$

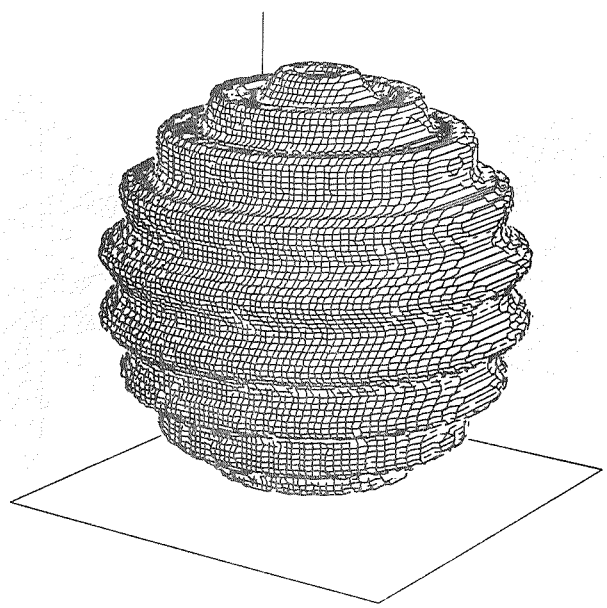

$T_{20}(-0.05)$

Figure 1 (Continued)

III. EBCM — THEORETICAL CONSIDERATIONS

We do not wish to review the EBCM in detail. For that, the reader is referred to the original references (Waterman, 1965, 1971; Barber, 1973; Barber and Yeh, 1975). But we do wish to clarify those concepts and formulas which are either relevant to the numerical computations, or inadequately discussed in the journal literature.

Reference frames

The problem is to find the scattered electromagnetic field produced by a plane wave incident upon a particle of arbitrary shape and size, in arbitrary orientation. The geometry of this scattering problem is shown in Figure 2.

Let us assume that a plane wave is always incident along the z–axis, while the orientation of the scatterer can vary. Let us take the x–z plane to be the 'scattering plane', containing the incident and scattering directions (z and s respectively) with an angle Θ between them. In this way we define the "laboratory frame" (x-y-z), within the origin 0 inside the particle (Fig. 2a).

Let us further define an (arbitrary) reference axis z' through the scatterer. (For axisymmetric particles such as ours, the problem simplifies immensely if the reference axis and the rotation axis are coincident.) Then the orientation of the particle in the laboratory frame is given by the zenith angle Θ_p and the azimuth angle ϕ_p of z' (see Fig. 2a again).

The "body frame" (x'–y'–z') is assumed rigidly fixed to the scatterer, with the same origin as the laboratory frame. It can be obtained by two successive rotations of the laboratory frame: first, as shown in Fig. 2b, a $(\pi - \phi_p)$ rotation around the z-axis in the y to x sense, to obtain a new frame $(x'' - y' - z)$; second, as shown in Fig. 2c, a Θ_p rotation around the y'-axis in the x'' to z sense. Therefore, as can be seen in Fig. 2c, y' lies on the x-y plane, while x'', x', z and z' are coplanar.

In the body frame, the direction of scattering s is characterized by zenith and azimuth angles Θ_b and ϕ_b respectively (see Fig. 2d).

Expansion of the electromagnetic field

In the EBCM, both the incident and scattered electric fields $\mathbf{E}^i$ and $\mathbf{E}^s$ are expanded in vector spherical harmonics:

$$\mathbf{E}^i(\mathbf{r}) = \sum_{\nu=1}^{\infty} D_\nu \left[a_\nu^i \mathbf{M}_\nu^1(k\mathbf{r}) + b_\nu^i \mathbf{N}_\nu^1(k\mathbf{r}) \right] \tag{4a}$$

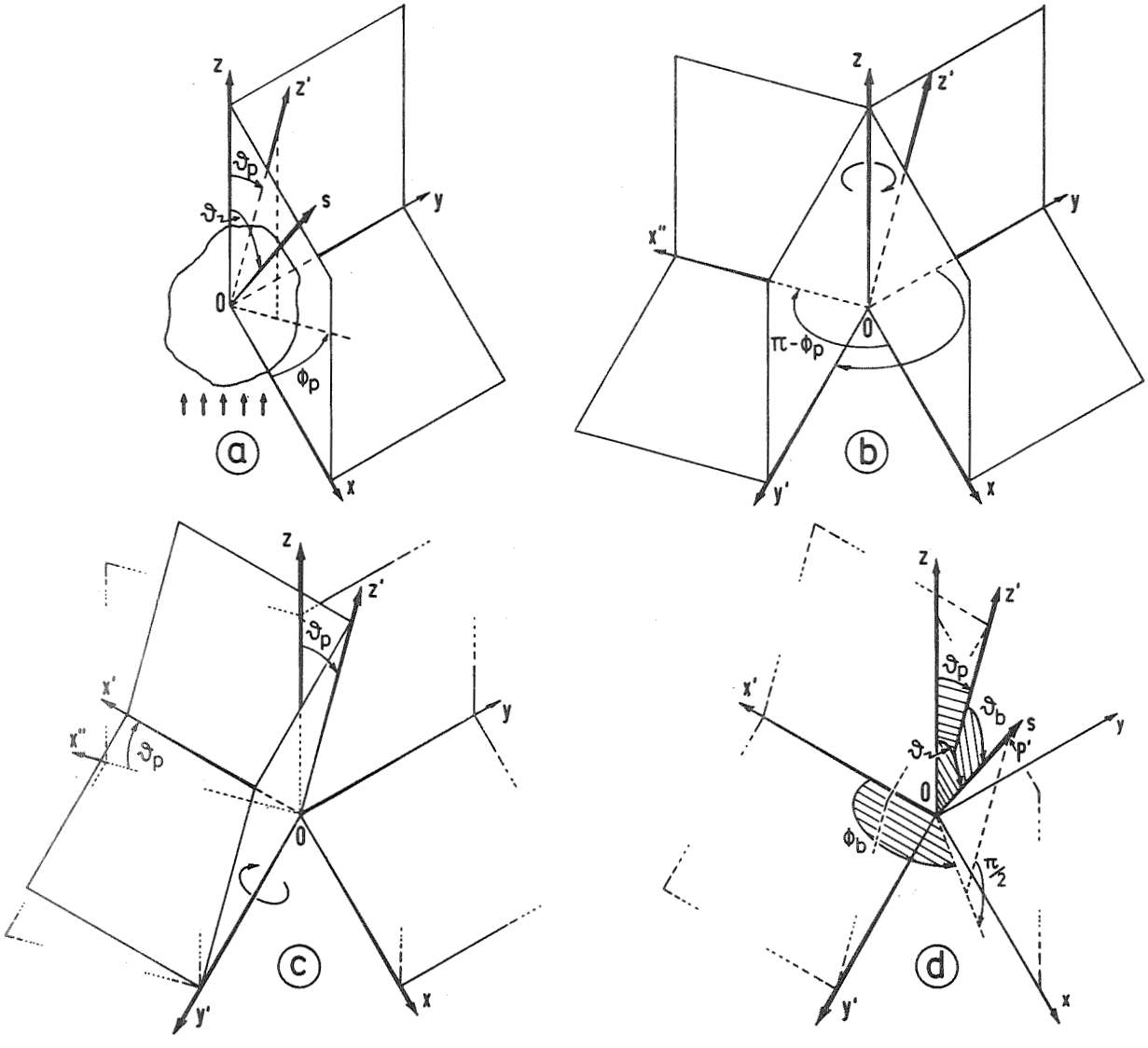

Figure 2. Successive rotations transforming the body frame into the laboratory frame. The various angles are defined in the text.

$$\mathbf{E}^s(\mathbf{r}) = \sum_{\nu=1}^{\infty} D_\nu \left[a_\nu^s \, \mathbf{M}_\nu^3(k\mathbf{r}) + b_\nu^s \, \mathbf{N}_\nu^3(k\mathbf{r}) \right] \tag{4b}$$

where $k = 2\pi/\lambda$; $\mathbf{r}$ is the radius vector; ν is a combined index incorporating the usual spherical harmonics indices σ,m,n (Morse and Feshbach, 1953, p. 1865), where σ is either 'e' (even) or 'o' (odd); D_ν is a normalization constant

$$D_\nu = \epsilon_m \frac{(2n+1)(n-m)!}{n(n+1)(n+m)!} \tag{5}$$

($\epsilon_0 = 1$, $\epsilon_m = 2$ otherwise); a_ν^i and b_ν^i are the known expansion coefficients of the incident field; a_ν^s and b_ν^s are the unknown coefficients of the scattered field (to be determined by the EBCM); and $\mathbf{M}$, $\mathbf{N}$ are the vector spherical harmonics

$$\mathbf{M}_\nu(\mathbf{r}) = \nabla \times \left[\mathbf{r} \begin{Bmatrix} \cos(m\phi) \\ \sin(m\phi) \end{Bmatrix} P_n^m(\cos\Theta) \, z_n(k\mathbf{r}) \right] \tag{6a}$$

$$\mathbf{N}_\nu(\mathbf{r}) = \frac{1}{k} \nabla \times \mathbf{M}_\nu \tag{6b}$$

(Morse and Feshbach, 1953, p. 1865). Here r, Θ, and ϕ are the usual spherical coordinates of the field point r; $\cos(m\phi)$ is used when the index σ is 'e' (even), $\sin(m\phi)$ when it is 'o' (odd); $P_n^m(\cos\Theta)$ is the associated Legendre function; and $z_n(kr)$ is a spherical Bessel function.

$\mathbf{M}^1$ and $\mathbf{N}^1$ must be finite at the origin $r = 0$, and therefore

$$z_n(kr) = j_n(kr) \tag{7a}$$

where j_n is the spherical Bessel function of the first kind. $\mathbf{M}^3$ and $\mathbf{N}^3$ must represent outgoing waves at infinity, and therefore

$$z_n(kr) = h_n^{(1)}(kr) = j_n(kr) + i\, y_n(kr) \tag{7b}$$

where $h_n^{(1)}$ is the spherical Hankel function of the first kind, and y_n is the spherical Neumann function.

We assume that $\mathbf{M}^3$ and $\mathbf{N}^3$ may be used to represent the scattered field even for concave particles, for which the scattered wave is not entirely an outgoing wave near the particle; by so doing, we apply the "Rayleigh hypothesis" (Millar, 1969, 1973), which had its origin in the theory of rough reflecting surfaces.

Since the incident field is assumed to be a plane wave, we have

$$\mathbf{E}^i = \mathbf{E}^o e^{ikz} \tag{8}$$

$\mathbf{E}^0$ is a unit vector along the direction of polarization (i.e., we normalize the incident field to unity).

Theoretical solution

A thorough formulation of the EBCM for dielectric scatterers can be found in Barber and Yeh (1975). Basically, their method of solution makes use of Schelkunoff's (1943) equivalence theorem, which says that the field scattered by a particle can be exactly reproduced by 'equivalent' (albeit fictitious) electric and magnetic currents on its surface. Then, applying the usual electromagnetic boundary conditions (continuity of the tangential components of the fields), and truncating the expansions (4) after N terms, one obtains a system of linear equations relating the scattered and incident field coefficients:

$$\begin{bmatrix} a^s \\ b^s \end{bmatrix} = - \begin{bmatrix} T \end{bmatrix} \begin{bmatrix} a^i \\ b^i \end{bmatrix} \tag{9}$$

This is a 2N x 2N system. The expansion coefficients of the scattered field are obtained by solving it.

In Eq. (9), the so-called "transition matrix" is given by

$$T = \begin{bmatrix} K' + \tilde{m}J' & L' + \tilde{m}I' \\ I' + \tilde{m}L' & J' + \tilde{m}K' \end{bmatrix} \begin{bmatrix} K + \tilde{m}J & L + \tilde{m}I \\ I + \tilde{m}L & J + \tilde{m}K \end{bmatrix}^{-1} \tag{10}$$

where $\tilde{m}$ is the refractive index of the particle. I, J, K, L and I', J', K', L' are two-dimensional integrals over the particle's surface, which define the particle from an electromagnetic point of view. For example, the surface integrals I are given by

$$I = \frac{k^2}{\pi} \int_S \mathbf{M}^3_\nu (kr_s) \times \mathbf{M}^1_{\nu'} (\tilde{m}kr_s) \bullet dS \tag{11}$$

Here, r_s is the radius vector from the origin to the surface element dS; and the combined index ν' incorporates σ',m',n'.

The surface integrals J, K, and L have a form similar to (11), but with different vector cross-products: $\mathbf{M}^3 \times \mathbf{N}^1$, $\mathbf{N}^3 \times \mathbf{M}^1$, and $\mathbf{N}^3 \times \mathbf{N}^1$, respectively. The surface integrals I', J', K', and L' have the same form as I, J, K, and L, respectively, except that all the vector spherical harmonics are of the first kind.

It is advantageous to calculate the surface integrals in the body frame because, in that frame, they are independent of the direction of the incident field. Thus, when we solve the system (9) in the body frame, we avoid recalculation of the transition matrix T when the orientation of the particle is changed. Moreover, in the next sub-section, we will see that for axisymmetric particles (like ours) the computation of surface integrals in the body frame can be dramatically simplified.

Surface integrals in the body frame

As an example of the formulas for the surface integrals in the body frame, let us consider:

$$I_{emnom'n'} = \frac{1}{\pi}\int_0^{2\pi} d\phi_s \int_{-1}^{1} h_n^{(1)}(kr_s)\, j_{n'}(\tilde{m}kr_s)\,(kr_s)^2 \tag{12}$$

$$\times \left[m\, A_{mnm'n'}(\cos\Theta_s)\sin(m\phi_s)\sin(m'\phi_s) \right.$$

$$\left. + m' A_{m'n'mn}(\cos\Theta_s)\cos(m\phi_s)\cos(m'\phi_s) \right]$$

$$d(\cos\Theta_s)$$

where

$$A_{m'n'mn}(\cos\Theta) = \frac{n(n+1)}{2n+1}\tilde{P}_{n'}^{m'}(\cos\Theta)\left[\frac{n-m+1}{n+1}\tilde{P}_{n+1}^{m}(\cos\Theta)\right. \tag{13}$$

$$\left. - \frac{n+m}{n}\tilde{P}_{n-1}^{m}(\cos\Theta)\right]$$

and

$$\tilde{P}_n^m(\cos\Theta) \equiv \frac{P_n^m(\cos\Theta)}{\sin\Theta} \tag{14}$$

Here, P_n^m is the associated Legendre polynomial. The other surface integrals have similar expressions, which can be easily obtained from Eq. (11) and the comments following it.

For axisymmetric particles, it is possible to perform the integral over azimuth ϕ_s analytically, since r_s, the radius of the particle surface, is a function of $\cos\Theta_s$ only (e.q., Eq. 1 for Chebyshev particles). As a consequence, many of the surface integrals vanish, depending on the relative parity of the indices σ and σ', and on the values of the azimuthal indices m and m'. For example, for the surface integrals I, we have (Barber, 1973, pp. 43-45):

$$I_{emnem'n'} = I_{omnom'n'} = 0 \tag{15a}$$

for all m and m'; and

$$I_{emnom'n'} = I_{omnem'n'} = 0 \tag{15b}$$

for $m' \neq m$.

Therefore, only the surface integrals $I_{emnomn'}$ and $I_{omnemn'}$ are non-vanishing. And because of the further simplification that

$$I_{omnemn'} = - I_{emnomn'} \tag{16a}$$

we need only calculate

$$I_{emnomn'} = m \int_{-1}^{1} h_n^{(1)}(kr_s)\, j_{n'}(\tilde{m}kr_s)\, (kr_s)^2 \times \left[A_{mnmn'}(\cos\Theta_s) + A_{mn'mn}(\cos\Theta_s) \right] d(\cos\Theta_s) \tag{16b}$$

Finally, for axisymmetric particles with a plane of symmetry perpendicular to the axis of rotation (like Eq. 1 for even 'n'), by virtue of the following property of associated Legendre functions:

$$P_n^m(-\cos\Theta) = (-1)^{n-m} P_n^m(\cos\Theta) \tag{17}$$

we have

$$I_{emnomn'} = 0 \tag{18}$$

if n and n' are both even, or both odd; otherwise, $I_{emnomn'}$ is still given by (16b), but the integral can be done just over the half-range (0,1) and doubled, if desired.

For axisymmetric particles, analogous simplifications exist for the other surface integrals as well (Barber, 1973, pp. 45–46).

Evaluation of the scattered field in the body frame

In order to evaluate the scattered field in the body frame, one must first express the expansion coefficients of the incident field in that frame.

The incident field coefficients are given by (Barber, 1973, pp. 137–139):

$$a^i_{\sigma mn} = i^n \sqrt{n(n+1)}\, \mathbf{E}^0 \cdot \mathbf{C}_{\sigma mn}(\Theta_i, \phi_i) \tag{19a}$$

$$b^i_{\sigma mn} = -i^{n+1} \sqrt{n(n+1)}\, \mathbf{E}^0 \cdot \mathbf{B}_{\sigma mn}(\Theta_i, \phi_i) \tag{19b}$$

Here, $\mathbf{E}^0$ is the unit vector in the direction of polarization of the incident electric field (8); Θ_i and ϕ_i are the zenith and azimuth angles of the direction of propagation of the incident field (in an arbitrary coordinate system); and the formulas for the vector functions $\mathbf{C}$ and $\mathbf{B}$ are given by Morse and Feshbach (1953, p. 1898).

Let us work in the body frame ($\Theta_i = \Theta_p$, $\phi_i = 0$), and define the auxiliary function

$$f_{mn}(x) = n\,x\,\tilde{P}_n^m(x) - (n+m)\,\tilde{P}^m_{n-1}(x) \tag{20a}$$

Then the incident field coefficients become

$$a^i_{emn} = -i^n f_{mn}(\cos\Theta_p)\,E^0_{y'} \tag{20b}$$

$$b^i_{emn} = -i^{n+1} f_{mn}(\cos\Theta_p)\,E^0_{x'}, \tag{20c}$$

$$a^i_{omn} = i^n m\,\tilde{P}_n^m(\cos\Theta_p)\,E^0_{x'}, \tag{20d}$$

$$b^i_{omn} = -i^{n+1} m\,\tilde{P}_n^m(\cos\Theta_p)\,E^0_{y'} \tag{20e}$$

where the components of $\mathbf{E}^0$ along the x'' and y' axes are:

$$E^0_{x'} = -E^0_x \cos\phi_p - E^0_y \sin\phi_p \tag{21a}$$

$$E^0_{y'} = E^0_x \sin\phi_p - E^0_y \cos\phi_p \tag{21b}$$

and E^0_x and E^0_y are the components of $\mathbf{E}^0$ in the laboratory frame.

Since we know the surface integrals I, J, etc., and therefore the transition matrix, we can now merely apply the linear transformation (9) to obtain the expansion coefficients a^s and b^s of the scattered field in the body frame.

The vector far-field ($kr \to \infty$) amplitude of the scattered field $\mathbf{F}$ is defined by

$$\mathbf{E}^s(kr) = \mathbf{F}(\mathbf{e}_s, \mathbf{e}_z)\,e^{ikr}/kr \tag{22}$$

where $\mathbf{e}_z$, $\mathbf{e}_s$ are unit vectors in the directions of the incident and scattered waves, respectively. The vector spherical harmonic expansion of $\mathbf{F}$ in the body frame is given by Barber (1973, pp. 148-150). Absorbing a factor $[n(n+)]^{1/2}$ into the spherical harmonics, the components of $\mathbf{F}$ parallel ($q = \ell$) and perpendicular ($q = r$) to the plane defined by z' and s are

$$F_b^q = \sum_{\nu=1}^{N} i^{-(n+1)} D_\nu \left[a^s_\nu C^q_\nu(\Theta_b, \phi_b) + i\,b^s_\nu B^q_\nu(\Theta_b, \phi_b)\right] \tag{23}$$

Θ_b and ϕ_b, the zenith and azimuth angles of the direction of scattering $\mathbf{e}_s$ in the body frame, are shown in Fig. 2d and are given by:

$$\Theta_b(\Theta) = \tan^{-1}\left\{\frac{[(\sin\Theta\cos\Theta_p\cos\phi_p - \cos\Theta\sin\Theta_p)^2 + (\sin\Theta\sin\phi_p)^2]^{1/2}}{\sin\Theta\sin\Theta_p\cos\phi_p + \cos\Theta\cos\Theta_p}\right\} \tag{24a}$$

$$\phi_b(\Theta) = \tan^{-1}\left\{\frac{\sin\Theta\sin\phi_p}{\cos\Theta\sin\Theta_p - \sin\Theta\cos\Theta_p\cos\phi_p}\right\} \tag{24b}$$

(Θ is the scattering angle in the laboratory frame). The modified vector spherical harmonics are

$$C^{\ell}_{emn} = B^{r}_{emn} = -m\sin(m\phi_b)\,\tilde{P}_n^m(\cos\Theta_b) \tag{25a}$$

$$C^{\ell}_{omn} = B^{r}_{omn} = m\cos(m\phi_b)\,\tilde{P}_n^m(\cos\Theta_b) \tag{25b}$$

$$C^{r}_{emn} = -B^{\ell}_{emn} = -\cos(m\phi_b)\,f_{mn}(\cos\Theta_b) \tag{25c}$$

$$C^{r}_{omn} = -B^{\ell}_{omn} = -\sin(m\phi_b)\,f_{mn}(\cos\Theta_b) \tag{25d}$$

The scattered field in the laboratory frame

The final step is to calculate the two components of **F** in the laboratory frame — one (F_ℓ) parallel to the scattering plane, the other (F_r) perpendicular to this plane:

$$F_\ell(\Theta) = F_b^{\ell}(\Theta_b, \phi_b)\cos\beta + F_b^{r}(\Theta_b, \phi_b)\sin\beta \tag{26a}$$

$$F_r(\Theta) = -F_b^{\ell}(\Theta_b, \phi_b)\sin\beta + F_b^{r}(\Theta_b, \phi_b)\cos\beta \tag{26b}$$

where

$$\beta = \tan^{-1}\left\{(\cos\Theta\cos\Theta_p\cos\phi_p\sin\phi_b + \sin\Theta\sin\Theta_p\sin\phi_b + \cos\Theta\sin\phi_p\cos\phi_b)/(\cos\Theta_p\sin\phi_p\sin\phi_b - \cos\phi_p\cos\phi_b)\right\} \tag{27}$$

The two components of the intensity of the scattered field (using the same notation as in Mie theory) are then simply

$$i_q(\Theta) = |F_q(\Theta)|^2 \tag{28}$$

where $q = \ell$ or r. The scattering and extinction cross-sections are given by (Waterman, 1965):

$$\sigma_{sca} = \frac{4\pi}{k^2}\sum_{\nu=1}^{N} D_\nu \left\{|a^s_\nu|^2 + |b^s_\nu|^2\right\} \tag{29a}$$

$$\sigma_{ext} = \frac{4\pi}{k^2} \text{Im} \left[\mathbf{E}^0 \bullet \mathbf{F}(0) \right] \tag{29b}$$

where $\mathbf{F}(0)$ is the far–field amplitude of the scattered electric field in the forward direction ($\Theta = 0$).

IV. EBCM — SPECIALIZATION TO AXISYMMETRIC SCATTERERS

For axisymmetric scatterers, all the surface integrals vanish for m = m' (recall that m and m' are components of the tripartite indices ν and ν' of the scattered and incident field expansions). As a consequence, by re-ordering $\nu = (\sigma,m,n)$ to $\nu = (\sigma,n,m)$ (and similarly for ν'), and allowing σ and n to run through their entire sequence before m is incremented, the transition matrix T in (9) becomes block diagonal. Therefore, due to the linearity of the equations, (9) splits into $(n_{max} + 1)$ independent subsystems, each corresponding to a different azimuthal mode m ($m = 0, \ldots, n_{max}$, where n_{max} is the highest n-value used):

$$\begin{bmatrix} a^s \\ b^s \end{bmatrix} = - \begin{bmatrix} T_m \end{bmatrix} \begin{bmatrix} a^i \\ b^i \end{bmatrix} \tag{30}$$

Here, T_m is the appropriate block of T for the given m-value, and the expansion coefficients a and b are for all possible combinations of σ and n (or σ' and n'), holding m (or m' = m) constant. In what follows, these expansion coefficients will be indicated by the subscript μ (or μ'), a combination of the two indices σ and n (or σ' and n').

Because of the linearity of the vector spherical harmonic expansions, the splitting over separate m–values carries through the entire calculation; thus, *the entire scattering problem can be replaced by $(n_{max} + 1)$ independent sub-problems, each corresponding to a different azimuthal mode m.* This is accompanied by a re-ordering of the sums over m and n in all spherical harmonic expansions, as follows:

$$\sum_{n=0}^{n_{max}} \sum_{m=0}^{n} \rightarrow \sum_{m=0}^{n_{max}} \sum_{n=m}^{n_{max}} \tag{31}$$

This means that the total scattered field can be calculated as the sum of partial fields $\mathbf{E}_m{}^s$:

$$\mathbf{E}^s = \sum_{m=0}^{n_{max}} \mathbf{E}_m{}^s \tag{32}$$

where each partial field is obtained from an analogue of (4b), but with coefficients obtained from (30), and a summation over μ rather than ν.

This result brings important simplifications and speed enhancements in the numerical solution. For, in the general case, the linear equations to be solved form a potentially very large 2Nx2N system (Eq. 9), where

$$N = n_{max}(n_{max} + 3) \tag{33}$$

is the total number of terms to be summed in the spherical harmonic expansions (4) (note that the $n = 0$ terms vanish and therefore are not taken into account when computing N). However, for axisymmetric scatterers, this system is replaced by the $(n_{max} + 1)$ sub-systems (30), each of dimension $2(n_{max} - m + 1)$. Note that the sub-system dimensions decrease as m increases, because, in the matrices T_m, n ranges from m to n_{max}. Also, the sub-system dimensions already account for parity relations among the surface integrals (e.g., 16a), which reduce the size of the matrices T_m by a factor of 4.

V. EBCM — NUMERICAL CONSIDERATIONS

There are four major numerical steps involved in calculating the scattered electric field for a given orientation of the particle; then, a fifth and sixth step are required for averaging over orientation. The organization of these six steps into an EBCM algorithm is shown in Figure 3. We developed this logical structure specifically to take advantage of the 'array processing' or 'vectorization' features of modern computers. (Figure 3 refers to axisymmetric particles only; for non-axisymmetric particles, important sections of this logical structure would have to be re-formulated.)

Step 1. Determination of n_{max} in nose-on orientation

The length N of the expansions of the incident and scattered fields in vector spherical harmonics (Eq. 4) is not known *a priori;* it depends on the shape, size, and refractive index of the particle. In general, one should guess an initial N value, solve the scattering problem, and then increase N in steps until 'satisfactory' convergence of the scattered field is obtained. This may, however, result in a prohibitively lengthy procedure.

Fortunately, for axisymmetric particles (see Sec. IV), it is possible to estimate the length of the expansions in a much faster way. For nose-on incidence (defined as $\Theta_p = 0$), by virtue of the rotational symmetry of the particle about the direction of incidence, the only contribution to the scattered field comes from the single azimuthal mode $m = 1$ (as for a sphere). Therefore, it is advantageous to utilize nose-on orientation to determine the length of the n-expansion sufficient for convergence. Then we merely use the same upper limit n_{max} for all the orientations.

By so doing, we assume that n_{max} is independent of the orientation of the particle — which is not true in general. For different orientations of the particle, deep downward spikes in the angular scattering pattern (representing a lot of cancellation among the terms in the spherical harmonic expansion) often require higher n_{max} values in order to converge. However, we usually ignored this problem; our interest was mainly in randomly-oriented particles, where the scattering pattern is rather smooth — the spikes wash out in the orientation-averaging process. (For further discussion of this spike-washing-out process, but for spheres, see Sec. VIII.)

We are not going to describe here the numerical procedures in the nose-on case, since they follow closely steps 2-4 in Fig. 3, which are described below. The only difference from the general case is that now the loop over the m_{max} disappears (m_{max} must be 1), and only the orientation ($\Theta_p = 0, \phi_p = 0$) is considered.

By solving the scattering problem for successively larger values of n_{max} in the nose-on case, and stopping when the changes become 'small enough', n_{max} is determined. Section VI (convergence procedures) will flesh out the details of this operation.

(STEP 1)	NOSE-ON	($\Theta_p = 0$)	
		find n_{max}	
	LOOP	$m_{max} = 0, 1, \ldots, n_{max}$	
(STEP 2)		I,J,K,L; I',J',K',L'	(vec. Θ_s)
(STEP 3)		T_m sub-matrices	(vec. n)
	LOOP	Θ_p: from 1 to N_Θ	
	LOOP	ϕ_p: from 1 to N_ϕ	
(STEP 4)		Θ_b, ϕ_b	(vec. Θ)
		a^i_μ, b^i_μ	(vec. n)
		a^s_μ, b^s_μ	(vec. n)
		$F_b^q(\Theta_b,\phi_b)$	(vec. Θ)
		$\sum_{m=0}^{m_{max}} F_q^{(m)}(\Theta)$	(vec. Θ)
		$i_q(\Theta,m_{max})$	(vec. Θ)
		σ_{sca}	(vec. n)
		σ_{ext}	
	END	ϕ_p LOOP	
	END	Θ_p LOOP	
(STEP 5)		$<i_q(\Theta)>$	(vec. Θ_p,ϕ_p)
(STEP 6)		$<\sigma_{sca}>, <\sigma_{ext}>$	(vec. n)
	IF	(convergence over m_{max}) EXIT	
	END	m_{max} LOOP	

Figure 3. Logical structure of EBCM algorithm. (vec. x) means that the indicated step is vectorized over the variable x. Other symbols are defined in the text.

Because of the splitting into (n_{max} + 1) sub-problems (see Sec. IV), steps 2-6 in Fig. 3 appear inside a loop over the azimuthal index 'm'. It is advantageous to check convergence of the series (32) at each step of this m-loop, since convergence usually occurs well before the theoretical upper limit n_{max}. Hence partial sums from m = 0 up to the current value of m (called m_{max} in Fig. 3) are calculated. When the newest terms being added to these sums are small compared to the values of the sums, this is called 'convergence over m_{max}', and the algorithm is finished. Details of this procedure may be found in Sec. VI.

Step 2: Calculation of the surface integrals

Rapid calculation of surface integrals (12-18) is important, since otherwise an inordinate amount of computer time will be wasted in assessing convergence over n_{max} (Step 1), as we shall see in Sec. VI. Hence, we used a Gaussian quadrature over the variable cos Θ_s, which requires about a factor of 10 fewer integrand evaluations than, for example, Simpson's or Bode's Rule (the latter was used in the EBCM code we received from Prof. Barber). Of course, Gauss rules assume a smooth particle shape, with no corners or edges; cubes and such-like are excluded.

We have found that, for the Chebyshev particles, the number of Gaussian quadrature points N_G must not be substantially smaller than n_{max}; otherwise, the surface integrals are not calculated accurately enough, and this may even cause the scattered field expansion to diverge. On the other hand, we have noticed that very high N_G values ($N_G >> n_{max}$) may also sabotage convergence, presumably because the error term R in the Gauss rule

$$\int_{-1}^{+1} f(x)\,dx = \sum_{i=1}^{N_G} w_i\, f(x_i) + R(N_G) \tag{34}$$

is proportional to a high-order derivative of the integrand (which is not true in Simpson's or Bode's Rule):

$$R(N_G) = \frac{2^{2n+1}\,(n!)^4}{(2n+1)\,[(2n)!]^3} f^{(2n)}(x_o) \tag{35}$$

(x_i and w_i are the absicissae and the weights, respectively, of the Gauss rule, and x_0 is a point in the interval of integration). Examples of inaccuracy in Gauss rules for overly-large numbers of quadrature points can be found in Davis and Rabinowitz (1975).

For the above-mentioned reasons, we have chosen to take $N_G = n_{max}$ throughout the calculations, even though this choice wastes computer time during the determination of n_{max} (because of the need to re-calculate surface integrals at each step of the iteration instead of just using the old values).

Step 3: Evaluation of the transition matrix

Once the surface integrals have been calculated, one is in a position to evaluate the transition sub-matrices T_m (33) in the body frame. This requires the inversion of the block-diagonal (axisymmetric-particle) form of the second matrix in (10), which is accomplished using the Gauss-Jordan method. We used Barber's routine for this, rather than a library subroutine from LINPACK, because it takes advantage of the large number of known zeroes in the matrix.

Barber (1977) discusses the ill-conditioning in this matrix inversion when any of the variables which define the scattering object (its size parameter, deviation from sphericity, and refractive index) is increased too far. This problem is a symptom that the transition matrix T (and therefore the scattered field coefficient vector) has become very sensitive to the length of the spherical harmonic expansions, so that no convergence can be determined.

In the present study, we fixed the Chebyshev deformation parameter ϵ at various values between -0.20 and $+0.20$; then, for each ϵ, we increased the size of the particle until ill-conditioning was encountered and convergence could no longer be achieved. Except for the very smallest size parameters, it was impossible to achieve convergence for magnitudes of ϵ significantly above 0.20.

Step 4. Evaluation of the scattered field for any orientation

We can now solve the scattering problem for any orientation (Θ_p, ϕ_p) of the particle. First of all, using (24) one must calculate the two arrays of angular coordinates (Θ_b, ϕ_b) which define the various scattering directions s in the body frame (see Fig. 2).

Then, the expansion coefficients of the incident field, (a_μ^i and b_μ^i) are evaluated in the body frame using (20). They are multiplied by the transition sub-matrix T_m (30) to obtain the expansion coefficients of the scattered field for the considered azimuthal mode m (a_μ^s and b_μ^s) in the body frame.

Next, the scattered field coefficients are used in (23) to obtain the components of the far-field amplitude in the body frame; and then, these components are transformed back to the laboratory frame (Eqs. 26). This is done for a whole array of scattering angles Θ at once, in vector loops, as indicated on the right-hand side of Fig. 3.

The computations carried out so far (Steps 2-4) all refer to a specific azimuthal mode m in the m_{max} loop in Fig. 3. One must also update the running sums of the components $F_q^{(m)}$ of the far-field amplitude vector corresponding to the partial fields E_m^s:

$$F_q(\Theta, m_{max}) = \sum_{m=0}^{m_{max}} F_q^{(m)}(\Theta) \tag{36}$$

Finally, the intensities i_q and extinction cross-sections σ_{ext} are evalulated from these running sums using (28) and (29b). For the computation of the scattering cross-section σ_{sca} (29a), all the a_ν^s and b_ν^s calculated so far must be considered; thus, in (29a), ν takes into account all possible combinations of σ, n and m for $n \leq n_{max}$ and $m \leq m_{max}$.

When studying scattering just in fixed particle orientation, convergence over m_{max} should be checked at the conclusion of Step 4. On the other hand, when our interest lies in randomly-oriented particles, this test must be postponed until after the average over orientation is made (Steps 5 and 6).

Step 5. Avering over orientation: intensities

Orientation-averaging is accomplished using a two-dimensional Gaussian quadrature over orientation angles (Θ_p, ϕ_p) of the following generic form:

$$<Y> = \frac{1}{4\pi} \int_0^{2\pi} d\phi \int_{-1}^{+1} Y(\Theta, \phi)\, d(\cos\Theta) \tag{37}$$

$$\cong \frac{1}{4\pi} \sum_{i=1}^{N_\Theta} \sum_{j=1}^{N_\phi} w_i \hat{w}_j\, Y(\Theta_i, \phi_j)$$

(This is actually just the product of two one-dimensional Gauss rules, not a general two-dimension rule, for which no exact solution for the weights and abscissae is known.) Y is any real scattering quantity, such as intensity or cross-section (averaging the complex scattering amplitude would preserve phase relations, which we assume does not occur). $\cos(\Theta_i)$ and w_i are the N_Θ abscissae and weights of the Gauss rule over $(-1,1)$; and ϕ_j and $\hat{w}_j$ are the N_ϕ abscissae and weights of the Gauss rule over $(0,2\pi)$.

In our computations, we have used a number of zenith orientations which depends on the particle size and on its deformation from a sphere:

$$N_\Theta = (0.5x + 3)(20\,|\epsilon| + 1)/3 \tag{38}$$

For each zenith orientation $\Theta_{p,i}$, the number of azimuth orientations is taken proportional to N_Θ and to the area of the spherical zone at that zenith angle:

$$N_\phi = 2\, N_\Theta \sin\Theta_{p,i} \tag{39}$$

Both (38) and (39) are purely empirical rules which we developed. There is no *a priori* reason to expect that they will be satisfactory for shapes very different from Chebyshev particles.

With only 750,000 words of memory on the CRAY-1, we were forced to set an upper bound of 10 on N_Θ (we also never let it fall below 3). This is due to the necessity of storing two complex matrices, of

dimension (no. scattering angles) x (no. orientations), containing the components of the vector far-field amplitude. This limits the total number of orientations to about 150, which may not be enough for large sizes and/or deformations. However, for axisymmetric particles, some simplifications enable us to double or quadruple the number of orientations.

This is because the axisymmetry of the particles leads to symmetry properties of the intensities. For any given zenith orientation Θ_p, the intensities corresponding to the ϕ_p and $(\phi_p + \pi)$ azimuth orientations are related as follows:

$$i_{\Theta_p, \phi_p + \pi}(\Theta) = i_{\Theta_p, \phi_p}(2\pi - \Theta) \tag{40}$$

Therefore, we only need to perform computations for Gauss quadrature azimuths $\phi_{p,j}$ in the interval $(0, \pi)$. Hence, in applying (37) to intensities, the ϕ-integration can be reduced to $(0, \pi)$ and the integrand taken as

$$Y(\Theta_p, \phi_p) = i_{\Theta_p, \phi_p}(\Theta) + i_{\Theta_p, \phi_p}(2\pi - \Theta) \tag{41}$$

This is a very important simplification, because it halves the number of azimuth orientations N_ϕ for any zenith angle $\Theta_{p,i}$. In turn, this allows us to double the number of zenith orientations N_Θ with no penalty in computer time or storage.

A further simplification is possible for particles with a plane of symmetry perpendicular to the rotational axis. In this case, one can integrate over $\cos(\Theta_p)$ from 0 to 1 rather than -1 to 1 in (37), then just multiply by two. This again doubles the allowable number of zenith orientations, for a net quadrupling.

Step 6. Averaging over orientation — cross-sections

The orientation-averaged cross-sections can be obtained by making use in (37) of the fixed-orientation cross-sections calculated in Step 4. However, if random-orientation intensities are not desired for some reason, there is a much faster procedure.

Since the cross-sections of randomly-oriented nonspherical particles do not depend on the polarization of the incident field, let us assume that the incident electric field is linearly polarized in the x-direction. For each zenith orientation Θ_p, symmetry considerations allow us to compute the azimuthally-averaged cross-section just by averaging the two cross-sections for azimuths

$$1)\ \phi_p = 90°\ (E^0_{x'} = 0, E^0_{y'} = 1)$$

$$2)\ \phi_p = 180°\ (E^0_{x'} = 1, E^0_{y'} = 0)$$

This simplification was found by Barber (personal communication).

Once the azimuthally-averaged cross-sections have been obtained by this trick, the orientation-averaged cross-sections follow directly from a Gauss quadrature over zenith orientation, as usual. If the particle has a plane of symmetry perpendicular to its rotation axis, this quadrature can be simplified as described in Step 5.

Calculation of associated Legendre and Bessel functions

In steps 2-4, it is necessary to calculate the associated Legendre function $P_n^m(\cos\Theta)$ with argument either $\cos\Theta_b$ (for obtaining the far-field amplitude) or $\cos\Theta_s$ (for obtaining the surface integrals). This is done by using forward recursion for fixed m, starting from $n = m+1$:

$$P^m_{n+1}(\cos\Theta) = \frac{1}{n-m+1}[(2n+1)\cos\Theta\, P_n^m(\cos\Theta) + (n+m)P^m_{n-1}(\cos\Theta)] \tag{42}$$

The recursion is initialized by:

$$P_m^m(\cos\Theta) = \sin^m\Theta \prod_{k=1}^{m}(2k-1) \tag{43a}$$

$$P^m_{m+1}(\cos\Theta) = (2m+1)\cos\Theta\, P_m^m(\cos\Theta) \tag{43b}$$

In step 2, it is necessary to calculate the spherical Bessel functions of the first kind, j_n, both for real ($k r_s$) and complex ($\tilde{m} k r_s$) arguments. It is also necessary to calculate the spherical Bessel function of the second kind y_n for real argument $k r_s$ only, since it enters into the expression of the spherical Hankel function.

For y_n, we use a forward recursion, which is stable for real arguments (Lentz, 1975). However, the use of forward recursion for j_n is unstable. For complex arguments, we calculated j_n using the continued fraction method of Lentz (1975), while for real arguments we have used a variation on the Miller backward recursion scheme proposed by Ross (1972).

In the original code provided to us by Prof. Barber, Bessel functions were generated, both for real and complex arguments, using the Miller backward recursion. We replaced such procedures because they can occasionally overflow for large arguments.

Vectorization

'Vectorization' means re-arranging an algorithm in order to make the longest loops the innermost ones. These innermost loops must also be free of recursions and other structures that would prevent their being executed all at once.

We have deeply modified the original code we received from Prof. Barber in order to take advantage of the vector features of a CRAY-1 computer. We have vectorized any section of the code which

timing tests revealed to be using more than 10% of the computer time. Super-speed vector routines (furnished by CRAY) were also used for performing some matrix operations. The code is now about ten times faster than the original one that we received. Even so, this research has required on the order of 10 hours of CRAY time.

Fig. 3 shows what loops were vectorized in the various steps of the numerical computation. The notation 'vec. x' means that loops over the variable 'x' were made innermost, and vectorized. (If only random-orientation cross-sections are desired, Step 4 is replaced by a simplified version in which only loops over n are vectorized.)

In the Bessel function routines, recursions prevent most of the loops over n from vectorizing. In the computation of the associated Legendre polynomials, either loops over Θ_s or over Θ were vectorized, depending on the context (surface integrals or spherical harmonics expansion, respectively).

Numerical checks

Since considerable modifications of the code were made, we repeatedly checked the modified code against some results obtained with the original one supplied to us by Barber. We also checked the original code against some exact calculations of Asano and Yamamoto (1975) for spheroids in fixed orientation, for which agreement within 0.01% had been found (Mugnai and Wiscombe, 1980).

After the modification of the code had been completed, we also checked it against exact calculations of Asano (1980) for randomly oriented spheroids. Very good agreement was still obtained (0.1%). However, we were not able to get convergence for elongations greater than 3:1 when the size parameter exceeded about 10. This is in line with a comment made by Waterman (1965) in his original paper on the EBCM:

> "One present drawback of the method is the poor numerical convergence of the truncation procedure in dealing with more elongated shapes. This is of course not surprising, since one is departing from the nearly spherical shapes most ideally suited to the vector wave functions employed. As a rough rule-of-thumb, it appears that obstacles having a length-to-width ratio ≤ 2 can be treated quite well by truncation to at most 20–25 terms. . . ."

Holt (private communication) has informed us that other investigators who use the EBCM have been able to obtain convergence for more elongated spheroids. The explanation may lie in our stringent convergence procedures (see next section), compared to the relatively lax definitions of convergence used by others. However, we did not concern ourselves with this difficulty, because the many sensitivity studies we carried out for Chebyshev particles convinced us that our numerical procedures are quite suitable for these particles.

VI. EBCM — CONVERGENCE PROCEDURES

In the EBCM, infinite series are truncated after a finite number of terms; integrals are numerically evaluated; and finite series may be truncated before their theoretical upper limit. The resulting solution may be more or less 'converged', depending on our skill (there is more than a little art involved as well) in selecting the following three parameters controlling convergence:

- the highest n-value, n_{max}, used in the spherical harmonic expansions;
- the number of Gauss quadrature points, N_G, for performing the surface integrals; and
- the number of different orientations of the particle, N_{or}, used for calculating an orientation average.

In addition, it is advantageous to check convergence on a fourth parameter: the highest m-value, m_{max}, used in the spherical harmonic expansions (this is not strictly necessary, since we know that, theoretically, $m_{max} = n_{max}$).

Our procedures for determining convergence over N_G and n_{max} have evolved from those used by Barber (private communication). We therefore begin by summarizing his method.

Barber looks only at nose-on orientation of the particle. He guesses initial values for n_{max} and N_G. N_G must be about 3-5 times n_{max}, depending on the deformation of the particle from a sphere (N_G must be large because Barber uses Bode's Rule for calculating surface integrals). Then, n_{max} is increased in unit steps, holding N_G fixed, until 'convergence' of the scattered intensities is reached.

'Convergence' is defined in the Cauchy sense: it occurs when two successive iterates are 'close'. For Barber, 'close' meant that the percentage difference between the scattered intensities for n_{max} and for $(n_{max} - 1)$ was less than 1% at <u>every</u> scattering angle. (Clearly, the exact convergence he reached depended on the set of scattering angles he chose.)

If convergence is slow, the Cauchy criterion can of course be misleading. Two successive iterates can be close, yet both can be far from the final solution. In practice, such pathological situations manifest themselves as a painfully slow downward trend in the inter-iterate difference.

If convergence didn't occur, Barber fixed n_{max} at the highest value it had attained, and iterated over N_G instead (by trial and error). If convergence over N_G was attained, iteration over n_{max} was re-started from its original (low) value, holding N_G constant at its converged value.

We have modified Barber's procedure for the following reason. Barber did EBCM calculations on a case-by-case basis, checking and tuning the convergence by hand until the results were satisfactory. Our goal was to study a *great many* cases, precluding the possibility of examining each one individually; therefore, we had to invent an automatic procedure. Of course, we could simply have enforced a very stringent Cauchy criterion (0.01%, say); but this would have allowed convergence in only the easiest cases (those with the smallest deviation from sphericity). Furthermore, since our interest was in random orientation, we did not care to enforce a stringent convergence at every particular orientation and for every scattering angle.

Convergence over N_G

In order to study convergence over N_G, we carried out many tests for Chebyshev particles in nose-on orientation. In these tests, N_G was either held fixed, or increased in direct proportion to n_{max}:

$$N_G = k_0 n_{max.} \tag{44}$$

k_0 was varied between 1 and about 3.

We found that, independent of n_{max}, convergence over N_G was reached for $1 \leq k_0 < 1.5$ (larger k_0 values were necessary when n_{max} was below its convergence value). In general, we found that N_G must be neither smaller, nor much bigger, than n_{max}; both extremes could sabotage convergence.

Based on our tests, we decided to take $k_0 = 1$ throughout our calculations, for the following reasons:

- increasing k_0 from 1 to 1.5 changes the intensities less than 1/10 as much as increasing the convergence value of n_{max} by one;
- this choice prevents the scattered field expansion from diverging; and
- taking $k_0 > 1$ sometimes lowers the n_{max} value for convergence, giving results of less accuracy than those obtained with $k_0 = 1$.

Eq. (44) is unfortunate in one sense: if N_G were held constant, then each of the 8 matrices of surface integrals (e.g. Eq. 12) could be preserved for the next step of the iteration over n_{max}; only two new rows, and two new columns, would need to be added. Instead, each matrix has to be recalculated *in toto*. But at least (44) eliminates Barber's trial-and-error double iteration (over N_G and n_{max}) in favor of a single automatic iteration (over n_{max}).

Convergence over n_{max}

The selection of n_{max} is critical in obtaining correct results, especially for fixed orientation of the particle. *Extreme caution is called for, first because bad results obtained with incorrect n_{max} values are*

difficult to detect; and second, because there are usually no independent methods to check the results (unless the particles are cylinders or spheroids).

We adopted Barber's suggestion to increase n_{max} in unit steps during convergence iteration. However, we found that his convergence criterion (1% at all the angles) failed when the angular scattering pattern developed deep down-spikes, signalling cancellation among the terms of the spherical harmonics expansion at the spike angles. Convergence at those angles could not usually be achieved at all.

However, our main interest was in random orientation, in which case the deep down-spikes one sees in fixed orientation are washed out. Therefore, we developed a convergence criterion with the following requirements in mind:

- convergence should not be tested in the spikes
- convergence should be summarized in a single number, representing some sort of average over all angles.

We met the first requirement by considering, not all the N_{sca} scattering angles, but only 90% of them, i.e. only

$$\tilde{N}_{sca} = 0.9\, N_{sca} \tag{45}$$

scattering angles. We throw out that 10% of the angles where the percentage differences from one iteration to the next are largest. This is always sufficient to get rid of the spike situations.

The second requirement is met by defining two numbers, δ_q ($q = \ell$ or r), which are the root mean square relative differences between the intensities when n_{max} is increased by one (but only at the 90% of the angles defined above):

$$\delta_q \equiv \left\{ \frac{1}{\tilde{N}_{sca}} \sum_{i=1}^{\tilde{N}_{sca}} \left[\frac{i_q(\Theta_i, n_{max}) - i_q(\Theta_i, n_{max}-1)}{i_q(\Theta_i, n_{max}-1)} \right]^2 \right\}^{1/2} \tag{46}$$

'Good' convergence is then defined as

$$\delta_\ell < \delta_{min} \text{ and } \delta_r < \delta_{min} \tag{47}$$

where $\delta_{min} = 0.001$ for our research. This corresponds to percentage differences in the intensities not exceeding about 0.1%, on the average. Thus we have relaxed Barber's criterion in one sense — by disregarding 10% of the angles — and made it stricter in another sense — by demanding 0.1% rather than 1% convergence at the remaining angles.

We have made many plots of the behavior of δ_q as a function of n_{max}. Figure 4.1 shows a small but representative sample of this information; δ_ℓ (dotted line) and δ_r (dashed line) are plotted vs. n_{max} for

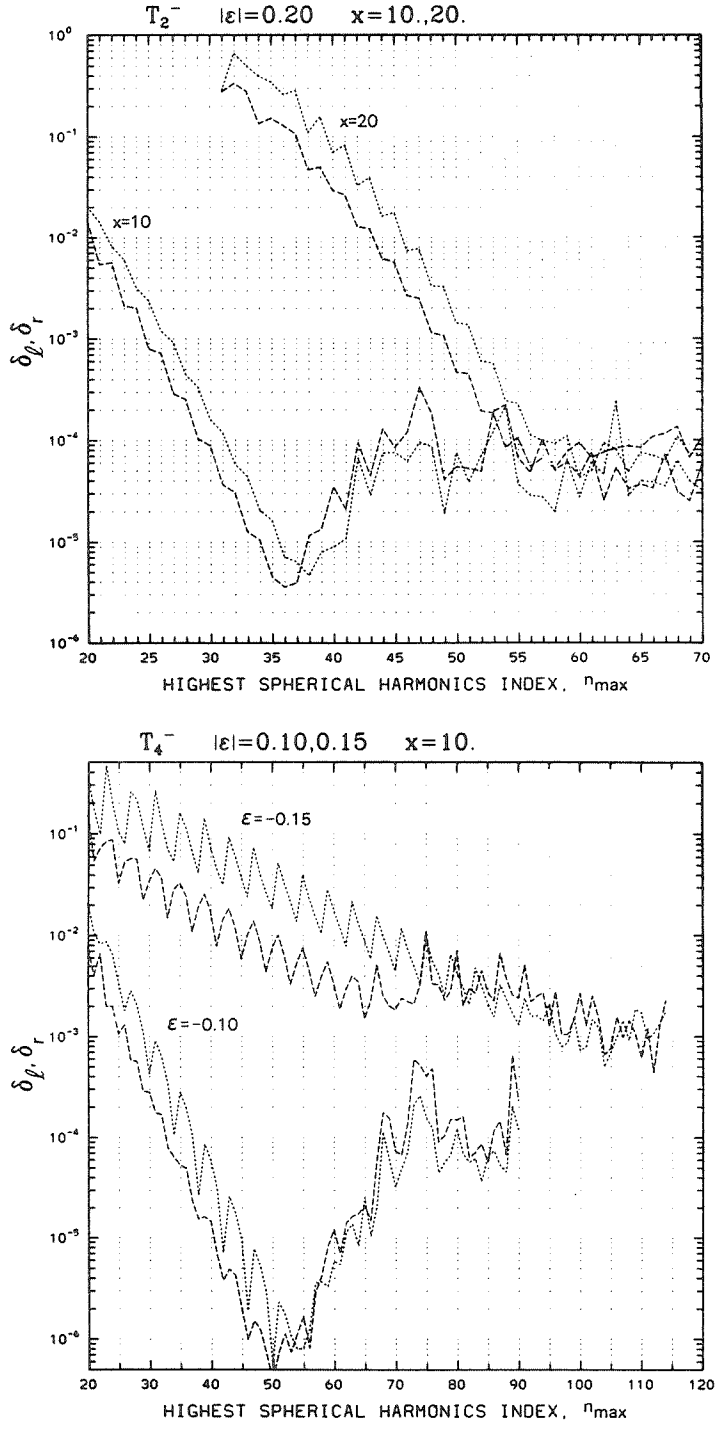

Figure 4.1. Convergence parameters δ_ℓ(dotted lines) and δ_r (dashed lines) vs. highest value n_{max} in spherical harmonics expansion over n: (a) $T_2(-0.20)$, x = 10 and 20; (b) $T_4(-0.10)$ and $T_4(-0.15)$, x = 10; (c) T_6 (0.10), x = 10; (d) T_8 (0.10), x = 8.

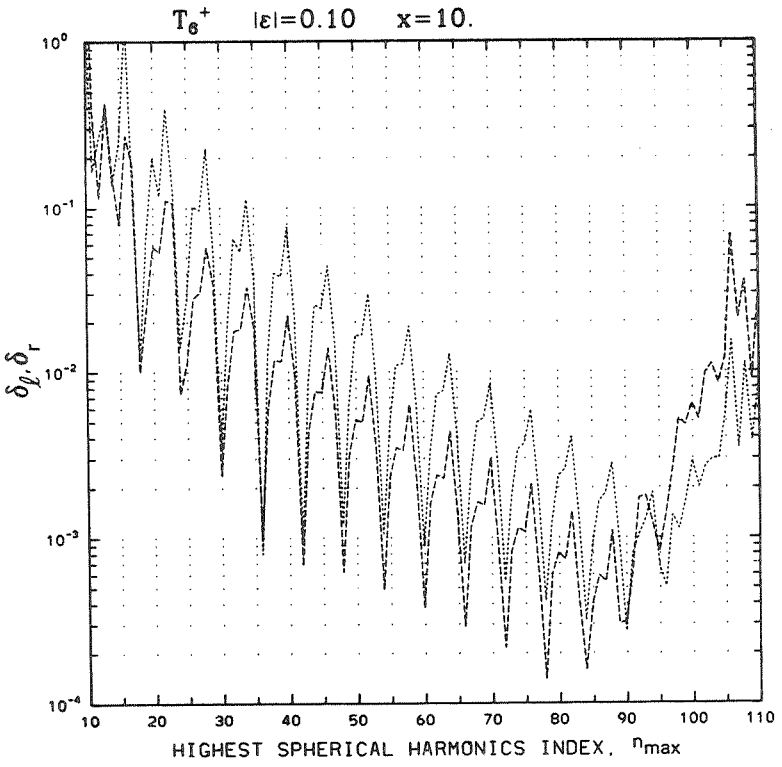

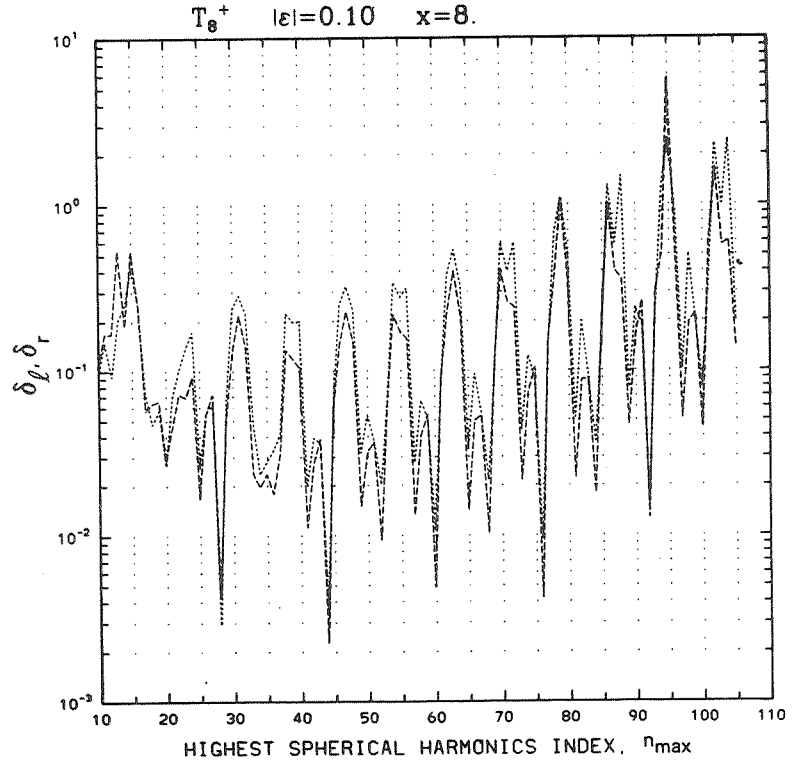

Figure 4.1 (Continued)

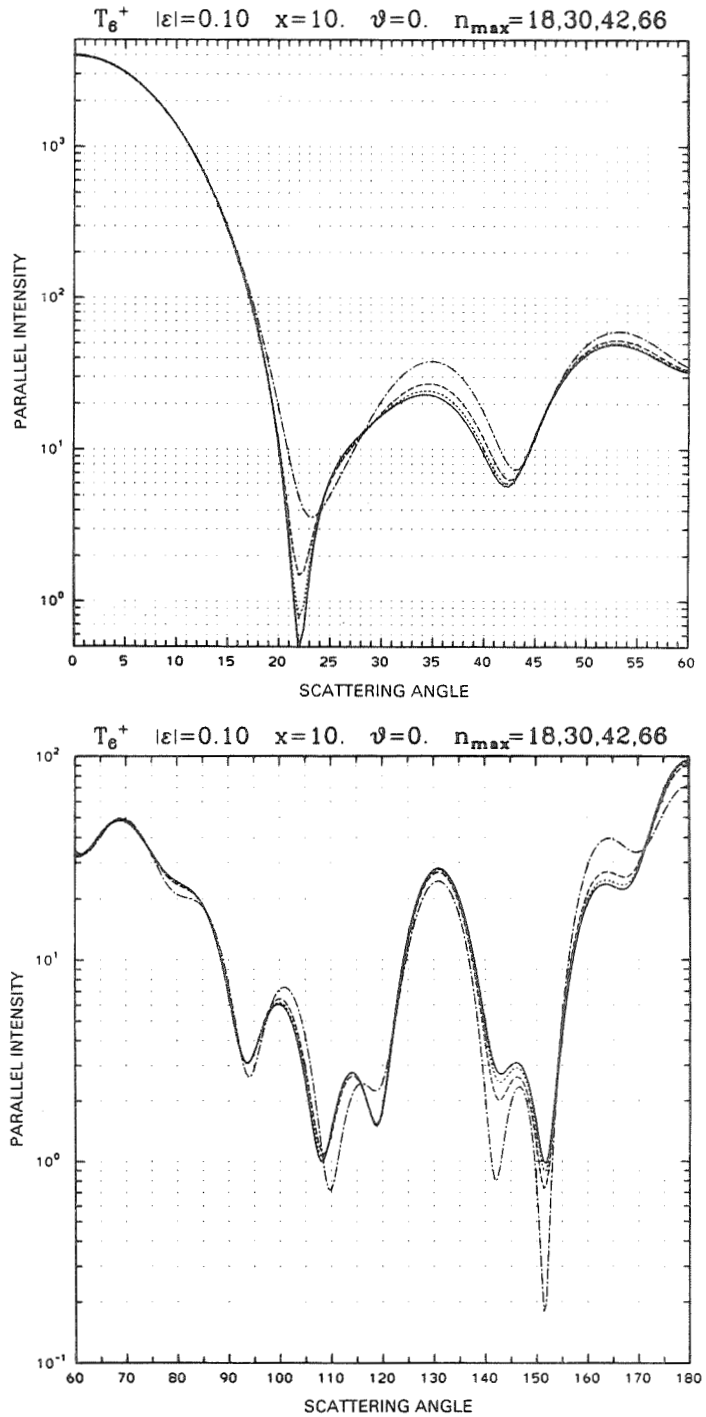

Figure 4.2. Parallel and perpendicular intensities i_ℓ and i_r vs. scattering angle Θ, for $T_6(0.10)$ particles in nose-on orientation with size parameter x = 10 and n_{max} = 18, 30, 42, and 66. (a-b) i_ℓ for 0-60 and 60-180 degrees respectively; (c-d) i_r for 0-60 and 60-180 degrees respectively. The solid line in each plot represents the "converged" result, corresponding to n_{max} = 66. The various dashed lines correspond to lower values of n_{max}: dot-dash, n_{max} = 18; dashed, n_{max} = 30; dotted, n_{max} = 42.

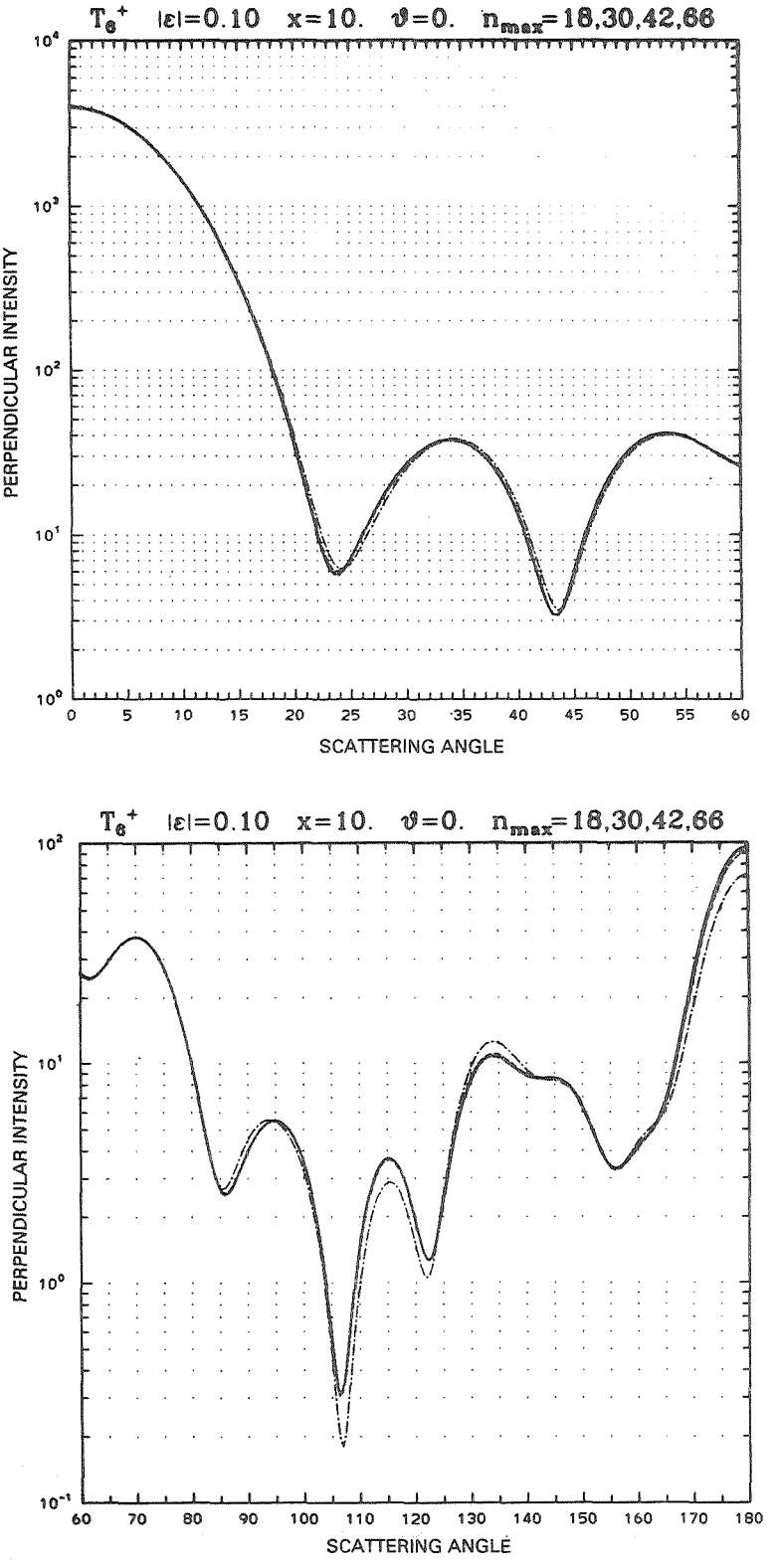

Figure 4.2 (Continued)

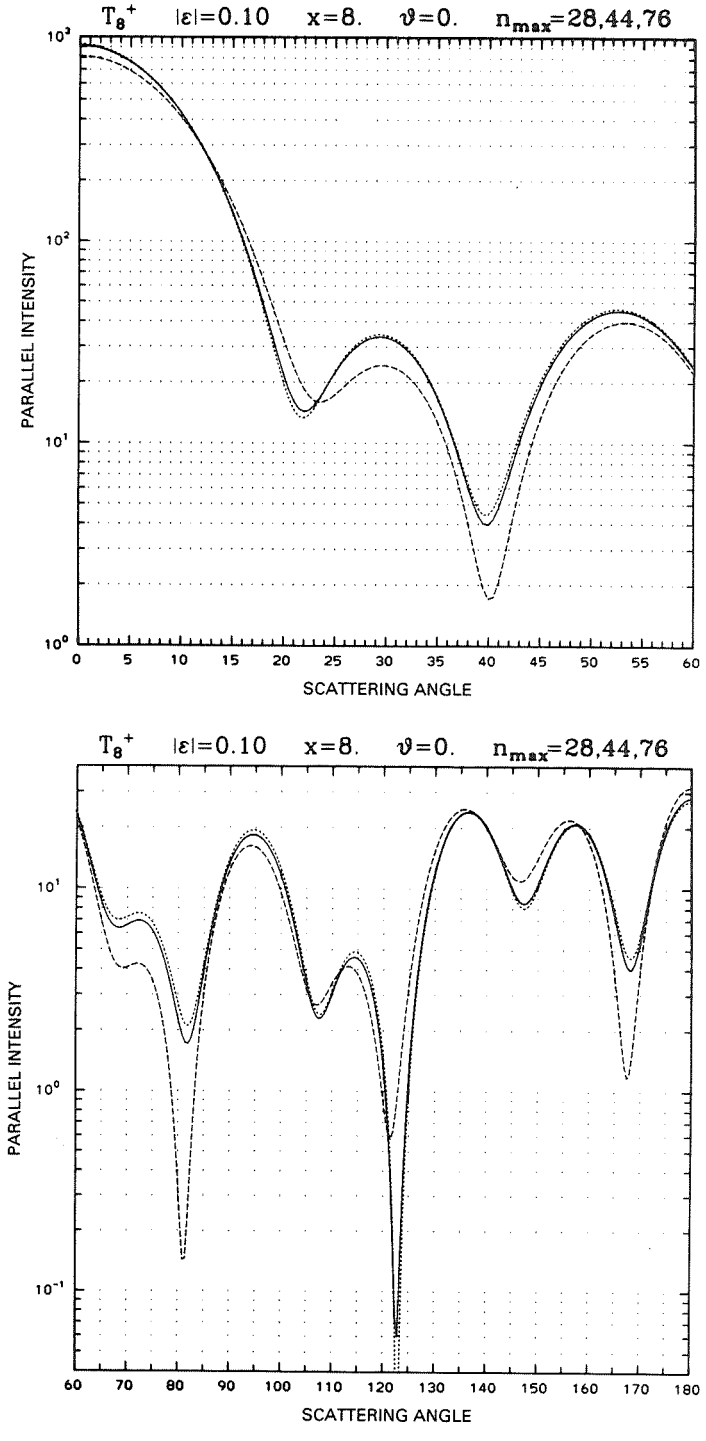

Figure 4.3. Parallel and perpendicular intensities i_{ℓ} and i_r vs. scattering angle Θ, for $T_8(0.10)$ particles in nose-on orientation with size parameter $x = 8$ and n_{max} = 28,44, and 76: (a-b) i_{ℓ} for 0-60 and 60-180 degrees, respectively; (c-d) i_r for 0-60 and 60-180 degrees, respectively. The solid line in each plot corresponds to the global minimum n_{max} = 44 in Figure 4.1(d). The dotted line corresponds to n_{max} = 28, the dashed line to n_{max} = 76.

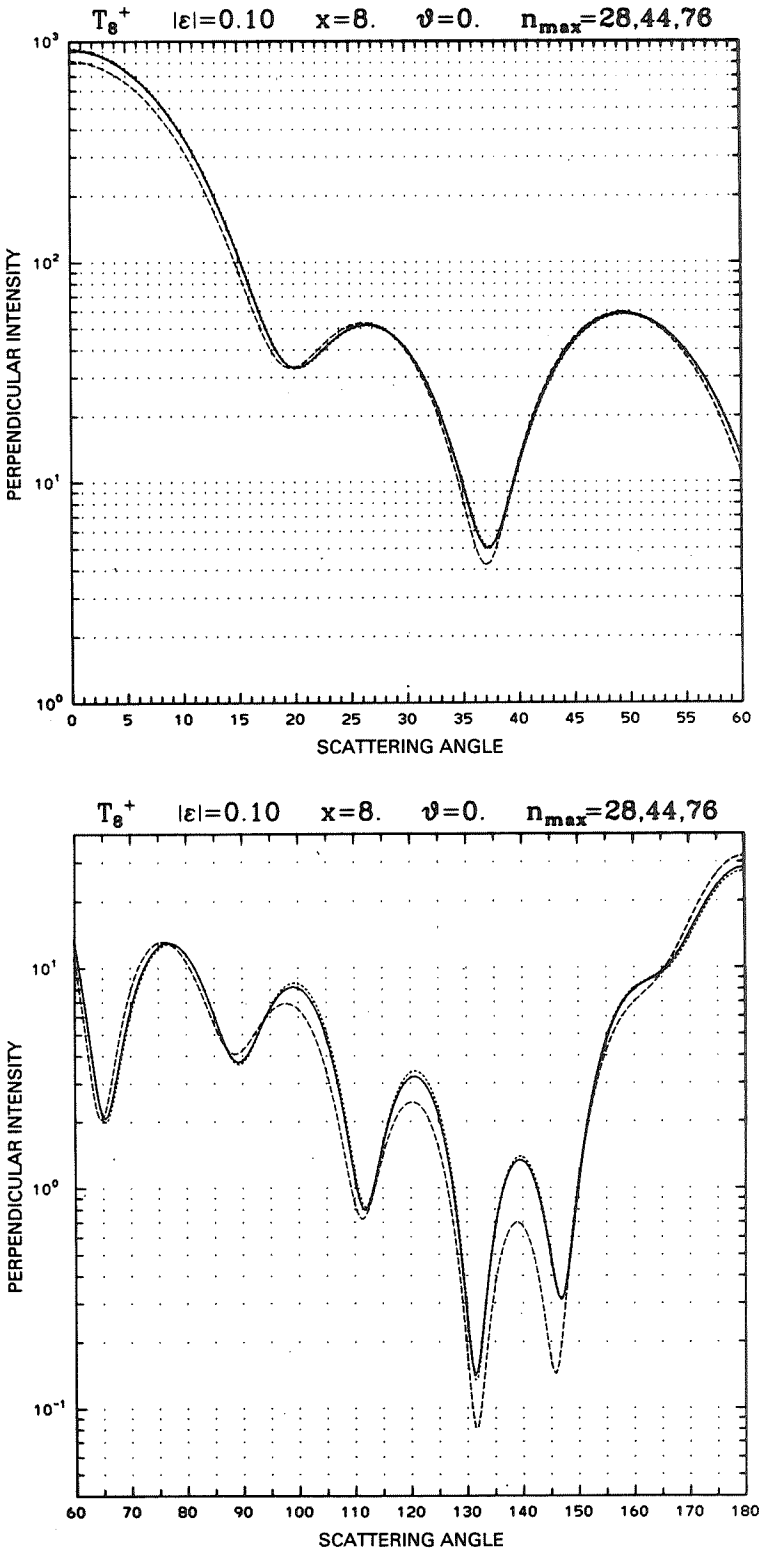

Figure 4.3 (Continued)

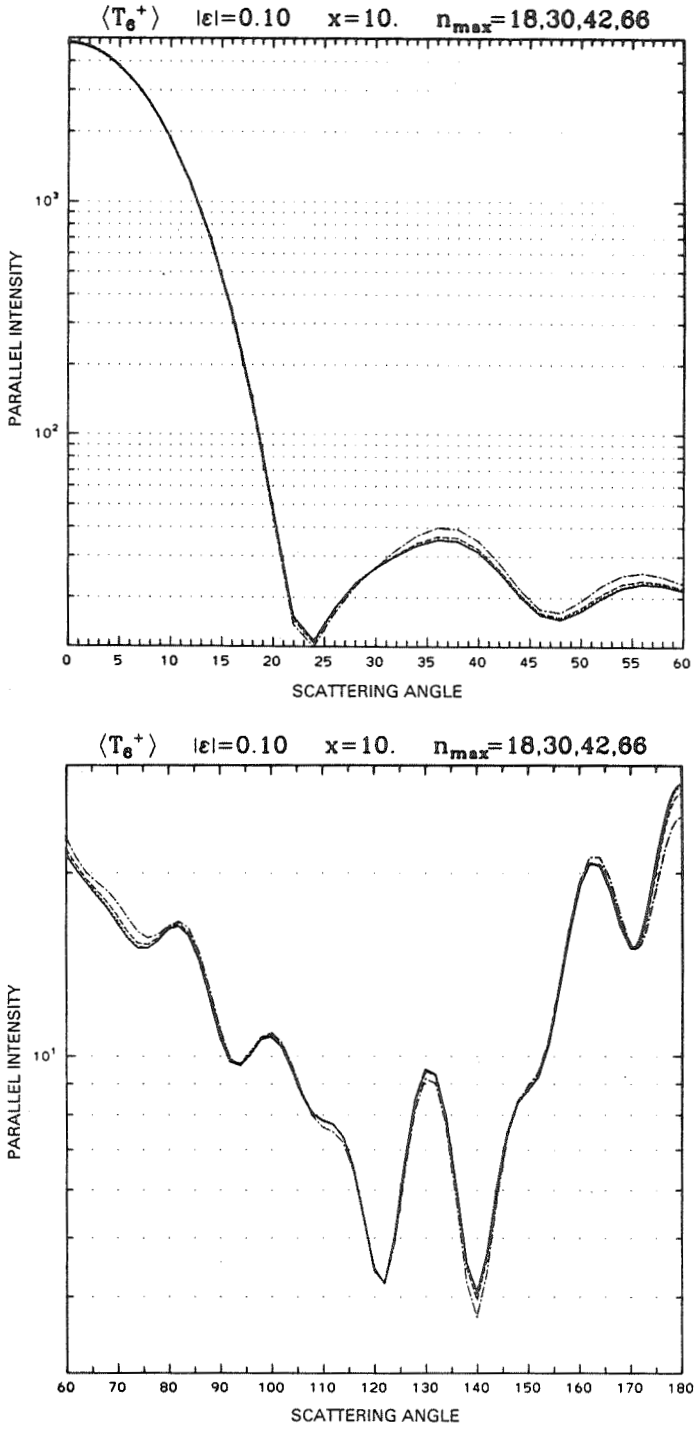

Figure 4.4. Parallel intensity i_{ℓ} vs. scattering angle Θ, for $T_6(0.10)$ particles in random orientation with size parameter $x = 10$ and $n_{max} = 18,30,42$, and 66: (a) 0-60 degrees; (b) 60-180 degrees. The solid line and the various dashed lines have the same meaning as in Figure 4.2

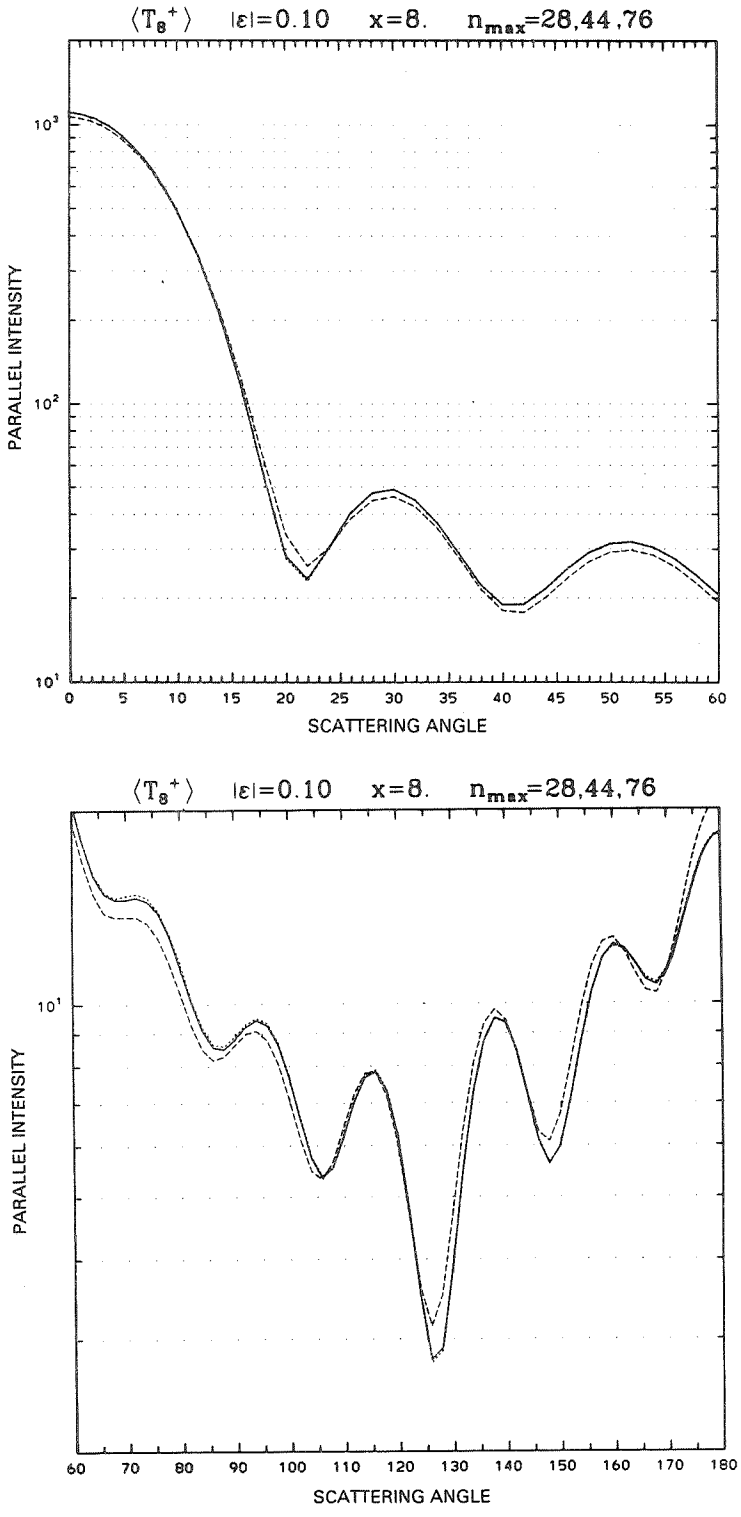

Figure 4.5. Parallel intensity i_{ℓ} vs. scattering angle Θ, for $T_8(0.10)$ particles in random orientation with size parameter $x = 8$ and $n_{max} = 28,44$, and 76: (a) 0-60 degrees; (b) 60-180 degrees. The solid line and the various dashed lines have the same meaning as in Figure 4.3.

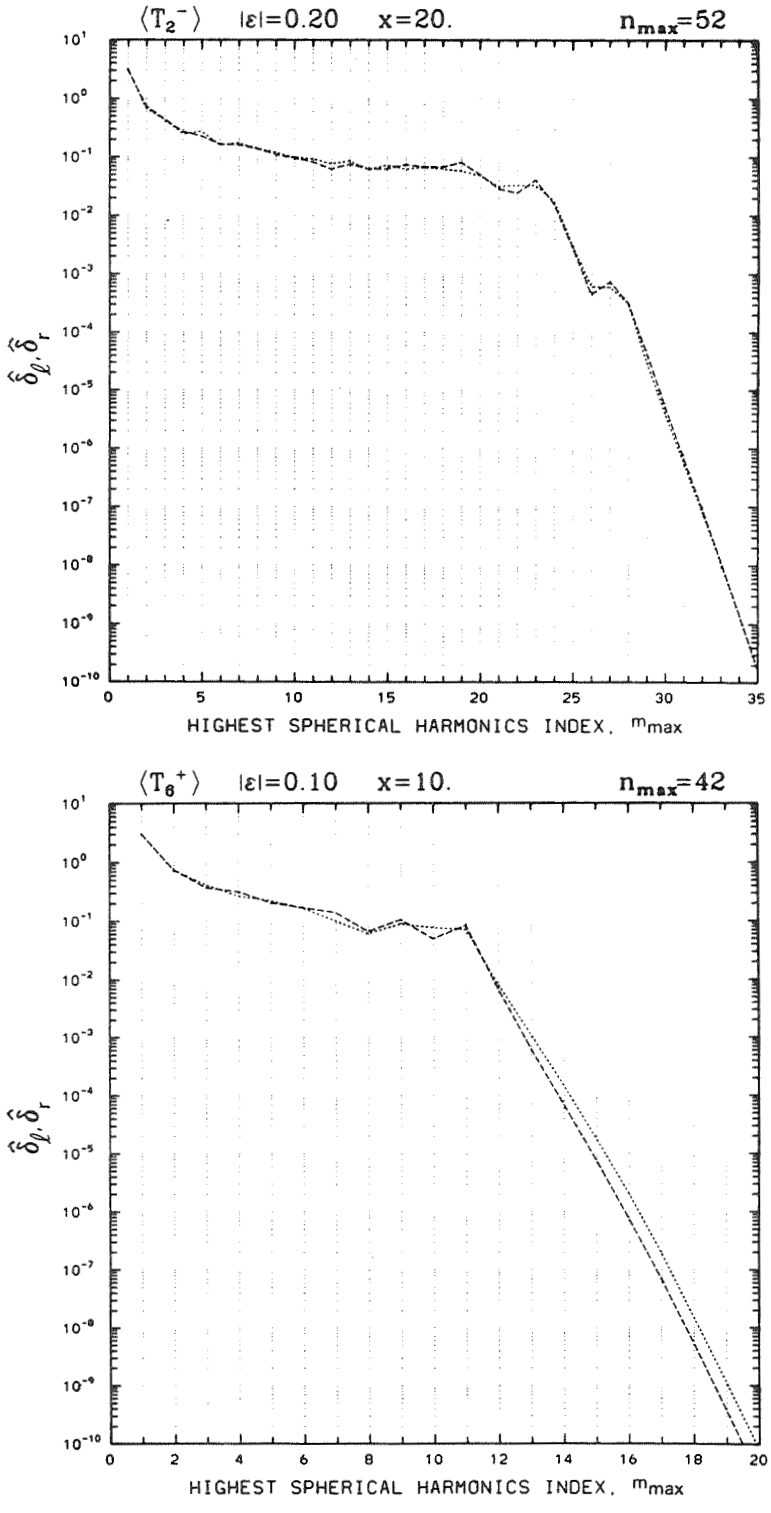

Figure 4.6. Convergence parameters $\hat{\delta}_\ell$ (dotted line) and $\hat{\delta}_r$ (dashed line) vs. highest value m_{max} in spherical harmonics expansion over m: (a) $T_2(-0.20)$ particles with $x = 20$; (b) $T_6(+0.10)$ particles with $x = 10$.

four different Chebyshev particles. Fig. 4.1(a) provides an example of how convergence becomes more difficult when the size of the particle increases; Fig. 4.1(b), of how it becomes much more difficult when the deformation from sphericity increases.

Figure 4.1 shows clearly that δ_q does not decrease monotically when n_{max} is increased, but rather has oscillations superimposed on its average downward trend. These oscillations have a period equal to the order n of the Chebyshev polynomial T_n defining the particle! This surprising (and so far unexplained) result explains why convergence over n_{max} is very slow for high Chevyshev orders.

Figure 4.1 also shows that δ_q eventually stops decreasing, and may actually start increasing again, as n_{max} continues to increase. This behavior may be due to

- accumulation of round-off errors; or
- the possibility that the spherical harmonics expansion, at least for concave particles, is an asymptotic rather than an exact series (this may be a consequence of the Rayleigh hypothesis which we have made); it is well known that there is an optimal number of terms to keep in an asymptotic series, beyond which it becomes less and less accurate.

These plots show explicitly how our definition of 'convergence' may fail: δ_q may 'bottom out' before (47) is satisfied. However, our convergence studies also revealed that satisfactory convergence of the scattered intensities can often be achieved even for n_{max} values violating (47).

For this reason, we have introduced a second, less stringent convergence criterion based on the quantity

$$\delta_{\ell r} \equiv \left[\tfrac{1}{2} (\delta_\ell^2 + \delta_r^2) \right]^{1/2} \tag{48}$$

We stop the n_{max} iteration before 'good' convergence is reached, if $\delta_{\ell r}$ reaches a minimum lower than 10 times δ_{min} ($=0.01$ in our study), then starts increasing again. We call this convergence 'fair'. It produces accurate enough results for a randomly oriented particle. However, it may give unacceptable errors for fixed orientation.

By introducing 'fair' convergence, it was possible to obtain results for many more cases than 'good' convergence would have allowed. It also shortens the iteration over n_{max} (which may otherwise be inordinately lengthy due to the oscillations in the δ_q vs. n_{max} curves). This in turn reduces computer time spent in orientation-averaging, which goes roughly as n_{max} to the 2.5 power.

We have singled out the two particles in Fig. 4.1(c-d) for particular consideration, since they are representative of cases of slow or difficult convergence, respectively. The first is a T_6 particle with $x = 10$; the second, a T_8 particle with $x = 8$. Both particles have deformation $\epsilon = 0.10$.

Parallel and perpendicular intensities for these two particles are shown in Figs. 4.2 and 4.3, respectively, for various n_{max} values and for nose-on orientation. (Studies we made for oblique orientation did not differ qualitatively.) There are separate plots for 0-60 and 60-180 degrees in order to gain resolution.

For the $T_6(+)$ particle, Fig. 4.1(c) shows that a deep local minimum, both for δ_ℓ and δ_r, is reached already for $n_{max} = 18$; 'fair' convergence is reached for $n_{max} = 30$; and 'good' convergence, for $n_{max} = 42$. For $n_{max} = 66$, δ_ℓ and δ_r are even lower yet. The solid curve in each plot in Fig. 4.2 represents the 'converged' result, corresponding to $n_{max} = 66$. The various dashed curves correspond to lower values of n_{max}. This enables us to watch the convergence process 'in action', so to speak.

The trend towards convergence in Fig. 4.2 is quite evident. Moreover, we find that:

- the main characteristics of the scattering pattern are already produced by $n_{max} = 18$
- perpendicular intensities converge much more rapidly than parallel ones
- 'fair' convergence does not produce accurate enough results for fixed orientation
- 'good' convergence produces almost perfectly converged intensities

The T_8 particle is truly a marginal case; even a small increase in its size or deformation causes convergence to fail entirely. As it is, Fig. 4.1(d) shows that 'fair' convergence is reached for $n_{max} = 28$, while 'good' convergence is not achieved at all. But there is a global minimum at $n_{max} = 44$. Beyond that, δ_ℓ and δ_r increase, but are still less than 0.01 in two local minima at $n_{max} = 60$ and 76. Therefore, in Fig. 4.3 we have plotted parallel and perpendicular intensities for $n_{max} = 28$, 44, and 76. We find that:

- intensities for $n_{max} = 28$ (dotted line) and 44 (solid line) are quite similar
- intensities for $n_{max} = 76$ (dashed line) are rather different from the first two.

This T_8 example clearly shows that taking too many terms in the spherical harmonics expansion is just as deadly as taking too few. Therefore, it is unwise just to arbitrarily choose a high value of n_{max} without checking convergence. For the same reason, even the first guess for n_{max} in the convergence iteration shouldn't be too high. But we have found that, even for 'fair' convergence, n_{max} is always bigger than the number of terms,

$$n_{sph} = x + 4x^{1/3} + 2 \tag{49}$$

required for convergence of the scattered field from an equal-volume sphere (Wiscombe, 1980). Therefore, we suggest utilizing $n_{max} = n_{sph}$ as a first guess.

Table 1 shows the n_{max} and $\delta_{\ell r}$ values corresponding to a selection of our Chebyshev particles, as well as what kind of convergence ('fair' or 'good') was obtained.

Figures 4.4 and 4.5 are analogous to Figs. 4.2 and 4.3, respectively, but for random orientation. Only parallel intensities are shown, because the curves for various n_{max} values are virtually indistinguishable for perpendicular intensity. Hence, for checking random-orientation convergence, it may be sufficient to look only at parallel intensity, although we have not done so in our calculations.

Table 1. Convergence parameters for a selection of Chebyshev particles. F and G refer to 'fair' and 'good' convergence, respectively. The other parameters are defined in the text.

x	particle	type	n_{max}	$n_{max}-n_{sph}$	$\delta_{\ell r}$	m_{max}	N_{or}
5	$T_3(0.05)$	G	14	1	5e-4	9	48
	$T_3(0.10)$	G	24	11	7e-4	9	132
	$T_3(0.15)$	F	37	24	3e-3	9	132
	$T_2(\pm 0.20)$	G	17	4	5e-4	8	400
	$T_4(\pm 0.05)$	G	13	0	2e-4	8	56
	$T_4(\pm 0.15)$	F	21	8	7e-3	9	284
	$T_6(\pm 0.05)$	G	13	0	3e-4	8	56
	$T_8(\pm 0.05)$	G	16	3	9e-4	8	56
	$T_8(\pm 0.10)$	F	20	7	8e-3	8	144
10	$T_3(0.05)$	F	20	0	2e-3	15	132
	$T_3(0.10)$	G	35	15	4e-4	15	132
	$T_3(0.15)$	F	43	23	9e-3	15	132
	$T_2(-0.20)$	G	28	8	4e-4	15	584
	$T_2(+0.20)$	F	24	4	5e-3	12	584
	$T_4(\pm 0.05)$	G	20	0	3e-4	14	144
	$T_4(-0.15)$	F	54	34	1e-2	13	584
	$T_6(\pm 0.05)$	F	21	1	4e-3	14	144
	$T_8(\pm 0.05)$	F	22	2	3e-3	14	144
	$T_8(\pm 0.10)$	F	46	26	9e-3	14	372
15	$T_3(0.05)$	F	27	0	3e-3	21	132
	$T_3(0.10)$	F	39	12	4e-3	21	132
	$T_2(\pm 0.20)$	G	41	14	9e-4	20	584
	$T_4(\pm 0.05)$	G	27	0	6e-4	20	284
	$T_6(\pm 0.05)$	F	28	1	6e-3	20	284
20	$T_3(0.05)$	F	34	1	3e-3	27	132
	$T_3(0.10)$	F	49	16	3e-3	27	132
	$T_2(\pm 0.20)$	F	47	14	9e-3	24	584
	$T_4(\pm 0.05)$	G	34	1	8e-4	26	372

There are several important observations to make about Figs. 4.4 and 4.5:

- the spread between the curves for various n_{max} values is an order of magnitude less than for nose-on orientation
- 'fair' convergence is good enough for random orientation; the worst errors are below 2% or so
- even the $n_{max} = 18$ intensities in Fig. 4.4 are within 10% of the converged values
- the $n_{max} = 28$ and 44 curves in Fig. 4.5 are virtually indistinguishable, whereas the $n_{max} = 76$ curve departs significantly from them.

This last observation (which was also noted in nose-on orientation) again shows the danger of taking too many terms in the spherical harmonic expansion.

Convergence over m_{max}

We have found that, for a given n_{max}, convergence over m is usually reached for $m_{max} < n_{max}$. It is therefore advantageous to introduce a convergence criterion over m_{max} in order to shorten the computation.

We adopted an m_{max} convergence criterion similar to 'good' convergence for n_{max} (46-47), except that all the scattering angles are now taken into account, because down-spikes do not seem to occur in the m-sum (apparently there is never the kind of massive cancellation of terms that occurs in the n-sum). For a particle in fixed orientation, the analogue to (46) is therefore:

$$\hat{\delta}_q = \left\{ \frac{1}{N_{sca}} \sum_{i=1}^{N_{sca}} \left[\frac{i_q(\Theta_i, m_{max}) - i_q(\Theta_i, m_{max}-1)}{i_q(\Theta_i, m_{max}-1)} \right]^2 \right\}^{1/2} \tag{50}$$

where

$$i_q(\Theta, m_{max}) = \left| \sum_{m=0}^{m_{max}} F_q^{(m)}(\Theta) \right|^2 \tag{51}$$

and $F_q^{(m)}$ is the q-component of the far-field amplitude of the partial field $\mathbf{E}_m^s$.

For a randomly-oriented particle, convergence over m_{max} is checked by making use of an exactly analogous criterion, except that i_q is replaced by $<i_q>$ (see 37).

$\hat{\delta}_\ell$ (dotted line) and $\hat{\delta}_r$ (dashed line) are plotted vs. m_{max} in Figure 4.6, for two different Chebyshev particles in random orientation. There is a striking trend towards convergence as soon as these quantities

become smaller than about 0.001; hence, convergence over m_{max} was assumed to have taken place as soon as $\hat{\delta}_\ell$ and $\hat{\delta}_r$ fell below this limit.

When only random-orientation cross-sections are desired, and the short-cut described in 'Step 6' of Sec. V is employed, m_{max} convergence is based on the following quantity:

$$\hat{\delta}_\phi = \left\{ \frac{1}{N_\Theta} \sum_{i=1}^{N_\Theta} \left[\frac{\sigma_\phi (\Theta_{p,i}, m_{max}) - \sigma_\phi (\Theta_{p,i}, m_{max}-1)}{\sigma_\phi (\Theta_{p,i}, m_{max}-1)} \right]^2 \right\}^{1/2} \tag{52}$$

where ϕ means one of the two azimuthal orientations (ϕ_p = 90, 180 degrees) used for computing the random-orientation cross-section (Sec. V), and N_Θ is the number of zenith orientations. In general, this leads to the same m_{max} values as applying the $\hat{\delta}_q$ criterion.

Table 1 shows m_{max} values for various particles. They range between about ¼ and ¾ of n_{max}, showing that checking convergence over a m_{max} reduces computer time by roughly a factor of two.

Convergence over N_Θ

When we compute the scattered field from a randomly-oriented particle, the number of azimuth orientations N_ϕ for any given zenith orientation is automatically assigned (39). Therefore, convergence is checked only over N_Θ.

Computer time and storage constraints have prevented us from testing convergence over orientation for many of the cases in this compendium. Ideally, computations should be done for successively larger N_Θ values until the final results converge to a specified accuracy. But in that case, in order to keep computer time within reasonable bounds, one would need to store all the T_m transition matrices; and this was beyond the capacity of the NCAR CRAY-1 (750,000 words).

We therefore resorted to testing the random-orientation results in selected cases in which N_Θ did not seem large enough. We temporarily modified the EBCM code to allow twice the usual maximum number of orientations (584 for T_n with even n, 132 for odd n). For a $T_2(-0.20)$ particle with x = 20, and a T_3 (0.15) particle with x = 10, the largest changes due to doubling the number of orientations were about 1-2%.

Suggested improvements in the convergence procedures

We wish now to suggest how the convergence criteria could be improved. However, in spite of our extensive experience, we are still unable to give general and completely automatic convergence procedures. Our suggestions are probably most appropriate to the Chebyshev particles; they may however serve as guidelines for other shapes.

We have not introduced the following changes in our computer code yet. However, we believe that they could speed up the convergence procedures and at the same time produce even more accurate results.

First, even though 'fair' convergence seems to produce accurate enough results for randomly-oriented Chebyshev particles, it might not be restrictive enough for other shapes. Besides, 'fair' convergence should always be avoided for fixed orientations. We suggest removal of the 'fair' convergence option and the raising of the value of δ_{min} instead. $\delta_{min} = 0.003$ should produce accurate enough results for random orientation; and $\delta_{min} = 0.001$ for fixed orientation.

Second, we propose an improvement in the iteration over n_{max} whenever the code discerns a periodicity in the variation of δ_{ℓ} and δ_r with n_{max}. The iteration over n_{max} should then proceed in steps equal to the periodicity, rather than in steps of one. This method could bring a considerable speed enhancement for those particles with long periodicities (See Fig. 4.1c). If 'good' convergence does not occur in this case, one should use the results from the overall minimum of δ_{ℓ_r}, comparing them with results for the previous and following minima to determine if the convergence is reliable (see Figs. 4.1(d), 4.3 and 4.5).

Third, the convergence over number of orientations could be handled in a more economic fashion, by using 'adaptive' Gaussian quadrature (Patterson, 1973). Here, one uses values of N_Θ in the sequence 1, 3, 7, 15, 31, 63, and so on. Each successive Gauss rule employs all the points used by its predecessor. Hence, one can select a high value (say 15) of N_Θ, and obtain orientation averages for the lower values (say 3, 7) for free. Comparing the various values will show how the convergence is going.

Finally, we propose yet another way to test convergence over number of orientations. We have noticed that backscattering at 180 degrees is very sensitive to number of orientations. Therefore, one could run the EBCM just for a scattering angle of 180 degrees, testing convergence for successively increasing values of N_Θ (perhaps as described in the previous paragraph). This would be relatively cheap, computationally, since computer time for calculating random-orientation intensities is roughly proportional to the number of scattering angles. Once convergence was achieved, the EBCM could be re-run with the full complement of scattering angles, holding N_Θ fixed at its converged value. In this procedure, it would be desirable to save all the T_m transition matrices to avoid recalculation.

VII. DEFINITIONS OF QUANTITIES TO BE PLOTTED

In order to deal with numbers of order unity, it is customary to define the efficiency factors

$$Q_{sca} = \sigma_{sca}/\pi\, r_{ev}^2 \tag{53a}$$

$$Q_{ext} = \sigma_{ext}/\pi\, r_{ev}^2 \tag{53b}$$

in which the cross-sections are normalized by the projected area of the equal-volume sphere. The single-scattering albedo is then defined as

$$\omega = Q_{sca}/Q_{ext} \tag{54}$$

The unpolarized phase function (which is proportional to the 'differential scattering cross-section' used by the inventors of the EBCM) is defined as

$$P(\cos\Theta) = 2\,(i_\ell + i_r)/(x^2\, Q_{sca}) \tag{55}$$

where i_ℓ and i_r are the parallel and perpendicular scattered intensities defined in (28). P, being essentially a probability of scattering at angle Θ from the direction of the incident unpolarized radiation, is normalized to unity:

$$(\tfrac{1}{2}) \int_{-1}^{+1} P(\cos\Theta)\, d(\cos\Theta) = 1 \tag{56}$$

In practice, we only calculate intensities at discrete angles; therefore, this normalization relation can test whether or not we have picked enough angles. With our usual 111 angles, and a Simpson Rule for the left-hand side of (56), we always obtained numbers in the range 0.997 to 1.003, indicating that our Simpson-Rule calculation of the asymmetry factor

$$g = (\tfrac{1}{2}) \int_{-1}^{+1} \cos\Theta\, P(\cos\Theta)\, d(\cos\Theta) \tag{57}$$

is probably accurate to 2 decimal places, with an angular-quadrature error of perhaps ± 1 in the 3rd place.

We use a trick to calculate unpolarized phase functions in the EBCM. The straightforward way would be to calculate i_ℓ and i_r first for incident parallel-polarized light, then for incident perpendicular-polarized light, and add them up. (For non-spheres, even in the random orientation, there is always

cross-polarization, meaning that incident parallel or perpendicular light produces non-zero values of both i_ℓ and i_r.) Instead, we assume incident light with linear polarization at 45 degrees to the scattering plane. This gives the same answer for i_ℓ and i_r (but not for the remaining two Stokes parameters), with only half the computation. This trick works because, in our cases, the 4x4 Mueller matrix has vanishing 2x2 sub-matrices in the upper right and lower left corners: nose-on orientation falls into case 2 of van de Hulst (1981), sec. 5.22; random orientation falls into case 6 of that same section.

Clearly, for a general non-spherical particle in fixed orientation, the phase function would depend on the azimuth angle between the scattering plane (variable) and the plane containing both the incident direction and the reference axis (fixed), as well as upon the scattering angle Θ. However, for the particular situations we consider — either nose-on (incident radiation along the particle's axis of rotation) or random orientation — this azimuthal dependence disappears. To show the phase function for arbitrary particle orientation would really require a 3-D plot.

The final quantity of interest is the degree of polarization:

$$d(\Theta) = (i_r - i_\ell)/(i_r + i_\ell) \tag{58}$$

Like the efficiency factors, this is of order unity, and in fact is bounded between -1 and $+1$.

Experimenters prefer looking at phase function and degree of polarization because both are independent of the absolute calibration of the instruments (provided the calibration is the same for i_ℓ and i_r). $d(\Theta)$ is particularly nice because, unlike the phase function, it can be determined accurately without knowing the scattering cross-section. By reading both phase function and degree of polarization from our plots, and looking up Q_{sca} in Table 3, the reader can recover i_ℓ and i_r. This is burdensome, we know, but this compendium would have been too long if phase function, degree of polarization, and intensities were all plotted.

Scattering cross-section requires an integration over all scattered intensities. Unfortunately, in the laboratory, it is nearly impossible to position the detector at scattering angles 0 to 5 degrees, because then it receives incident as well as scattered radiation. Angles 175–180 degrees are generally unreachable as well, since here the detector either blocks the incident beam, or is blocked by the device emitting it. The loss of 0–5 degree information is particularly harmful, because this is in the diffraction region, where intensities are largest.

VIII. SIZE-AVERAGING OF SPHERICAL RESULTS

After examining many hundreds of plots comparing spherical to non-spherical scattering results, we came to feel that comparing to a sphere for a specific value of size parameter 'x', far from being the most honest comparison, was in fact the most misleading. Often the pattern of spherical-nonspherical differences would alter radically with only a slight change in x; and invariably that alteration was caused by the sphere. The random-orientation nonspherical results were rock-steady by comparison.

The problem lies, of course, in the multiple periodicities and spikes in the Mie results as a function of x. This is collectively known as the "ripple structure". It is very special to a sphere, and is caused by the interference between surface waves and the internally transmitted and reflected radiation. Ripple tends to be damped out by nonsphericity, and especially by nonsphericity plus averaging over orientation. (However, a high imaginary index will damp the 'short-cutting' surface waves, and hence the ripple, even for a sphere (van de Hulst, 1981).)

The fastest oscillation in Mie quantities has a period of about 0.8 in x for refractive indices typical of aerosols in the shortwave spectrum (Dave, 1969). This has recently been explained as a 'forward glory oscillation' by Nussenzveig and Wiscombe (1980), who give an analytic formula for the period as a function of real refractive index. For $\tilde{m}_{re} = 1.5$, this period is 0.7393 for spheres with size parameter $x >> 1$.

To see the extent to which this period applied for smaller values of x, we made a number of high-resolution plots of Mie single-scattering albedo, ω, and asymmetry factor, g, as a function of x, using the Mie algorithms of Wiscombe (1979, 1980). The complete course of these quantities, from $x = 0$ to 30, is shown in Fig. 5(a); then, in Figs. 5(b-i), the sub-ranges x = 2-6, 6-10, 10-15 and 15-20 are shown in detail (solid lines). For ω below $x = 10$, the peak-to-peak period is about 0.85, while the trough-to-trough period is in the range 0.71 to 0.76. Both periods settle down to around 0.74 ± 0.02 for $x > 10$. For g, the period is consistently around 0.78 for all $x < 25$.

Since the deviations from the theoretical period are relatively small, we averaged the Mie single-scattering albedo and asymmetry factor over an interval $\delta x = 0.7393$, using 201 equally-spaced points centered on each value of x. These averages are tabulated for integer values of x in Table 2 alongside the exact (unaveraged) values. Then, they are plotted as dotted lines in Figs. 5(b-i). The resulting curves are almost completely smooth, with only a faint residual oscillation due to not averaging over the exact period.

The averaging was actually done over cross-sections and intensities (which makes more physical sense) rather than directly on ω and g:

$$\overline{Q_{sca}} = \overline{x^2 Q_{sca}} / \overline{x^2} \qquad (59a)$$

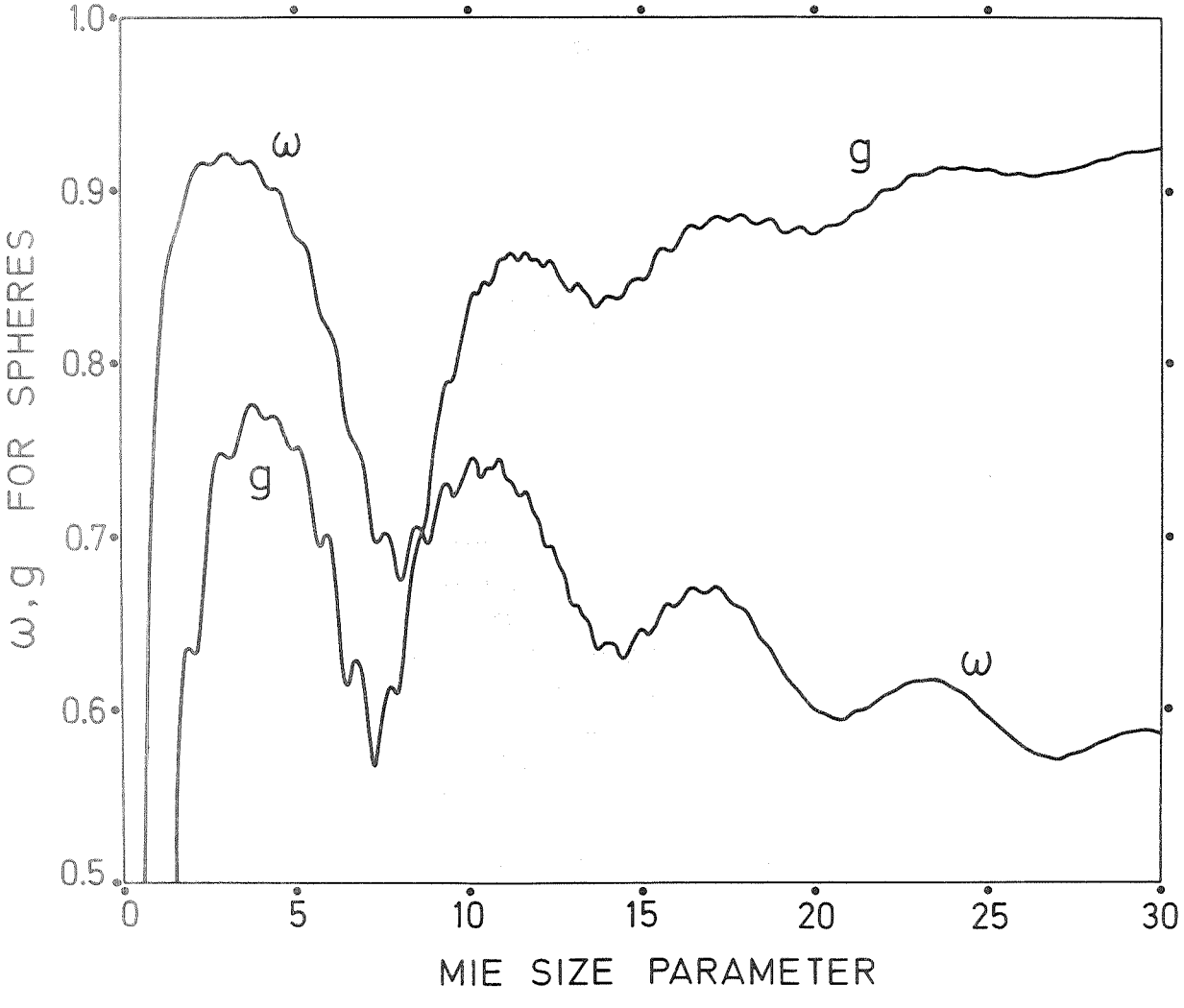

Figure 5. Mie single scattering albedo ω and Mie asymmetry factor g vs. Mie size parameter x: (a) for the full range x = 0-30 considered in this study; (b-e) exact (solid line) and size-averaged (dotted line) ω in the sub-ranges x = 2-6, 6-10, 10-15, and 15-20; (f-i) exact (solid line) and size-averaged (dotted line) g in the same sub-ranges.

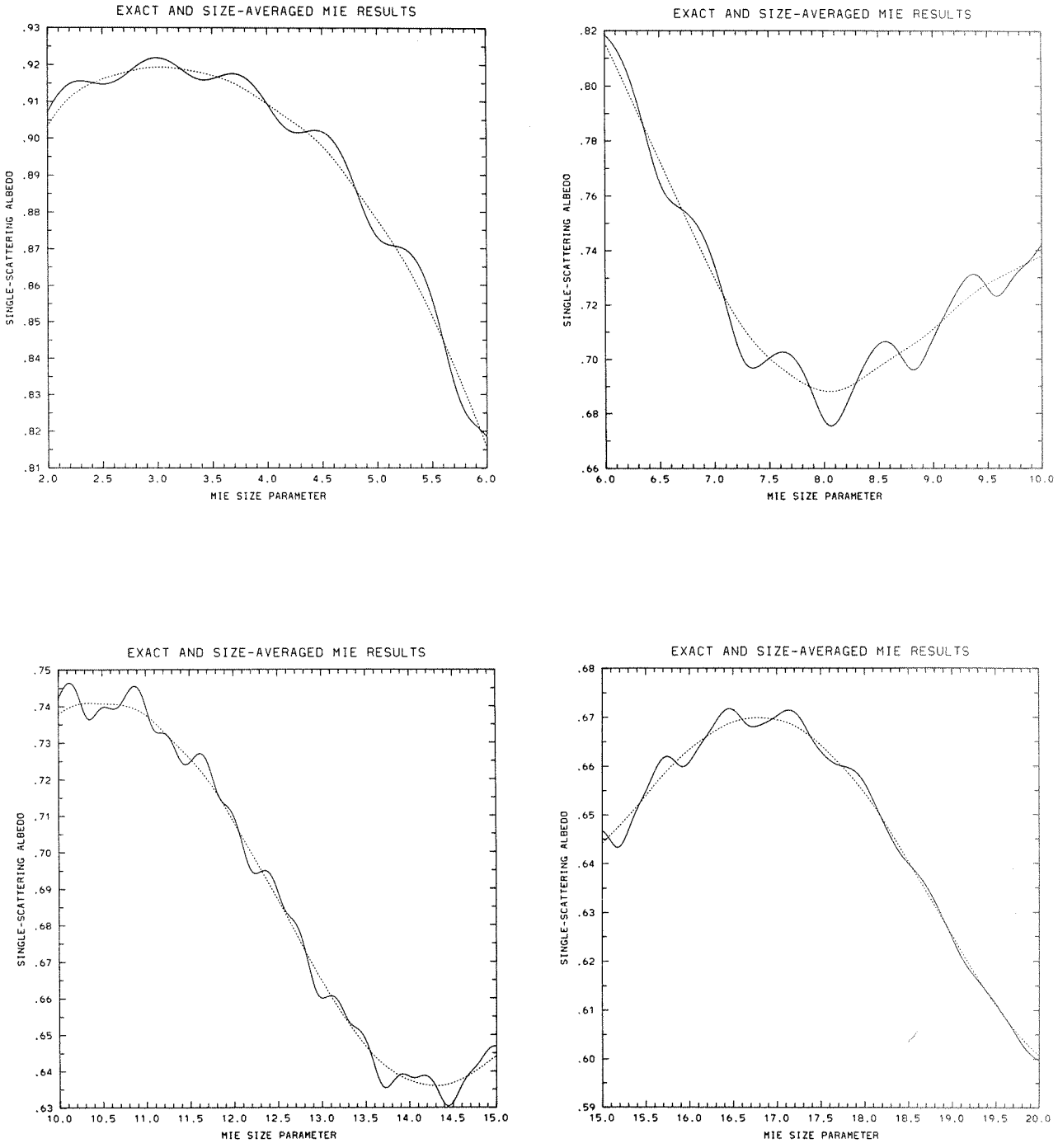

Figure 5 (Continued)

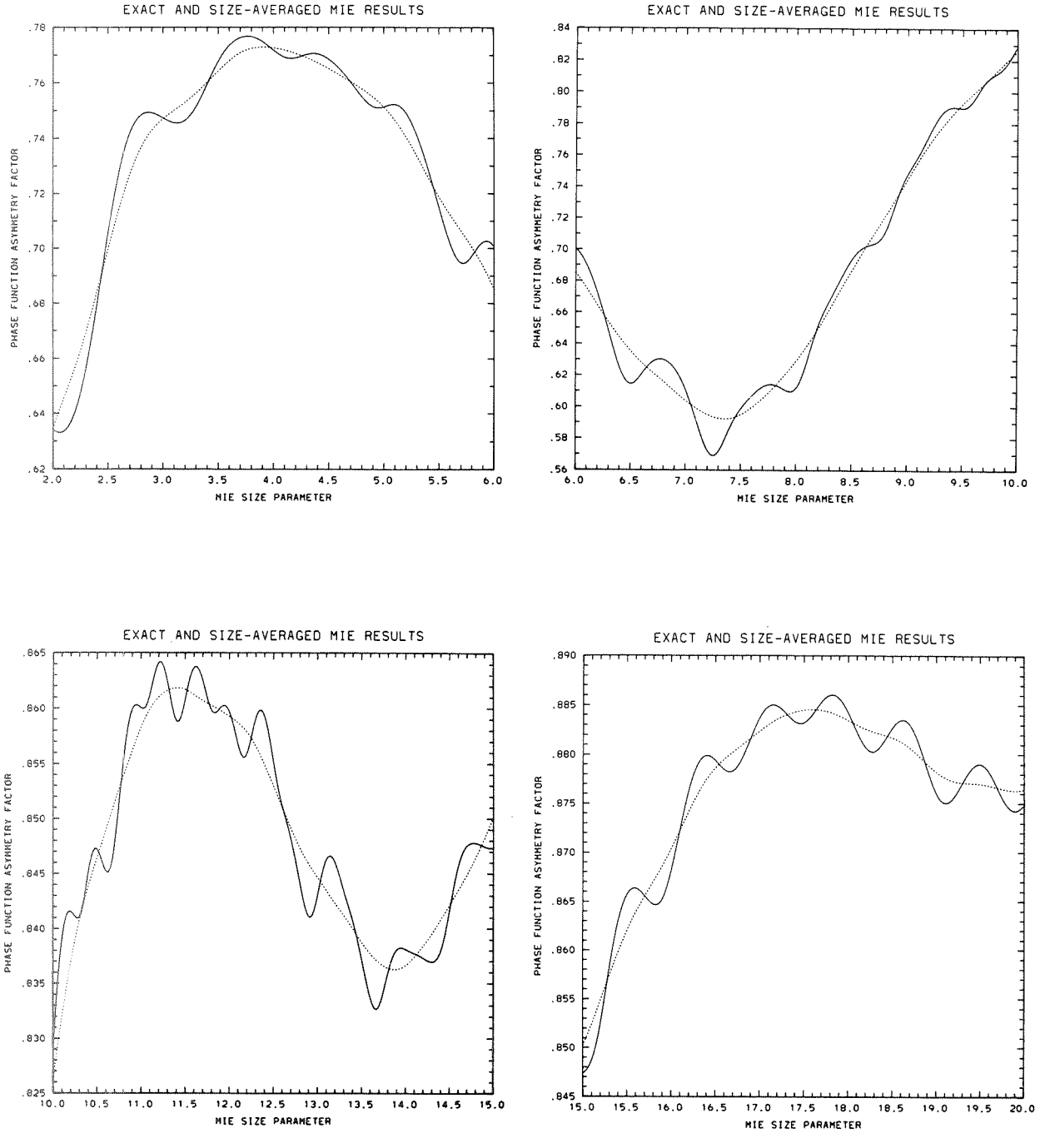

Figure 5 (Continued)

$$\overline{Q_{ext}} = \overline{x^2 Q_{ext}}/\overline{x^2} \tag{59b}$$

$$\omega_{avg} = \overline{Q_{sca}}/\overline{Q_{ext}} \tag{59c}$$

$$g_{avg} = \overline{x^2 g Q_{sca}}/\overline{x^2 Q_{sca}} \tag{59d}$$

The overbar indicates size-averaging over a rectangular size distribution of spheres spanning the range Δx.

Turning now to the phase function, we observe that the deep downward spikes in exact Mie phase functions, separating the (approximately) 'x' peaks between 0 and 180 degrees, must be due to very particular cancellations of terms in the Mie series. Small changes in x cause big changes in the location of these spikes. Hence even a modest amount of size-averaging reduces them considerably. The peaks between the spikes, on the other hand, are less affected by size-averaging. Thus, the general effect of size-averaging is to smooth the Mie curves considerably.

Figure 6 illustrates this phenomenon. The thin solid curve is a size-averaged ($\Delta x = 1$) Mie phase function for $x = 15$ in the angular range 80-180 degrees; the thick solid curve, the exact Mie result. The dotted and dashed lines show the exact and size-averaged $< T_4(-0.10) >$ phase function; these bear out our remark above, that nonspherical results tend to be rock-steady under size-averaging, compared to spherical results.

Away from scattering angle $\Theta = 0$, Mie phase function values tend to have several incommensurate periods as a function of x — not just 0.8. For example, at 180 degrees (the worst angle), Shipley and Weinman (1979) find periodicities of 0.42, 0.81, 1.1, etc. using power-spectrum analysis. Thus, there is no clear theoretical justification for averaging over an interval $\Delta x = 0.7393$. In fact, when we used this fixed averaging interval, it gave too much averaging for small x, and not enough for large x. Hence, we found it more convenient to use $\Delta x = 0.1x$ for all size-averaged spherical phase functions. This of course aliases all the oscillations, but still leads to an acceptable degree of smoothing of the most unrepresentative parts of the Mie curves.

To maintain consistency between our treatment of single-scattering albedo, asymmetry factor, and phase function, we will also compare (in Sec. IX) nonspherical ω and g with their spherical counterparts averaged over $\Delta x = 0.1x$. That is why the latter values were also included in Table 2. Except for $x \leq 3$, this causes very little change in the spherical-nonspherical percentage difference plots.

Goedecke, in a comment at the end of Wiscombe and Mugnai (1980), suggested using the projected-area distribution of the non-spherical particles as the size distribution for averaging the spherical results. Since many of our particles exhibit 10% deviations from a sphere, we had something like this in mind in picking $\Delta x = 0.1x$. However, in detail, Goedecke's idea would seem more applicable to large particles ($x >> 1$) than to the ones we studied, because projected area and scattering cross-section are closely related only in the geometric-optics limit.

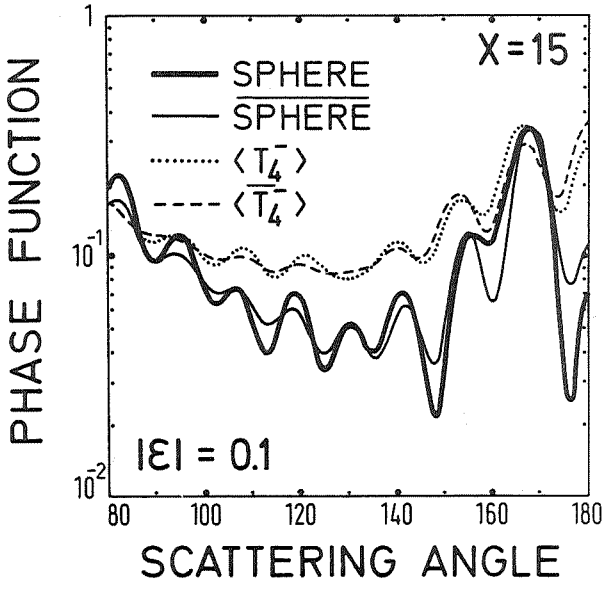

Figure 6. Exact (thick solid line) and size-averaged (thin solid line) Mie phase functions, and exact (dotted line) and size-averaged (dashed line) $<T_4(-0.10)>$ phase functions, for size parameter x = 15. Shows the relatively small effect of size-averaging on nonspherical results.

Since we will not be showing size-averaged scattered intensities, it is worth noting that the effect of size-averaging is much greater on i_r than on i_ℓ. For i_r, it is typical for down-spikes to be raised by factors of 5 to 10, and sometimes even by factors of 100. For both intensities, the smoothing is usually greatest in the angular region 80-150 degrees. The oscillatory structure in the 0-80 and 150-180 degree regions is more resistant to size-averaging.

Looking ahead to Figures 9 and 10, the reader can see examples of exact and $\Delta x = 0.1x$ size-averaged spherical phase functions and degrees of polarization.

Table 2. Mie single-scattering albedo (ω) and asymmetry factor (g): exact, $\Delta x = 0.7393$ size-averaged and $\Delta x = 0.1x$ size-averaged. x is Mie size parameter.

x	ω	ω_{avg} ($\triangle x = 0.74$)	ω_{avg} ($\triangle x = 0.1x$)	g	g_{avg} ($\triangle x = 0.74$)	g_{avg} ($\triangle x = 0.1x$)
1	0.787	0.824	0.788	0.200	0.304	0.203
2	0.907	0.908	0.907	0.634	0.640	0.634
3	0.922	0.919	0.921	0.747	0.748	0.747
4	0.910	0.909	0.909	0.772	0.772	0.772
5	0.873	0.877	0.876	0.751	0.751	0.752
6	0.819	0.816	0.816	0.701	0.686	0.690
7	0.736	0.729	0.730	0.611	0.604	0.604
8	0.678	0.688	0.689	0.612	0.631	0.633
9	0.707	0.712	0.713	0.748	0.748	0.749
10	0.742	0.738	0.737	0.829	0.827	0.826
12	0.709	0.708	0.708	0.860	0.859	0.859
14	0.638	0.637	0.639	0.838	0.837	0.839
15	0.647	0.645	0.645	0.847	0.850	0.852
16	0.660	0.663	0.663	0.868	0.871	0.871
18	0.656	0.654	0.653	0.884	0.883	0.883
20	0.600	0.600	0.603	0.875	0.876	0.878
22	0.609	0.608	0.608	0.900	0.899	0.899
24	0.612	0.612	0.609	0.913	0.913	0.912

IX. SINGLE-SCATTERING ALBEDO AND ASYMMETRY FACTOR

Single-scattering albedo and asymmetry factor, aside from their intrinsic interest, play a crucial role in all simple models of multiple scattering (e.g., Joseph, et. al., 1976). Figure 7 shows percentage differences between spherical and nonspherical single-scattering albedo. Figure 8 is similar, but for the axymmetry factor. Results are shown only for the MIXTURE, and for T_n particles up through T_4; we had much less data for T_6, T_8 and T_{20} particles, and it showed deviations of less than 1-2% from the spherical results. Because of computer time limitations, we could not collect enough data to make these curves smooth; however, we believe that they are not seriously aliased, even if they present a rather unattractive appearance.

Percentage differences for the MIXTURE (Figs. 7a and 8a) are with respect to exact (dotted line), $\Delta x = 0.1x$ size-averaged (dashed line) and $\Delta x = 0.7393$ size-averaged (dot-dash line) spherical results. It doesn't matter much which Mie curve is used, as the reader can easily see, and the differences from the sphere are generally below 3%.

In Figs. 7(b-d) and 8(b-d), percentage differences for T_n particles are only with respect to the $\Delta x = 0.1x$ size-averaged Mie results; on each of these plots, the dotted, dashed, and dot-dash lines represent the various $|\epsilon|$ values shown, in increasing order. In the T_2 and T_4 cases, there are two of each kind of curve; one is for the positive value of ϵ, the other for the negative value. The two curves are not separately identified because they are so close to one another.

The spherical–nonspherical differences in Figs. 7 and 8 were usually much greater than the spread between the exact and size-averaged spherical curves in Fig. 5. Also, spherical and nonspherical asymmetry factors almost always differed in the second decimal place, so the angular–quadrature error in computing nonspherical g's (in the 3rd decimal place) is not significant either. This gives our conclusions about the effect of nonsphericity on ω and g a certain robustness.

The 'noise level' on the percentage differences in Figs. 7 and 8 is somewhere between 0.1 and 1%. The lower limit has to be 0.1% because we always rounded the nonspherical quantities to 3 significant digits. The upper limit is due to obtaining only 'fair' rather than 'good' EBCM convergence in some cases.

Because we only present plots of spherical-nonspherical differences in ω and g, and because plots of ω and g are difficult to read to 3 significant digits, we have tabulated them, as well as Q_{sca} and Q_{abs}, for each Chebyshev particle studied, in Table 3. (Q_{sca} is necessary to convert phase functions back to intensities; see Eq. 55.) The particular value of 'x' at which each tabular column ends generally represents the largest integer for which we were able to obtain at least 'fair' convergence in the EBCM. For $\epsilon = 0.05$ (and sometimes even for $\epsilon = 0.10$), however, calculations are stopped before this barrier is reached.

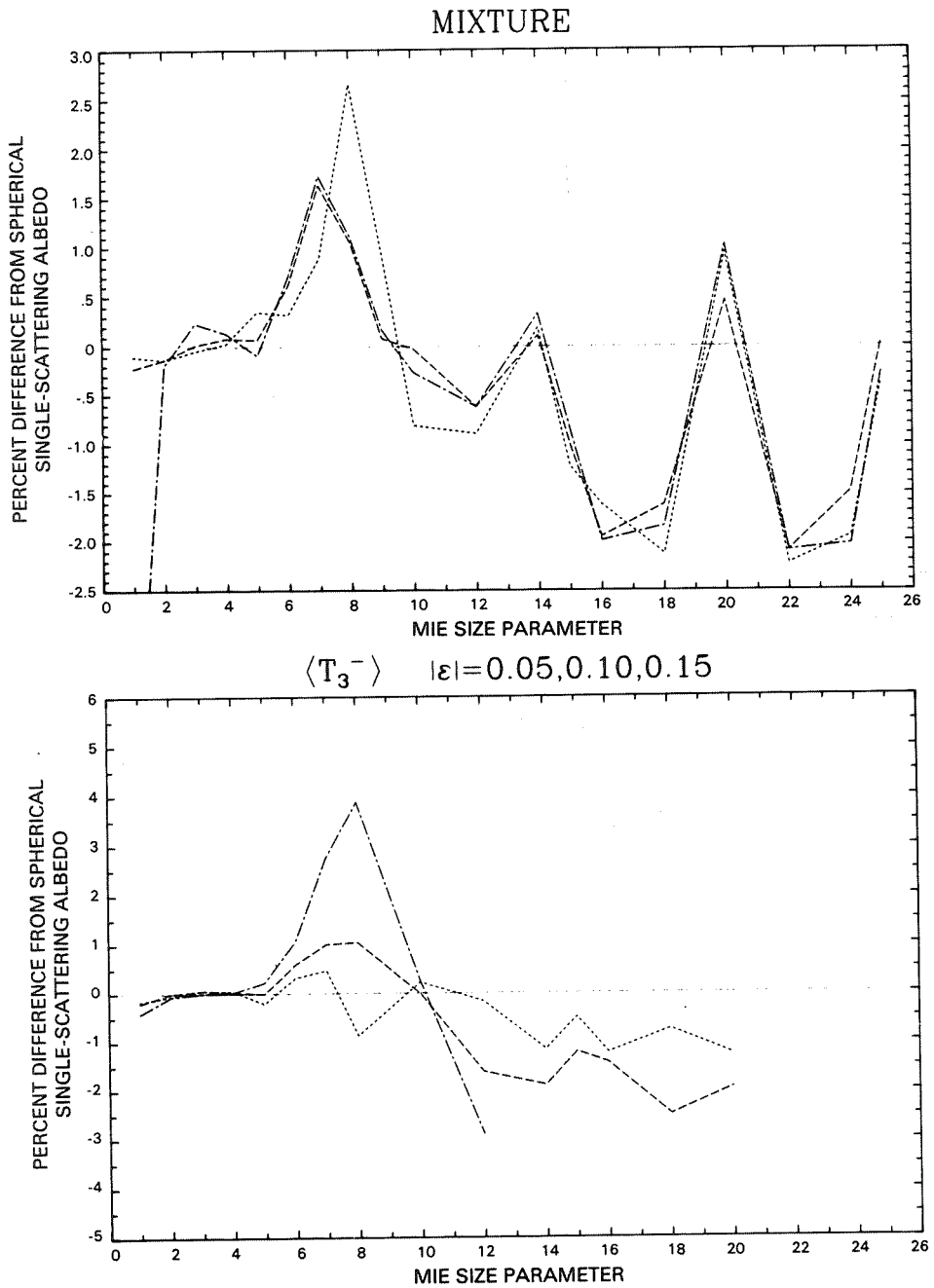

Figure 7. Percentage difference between spherical and nonspherical single-scattering albedo, vs. size parameter x: (a) MIXTURE (a uniform blend of all particle shapes considered); (b) T_3 for $\epsilon = 0.05, 0.10$, and 0.15; (c) T_2 for $\epsilon = -0.10, +0.10$, and $-0.20, +0.20$; (d) T_4 for $\epsilon = 0.05, +0.05, -0.10, +0.10$, and $-0.15, +0.15$. In (a), differences are with respect to exact (dotted line), $\Delta x = 0.1x$ size-averaged (dashed line), and $\Delta x = 0.7393$ size-averaged (dot-dash line) spherical results. In (b-d), differences are only with respect to the $\Delta x = 0.1x$ size-averaged spherical results; the dotted, dashed, and dot-dash lines represent the various ϵ values shown, in increasing order. Dog-legs are due to large steps between computations; there may be finer structure not revealed by these plots.

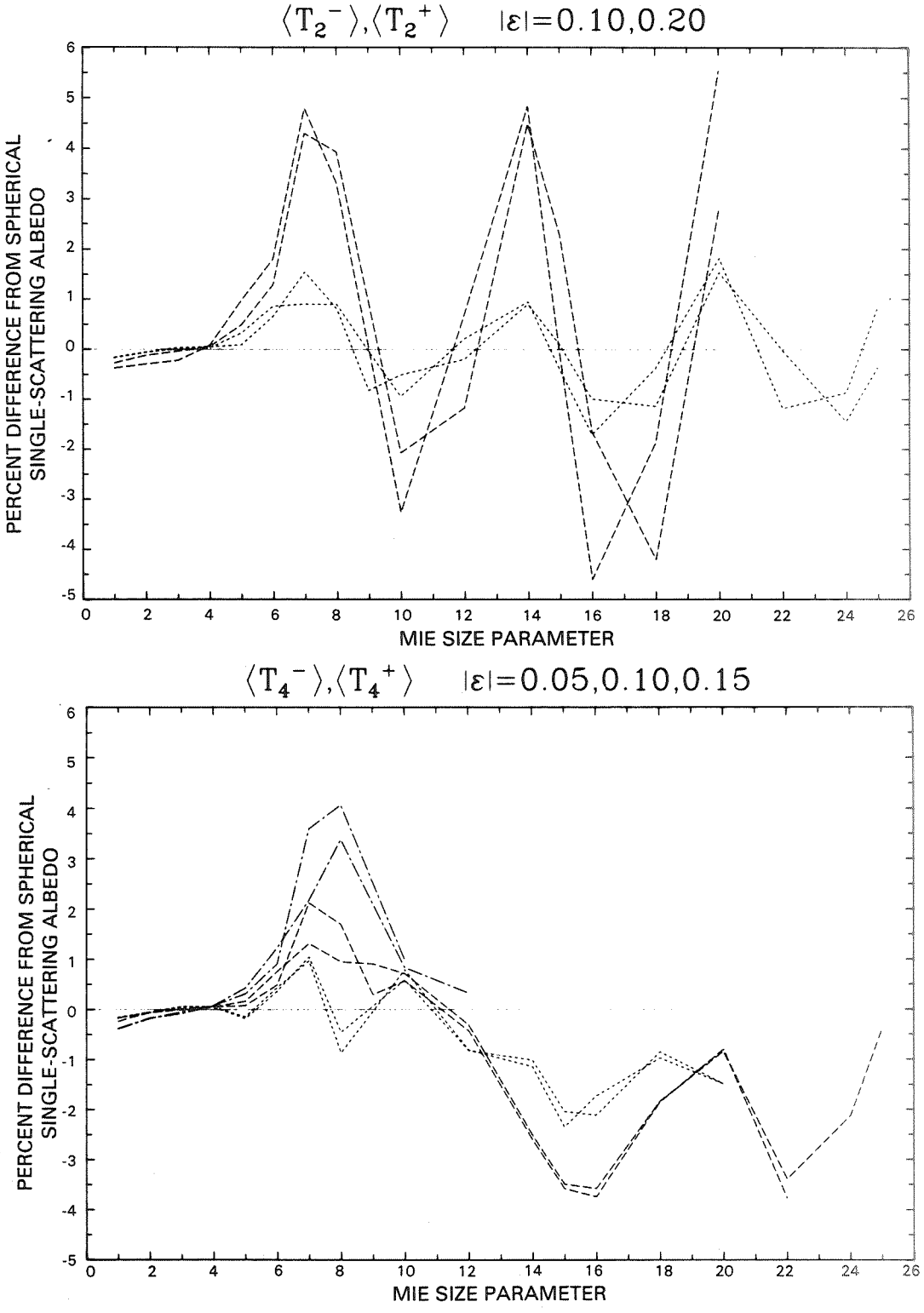

Figure 7 (Continued)

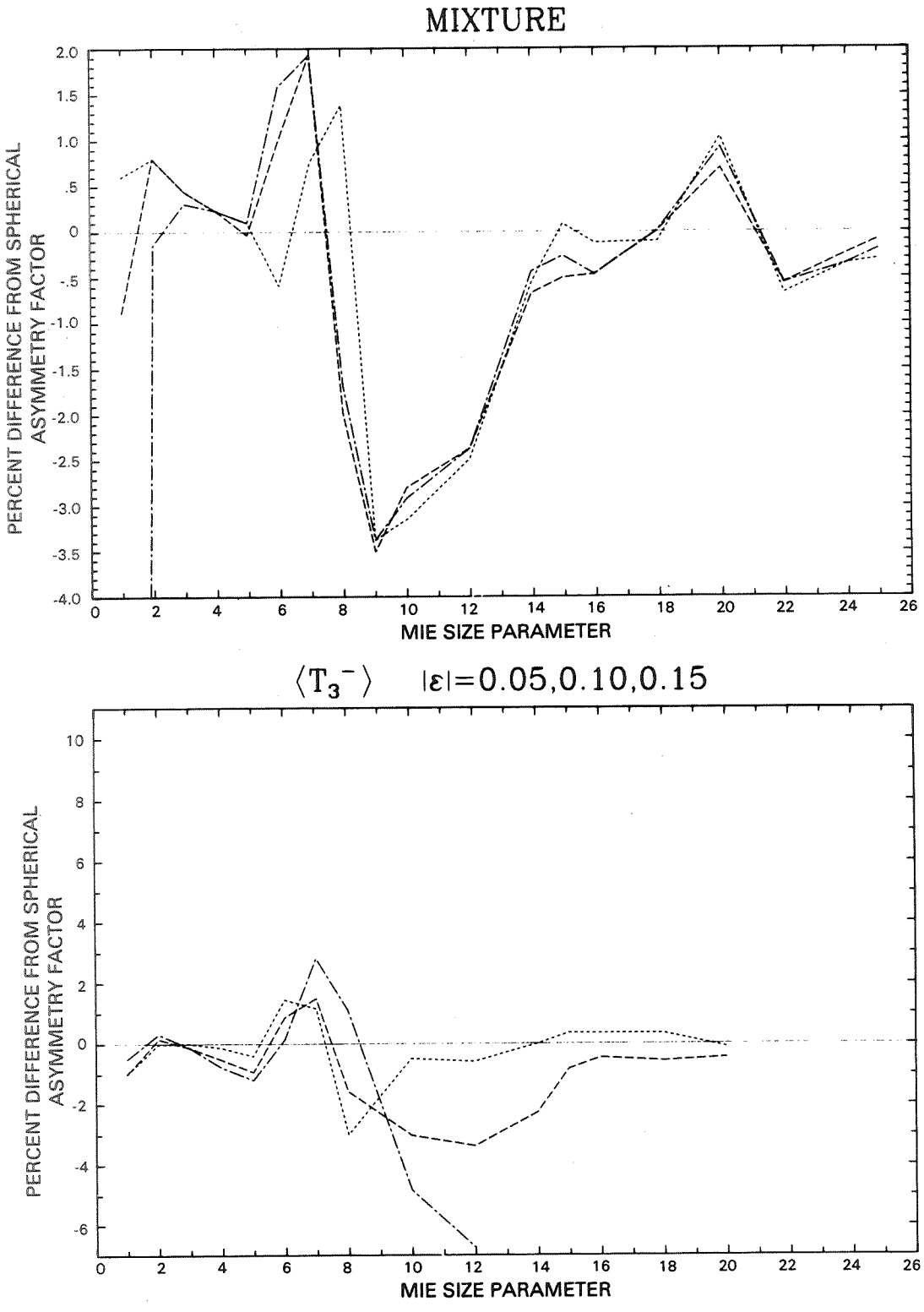

Figure 8. Percentage difference between spherical and nonspherical asymmetry factor, vs. size parameter. Same cases, and same meanings for the lines, as in Fig. 7.

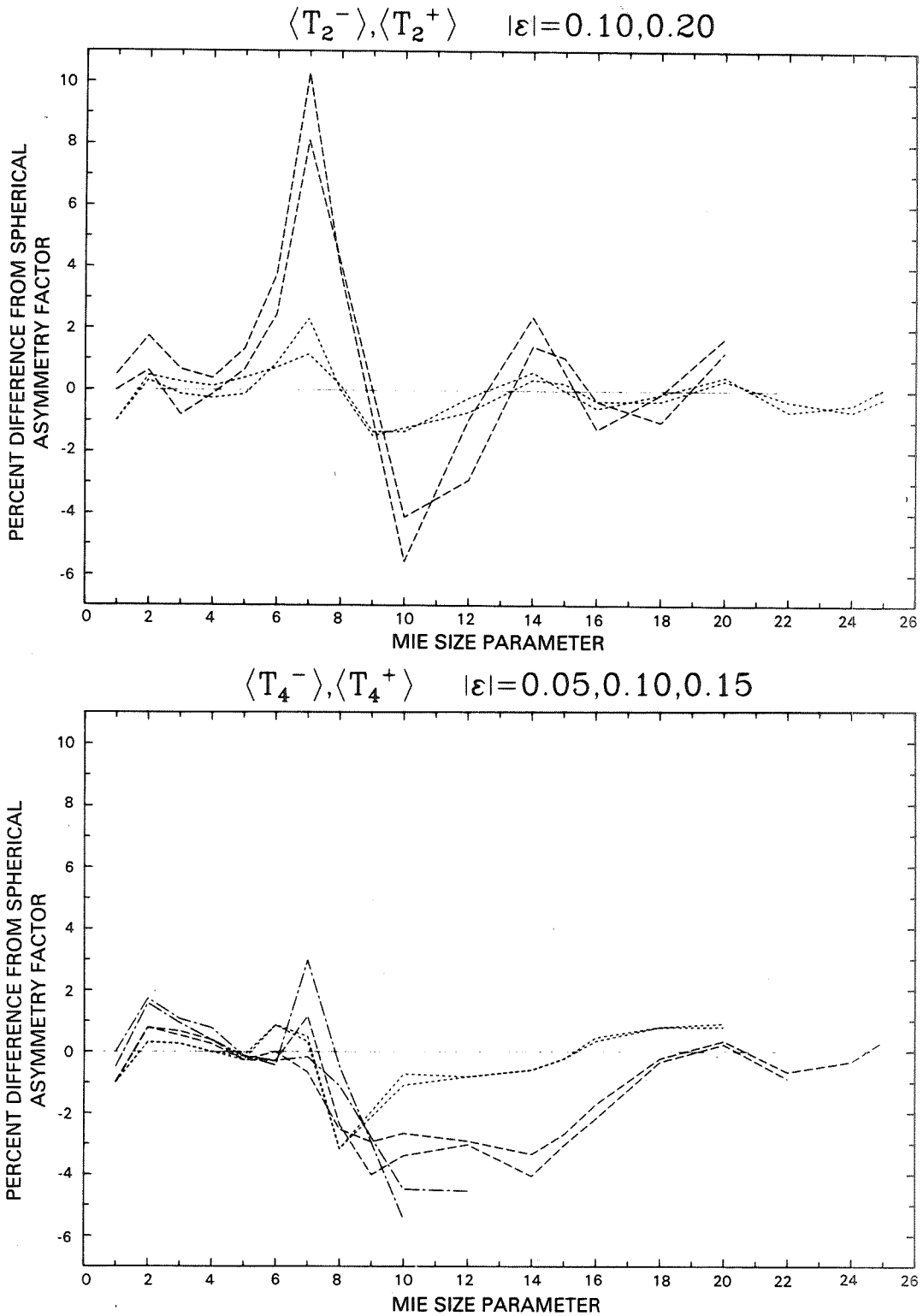

Figure 8 (Continued)

The set of data in Table 3 is one of the key products of this study. It is much more extensive than any which has been computed before; and the entire experimental literature does not contain even 1/10 this much data on nonspherical ω and g. Furthermore, together with Asano's (1980) study for spheroids, this is the only study to show the effect of nonsphericity plus random orientation on both ω and g simultaneously.

It may be of some interest for the reader to compare these results with the predictions of the Pollack/Cuzzi (1980) semi-empirical theory, which are that:

$$\omega_{\text{nonspher}} > \omega_{\text{spher}} \tag{60a}$$

$$g_{\text{nonspher}} < g_{\text{spher}} \tag{60b}$$

where 'spher' refers to an equal-volume sphere, as in our case.

Table 3. Scattering efficiency Q_{sca}, absorption efficiency Q_{abs}, single-scattering albedo ω, and asymmetry factor g for spheres (S), $\Delta x = 0.1x$ size-averaged spheres (S_{avg}), and various Chebyshev particles as a function of size parameter x (equal-volume size parameter for the nonspherical particles).

SCATTERING EFFICIENCY Q_{sca}

x	S	S_{avg}	$T_3(0.05)$	$T_3(0.10)$	$T_3(0.15)$	$T_2(-0.10)$	$T_2(0.10)$
2	1.66	1.66	1.65	1.65	1.63	1.64	1.64
3	3.05	3.05	3.05	3.05	3.04	3.04	3.04
4	3.54	3.57	3.54	3.53	3.53	3.57	3.59
5	3.25	3.21	3.24	3.23	3.22	3.24	3.26
6	2.34	2.29	2.35	2.38	2.42	2.37	2.36
7	1.51	1.55	1.52	1.59	1.73	1.62	1.62
8	1.35	1.39	1.38	1.47	1.61	1.42	1.44
9	1.65	1.65	—	—	—	1.64	1.64
10	2.00	1.96	1.98	1.99	2.03	1.92	1.90
12	1.78	1.79	1.78	1.75	1.71	1.79	1.82
14	1.35	1.36	1.35	1.36		1.42	1.42
15	1.41	1.43	1.43	1.46		1.45	1.43
16	1.57	1.57	1.56	1.59		1.54	1.51
18	1.57	1.56	1.56	1.53		1.53	1.56
20	1.30	1.31	1.29	1.30		1.37	1.38

x	$T_2(-0.20)$	$T_2(0.20)$	$T_4(-0.05)$	$T_4(0.05)$	$T_4(-0.10)$	$T_4(0.10)$
2	1.61	1.59	1.65	1.65	1.64	1.64
3	3.00	3.00	3.05	3.05	3.04	3.04
4	3.59	3.65	3.55	3.55	3.57	3.57
5	3.26	3.32	3.25	3.24	3.26	3.23
6	2.48	2.54	2.35	2.35	2.36	2.38
7	1.82	1.87	1.54	1.55	1.60	1.65
8	1.57	1.55	1.38	1.37	1.47	1.45
9	—	—	—	—	1.76	1.75
10	1.83	1.75	2.00	2.01	2.04	2.06
12	1.76	1.89	1.80	1.79	1.86	1.85
14	1.60	1.62	1.34	1.35	1.36	1.36
15	1.58	1.48	1.39	1.39	1.39	1.39
16	1.55	1.42	1.55	1.54	1.51	1.51
18	1.43	1.52	1.57	1.57	1.58	1.59
20	1.44	1.54	1.30	1.30	1.36	1.36

Table 3 (Continued)

SCATTERING EFFICIENCY Q_{sca}

x	$T_4(-0.15)$	$T_4(0.15)$	$T_6(-0.05)$	$T_6(0.05)$	$T_6(-0.10)$	$T_6(0.10)$
2	1.62	1.61	1.65	1.65	1.63	1.63
3	3.02	3.02	3.06	3.06	3.06	3.06
4	3.59	3.58	3.55	3.55	3.57	3.57
5	3.28	3.22	3.24	3.24	3.25	3.23
6	2.40	2.46	2.35	2.35	2.37	2.37
7	1.68	1.76	1.54	1.54	1.62	1.61
8	1.60	1.61	1.38	1.38	1.46	1.46
9	—	—	—	—	1.71	1.72
10	2.11	2.14	2.00	1.99	2.04	2.00
12	1.93		1.79	1.80	1.84	1.86
14			1.37	1.38	1.50	1.51
15			1.44	1.44	1.55	1.55
16			1.59	1.59	1.65	1.65

x	$T_8(-0.05)$	$T_8(0.05)$	$T_8(-0.10)$	$T_8(0.10)$
2	1.65	1.65	1.62	1.61
3	3.06	3.05	3.05	3.05
4	3.56	3.56	3.59	3.61
5	3.24	3.25	3.23	3.26
6	2.35	2.35	2.37	2.36
7	1.53	1.53	1.59	1.58
8	1.36	1.37	1.42	1.43
9	—	—		—
10	2.00	2.00		1.98

Table 3 (Continued)

ABSORPTION EFFICIENCY Q_{abs}

x	S	S_{avg}	$T_3(0.05)$	$T_3(0.10)$	$T_3(0.15)$	$T_2(-0.10)$	$T_2(0.10)$
2	.170	.170	0.170	0.169	0.168	0.169	0.169
3	.259	.261	0.259	0.259	0.260	0.259	0.260
4	.352	.357	0.352	0.352	0.352	0.355	0.358
5	.471	.455	0.467	0.458	0.448	0.456	0.450
6	.518	.515	0.519	0.518	0.513	0.514	0.506
7	.543	.573	0.552	0.566	0.576	0.565	0.579
8	.641	.628	0.641	0.642	0.640	0.625	0.632
9	.684	.664	—	—	—	0.679	0.661
10	.695	.702	0.703	0.713	0.720	0.701	0.705
12	.729	.740	0.740	0.764	0.779	0.745	0.747
14	.765	.769	0.788	0.810		0.783	0.782
15	.768	.784	0.795	0.828		0.793	0.793
16	.808	.800	0.824	0.845		0.808	0.809
18	.823	.830	0.848	0.874		0.841	0.839
20	.865	.861	0.875	0.897		0.866	0.866

x	$T_2(-0.20)$	$T_2(0.20)$	$T_4(-0.05)$	$T_4(0.05)$	$T_4(-0.10)$	$T_4(0.10)$
2	0.167	0.168	0.170	0.170	0.169	0.169
3	0.258	0.264	0.259	0.259	0.260	0.260
4	0.357	0.362	0.353	0.353	0.355	0.355
5	0.444	0.434	0.466	0.466	0.456	0.455
6	0.519	0.516	0.516	0.518	0.509	0.521
7	0.570	0.574	0.549	0.551	0.563	0.563
8	0.623	0.628	0.641	0.628	0.644	0.620
9	—	—	—	—	0.686	0.697
10	0.708	0.707	0.695	0.704	0.711	0.722
12	0.757	0.763	0.765	0.761	0.777	0.776
14	0.797	0.799	0.782	0.785	0.824	0.826
15	0.812	0.814	0.814	0.807	0.840	0.842
16	0.829	0.827	0.831	0.835	0.854	0.858
18	0.857	0.853	0.859	0.856	0.886	0.892
20	0.881	0.878	0.887	0.887	0.913	0.912

Table 3 (Continued)

ABSORPTION EFFICIENCY Q_{abs}

x	$T_4(-0.15)$	$T_4(0.15)$	$T_6(-0.05)$	$T_6(0.05)$	$T_6(-0.10)$	$T_6(0.10)$
2	0.169	0.168	0.170	0.170	0.169	0.169
3	0.261	0.260	0.259	0.259	0.260	0.260
4	0.356	0.355	0.353	0.353	0.354	0.354
5	0.449	0.445	0.468	0.468	0.462	0.459
6	0.504	0.526	0.520	0.521	0.520	0.526
7	0.572	0.567	0.549	0.550	0.564	0.571
8	0.647	0.636	0.635	0.632	0.632	0.629
9	—	—	—	—	0.697	0.681
10	0.732	0.738	0.705	0.704	0.737	0.735
12	0.789		0.761	0.761	0.791	0.777
14			0.795	0.795	0.835	0.840
15			0.814	0.816	0.860	0.857
16			0.835	0.833	0.879	0.874

x	$T_8(-0.05)$	$T_8(0.05)$	$T_8(-0.10)$	$T_8(0.10)$
2	0.169	0.170	0.168	0.169
3	0.259	0.259	0.259	0.259
4	0.353	0.351	0.350	0.351
5	0.468	0.467	0.458	0.459
6	0.522	0.522	0.526	0.527
7	0.550	0.550	0.563	0.566
8	0.631	0.634	0.624	0.636
9	—	—		—
10	0.704	0.702		0.711

Table 3 (Continued)

SINGLE-SCATTERING ALBEDO

x	S	S_{avg}	$T_3(0.05)$	$T_3(0.10)$	$T_3(0.15)$	$T_2(-0.10)$	$T_2(0.10)$
2	.907	.907	0.907	0.907	0.907	0.907	0.907
3	.922	.921	0.922	0.922	0.921	0.921	0.921
4	.909	.909	0.910	0.909	0.909	0.910	0.909
5	.873	.876	0.874	0.876	0.878	0.877	0.879
6	.819	.816	0.819	0.821	0.825	0.822	0.823
7	.735	.730	0.734	0.737	0.750	0.741	0.737
8	.677	.689	0.683	0.696	0.716	0.694	0.695
9	.708	.713	—	—	—	0.707	0.713
10	.742	.737	0.738	0.736	0.738	0.733	0.729
11	.740	.736	—	—	—	0.733	0.731
12	.710	.708	0.706	0.696	0.687	0.706	0.709
13	.660	.666	—	—		0.670	0.673
14	.639	.639	0.631	0.627		0.645	0.645
15	.647	.645	0.643	0.638		0.646	0.643
16	.661	.663	0.654	0.653		0.656	0.651
17	.670	.667	—	—		0.657	0.657
18	.657	.652	0.648	0.636		0.645	0.650
19	.625	.625	—	—		0.627	0.633
20	.600	.603	0.596	0.592		0.613	0.614

x	$T_2(-0.20)$	$T_2(0.20)$	$T_4(-0.05)$	$T_4(0.05)$	$T_4(-0.10)$	$T_4(0.10)$
2	0.906	0.904	0.907	0.907	0.907	0.907
3	0.921	0.919	0.922	0.922	0.921	0.921
4	0.910	0.910	0.910	0.910	0.910	0.910
5	0.880	0.884	0.875	0.874	0.877	0.877
6	0.827	0.831	0.820	0.819	0.823	0.820
7	0.762	0.765	0.737	0.738	0.740	0.746
8	0.716	0.712	0.683	0.686	0.695	0.700
9	—	—	—	—	0.720	0.715
10	0.721	0.712	0.742	0.741	0.742	0.740
11	—	—	—	—	0.735	0.738
12	0.699	0.712	0.702	0.702	0.705	0.704
13	—	—	—	—	0.659	0.655
14	0.668	0.670	0.631	0.632	0.623	0.622
15	0.661	0.645	0.631	0.633	0.623	0.623
16	0.652	0.632	0.651	0.648	0.639	0.638
17	—	—	—	—	0.647	0.646
18	0.625	0.641	0.646	0.647	0.641	0.641
19	—	—	—	—	0.621	0.621
20	0.620	0.637	0.594	0.594	0.598	0.599

Table 3 (Continued)

SINGLE-SCATTERING ALBEDO

x	$T_4(-0.15)$	$T_4(0.15)$	$T_6(-0.05)$	$T_6(0.05)$	$T_6(-0.10)$	$T_6(0.10)$
2	0.906	0.906	0.907	0.907	0.906	0.906
3	0.920	0.921	0.922	0.922	0.922	0.922
4	0.910	0.910	0.910	0.910	0.910	0.910
5	0.880	0.879	0.874	0.874	0.876	0.876
6	0.826	0.824	0.819	0.819	0.820	0.818
7	0.746	0.756	0.737	0.737	0.742	0.738
8	0.712	0.717	0.685	0.686	0.698	0.699
9	0.729	0.731	—	—	0.710	0.716
10	0.742	0.744	0.739	0.739	0.735	0.731
11	0.737	0.740	—	—	0.733	0.731
12	0.710		0.702	0.703	0.699	0.705
13	0.666		—	—	0.664	0.667
14			0.633	0.634	0.642	0.643
15			0.639	0.638	0.643	0.644
16			0.656	0.656	0.652	0.654
17					0.650	0.651

x	$T_8(-0.05)$	$T_8(0.05)$	$T_8(-0.10)$	$T_8(0.10)$
2	0.907	0.907	0.906	0.905
3	0.922	0.922	0.922	0.922
4	0.910	0.910	0.911	0.911
5	0.874	0.874	0.876	0.877
6	0.818	0.818	0.818	0.817
7	0.736	0.736	0.739	0.736
8	0.683	0.684	0.695	0.692
9	—	—		—
10	0.740	0.740		0.736

Table 3 (Continued)

ASYMMETRY FACTOR g

x	S	S_{avg}	$T_3(0.05)$	$T_3(0.10)$	$T_3(0.15)$	$T_2(-0.10)$	$T_2(0.10)$
2	.634	.634	0.634	0.635	0.636	0.636	0.637
3	.747	.747	0.747	0.746	0.746	0.746	0.749
4	.772	.772	0.771	0.768	0.766	0.770	0.773
5	.751	.752	0.749	0.745	0.743	0.751	0.755
6	.701	.690	0.700	0.696	0.691	0.696	0.695
7	.611	.604	0.611	0.613	0.621	0.618	0.611
8	.612	.633	0.614	0.623	0.640	0.633	0.634
9	.748	.749	—	—	—	0.738	0.739
10	.829	.826	0.822	0.801	0.786	0.816	0.815
11	.860	.857	—	—	—	0.848	0.849
12	.860	.859	0.854	0.830	0.801	0.853	0.857
13	.843	.845	—	—		0.845	0.849
14	.838	.839	0.839	0.820		0.842	0.844
15	.847	.852	0.855	0.845		0.854	0.852
16	.868	.871	0.874	0.867		0.868	0.866
17	.884	.882	—	—		0.878	0.877
18	.884	.883	0.886	0.878		0.880	0.882
19	.876	.879	—	—		0.880	0.882
20	.875	.878	0.877	0.874		0.881	0.882

x	$T_2(-0.20)$	$T_2(0.20)$	$T_4(-0.05)$	$T_4(0.05)$	$T_4(-0.10)$	$T_4(0.10)$
2	0.638	0.645	0.636	0.636	0.639	0.639
3	0.741	0.752	0.749	0.749	0.751	0.752
4	0.771	0.775	0.772	0.772	0.774	0.775
5	0.757	0.762	0.751	0.750	0.750	0.750
6	0.707	0.716	0.696	0.696	0.690	0.688
7	0.653	0.666	0.606	0.607	0.600	0.611
8	0.659	0.657	0.613	0.613	0.617	0.618
9	—	—	—	—	0.727	0.719
10	0.792	0.780	0.820	0.817	0.804	0.798
11	—	—	—	—	0.835	0.832
12	0.834	0.851	0.852	0.852	0.834	0.833
13	—	—	—	—	0.818	0.813
14	0.851	0.859	0.834	0.834	0.811	0.805
15	0.861	0.857	0.850	0.850	0.829	0.826
16	0.868	0.860	0.875	0.874	0.856	0.852
17	—	—	—	—	0.874	0.870
18	0.874	0.882	0.890	0.890	0.881	0.880
19	—	—	—	—	0.882	0.881
20	0.889	0.893	0.886	0.885	0.881	0.880

Table 3 (Continued)

ASYMMETRY FACTOR g

x	$T_4(-0.15)$	$T_4(0.15)$	$T_6(-0.05)$	$T_6(0.05)$	$T_6(-0.10)$	$T_6(0.10)$
2	0.644	0.645	0.637	0.637	0.644	0.644
3	0.754	0.755	0.749	0.749	0.753	0.753
4	0.775	0.778	0.773	0.773	0.777	0.777
5	0.751	0.751	0.752	0.753	0.754	0.753
6	0.688	0.687	0.698	0.698	0.691	0.693
7	0.603	0.622	0.607	0.607	0.602	0.607
8	0.626	0.630	0.605	0.607	0.605	0.614
9	—	—	—	—	0.705	0.712
10	0.789	0.781	0.817	0.817	0.788	0.787
11	0.818	0.813	—	—	0.819	0.821
12	0.820		0.845	0.845	0.809	0.826
13	0.808		—	—	0.816	0.816
14			0.838	0.836	0.822	0.820
15			0.853	0.852	0.841	0.840
16			0.875	0.873	0.862	0.860

x	$T_8(-0.05)$	$T_8(0.05)$	$T_8(-0.10)$	$T_8(0.10)$
2	0.637	0.637	0.644	0.647
3	0.750	0.750	0.756	0.756
4	0.774	0.774	0.776	0.778
5	0.751	0.751	0.750	0.753
6	0.700	0.701	0.694	0.694
7	0.613	0.614	0.607	0.608
8	0.610	0.610	0.602	0.603
9	—	—		—
10	0.820	0.818		0.787

X. SCATTERED INTENSITIES IN FIXED ORIENTATION

One goal of this research was to provide a set of results against which the validity of the EBCM could be tested, either by other exact theoretical techniques or by laboratory experiments. All our random-orientation results are available for this purpose. However, they may not be the best choice, for several reasons:

- random-orientation intensities are rather smooth functions of angle; correctness of the EBCM could be more incisively tested against more highly structured angular patterns, differing more from a sphere;

- random-orientation results depend to some extent on the quadrature over orientation, which introduces an unknown error;

- comparison with microwave-analogue measurements (see Appendix A) would be easier in fixed orientation;

- it is intensities which are measured in the laboratory, while all our random-orientation plots are for phase function and degree of polarization; it requires some effort to deconvolve intensities from these plots

- our random-orientation results are for unpolarized incident radiation, whereas laboratory sources (esp. lasers) are frequently polarized.

Hence, we have decided to include a small selection of fixed-orientation intensities, using both parallel and perpendicular polarized incident light, in Appendix B. These are for Chebyshev particles with $\epsilon = 0.10$ and $x = 5,10$. Shapes were chosen so that the EBCM could be tested for convex [T_2], concave [T_3, T_4, T_6], and asymmetric [T_3] particles. Two fixed orientations for which no cross-polarization occurs were chosen: nose-on and 'perpendicular-to-nose-on' ($\Theta_p = 90°$, $\phi_p = 0$).

Solid lines in App. B refer to the equal-volume sphere; dotted lines to the nose-on orientation; and dashed lines to the 'perpendicular-to-nose-on' orientation. The 'fair' convergence criterion was not used to produce any of these results.

XI. PHASE FUNCTION AND DEGREE OF POLARIZATION IN RANDOM ORIENTATION

MIXTURE

Figures 9 and 10 show the phase function (55) and degree of polarization (58), respectively, for the MIXTURE of 23 particles. These are the most general results of our study, vis a vis the 'net' effect of nonsphericity plus random orientation on the angular variation of scattering.

The arrangement of these plots is similar to that in Appendices C and D (described below). Each phase function plot (for 60–180°) is on the same page with its corresponding percentage-difference-from-a-sphere plot (for 0–180°). The MIXTURE phase function for x = 2,3,4,5,6,8,10,15, and 20 (solid line) can be compared with the exact (dotted line) and $\Delta x = 0.1x$ size-averaged (dashed line) spherical phase functions. The solid, dashed, and dotted lines have the same meaning on the degree of polarization plots (Fig. 10). The percentage differences in Fig. 9 are with respect to the exact (dotted) and size-averaged (dashed) Mie phase functions.

Although we calculated results for many more integer values of 'x' in the range 10–25 than we show here, the decision was made to omit these results because, too often, the changes from one value of 'x' to the next were not noteworthy.

The two spherical curves in Figure 9 bear out our remarks in Sec. VIII, to the effect that down-spikes in the angular range 80–150° tend to be washed out by size-averaging. One should be cautious of the visual impression that size-averaging biases the phase function upward, however; often, this is due only to plotting on a logarithmic vertical scale.

T_n particles

The bulk of our results for phase function (60–180° only) and degree of polarization are contained in Appendices C and D, respectively. On each such plot, the solid line shows the $\Delta x = 0.1x$ size-averaged spherical result, while the dotted, dashed, and dot-dash lines refer to T_n particles with successively increasing values of $|\epsilon|$. Note the change of convention relative to the MIXTURE; there, we used a solid line for the nonspherical result because we wanted to show two spherical results (exact and size-averaged).

These Appendices were designed to allow the reader to flip through them rapidly, generating almost a moving picture of spherical-nonspherical differences as a function of particle size. Thus, a rapid feeling for the results can be obtained. In Appendix C, the phase functions are plotted at the top of each page, and their percent differences from a sphere at the bottom; thus, the 'action' can be stopped at any point to compare the two.

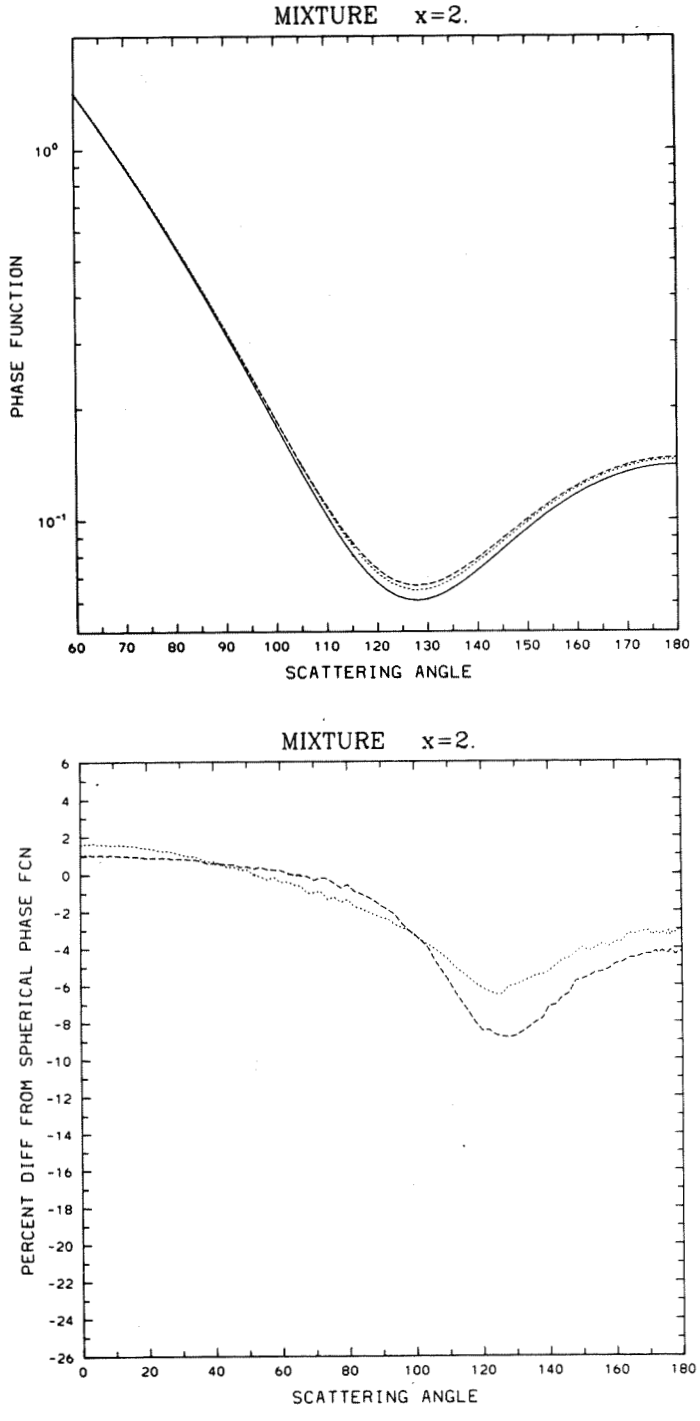

Figure 9. 60–180 degree phase function for nonspherical MIXTURE (solid line), exact sphere (dotted line), and $\Delta x = 0.1x$ size distribution of spheres (dashed line) for x = 2,3,4,5,6,8,10,15, and 20. Companion plots show percent differences of the nonspherical phase functions from the spherical ones for the full range of angles (0–180 degrees); interrupted lines refer to the same spherical cases as in the corresponding phase function plot. Note how size-averaging the spherical results frequently mimics the effect of nonsphericity.

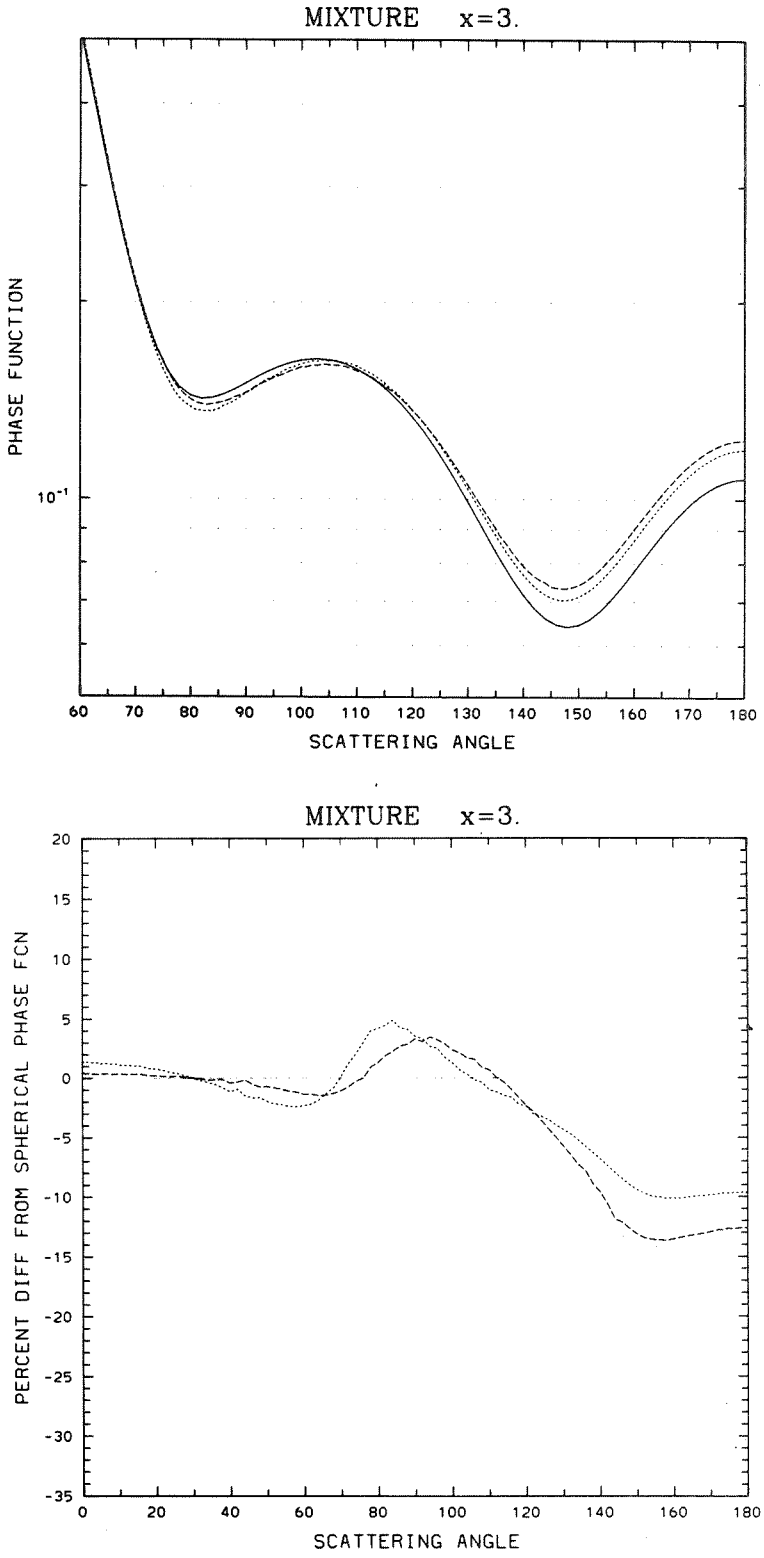

Figure 9 (Continued)

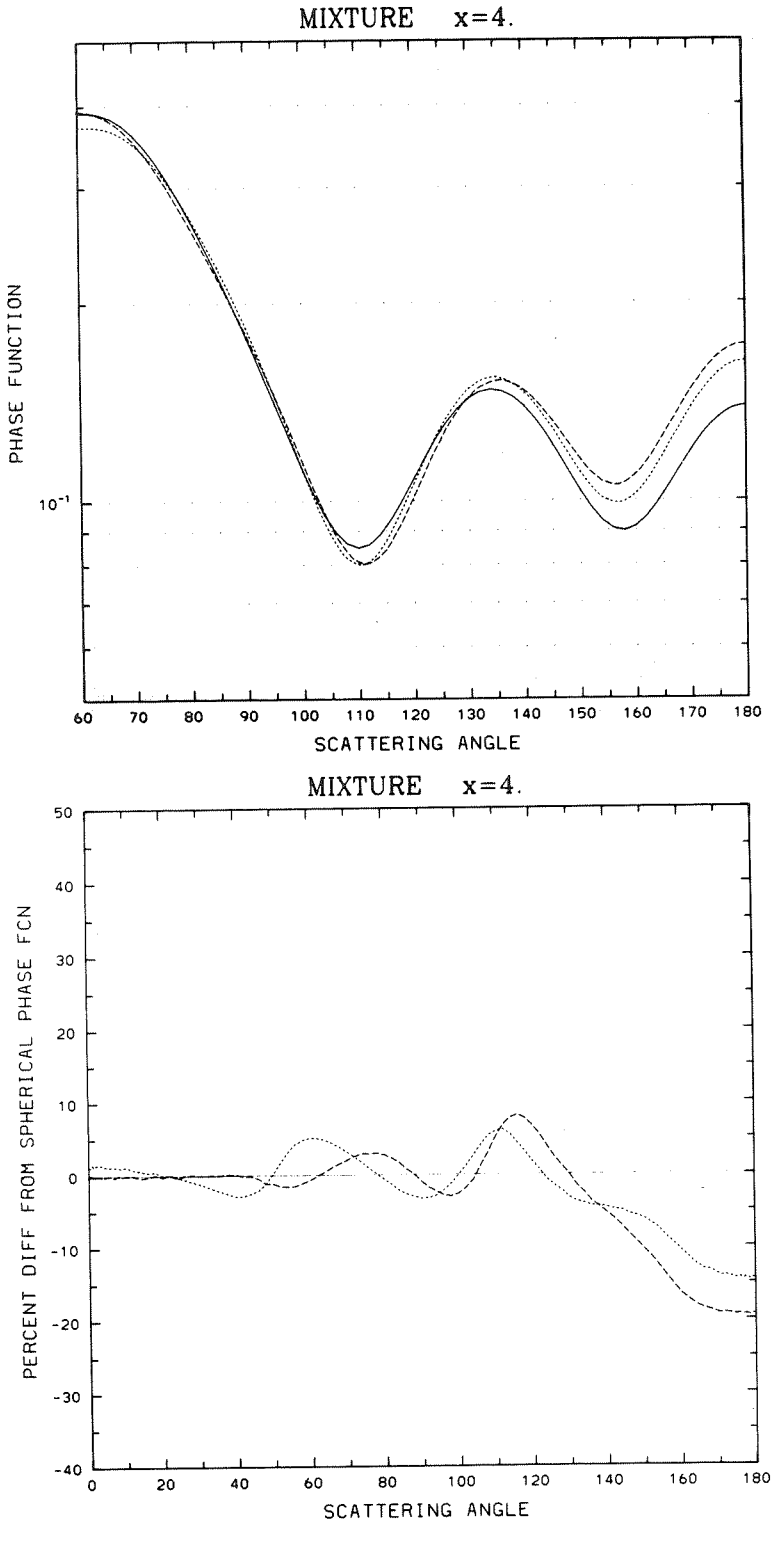

Figure 9 (Continued)

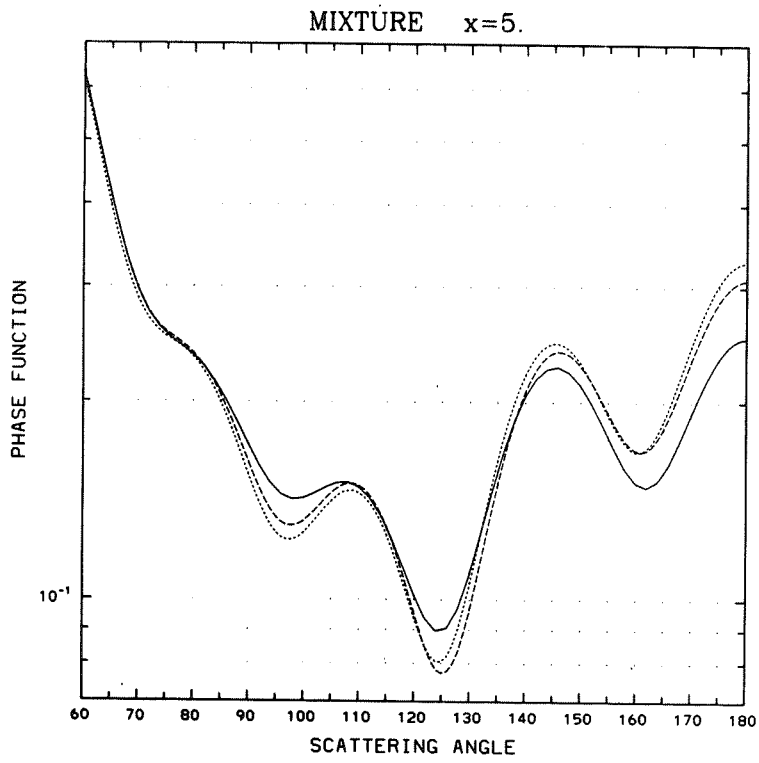

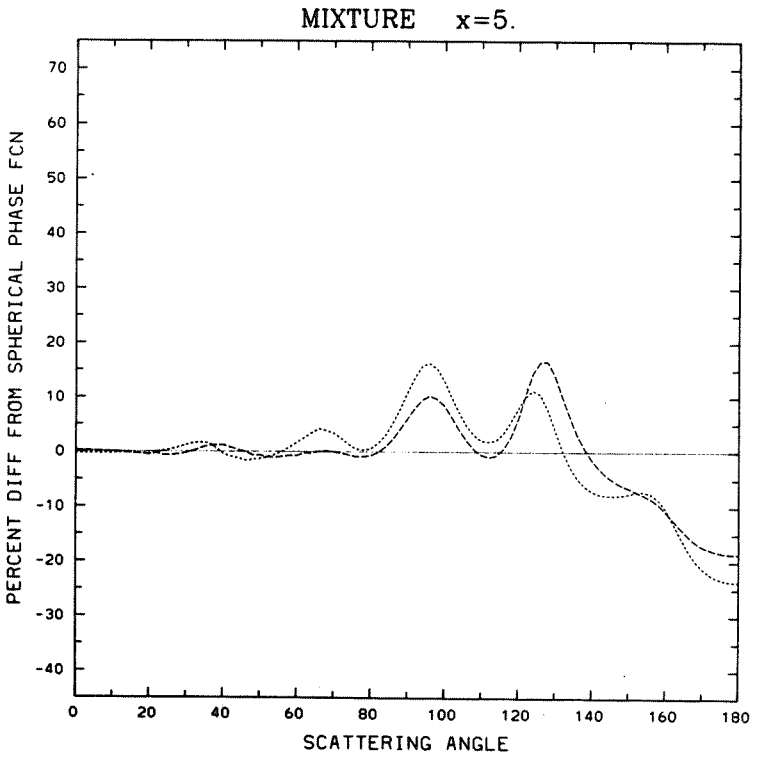

Figure 9 (Continued)

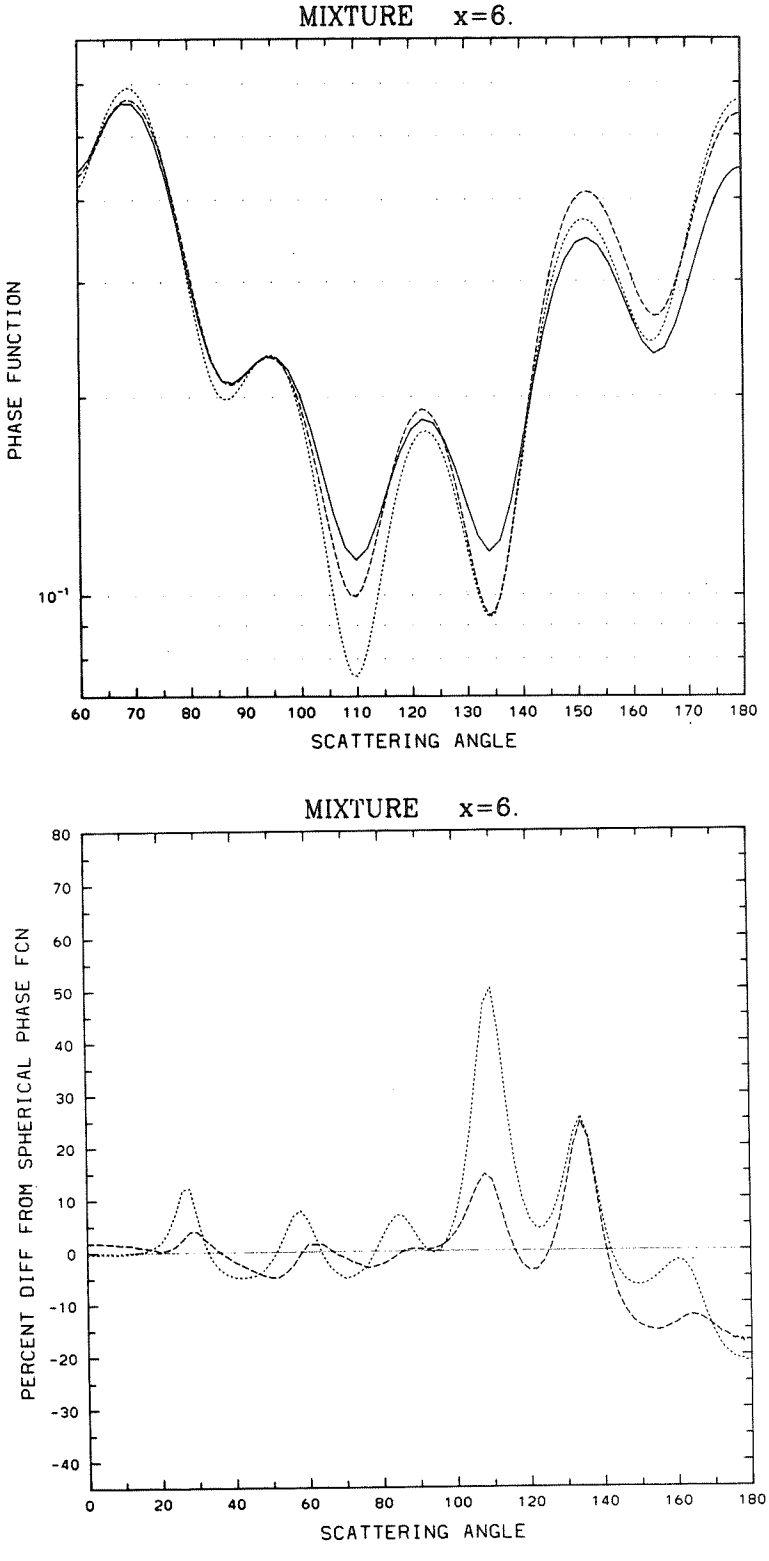

Figure 9 (Continued)

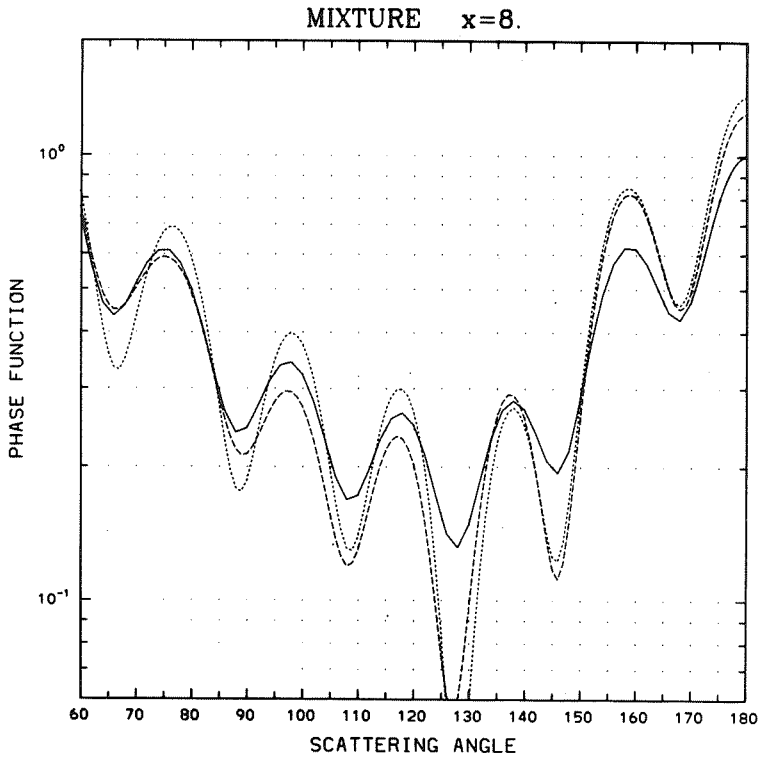

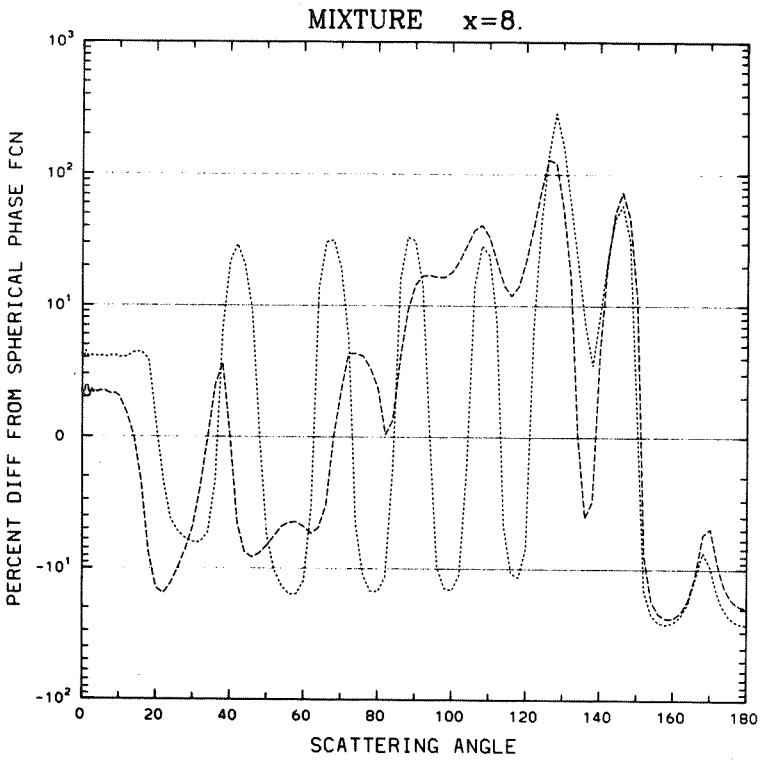

Figure 9 (Continued)

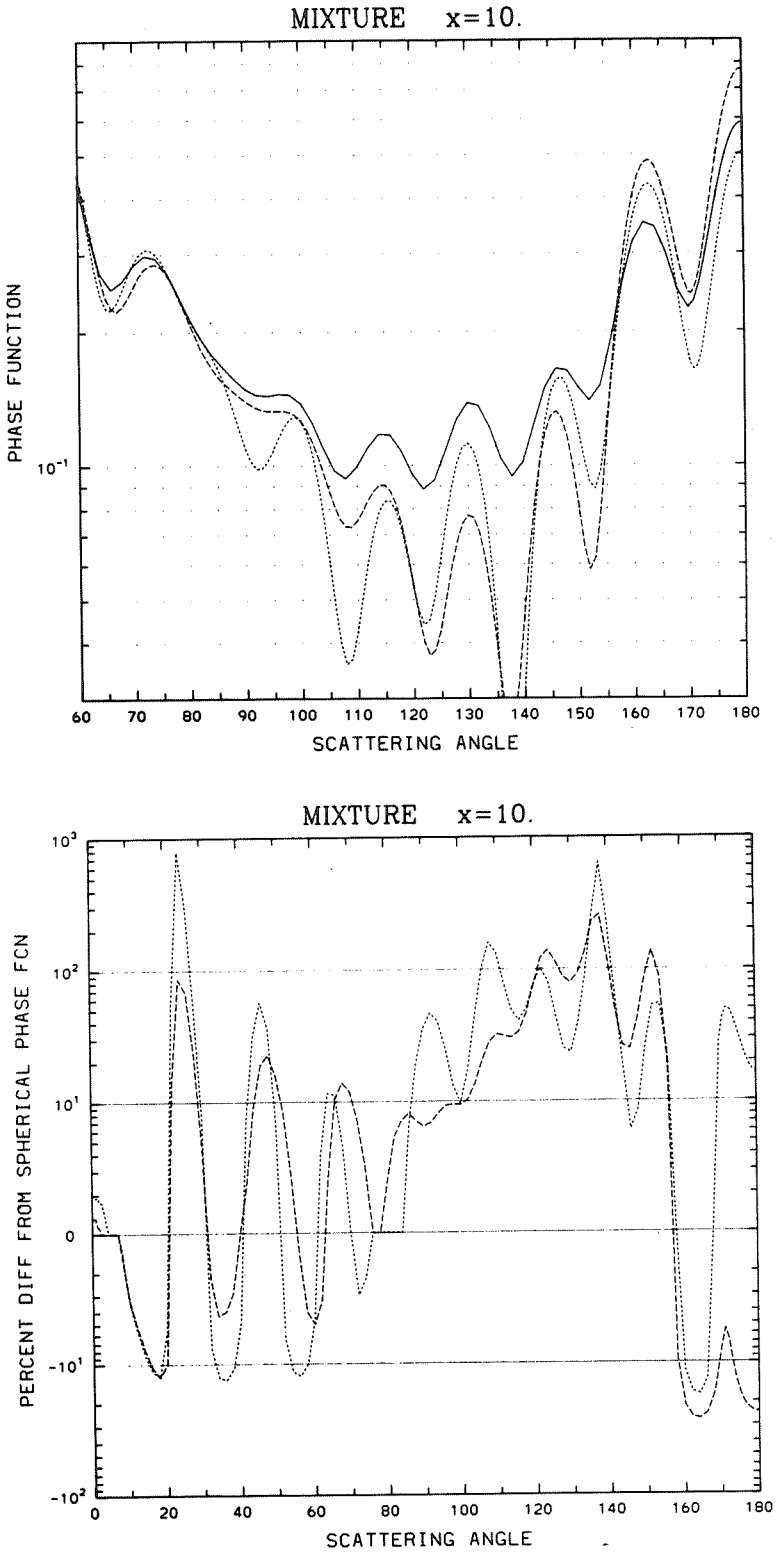

Figure 9 (Continued)

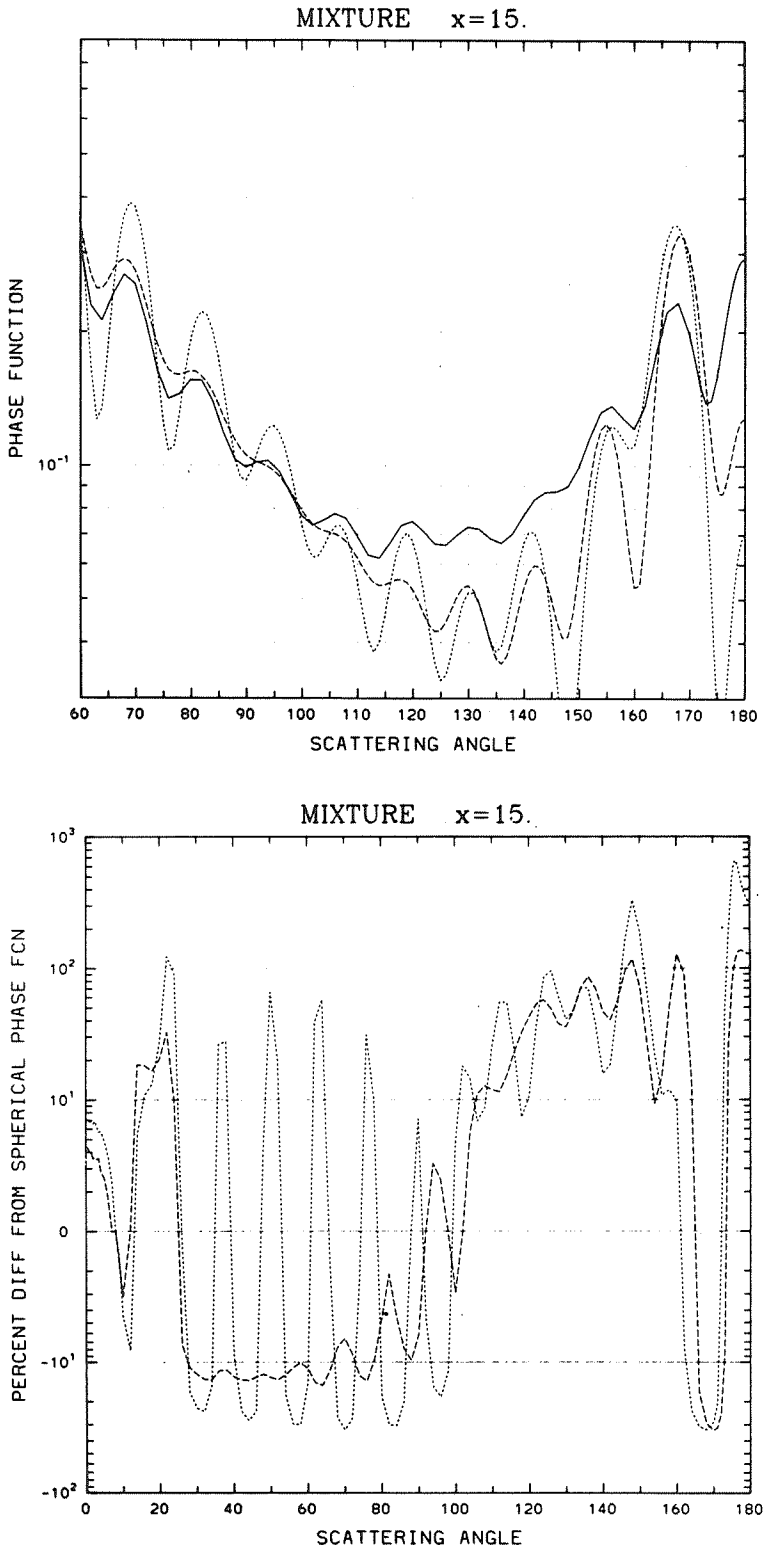

Figure 9 (Continued)

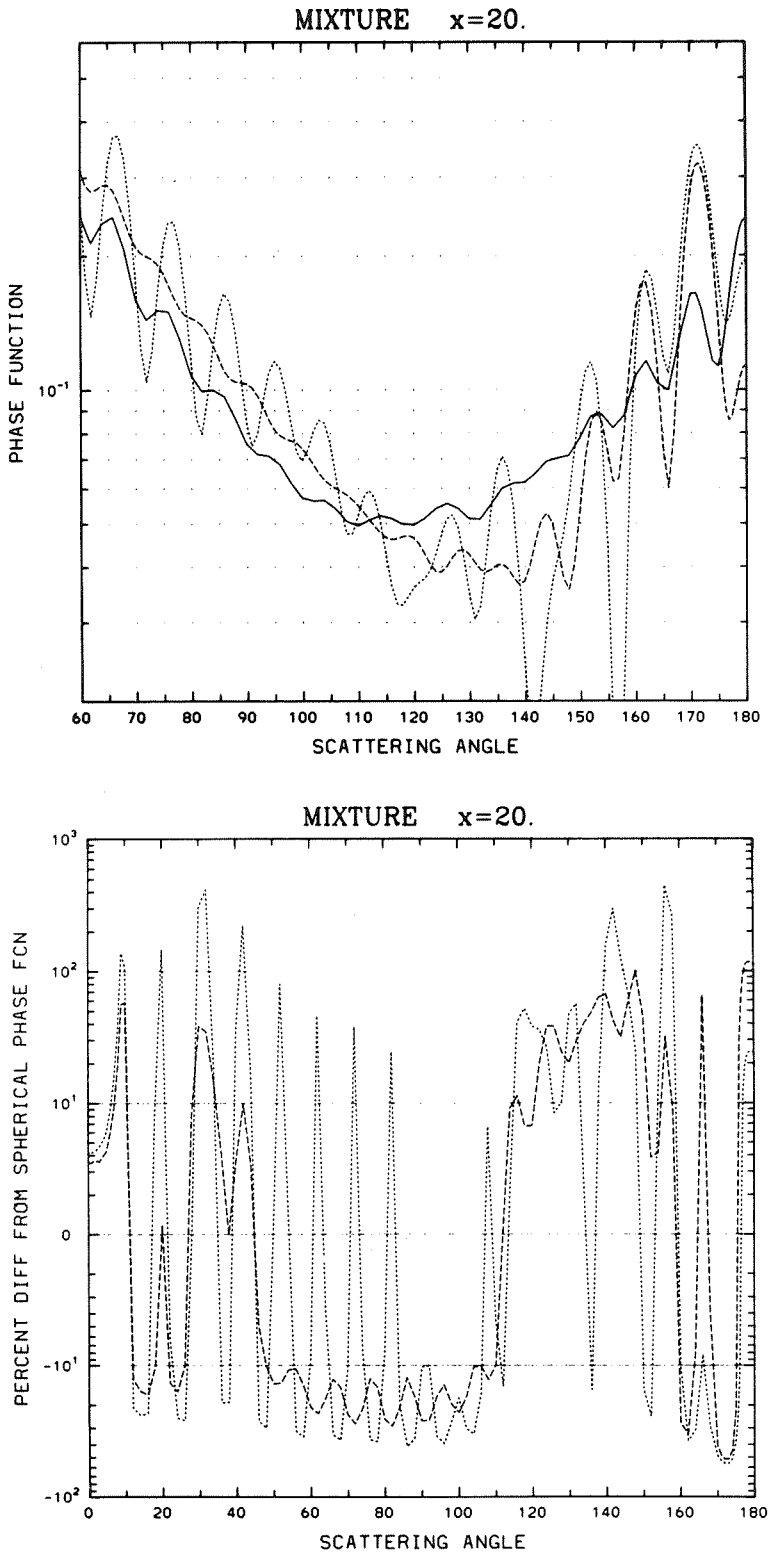

Figure 9 (Continued)

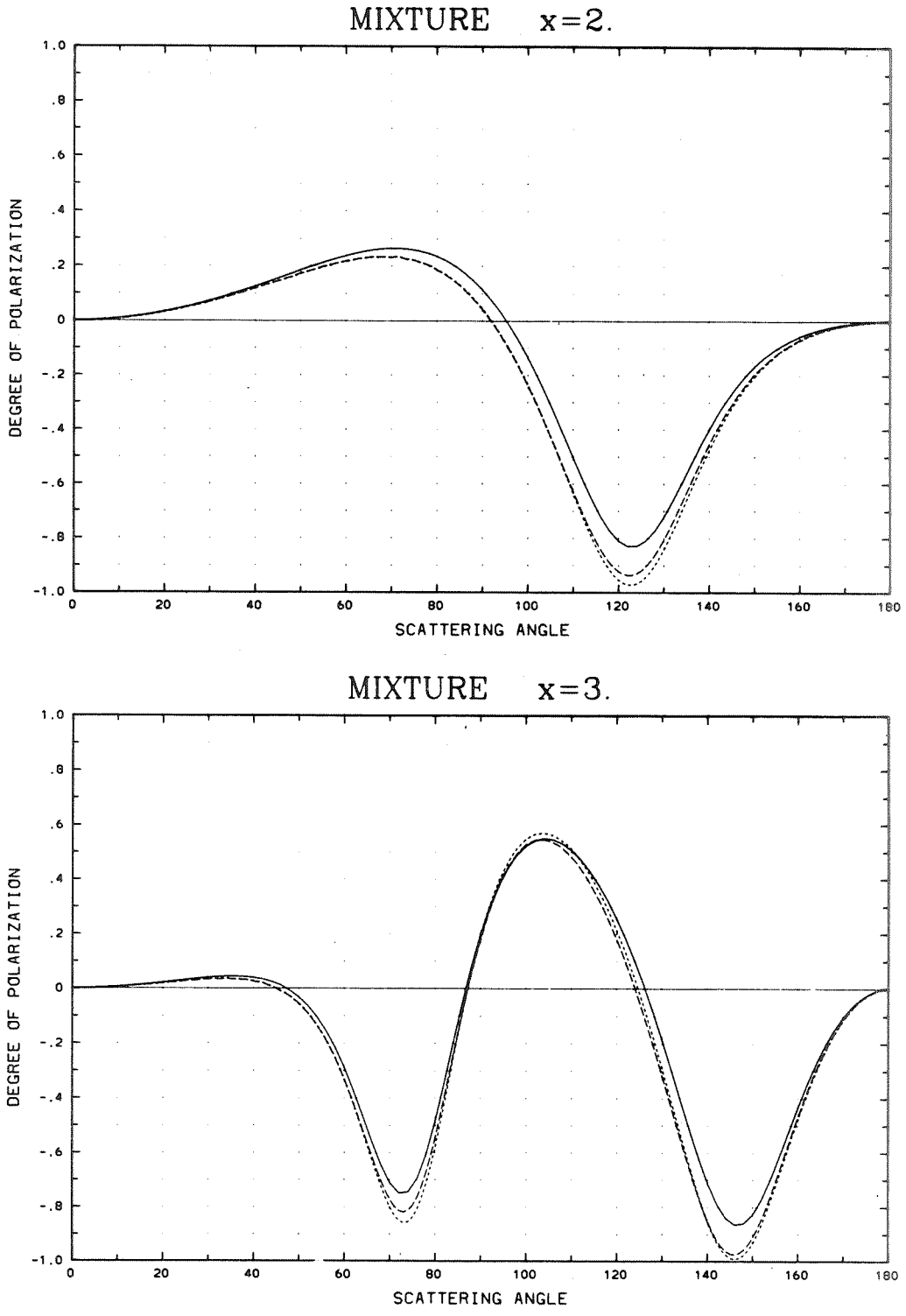

Figure 10. Degree of polarization for nonspherical mixture (solid line), exact sphere (dotted line), and $\Delta x = 0.1x$ size distribution of spheres (dashed line) for x = 2,3,4,5,6,8,10,15 and 20. Note how, as in Fig. 9, size-averaging the spherical results frequently mimics the effect of nonsphericity.

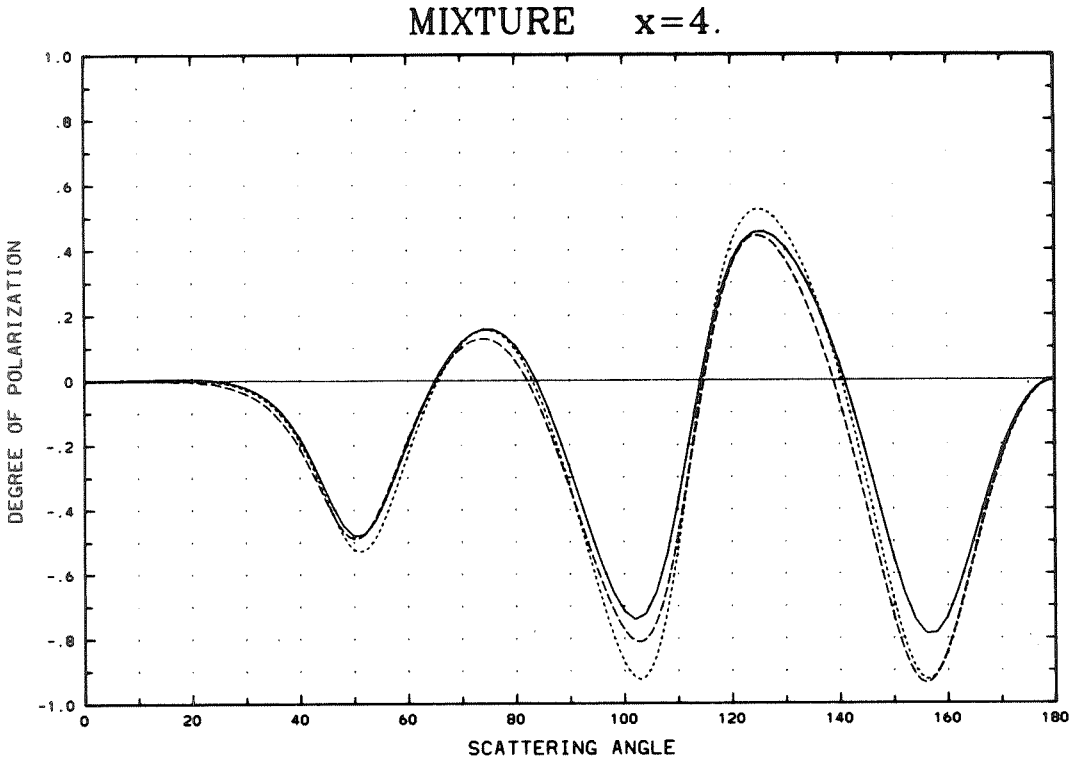

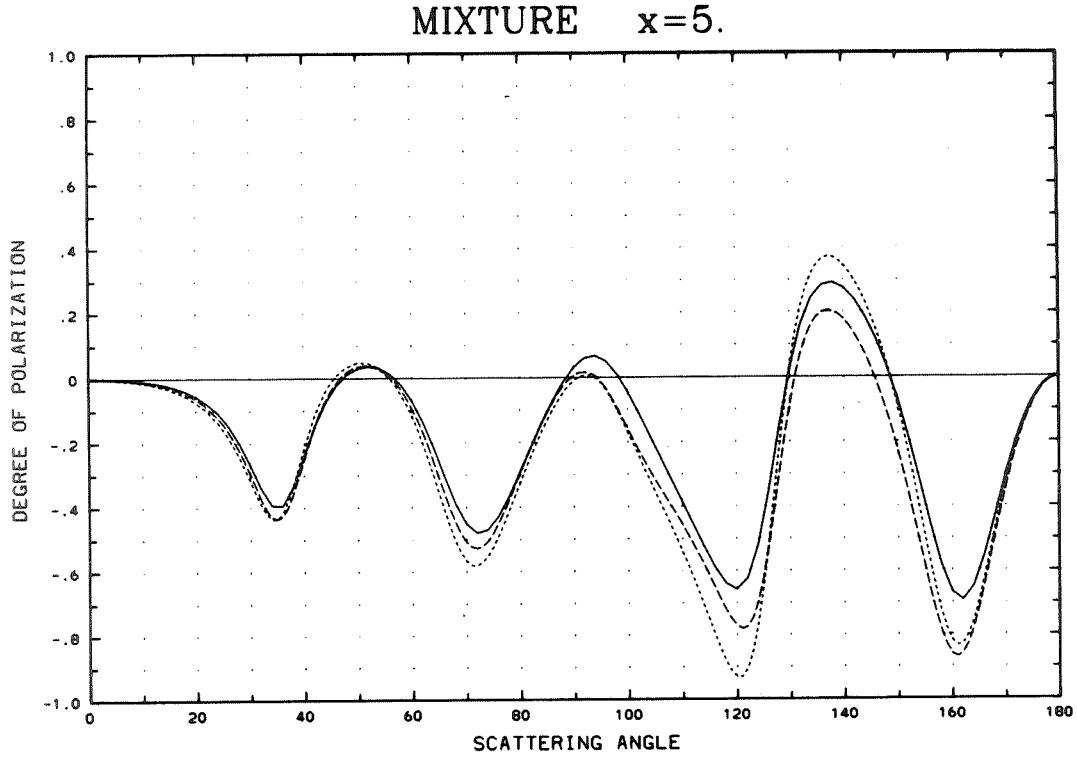

Figure 10 (Continued)

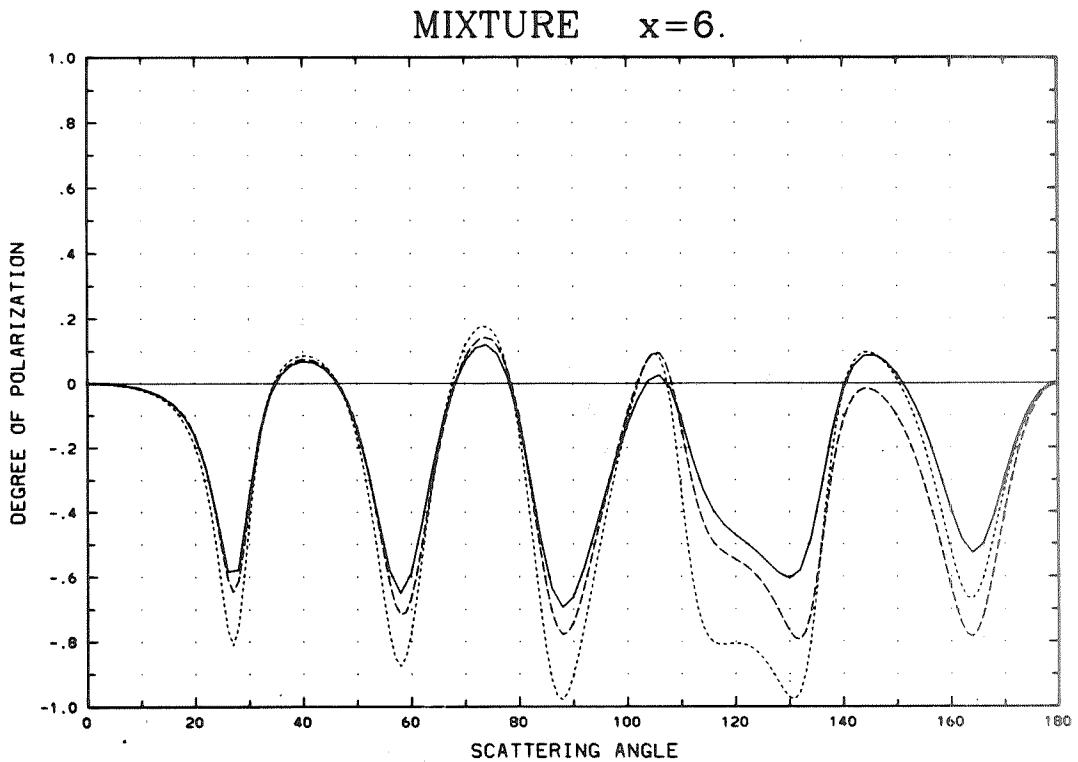

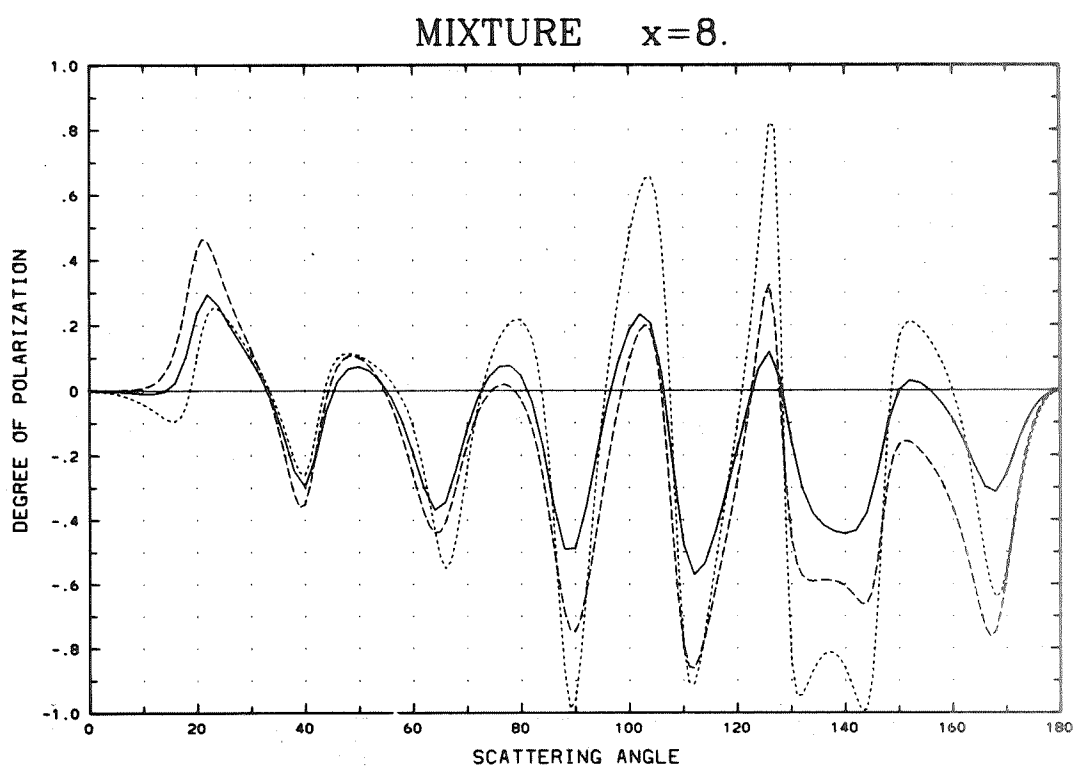

Figure 10 (Continued)

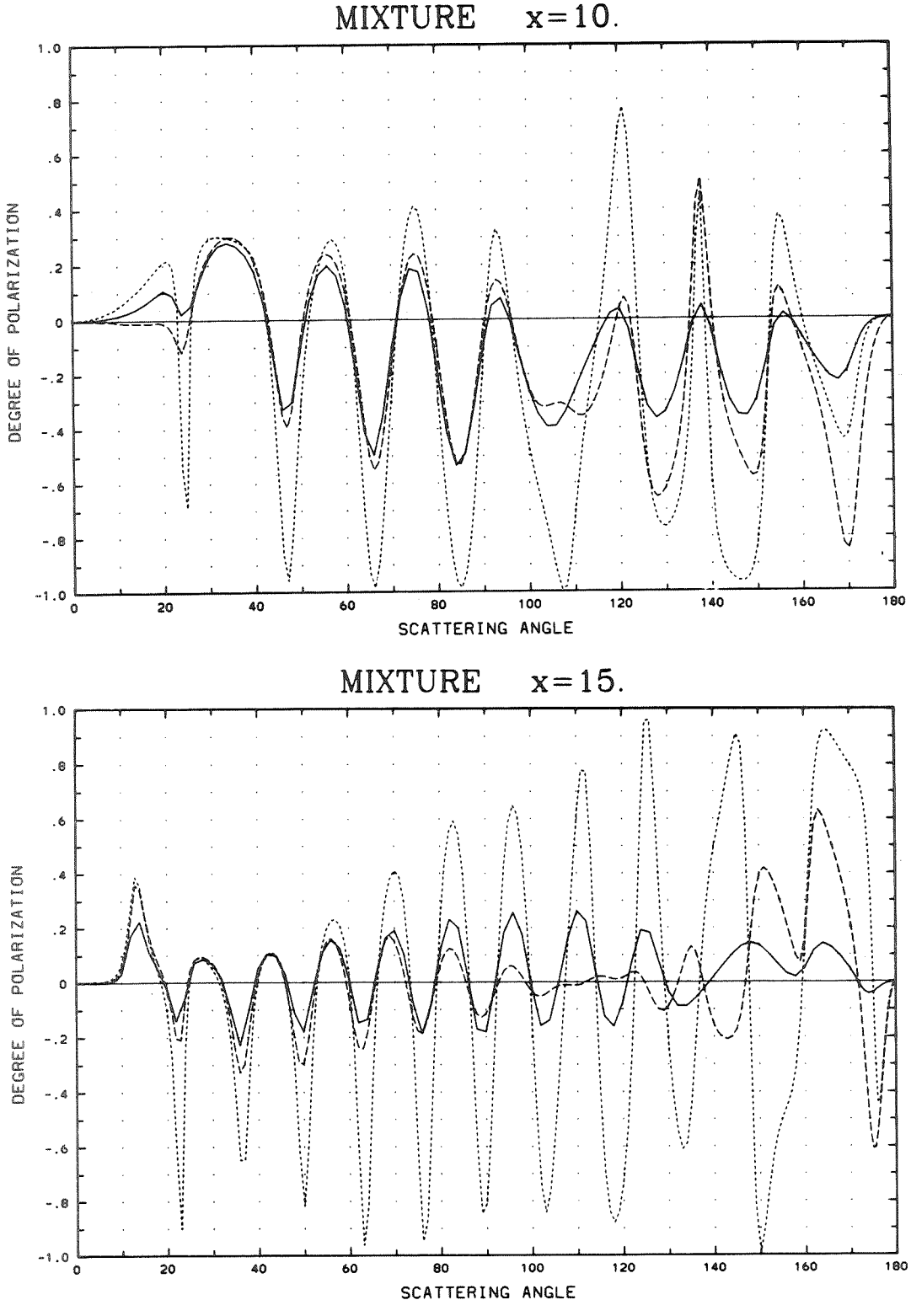

Figure 10 (Continued)

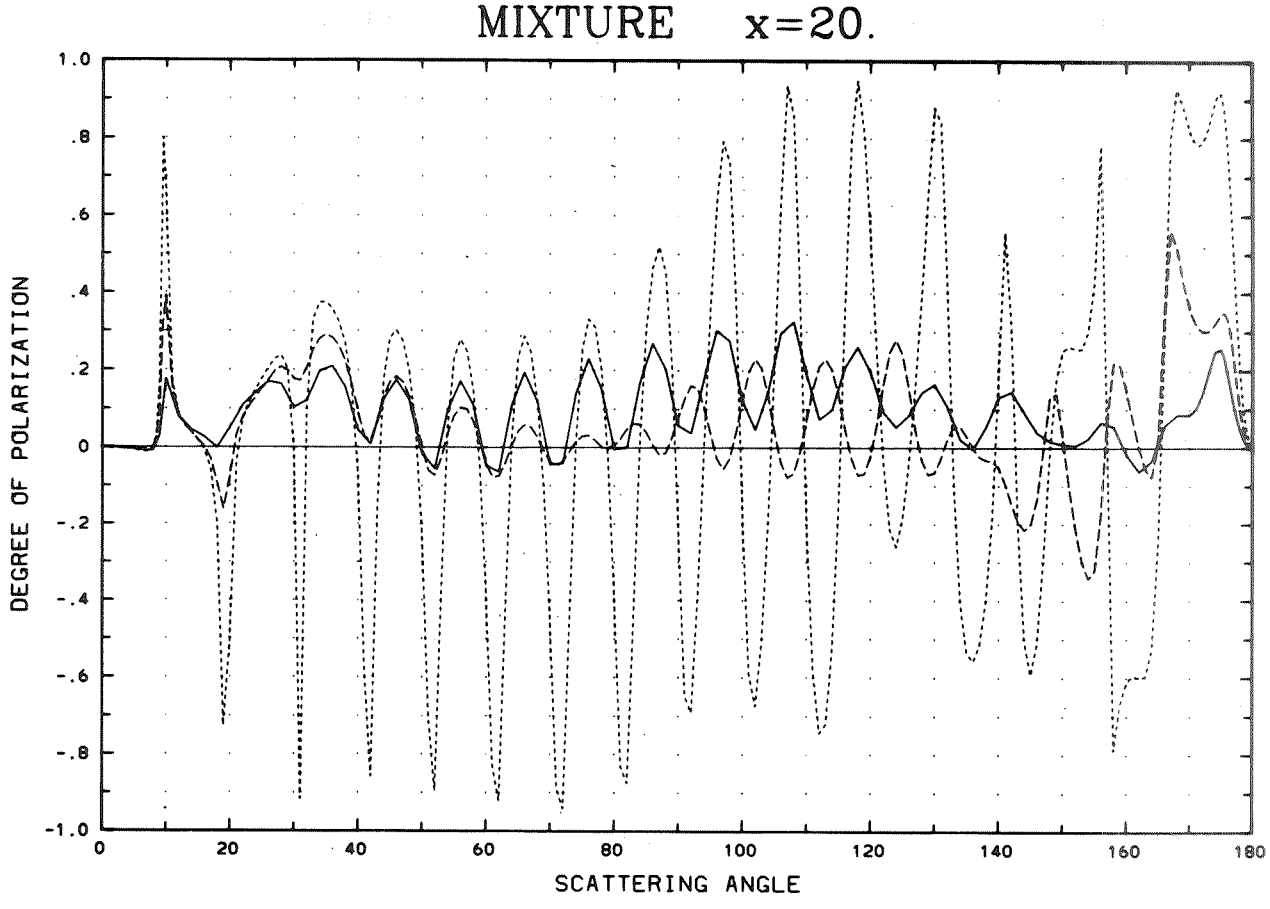

Figure 10 (Continued)

The organization of the Appendices can be likened to a sequence of 3 nested loops. The idea was, to group the most similar results closest together, then the next most similar, and so forth. Thus, the innermost 'loop' is over the magnitude of the deformation parameter ϵ of a Chebyshev particle; results from those values of ϵ for which the EBCM converged are plotted on the same frame.

The reason for grouping different values of ϵ closest together, is to test our intuitive notions of perturbation theory. When ϵ doubles, so these notions go, the differences from the spherical phase function and degree of polarization should double also. Thus, dividing the percent differences by the corresponding $|\epsilon|$ should cause them to fall almost on top of one another. This does not in fact happen — far from it — else we should have presented the percentages in this way.

The middle 'loop' is over particle type. Since $T_n{}^+$ and $T_n{}^-$ particles bear a subtle similarity, as described in Sec. II, they are placed on facing pages, for easy comparison. The first particle in each group is T_3, since it is the only unsymmetric one; then the other T_n's follow in order of n — 2, 4, 6, 8. T_{20} results are omitted because only the $|\epsilon| = 0.05$, $x < 8$ cases could be converged, and they did not differ much from a sphere.

The outermost loop is over size parameter x (from 2 to 20), because the biggest changes occur as size changes. As noted above, we omitted all of our results from $x = 11$ to $x = 25$ except $x = 15$ and 20, because we were unable to see big enough differences among the $x > 10$ plots — just an increasingly complex jumble of oscillations. We feel that further filtering — perhaps the subtraction of a common oscillatory term from all curves — is necessary to make any sense out of this data. Or perhaps phase function and degree of polarization are the wrong quantities to look at; they just do not make spherical-nonspherical differences stand out in stark relief.

Until a better way is found to look at spherical-nonspherical differences for $x > 10$, our use of the EBCM all the way up to $x = 25$ (no one had gone beyond $x = 10$ before) remains more of a *tours de force* than a way to gain fundamentally new insights.

We tried to keep the vertical-axis range of our plots as small as possible, in order to magnify spherical-nonspherical differences. At the same time, we wanted to avoid having a different scale for every plot. The compromise we struck was to fix the range for large groups of plots (for example, at one full decade), but to slide this range up or down to match the quantities being plotted, as necessary. This way, the spread between curves on neighboring plots is comparable, even when the vertical scales are not identical.

It was also the question of vertical resolution which drove us to plot phase function separately for 0–60° and 60–180°. The forward peak of the phase function takes several decades to contain it, yet spherical-nonspherical differences are all but negligible there. Meanwhile, the important differences in side-scattering were shrunk to Lilliputian proportions.

Note that the percentage difference plots in App. C change from a linear to a logarithmic vertical scale past $x = 6$. This is because the percentages become very large — over 100% in many cases — in spite of the relatively small deviations from sphericity. Percentages below about 1%, we regard as in the

noise level, and have explicitly accounted for this in the logarithmic plots by starting the scale at 1% (which is labelled '0').

0–60° phase function

We present in Fig. 11 only a sparse sampling of our phase function results in the angular range 0–60°. (The corresponding percentage differences from a sphere for 0–60° can be found in Appendix C.) The meanings of the various lines are the same as in Fig. 9 (for the MIXTURE cases) and as in Appendix C (for the T_n cases).

The reason for omitting much of this data, is simply that it proved uninstructive. After all, 0–60° is primarily a diffraction region, dominated by 'rays' that do not actually 'hit' a particle but merely bend around it. (One cannot really talk of 'rays' at $x = 1$, but already by $x = 10$ the concept has some utility.) These 'rays' are insensitive to particle shape and refractive index. They are sensitive primarily to projected area (van de Hulst, 1981); and the differences in projected area between randomly-oriented Chebyshev particles and equal-volume spheres are minute.

Hence, as might be expected, the spherical and nonspherical phase functions tracked each other very closely in this region — so closely, often, that they were indistinguishable. Some of the plots in Fig. 11 were selected to illustrate this point. The remainder show cases where the differences are more substantial.

Acknowledgments: We are indebted to the National Center for Atmospheric Research for providing the computer time for these studies; to David Kennison of NCAR for assistance with some of the graphical presentations; and to NASA for publishing this compendium, whose completion spanned over 5 years and hence came to be affectionately known as 'The Eternal Project'.

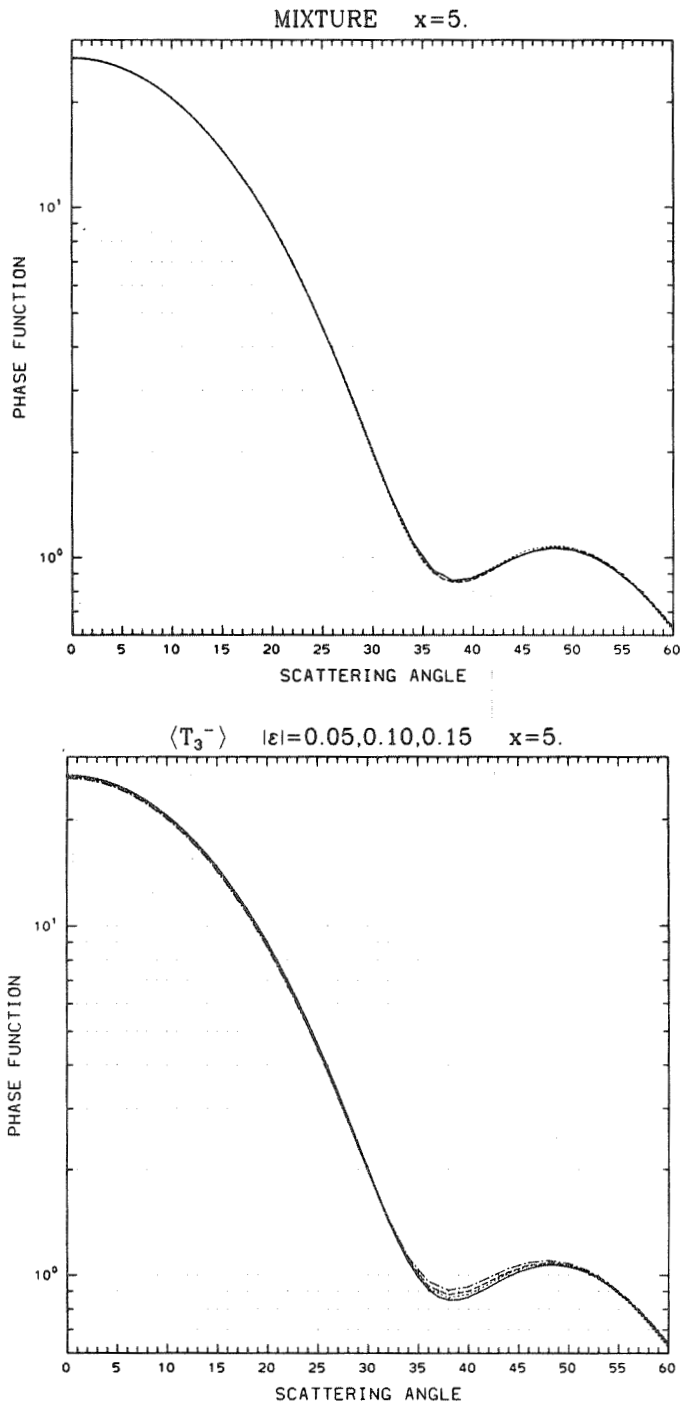

Figure 11. 0–60 degree phase function for nonspheres (solid line for MIXTURE, interrupted lines in other cases — dotted, dashed, and dot-dash lines correspond to the various ϵ values shown, in increasing order) and for $\Delta x = 0.1x$ size distribution of spheres (dashed line for MIXTURE, solid line in other cases). Exact sphere result (dotted line) is shown only for MIXTURE. Size parameters $x = 5$, 10, 15, and 20 only.

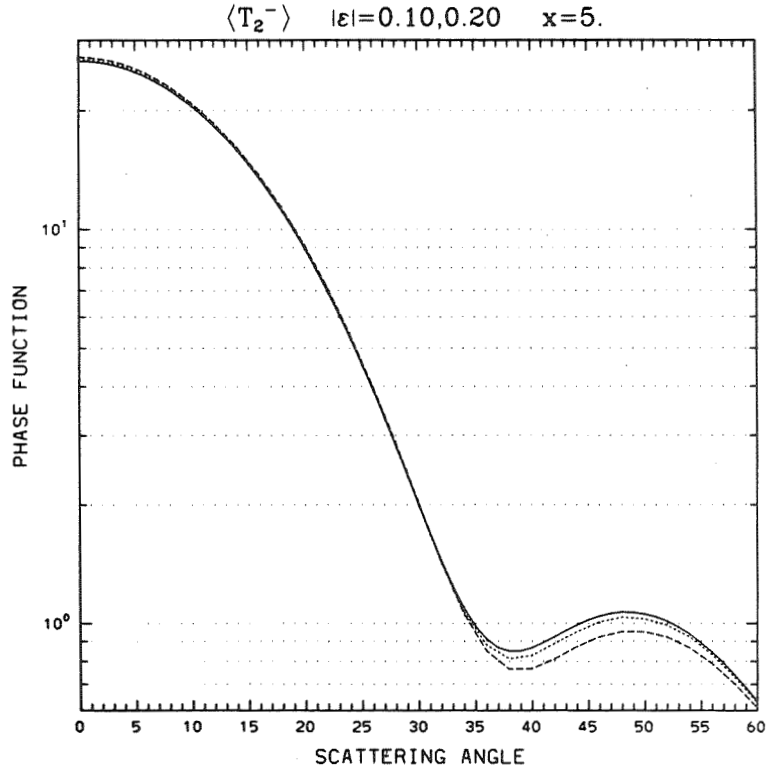

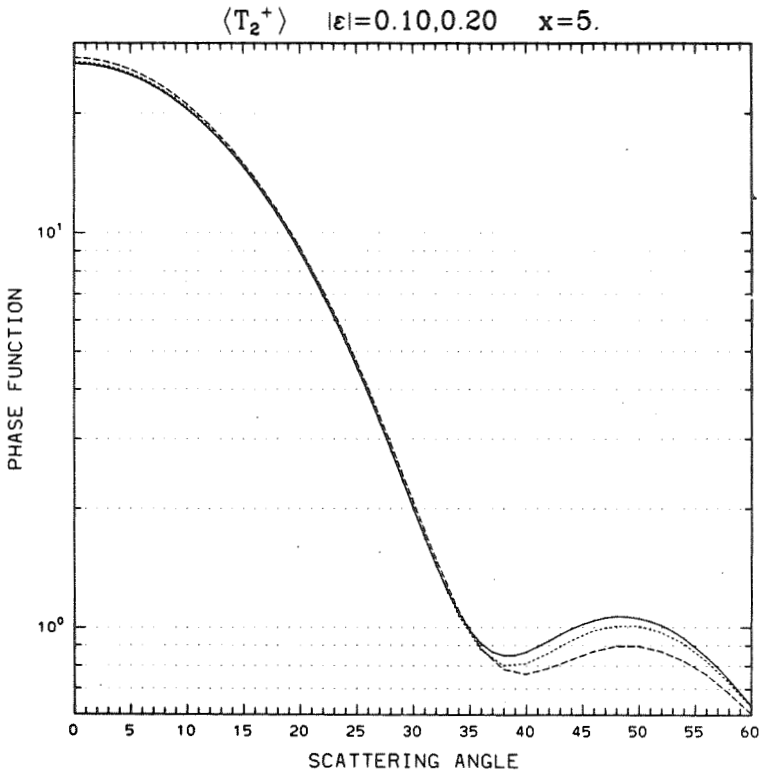

Figure 11 (Continued)

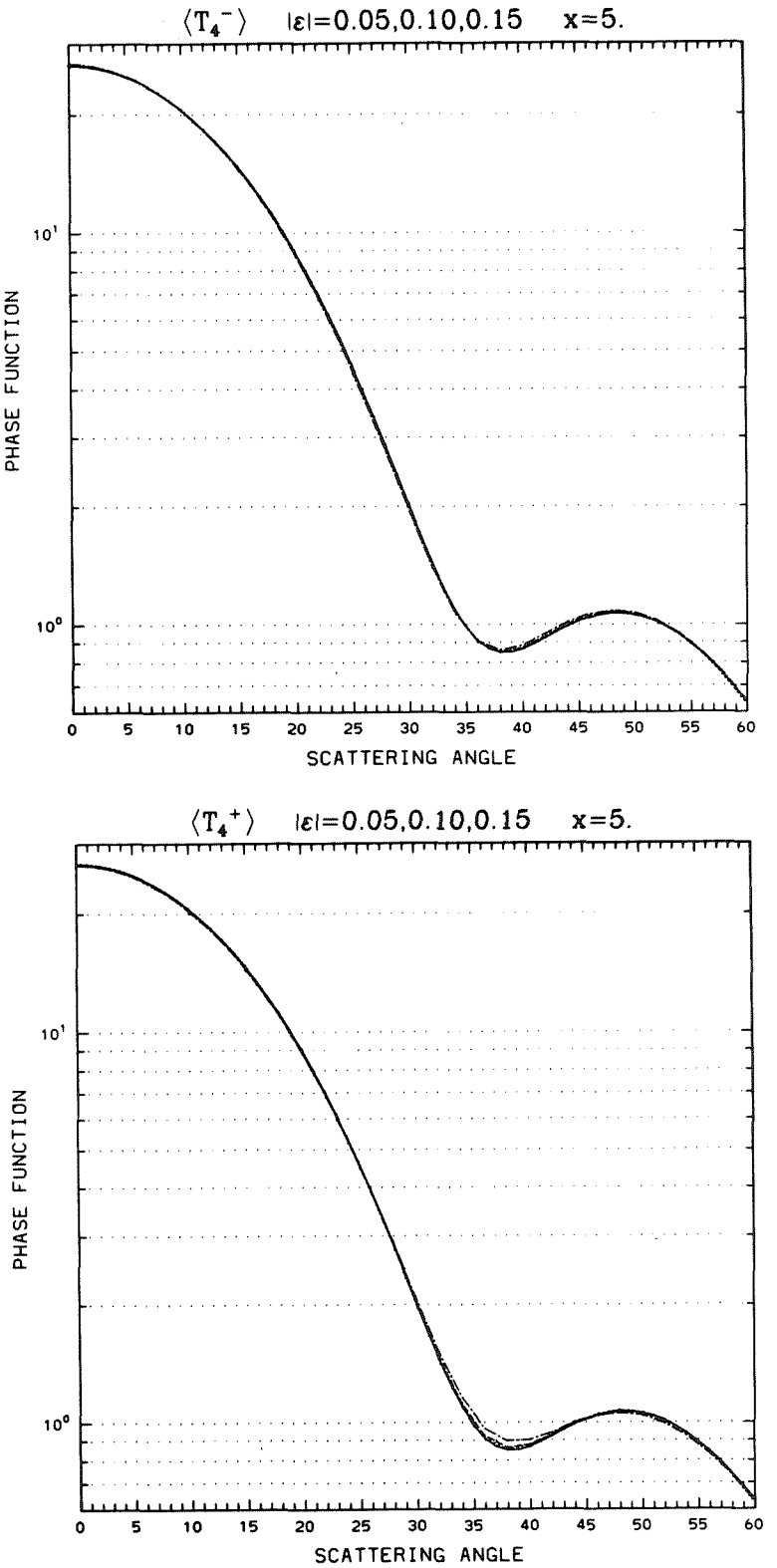

Figure 11 (Continued)

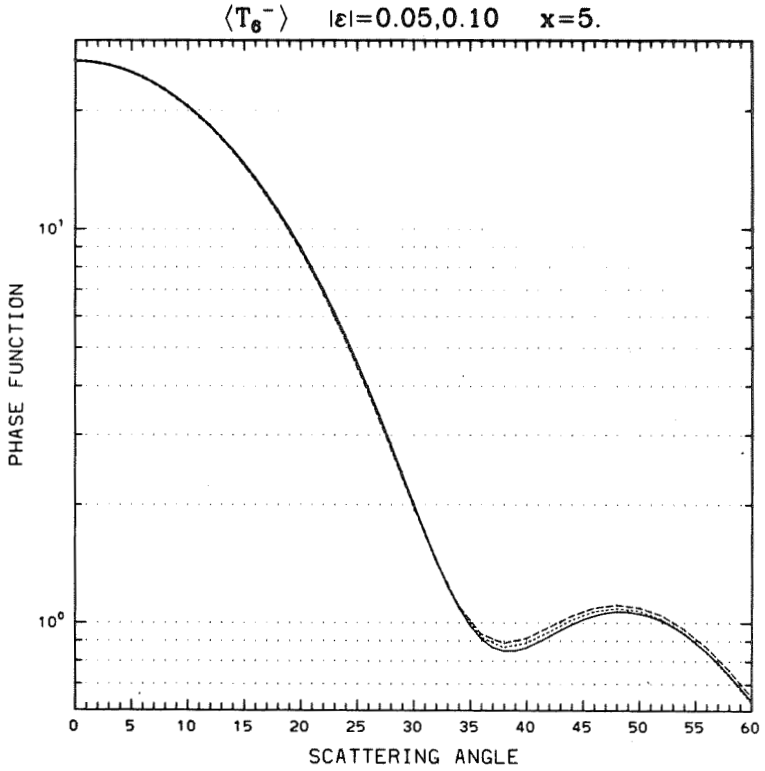

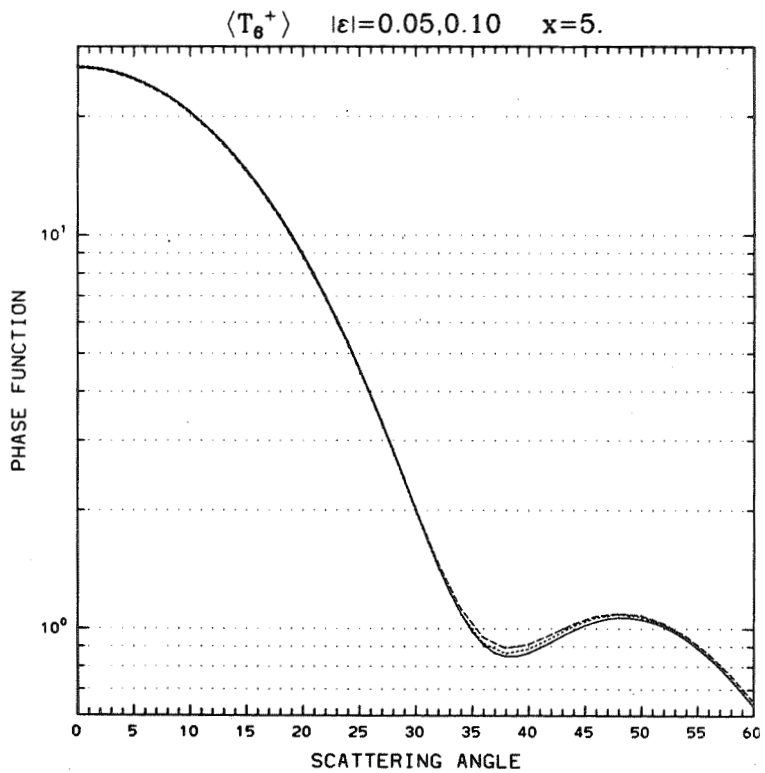

Figure 11 (Continued)

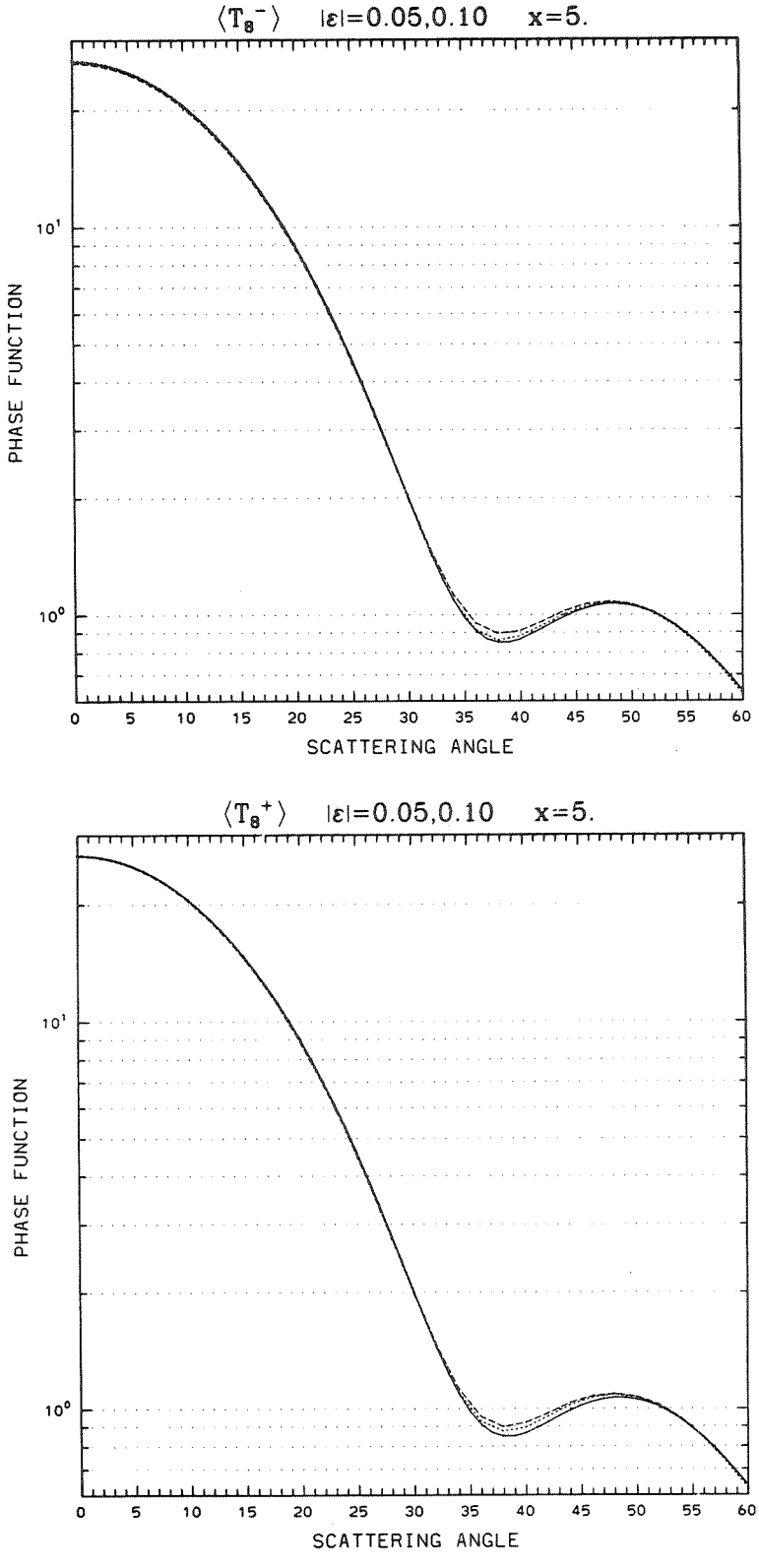

Figure 11 (Continued)

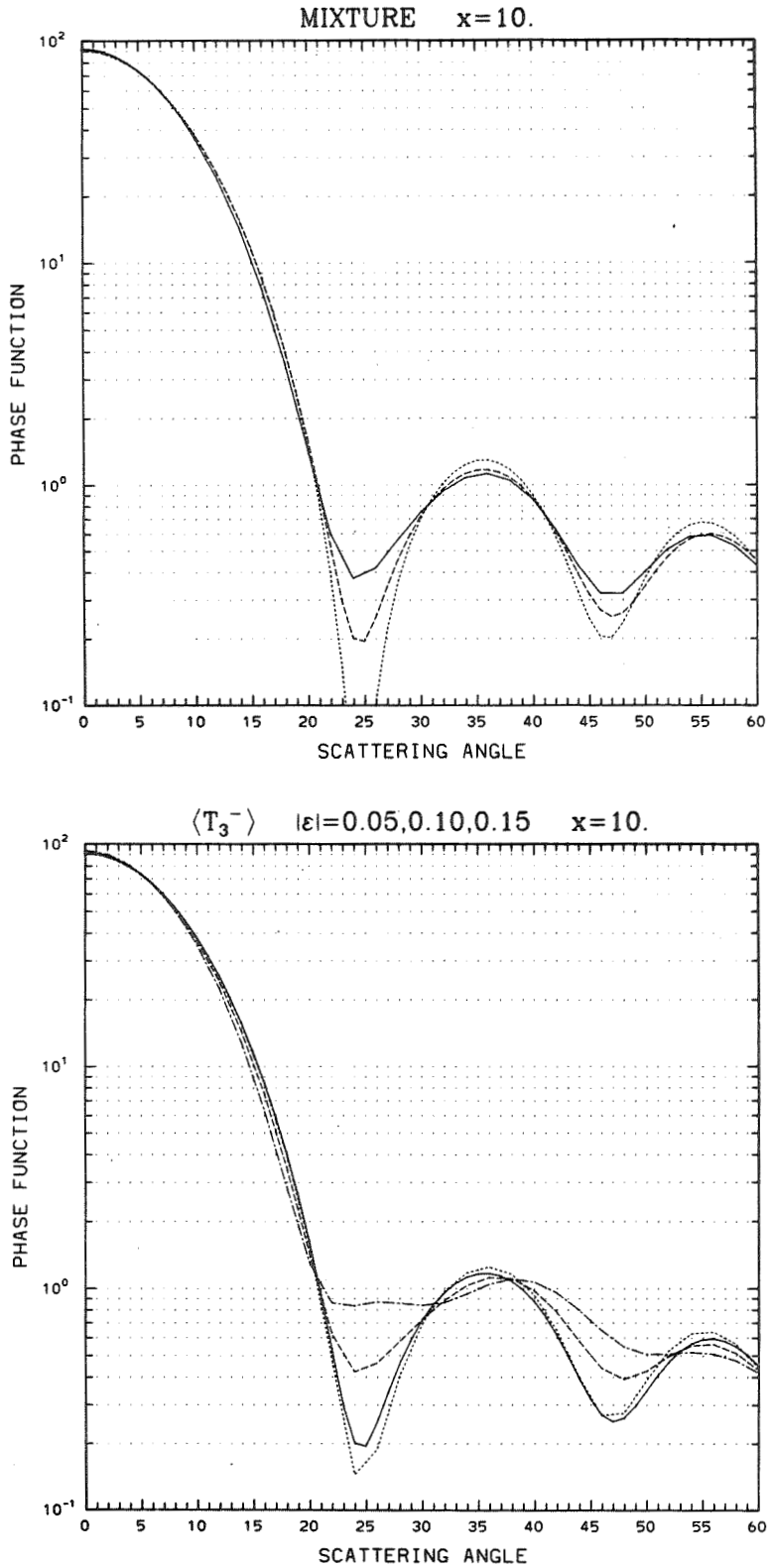

Figure 11 (Continued)

C-2

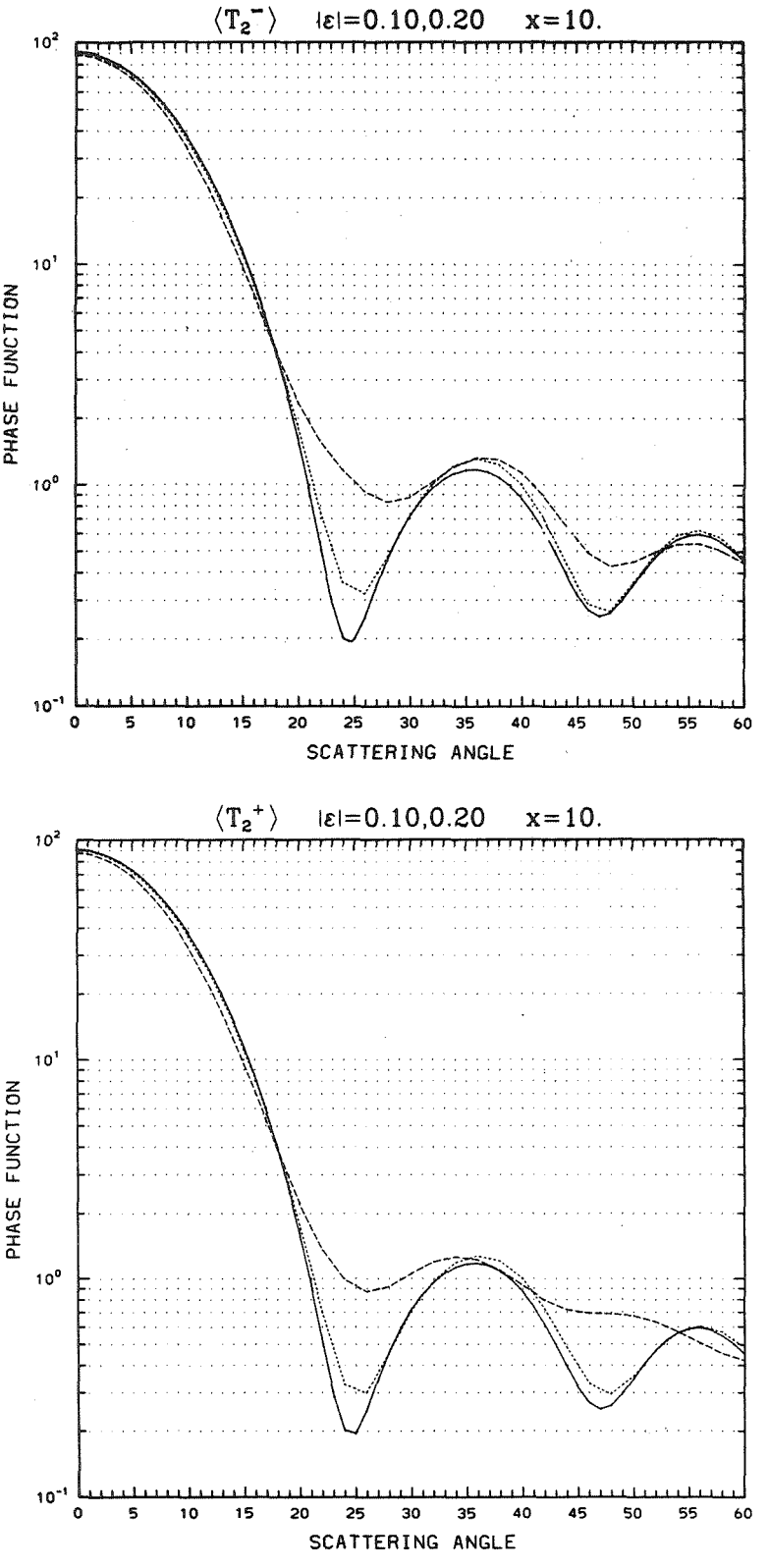

Figure 11 (Continued)

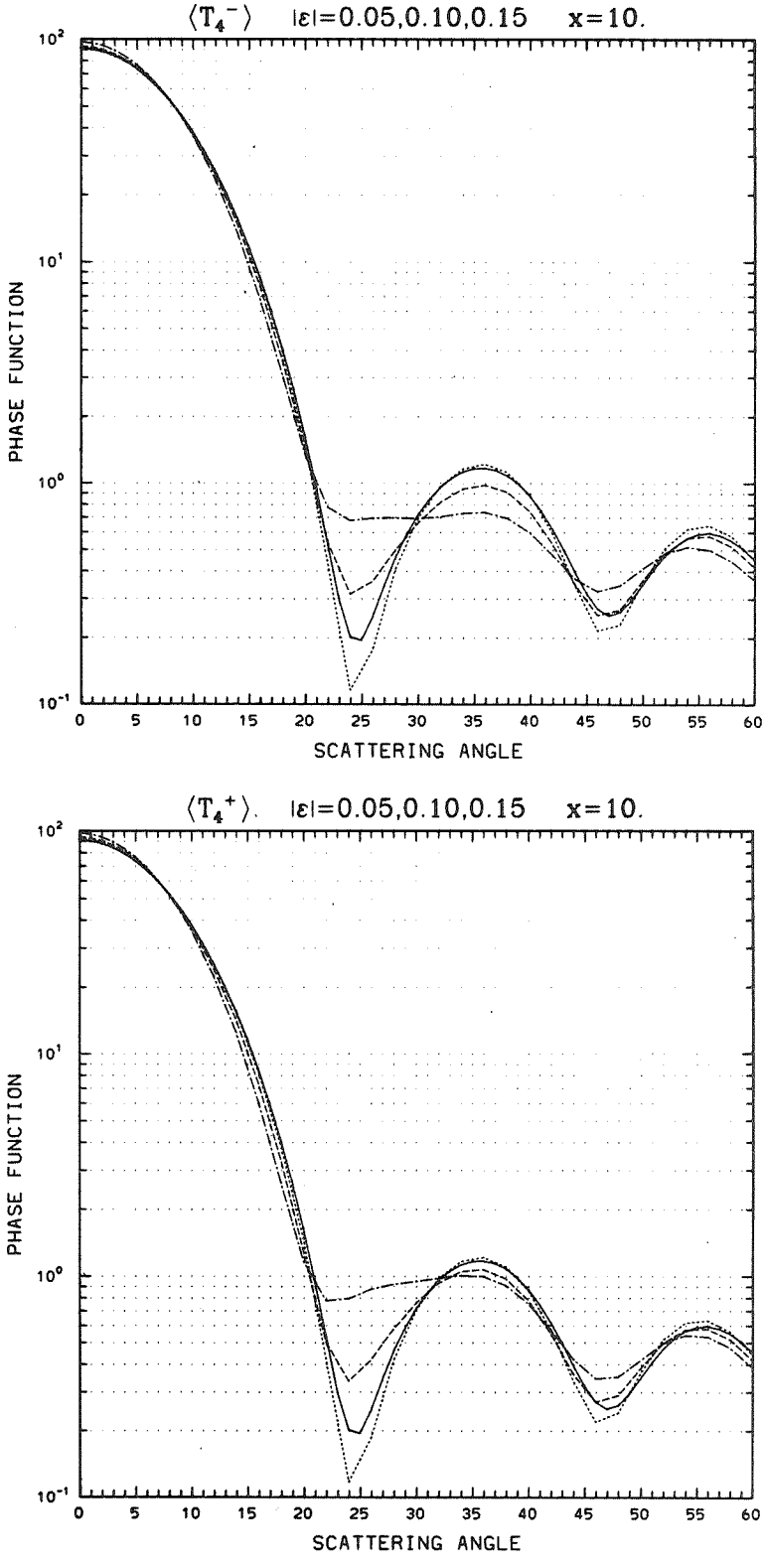

Figure 11 (Continued)

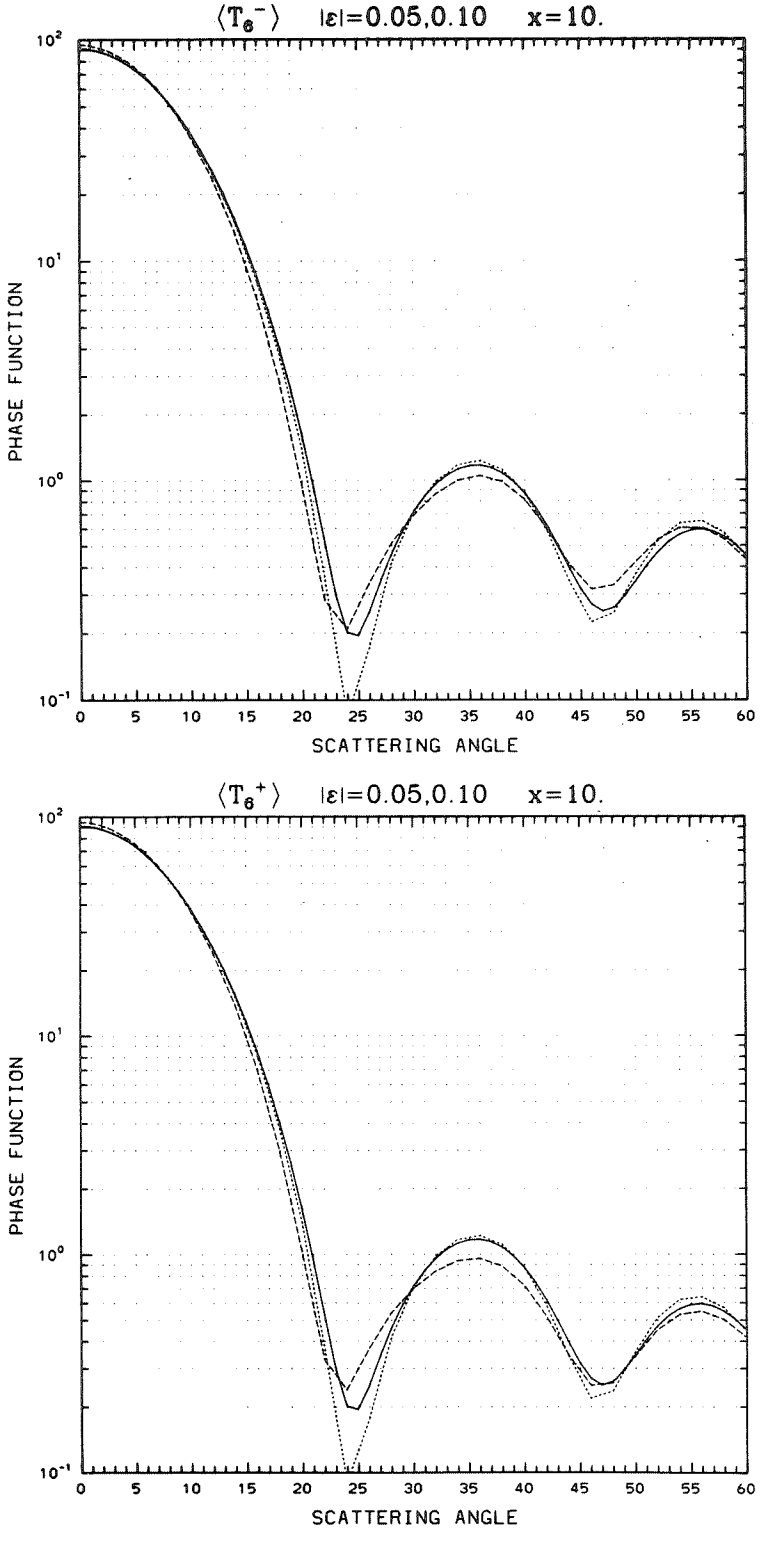

Figure 11 (Continued)

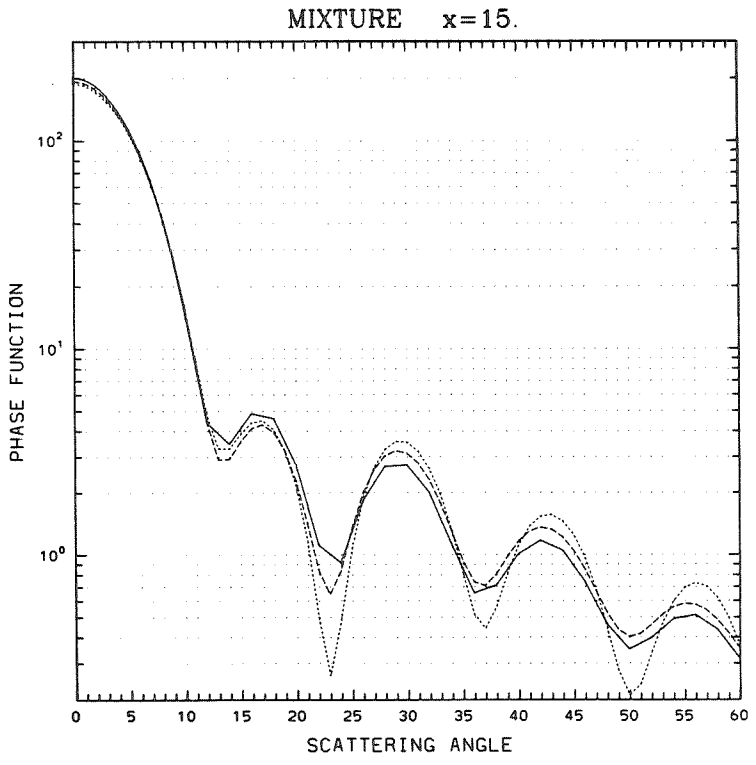

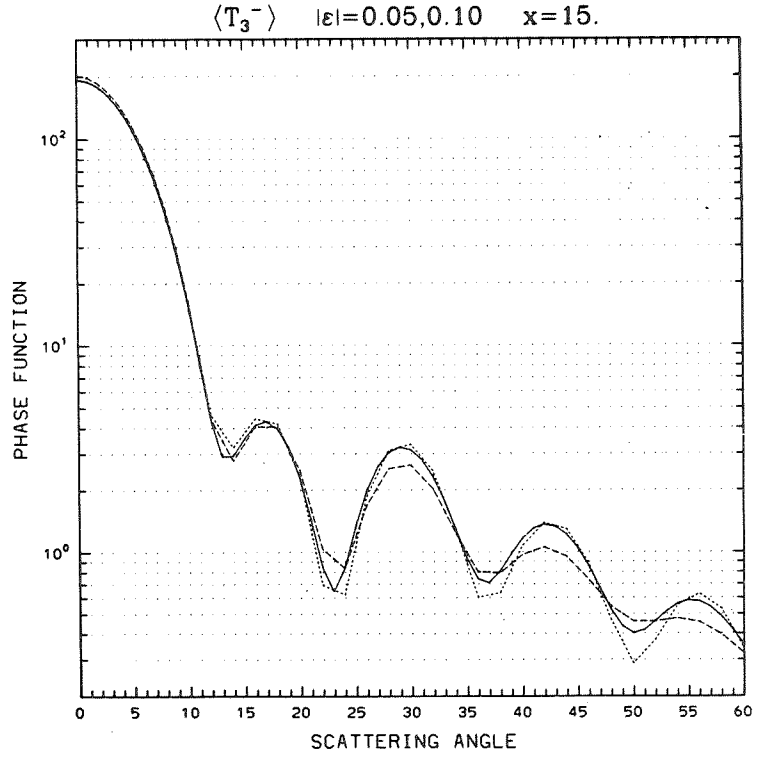

Figure 11 (Continued)

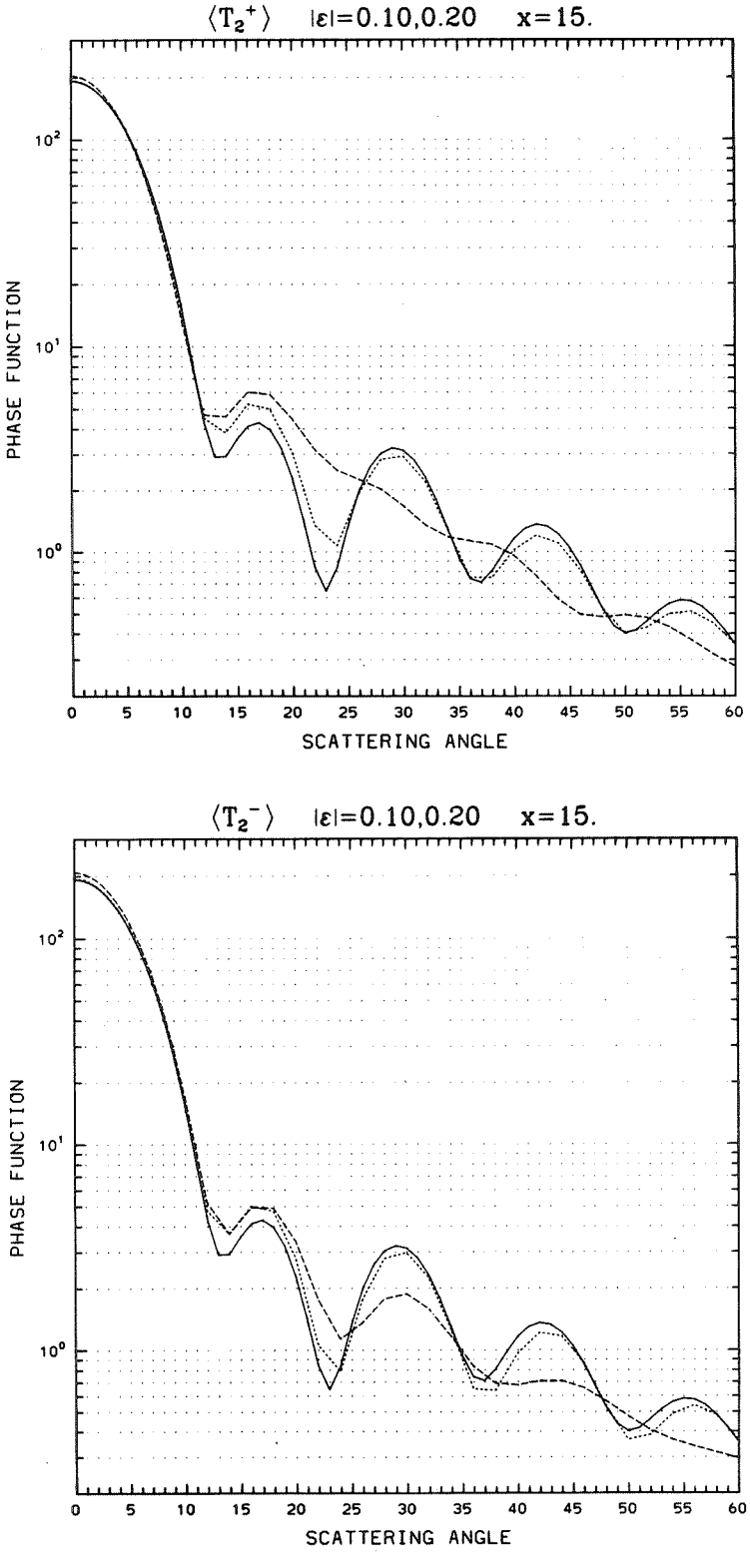

Figure 11 (Continued)

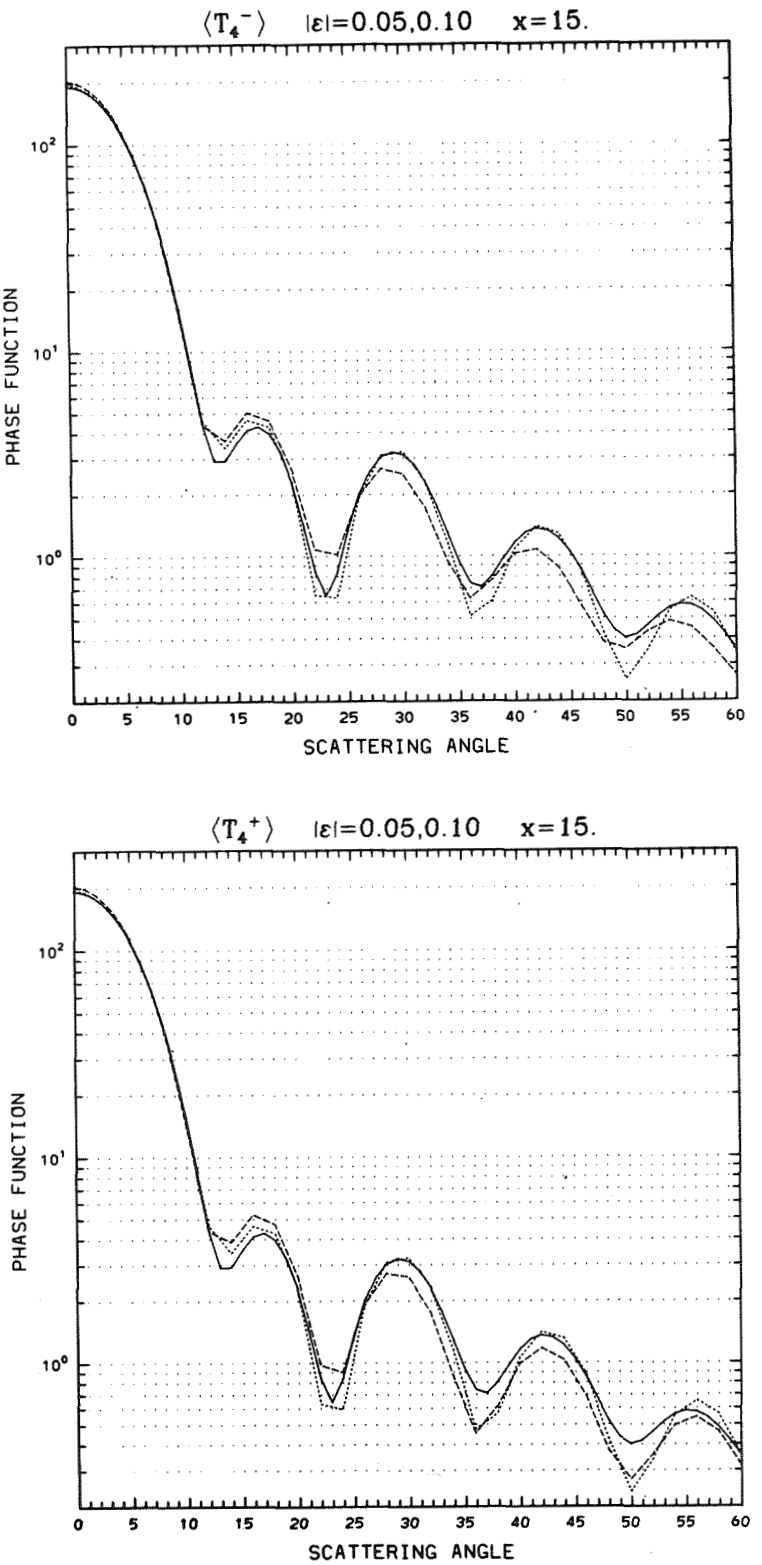

Figure 11 (Continued)

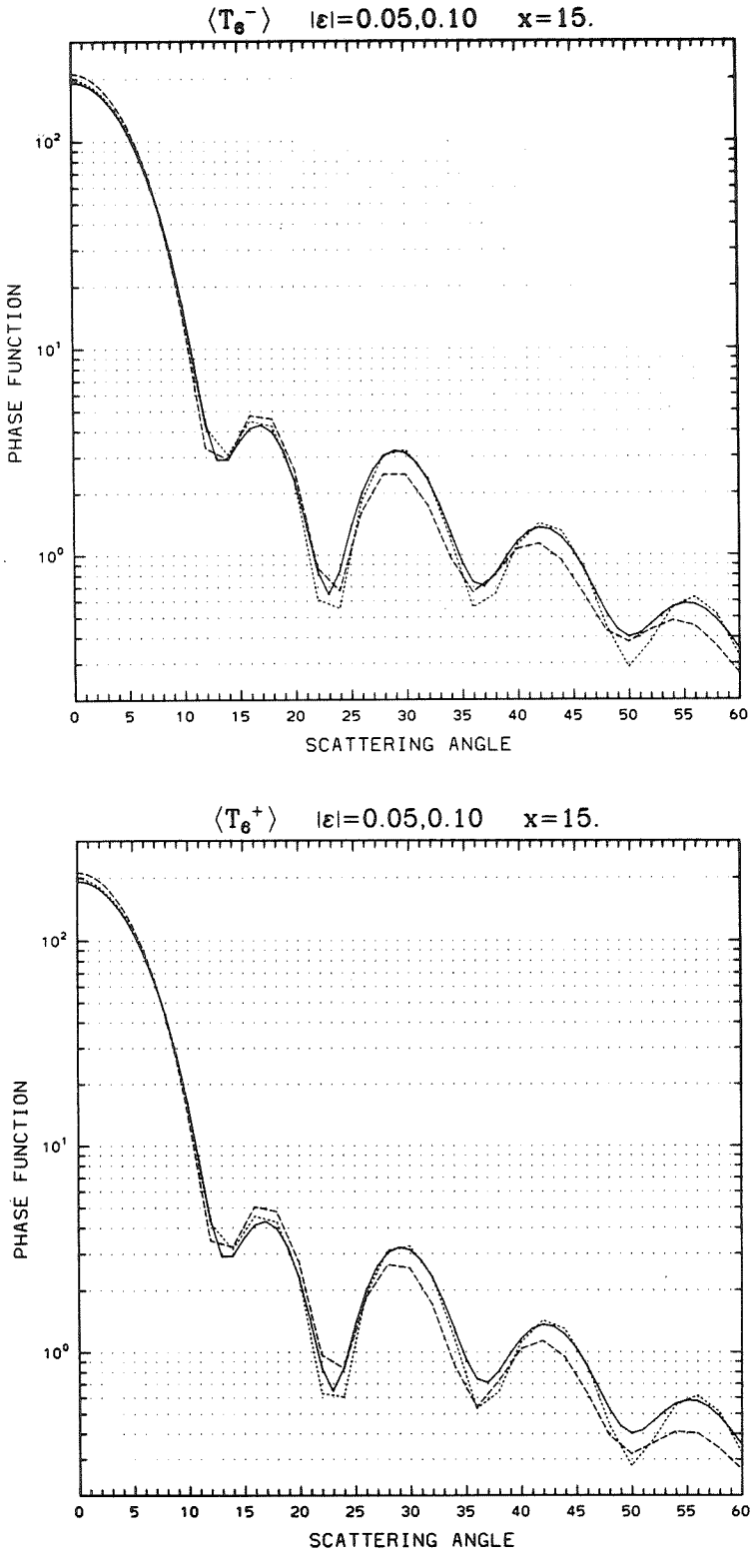

Figure 11 (Continued)

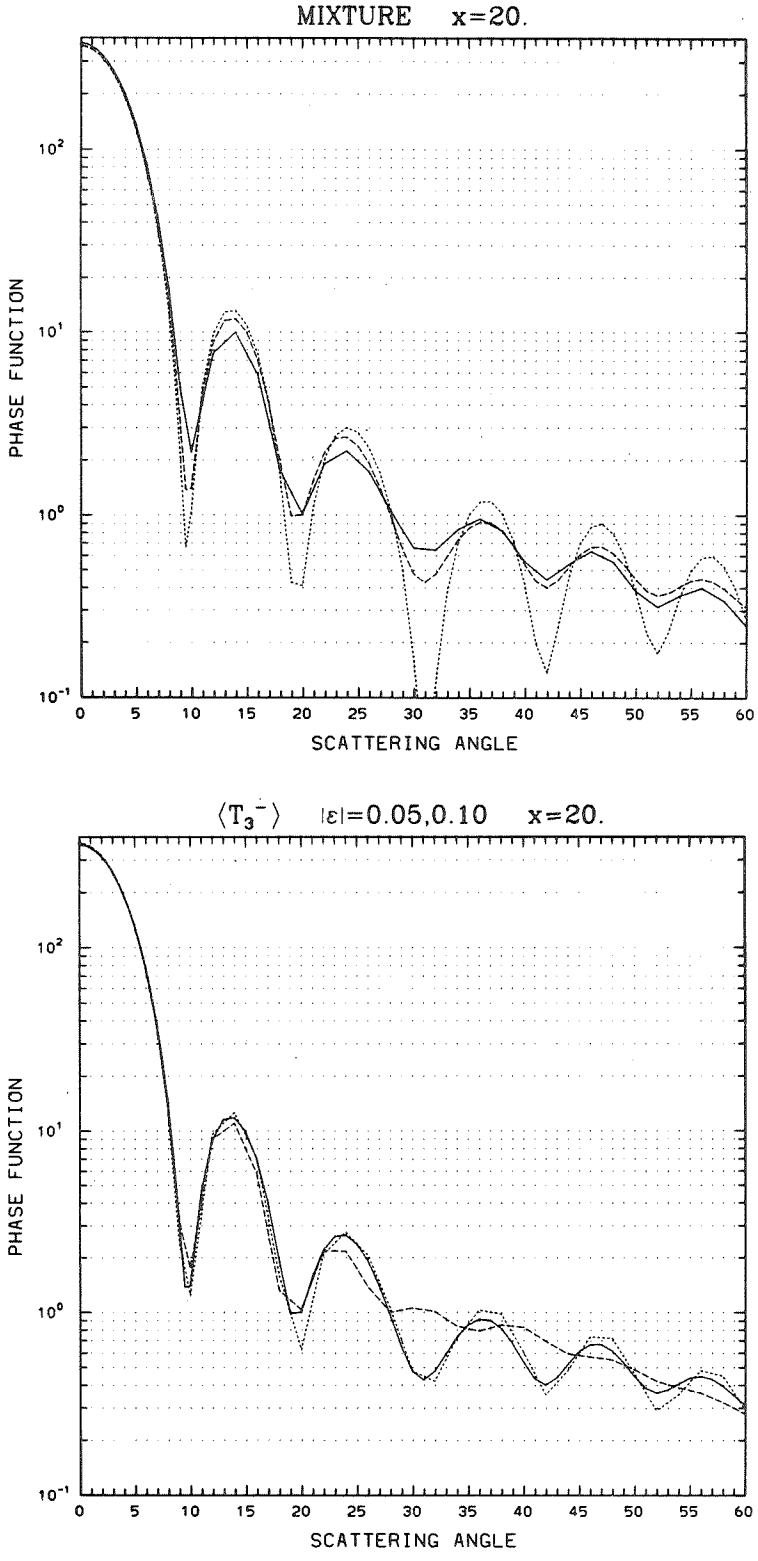

Figure 11 (Continued)

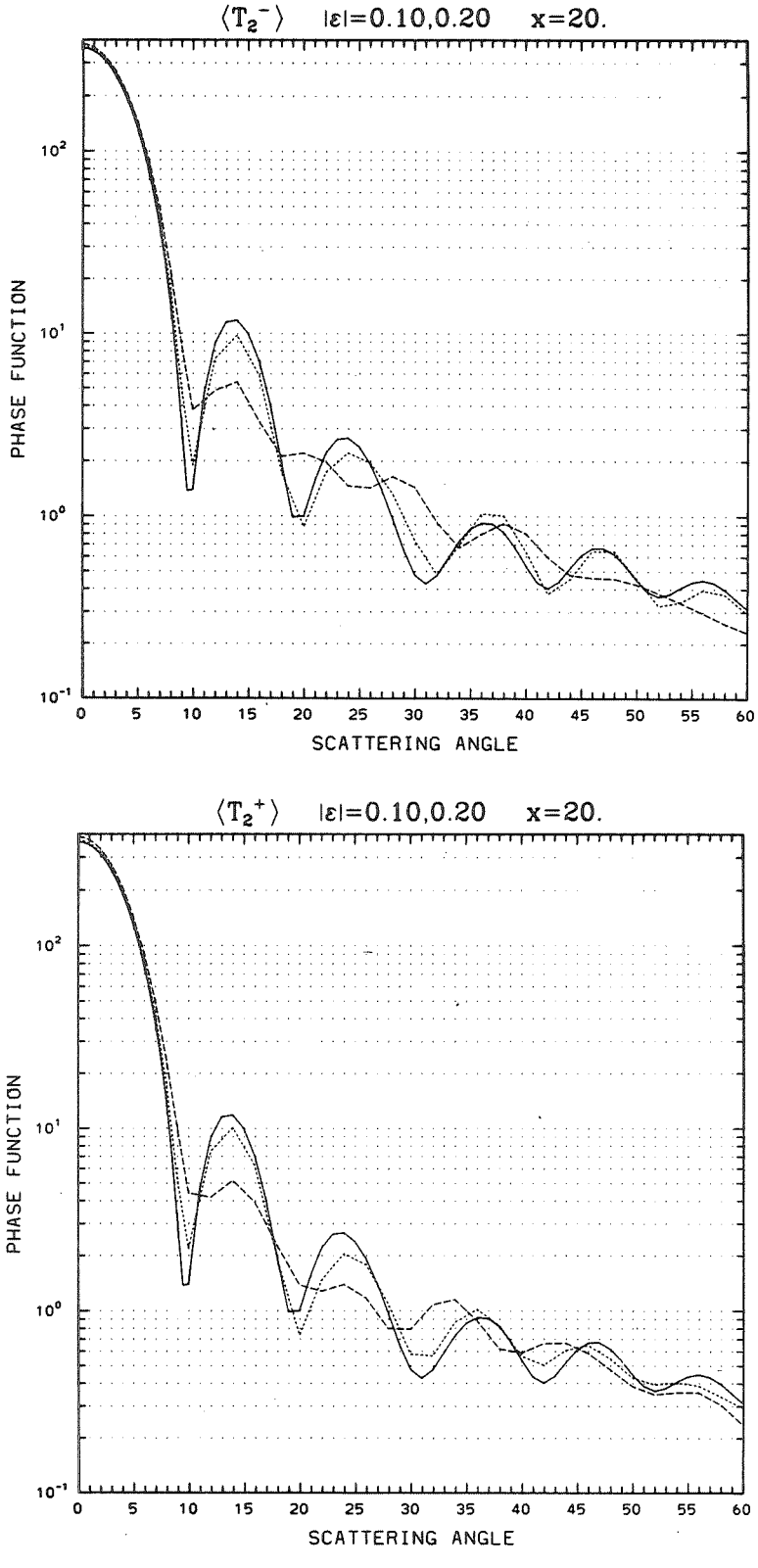

Figure 11 (Continued)

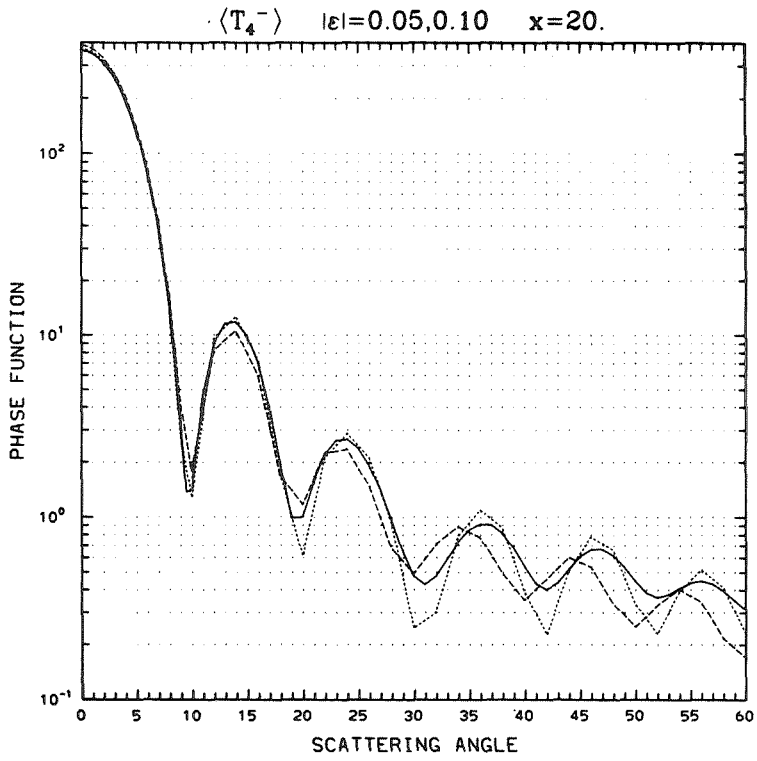

Figure 11 (Continued)

REFERENCES

Asano, S. and G. Yamamoto, 1975: Light scattering by a spheroidal particle, Appl. Opt. 14, 29–49.

Asano, S., 1980: Light scattering by randomly oriented spheroidal particles, Appl. Opt. 19, 962–974.

Barber, P., 1973: "Differential scattering of electromagnetic waves by homogeneous isotropic dielectric bodies", Ph.D. Thesis, UCLA, Los Angeles, Calif. (available from University Microfilms, Ann Arbor, Mich.)

Barber, P., 1977: Resonance electromagnetic absorption by nonspherical dielectric objects, IEEE Transac. Microwave Theory & Tech. MTT-25, 373–381.

Barber, P. and C. Yeh, 1975: Scattering of electromagnetic waves by arbitrarily shaped dielectric bodies, Appl. Opt. 14, 2864–2872.

Bowman, J., Senior, T. and P. Uslenghi, eds., 1969: Electromagnetic and Acoustic Scattering By Simple Shapes, American Elsevier, New York.

Chylek, P., V. Ramaswamy and W. Wiscombe, 1982: Note on "The scattering of radiation by moderately nonspherical particles", J. Atmos. Sci. 39, 1886–1889.

Collis, R. and P. Russell, 1976: Lidar measurement of particles and gases by elastic backscattering and differential absorption, in Laser Monitoring of the Atmosphere, E. Hinkley, ed., Springer-Verlag, New York, pp. 71–151.

Dave, J., 1969: Effect of coarseness of the integration increment on the calculation of the radiation scattered by polydispersed aerosols, Appl. Opt. 8, 1161–1167.

Davis, P. and P. Rabinowitz, 1975: Methods of Numerical Integration, Academic Press, New York, 258 pp.

Gerber, H., 1979: Absorption of 632.8 nm radiation by maritime aerosols near Europe, J. Atmos. Sci. 36, 2502–2506.

Joseph, J., W. Wiscombe and J. Weinman, 1976: The delta-Eddington approximation for radiative flux transfer, J. Atmos. Sci. 33, 2452–2459.

Lentz, W., 1975: Generating Bessel functions in Mie scattering calculations using continued fractions, Appl. Opt. 15, 668–671.

Millar, R., 1969: Rayleigh hypothesis in scattering problems, Elec. Lett. 5, 416–418.

Millar, R., 1973: The Rayleigh hypothesis and a related least-squares solution to scattering problems for periodic surfaces and other scatterers, Radio Sci. 8, 785–796.

Morse, P. and H. Feshbach, 1953: Methods of Theoretical Physics, McGraw-Hill, New York.

Mugnai, A. and W. Wiscombe, 1980: Scattering of radiation by moderately non-spherical particles, J. Atmos. Sci. 37, 1291–1307.

Nussenzveig, H. and W. Wiscombe, 1980: Forward optical glory, Opt. Lett. 5, 455–457.

Patterson, T., 1973: Algorithm for automatic numerical integration over a finite interval, Commun. ACM 16, 694–699.

Pollack, J. and J. Cuzzi, 1980: Scattering by nonspherical particles of size comparable to a wavelength: a new semi-empirical theory and its application to tropospheric aerosols, J. Atmos. Sci. 37, 868–881.

Pruppacher, H. and R. Pitter, 1971: Calculations and measurements of the shape of deformed raindrops, J. Atmos. Sci. 28, 86–94.

Ross, W., 1972: Computation of Bessel functions in light scattering studies, Appl. Opt. 11, 1919–1923.

Schelkunoff, S., 1943: Electromagnetic Waves, van Nostrand, New York.

Schuerman, D., ed., 1980: Light Scattering by Irregularly Shaped Particles, Plenum Press, New York.

Schuerman, D., R. Wang, B. Gustafson and R. Schaefer, 1981: Systematic studies of light scattering. 1: Particle shape, Appl. Opt. 20, 4039–4050.

Shipley, S. and J. Weinman, 1979: A numerical study of scattering by large dielectric spheres, J. Opt. Soc. Amer. 68, 130–134.

Van de Hulst, H., 1981: Light Scattering by Small Particles, Dover, New York.

Waterman, P., 1965: Matrix formulation of electromagnetic scattering, Proc. IEEE 53, 805–812.

Waterman, P., 1971: Symmetry, unitarity, and geometry in electromagnetic scattering, Phys. Rev. D3, 825–839.

Wiscombe, W., 1979: Mie Scattering Calculations: Improvements in Technique and Fast, Vector-Speed Computer Codes, NCAR Technical Note TN-140+STR, National Center for Atmospheric Research, Boulder, Colorado.

Wiscombe, W., 1980: Improved Mie scattering algorithms, Appl. Opt. 19, 1505–1509.

Wiscombe, W. and A. Mugnai, 1980: Exact calculations of scattering from moderately-nonspherical Chebyshev particles: comparisons with equivalent spheres, in Light Scattering by Irregularly Shaped Particles, D. Schuerman, ed., Plenum Press, New York, pp. 141–152.

Zerull, R., 1976: Scattering measurements of dielectric and absorbing nonspherical particles, Beitr. Phys. Atmos. 49, 166–188.

Zerull, R., Giese, R. and K. Weiss, 1977: Scattering functions of nonspherical dielectric and absorbing particles vs. Mie theory, Appl. Opt. 16, 777–778.

APPENDIX A: REVIEW OF NONSPHERICAL SCATTERING

There is barely a field of science or engineering that does not have some interest in scattering of radiation. In many of these fields, the problem can be separated into single scattering by individual objects, followed by multiple scattering among them. But rarely do scattering objects have those ideal shapes — sphere, spheroid, circular cylinder, and so forth — that allow an 'exact' solution of Maxwell's Equations in infinite series of eigenfunctions (Morse and Feshbach, 1953, pp. 492–523).

Instead, the problem of scattering by rather nasty-looking shapes constantly presents itself. Mostly, the effect of shape is ignored; as van de Hulst (1981) says, "the formulae for spherical particles are used in 95% of all applications." Assuming sphericity is certainly the path of least resistance; well-documented computer algorithms for spherical ('Mie') scattering are available (Wiscombe, 1979, 1980) and have been available since Dave produced the first ones in 1968. Circular cylinder and spheroidal algorithms are also available, although less widely used.

But the assumption of sphericity is rarely made after first studying the effect of nonsphericity, then discounting it. Instead, it is almost invariably made *a priori*. Hence, there is an increasing desire to go back and check this assumption, and find out where it breaks down.

The questions one asks about nonspherical scattering depend, of course, on one's research interests. Those who use lidar and radar to sound the atmosphere, for example, want to know only about the intensity and polarization in direct backscatter. Military planners want to block enemy radar and communications with airborne 'chaff', whose shape (among other factors) is adjusted to obtain the maximum extinction cross-section with the minimum amount of material.

Medical researchers want to side-scatter laser light off blood samples and determine the state of the suspended cells. And they want to know the absorption cross-section of human organs in the microwave region. Aerosol specialists want to infer aerosol size distributions from the angular distribution of near-forward-scattered light. Climate theorists want to know how ice crystals in cirrus clouds control the Earth's radiative fluxes.

Each group has a different set of questions it wants answered. We shall begin by reviewing the questions that are being asked about nonspherical scattering, in order to set the stage for the following discussions of experimental and theoretical results.

A.1 CURRENT QUESTIONS

Neglecting quantum and non-linear effects, the questions revolve around one or more of the following list of classical scattering quantities, arranged in order of increasing complexity:

extinction cross-section

scattering cross-section

absorption cross-section

single-scattering albedo

radiation pressure cross-section

asymmetry factor

unpolarized scattered intensity at any angle from the direction of the incident radiation

unpolarized phase function

Legendre moments of unpolarized phase function

polarized scattered intensities, parallel and perpendicular to the plane of scattering (the plane of the incident and scattered beams)

Stokes parameters

Mueller matrix

Legendre moments of Mueller matrix elements

To add to this list, there are different possible states of the incident radiation: plane wave, spherical wave, finite beam, and so forth. And while the above quantities all traditionally refer to the 'far-field' (far enough from the particle that radial components of the scattered field can be neglected), there are also important problems of near-field scattering as well — for example in paint or snow.

The orientation of the particle is another complexifying factor. Some particles are simply in fixed orientations, as in microwave-analogue experiments. Others are partially randomly oriented, as ice needles in a cirrus cloud, or falling raindrops. Most are completely randomly oriented, as aerosol particles.

Generally, as one moves down the above list, the effect of nonsphericity may be expected to become more and more important. Those who are interested only in cross-sections may be justified in ignoring nonsphericity in 95% of the cases. On the other hand, those who need the lower right-hand 2x2 sub-matrix of the Mueller matrix may find it almost impossible to ignore nonsphericity. Those whose problem areas lie in between, are in a grey area where they may or may not ignore it, depending on the size, deviation from sphericity, and refractive index of their scattering objects.

Refractive index plays a particularly important role. When the real index differs significantly from unity, and the imaginary index is nearly zero, nonsphericity exerts its maximum effect. On the other hand, when real index is near unity (as for a bacterium suspended in water), or the imaginary index is large (as for a carbon particle), nonsphericity can often be safely neglected.

Questions of nonsphericity may also be embedded in a larger context: for example, multiple scattering, or size-averaging. Size-averaging and shape-averaging wash out the fine details of nonspherical scattering, making the ensemble (we assume) look more like a collection of spheres. And the greater the extent of multiple scattering, the less the fine details of the phase function matter; only the cross-sections and the first few Legendre moments play a role. In such settings, nonsphericity may be more or less important, depending on the width of the size distribution and the total optical thickness of the scattering medium.

Looking at the list of scattering quantities above, and the variety of complexifying factors, it is clear that a program of research in nonspherical scattering must be carefully focussed to address very specific questions. Otherwise, it risks being swamped by the sheer number of possible variables, and the variety of parameters which can influence those variables. Up to the present, the foci have been:

- Can the nonspherical particle be replaced by an 'equivalent sphere'? If so, which equivalent sphere (equal-volume, equal-area, . . .) is best?
- Can we make simple, empirical adjustments to Mie theory to mimic nonspherical scattering?
- When Mie theory just won't work, can we use either an exact solution for cylinders or spheroids, or a small- or large-particle approximation?
- Can we discern general features of nonspherical scattering just by looking at a few canonical shapes (in the lab or theoretically)?
- What impact does nonsphericity have on our remote sensing capabilities, ranging from interstellar dust effects on astronomical observations to ice particle effects on radar?

The general tenor of the questions in nonspherical scattering is therefore somewhat as follows: What is the least amount of shape information we need to know? Can we just make simple modifications to existing theories to get what we want? For the fact of the matter is, few people outside of electrical engineering (where unusual antenna shapes are routinely studied) want to know the exact scattering from a doughnut or a dodecahedron in fixed orientation. They just want to know the general effect of nonsphericity, shorn of its details. In what follows, this is the tack we shall take in describing experiments and theoretical results.

A.2 MEASUREMENTS

We will survey only a selection of measurements specifically aimed at studying nonsphericity. There are a large number of instruments which routinely measure the scattering from nonspherical particles. Yet these are of no use for our purposes, because they all make simple empirical adjustments to account for nonsphericity (if they account for it at all). Thus, their goal is not to study nonsphericity, but to get rid of it, like an unwelcome dinner guest.

Traditionally, the measurements have tended to fall into two categories:

- visible light scattering from micron-sized particles
- microwave scattering by centimeter-sized objects

In the future, much more of the electromagnetic spectrum will be available, using tuneable lasers and cryogenically cooled detectors; but until recently, experimenters were strongly constrained by the relatively primitive state of source and detector technology, and by the lack of windows in the spectrum of the Earth's atmosphere.

Visible light scattering experiments involve relatively simple and cheap instrumentation, and have just as frequently been done in the field as in the laboratory. Microwave scattering experiments, by contrast, require expensive instrumentation and large laboratories, and have as a consequence been undertaken by only a few groups.

Microwave

The "microwave-analogue method" was pioneered by Greenberg (1960, 1961), with the application of interstellar dust in mind. The idea was, to manufacture centimeter-sized scattering objects with desired shapes and refractive indices. Then, in a large, anechoic chamber, perhaps 100 feet across, one directed a microwave beam at the object and measured the scattering at all angles. By special techniques, even the extinction cross-section could be measured; and for independent confirmation, one could place temperature sensors in the object and measure the Joule heating directly (to get absorption cross-section).

The 'analogue' part of the method meant simply that the results could be extrapolated to smaller or larger sized scatterers, keeping the ratio size/wavelength fixed, in much the same way as aerodynamicists extrapolate wind tunnel model results to full-sized aircraft.

Very few published results came out of Greenberg's effort. Greenberg, et. al. (1971) presented a few measurements of extinction cross-section for spheroids, while Greenberg (1972) made measurements for stacked cylinder configurations. Wang (1980) has given extinction cross-sections for aggregates of 2, 4, and 8 spheres, as well as stacked cylinders.

Waterman (1965, 1971) measured scattered microwave intensities from hemispherically capped cylinders and cones made of metal, primarily in order to verify his EBCM calculations.

Zerull (1976) and Schuerman, et. al. (1981) have published by far the largest collection of microwave analogue measurements. They measured scattered intensities from roughened spheres, cubes, octahedra, and irregular convex and concave particles, with various effective size parameters up to 20. Comparing to equal-volume spheres, their main conclusions were that:

- for size parameters $x < 6$, agreement is within a factor of two; as x increases beyond 6, differences escalate dramatically

- nonspherical curves have greatly damped oscillations as a function of angle
- agreement is very good in the forward peak (scattering angles 0–30°), with nonspherical particles probably scattering somewhat less than spheres there
- nonspherical particles side-scatter (angles 30–140°) as much as an order of magnitude more
- transparent nonspherical particles backscatter less, and their backscattering exhibits a much milder variation with angle
- backscatter from opaque nonspherical particles shows an increase toward 180°, while the backscattering for spheres shows no such rise

Zerull also found that concave particles tended to scatter more energy at most angles than equal-volume convex particles.

Visible

Visible light measurements have traditionally suffered from an inability to calibrate the instrumentation using particles of known shape, size and refractive index. This problem has been somewhat alleviated of late, however, as monodisperse polystrene latex spheres have been more reliably manufactured (e.g., Bottiger, et. al., 1980). Also, the 'vibrating-orifice aerosol generator' can generate quasi-monodispersions of various water-soluble aerosols (Pinnick, et. al., 1976; Coletti, 1984).

There are many more visible than microwave measurements, reflecting the relative simplicity and compactness of sources and detectors at visible wavelengths; but these measurements are almost exclusively of scattered intensity in the 10–170 degree angular range. The arrangement of source and detector precludes measurements near the forward or backward directions, although Ashkin and Dziedzic (1980, 1981), in their 'optical levitation' technique involving suspension of particles by laser light pressure alone, have obtained direct backscatter measurements.

Lacking especially the important 0–10 degree scattering, it is difficult to obtain an accurate estimate of scattering cross-section (and hence of phase function) from integrating the scattered intensities over angle. As a result, there has been a tendency to normalize experimental results to the equal-volume sphere phase function at 10°, which may introduce biases into some of the conclusions drawn. Recently, however, Coletti (1984) has used Fraunhofer diffraction theory to extrapolate his results into 0–10°, which goes far toward correcting this problem.

Extinction cross-section measurements have suffered from the classic problem that a detector with a finite aperture picks up some of the diffracted light. Depending on how much of this light is detected, the extinction can be mis-estimated by as much as a factor of two. Careful correction for the diffraction can eliminate this effect if the particle projected area is known, but too often this is not the case. And with large errors in both extinction and scattering cross-section, almost nothing can be said about absorption cross-section, and hence the single-scattering albedo.

A number of early results on nonspherical scattering were reported at the First International Conference on Electromagnetic Scattering in 1963. Hodkinson (1963) measured extinction and forward-hemisphere scattering for quartz, diamond, flint, and coal dust particles of sizes 1 to 6 microns, in aqueous suspension. The curve of extinction as a function of size parameter x (= 10–50) did not display the large oscillations found in its Mie theory counterpart; instead, it just rose monotonically to an asymptote. Fraunhofer diffraction plus geometrical optics for a sphere gave a fair fit to the results for 0–60°, but not for 60–90°.

Napper and Ottewill (1963) measured scattered intensities from transparent cubes and octahedra of size 0.5–0.7 microns. The octahedral and equal-volume Mie results agreed well in 60–120 degrees, but the cubes side-scattered much more in both polarizations.

Huffman and Thursby (1969) measured scattered intensities from irregular ice crystals, as well as hexagonal plates and columns, in the angular range 10–150°. They showed that if they picked a size of sphere with equal scattering at 10 degrees, that sphere scattered considerably less to the side (around 90°).

In a well-done classic study, Holland and Gagne (1970) measured the Stokes parameters of light scattered from 0.1 to 1 micron plate-like, randomly oriented quartz crystals. They argue for comparing to equal-projected-area rather than equal-volume spheres, which gives good agreement out to 40° but underestimates the nonspherical side-scattering from there to 140 degrees or so. Past 140°, the situation was reversed: Mie theory was more than a factor of 3 higher. Waggoner, et. al. (1972) also found that nonsphericity depressed backscattering, although it must be emphasized that neither study could reach 180°.

Proctor and Harris (1974) and Proctor and Barker (1974) measured extinction for numerous size distributions (spanning 0.1 to 50 microns) of quartz and diamond dust suspended in water. When they plotted extinction vs. the phase shift parameter

$$\rho = 2\,x\,(\tilde{m} - 1)$$

they found no oscillations, unlike Mie theory; only the first main peak showed up.

Chylek, et. al. (1976) measured scattered intensities for transparent salt particles of size 0.04 to 2 microns. They showed a result which seemed contrary to everyone else's, namely less side-scattering for non-spheres than for spheres. However, it seems that they used polarized incident light, whereas the previous measurements used unpolarized light. In fact, for one of the two incident polarizations in Holland and Gagne's experiment, a similar result to Chylek, et. al. was obtained. Pinnick, et. al. (1976) continued this work, and found that either assuming voids in the particles, or averaging over sizes in Mie theory, improved agreement with spherical results.

Perry, et. al. (1978) made one of the rare studies of the complete Mueller matrix. They used cubic salt and rounded ammonium sulfate particles of size 0.1 to 2 microns. They found that Mie theory could fit results for the rounded particles all the way up to x = 12, but for the cubes only up to x = 3. The nonspherical particles always had higher side-scatter, and lower backscatter, than equal-volume spheres.

Bottiger, et. al. (1980) also measured the Mueller matrix. Their scatterers were not 'natural' aerosol particles, but rather aggregates of 2, 3, or 4 polystyrene latex spheres, levitated electrostatically. They thus achieved a much greater degree of shape control than in previous experiments. They found that the strong angular oscillations in spherical Mueller matrix elements tend to be washed out — the more so, the more spheres were in the nonspherical aggregate.

Saunders (1980) suspended 50 micron salt crystals on spider webs and measured scattered intensity at 180° as they hydrated. He also subjected the hydrating particle to an electric field, causing distortions undetectable by microscope yet sufficient to cause large variations in backscattered intensity. This proved that direct backscatter is very sensitive to even slight nonsphericity.

Coletti (1984) has scattered laser light from quasi-monodispersions of transparent salt particles and absorbing dye particles. He finds almost a complete washing-out of the angular structure in Mie theory, with the only remnant being the first side-peak in the diffraction region. The difference between the scattering for two orthogonal incident polarizations is also much less than in Mie theory, and sometimes vanishes entirely.

Other sources of experimental information include Berry (1962), Donn and Powell (1963), Kirmaci and Ward (1979), Sassen and Liou (1979), and the book edited by Schuerman (1980).

Summary

This is but a limited survey of nonspherical scattering experiments, and one oriented toward atmospheric science, but it should be sufficient to give a flavor of the results.

All the measurements to date show the following tendencies, relative to Mie theory:

(i) damping of the oscillations vs. angle and vs. size parameter

(ii) more side-scattering (60–120°), for unpolarized incident light

(iii) less backscattering (140–180°) unless the particle is opaque

(iv) nearly equal forward scattering (0–50°)

(v) rapidly worsening agreement as size parameter increases past $x = 3$ to 5

(vi) less difference between scattering resulting from the two possible orthogonal polarizations of the incident radiation

A.3 THEORIES — EXACT OR NUMERICAL

In the past 25 years, numerical techniques for scattering and absorption by variously-shaped objects have proliferated like weeds. This is due to the relatively few exact solutions of Maxwell's Equations for the 'simplest-case' scattering problem (an incident plane wave). The exact solution for a circular

cylinder in perpendicular incidence was given by Rayleigh in 1888, and extended to oblique incidence by Wait in 1955 (see also Liou, 1972; Cohen and Alpert, 1979, 1980). Lorenz in the 1890's, and independently Mie in 1908, and Debye in 1909, gave the solution for a sphere. Yeh (1965) gave a partial solution for elliptic cylinders. Asano and Yamamoto (1975), in a much-acclaimed paper, gave the solution for a spheroid.

It is unlikely that this arsenal will be enlarged much in the future. The reason is simple: the solution even for a spheroid is already so complex that it offers very little advantage over a good numerical solution (except to furnish an independent check). The spheroidal solution suffers from numerical ill-conditioning, preventing its use above size parameter $x = 30$ or so (Asano, 1979); and in random orientation, it gobbles up monstrous amounts of computer time (Asano, 1980). Thus, even for this simplest of all nonspherical shapes, the exact solution behaves in many ways like a numerical solution.

The better numerical solutions, in turn, behave in many ways like an 'exact' solution — for example, by expanding the solution in a set of orthogonal eigenfunctions. This is all symptomatic, we believe, of a general crumbling of the formerly rigid barriers between 'exact' and 'numerical' solutions.

For those who wish to pursue the question of 'exact' solutions in more detail, we offer a few more remarks. The problem boils down to solving the "vector Helmholtz equation" (Morse and Feshbach, 1953, Ch. 13) for the electric field. This is done by expanding the electric field in an infinite series of eigenfunctions in one of the 11 coordinate systems in which the vector Helmholtz equation is separable. (These series are double series in general; only for the sphere and circular cylinder do they degenerate to single series.) The eigenfunctions used inside the scatterer are different from those used outside of it, because the 'inside' expansion must be finite at the origin, while the 'outside' expansion must produce outgoing waves at infinity.

Then, the usual Maxwell boundary condition (continuity of the tangential component of the electric field) is applied on the surface of the scatterer; the inside and outside expansions must be 'matched up' there. This is where all the difficulties arise. In every case but the few which have already been solved, the boundary condition leads to a set of equations which cannot be solved analytically. (If boundary conditions were not the major hang-up, scattering from a cube, involving only simple Cartesian coordinates, would have been solved long ago. Instead, it remains an unsolved problem.)

Those who wish to see exact solutions for metallic scatterers in various unusual coordinate systems may consult the book by Bowman, et. al. (1969), where the main thrust is antenna design. Kouyoumjian (1965) gives the original references for solutions for metallic cones, disks, strips, and parabolic cylinders. Of greater interest, perhaps, is the solution by Borghese, et. al. (1979) for an arbitrary cluster of spheres; indeed, it seems to this author that sphere clusters would be excellent archetypes for general nonspherical particles. Apparently, however, the solution of Borghese et. al. is nightmarish to put into practice.

Returning now to numerical solutions, we observe that they are primarily used in the range 1 to 10 of size parameter (the so-called 'resonance region'). Below 1, small-particle approximations are useful; above 10, large-particle approximations. Very few numerical methods have been applied for size

parameters above 15 or so, partly because, in general, the computational demands escalate as some high power of size parameter.

Fortunately, the seemingly innumerable numerical techniques fall into two rather broad classes: differential equation (including finite element) methods, and integral equation methods. Each 'new' technique is usually only a minor variation on a familiar theme. It is these themes which we shall attempt to highlight here. But first we shall deal with a method that defies classification.

Purcell-Pennypacker: aggregates of dipoles

Purcell and Pennypacker (1977) suggested replacing a scatterer by a cubic array of point dipoles spaced no farther than (wavelength/4 π) apart. Each dipole has a polarizability such that the correct bulk refractive index is predicted by the Clausius–Mosotti relation. Exact account is taken of all mutual dipole–dipole interactions, leading to a set of 6N linear equations for N dipoles.

In this method, the surface disappears, and with it all the nastiness associated with surface boundary conditions. That is the beauty of the method. It is elegant in its simplicity, and therefore has attracted a good deal of attention. Kattawar and Humphreys (1980), for example, have applied the method to two nearby spheres.

Purcell and Pennypacker themselves considered no more than 100 dipoles. Yung (1978), however, has been able to reformulate the method as a variational principle, enabling him to use the prodigious number of 16,000 dipoles (corresponding to a size parameter of about $x = 6$). Until computer memory and speed become very much larger, $x = 10$ is probably a practical upper limit to this method.

Rayleigh hypothesis

Rayleigh was interested in the scattering of a plane wave from a sinusoidal diffraction grating. Between the peaks and valleys of the grating, there are both upgoing and downgoing waves. Rayleigh made the hypothesis, now associated with his name, that only the upgoing wave eigenfunctions need be considered in the solution. This hypothesis was accepted without question until about 1950, when it became embroiled in controversy (Millar, 1973).

As it applies to scattering by a finite object, this controversy still raged through the 1960's (Bates, 1969; Bates, et. al., 1973; Millar, 1969; Millar and Bates, 1970). Consider a scattering object C with its inscribed (S_{in}) and circumscribed (S_{out}) spheres, as in Fig. A.1. At any point P outside C, but inside S_{out}, there are both incoming and outgoing waves; after all, part of C is outside the sphere passing through P, and thus can radiate inwards towards P . . . .

If we think in terms of rays, of course, this could only happen if C were concave. But, mathematically speaking, the problem exists for all objects, and the solution ought really to be of the form (see Fig. A.1 for region designations):

(Region I) expansion in eigenfunctions regular at the origin

(Region II) expansion in incoming and outgoing eigenfunctions

(Region III) expansion in outgoing eigenfunctions.

For some very simple problems, including Rayleigh's sinusoidal grating, Millar (1973) has actually succeeded in showing the quantitative limits of validity of the Rayleigh hypothesis. If the grating is described by

$$f(z) = a \cos kz$$

where 'z' is height, then the Rayleigh hypothesis fails if $ka > 0.448$, or, loosely speaking, if the waves on the surface become too 'violent'. By naively comparing this case to the case of Chebyshev particles (Eq. 1 of the text), and analogizing z with theta, one might expect the Rayleigh hypothesis to fail also for Chebyshev particles such than $n\epsilon > 0.05$ or so. This is curiously close to the actual limits found on EBCM convergence for size parameters exceeding 5 or so.

Millar shows that a necessary and sufficient condition for the Rayleigh hypothesis to be valid is that the singularities of the Region III expansion all lie in Region I. Thus the hypothesis may be valid with one origin of coordinates, and not with another. Its validity may also change, depending on which eigenfunctions are used in the Region III expansion. And if the scatterer has corners or edges, this almost always causes singularities to occur in Region II, invalidating the Rayleigh hypothesis.

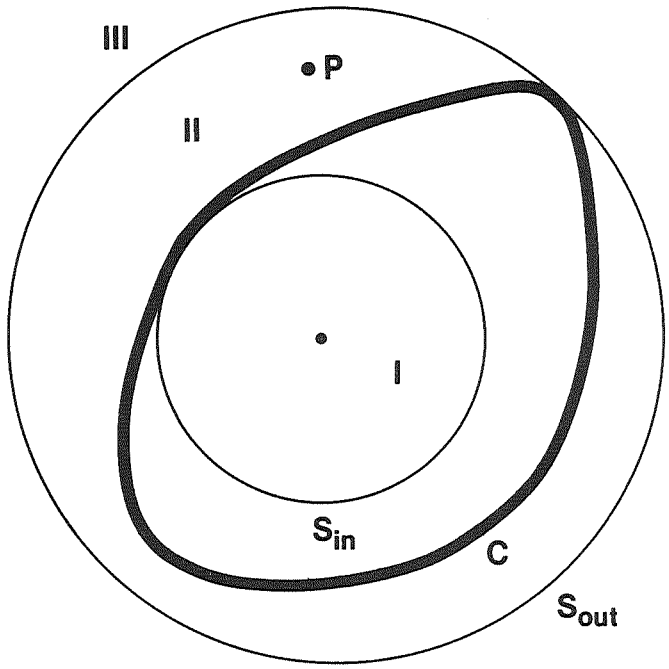

Figure A.1. Cross-section of a general scattering object with surface C, inscribed sphere S_{in}, and circumscribed sphere S_{out}.

But following this gloomy prognosis, Millar offers a way out which seems almost too good to be true. We merely have to abandon our craving for an 'exact' solution, and satisfy the boundary conditions only in the least-squares sense. Then an expansion in any complete set of outgoing eigenfunctions is satisfactory in Region II. It will even converge uniformly in Region III (although the convergence may be slow, if the eigenfunctions chosen are ill-suited to the geometry).

In the various debates over the Rayleigh hypothesis in the literature, the EBCM was always regarded as immune to these difficulties — apparently, because it sidesteps the whole issue of making an expansion of the scattered field in Region II. One is left with an uneasy feeling, however, that the problem has perhaps been papered over rather than resolved.

Differential equation approaches

According to Mei, et. al. (1978):

> "During the last 15 years, computation in electromagnetic scattering has been actively pursued almost entirely in terms of integral equations. . . .this drift to integral equations is very natural — and for good reasons. In integral equations, the computations are limited to the scatterer itself; while in the finite methods they are generally spread over the entire space. In integral equations, the radiation conditions are automatically satisfied, while in the finite methods they require special numerical treatments which are often unsatisfactory. But recent advances . . . have urgently demanded the results of scattering by . . . inhomogeneous bodies. The only practical approach to such problems appears to be direct solution of partial differential equations rather than solution by integral equations, the formulation of which in an inhomogeneous medium is a difficult task."

This explains why methods which proceed directly from the vector Helmholtz equation, without reformulating it as an integral equation, have recently regained some popularity.

Differential-equation methods are invariably simpler in concept, and simpler in execution, than integral-equation methods, and they avoid the singular-kernel problems in those approaches. They tend, however, to consume much more computer time. A well-thought-out-example is the method of Patwari and Davies (1966). They assume an expansion in outgoing-wave eigenfunctions in Region III. Then they carry this solution from S_{out} to C (the scatterer's surface) using a finite-difference form of the vector Helmholtz equation. The expansion coefficients are then determined by boundary conditions at C.

Reilly's (1973) method is an interesting variation. He uses a Galerkin method, and applies boundary conditions on S_{out} rather than on C.

Perhaps the simplest method of all is 'point-matching', reviewed by Richmond (1965). The scattered field is expanded in an N-term series of outgoing-wave eigenfunctions, then the boundary conditions are enforced at N points on C, leading to a set of N linear equations for the expansion coefficients. Point-matching has been used by Greenberg, et. al. (1965), among others, to study nonspherical scattering. However, the validity of point-matching became the subject of a heated debate (Bates, 1967,

1969; Bates, et. al., 1973; Millar and Bates, 1970) connected with the Rayleigh hypothesis. The general feeling nowadays seems to be that it has uncertain convergence, is inaccurate, and uses too much computer time.

There have been efforts to rescue point-matching by generalizing it. In 'least-squares matching', one enforces boundary conditions at $M >> N$ points in a least-squares sense. In 'spectral-component matching' (Millar, 1973), one picks a set of smooth basis functions, multiplies the boundary condition by each of these in turn, and integrates over C. (If the basis functions are delta-functions, this reduces to point-matching.) This can make the Rayleigh hypothesis valid even when it fails for point-matching. Of course, computation is increased considerably, because many surface integrals must be done. Spectral-component and least-squares matching are closely related from a mathematical point of view.

As Mei, et. al. (1978) have noted in the quote above, the necessity to calculate scattering from inhomogeneous objects has breathed new life into differential equation methods. But they have revived mostly in the form of 'finite-element' methods (e.g. Morgan and Mei, 1979; Yeh and Mei, 1980), which Mei et. al. review in detail.

Integral equation methods

Integral equation methods reformulate the vector Helmholtz equation as an integral equation using Green's functions (Morse and Feshbach, 1953, p. 1769 ff.). The boundary conditions are included automatically. Within and/or on the surface of the scatterer C, one solves either for

- the induced current $\mathbf{J}$, or
- the electric field $\mathbf{E}_{in}$.

The scattered field is then found from the vector form of Huyghens' principle or its equivalent.

There are three variants, involving:

(A) volume and surface integrals for either $\mathbf{J}$ or $\mathbf{E}_{in}$ in one vector equation;

(B) surface integral equations only

(1) coupled equations for $\mathbf{J}$ and its spatial derivatives, with singular kernels;

(2) coupled equations for $\mathbf{J}$ alone, with a higher-order singularity than in (1).

The singularities in (B) come from the so-called 'free-space Green's function'. They are the cross that integral equation methods are forced to bear, in return for escaping the boundary condition nightmares of differential equation methods.

Livesay and Chen (1974) do nothing fancy at all. They just calculate $\mathbf{E}_{in}$ by directly evaluating the volume integrals in a type (A) formulation. A second quadrature over $\mathbf{E}_{in}$ then yields the scattered field. They can end up with huge matrices compared to the EBCM, but they do avoid the surface integrals required in the EBCM.

Some methods avoid numerical evaluation of the singular integrals in type (B1) formulations by analytic methods. The EBCM (Waterman, 1965, 1971; Barber and Yeh, 1975; Mugnai and Wiscombe, 1980) uses different spherical harmonic expansions inside and outside the sphere passing through the singularity. Chu and Weil (1976) and Holt, et. al. (1978) evaluate the integrals analytically just in the neighborhood of the singularity. Actually, since the (B1) singularities are integrable in the principal value sense, sophisticated modern quadrature techniques could probably handle them; but no one has tried this.

The singularities in type (B2) formulations are non-integrable. The only approach which has so far been used is the Hadamard finite part idea (Senior and Weil, 1977), although the physical interpretation of this procedure is elusive.

"Moment methods" are a particular variant of integral equation methods (cf. the book by Harrington, 1968, and the review article by Miller and Poggio, 1978). If the integral equation to be solved is written schematically as

$$LF = G$$

where L is a linear operator, then the idea is to expand F in a set of basis functions f_n

$$F = \sum_{n=1}^{N} a_n f_n$$

and then to take M weighted moments of the resulting equation:

$$\sum_{n=1}^{N} a_n \int W_m L(f_n) = \int W_m G$$

Taking $M < N$, one then solves this set of linear equations for the coefficients a-sub-n in the least-squares sense.

Moment methods are frequently applied to 'wire structures', either actual (like antenna arrays), or simulacrams of real objects.

In spite of the revival of differential equation methods for inhomogeneous scatterers, it is worth noting that Wang and Barber (1979) have extended the EBCM to such objects (see also Druger, et. al., 1979).

A.4 THEORETICAL — APPROXIMATE

Approximate methods fall into the following general categories:

- Rayleigh or Rayleigh–Gans limit
- geometrical optics and extensions thereof
- perturbation theory
- thin in one dimension
- semi–empirical
- replace by a simpler shape

Small particles

Stevenson (1953) gives the general theory for scattering by arbitrarily–shaped bodies in the Rayleigh limit where size divided by wavelength is small. Kleinman (1967, 1978) made important improvements in this theory (see also Herrick and Senior, 1977; Senior, 1976, 1980). A completely analytic solution still eludes us, except for 5 simple shapes, including ellipsoids. The ellipsoid solution has been widely exploited (e.g., Huffman and Bohren, 1980). For general shapes, one must solve a simple integral equation for the polarizability tensor by numerical methods.

The Rayleigh–Gans approximation is even more restricted, requiring not only small particles but a refractive index near unity as well (van de Hulst, 1981). The trade–off is that great analytical progress can be made in this case, and, like many asymptotic approximations, it is useful outside its strictly defined range of validity. Barber and Wang (1978) found it reasonably accurate up to refractive indices of 1.1 and size parameters of 1. And there are more applications than one might imagine; for example, to scattering by cells in aqueous solution.

Acquista (1976, 1980) developed an extended Rayleigh–Gans approximation, based on an iterative solution to Shifrin's integro–differential formulation of scattering. It is valid all the way up to size parameters of 5 or so.

Large particles

The class of methods for particles large compared to the wavelength is extensive. Kouyoumjian (1965) gives an excellent review. He notes that progress in developing large–particle asymptotic solutions to Maxwell's Equations (or to particular solutions like Mie theory) has been excruciatingly slow, due to the great mathematical difficulties (see also Kline, 1962).

"Geometric optics" is the simplest large–particle approximation. It refers to the calculation of intensity along ray paths as those rays experience reflection and refraction at the boundaries of a scatterer,

and absorption within it. The Fraunhofer diffraction pattern is normally added to the geometrical optics approximation, to account for the strong forward peak in scattering from large particles. Phase and polarization information can be carried along with the intensity, as van de Hulst (1981) shows, but usually the interference between rays is ignored, since even a slight spread in size or wavelength will wash it out.

Geometric optics is particularly simple for a sphere (Liou and Hansen, 1971), because the ray paths remain in a plane. For any other shape, the ray paths are twisted 3-D curves, and an analytical solution borders on the impossible. Instead, a Monte Carlo approach is normally taken: the scatterer is bombarded with enough rays to give decent statistics on the scattered energy at each angle. Jacobowitz (1971), Wendling et. al. (1979), and Coleman and Liou (1981) all did this for a hexagonal ice cylinder. Takano and Tanaka (1980) did it for circular cylinders.

Concave particles greatly complexify geometric optics. A ray emerging from the scatterer cannot be logged and forgotten; this can only be done when it finally leaves the circumscribing sphere, since there is always the possibility that it may re-enter the particle. Thus, the ray paths may ramify almost endlessly.

Reflection from a large, randomly-oriented, convex particle is rigorously identical to the reflection from a large sphere (van de Hulst, 1981; Hodkinson, 1963). The diffraction is close to that from an equal-projected-area sphere. Hence, if the particle absorbs enough to extinguish transmitted rays, reflection plus diffraction from an equal-projected-area sphere is an excellent approximation to the nonspherical scattering.

Some authors (e.g. Pollack and Cuzzi, 1980) postulate that the transmitted rays suffer greater deviations for any non-sphere than for a sphere, accounting for the higher side-scattering from nonspheres.

Chylek (1977), drawing on a result of Vouk (1948), notes that the extinction cross-section of a large, randomly-oriented particle always exceeds that of an equal-volume sphere.

Maxwell's Equations can in principle be expanded as wavelength tends toward zero (the so-called 'Luneberg-Kline expansion'), leading in zeroth order to the famous 'eikonal equation' (Kline, 1962). But the eikonal equation is non-linear, and the equations for the higher-order terms of the Luneberg-Kline expansion become increasingly complicated and non-linear; furthermore, these equations break down near light-shadow boundaries, where diffraction occurs. Little progress has been made on these higher-order equations.

Keller (1962), in a famous piece of work, developed a theory which extends geometric optics by adding "diffracted rays". These are produced whenever an incident ray hits an edge, vertex, or shadow boundary, and behave according to their own laws, different from ordinary rays.

Perturbation theory

The idea of perturbation theory is simple enough: assume the scatterer is bounded by the surface

$$r_s = r_0 [1 + e\, f(\Theta,\phi)]$$

where $e << 1$. Then expand everything in powers of e. Yeh (1964, 1965) worked out the order e correction terms for deviations from a cylinder as well as a sphere. Erma (1968a,b) corrected Yeh's formulation and extended it to arbitrary orders. Neither author gave any numerical results. The formulas for scattering quantities are complicated; double series for order e, triple series for order e^2, and so on.

Chylek, et. al. (1978) made some first-order perturbation theory calculations and generally found unacceptably large errors for $e > 0.10$. For $e = 0.05$, they found roughly 1% errors compared to the exact spheroidal results of Asano and Yamamoto (1975). They also pointed out that perturbation series become useless, and may in fact diverge, once the Mie coefficients a_n and b_n develop sharp spikes (beyond size parameter $x = 6$ or so). This is because perturbation theory involves derivatives of a_n and b_n. When these derivatives become large, the omitted terms in the perturbation series become larger than the ones which are kept.

Two particles are 'conjugate' if they are described by

$$r_s = r_0 \pm g(\Theta,\phi)$$

(with g such that $r_s > 0$). Using perturbation theory, Chylek, et. al. (1979) showed that, for small g, the two conjugate particles have an average scattering equal to that of a sphere of radius r_0. This is an interesting twist on the idea of replacing a particle by an equivalent sphere; here two particles (or a single "self-conjugate" particle) can be replaced by an equivalent sphere.

Thin particles

If a particle is thin in one of its dimensions, it is possible to approximate the integral equations describing scattering. The work of Chu and Weil (1976), Weil and Chu (1976, 1980), and Senior and Weil (1977) is an example of this approach. They have applied it to both ice crystal plates and aerosol particles.

Semi-empirical

The word 'semi-empirical' denotes a class of methods containing a mixture of experimental and theoretical results.

Emslie and Aronson (1973) and Aronson and Emslie (1980) developed such a method for the dust blanketing the Moon and Mars. They modeled the small dust grains as ellipsoids in the small-particle limit and the large grains as spheres in the geometric optics limit. Roughness on the spheres was

mimicked by distributing absorbing dipoles over their surfaces, which could interact with the geometric optics rays. Intermediate-sized particles were treated by interpolation between these two extremes. There were probably too many tuneable parameters in this model, but it did yield agreement with measured emission and reflection spectra which had not been previously explained.

An abortive semi-empirical theory which involved truncating the sharp spikes in the Mie coefficients a_n and b_n was proposed by Chylek, et. al. (1976). The idea was that these spikes were associated with 'surface waves', which would be suppressed on nonspherical particles. Unfortunately, the spikes do not correspond to surface waves, and in any case exact calculations by Mugnai and Wiscombe (1980), among others, show that surface waves persist even on rather nonspherical particles. This theory became embroiled in controversy (Acquista, 1978; Chylek and Pinnick, 1979) from which it has never recovered.

Pollack and Cuzzi (1980) suggested a theory based primarily on the measurements of Zerull (1976). They use equal-volume Mie theory for nonspherical particles with size parameter $x < x_0$, where x_0 is tuned in the range 3 to 10. For $x > x_0$, the absorption cross-section is still gotten from Mie theory, while the phase function is gotten from a sum of

- Fraunhofer diffraction
- reflected rays from a sphere
- transmitted rays fitted to mimic Zerull's measurements (involving a second tuneable parameter).

The single-scattering co-albedo of the sphere is multiplied by the ratio

surface area of particle/surface area of sphere

to get the co-albedo for the particle.

Coletti (1984) has devised another semi-empirical theory based on his own measurements, and similar in some respects to that of Pollack and Cuzzi.

Replace by a simpler shape

Perhaps the simplest approximation is to replace the particle by a simpler shape, which however has to fulfill two sometimes contradictory requirements:

- the scattering properties of the simpler shape have to be relatively easy to calculate, and
- they have to resemble those of the actual particle.

Spheres are by far and away the most popular replacement. The only question then is: of what radius? Equal-volume spheres are the choice of 90% of all investigators. Equal-surface-area and equal-projected-area spheres also have their devotees. A less well-explored option is to match, not a material property of the particle, but an optical property: extinction cross-section, for example.

The argument for equal-volume spheres (aside from the relative ease of measuring particle masses) is that, at least for particles of small size parameter, scattering depends primarily on volume, not shape. This is gainsaid, however, by Aronson and Emslie (1980) and by Huffman and Bohren (1980), who find that, even when one averages over shape and orientation, ellipsoids do not behave like spheres. Likewise, Liou (1974) has found that equal-volume spheres are a poor substitute for ice cylinders in the 8–12 micron infrared window region.

Equal-projected-area spheres are generally regarded as the best replacement for particles of large size parameter, because the forward diffraction peak depends primarily on projected area (Hodkinson, 1963). Since this peak is the prime determinant of the low-order phase function moments, and since these moments are the prime determinants of multiple scattering, it is worth considering the equal-projected-area sphere for that application. Holland and Gagne (1970), among others, find that the scattering from 0 to 40–50° is best approximated by equal-projected-area spheres.

A.5 SPECULATIONS AND IDEAS

Nonspherical particle scattering is so exceedingly rich and various that there is no hope of jumping immediately, by a sort of Aristotelian contemplation, to an all-embracing theory. The rush to 'semi-empirical' theories is, in our opinion, premature; it has already led to one bad mistake, and is likely to lead to more. Instead, we should proceed inductively, examining many special cases first.

Mie theory should be abandoned only grudgingly. Single equal-volume spheres are surely not an adequate replacement for all, or even most, nonspherical particles. But we are far from having exhausted Mie theory. There are still several largely unexplored replacement possibilities:

- a sphere having the same volume-to-surface-area ratio
- a size distribution of spheres (e.g., Wang et. al., 1979)
- a multi-layer sphere (e.g., Kerker, 1969, Ch. 5)
- a sphere with continuously-varying refractive index (e.g., Kerker, 1969, Ch. 5).

The last two possibilities are based on the simple idea of trading off nonsphericity against inhomogeneity. Imagine a tumbling nonspherical particle as a 'fuzzy sphere', with a solid core shading gradually outwards. Between the core and the periphery, the refractive index would gradually change to that of the surrounding medium. By picking a functional form for this change that allowed a reasonably simple radial solution, with one or two adjustable parameters, it might be possible to match nonspherical scattering properties. Because scattering from an inhomogeneous sphere is orders

of magnitude easier to calculate than scattering from any non-sphere, this idea is immensely attractive.

Modifications to Mie theory to account for non-sphericity may also be possible; but not until a definite physical interpretation can be assigned to the terms. In this regard, Complex Angular Momentum Theory (Nussenzweig, 1979) may prove useful for larger particles, since it replaces the Mie expansion with a series of only a few terms, each of which can be assigned a simple physical meaning.

If we are finally forced to abandon Mie theory for some particularly recalcitrant cases, we should at least try to use equivalent spheroids. This gives us two parameters to tune to match the actual nonspherical results, and that may be enough.

Concave particles, and particles with voids, may defy all our attempts to replace them with equivalent spheres or spheroids. Since such particles are of great practical importance, we should make every effort to find their scattering properties, both experimentally and from exact theory. Our own EBCM calculations have shown great differences between the phase functions of convex and even mildly concave particles.

We need to develop a minimal, prototypical set of shape parameters. Up to now, we have either picked shapes which were easy to calculate for, or which Nature thrust upon us. Very little thought has been devoted to the abstract concept of 'Shape', and what characterizes it. Greenberg (1980) has suggested some of the shape information which may be important. Our own list would include:

- some measure of surface roughness
- the 3 semi-axes of the ellipsoid which best approximates the particle
- the hole volume or 'porosity'.

Present numerical methods need to be speeded up dramatically. Even the fastest of them, like our vectorized EBCM code, consume far too much computer time. At the same time, faster ways of averaging over orientation need to be found; this is a real roadblock in present scattering calculations.

Once faster numerical methods are available, it will become possible to routinely average over shape, size, and orientation, something which is now impractical except in test cases. Then we can more incisively answer questions as to how much each kind of averaging reduces spherical-nonspherical differences.

REFERENCES: APPENDIX A

General

Greenberg, J., 1980: "Focusing in on particle shape", Light Scattering from Irregularly Shaped Particles, D. Schuerman, ed., Plenum Press, New York, 7–23.

Kerker, M., 1969: The Scattering of Light and Other Electromagnetic Radiation, Academic Press, New York.

Nussenzweig, H., 1979: Complex angular momentum theory of the rainbow and the glory, J. Opt. Soc. Amer. 69, 1068–1079.

Schuerman, D., ed., 1980: Light Scattering by Irregularly Shaped Particles, Plenum Press, New York.

Van de Hulst, H., 1981: Light Scattering by Small Particles, Dover, New York.

Wiscombe, W., 1979: Mie Scattering Calculations: Improvements in Technique and Fast, Vector-Speed Computer Codes, NCAR Technical Note TN-140+STR, National Center for Atmospheric Research, Boulder, Colorado.

Wiscombe, W., 1980: Improved Mie scattering algorithms, Appl. Opt. 19, 1505–1509.

Experimental

Ashkin, A. and J. Dziedzic, 1980: Observation of light scattering from nonspherical particles using optical levitation, Appl. Opt. 19, 660–668.

_____, 1981: Observation of optical resonances of dielectric spheres by light scattering, Appl. Opt. 20, 1803–1813.

Berry, C., 1962: Turbidity of monodisperse suspensions of AgBr, J. Opt. Soc. Amer. 52, 888–895.

Bottiger, J., E. Fry and R. Thompson, 1980: "Phase matrix measurements for electromagnetic scattering by sphere aggregates", Light Scattering by Irregularly Shaped Particles, D. Schuerman, ed., Plenum Press, New York, 283–290.

Chylek, P., G. Grams and R. Pinnick, 1976: Light scattering by irregular randomly oriented particles, Science 193, 480-482.

Donn, B. and R. Powell, 1963: "Angular scattering from irregular particles with application to astronomy", Electromagnetic Scattering, Proc. ICES I, M. Kerker, ed., Pergamon Press, New York, 151–158.

Greenberg, J., 1960: Scattering by nonspherical particles, J. Appl. Phys. 31, 82-90.
_____, 1961: Microwave analog to the scattering of light by nonspherical particles, J. Appl. Phys. 32, 233-242.
_____, 1972: Absorption and emission of radiation by nonspherical particles, J. Coll. Interface Sci. 39, 513-519.
_____, R. Wang and L. Bangs, 1971: Extinction by rough particles and the use of Mie theory, Nature Phys. Sci. 230, 110-112.

Holland, A. and G. Gagne, 1970: The scattering of polarized light by polydisperse systems of irregular particles, Appl. Opt. 9, 1113-1121 (see also "Comment", Appl. Opt. 10, 1173-1174).

Huffman, P. and W. Thursby, 1969: Light scattering by ice crystals, J. Atmos. Sci. 26, 1073-1077.

Janzen, J., 1980: Extinction of light by highly nonspherical strongly absorbing colloidal particles: spectrophotometric determination of volume distributions for carbon blacks, Appl. Opt. 19, 2977-2985.

Kirmaci, I. and G. Ward, 1979: Scattering of 0.627 micron light from spheroidal 2-micron cladosporium and cubical NaCl particles, Appl. Opt. 18, 3328-3331.

Napper, D. and R. Ottewill, 1963: "Light scattering studies on monodisperse AgBr sols", Electromagnetic Scattering, Proc. ICES I, M. Kerker, ed., Pergamon Press, New York, 377-385.

Perry, R., A. Hunt and D. Huffman, 1978: Experimental determinations of Mueller scattering matrices for nonspherical particles, Appl. Opt. 17, 2700-2710.

Pinnick, R., D. Carroll and D. Hofmann, 1976: Polarized light scattered from monodisperse randomly oriented nonspherical aerosol particles: measurements, Appl. Opt. 15, 384-393.

Proctor, T. and G. Harris, 1974: The turbidity of suspensions of irregular quartz particles, J. Aerosol Sci. 5, 81-90.
_____ and D. Barker, 1974: The turbidity of suspensions of irregular diamond particles, J. Aerosol Sci. 5, 91-99.

Sassen, K. and K. Liou, 1979: Scattering of polarized laser light by water droplet, mixed-phase and ice crystal clouds. Part I. Angular scattering patterns, and Part II: Angular depolarizing and multiple scattering behavior, J. Atmos. Sci. 36, 838-861.

Saunders, M., 1980: "The effect of a distorting electric field on the backscattered radiance from a single water drop", Light Scattering by Irregularly Shaped Particles, D. Schuerman, ed., Plenum Press, New York, 237-242.

Schuerman, D., R. Wang, B. Gustafson and R. Schaefer, 1981: Systematic studies of light scattering. 1: Particle shape, Appl. Opt. 20, 4039-4050.

Waggoner, A., N. Ahlquist and R. Charlson, 1972: Measurement of the aerosol total scatter-backscatter ratio, Appl. Opt. 11, 2886-2889.

Wang, R., 1980: Extinction signatures of nonspherical/nonisotropic particles, in Light Scattering by Irregularly Shaped Particles, D. Schuerman, ed., Plenum Press, New York, pp. 255-272.

Zerull, R., 1976: Scattering measurements of dielectric and absorbing nonspherical particles, Beitr. Phys. Atmos. 49, 166-188.

Zerull, R., Giese, R. and K. Weiss, 1977: Scattering functions of nonspherical dielectric and absorbing particles vs. Mie theory, Appl. Opt. 16, 777-778.

Theoretical — exact

Asano, S. and G. Yamamoto, 1975: Light scattering by a spheroidal particle, Appl. Opt. 14, 29-49.

Asano, S., 1979: Light scattering properties of spheroidal particles, Appl. Opt. 18, 712-723.

Asano, S., 1980: Light scattering by randomly oriented spheroidal particles, Appl. Opt. 19, 962-974.

Barber, P. and C. Yeh, 1975: Scattering of electromagnetic waves by arbitrarily shaped dielectric bodies, Appl. Opt. 14, 2864-2872.

Bates, R., 1967: The point-matching period for interior and exterior 2-D boundary-value problems, IEEE Trans. MTT-15, 185-187.

_____, 1969: Rayleigh hypothesis, the extended boundary condition, and point matching, Elec. Lett. 5, 654-655.

_____, James, J., Gallett, I. and R. Millar, 1973: An overview of point matching, Radio and Elec. Eng. 43, 193-200.

Borghese, F., Denti, P., Toscano, G. and O. Sindoni, 1979: Electromagnetic scattering by a cluster of spheres, Appl. Opt. 18, 116-120.

Bowman, J., Senior, T. and P. Uslenghi, eds., 1969: Electromagnetic and Acoustic Scattering By Simple Shapes, American Elsevier, New York.

Cohen, A. and P. Alpert, 1979: Cross sections for extinction of tilted infinite circular cylinders, Appl. Opt. 18, 2728.

_____, 1980: Radiation pressure on randomly oriented infinite cylinders, Appl. Opt. 19, 558-560.

Druger, S., M. Kerker, D. Wang and D. Cooke, 1979: Light scattering by inhomogeneous particles, Appl. Opt. 18, 3888-3889.

Greenberg, J., A. Lind, R. Wang and L. Libelo, 1965: "Scattering by nonspherical systems", Electromagnetic Scattering, Proc. of ICES II, Rowell and Stein, eds., Gordon and Breach, New York, pp. 3–49.

Harrington, R., 1968: Field Computations by Moment Methods, MacMillan, New York, 450 pp.

Holt, A., N. Uzunoglu and B. Evans, 1978: An integral equation solution to the scattering of electromagnetic radiation by dielectric spheroids and ellipsoids, IEEE Transac, AP-26, 706–712.

Kattawar, G. and T. Humphreys, 1980: "Electromagnetic scattering from two identical pseudospheres", Light Scattering by Irregularly Shaped Particles, D. Schuerman, ed., Plenum Press, New York, 177–190.

Liou, K., 1972: Electromagnetic scattering by arbitrarily oriented ice cylinders, Appl. Opt. 11, 667–674.

Livesay, D. and K. Chen, 1974: Electromagnetic fields induced inside arbitrarily shaped biological bodies, IEEE Transac. MTT-22, 1273–1280.

Mei, K., M. Morgan and S. Chang, 1978: "A review of finite element methods in electromagnetic scattering", Electromagnetic Scattering, P. Uslenghi, ed., Academic Press, New York, 359–392.

Millar, R., 1969: Rayleigh hypothesis in scattering problems, Elec. Lett. 5, 416–418.
_____, 1973: The Rayleigh hypothesis and a related least-squares solution to scattering problems for periodic surfaces and other scatterers, Radio Sci. 8, 785–796.
_____ and R. Bates, 1970: On the legitimacy of an assumption underlying the point-matching method, IEEE Trans. MTT-18, 325–327.

Miller, E. and A. Poggio, 1978: "A review of moment-method techniques in electromagnetics from an applications viewpoint", Electromagnetic Scattering, P. Uslenghi, ed., Academic Press, New York, 315–357.

Morgan, M. and K. Mei, 1979: Finite-element computation of scattering by inhomogeneous penetrable bodies of revolution, IEEE Transac. AP-27, 202–214.

Morse, P. and H. Feshbach, 1953: Methods of Theoretical Physics, McGraw-Hill, New York.

Mugnai, A. and W. Wiscombe, 1980: Scattering of radiation by moderately non-spherical particles, J. Atmos. Sci. 37, 1291–1307.

Patwari, A. and J. Davies, 1966: Scattering by infinite cylinders of arbitrary cross-section by the method of finite differences, Elec. Lett. 2, 470–471.

Purcell, E. and C. Pennypacker, 1977: Scattering and absorption of light by nonspherical dielectric grains, Astrophys. J. 186, 705–714.

Reilly, E., 1973: Resonant scattering from inhomogeneous nonspherical targets, J. Comp. Phys. 11, 463–492.

Richmond, J., 1965: Digital computer simulations of the rigorous equations for scattering problems, Proc. IEEE 53, 796–804.

Wait, J., 1955: Scattering of a plane wave from a circular dielectric cylinder at oblique incidence, Can. J. Phys. 33, 189–195.

Wang, D. and P. Barber, 1979: Scattering by inhomogeneous nonspherical objects, Appl. Opt. 18, 1190–1197.

_____, H. Chen, P. Barber and P. Wyatt, 1979: Light scattering by polydisperse suspensions of inhomogeneous nonspherical particles, Appl. Opt. 18, 2672–2678.

Waterman, P., 1965: Matrix formulation of electromagnetic scattering, Proc. IEEE 53, 805–812.

_____, 1971: Symmetry, unitarity, and geometry in electromagnetic scattering, Phys. Rev. D3, 825–839.

Yeh, C., 1965: Backscattering cross-section of a dielectric elliptical cylinder, J. Opt. Soc. Amer. 55, 309–315.

_____ and K. Mei, 1980: "On the scattering from arbitrarily shaped inhomogeneous particles — exact solution by finite element method", Light Scattering from Irregularly Shaped Particles, D. Schuerman, ed., Plenum Press, New York, 201–206.

Yung, Y., 1978: Variational principle for scattering of light by dielectric particles, Appl. Opt. 17, 3707–3709.

Theoretical — approximate

Acquista, C., 1976: Light scattering by tenuous particles: a generalization of the Rayleigh–Gans approach, Appl. Opt. 15, 2932–2936.

_____, 1978: Validity of modifying Mie theory to describe scattering by nonspherical particles, Appl. Opt. 17, 3851–3852.

_____, 1980: "Shifrin's method applied to scattering by tenuous nonspherical particles", Light Scattering by Irregularly Shaped Particles, D. Schuerman, ed., Plenum Press, New York, 165–168.

Aronson, J. and A. Emslie, 1980: "Absorption by particle edges and asperities", Light Scattering by Irregularly Shaped Particles, D. Schuerman, ed., Plenum Press, New York, 191–200.

Barber, P. and D. Wang, 1978: Rayleigh–Gans–Debye applicability to scattering by nonspherical particles, Appl. Opt. 17, 797–803.

Chu, C. and H. Weil, 1976: Integral equation method for scattering and absorption of radiation by thin lossy dielectric disks, J. Comp. Phys. 22, 111–124.

Chylek, P., 1977: Extinction cross-sections of arbitrarily shaped randomly oriented nonspherical particles, J. Opt. Soc. Amer. 67, 1348–1350.
_____, J. Kiehl and M. Ko, 1978: Light scattering by almost spherical particles, in Proc. Third Conf. on Atmospheric Radiation, Davis, Calif., June 28–30, 1978, American Meteorological Society, 45 Beacon St., Boston, Mass.
_____ and R. Pinnick, 1979: Non–unitarity of the light scattering approximations, Appl. Opt. 18, 1123–1124.
_____, J. Kiehl and A. Mugnai, 1979: Light scattering by a pair of conjugate nonspherical particles, J. Opt. Soc. Amer. 69, 1231–1233.

Coleman, R. and K. Liou, 1981: Light scattering by hexagonal ice crystals, J. Atmos. Sci. 38, 1260–1271.

Coletti, A., 1984: Light scattering by nonspherical particles: a laboratory study, Aerosol Sci. and Tech. 3, 39–52.

Erma, V., 1968a: Perturbation solution for the scattering of electromagnetic waves from conductors of arbitrary shape. I. Case of cylindrical symmetry, Phys. Rev. 173, 1243–1257.
_____, 1968b: Perturbation solution for the scattering of electromagnetic waves from conductors of arbitrary shape. II. General case, Phys. Rev. 176, 1544–1553.

Emslie, A. and J. Aronson, 1973: Spectral reflectance and emittance of particulate materials 1: Theory, Appl. Opt. 12, 2563–2572.

Herrick, D. and T. Senior, 1977: Low–frequency scattering by rectangular dielectric particles, Appl. Phys. 13, 175–183.

Hodkinson, J., 1963: "Light scattering and extinction by irregular particles larger than the wavelength", Electromagnetic Scattering, Proc. ICES I, M. Kerker, ed., Pergamon Press, New York, 87–100.

Huffman, D. and C. Bohren, 1980: "Infrared absorption spectra of nonspherical particles treated in the Rayleigh–ellipsoid approximation", Light Scattering by Irregularly Shaped Particles, D. Schuerman, ed., Plenum Press, New York, 103–112.

Jacobowitz, H., 1971: A method for computing the transfer of solar radiation through clouds of hexagonal ice crystals, JQSRT 11, 691–695.

Keller, J., 1962: Geometrical theory of diffraction, J. Opt. Soc. Amer. 52, 116–130.

Kiehl, J., M. Ko, A. Mugnai and P. Chylek, 1980: "Perturbation approach to light scattering by nonspherical particles", Light Scattering by Irregularly Shaped Particles, D. Schuerman, ed., Plenum Press, New York, 135–140.

Kleinman, R., 1967: Far-field scattering at low frequencies, Appl. Sci. Res. 18, 1–8.
_____, 1978: "Low-frequency electromagnetic scattering", Electromagnetic Scattering, P. Uslenghi, ed., Academic Press, New York.

Kline, M., 1962: "Electromagnetic theory and geometrical optics", Electromagnetic Waves, R. Langer, ed., University of Wisconsin Press, Madison, Wisconsin.

Kouyoumjian, R., 1965: Asymptotic high-frequency methods, Proc. IEEE 53, 864–876.

Latimer, P., 1980: Predicted scattering by spheroids: comparison of approximate and exact methods, Appl. Opt. 19, 3039–3041.

Liou, K., 1974: On the radiative properties of cirrus in the window region and their influence on remote sensing of the atmosphere, J. Atmos. Sci. 31, 522–532.
_____ and J. Hansen, 1971: Intensity and polarization for single scattering by polydisperse spheres: comparison of ray optics and Mie theory, J. Atmos. Sci. 28, 995–1004.

Pollack, J. and J. Cuzzi, 1980: Scattering by nonspherical particles of size comparable to a wavelength: a new semi-empirical theory and its application to tropospheric aerosols, J. Atmos. Sci. 37, 868–881.

Senior, T., 1976: Low-frequency scattering by a dielectric body, Radio Sci. 11, 447–482.
_____, 1980: Effect of particle shape on low-frequency absorption, Appl. Opt. 19, 2483–2485.
_____ and H. Weil, 1977: Electromagnetic scattering and absorption by thin dielectric cylinders with application to ice crystals, Appl. Opt. 16, 2979–2985.

Stevenson, A., 1953: Solution of electromagnetic scattering problems as power series in the ratio (dimension of scatterer/wavelength), J. Appl. Phys. 24, 1134–1142.

Takano, Y. and M. Tanaka, 1980: Phase matrix and cross-sections for single scattering by circular cylinders: comparison of ray optics and wave theory, Appl. Opt. 19, 2781–2793.

Vouk, V., 1948: Projected area of convex bodies, Nature 162, 330–331.

Weil, H. and C. Chu, 1976: Scattering and absorption of electromagnetic radiation by thin dielectric disks, Appl. Opt. 15, 1832–1836.
_____, 1980: Scattering and absorption by thin flat aerosols, Appl. Opt. 19, 2066–2071.

Wendling, P., R. Wendling and H. Weickmann, 1979: Scattering of solar radiation by hexagonal ice crystals, Appl. Opt. 18, 2663–2671.

Yeh, C., 1964: Perturbation approach to the diffraction of electromagnetic waves by arbitrarily shaped dielectric obstacles, Phys. Rev. 135, 1193–1201.

_____, 1965: Perturbation method in the diffraction of electromagnetic waves by arbitrarily shaped penetrable obstacles, J. Math. Phys. 6, 2008–2013.

APPENDIX B

Parallel and perpendicular scattered intensities vs. scattering angle for two fixed orientations, nose-on (dotted line) and perpendicular to nose-on (dashed line); for Chebyshev particles $T_3(+0.10)$, $T_2(-0.10)$, $T_4(+0.10)$, and $T_6(-0.10)$; and for size parameters $x = 5$ and 10. Spherical results (solid line) are shown for comparison. Note the much larger spherical-nonspherical differences in fixed orientation than in random orientation. These results are intended for direct comparison with experiment.

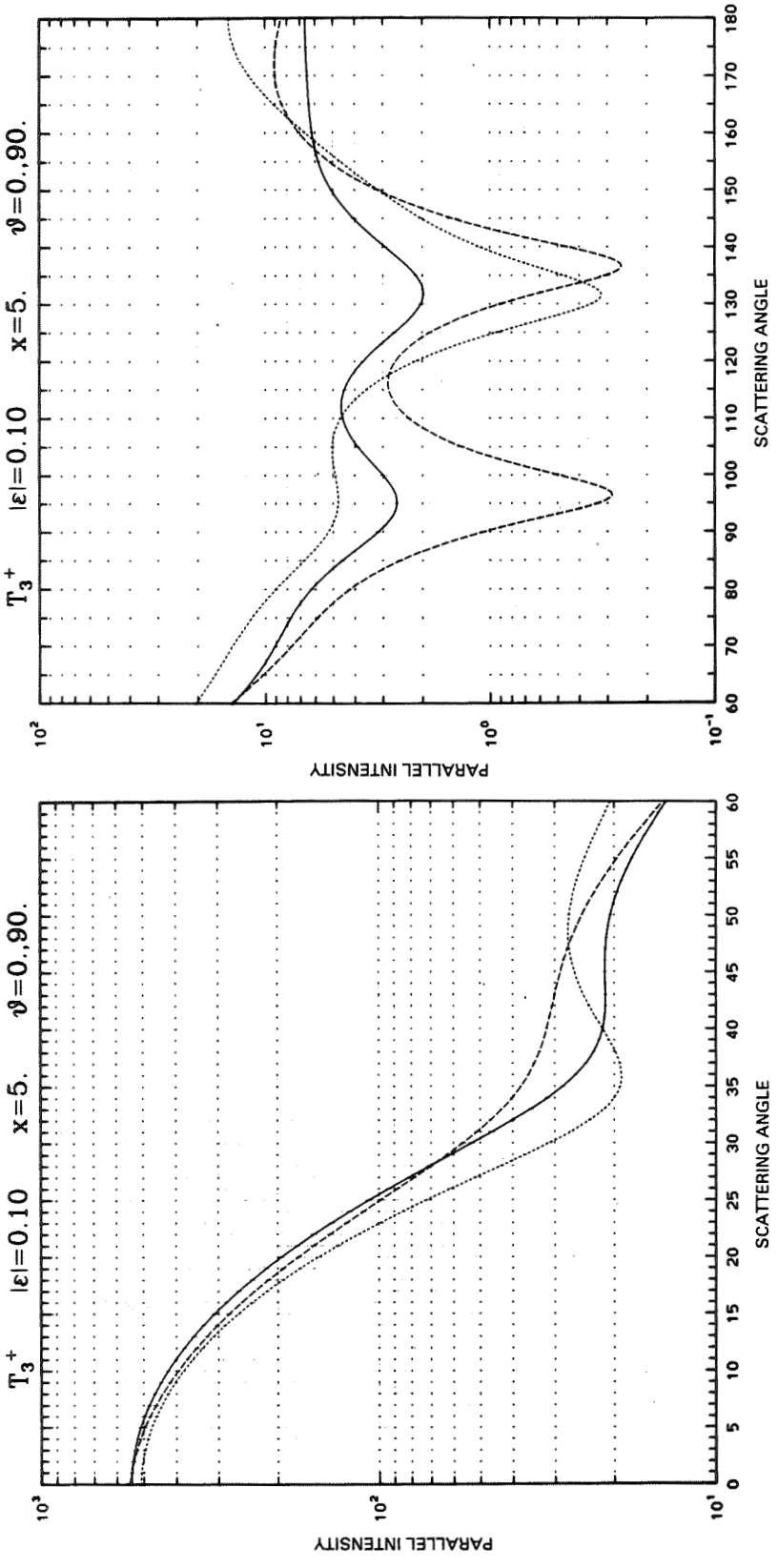

Appendix B. Nonspherical SCATTERED INTENSITIES (parallel and perpendicular) vs. ANGLE for Chebyshev particles in two fixed orientations

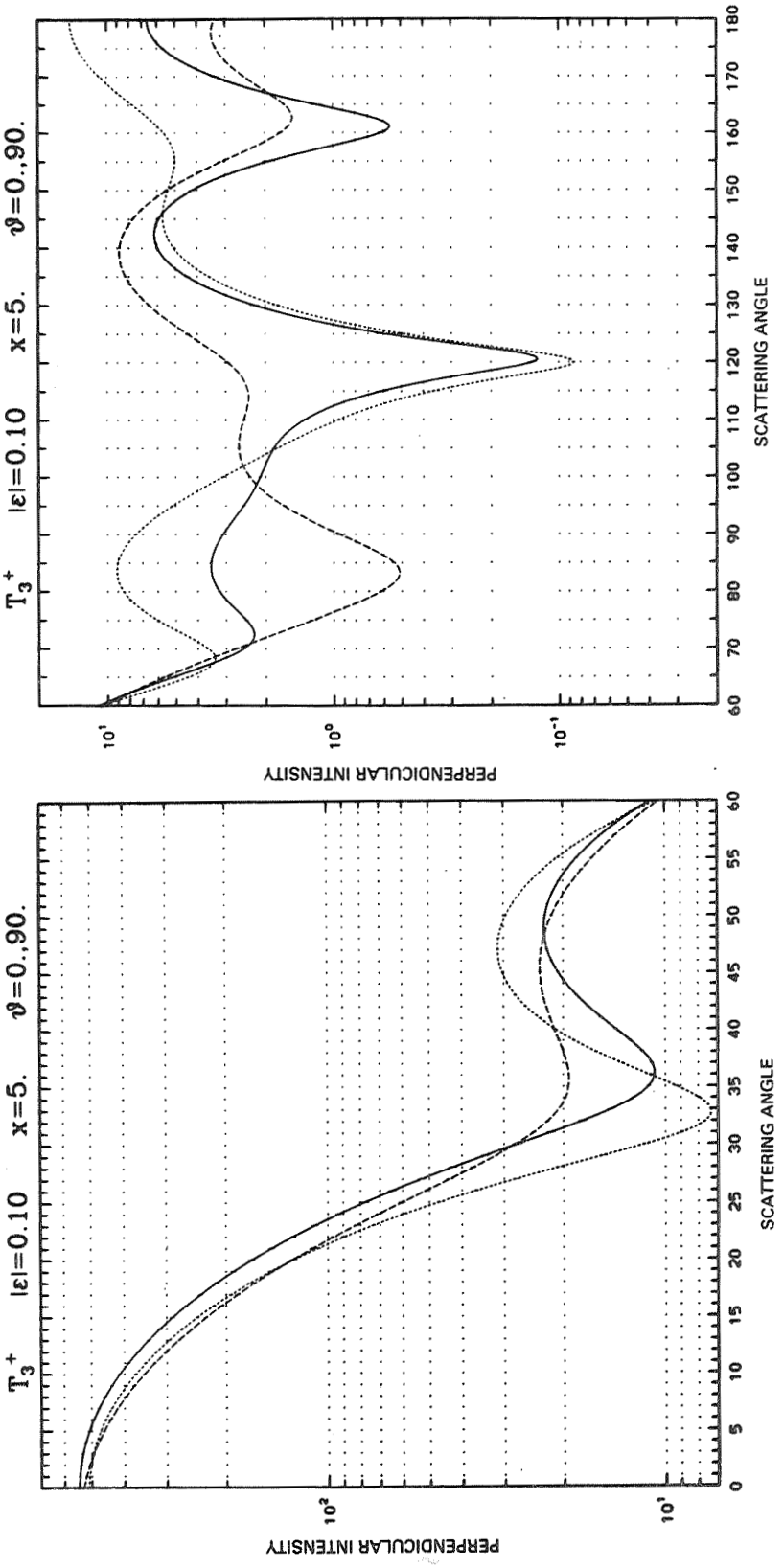

Appendix B (Continued)

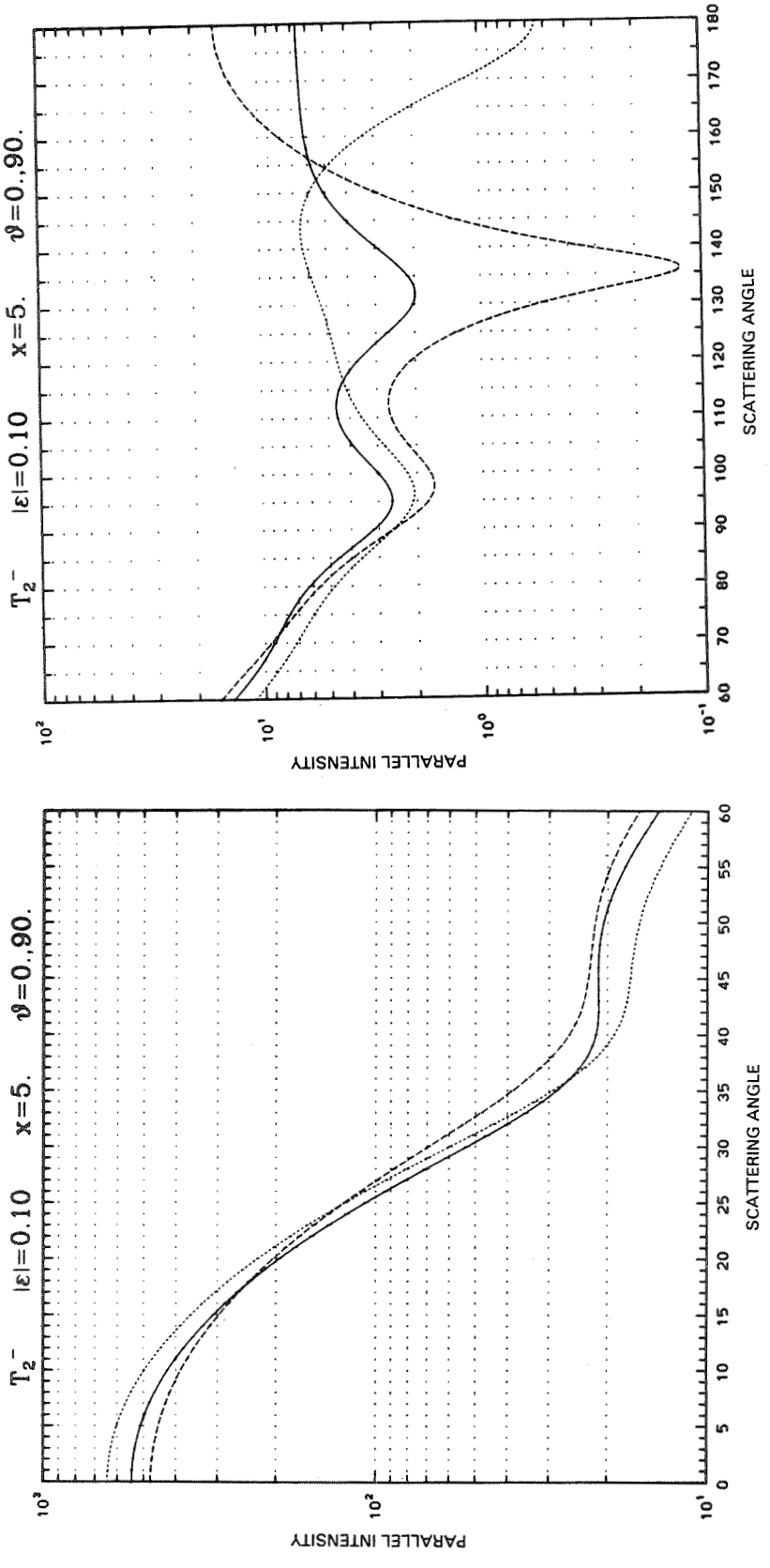

Appendix B (Continued)

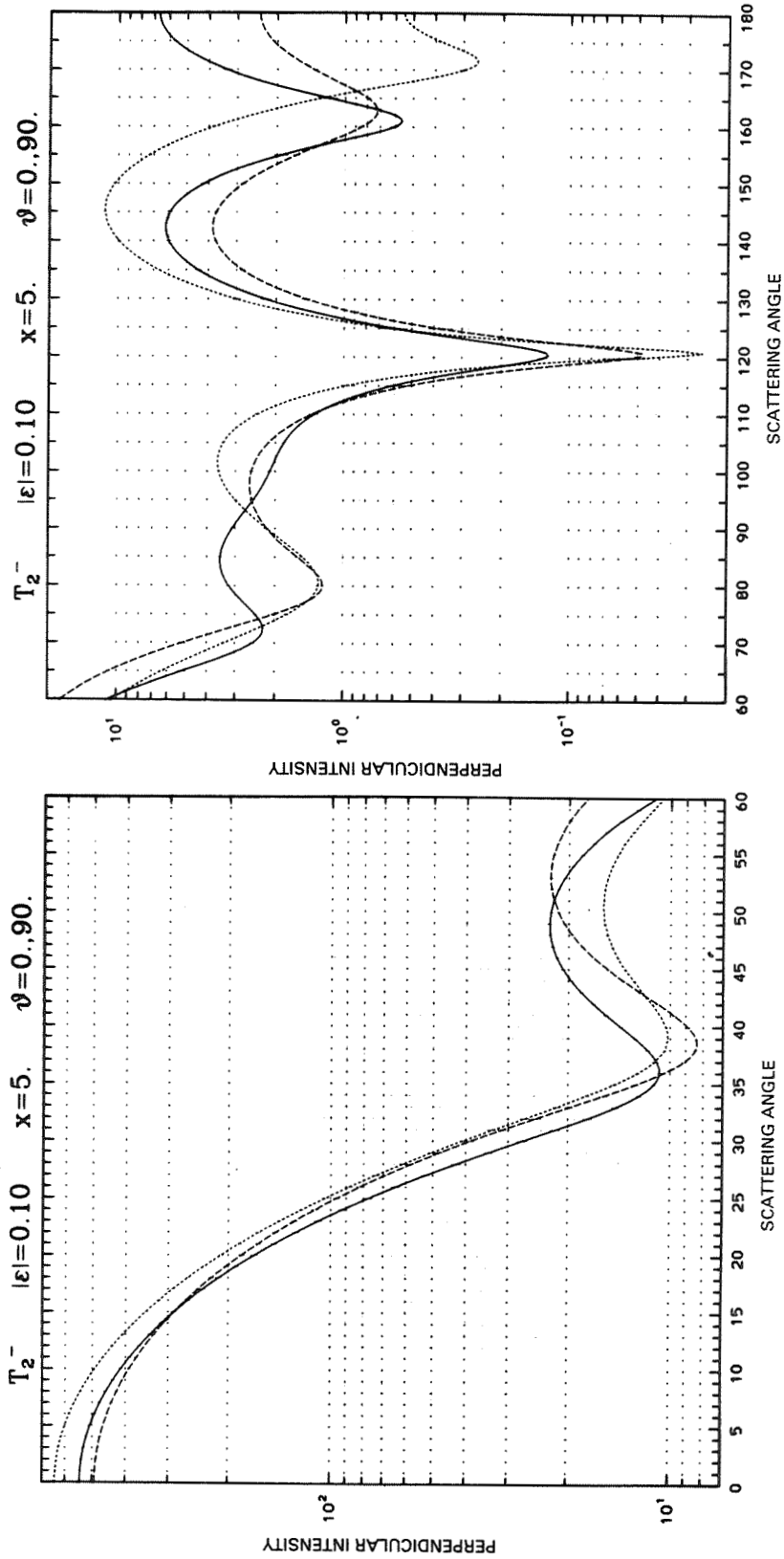

Appendix B (Continued)

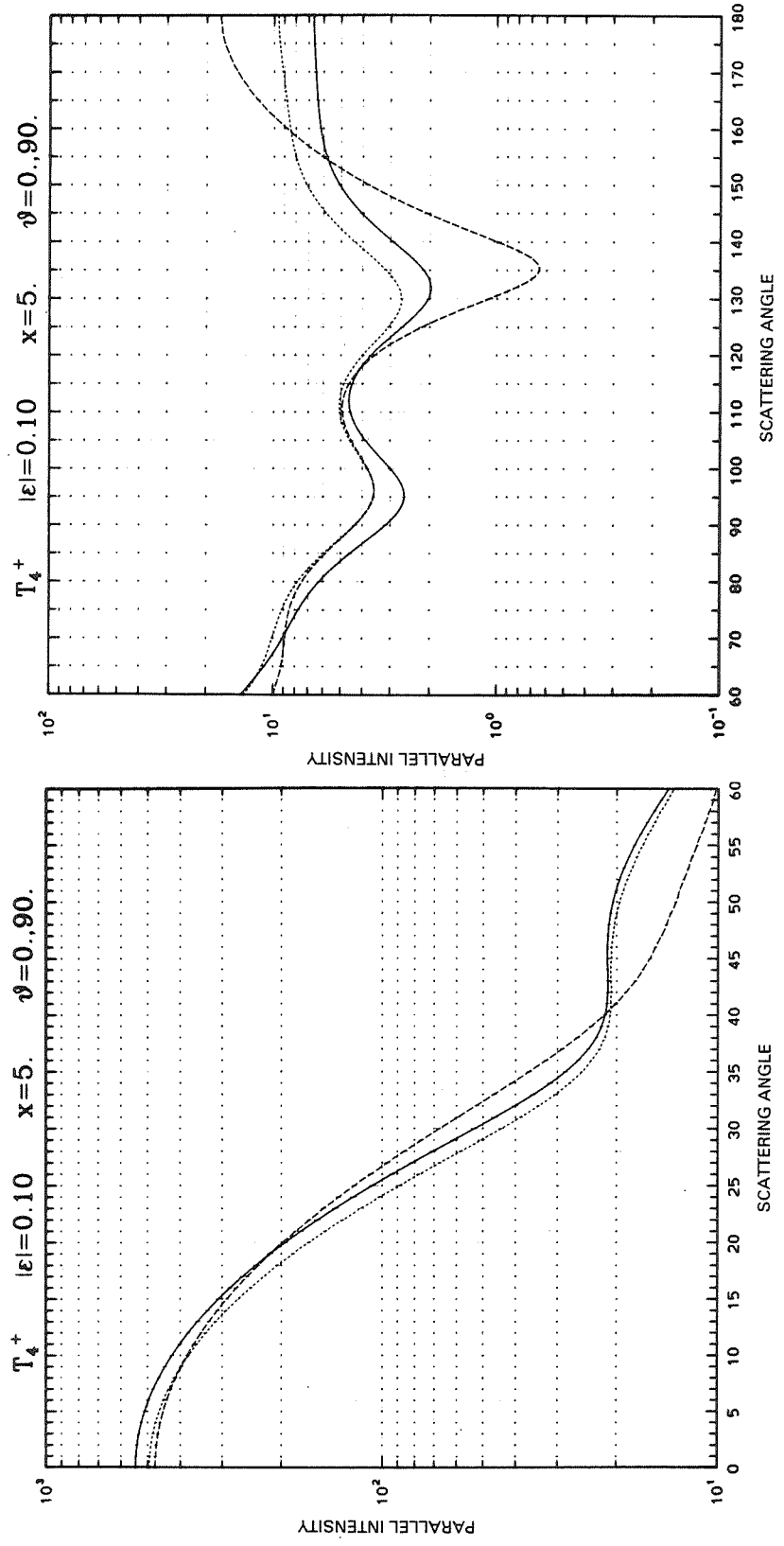

Appendix B (Continued)

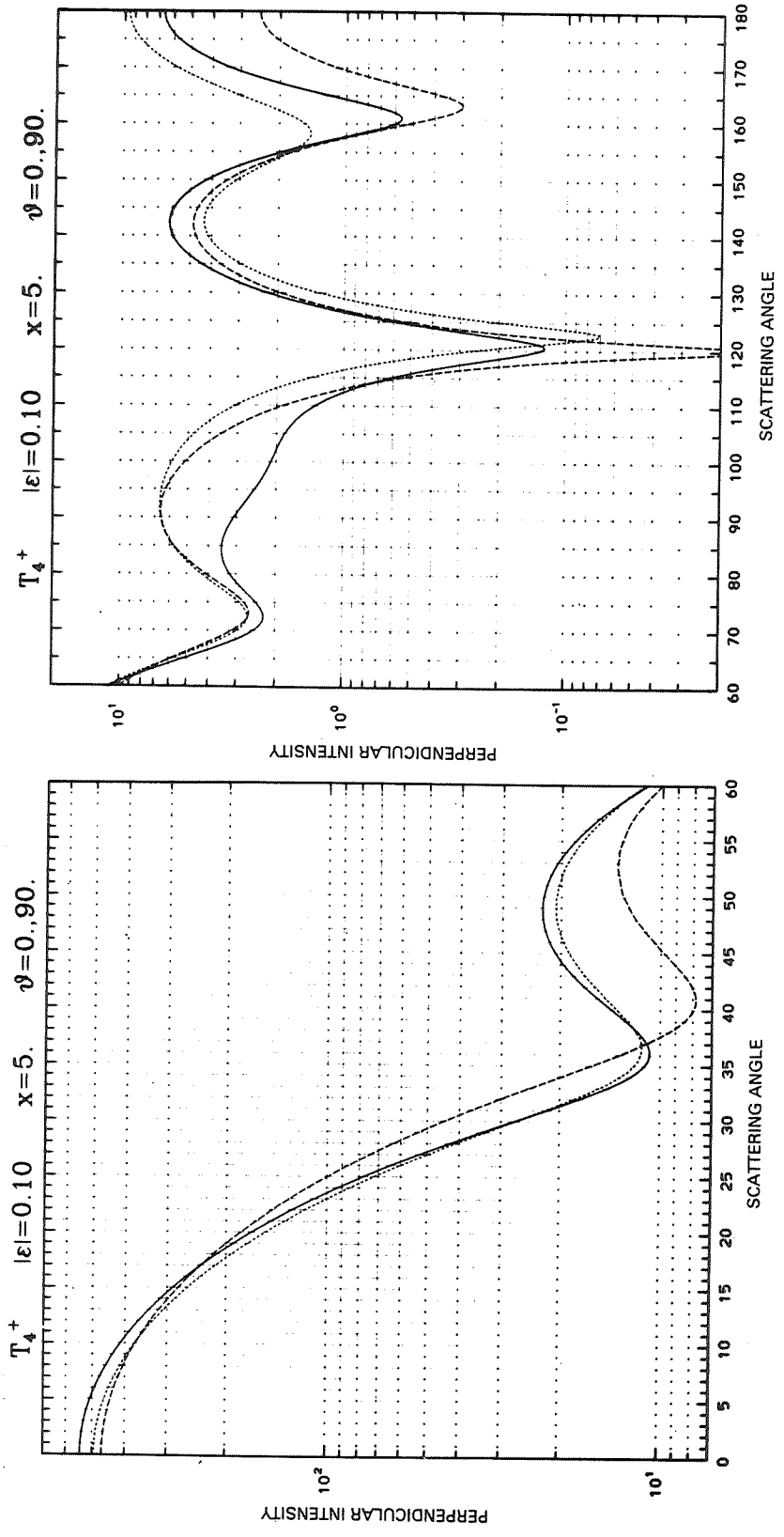

Appendix B (Continued)

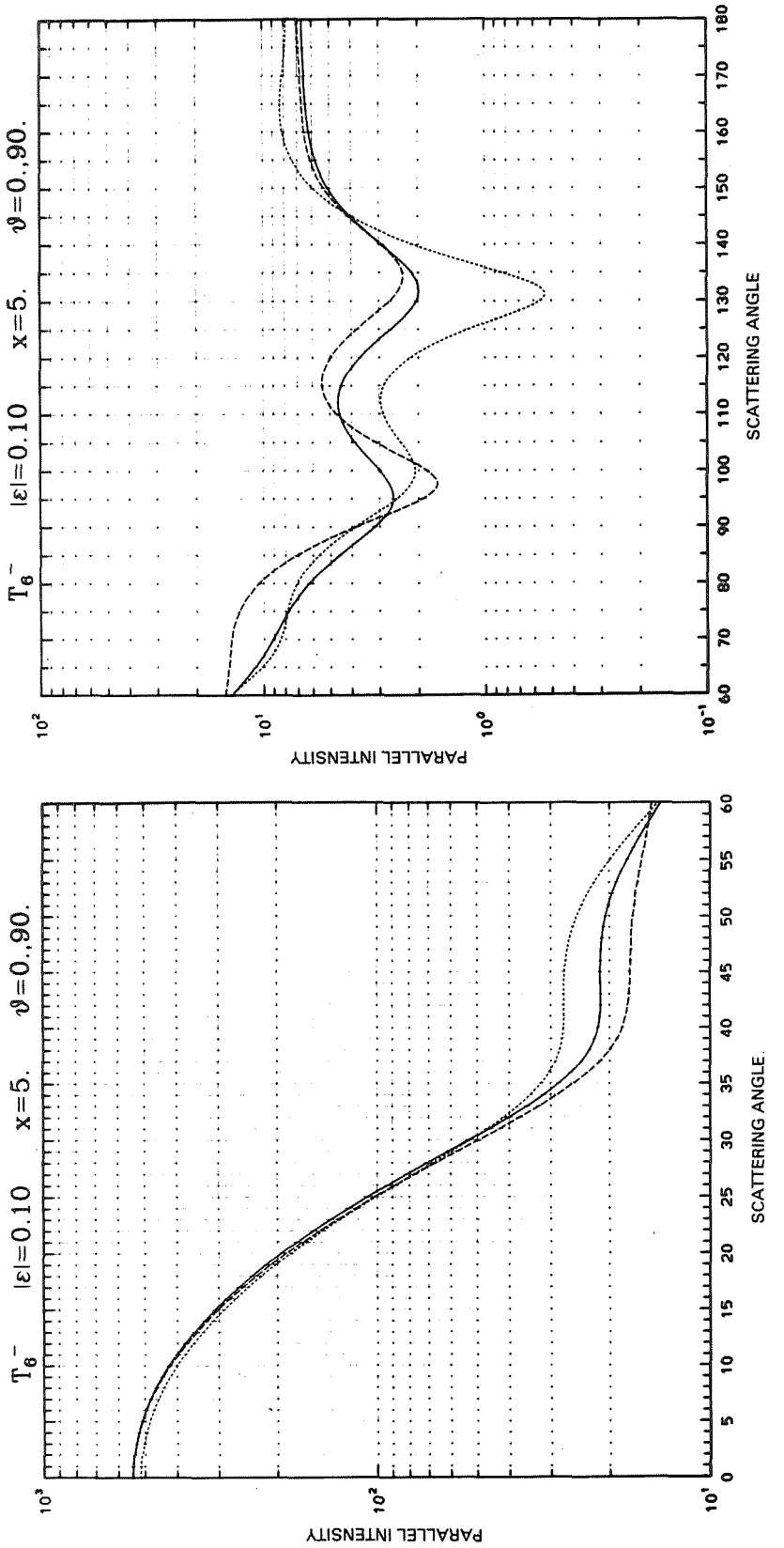

Appendix B (Continued)

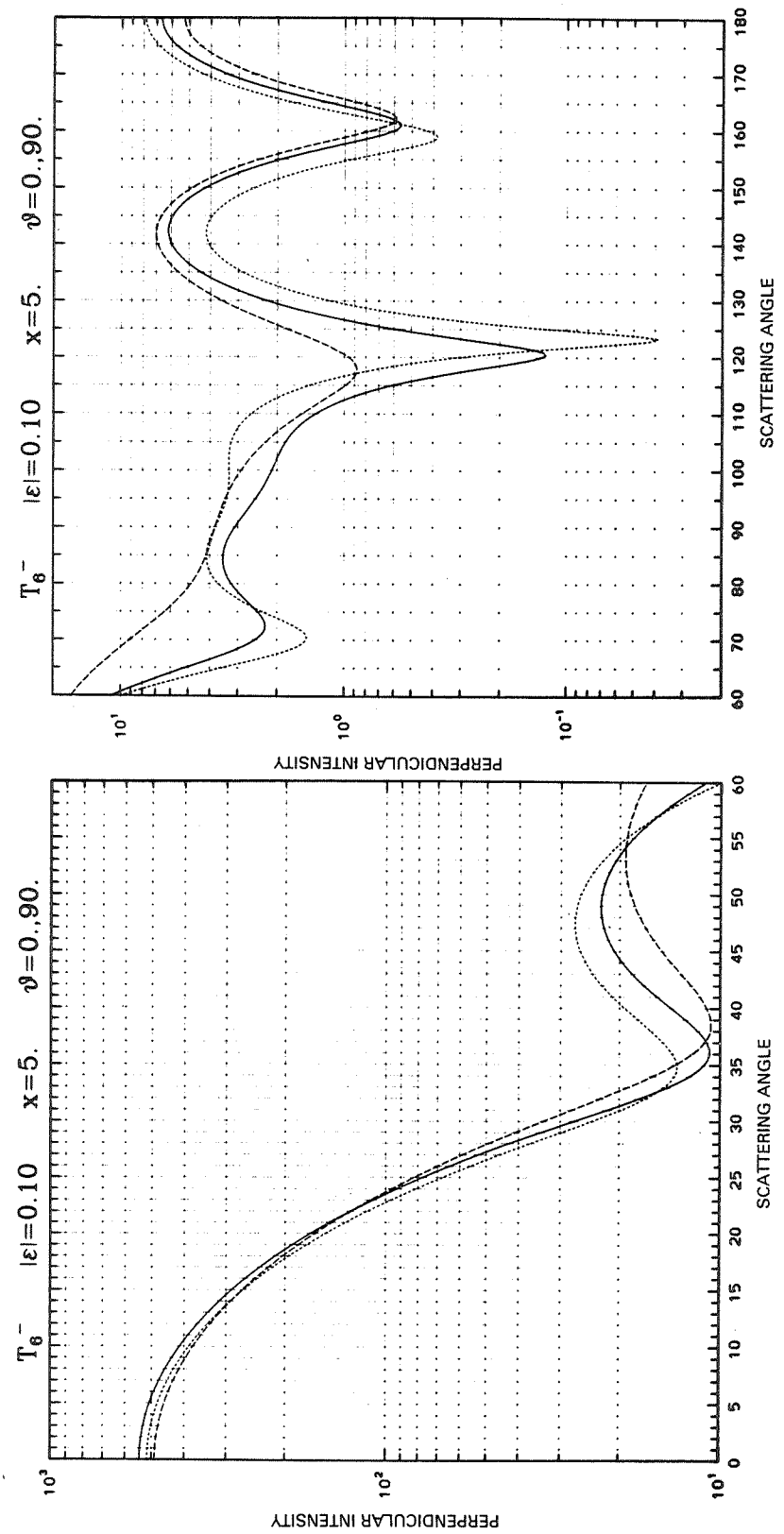

Appendix B (Continued)

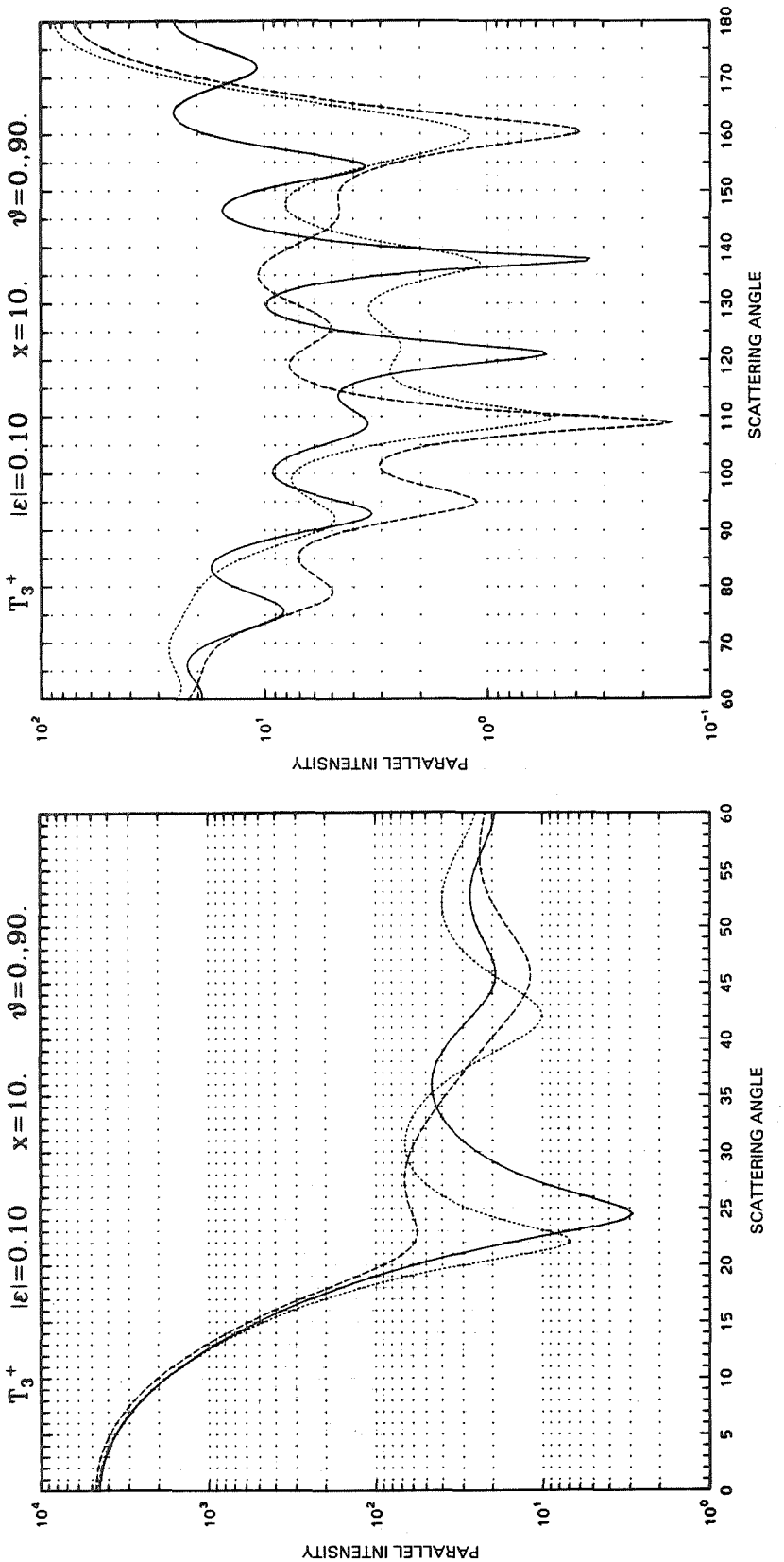

Appendix B (Continued)

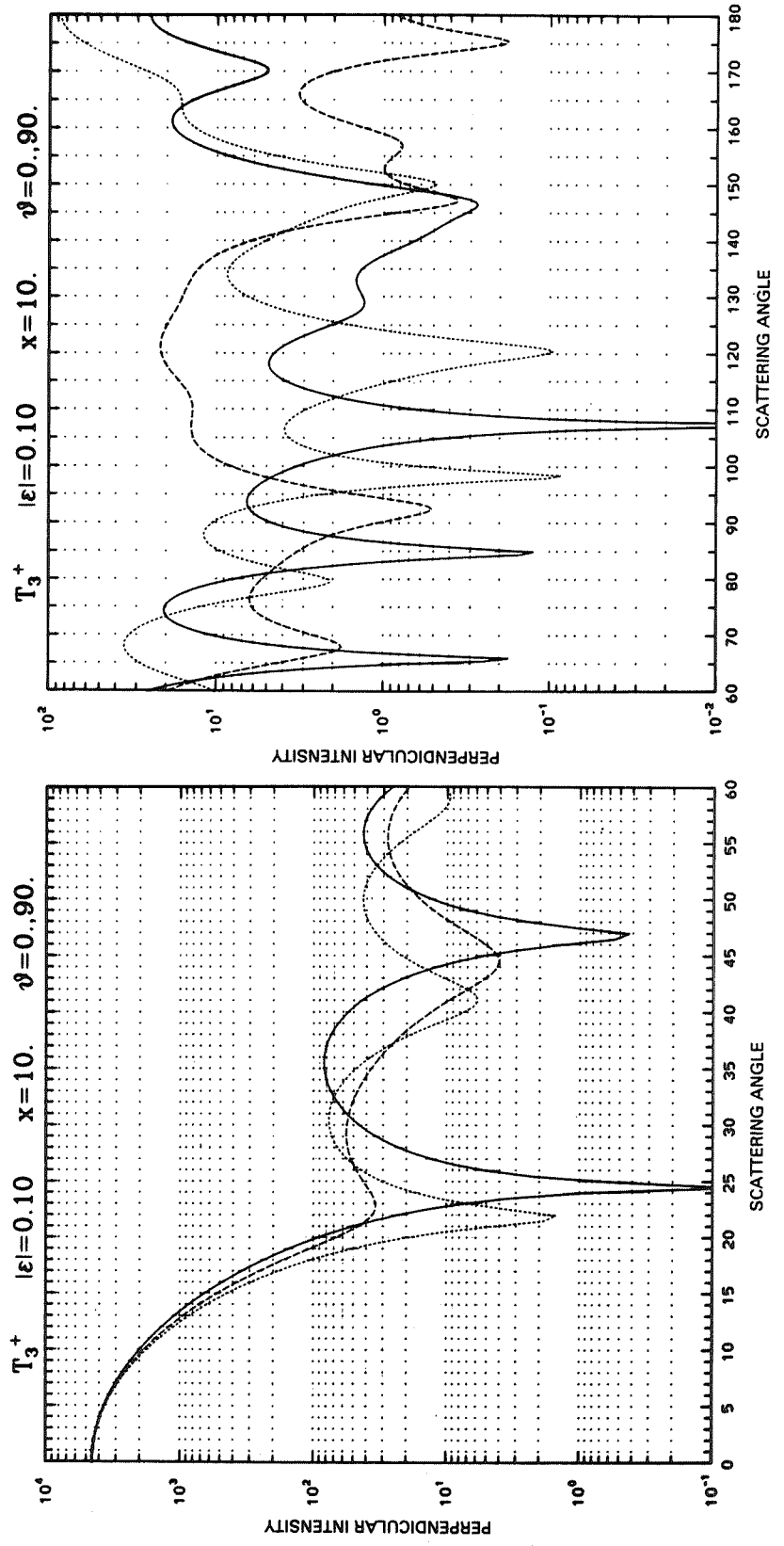

Appendix B (Continued)

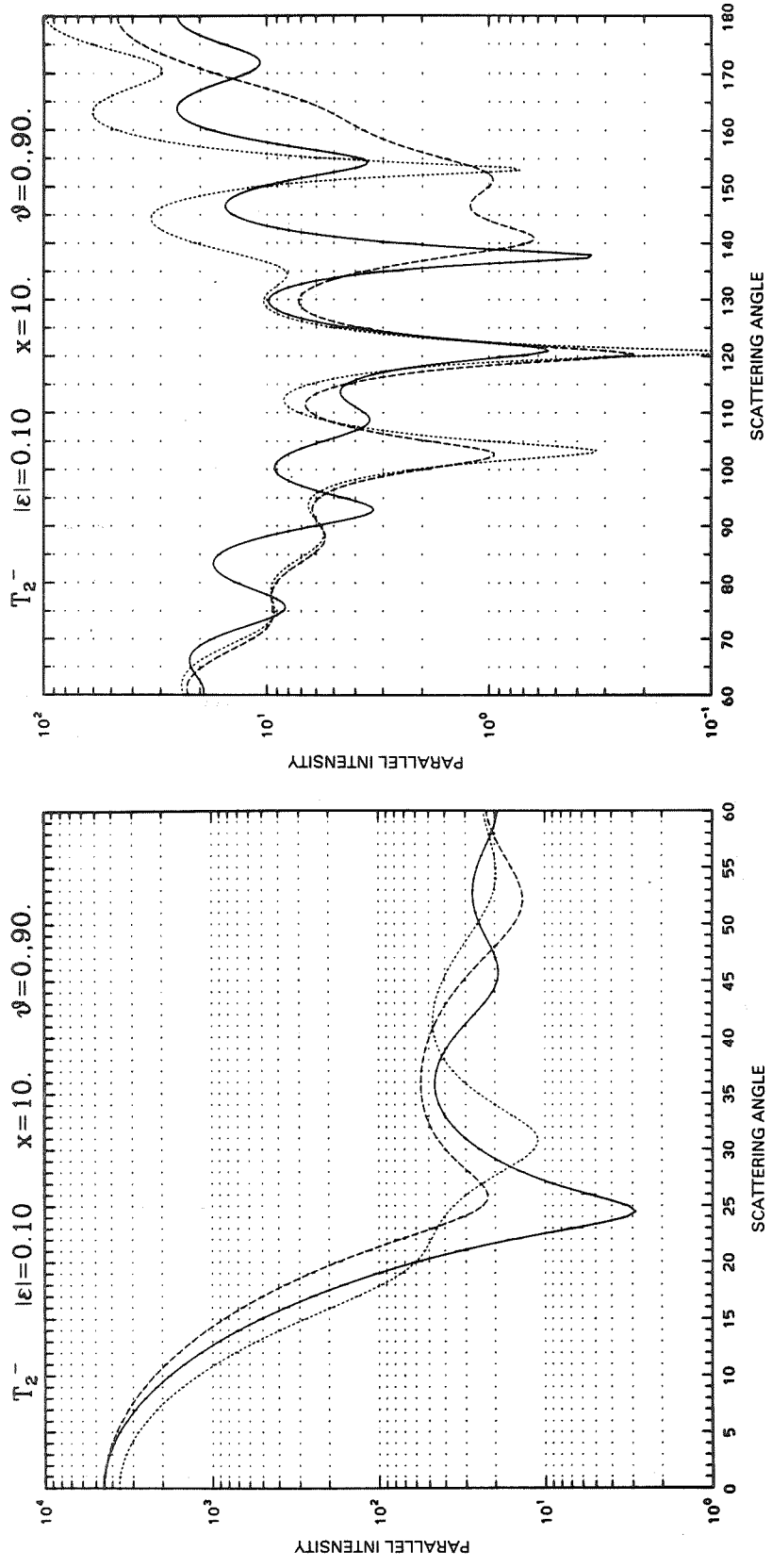

Appendix B (Continued)

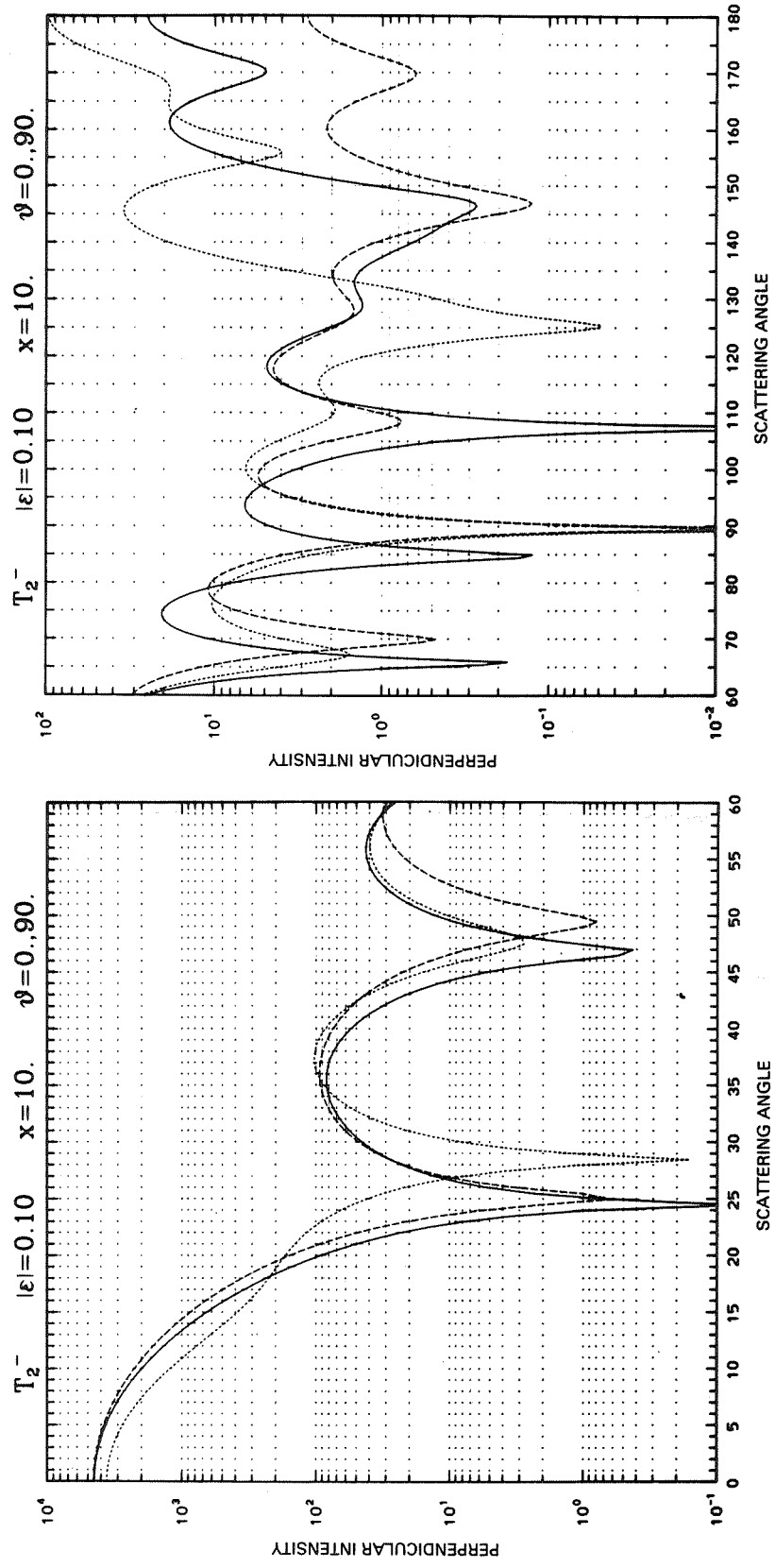

Appendix B (Continued)

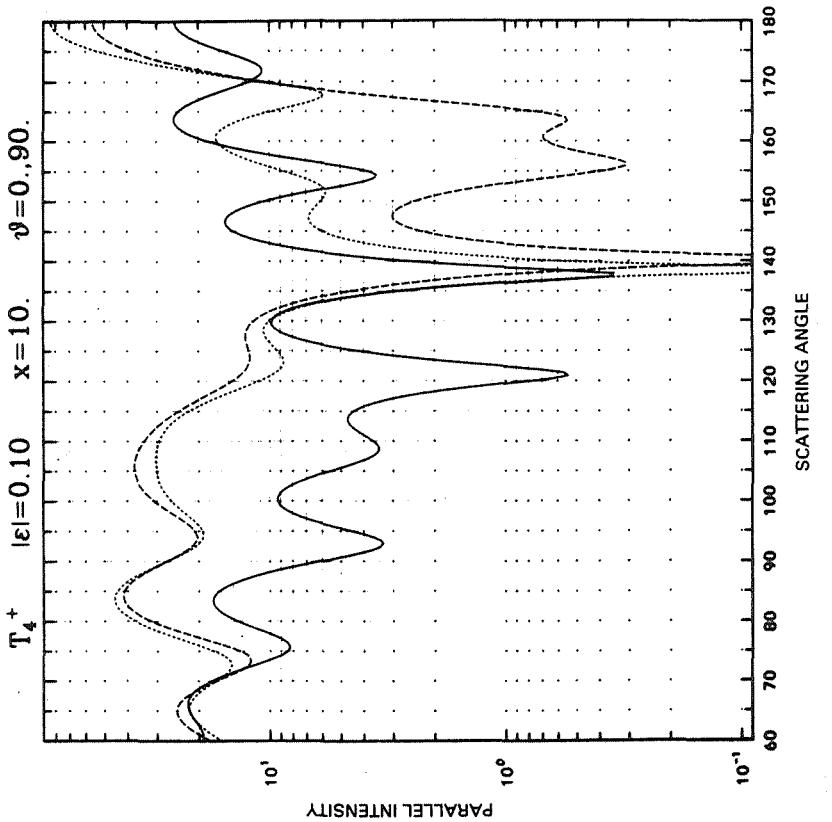
T_4^+ |ε|=0.10 x=10. ϑ=0.,90.
PARALLEL INTENSITY
SCATTERING ANGLE

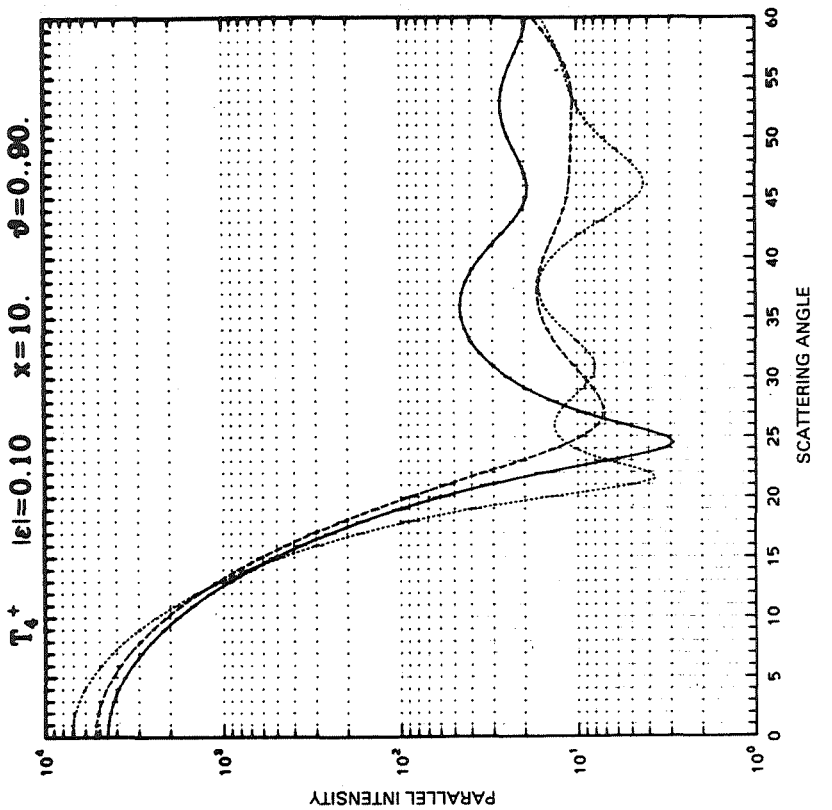
T_4^+ |ε|=0.10 x=10. ϑ=0.,90.
PARALLEL INTENSITY
SCATTERING ANGLE

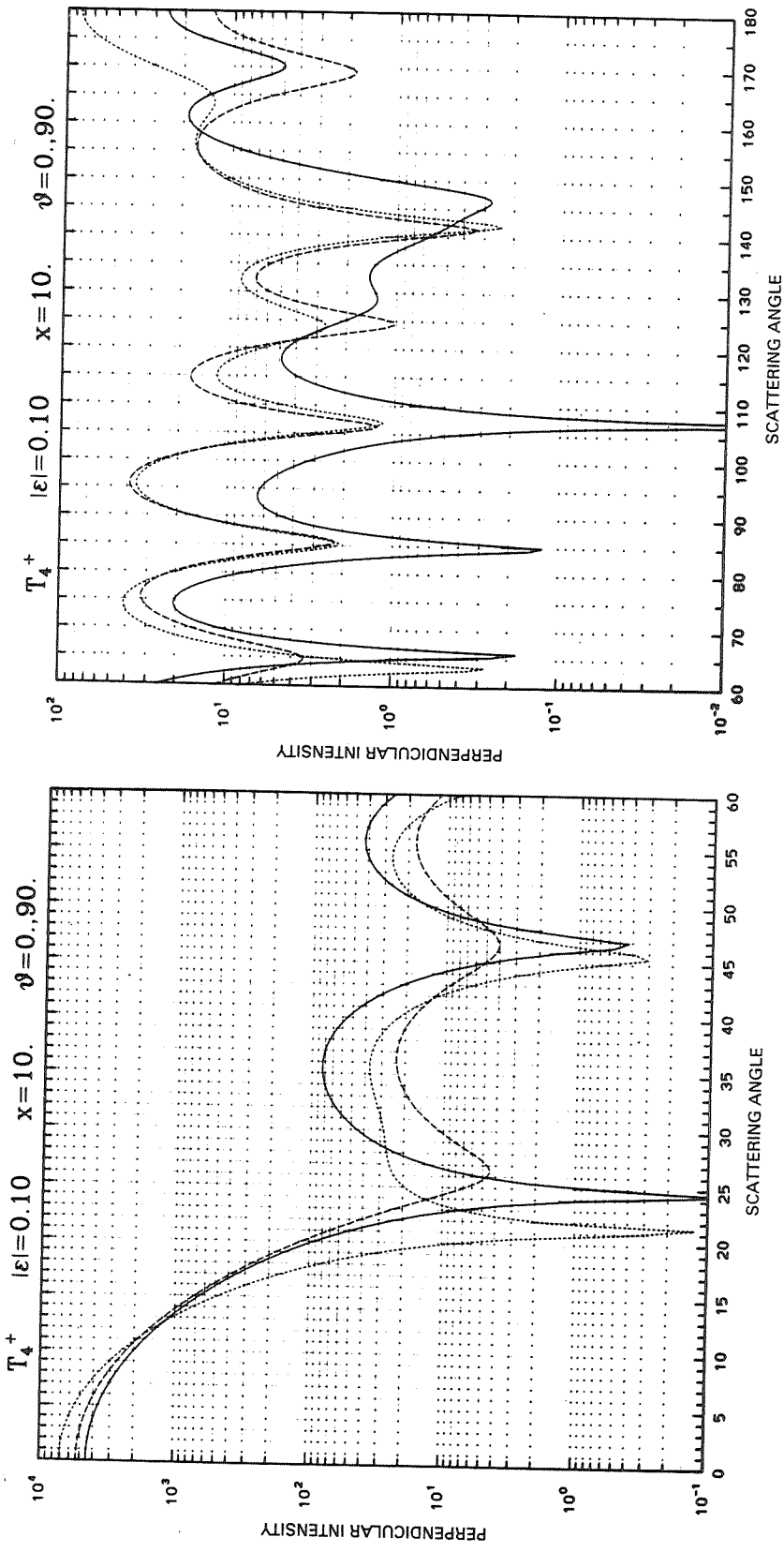

Appendix B (Continued)

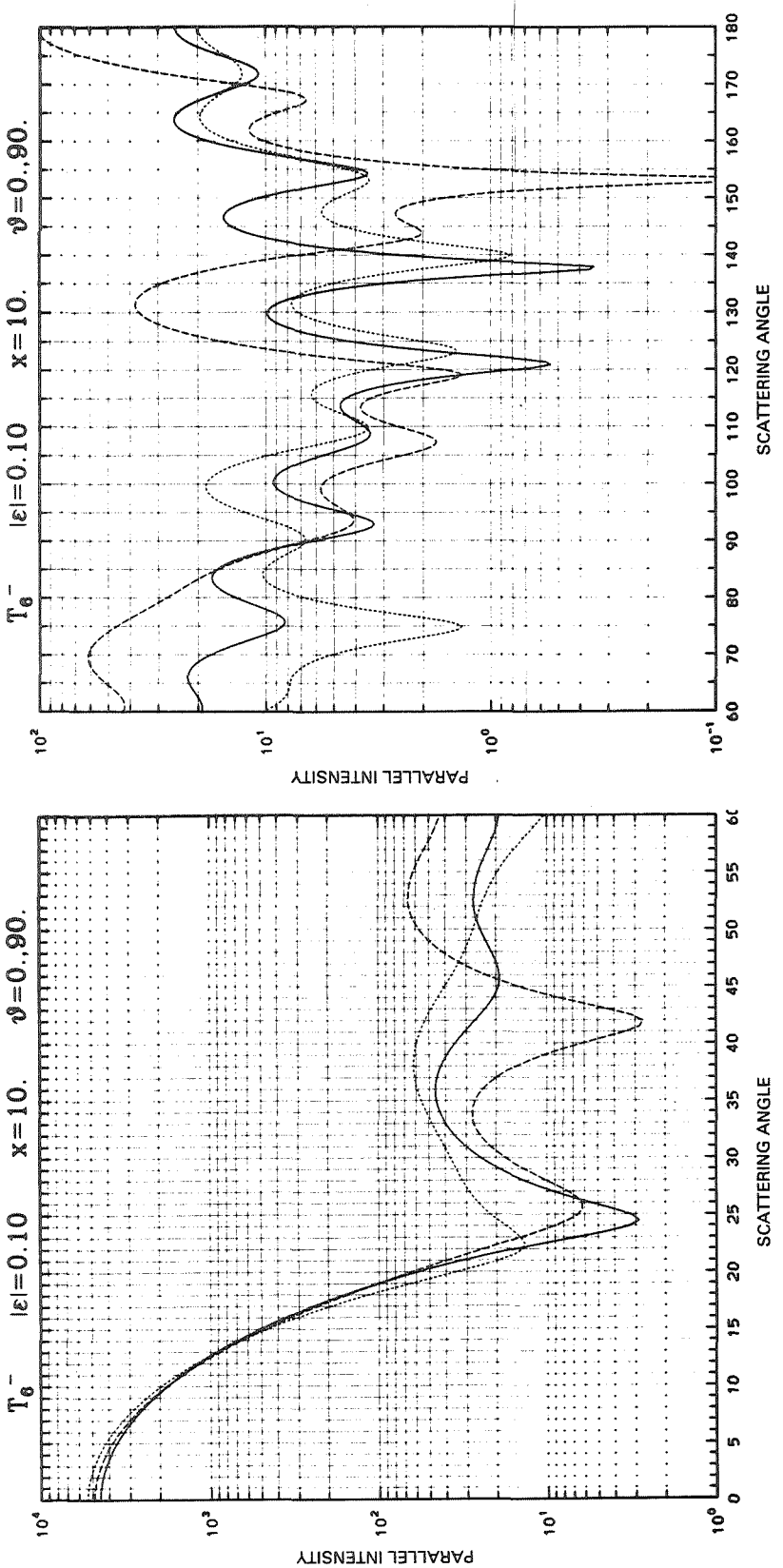

Appendix B (Continued)

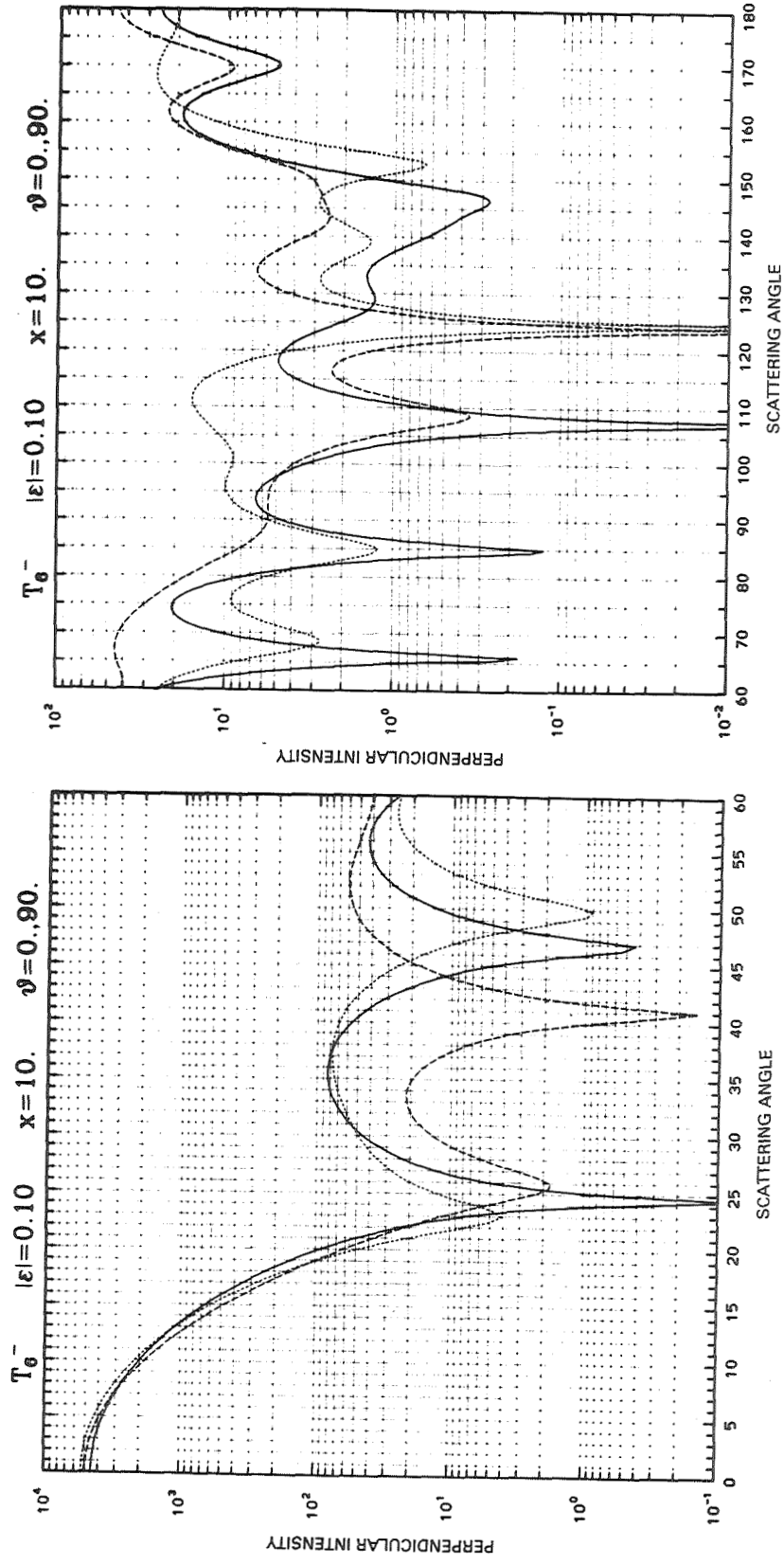

Appendix B (Continued)

APPENDIX C

Phase functions in the side- and back-scattering regime (60-180 degrees) vs. scattering angle for randomly oriented Chebyshev particles T_3, T_2, T_4, T_6, and T_8; for various deformation parameters between -0.20 and 0.20 (as shown above each plot); and for size parameters $x = 2,3,4,5,6,8,10,15$, and 20. Solid line is for $\Delta x = 0.1x$ size-averaged spherical result, interrupted lines are for non-sheres: dotted, dashed, and dot-dash lines refer to the various ϵ values shown, in increasing order (in general, the larger the value of $|\epsilon|$, the greater the general deviation from the spherical result). Not all particles are represented at larger values of x because of an inability to achieve satisfactory convergence of the EBCM.

Next to each phase function plot is a plot of the percentage deviations of the nonspherical phase functions from the spherical one, but for the full range of angles (0–180 degrees) rather than just 60–180 degrees. The interrupted lines in these plots refer to the same nonspherical particles as in the adjacent phase function plot. Note that when the percentage differences become larger than about 100% the vertical scale becomes logarithmic, and in order to display both positive and negative values, percentages smaller than 1% in magnitude are assumed to be zero.

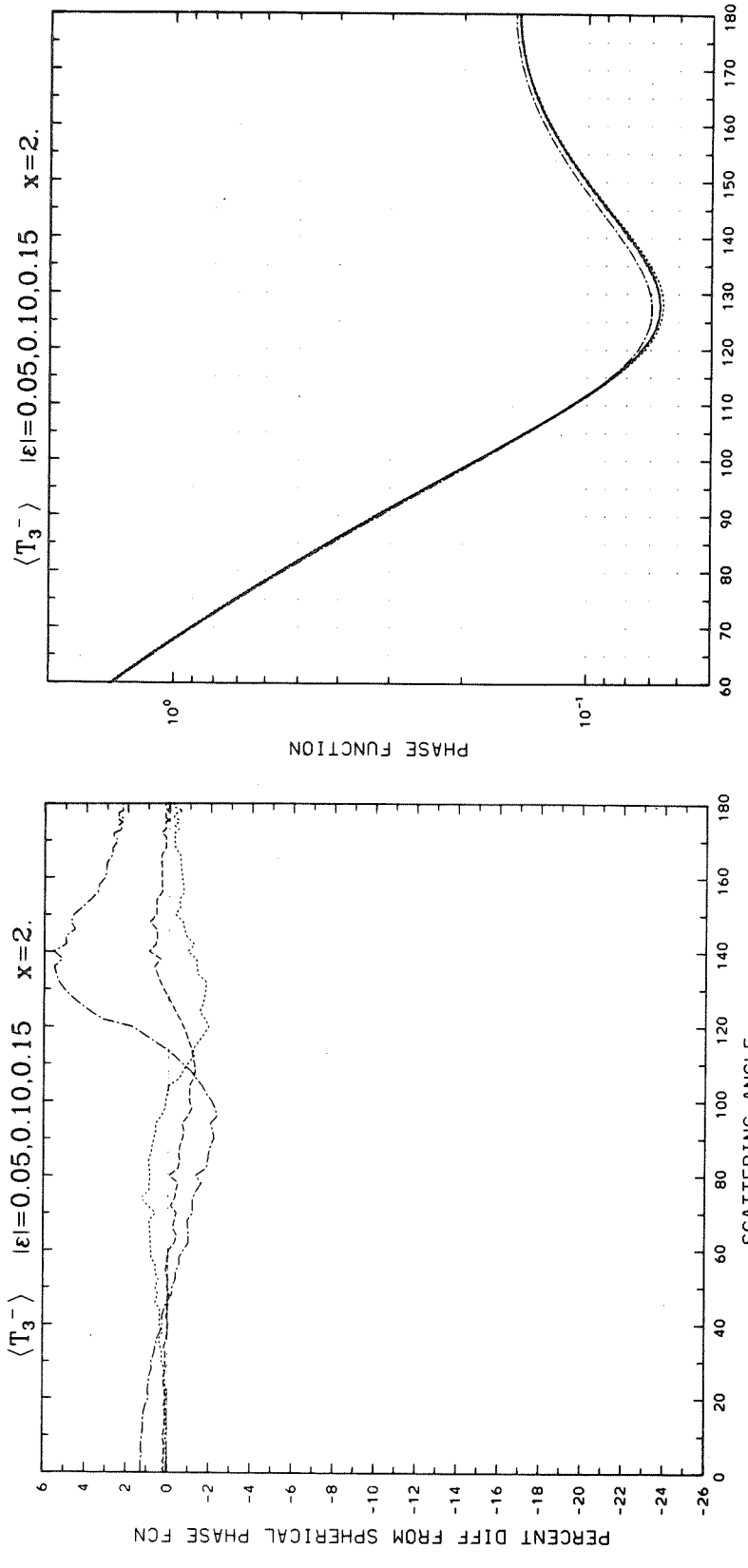

Appendix C. PHASE FUNCTIONS for Chebyshev particles in random orientation vs. ANGLE (60°-180°); PERCENT DIFFERENCES between these nonspherical and various spherical phase functions, vs. ANGLE (0°-180°).

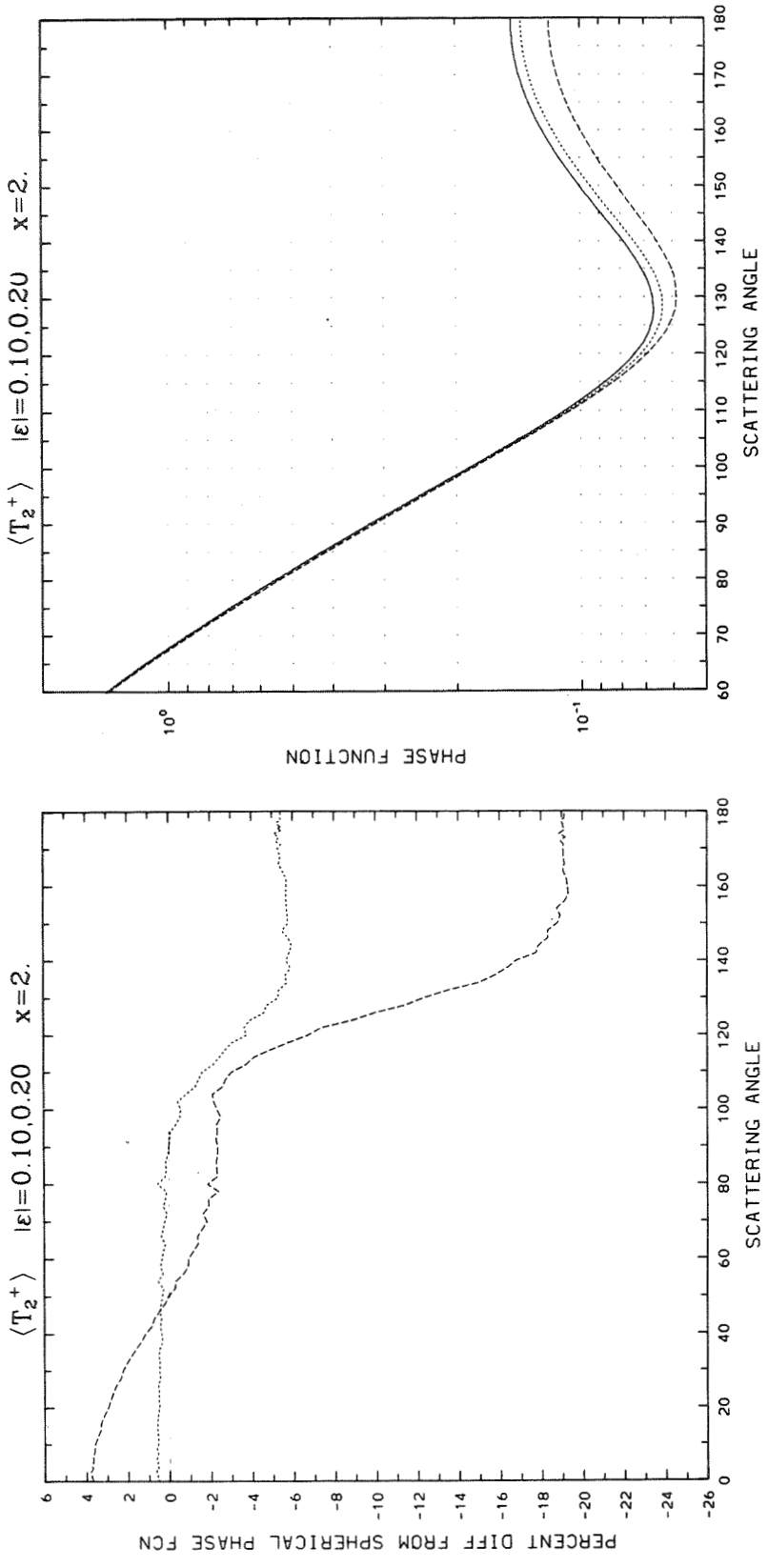

Appendix C (Continued)

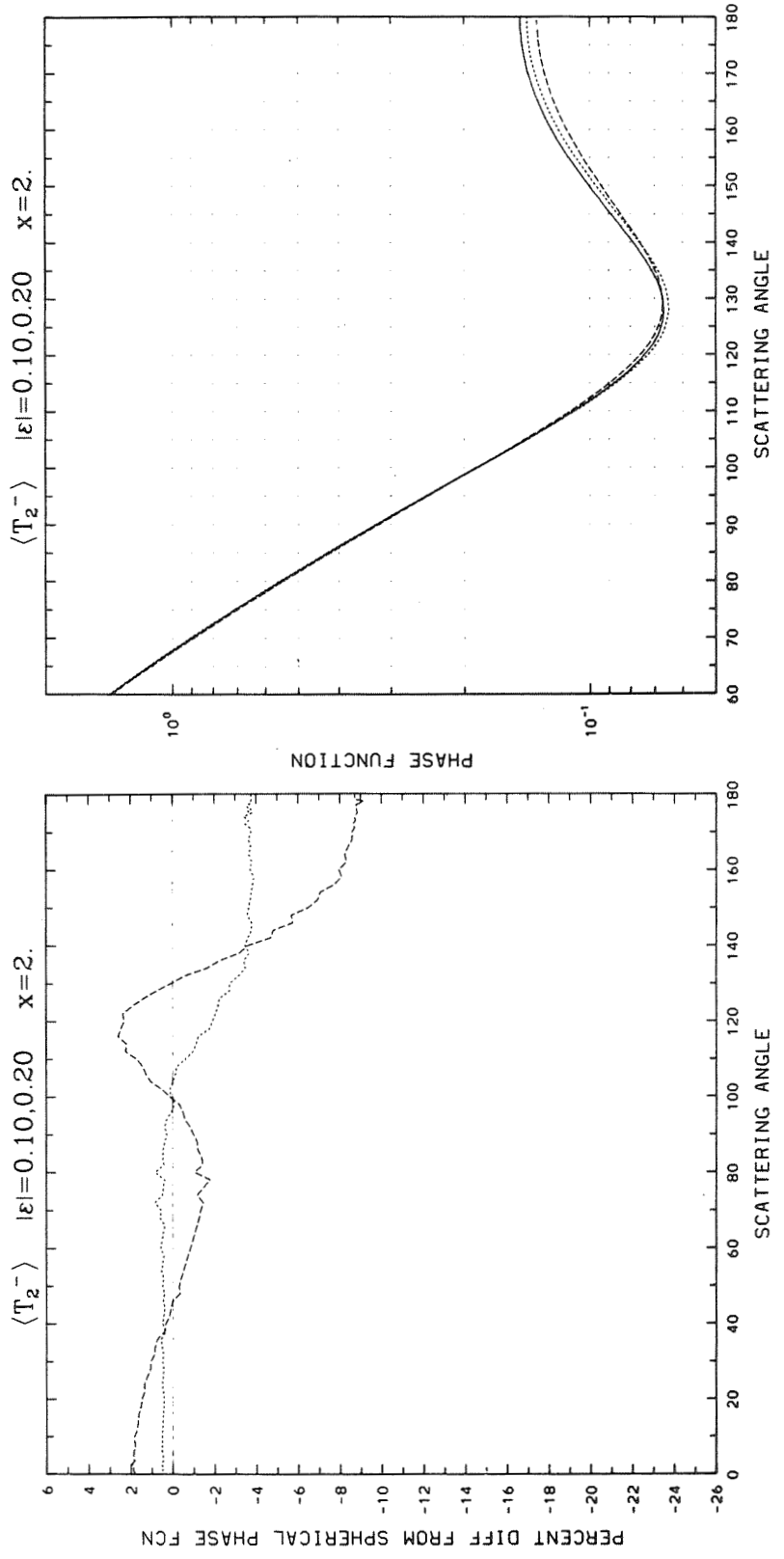

Appendix C (Continued)

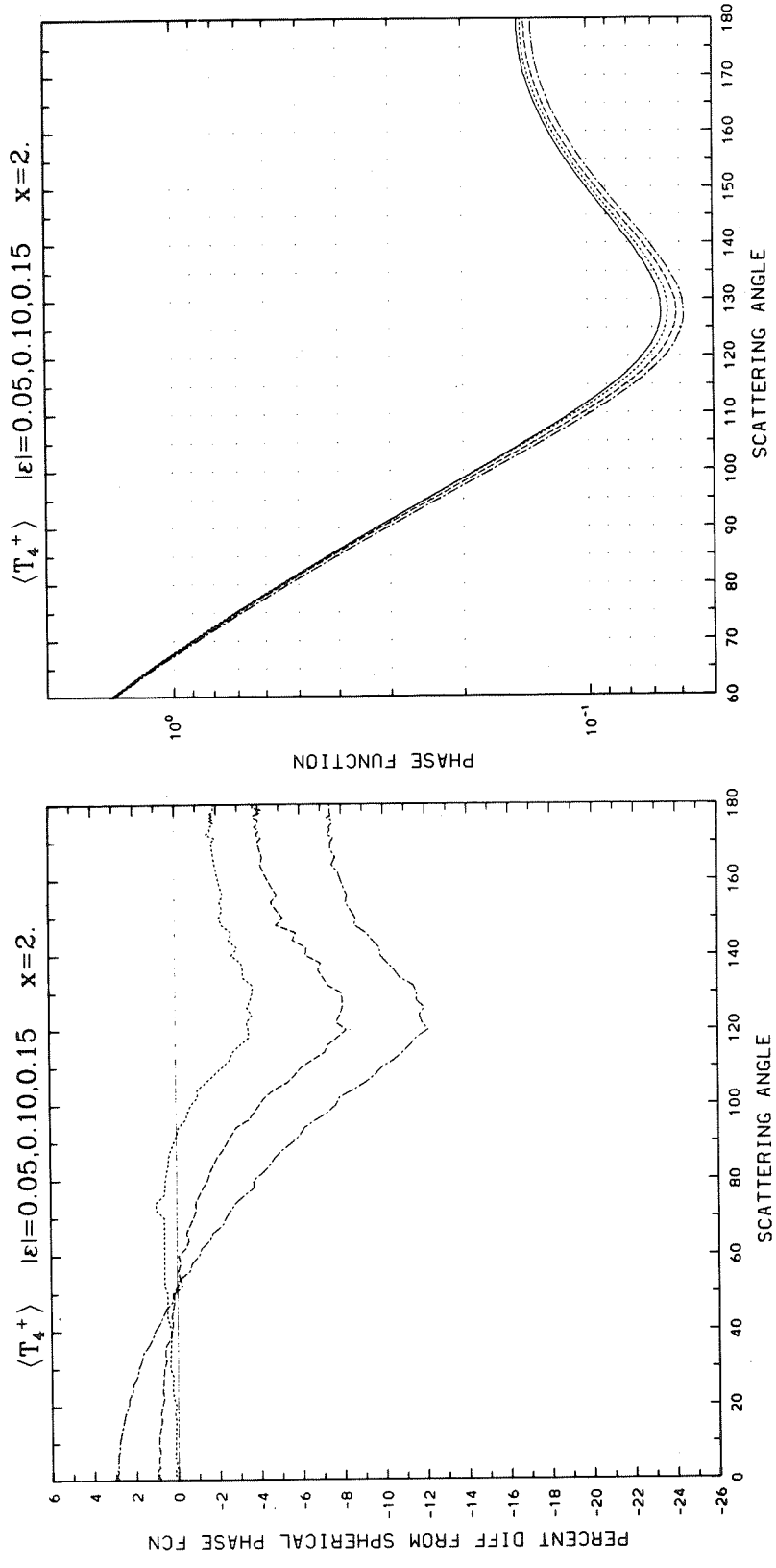

Appendix C (Continued)

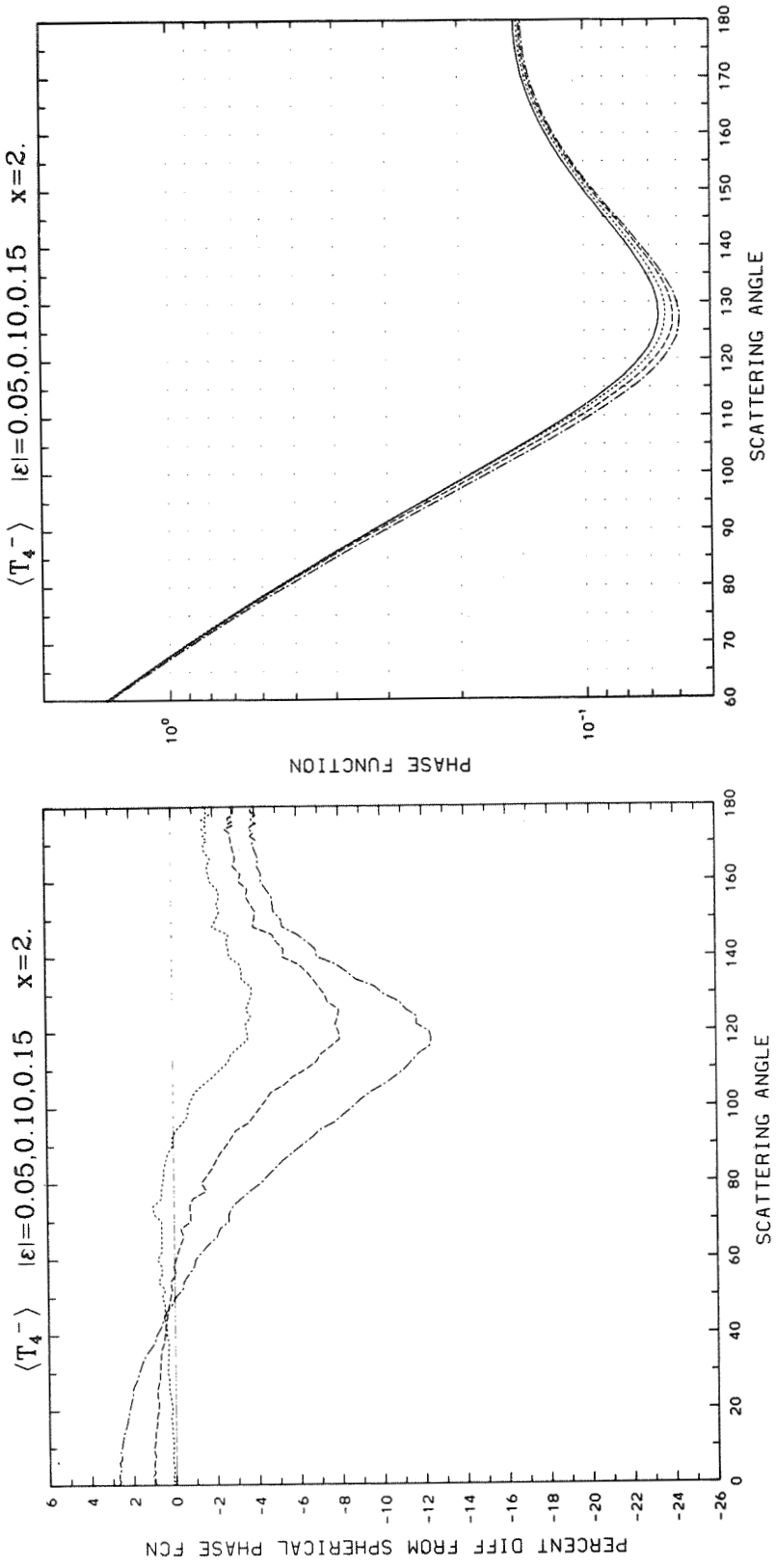

Appendix C (Continued)

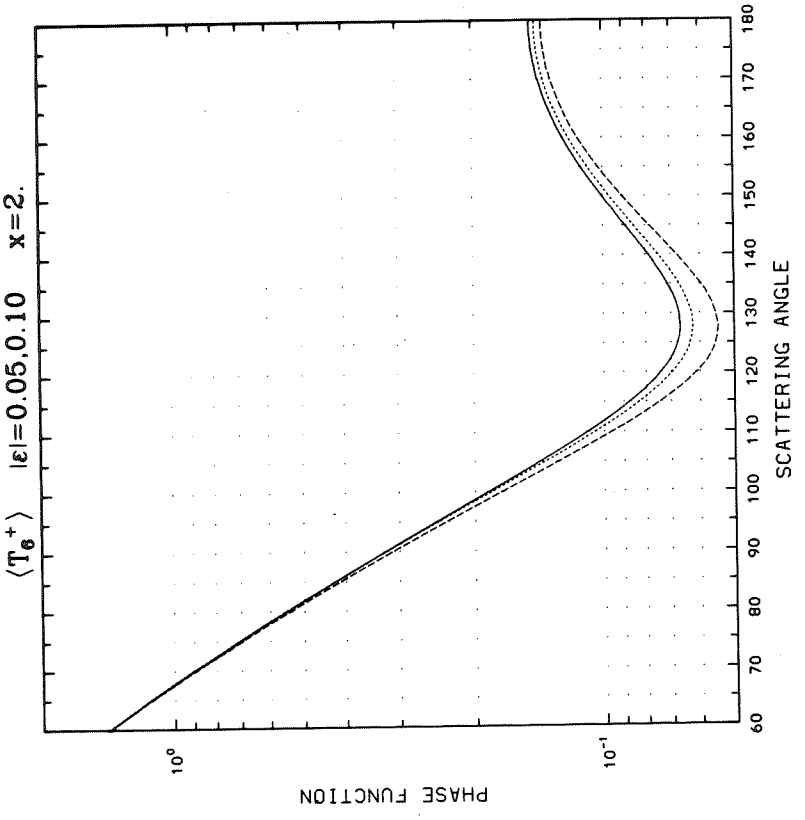

Appendix C (Continued)

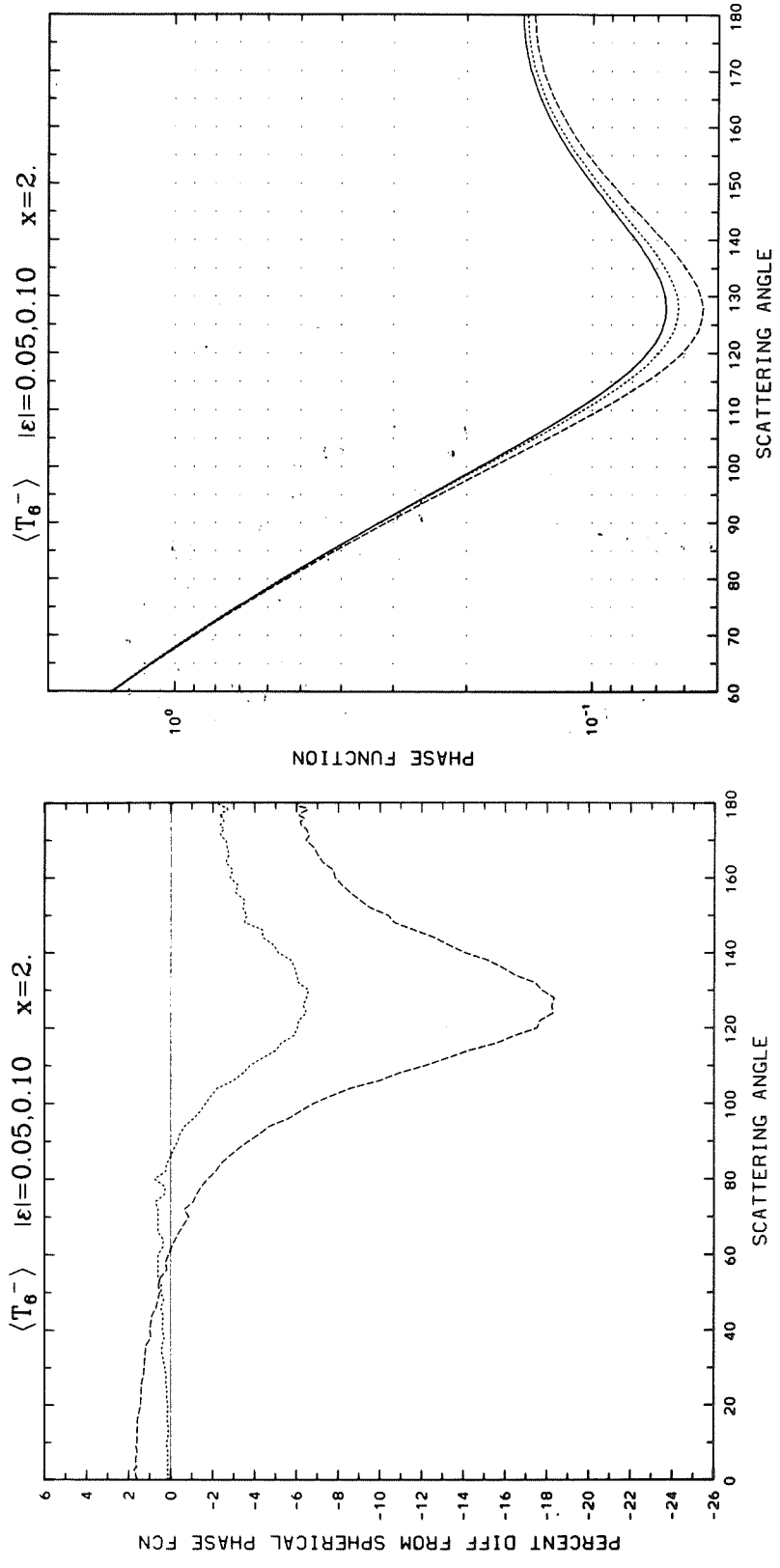

Appendix C (Continued)

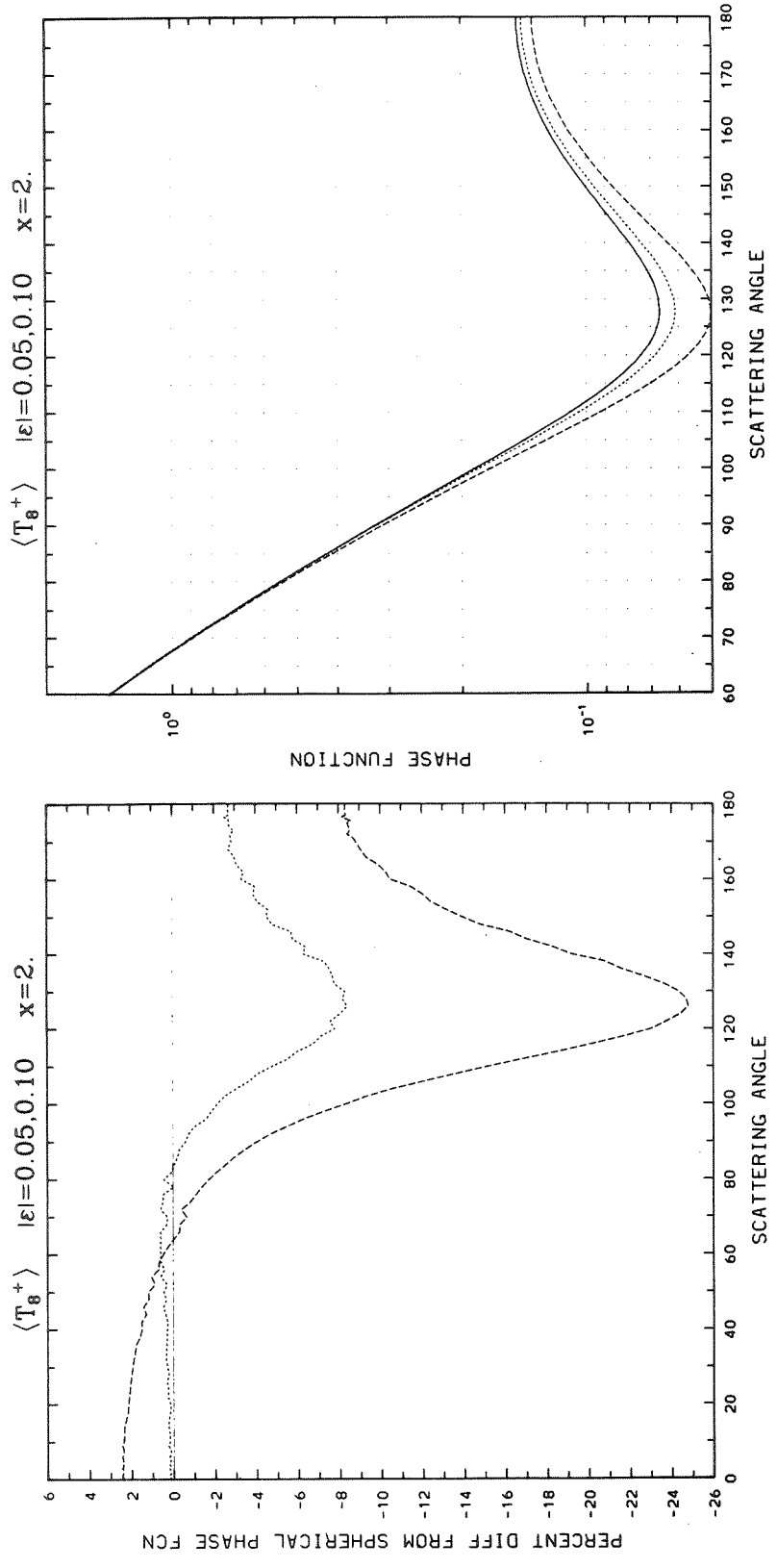

Appendix C (Continued)

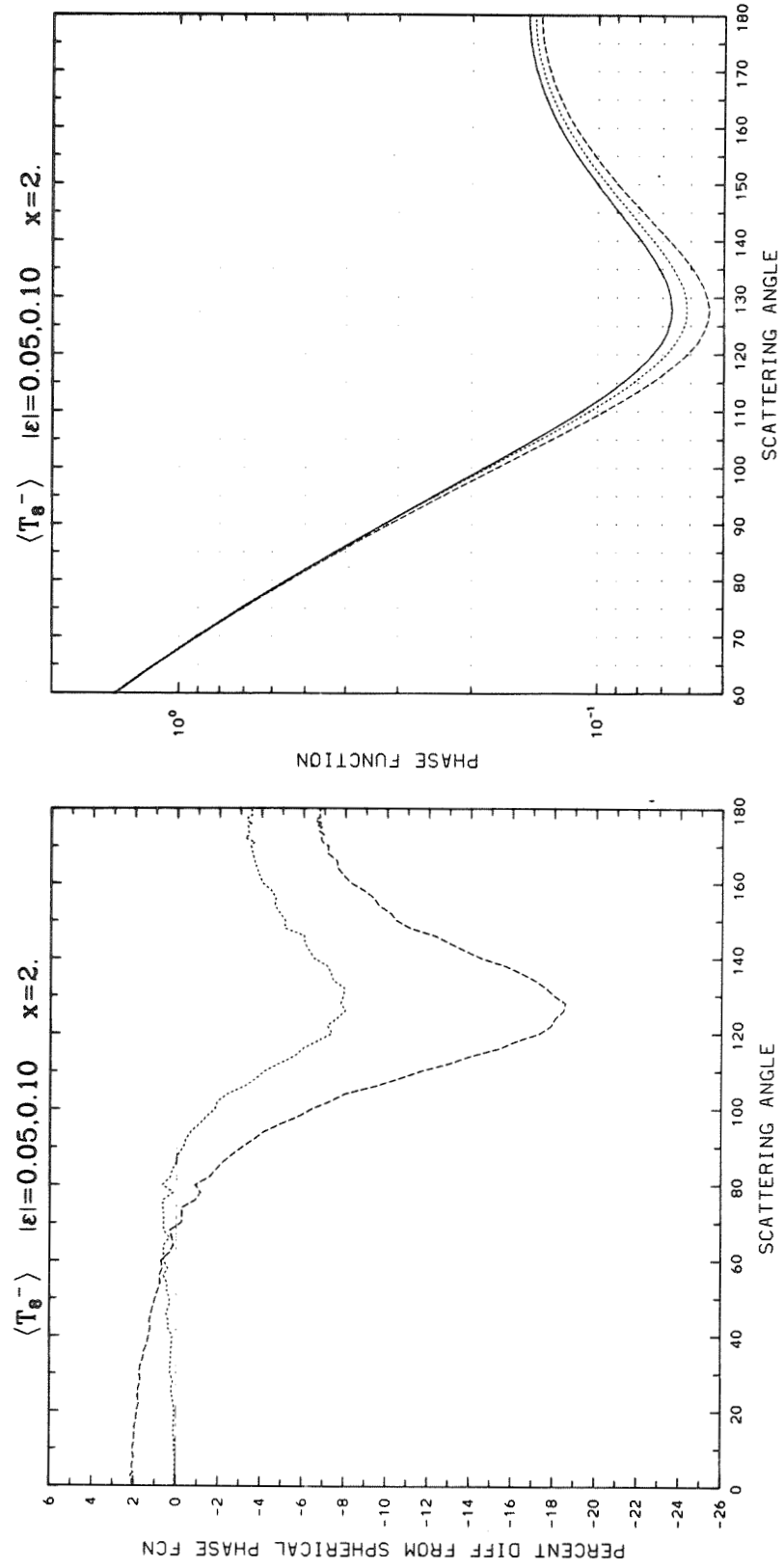

Appendix C (Continued)

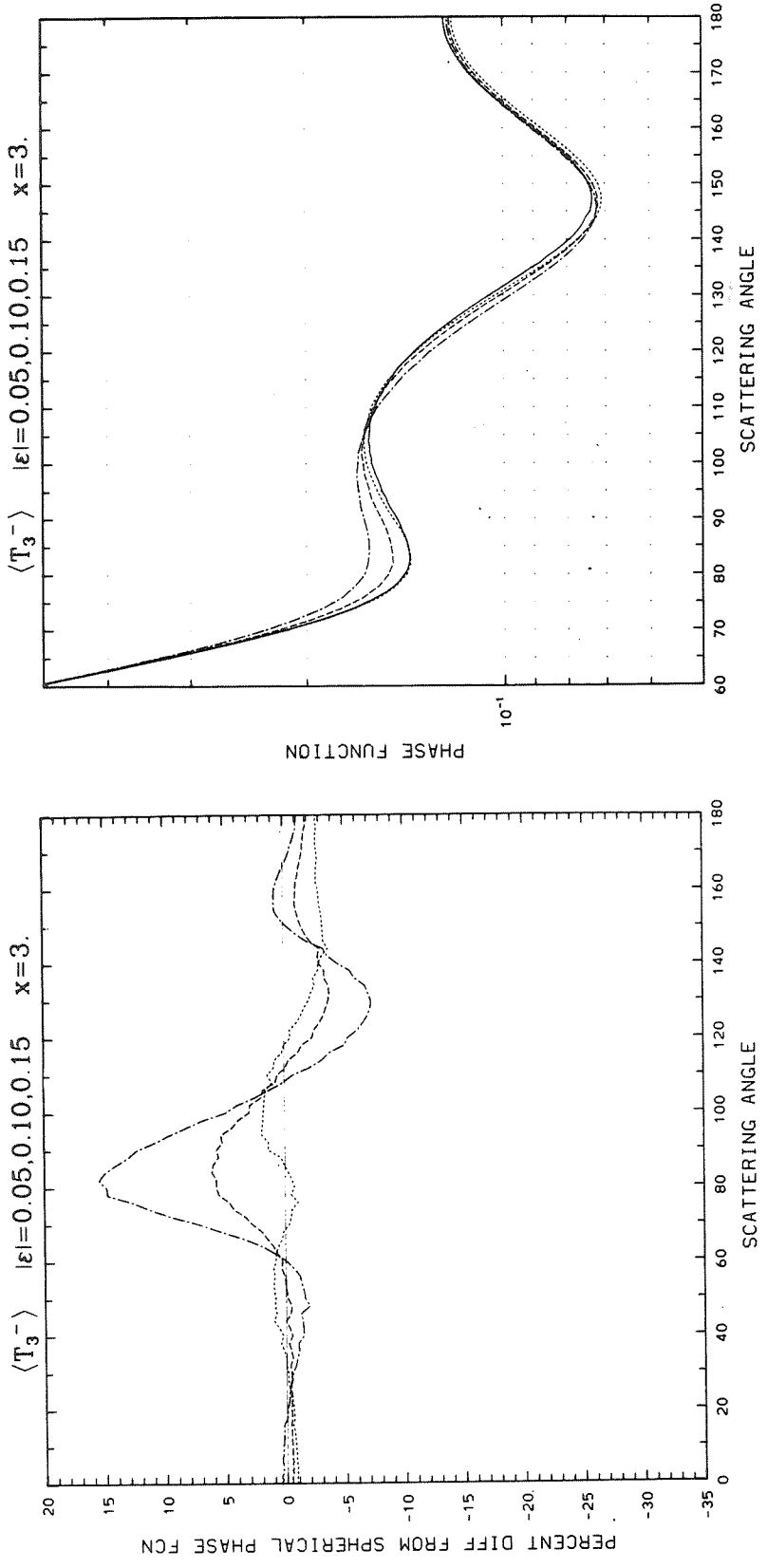

Appendix C (Continued)

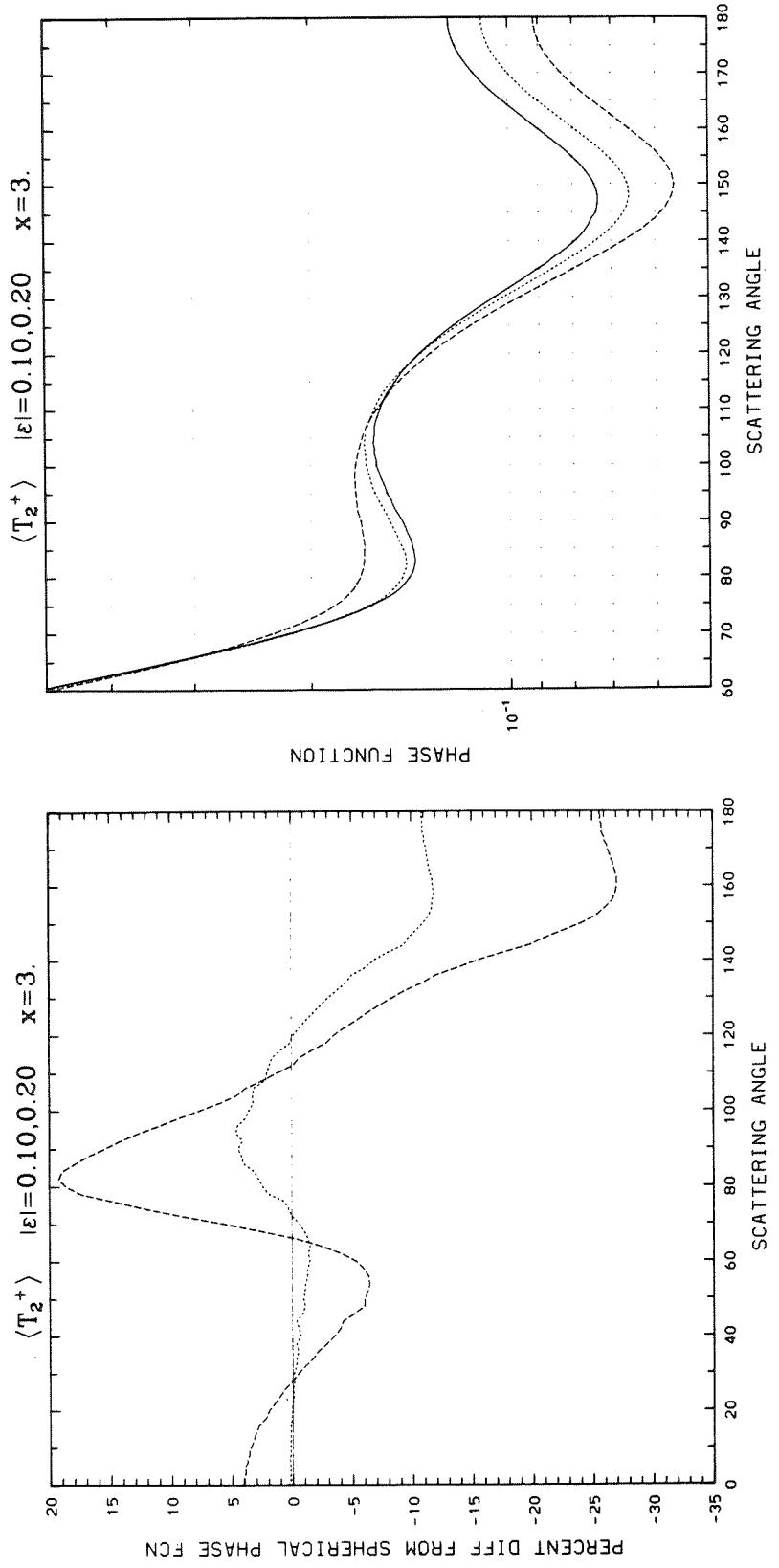

Appendix C (Continued)

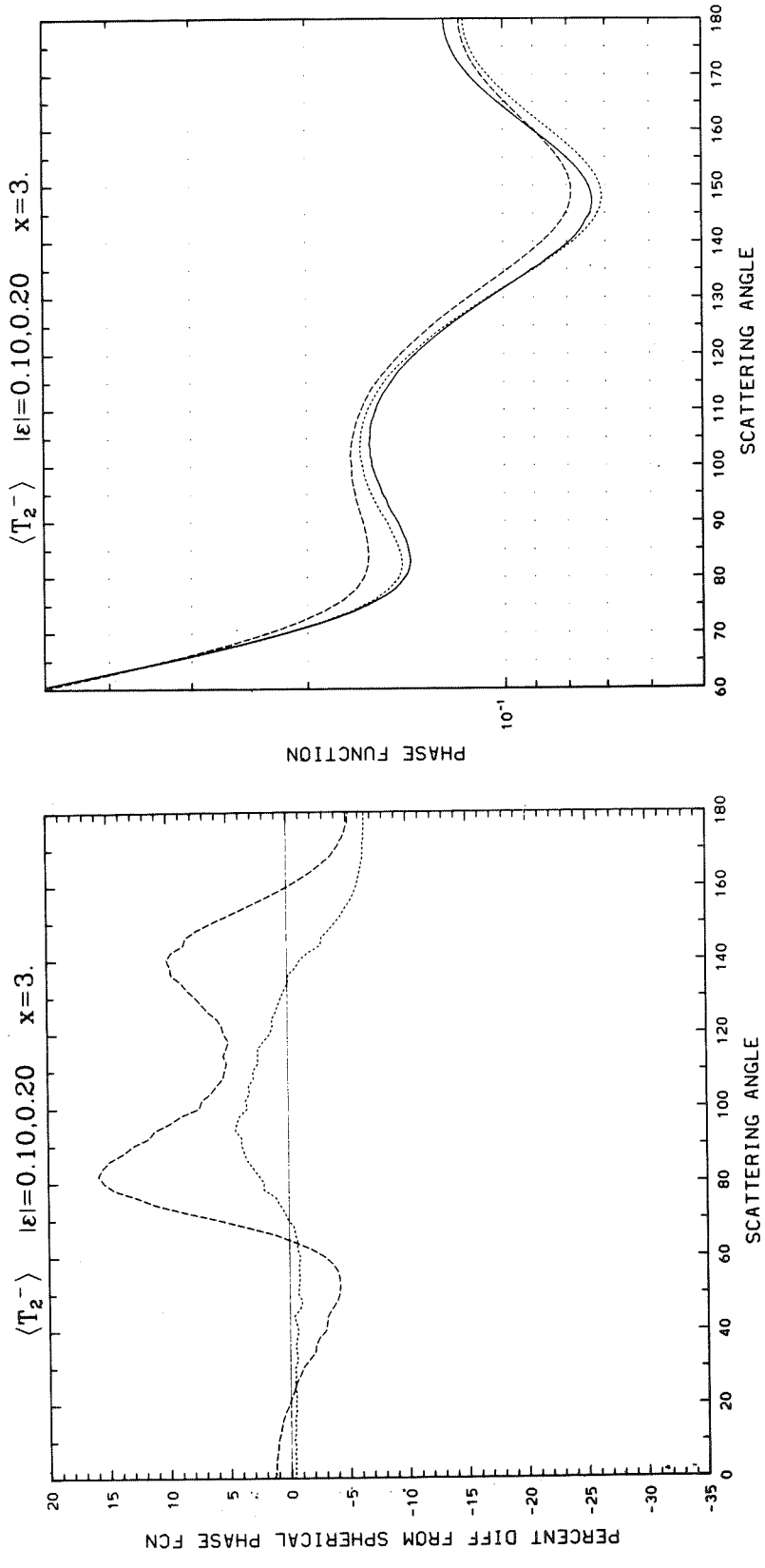

Appendix C (Continued)

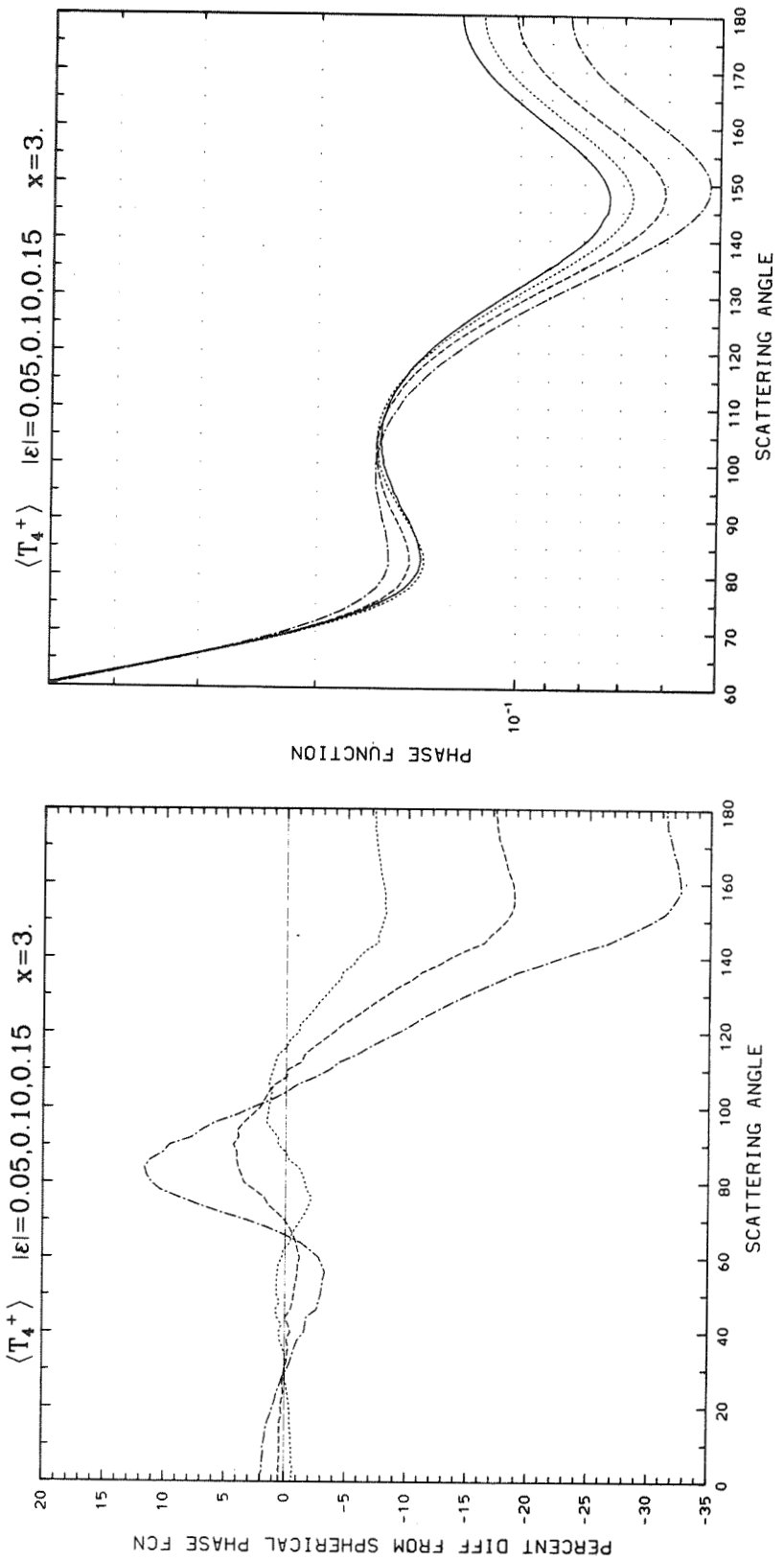

Appendix C (Continued)

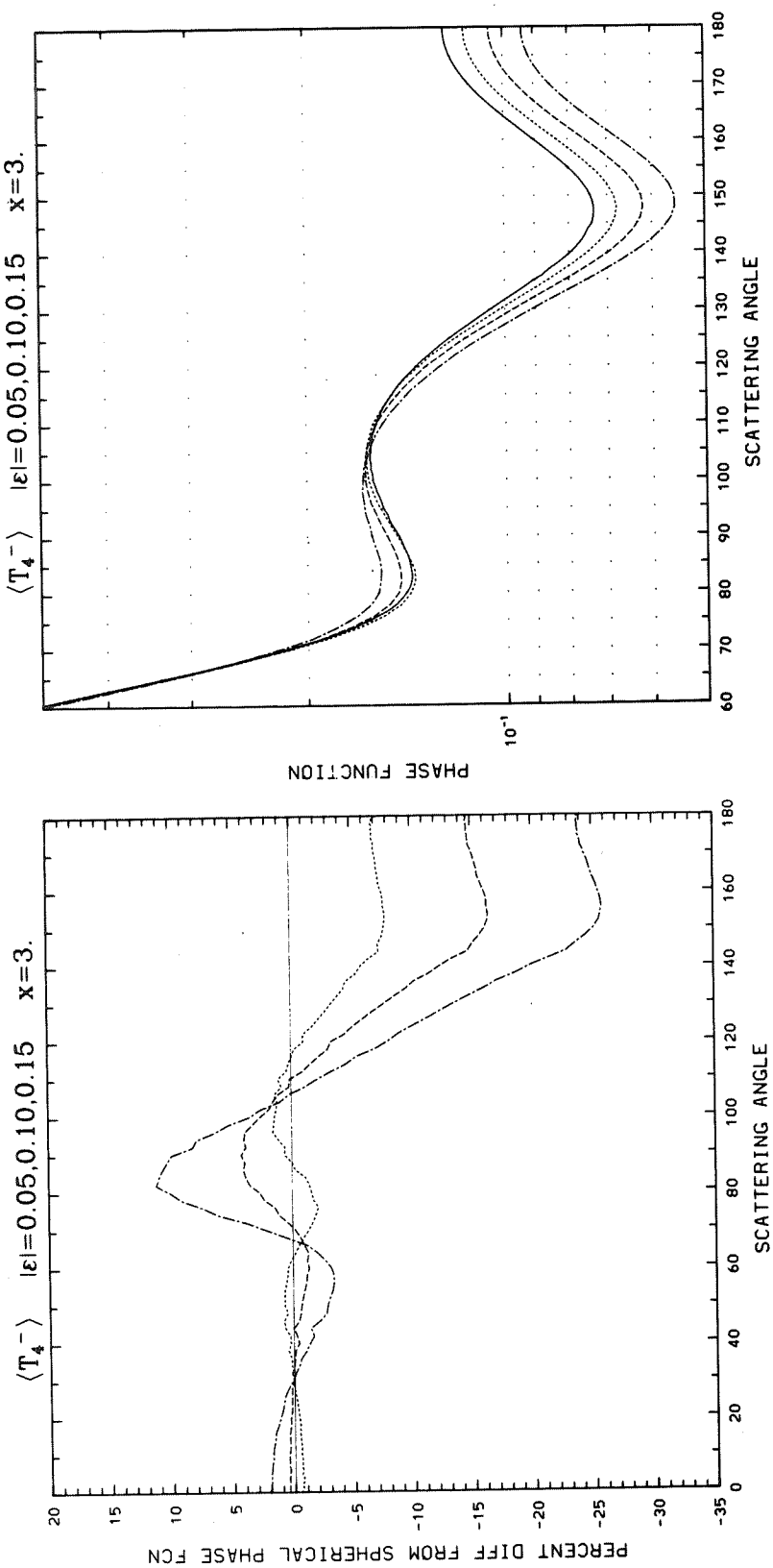

Appendix C (Continued)

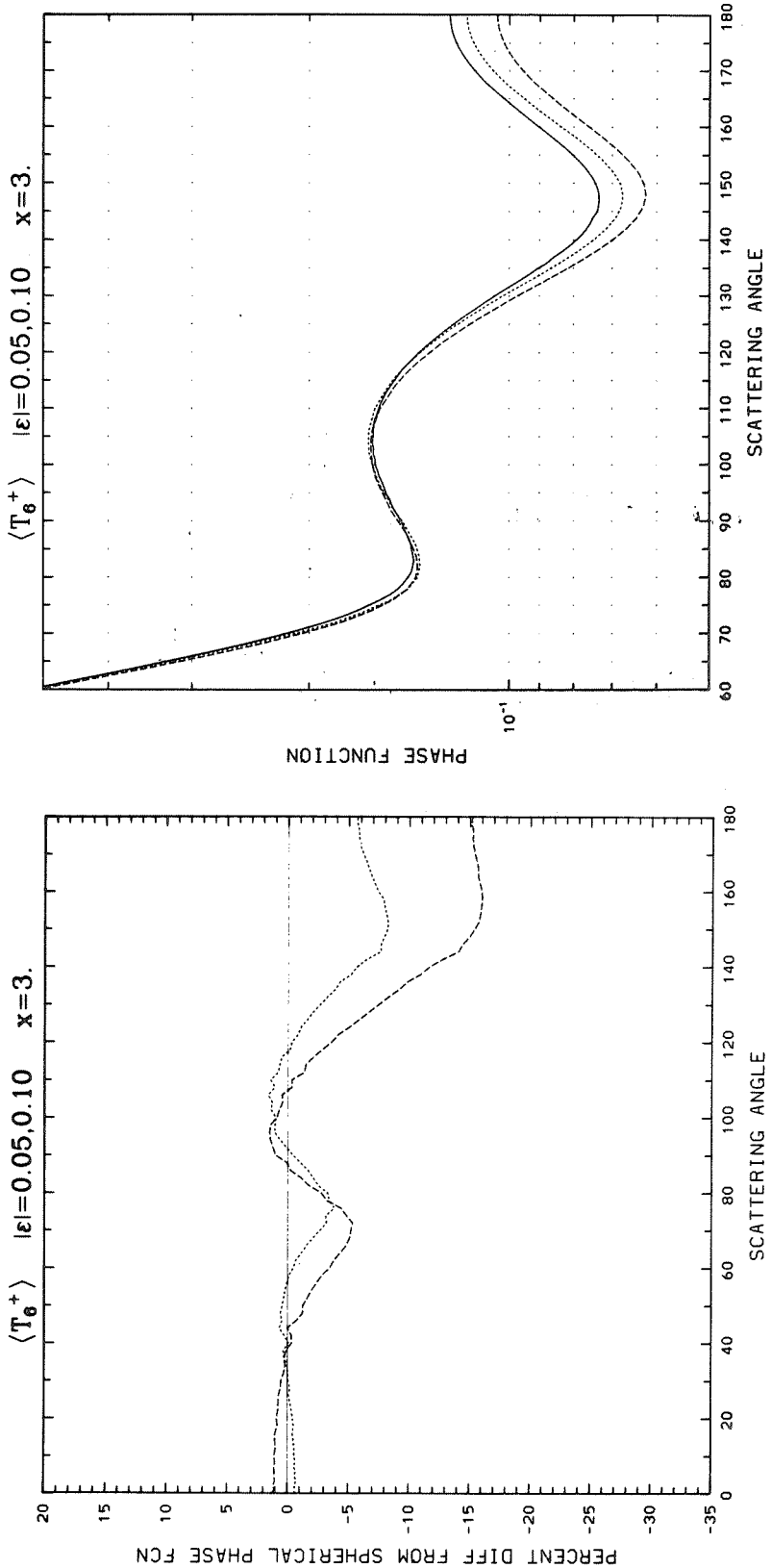

Appendix C (Continued)

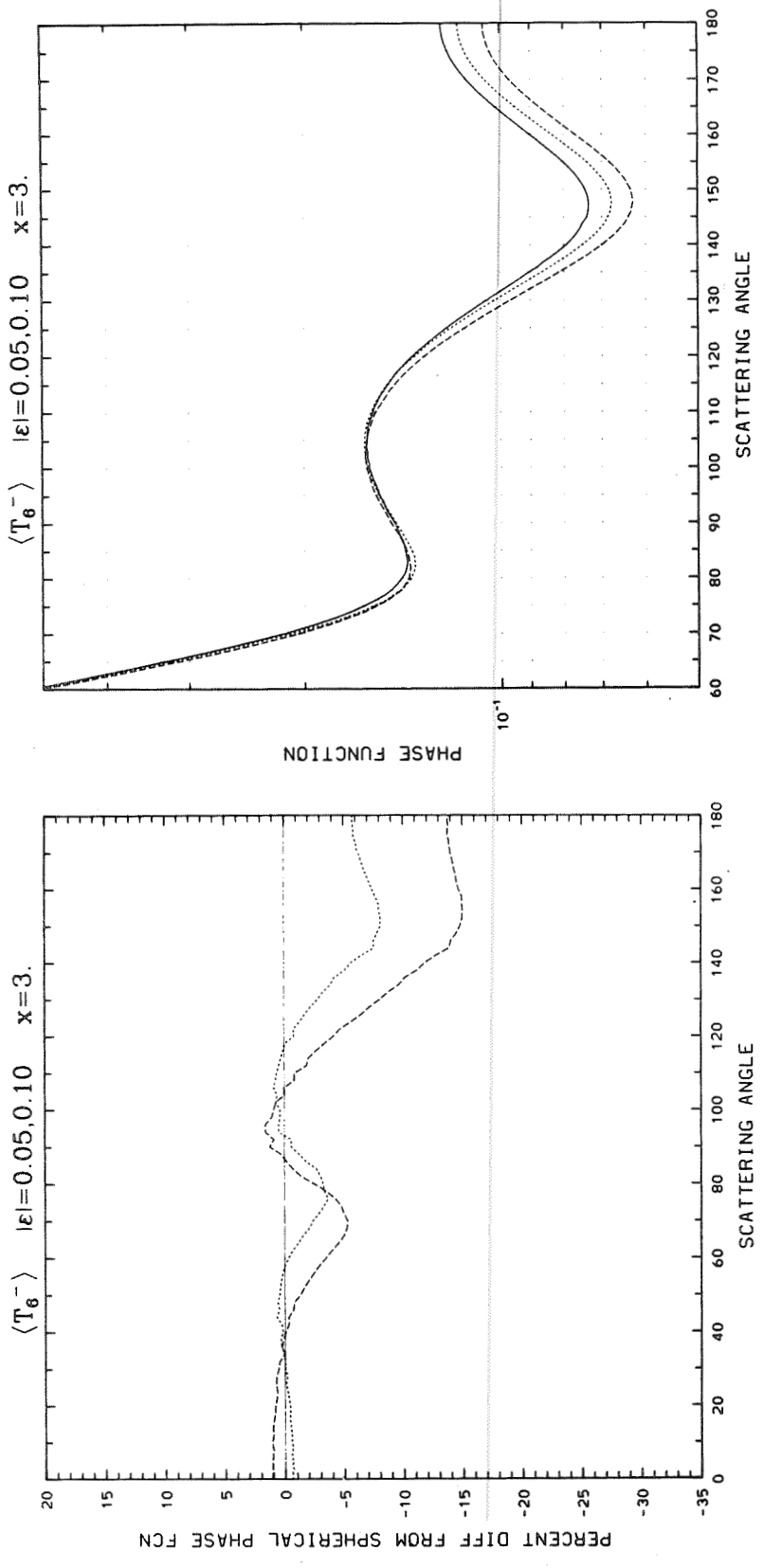

Appendix C (Continued)

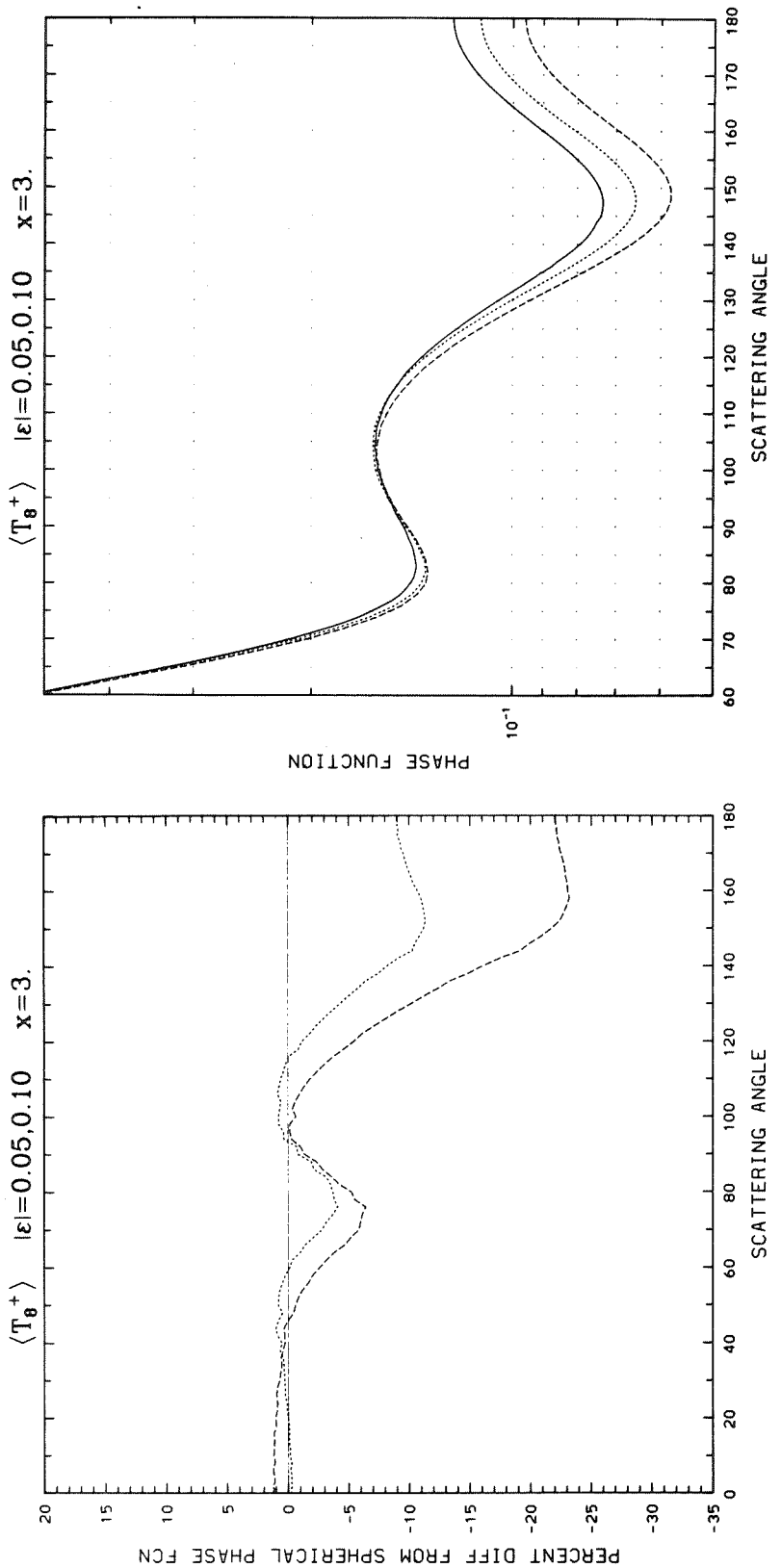

Appendix C (Continued)

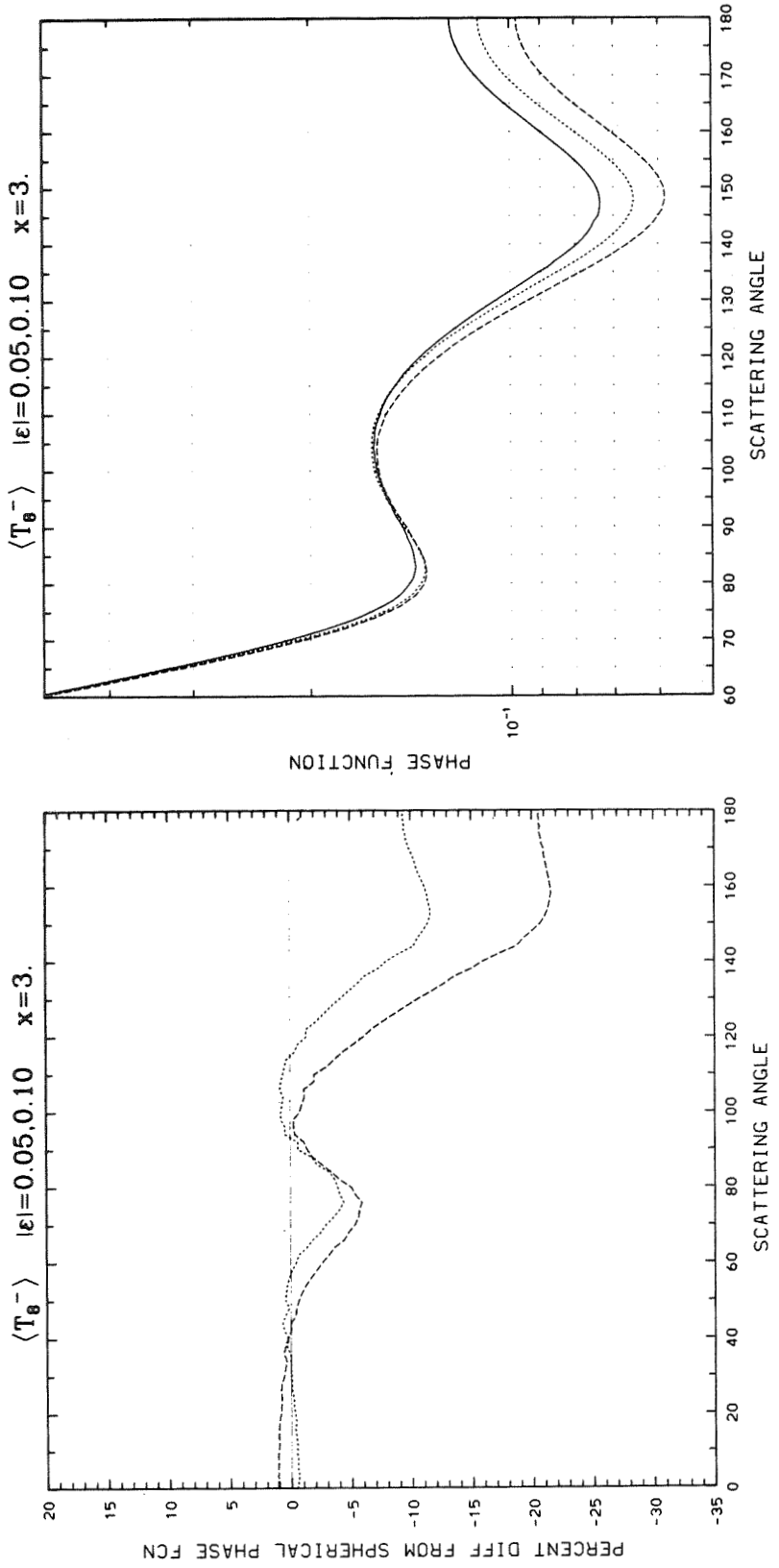

Appendix C (Continued)

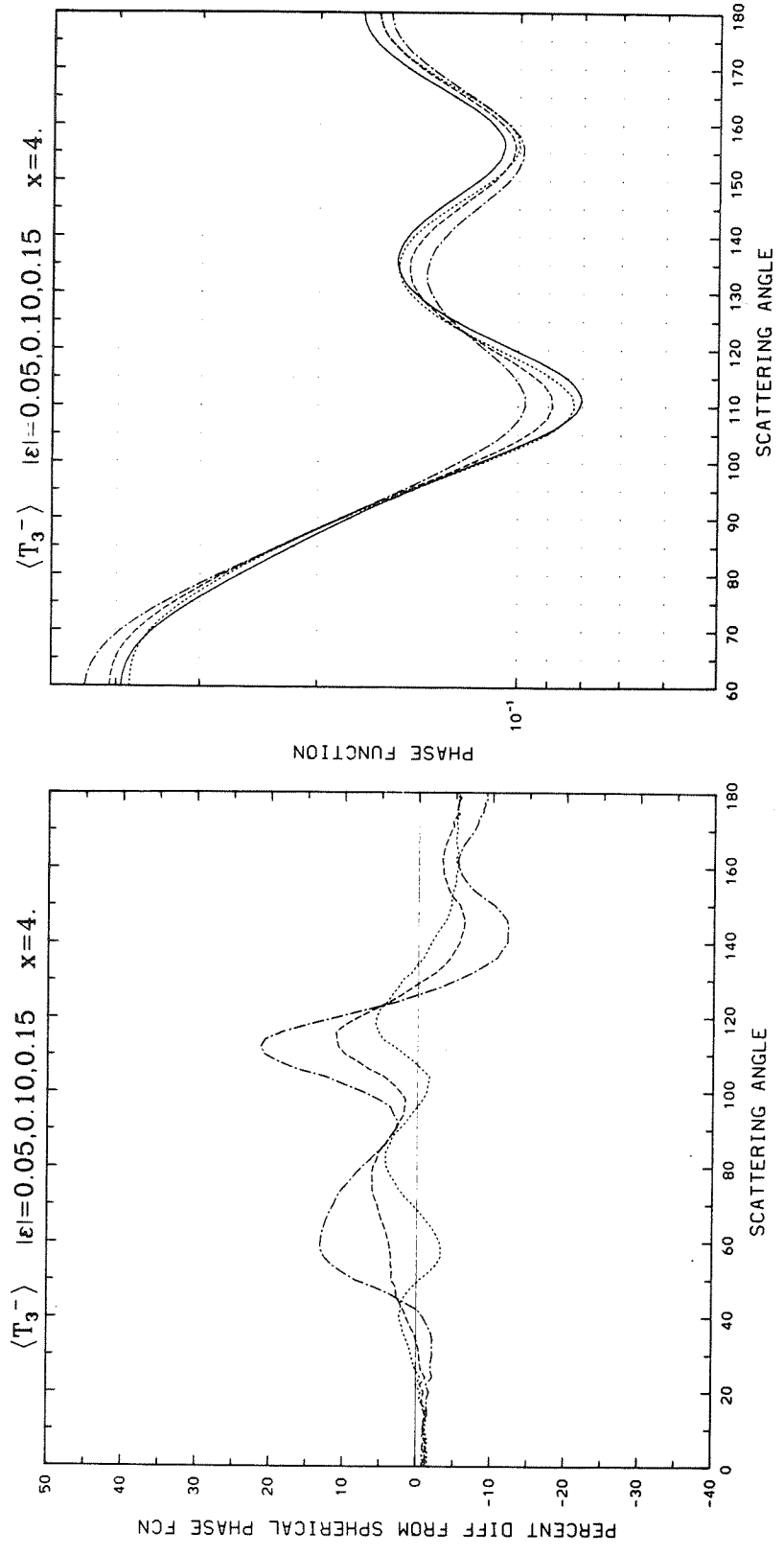

Appendix C (Continued)

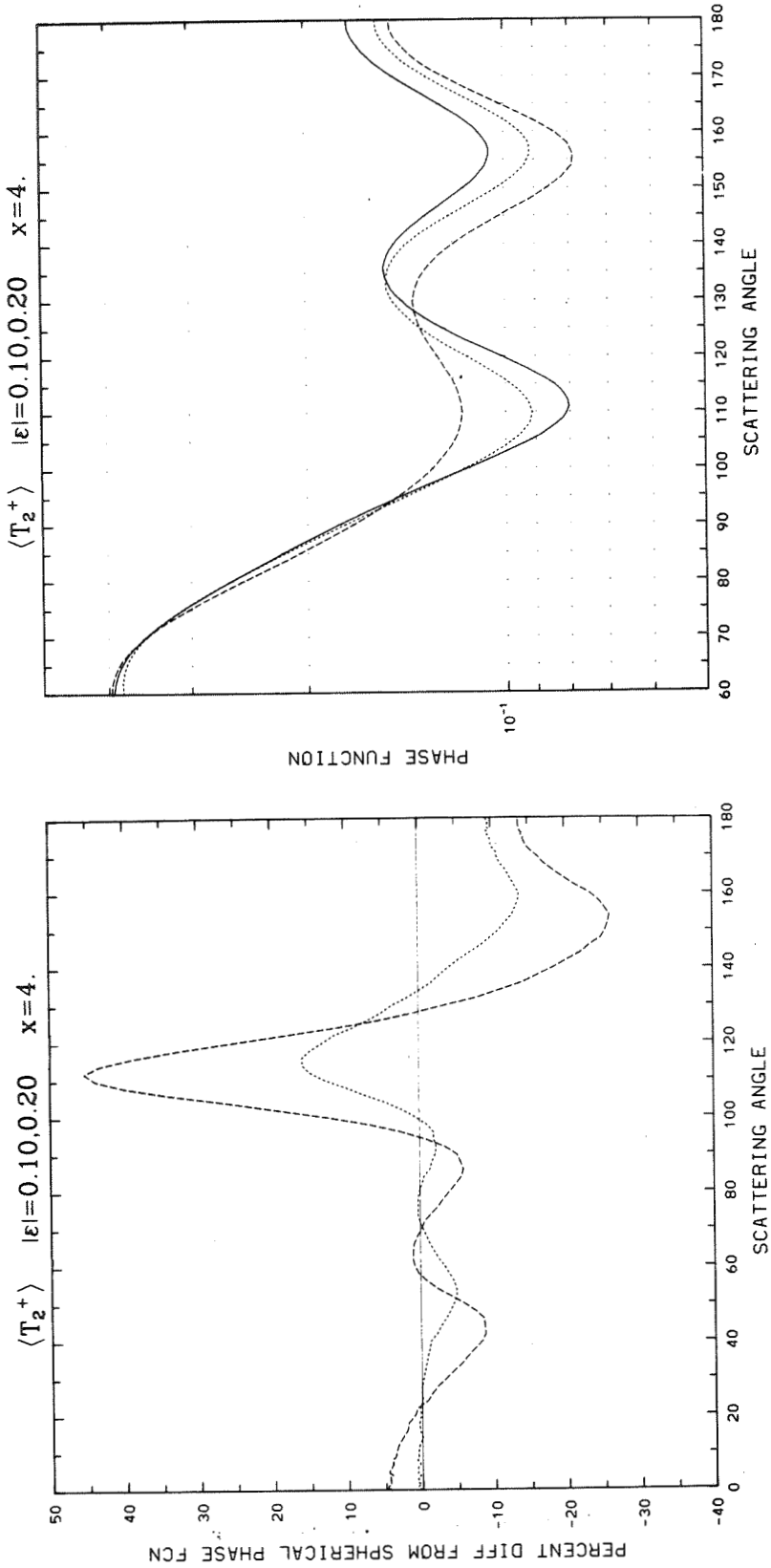

Appendix C (Continued)

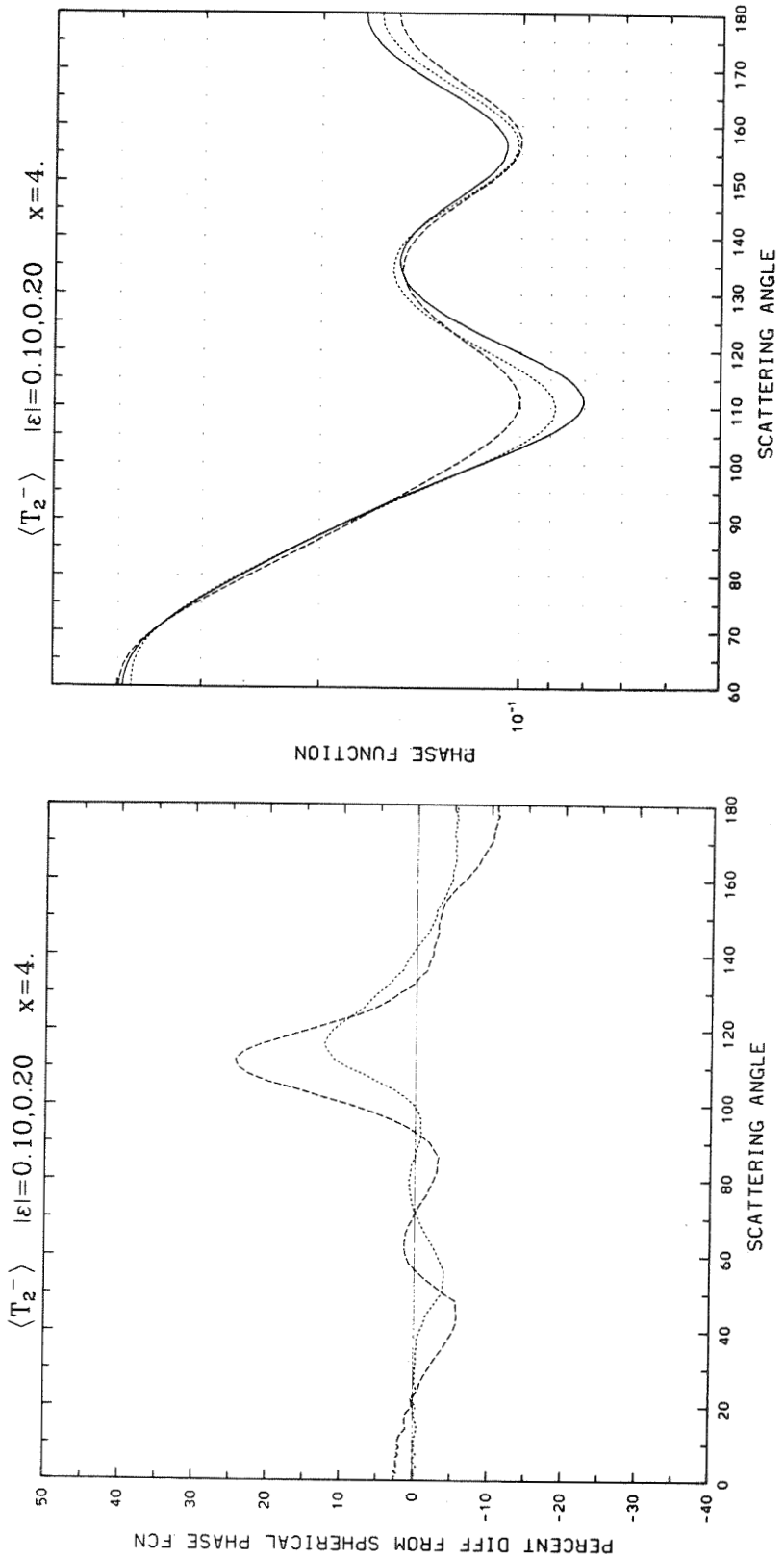

Appendix C (Continued)

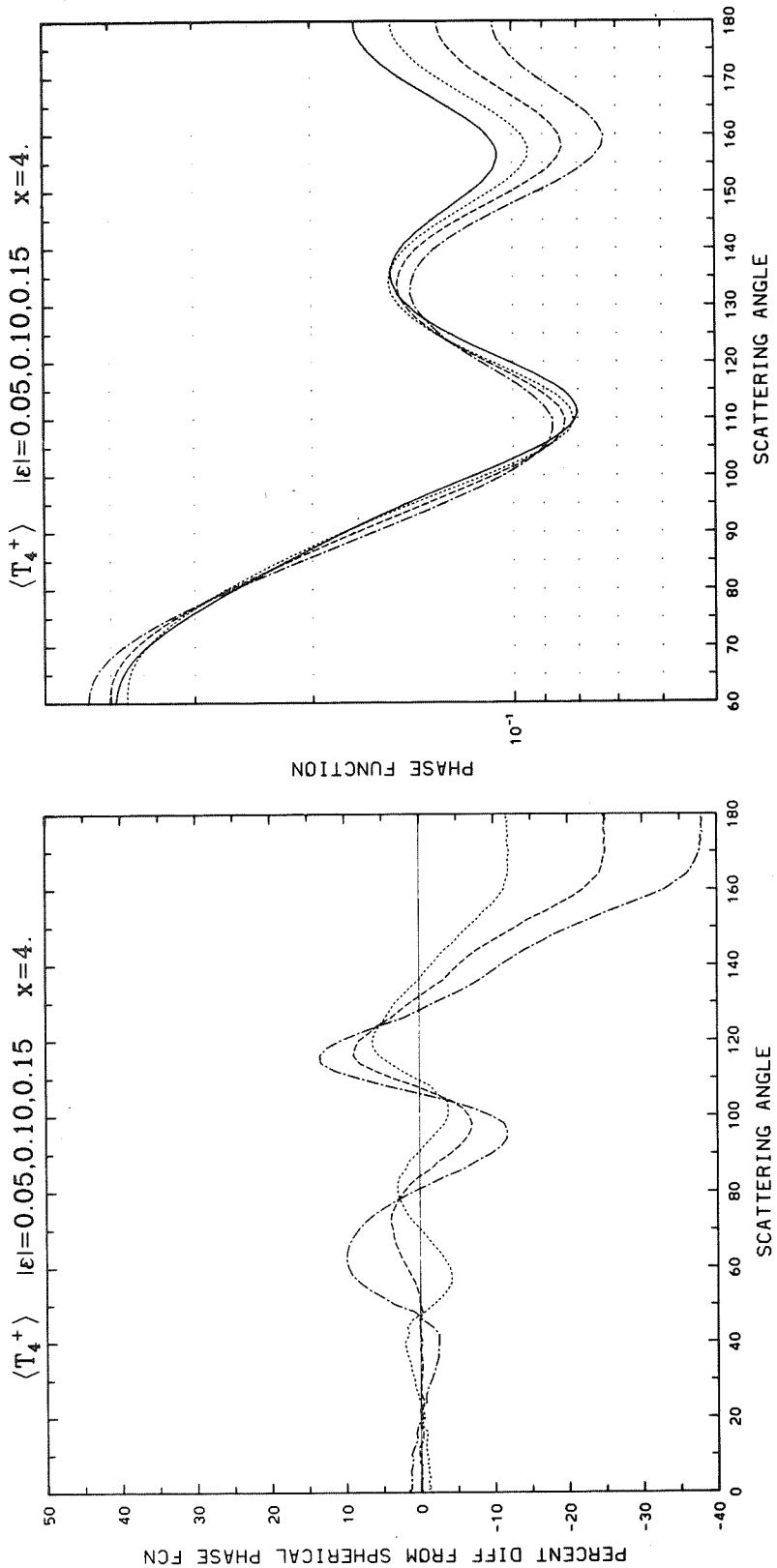

Appendix C (Continued)

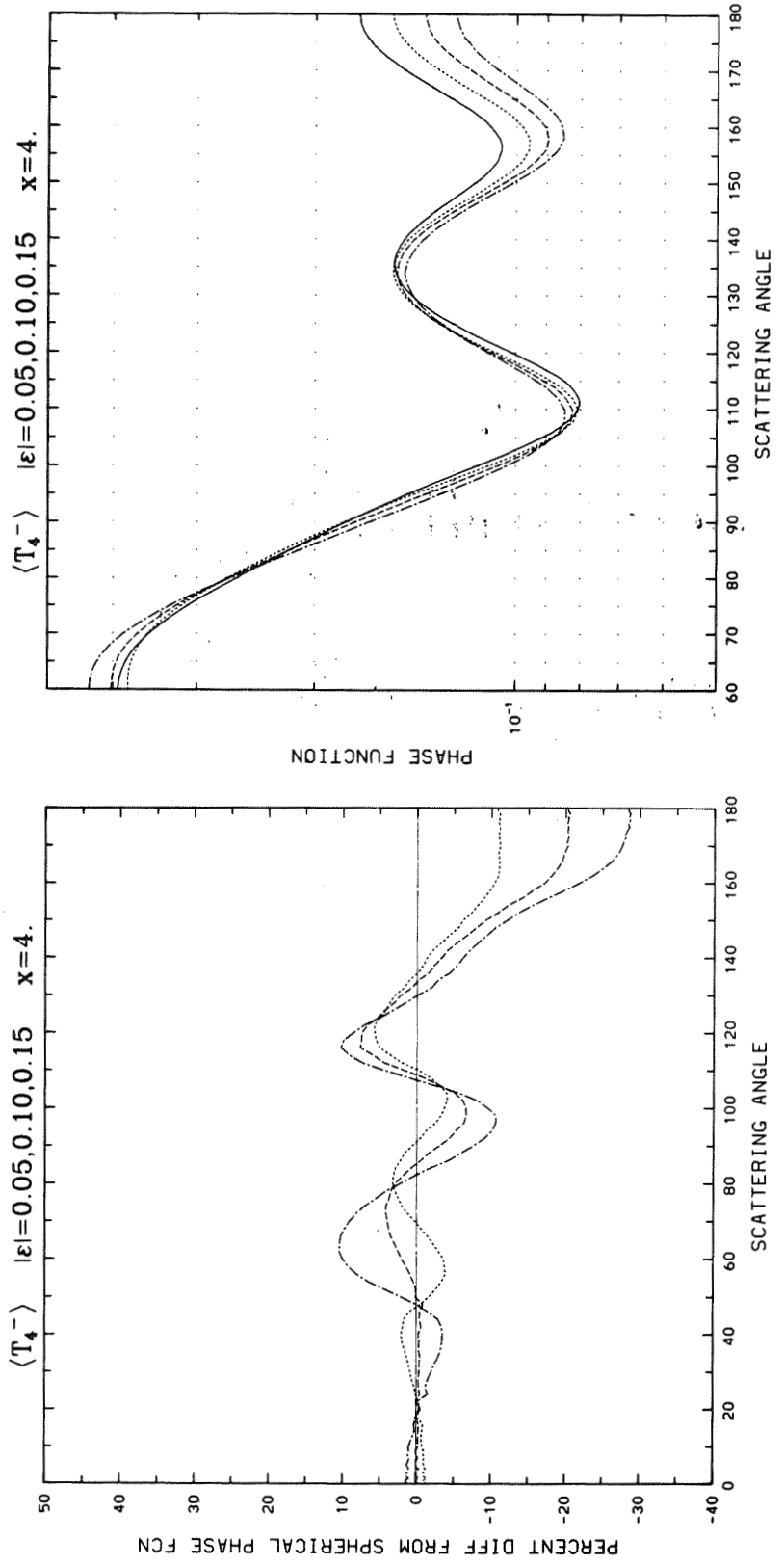

Appendix C (Continued)

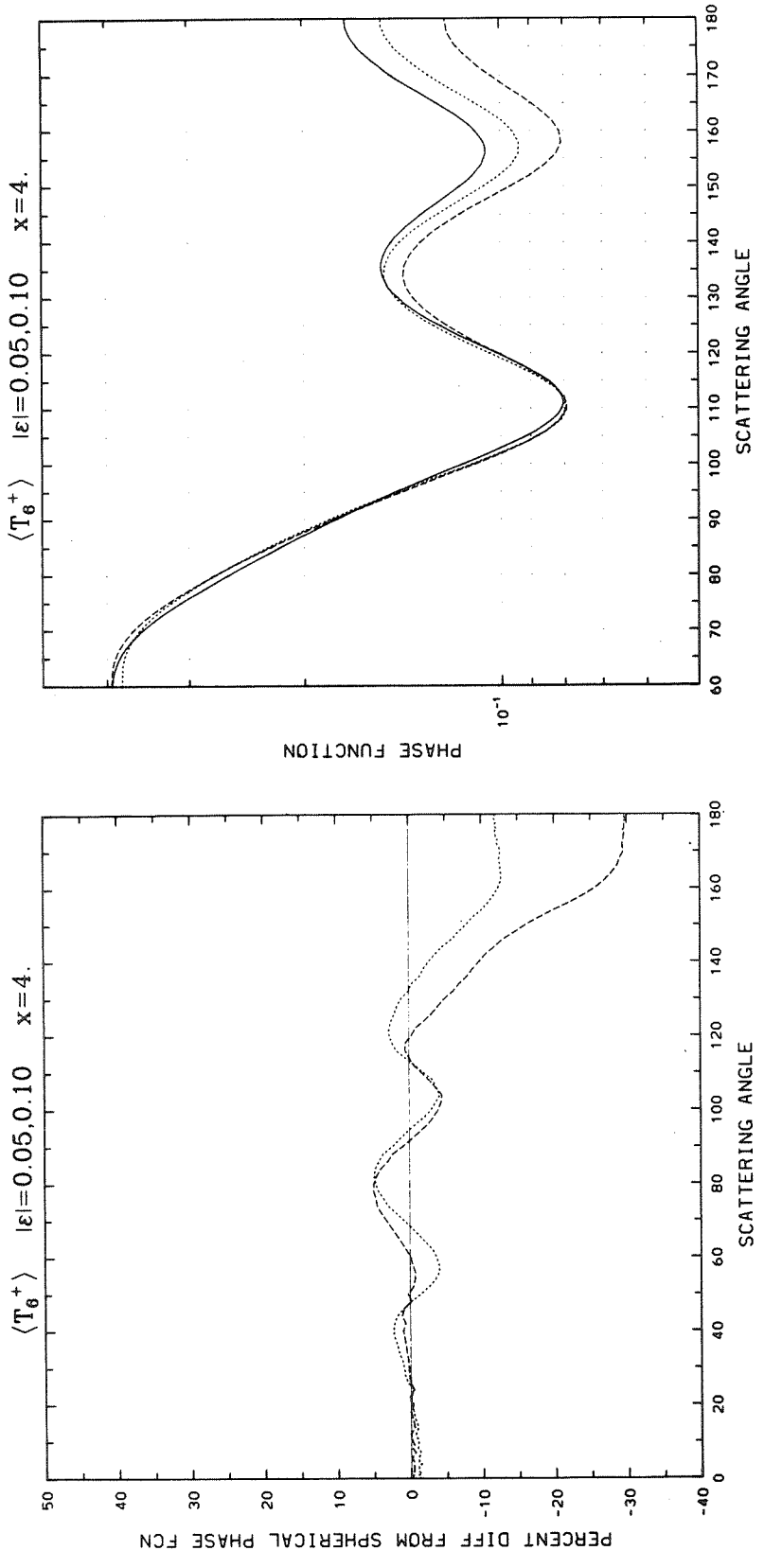

Appendix C (Continued)

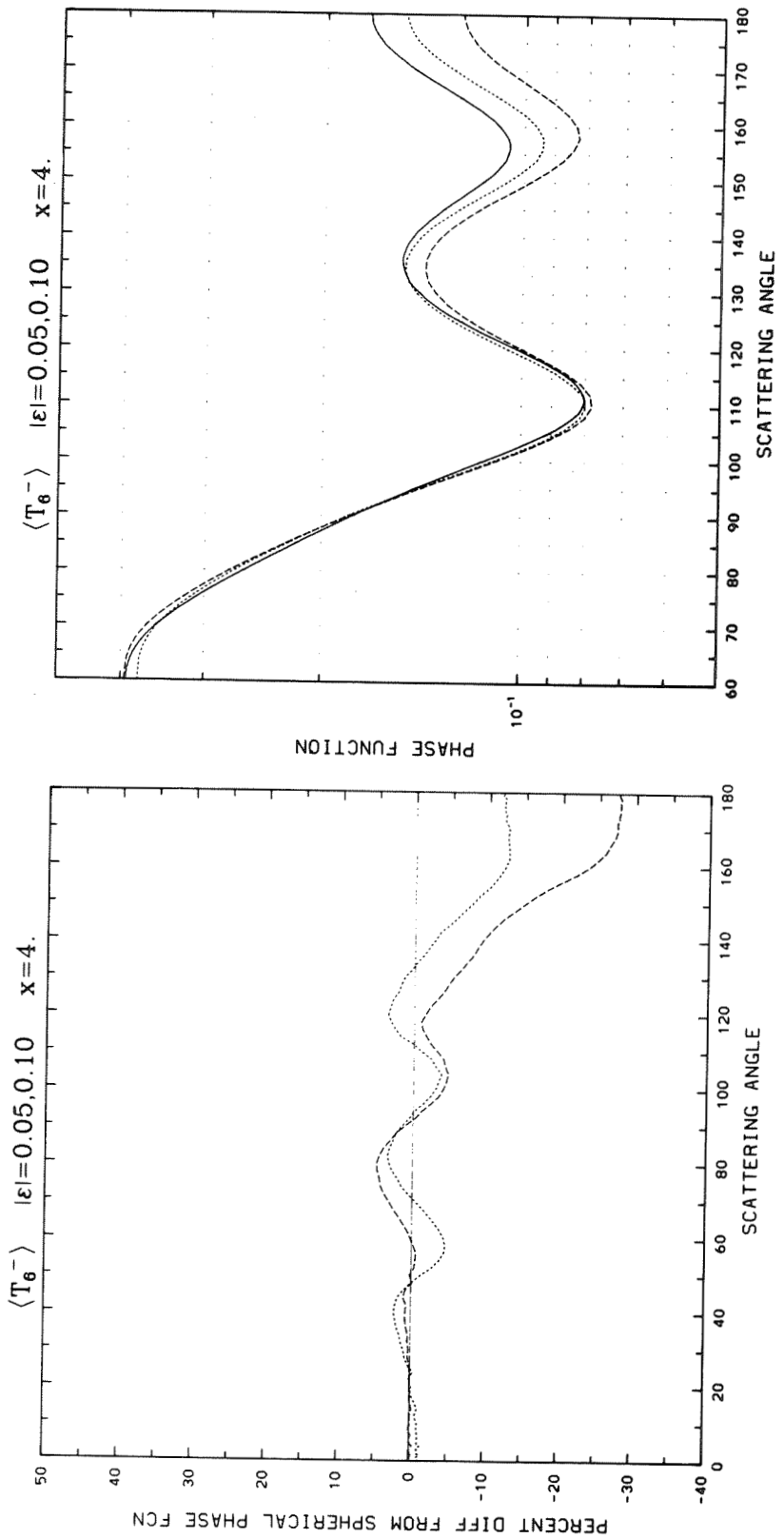

Appendix C (Continued)

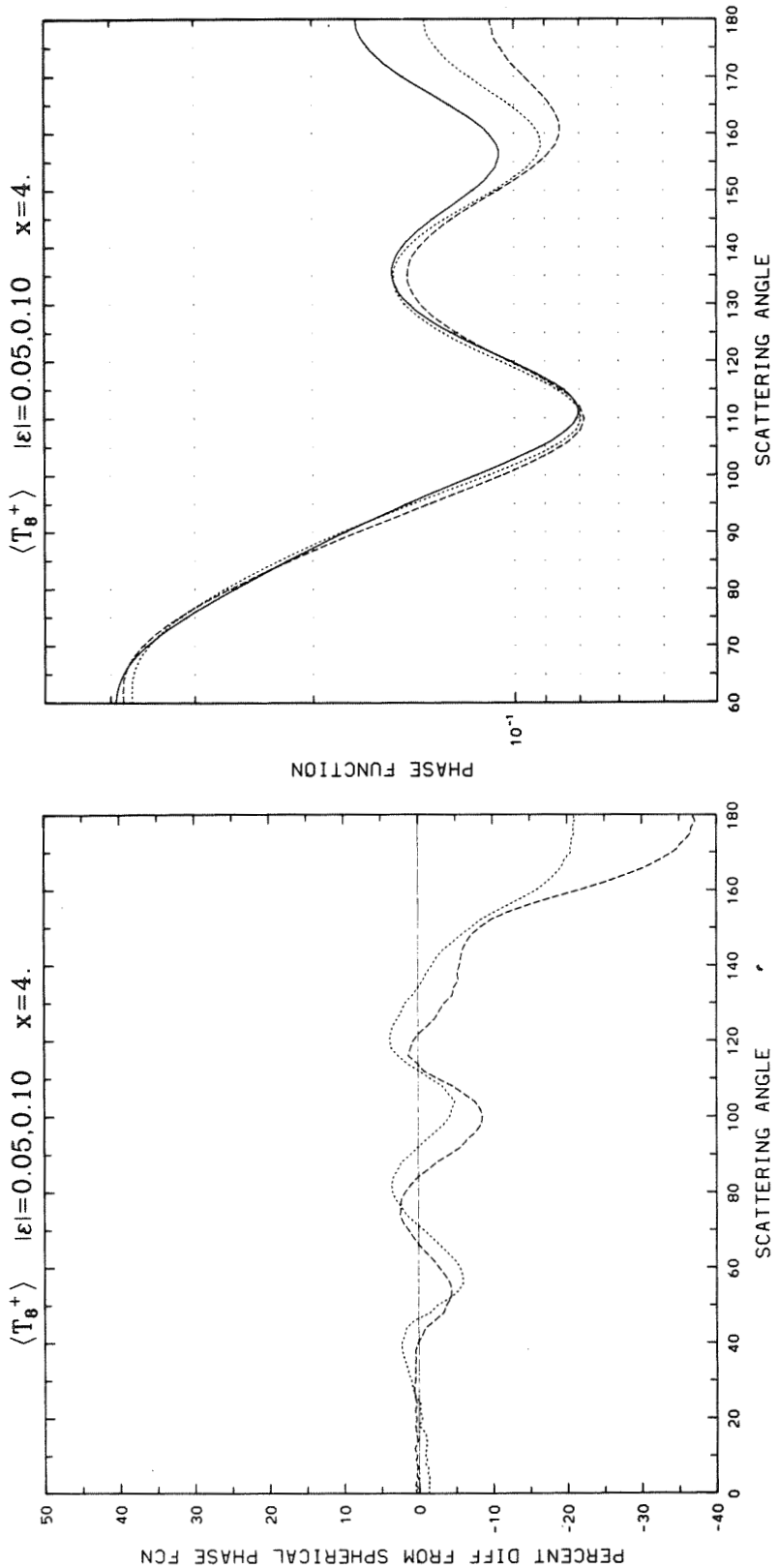

Appendix C (Continued)

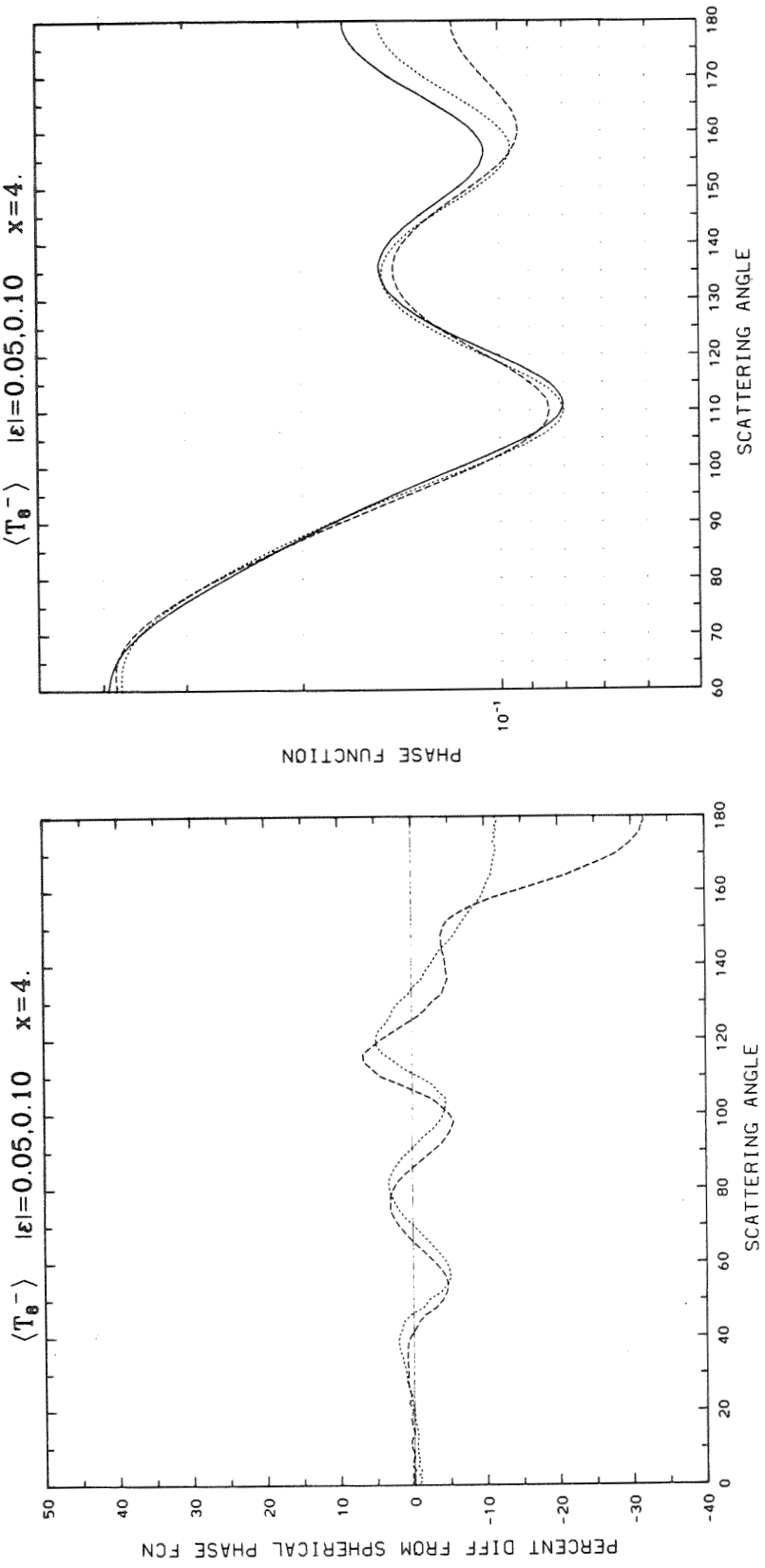

Appendix C (Continued)

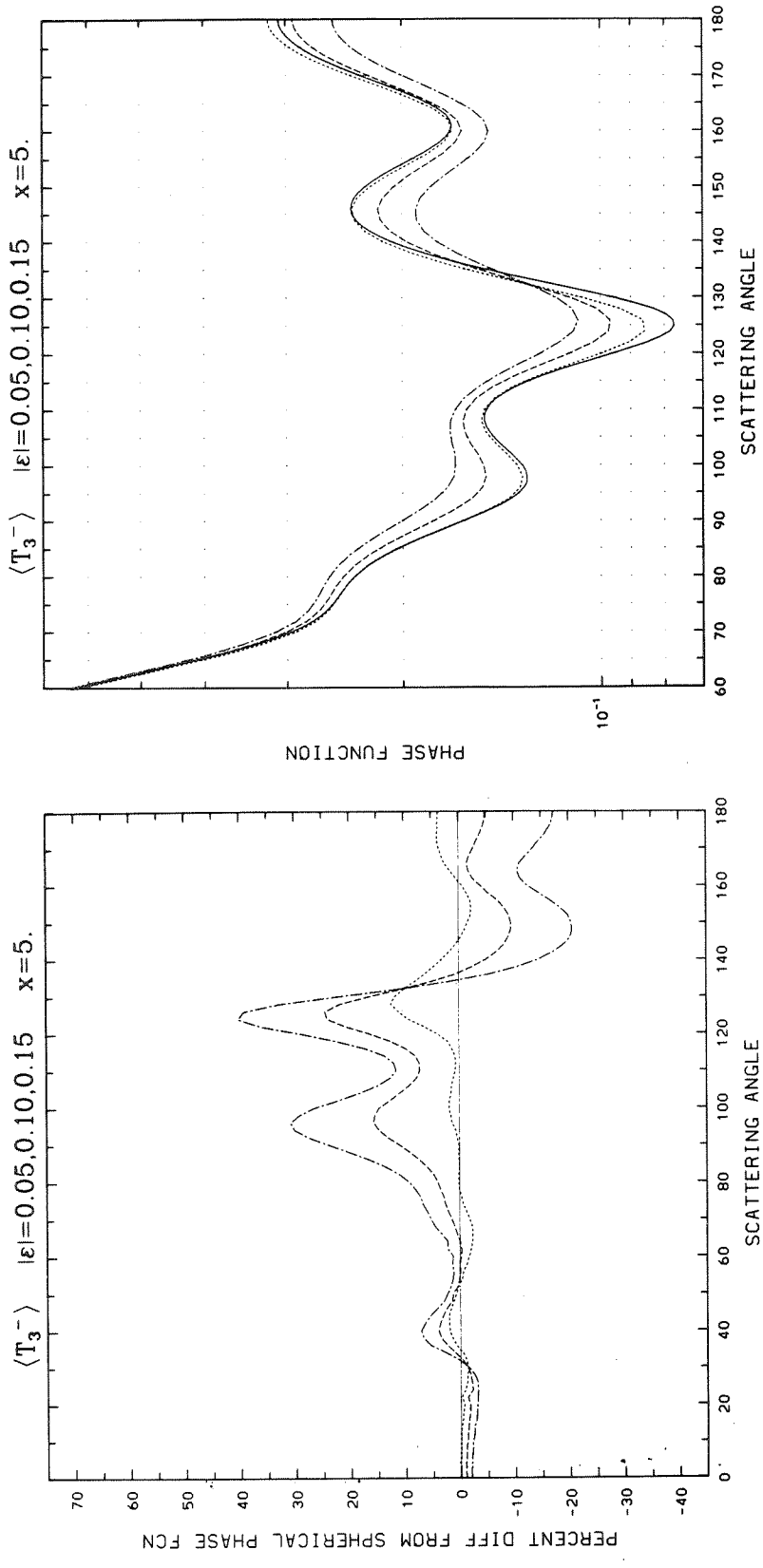

Appendix C (Continued)

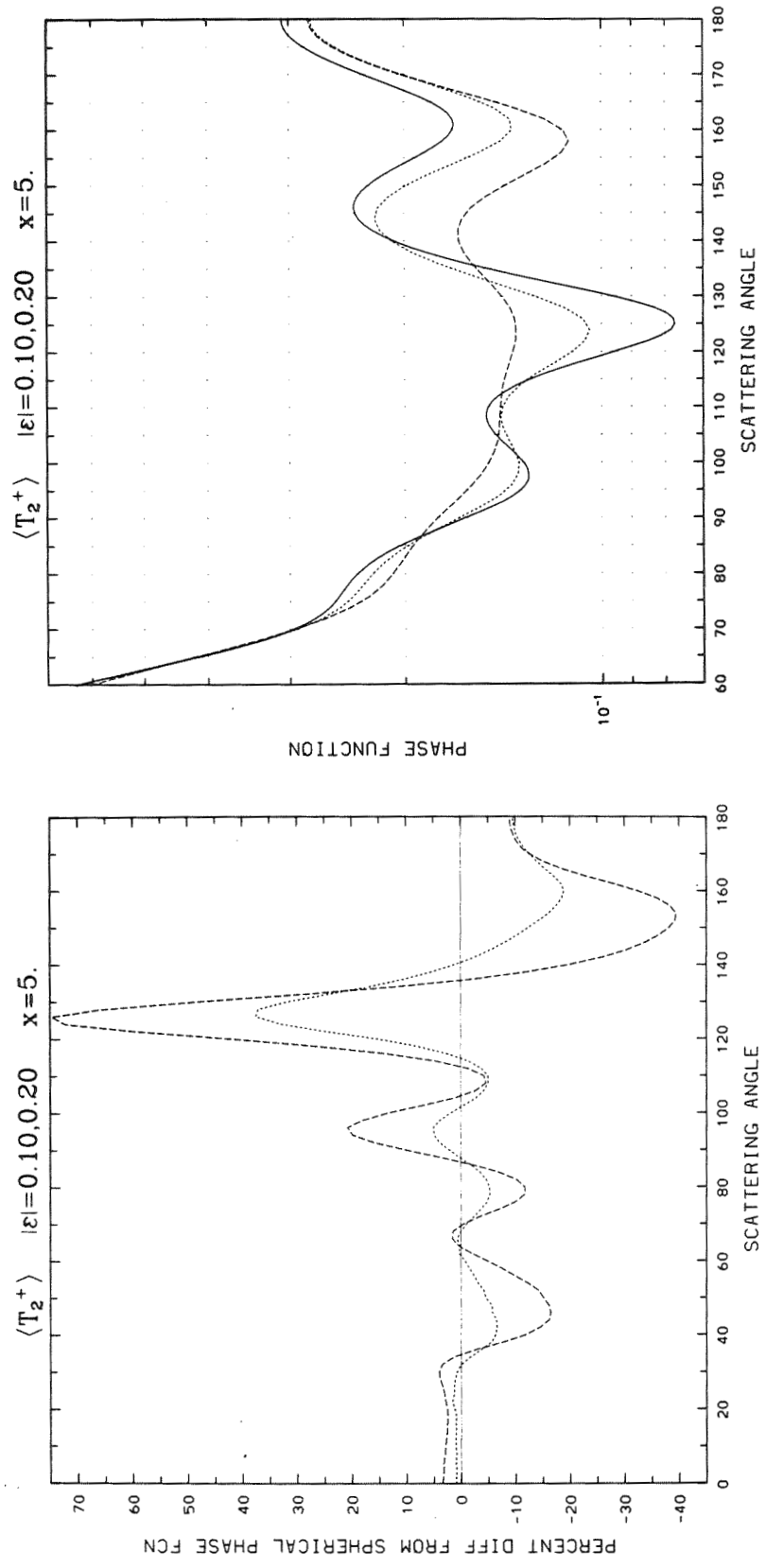

Appendix C (Continued)

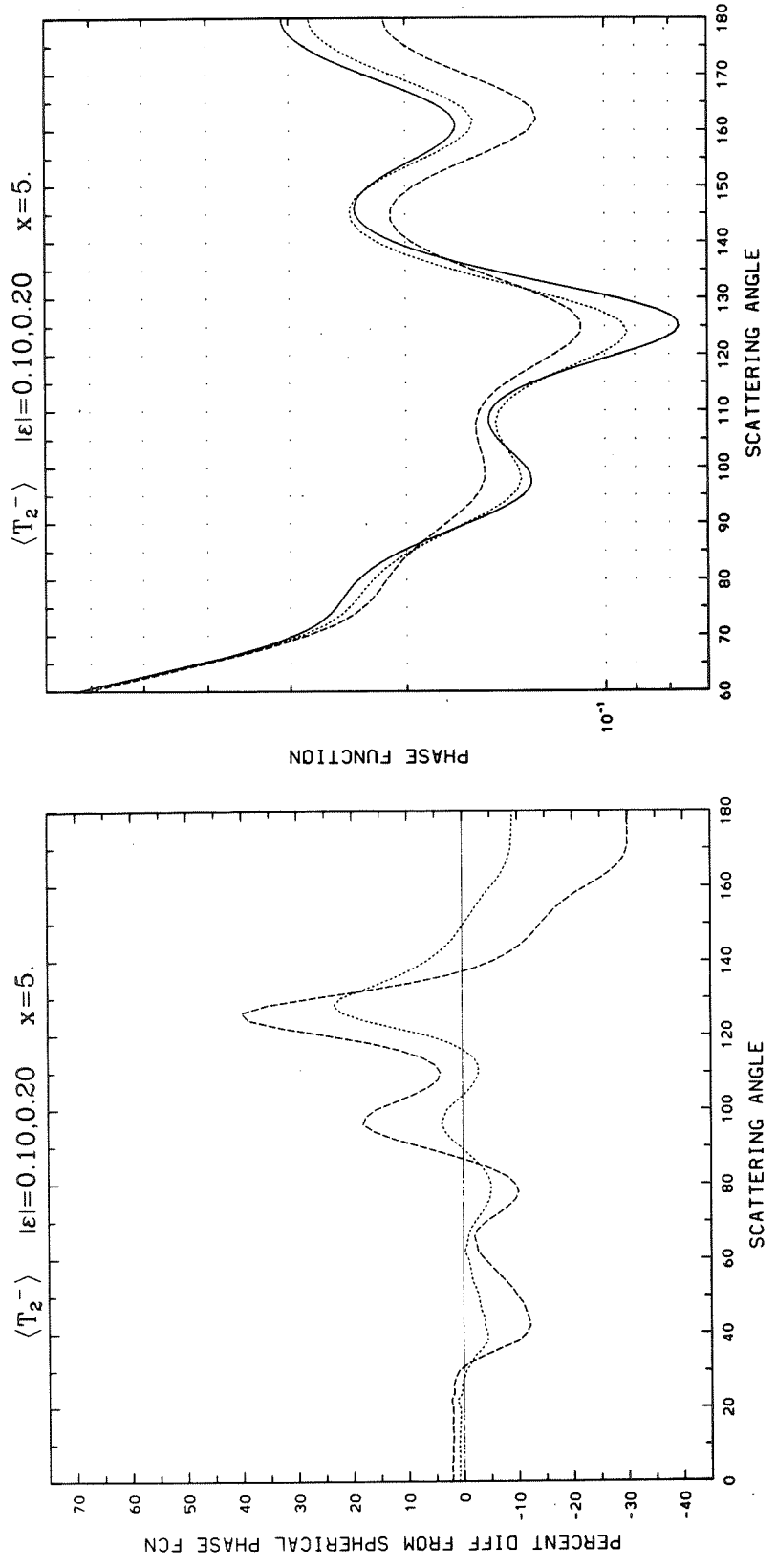

Appendix C (Continued)

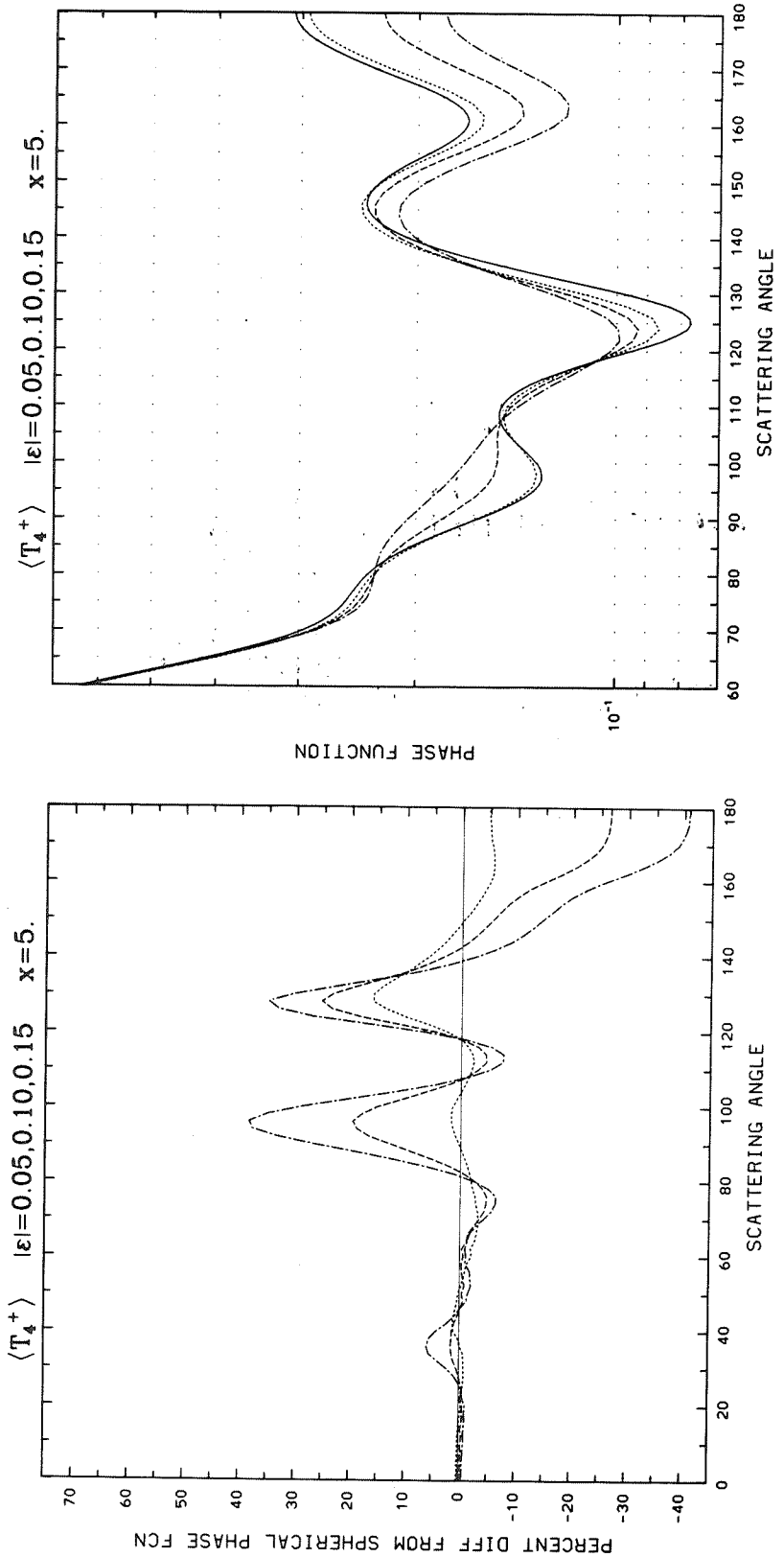

Appendix C (Continued)

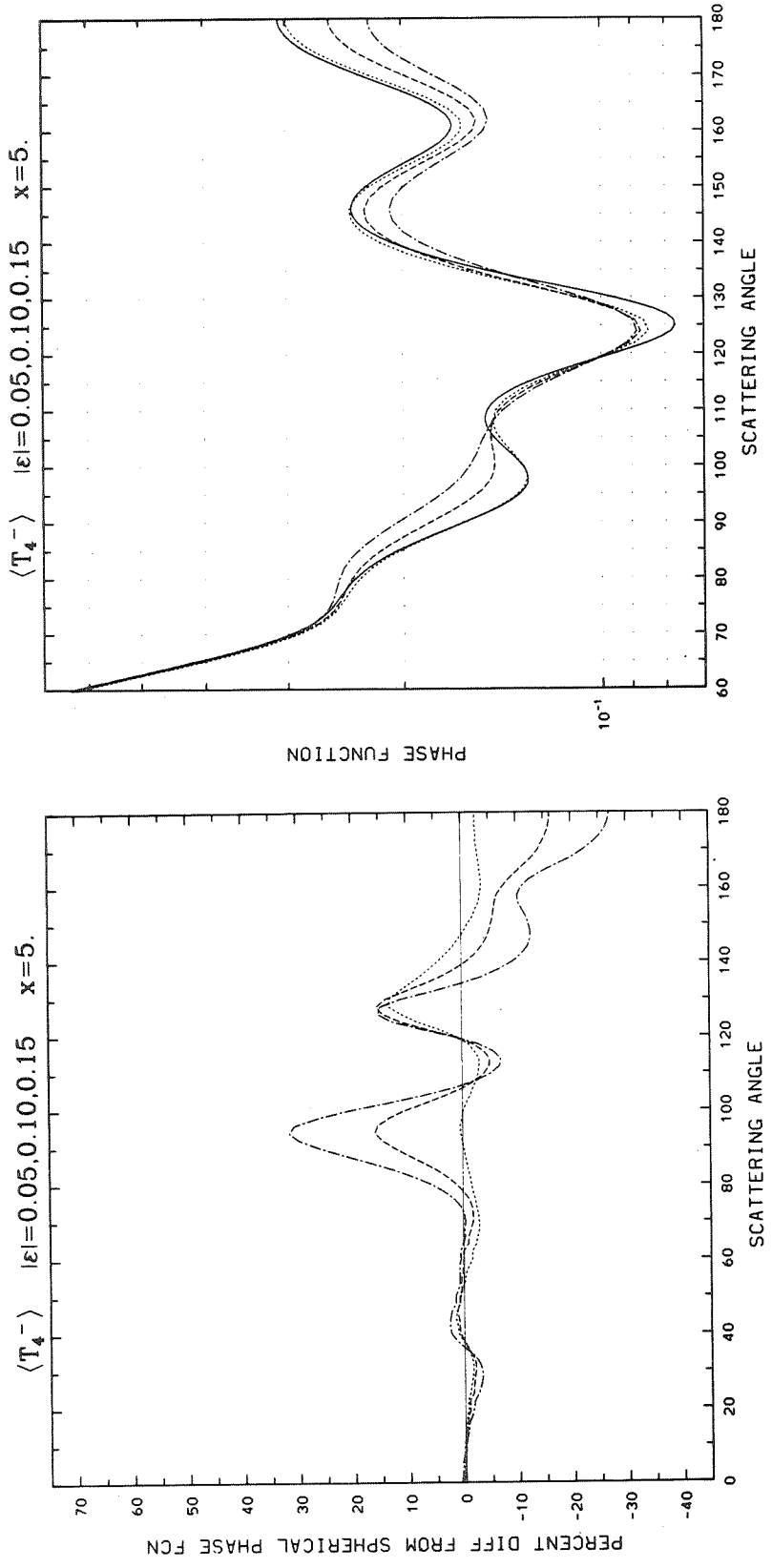

Appendix C (Continued)

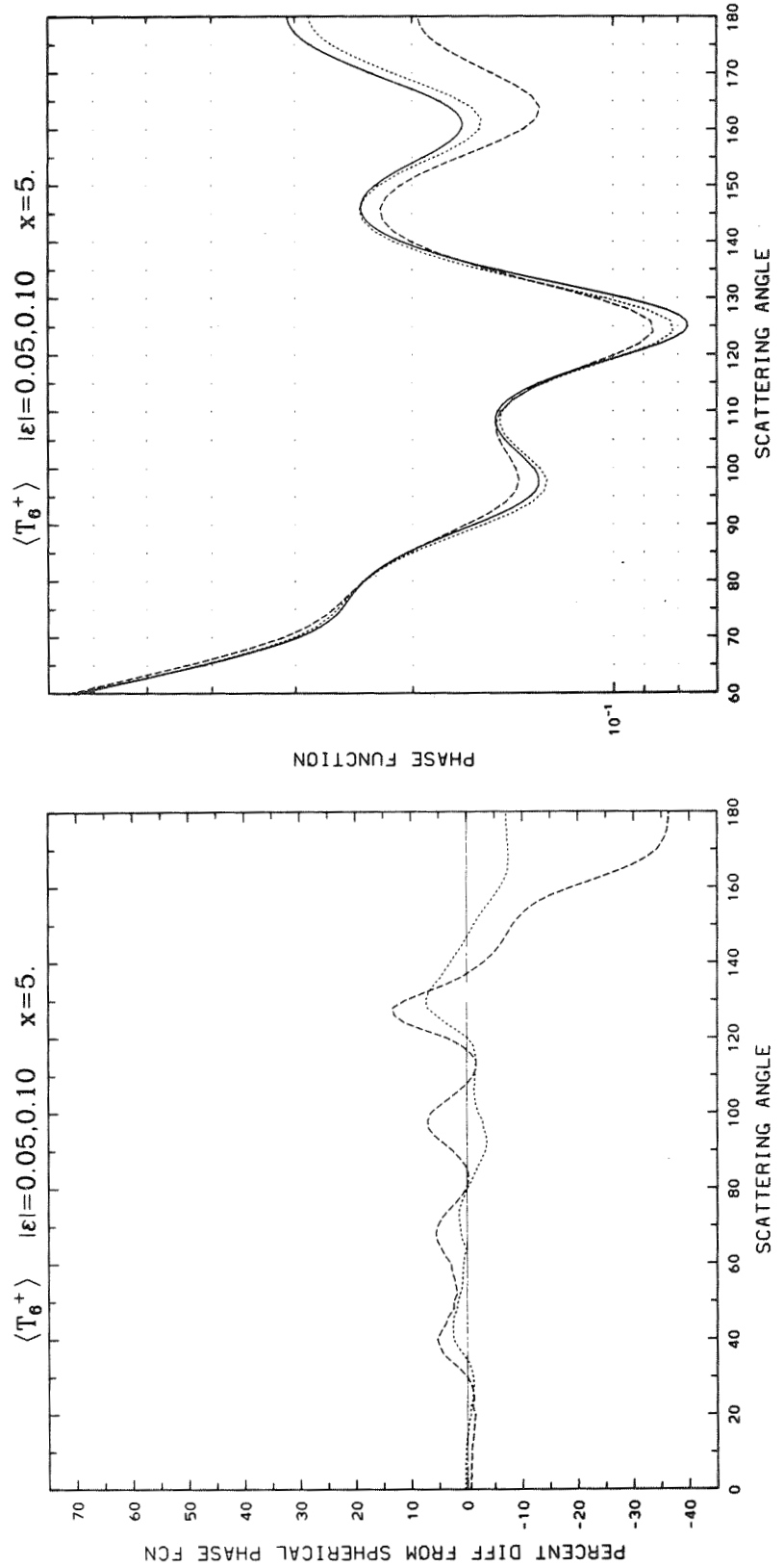

Appendix C (Continued)

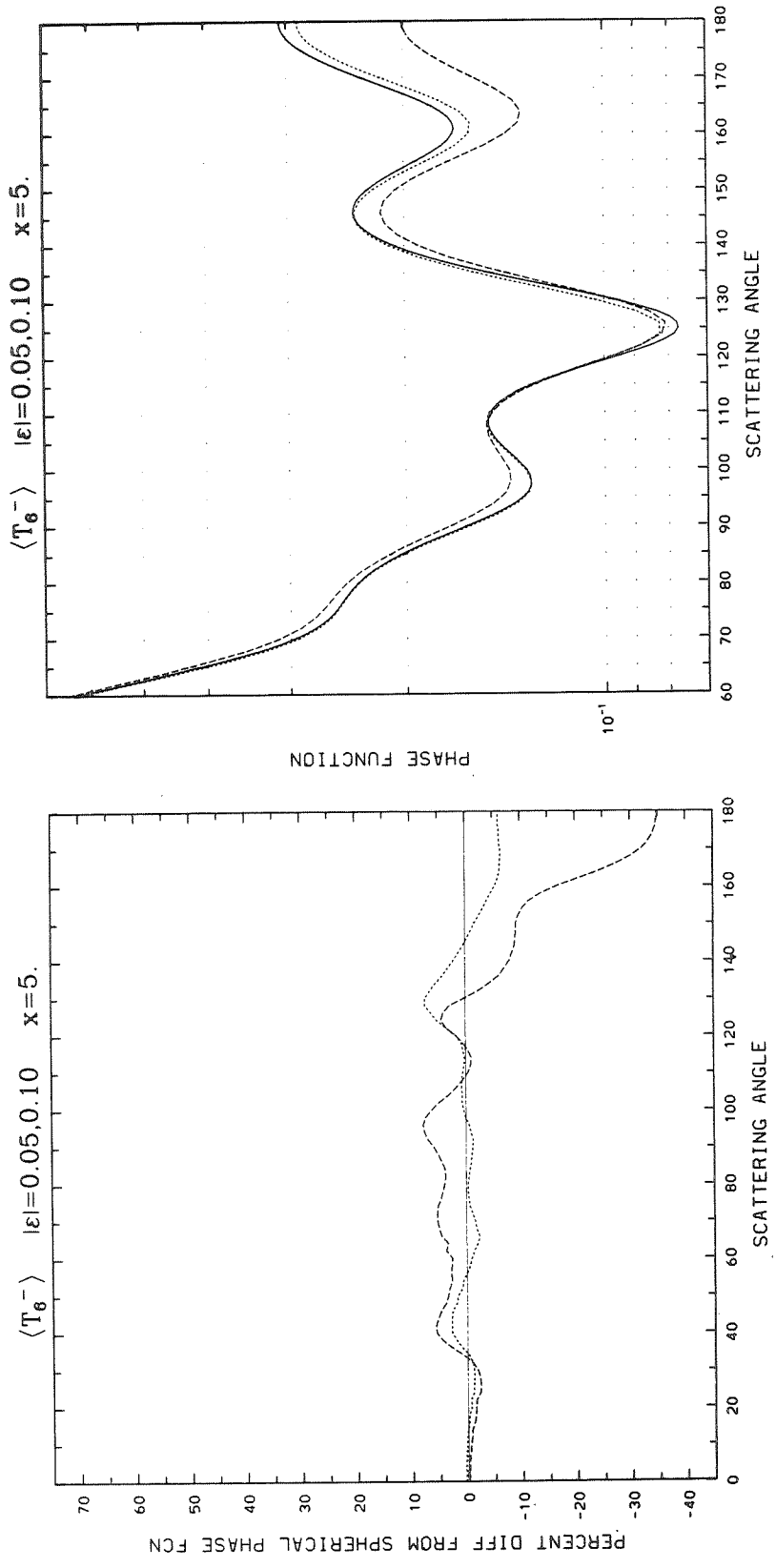

Appendix C (Continued)

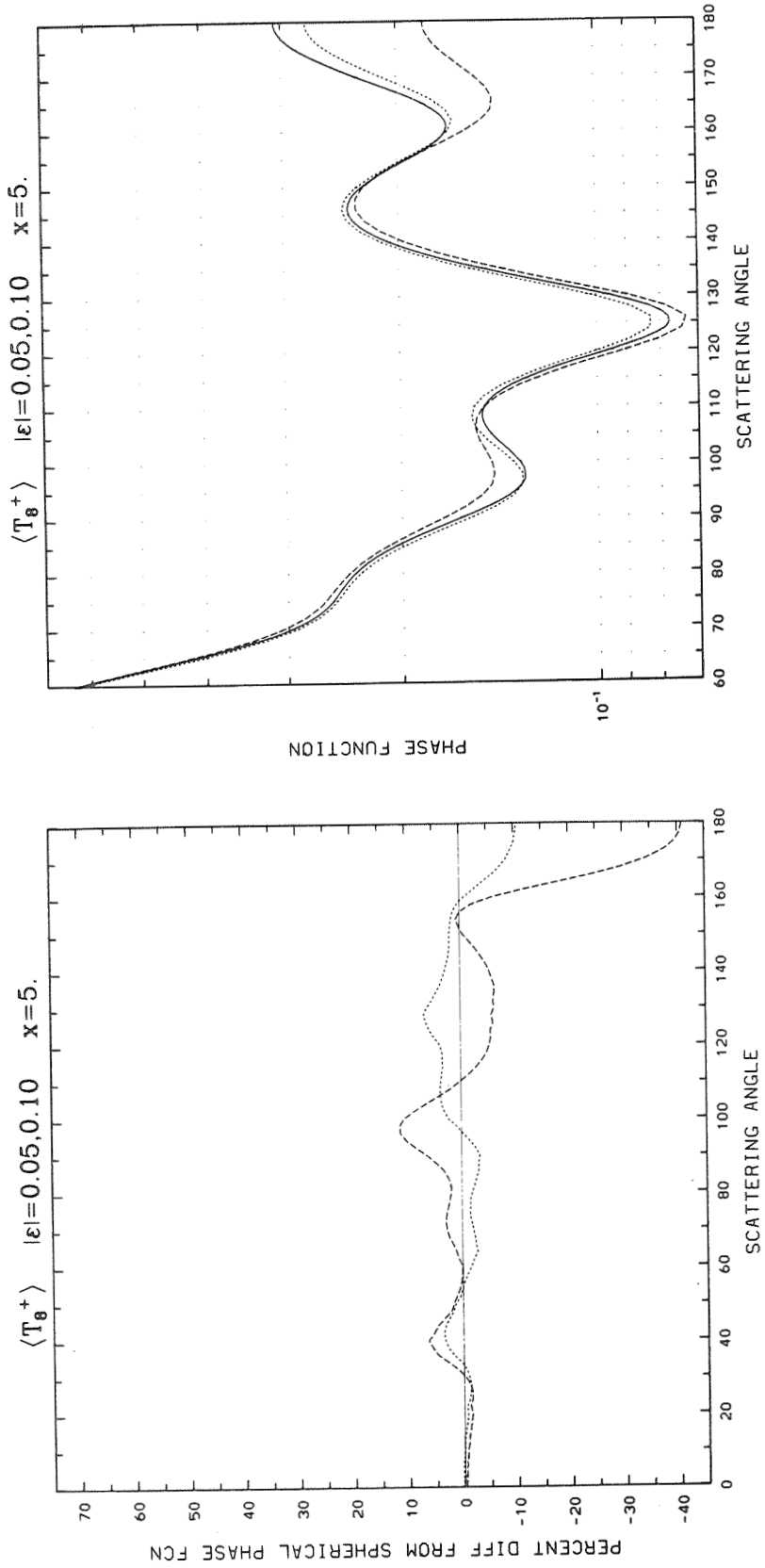

Appendix C (Continued)

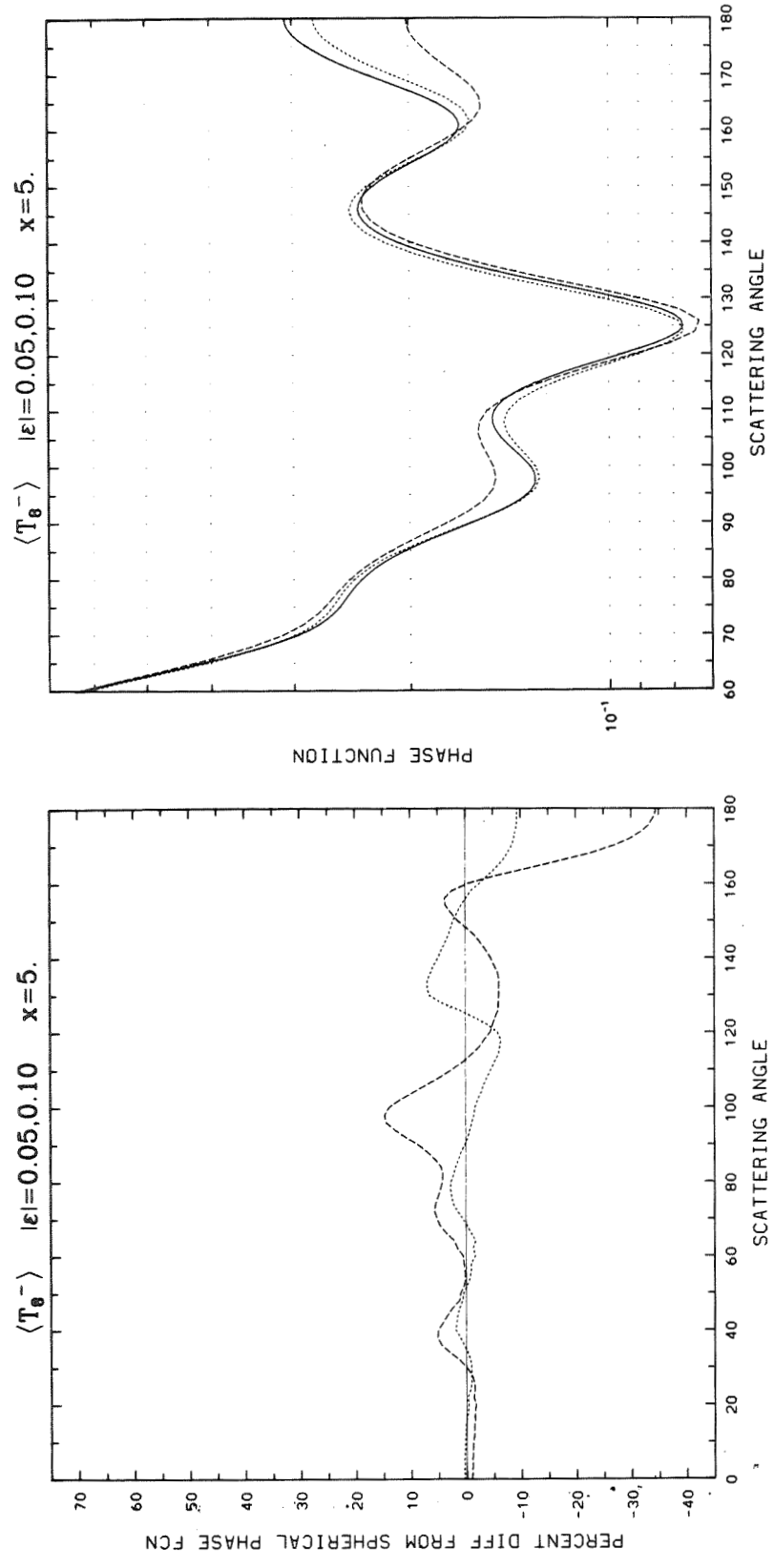

Appendix C (Continued)

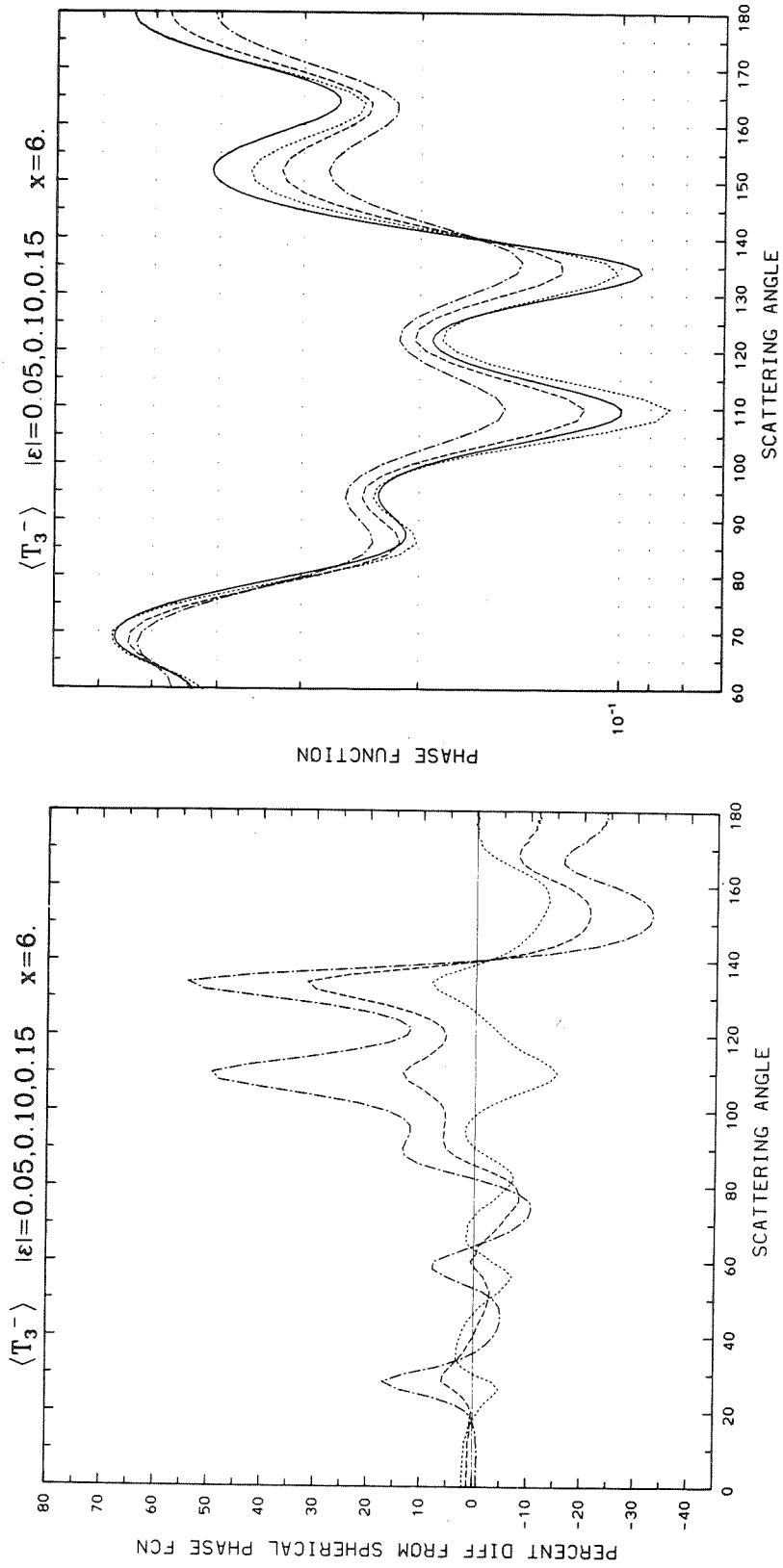

Appendix C (Continued)

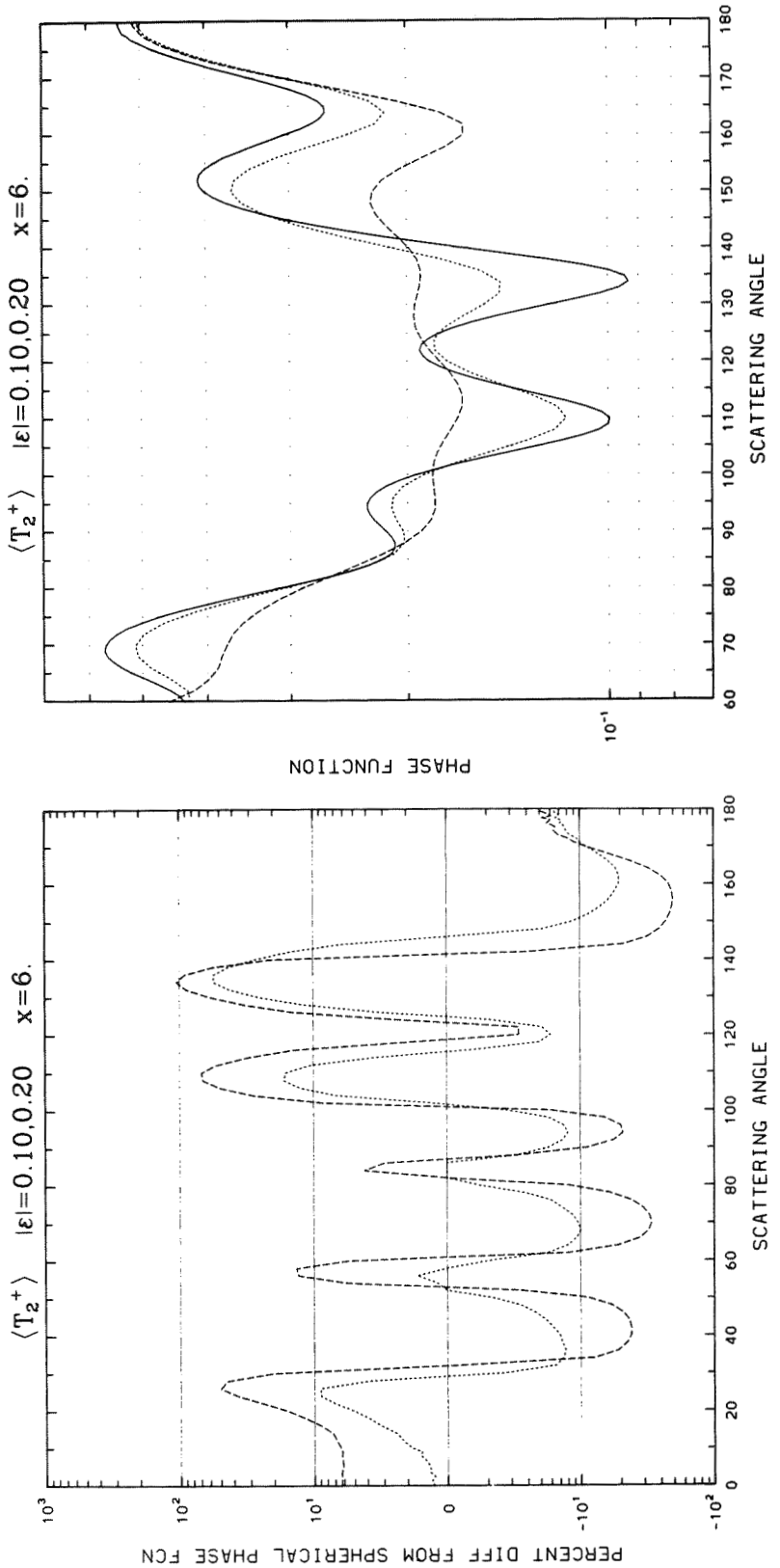

Appendix C (Continued)

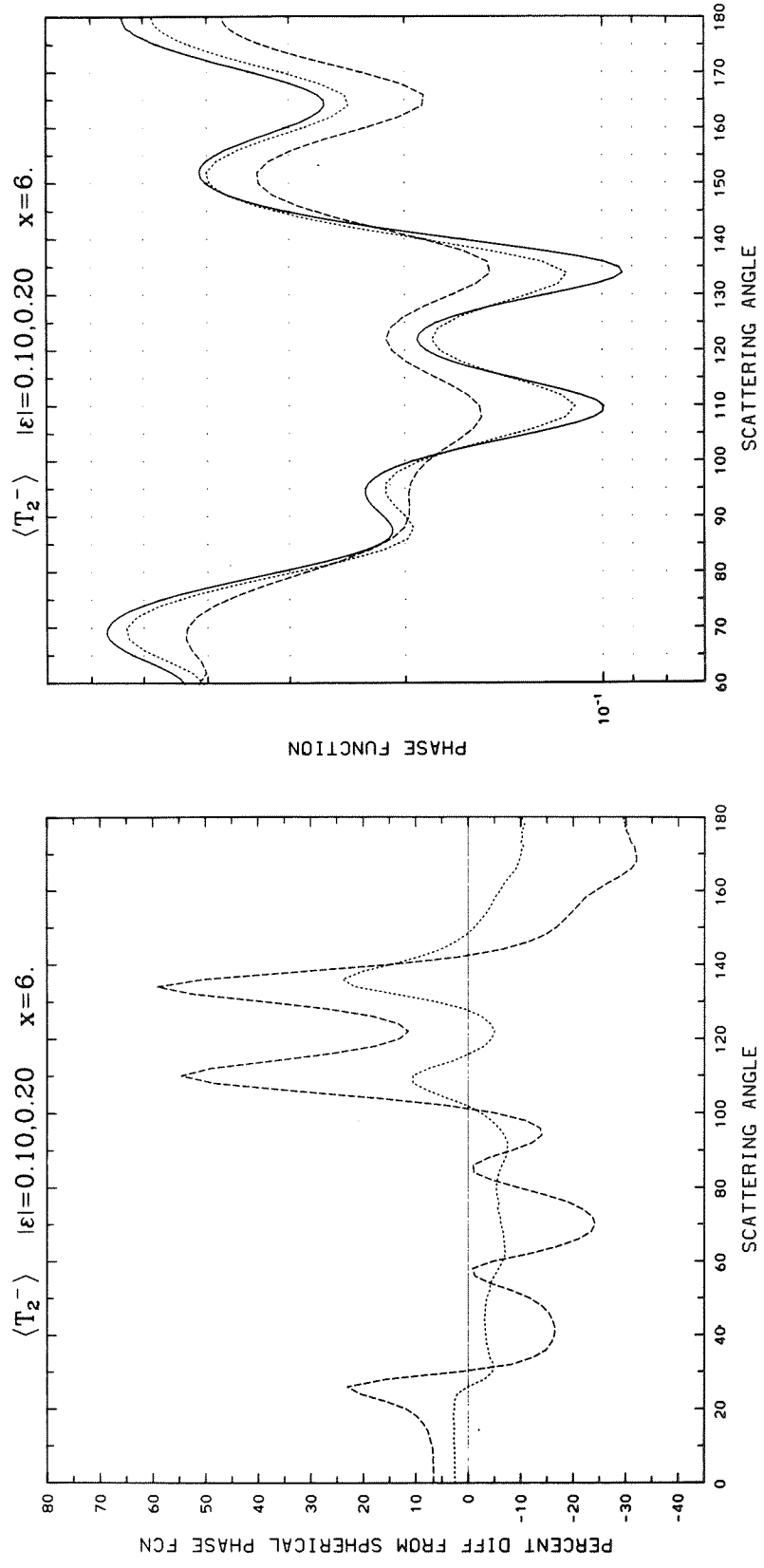

Appendix C (Continued)

C-3

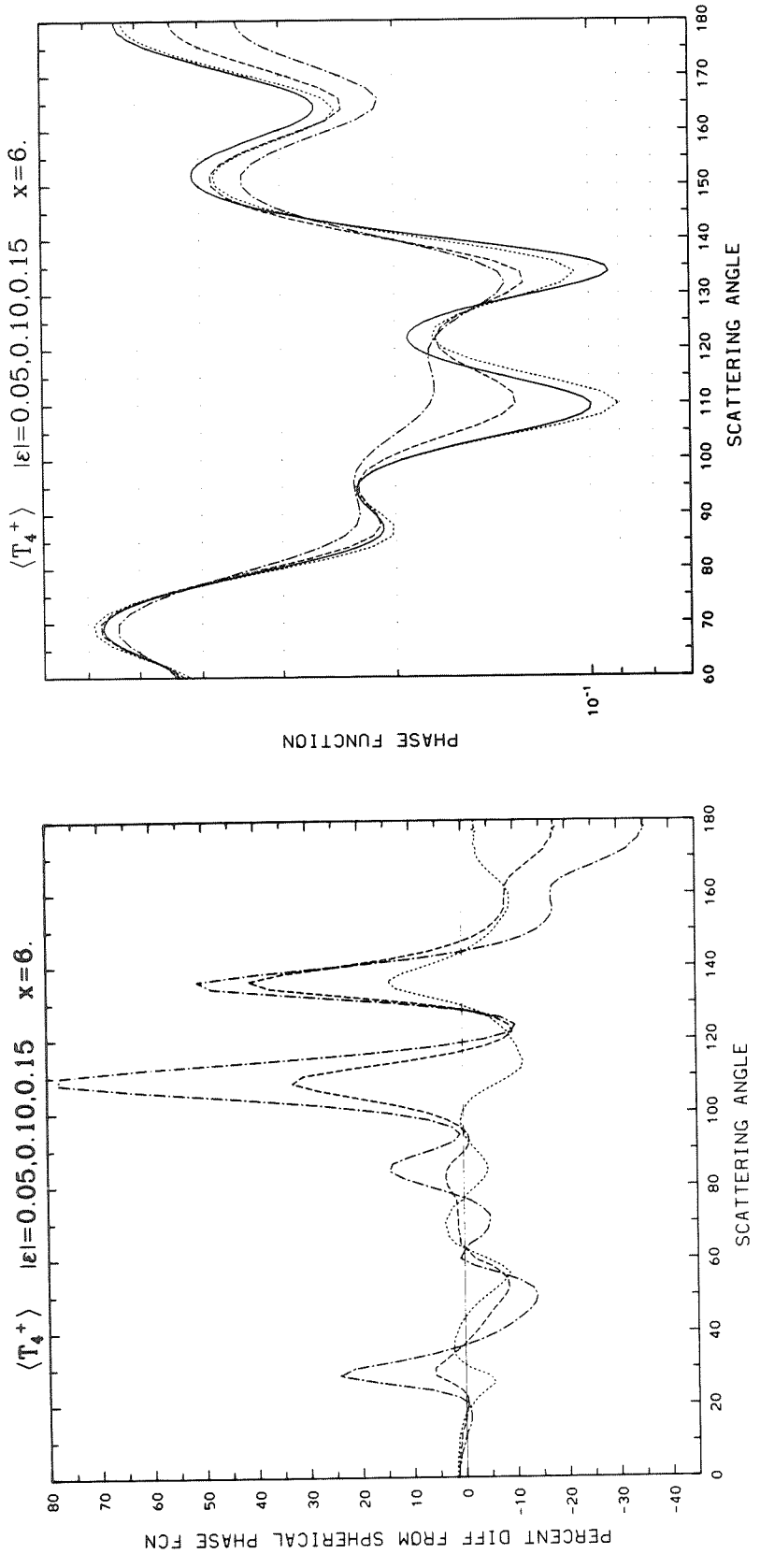

Appendix C (Continued)

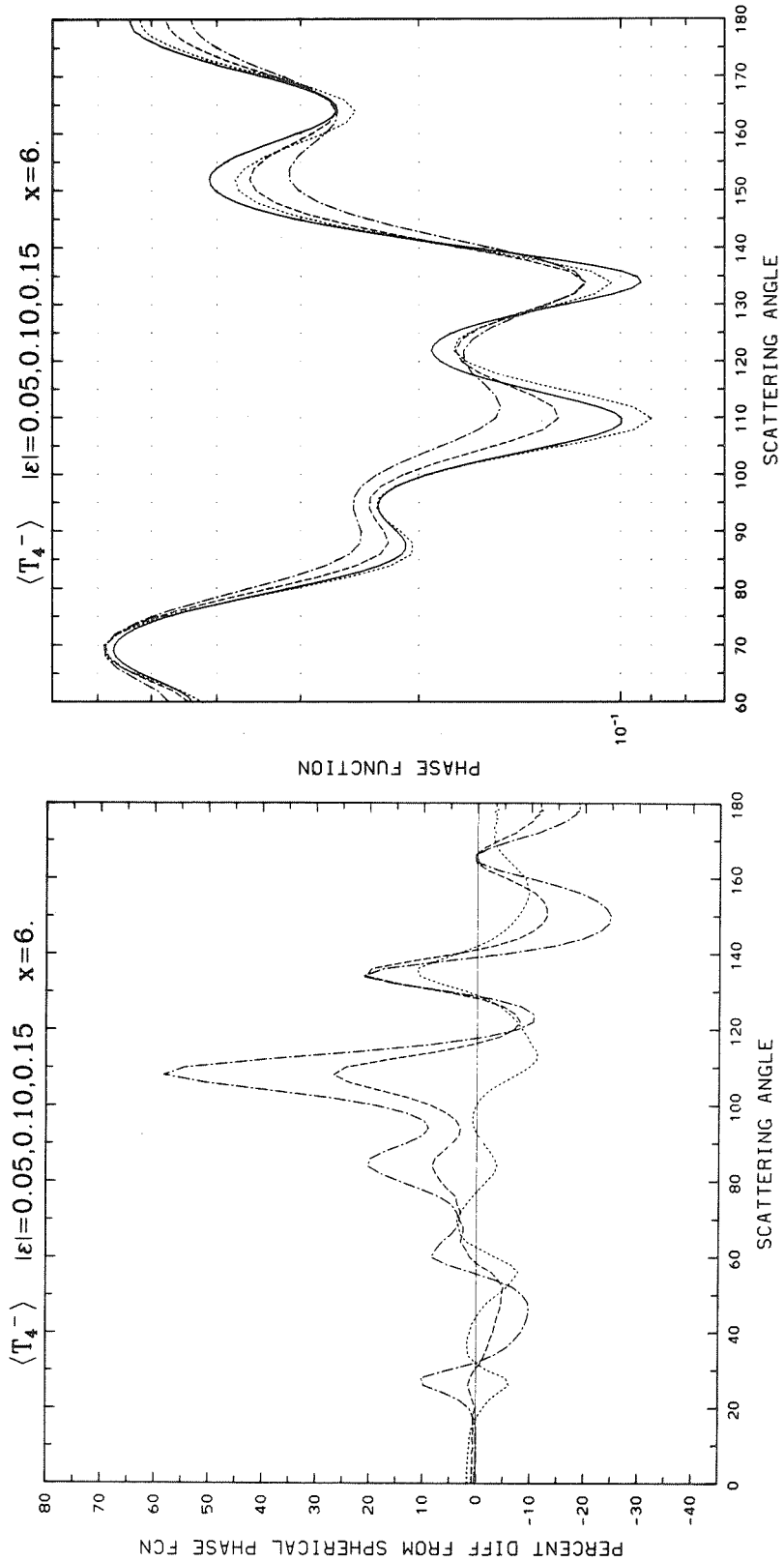

Appendix C (Continued)

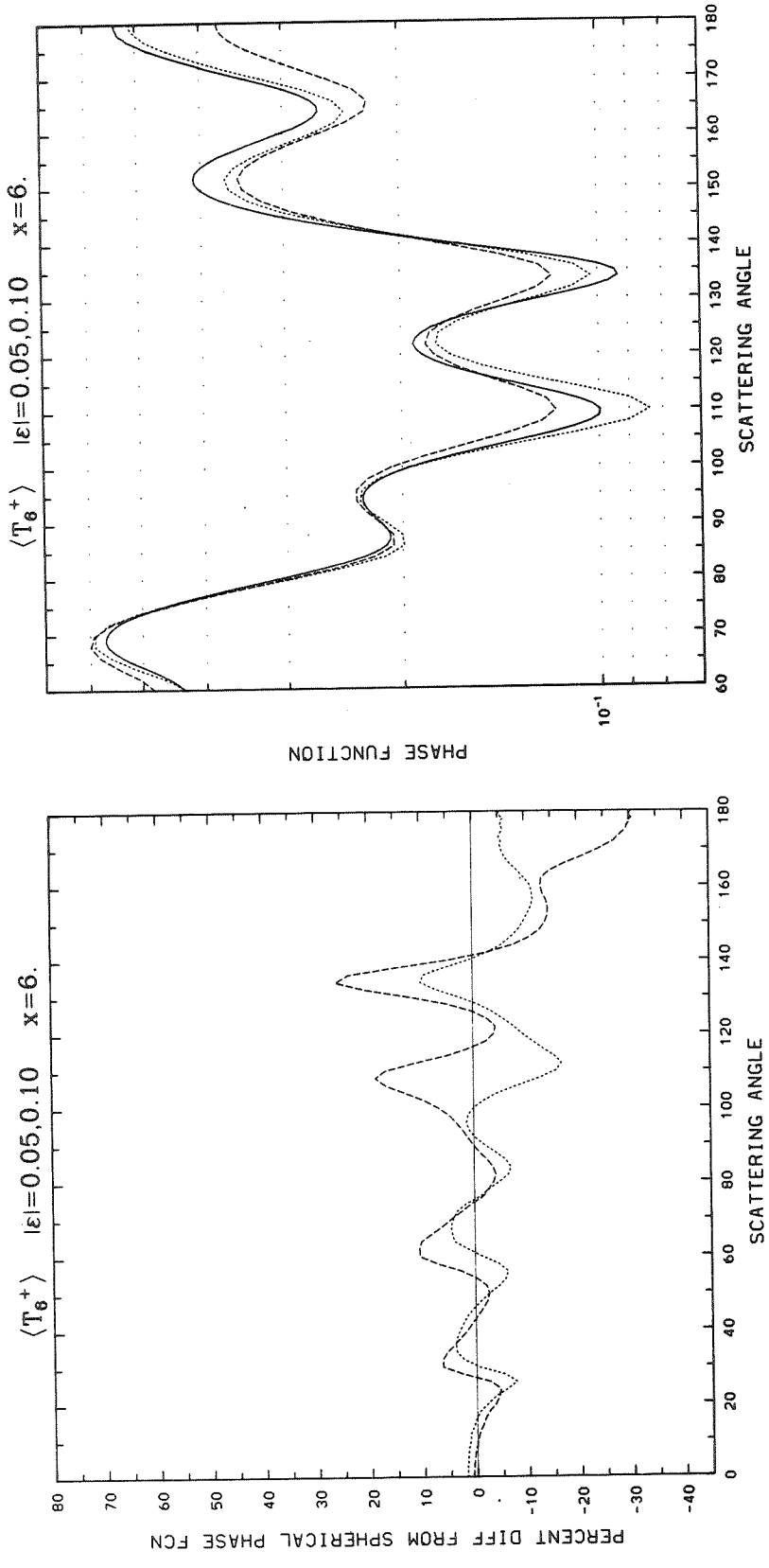

Appendix C (Continued)

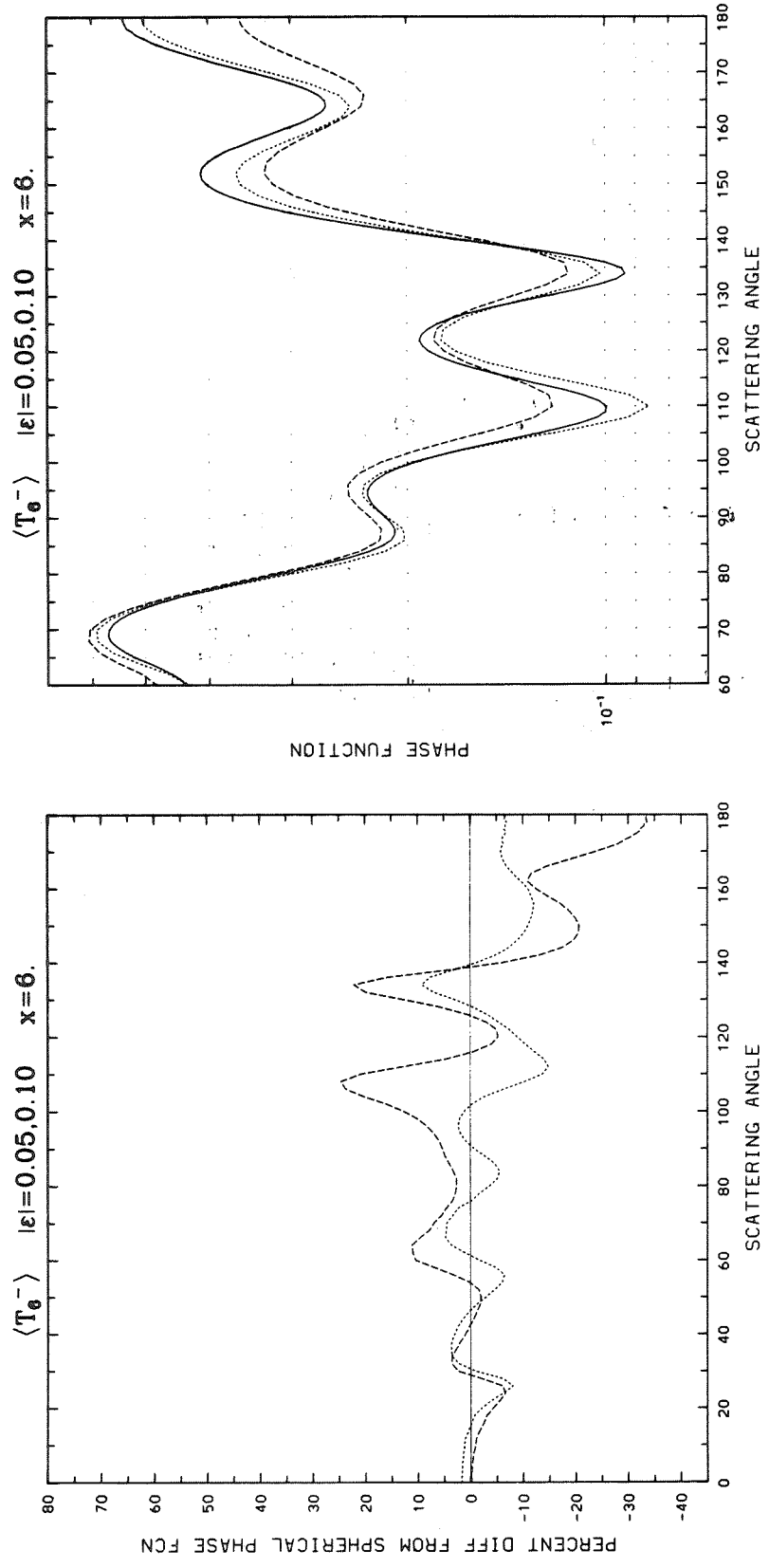

Appendix C (Continued)

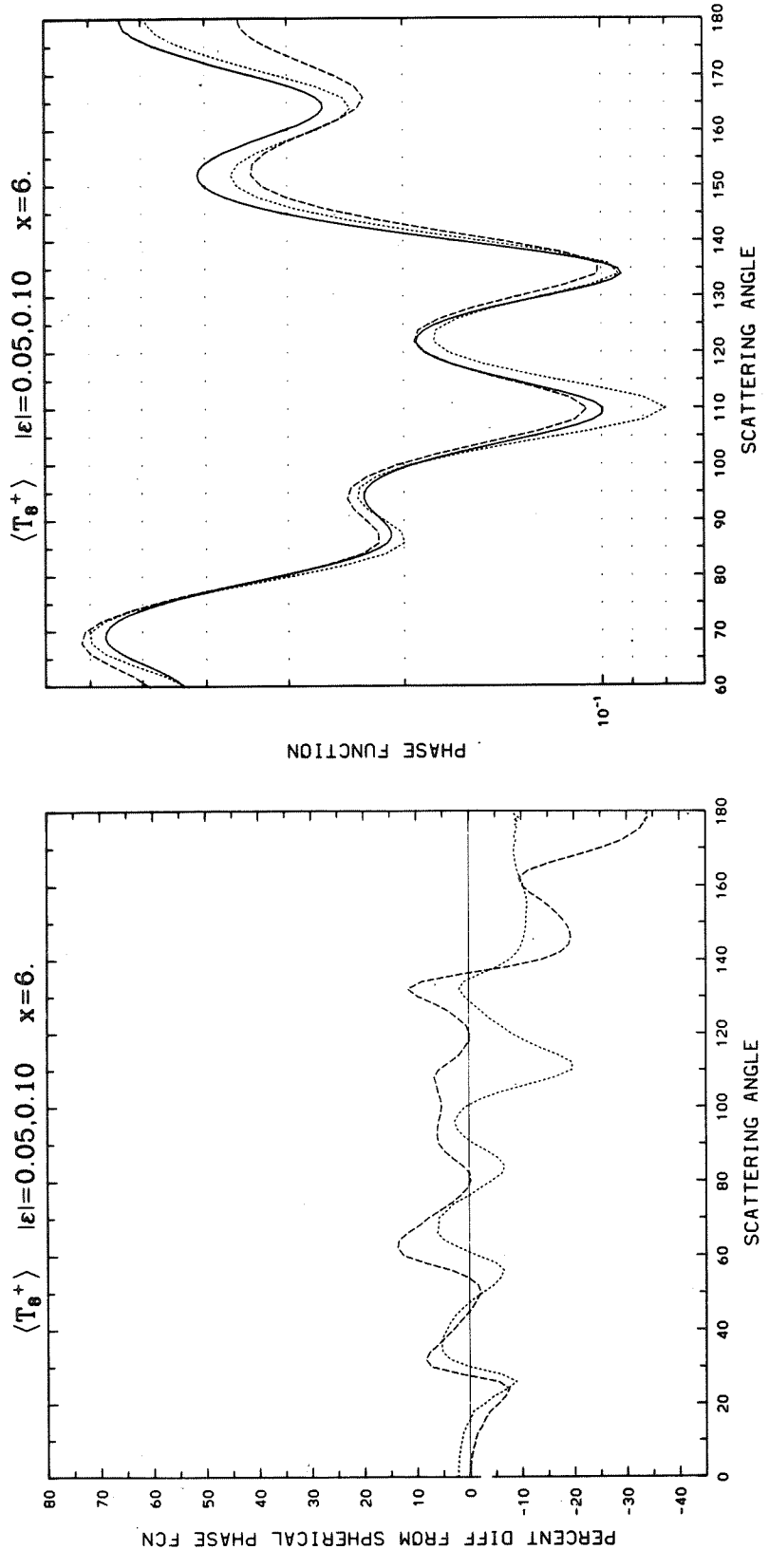

Appendix C (Continued)

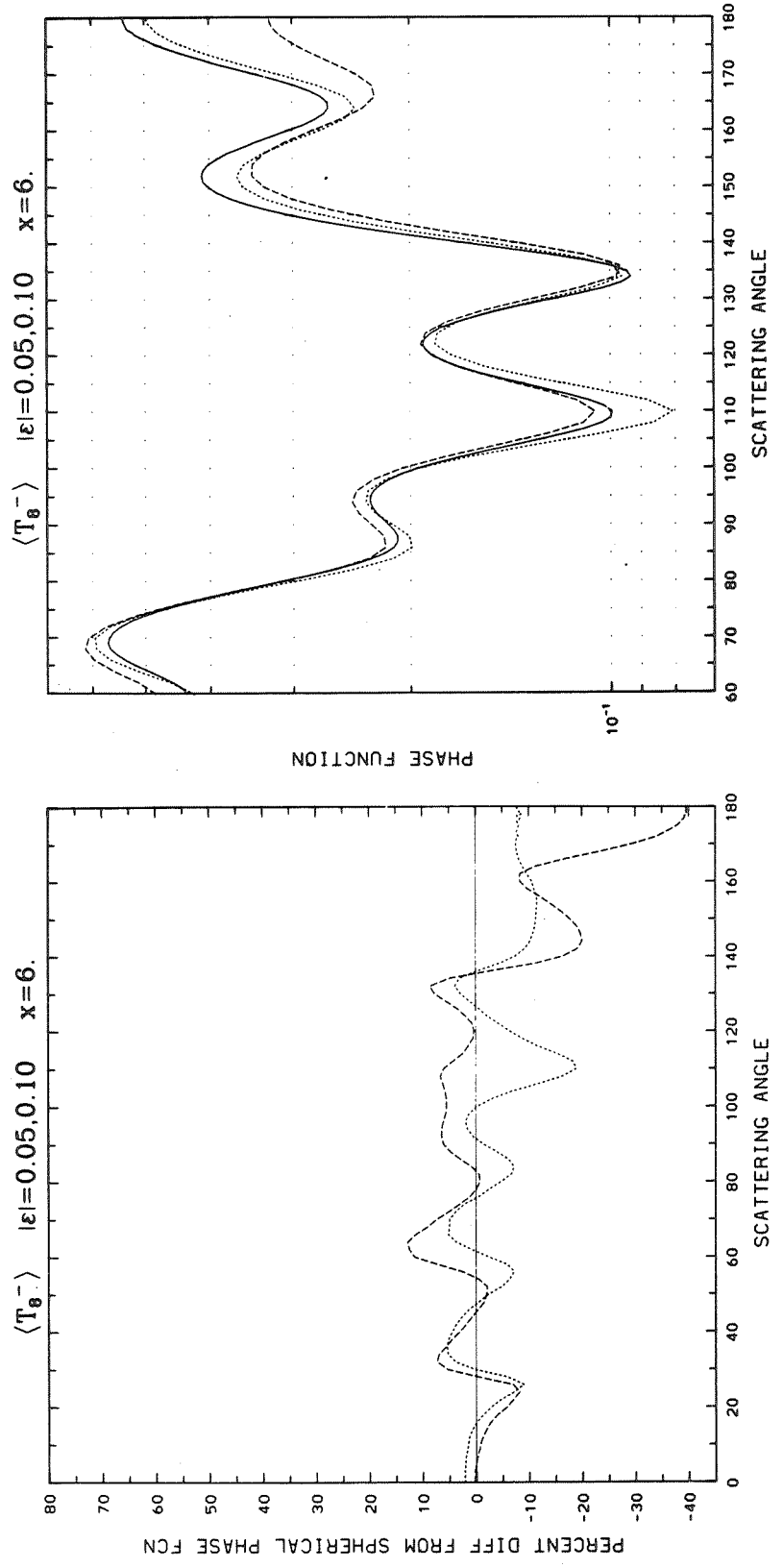

Appendix C (Continued)

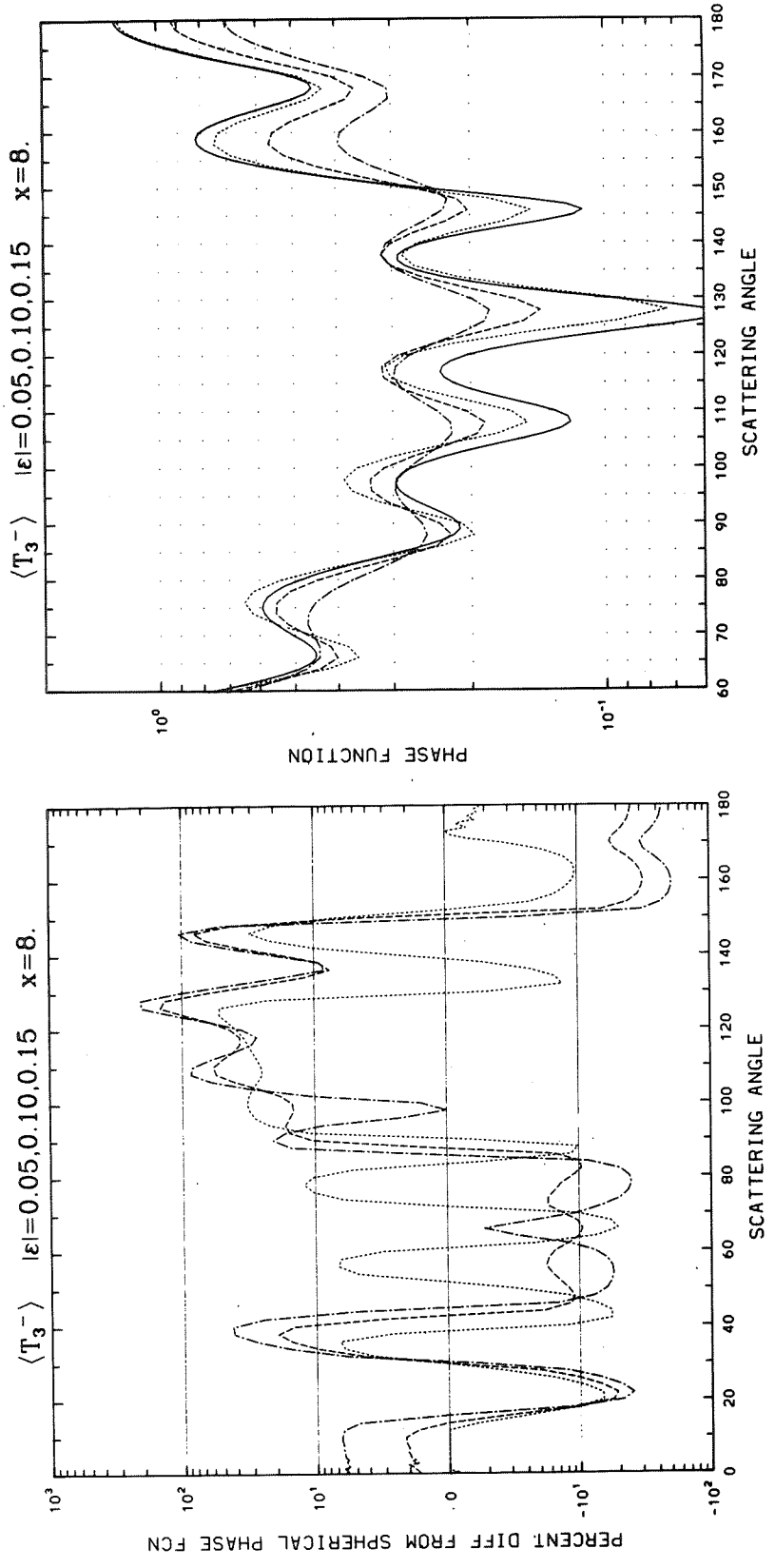

Appendix C (Continued)

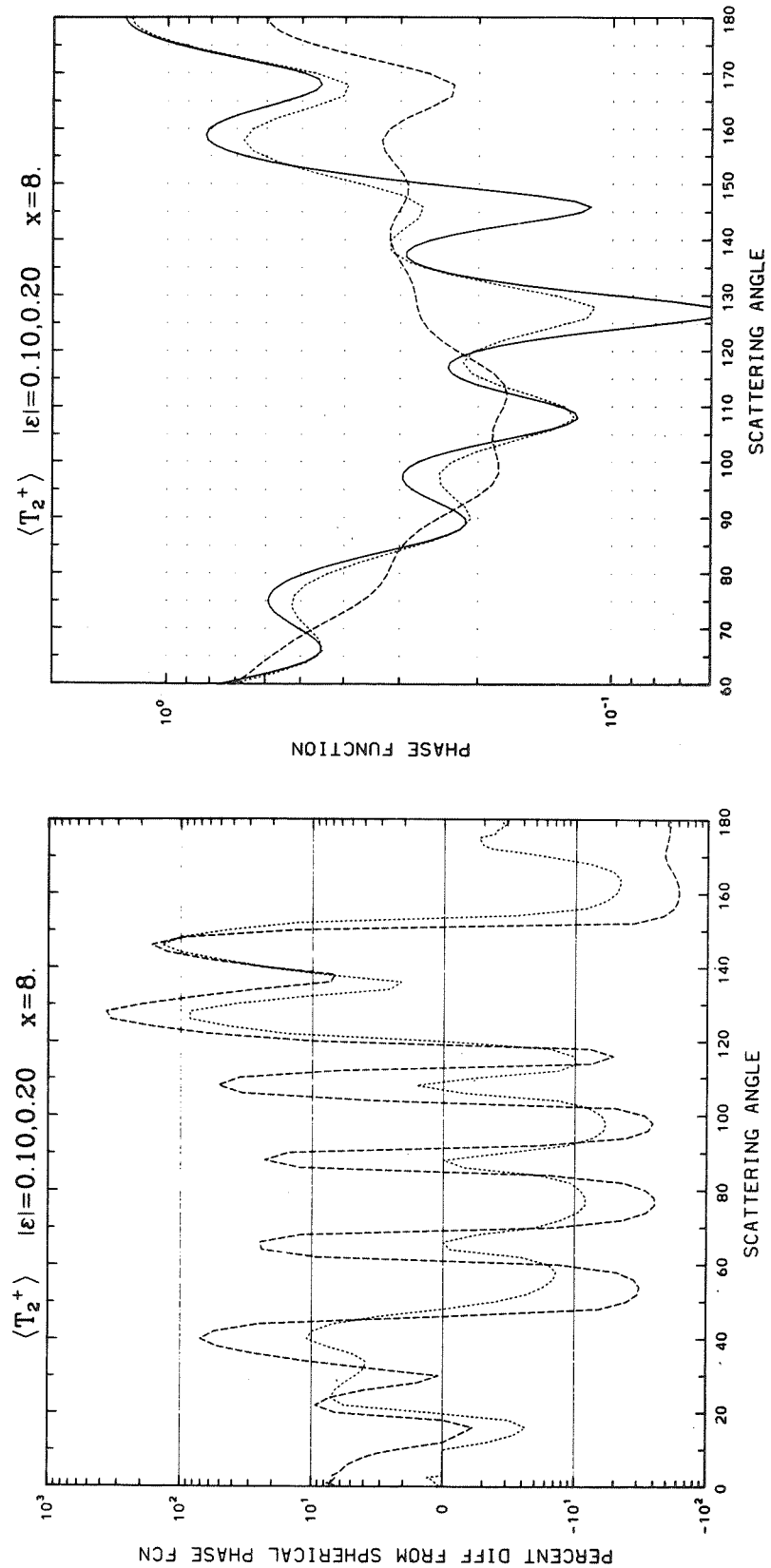

Appendix C (Continued)

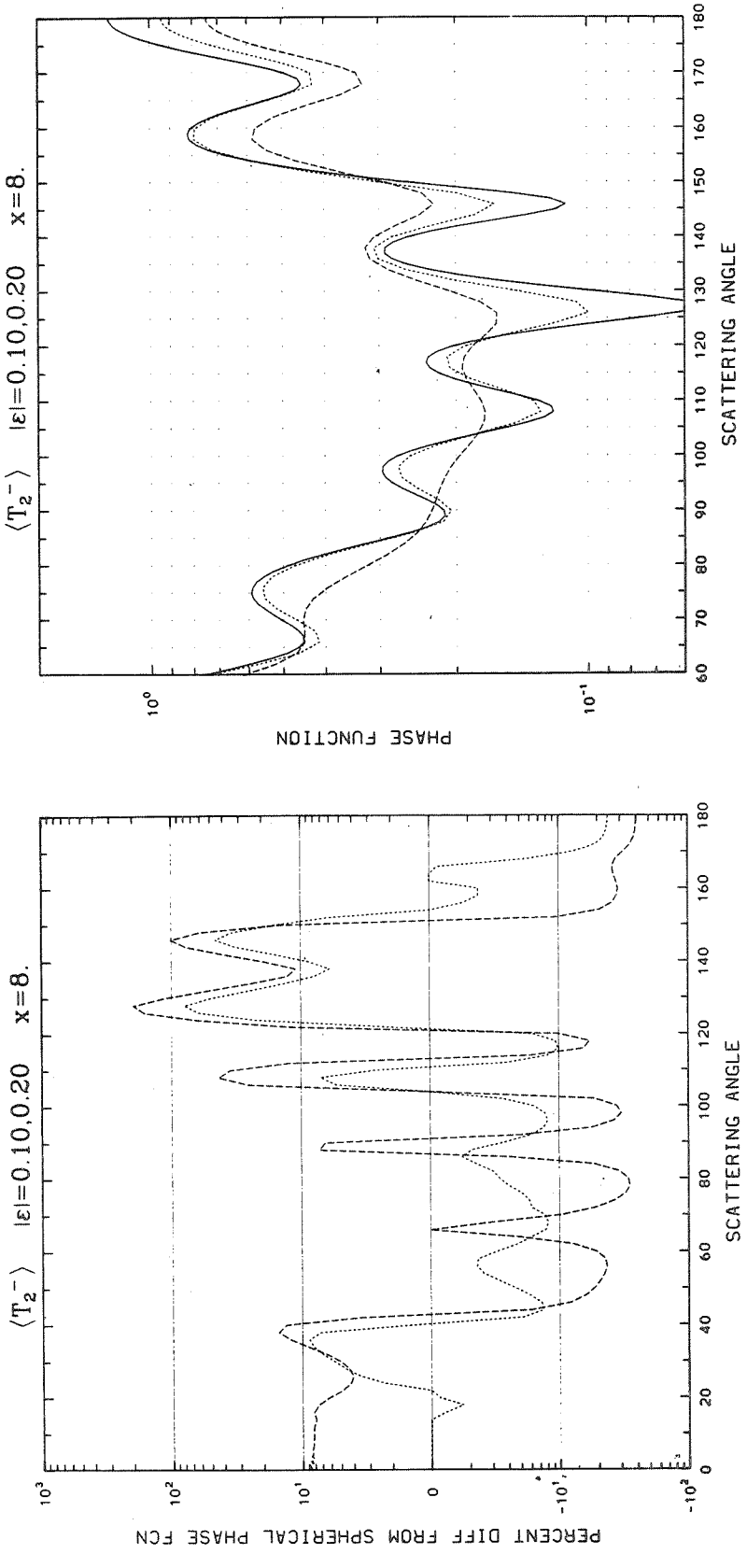

Appendix C (Continued)

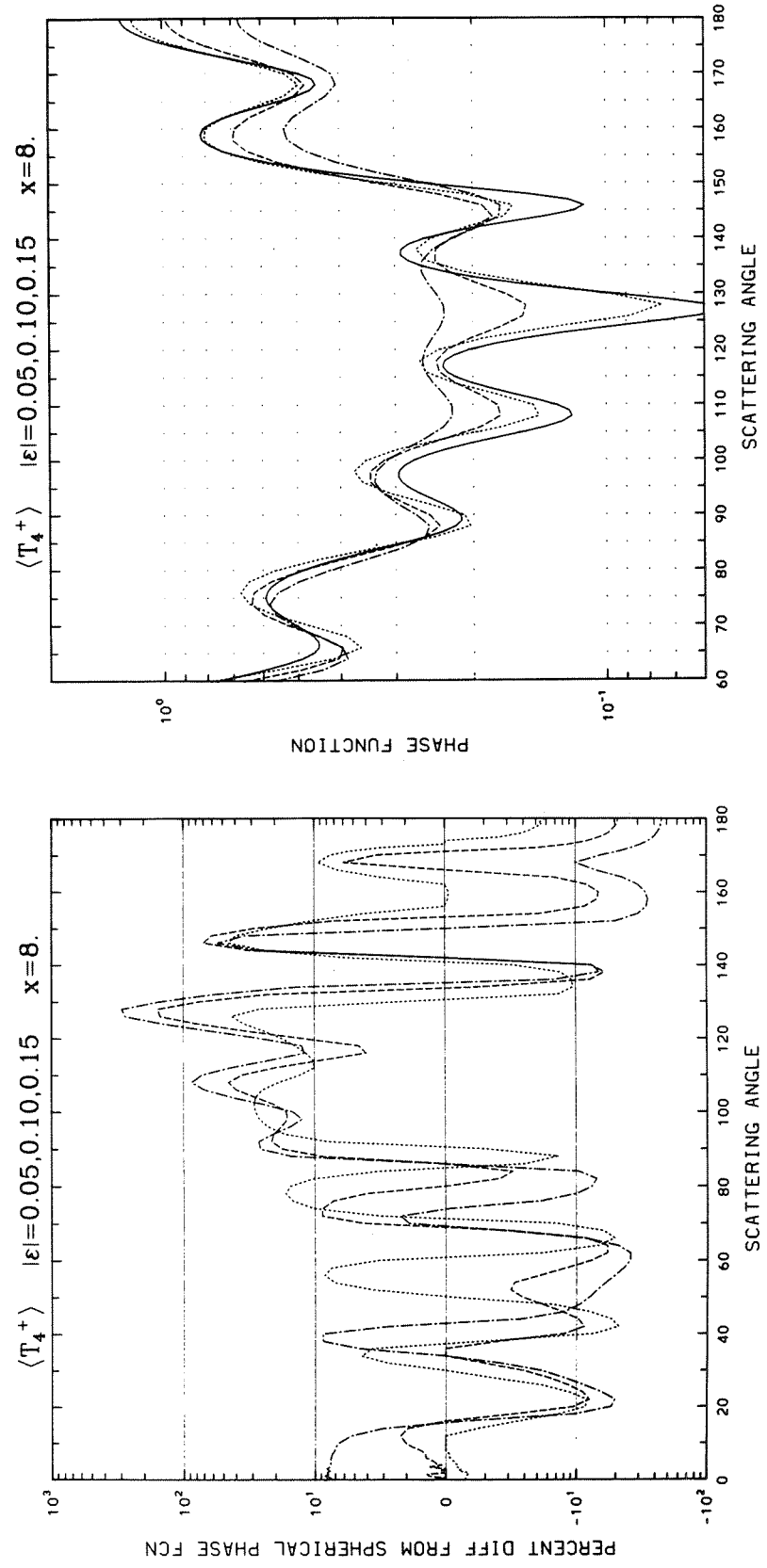

Appendix C (Continued)

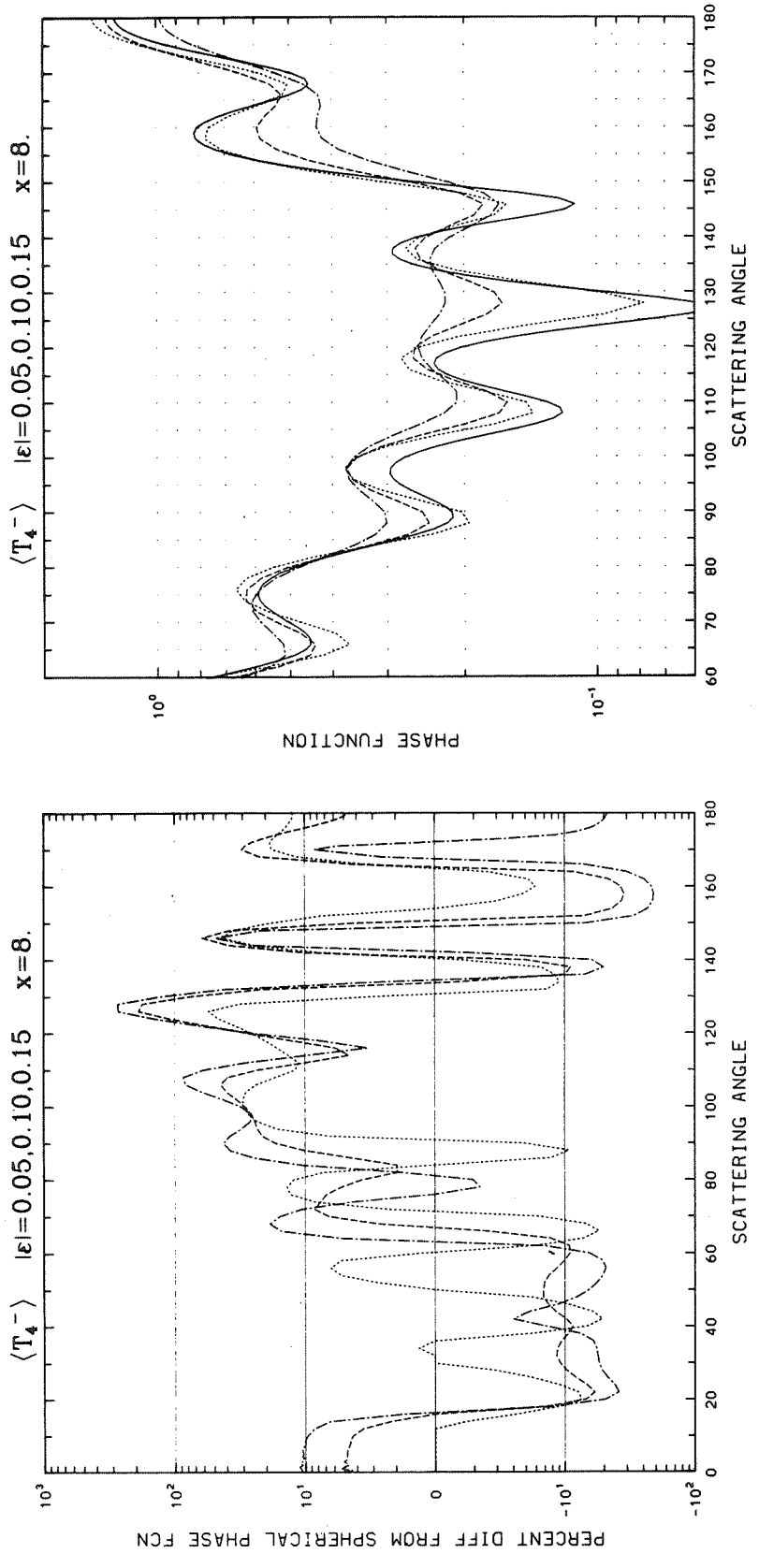

Appendix C (Continued)

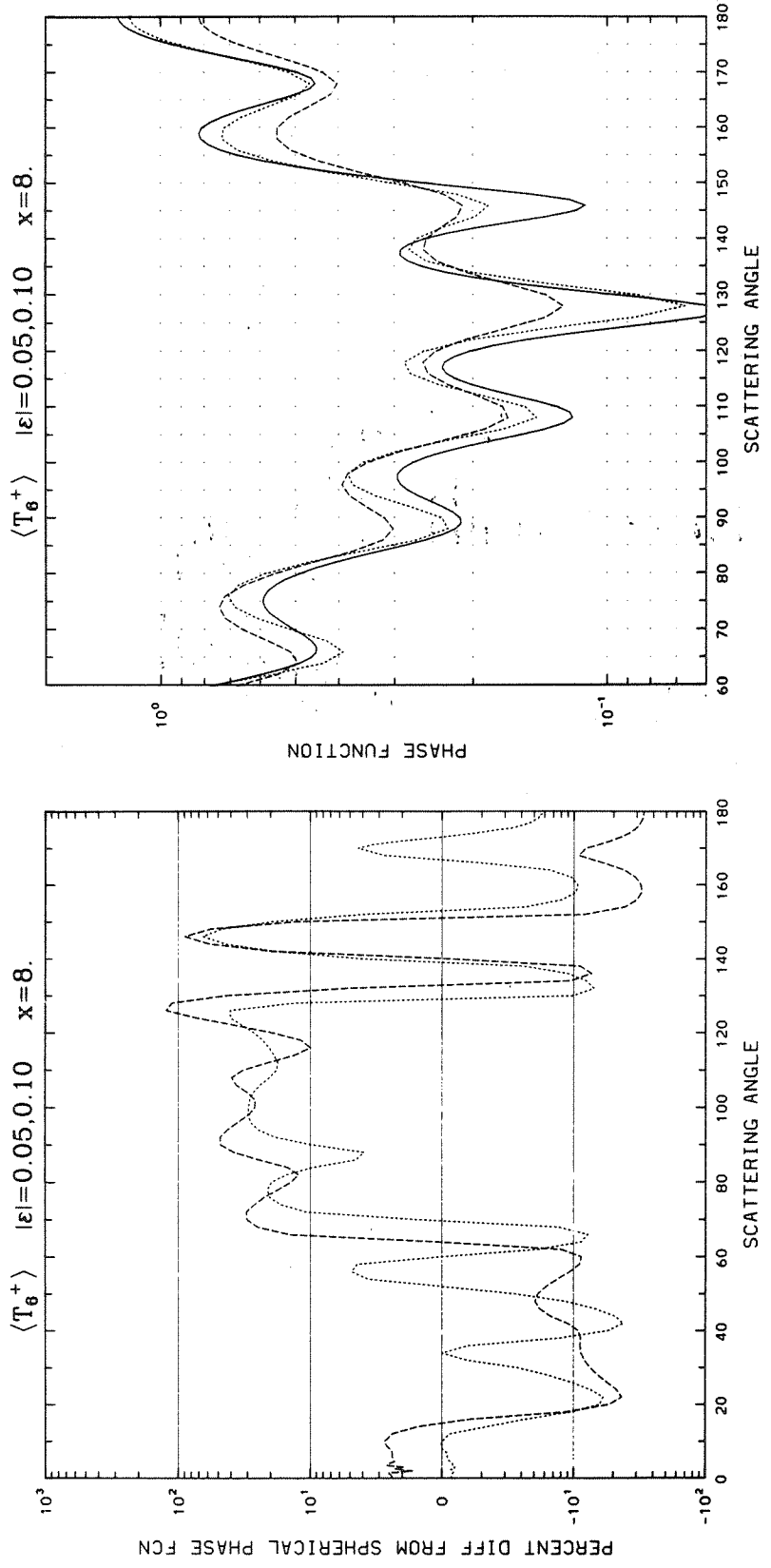

Appendix C (Continued)

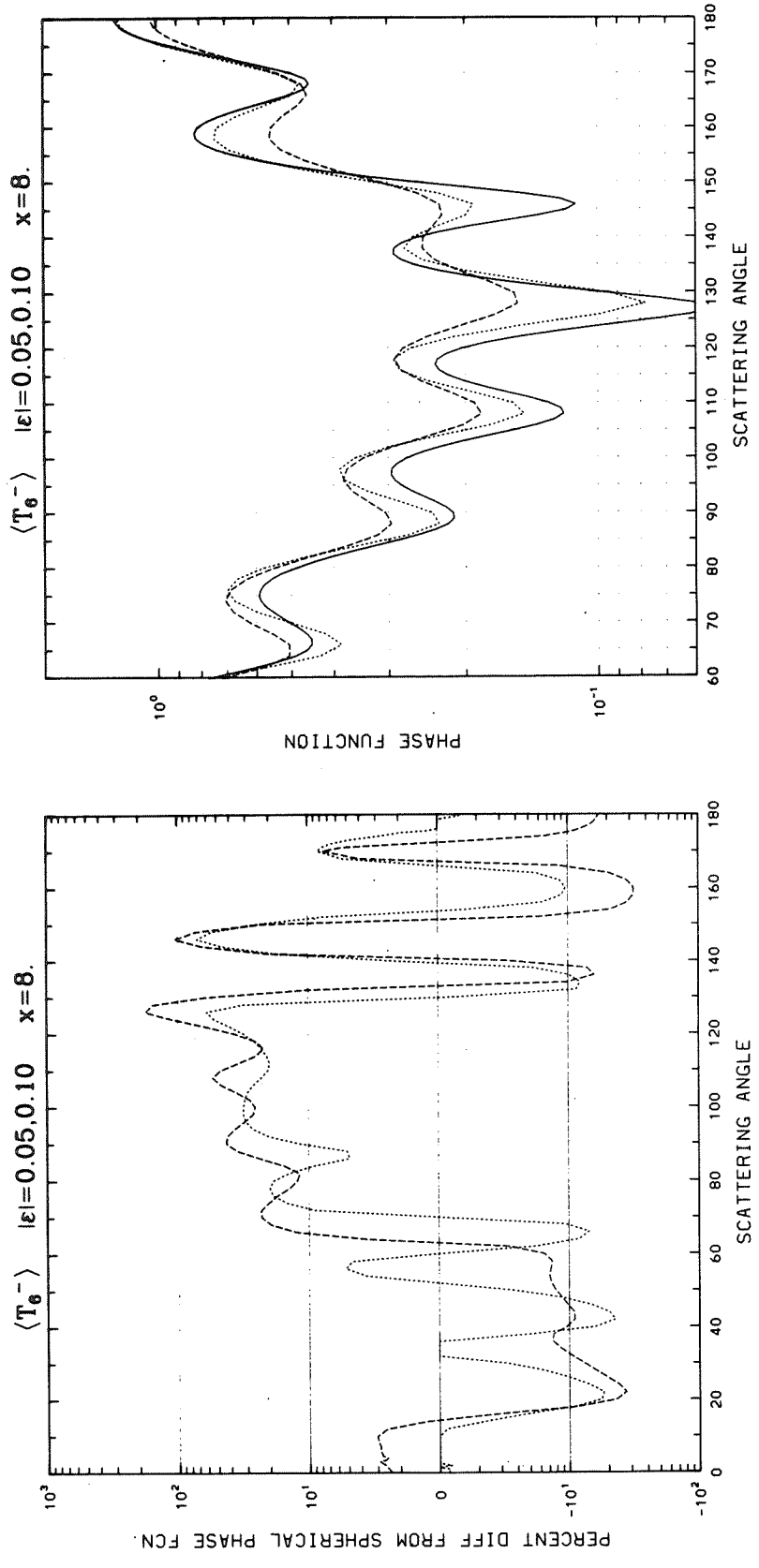

Appendix C (Continued)

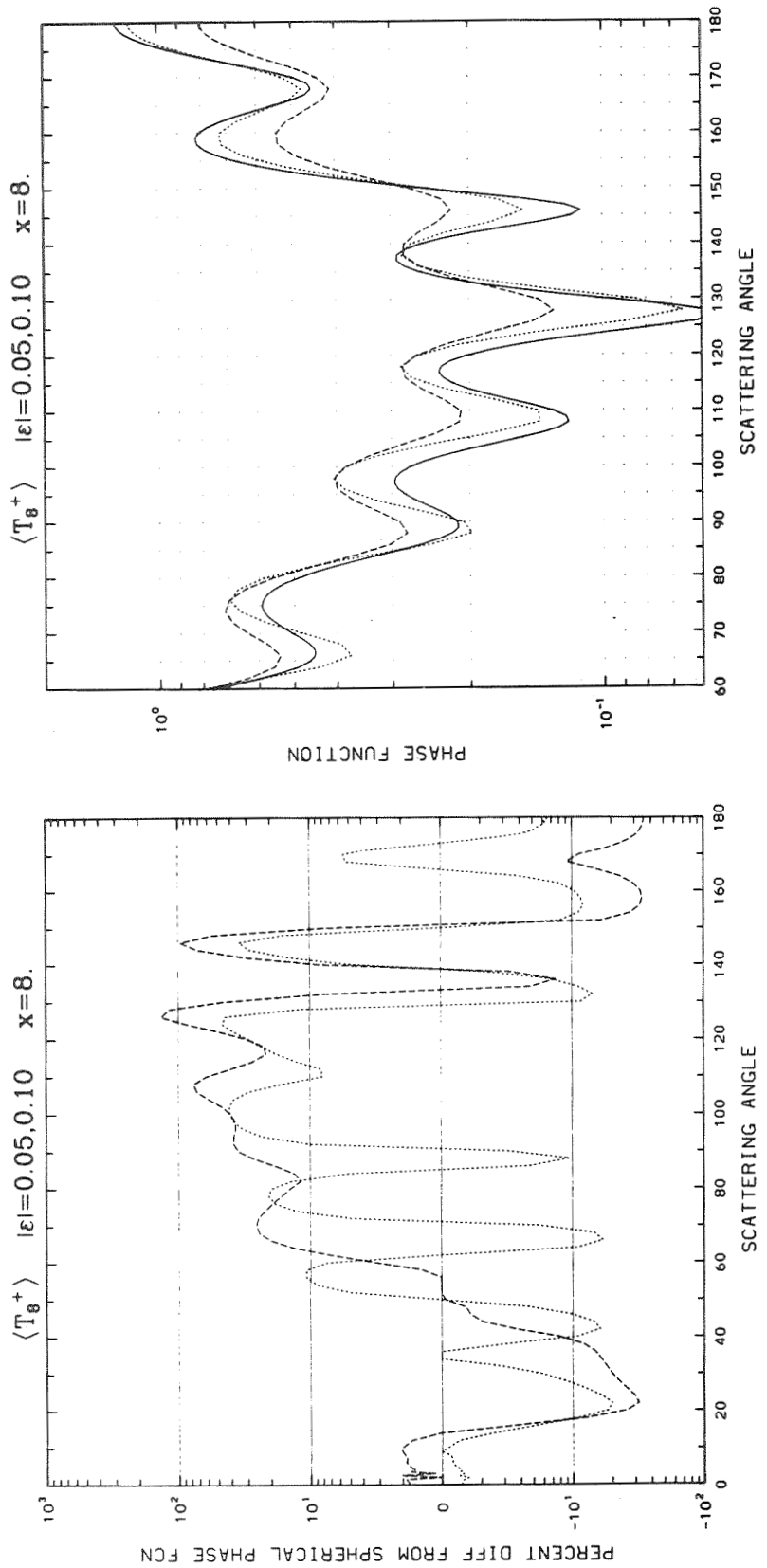

Appendix C (Continued)

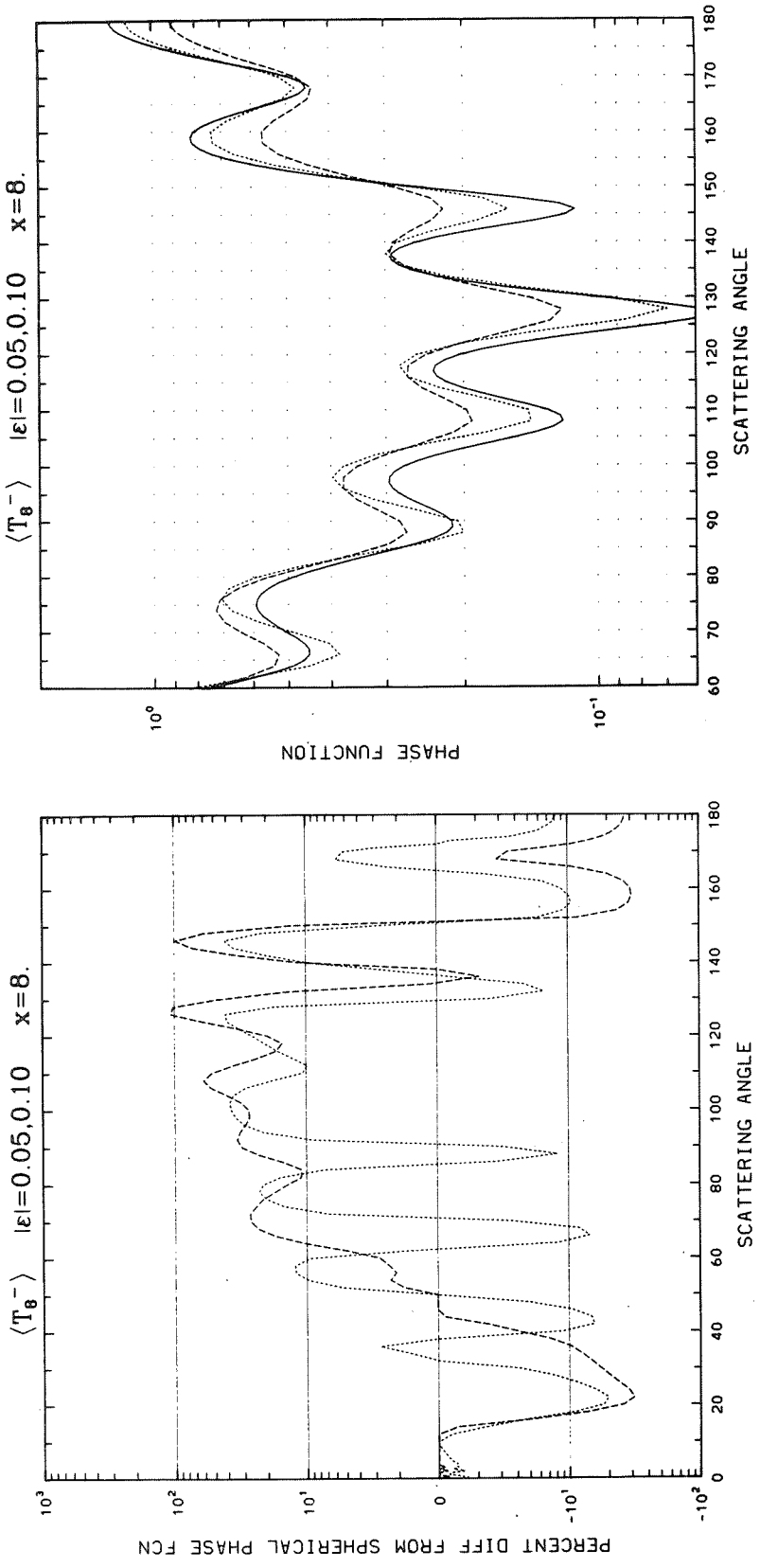

Appendix C (Continued)

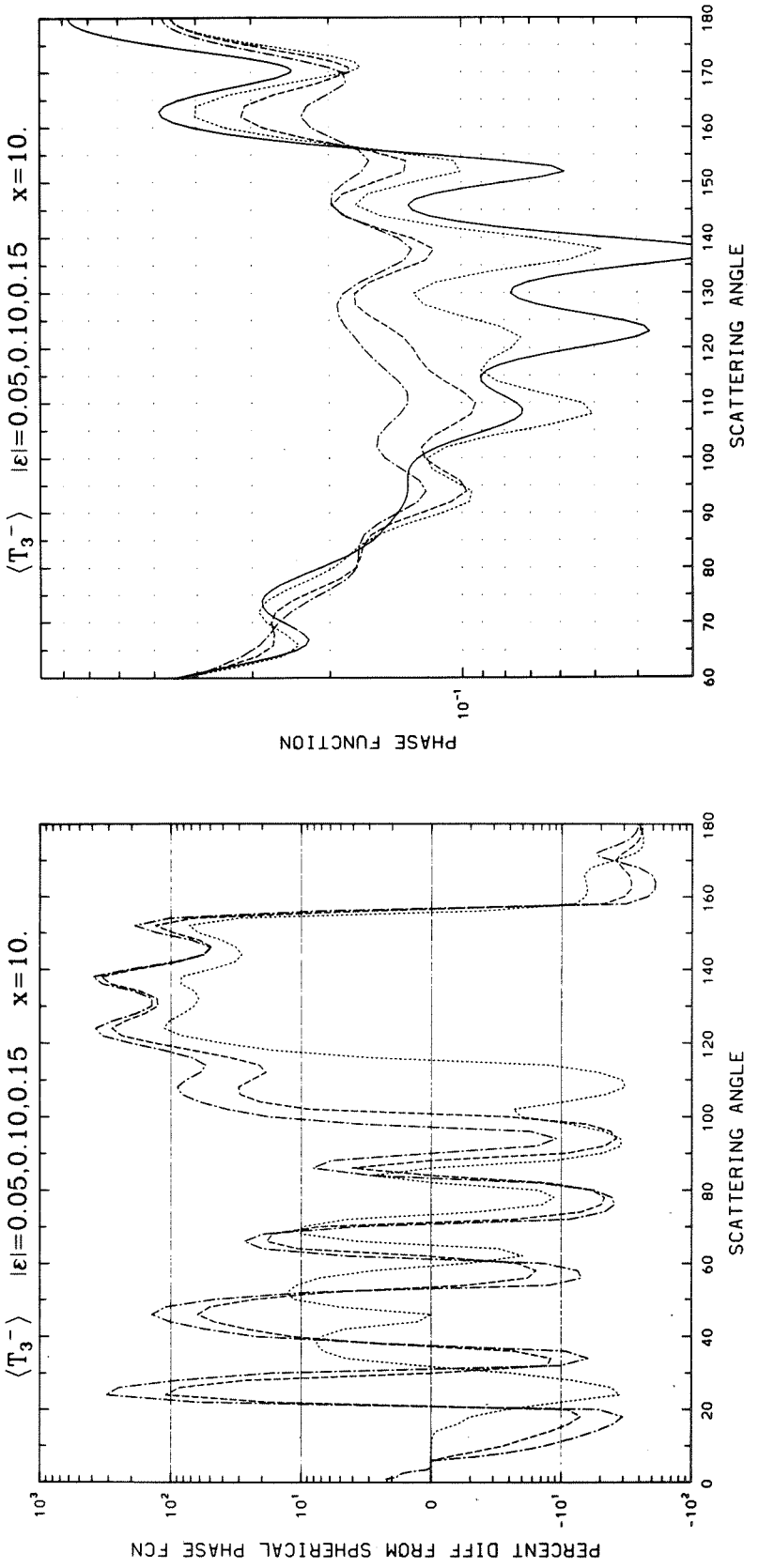

Appendix C (Continued)

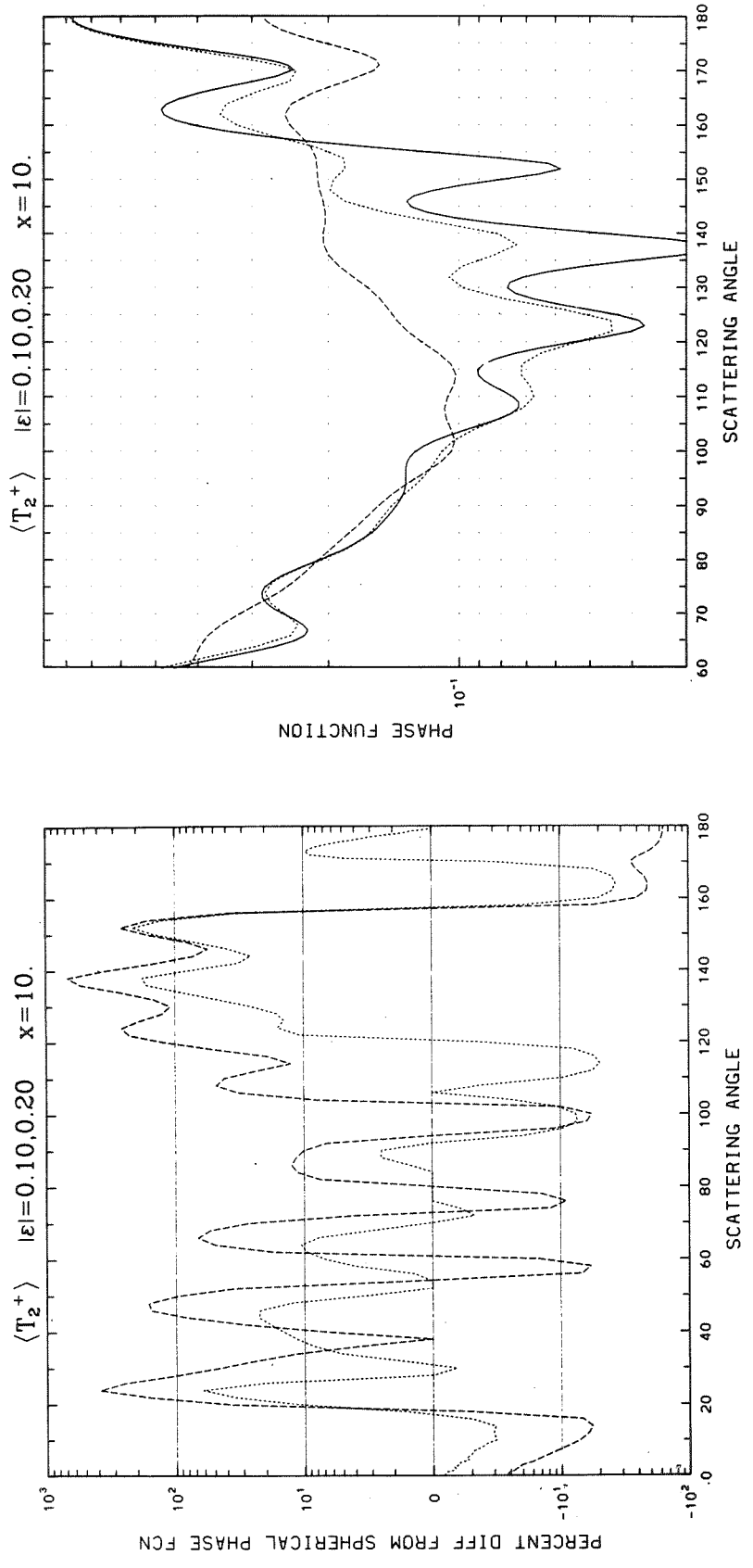

Appendix C (Continued)

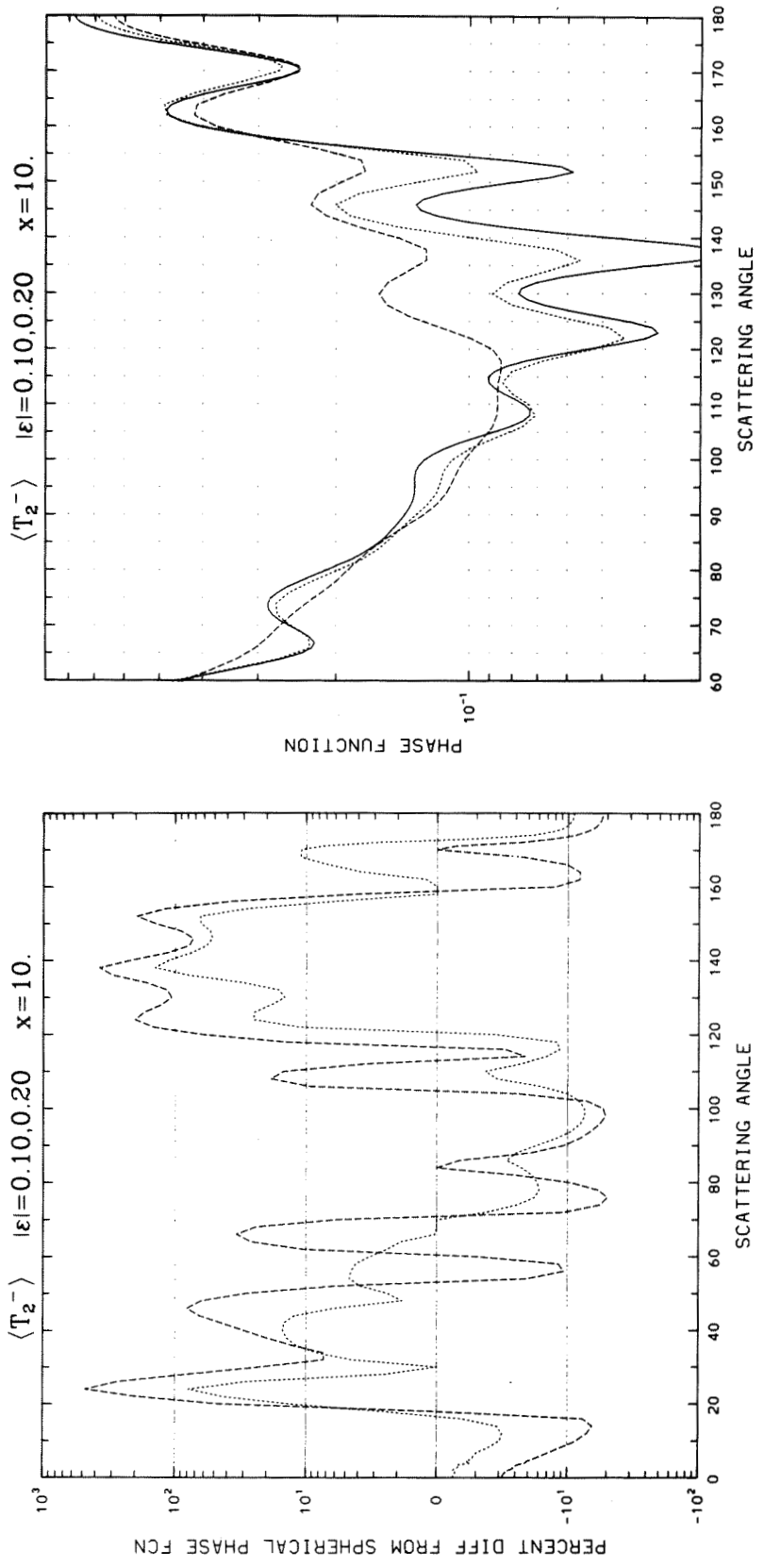

Appendix C (Continued)

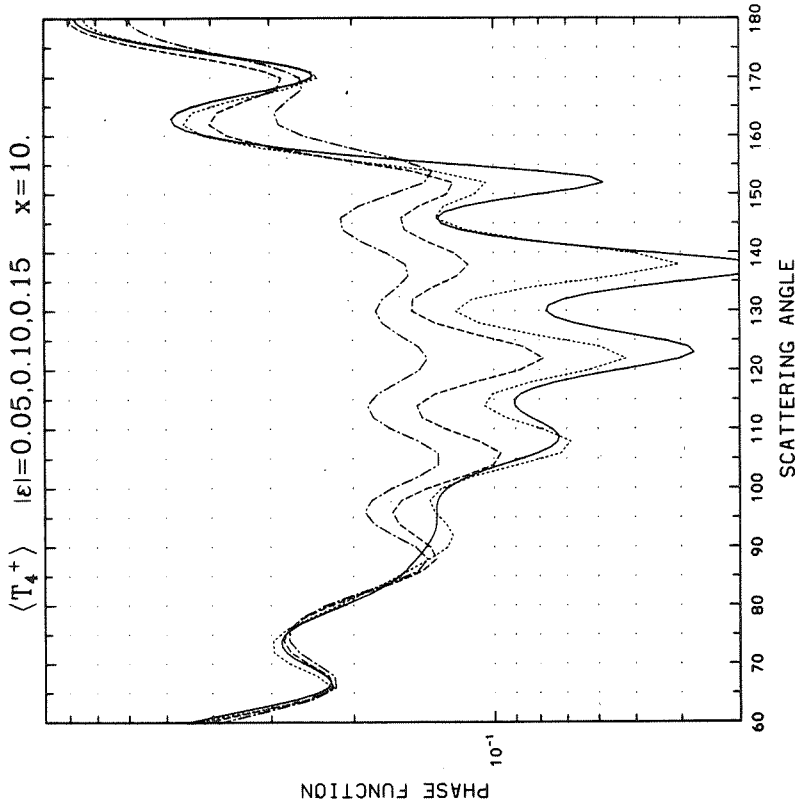

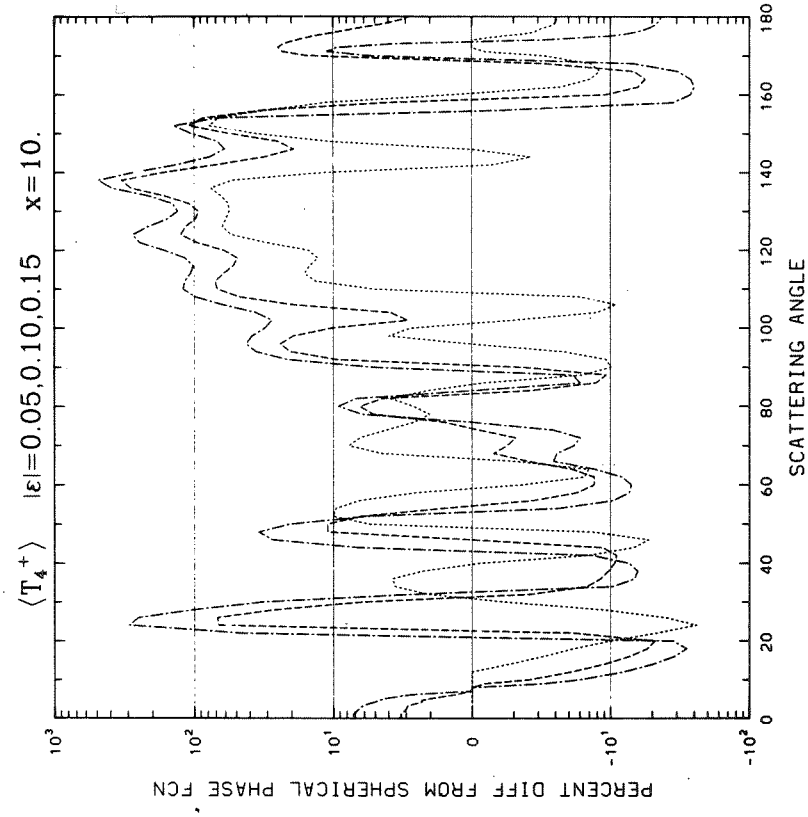

Appendix C (Continued)

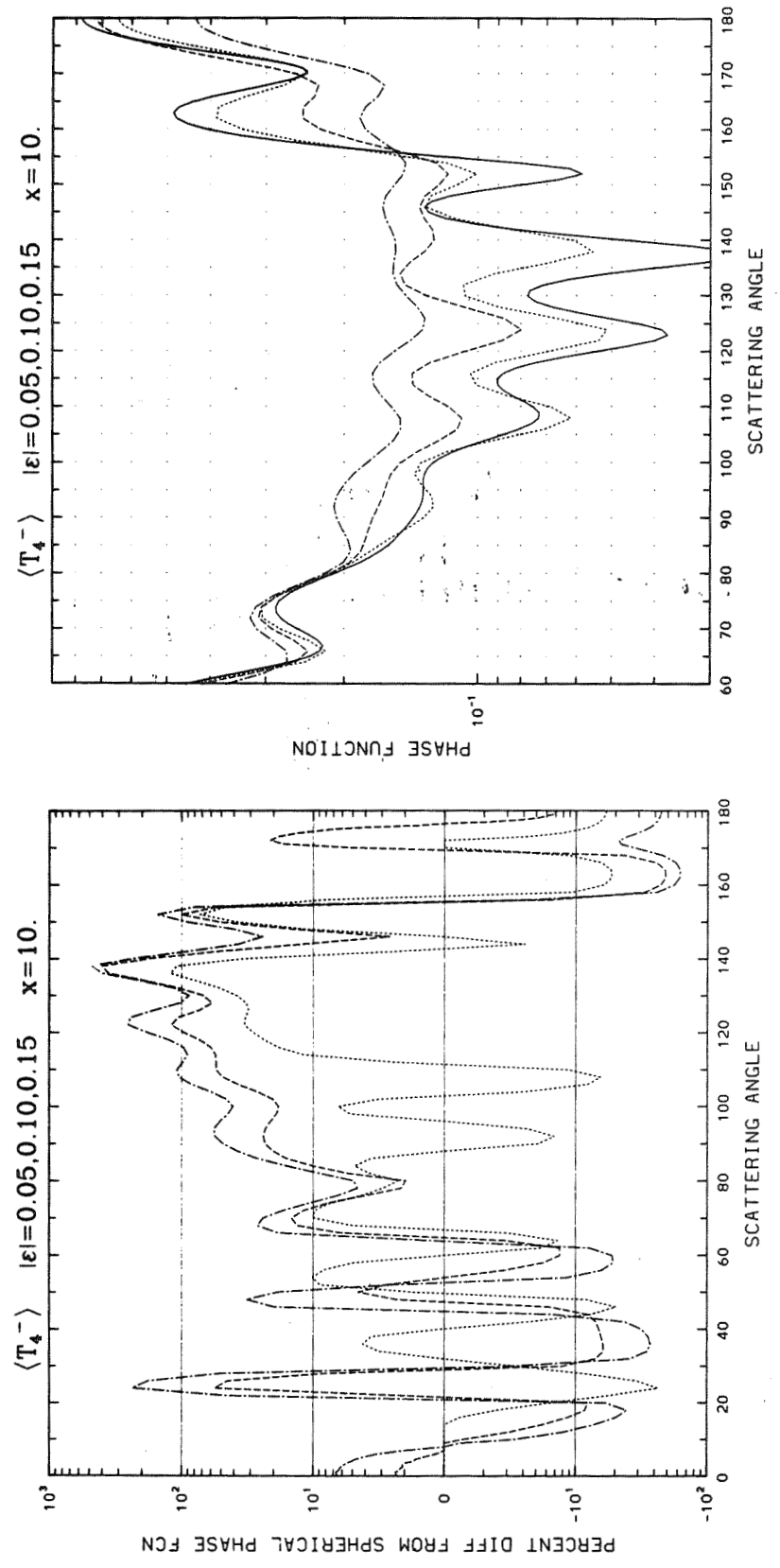

Appendix C (Continued)

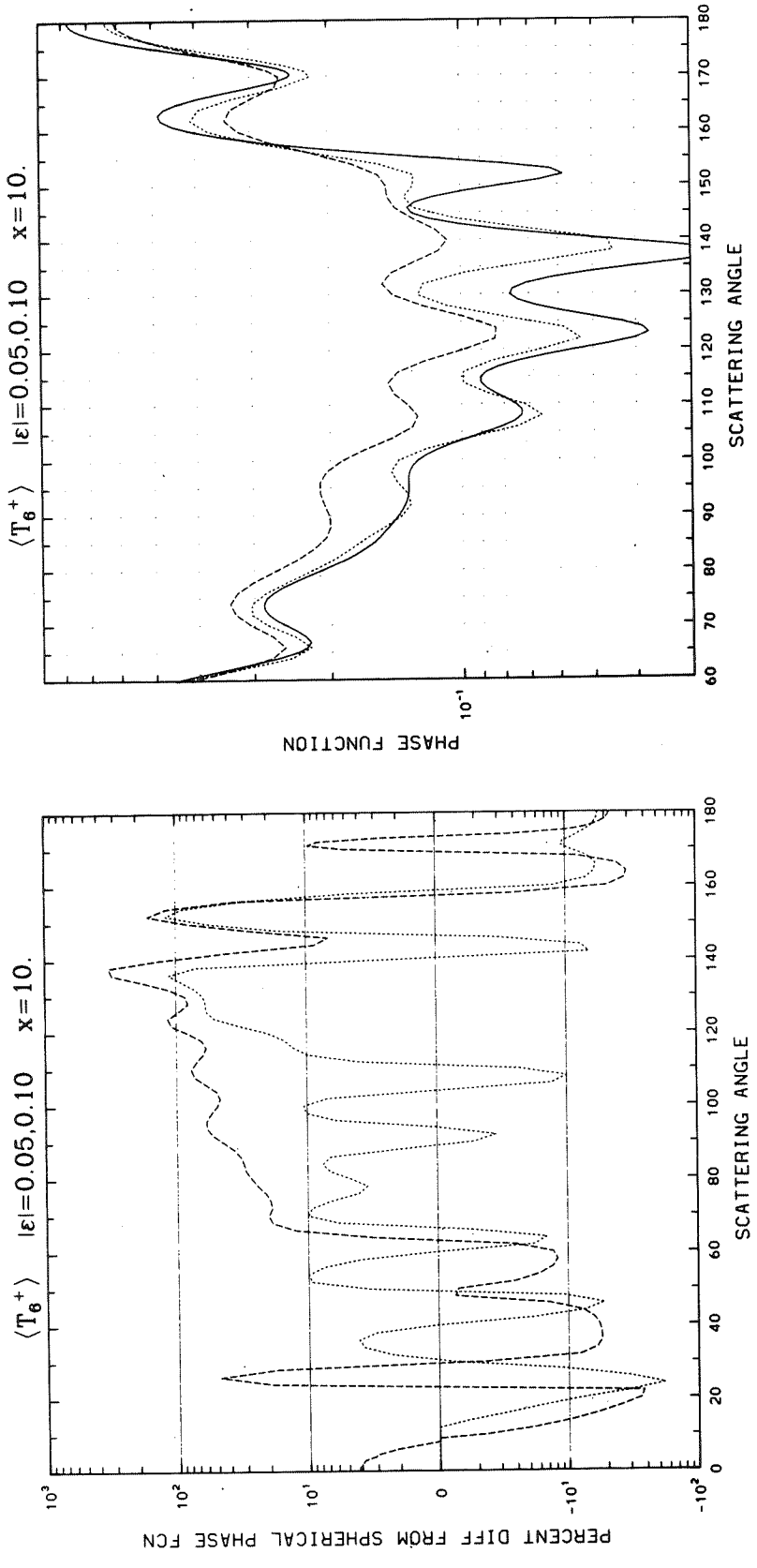

Appendix C (Continued)

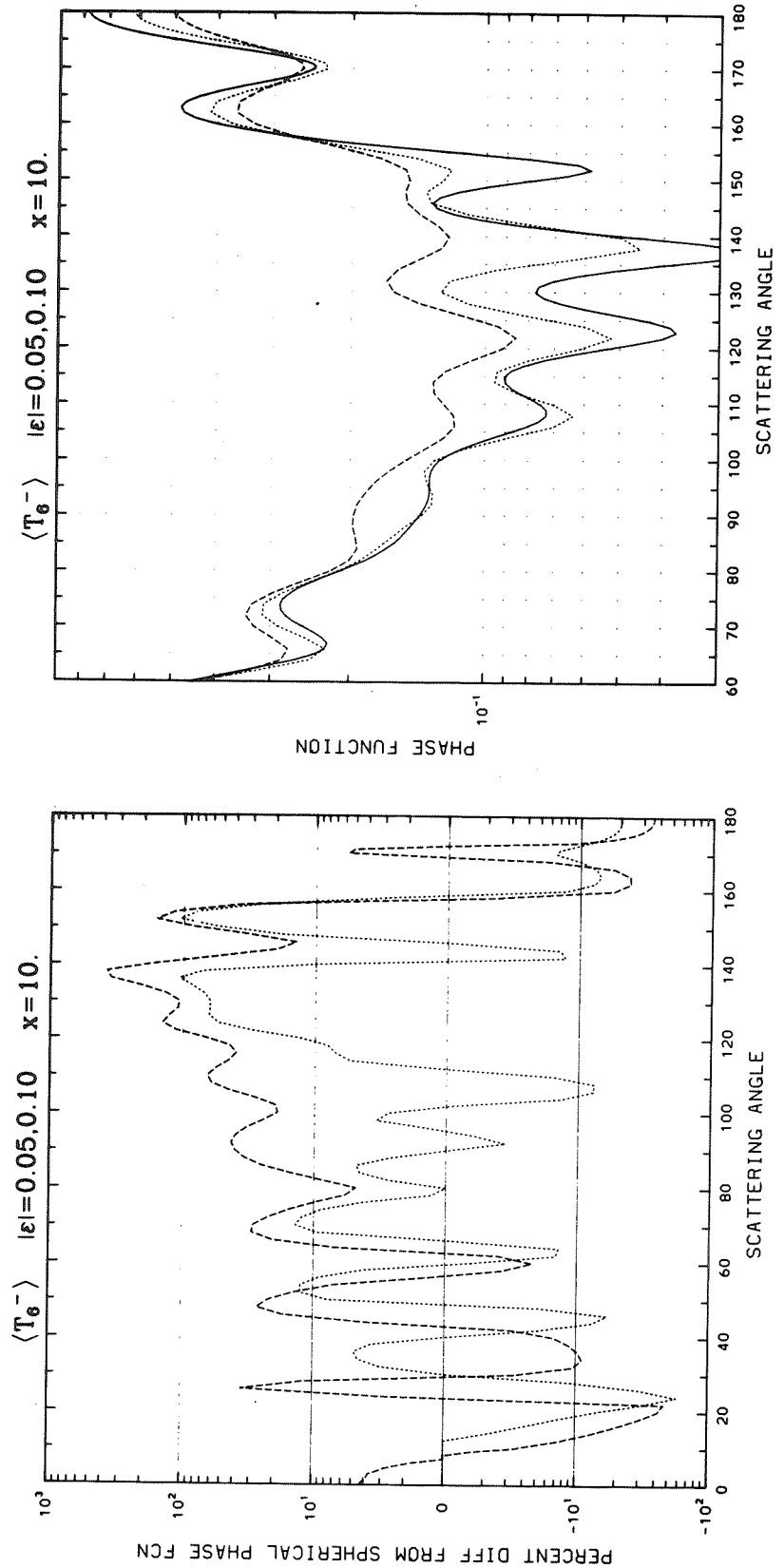

Appendix C (Continued)

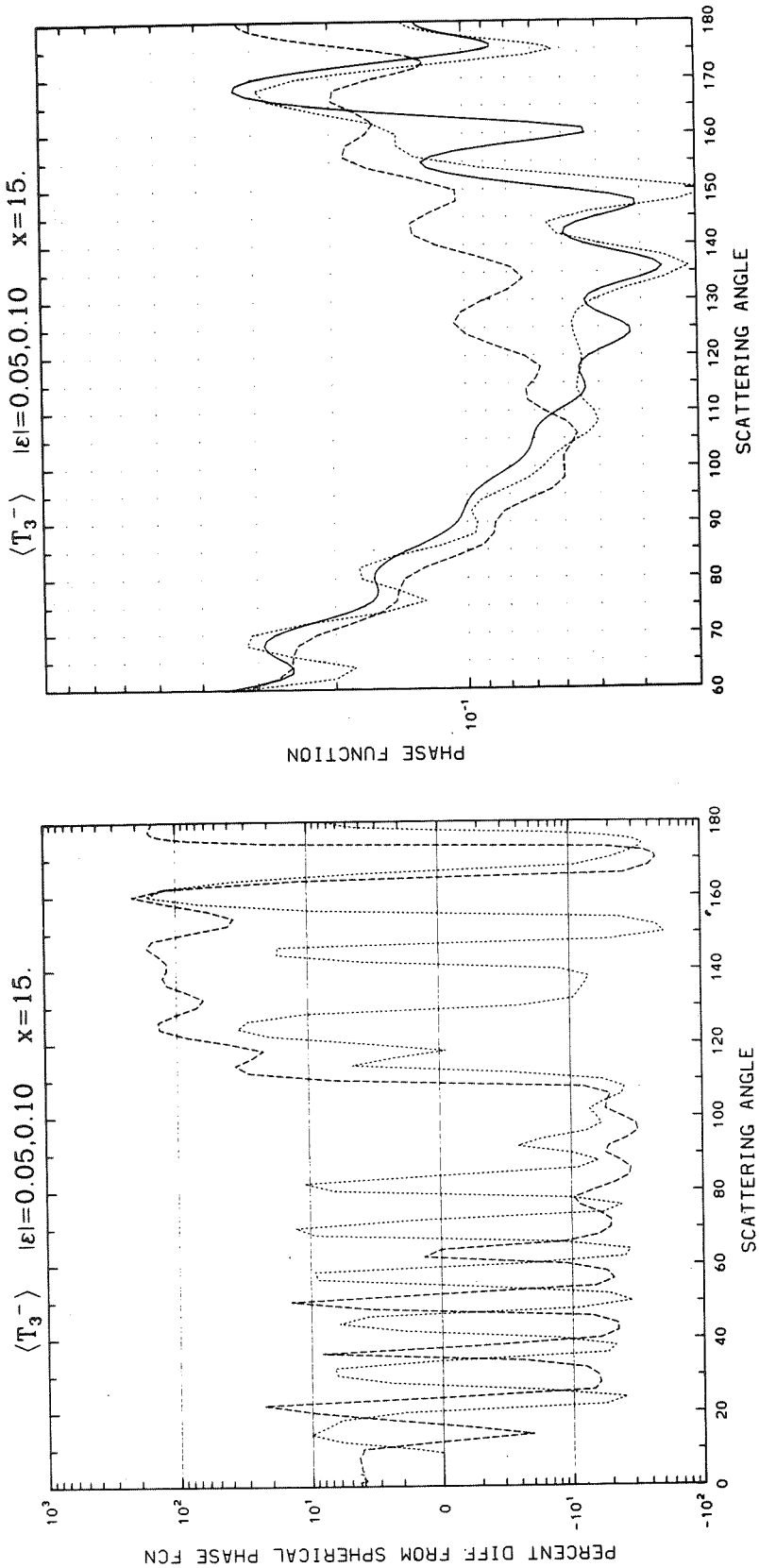

Appendix C (Continued)

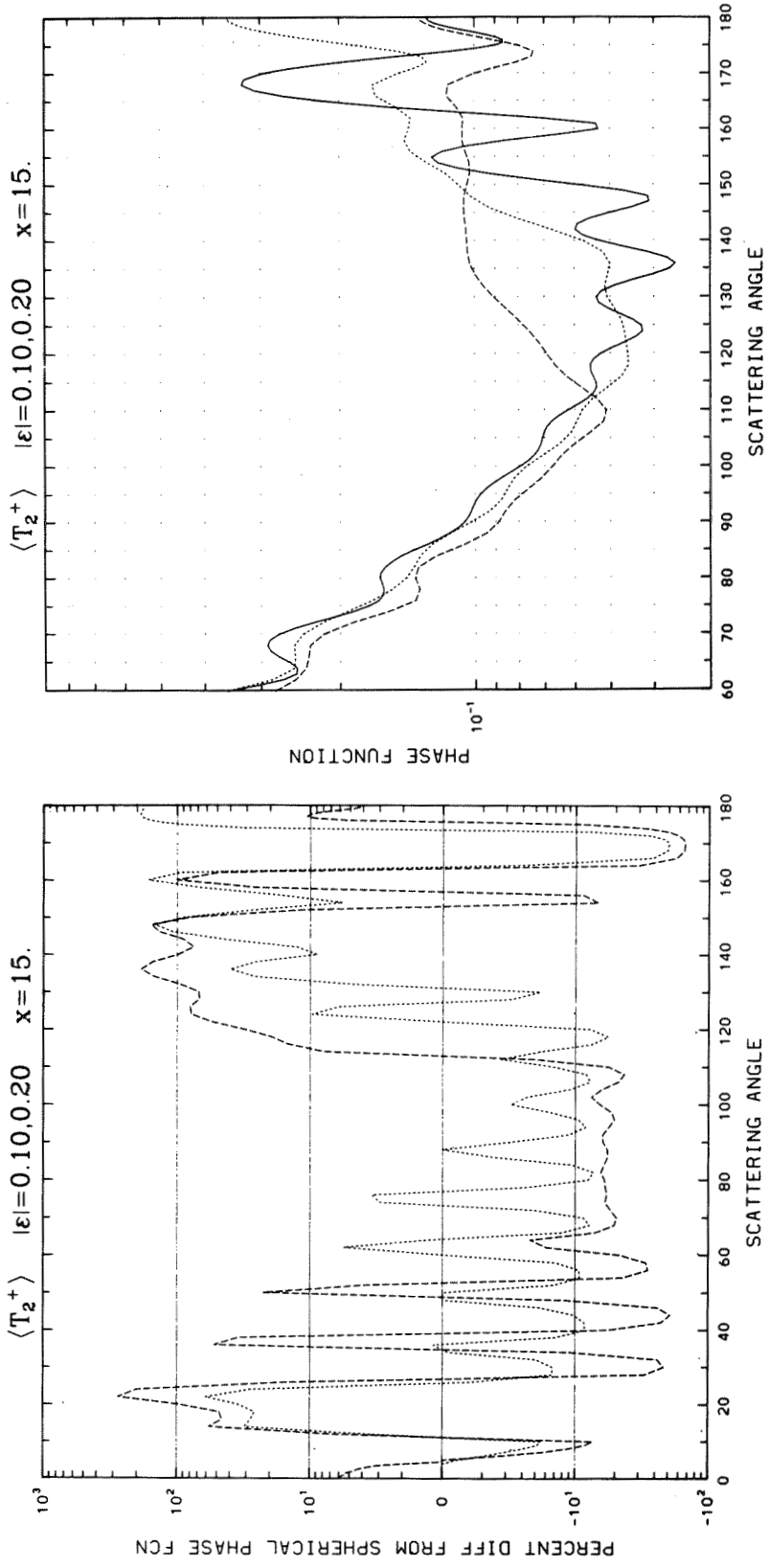

Appendix C (Continued)

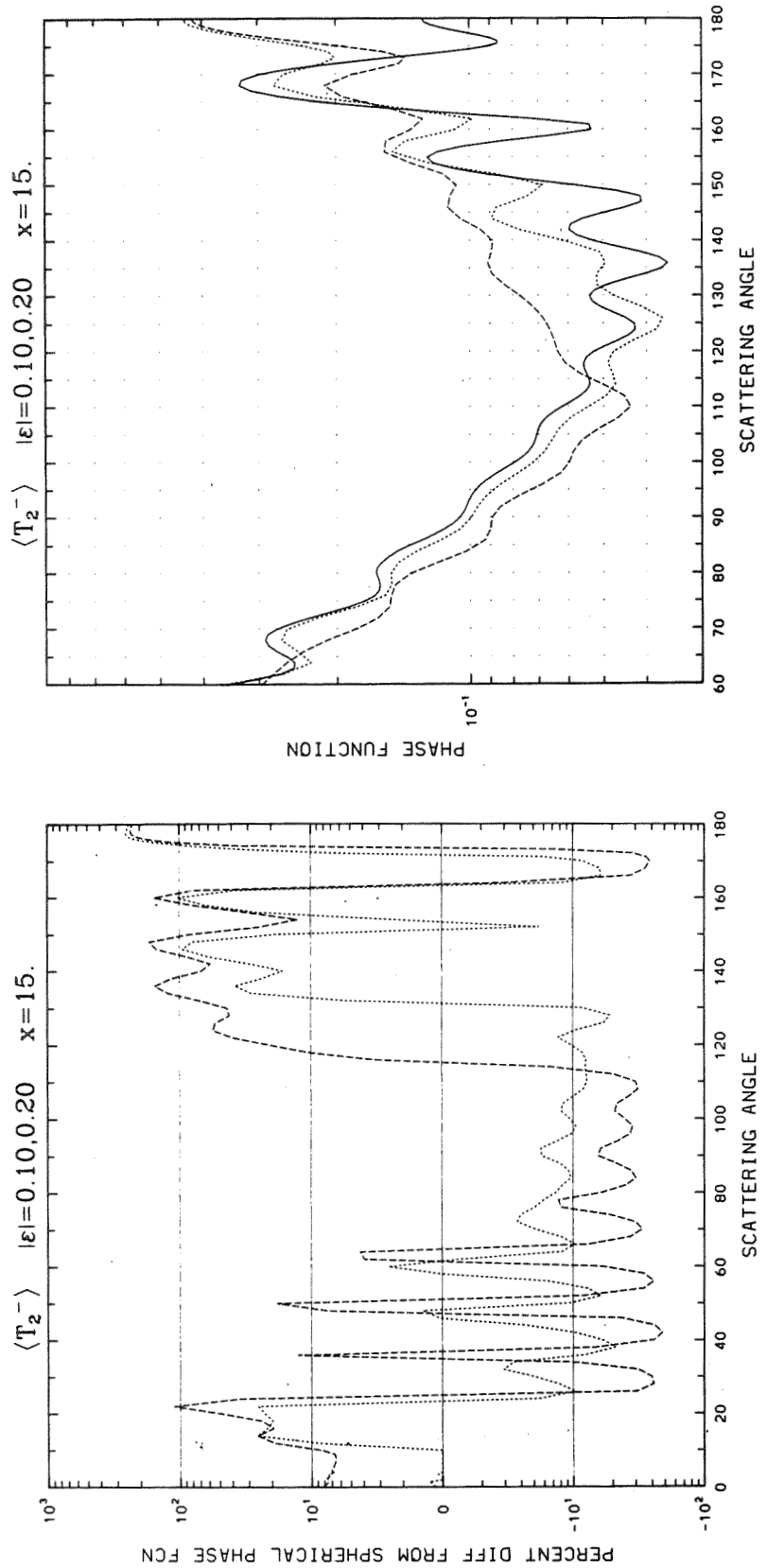

Appendix C (Continued)

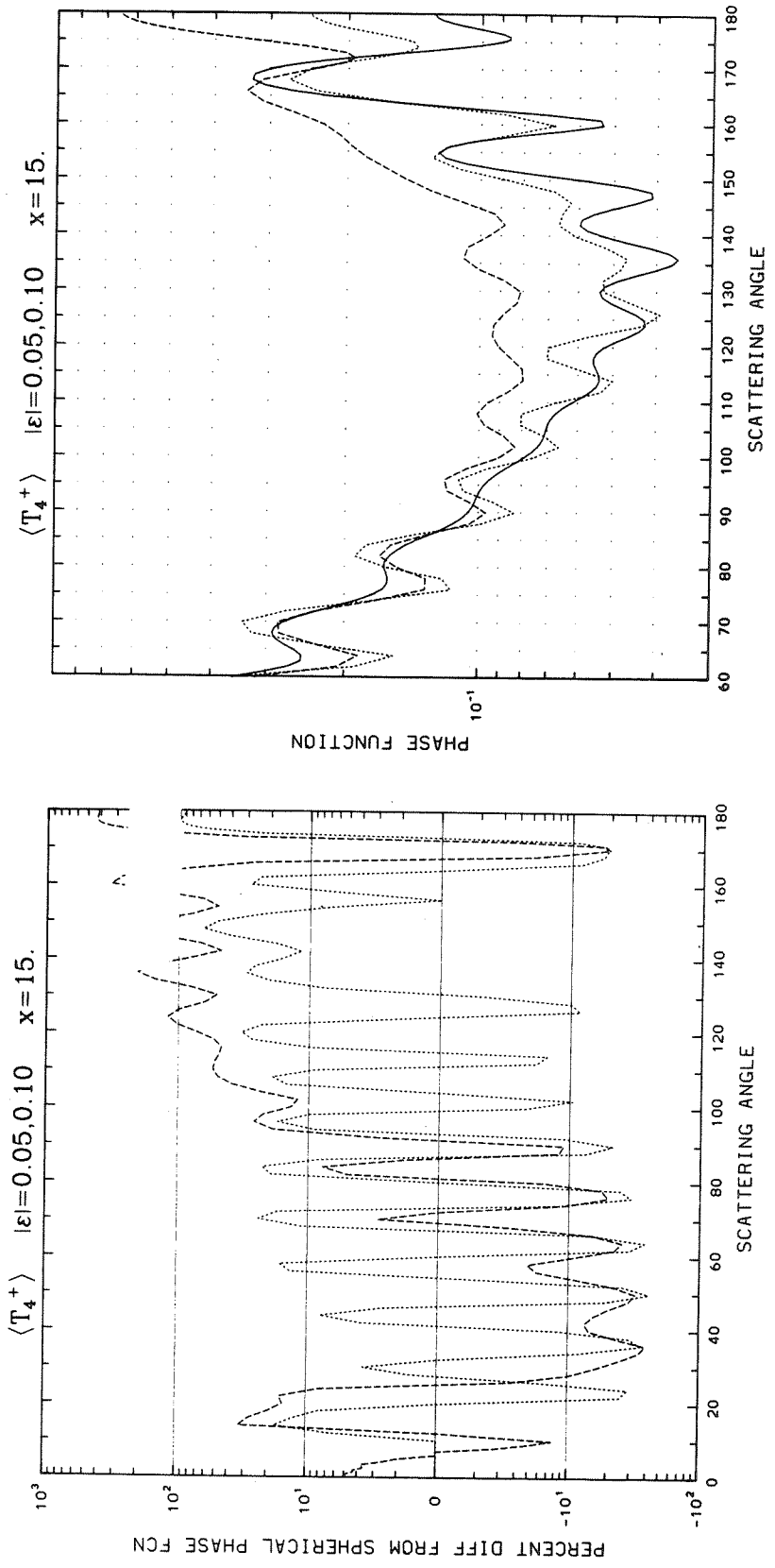

Appendix C (Continued)

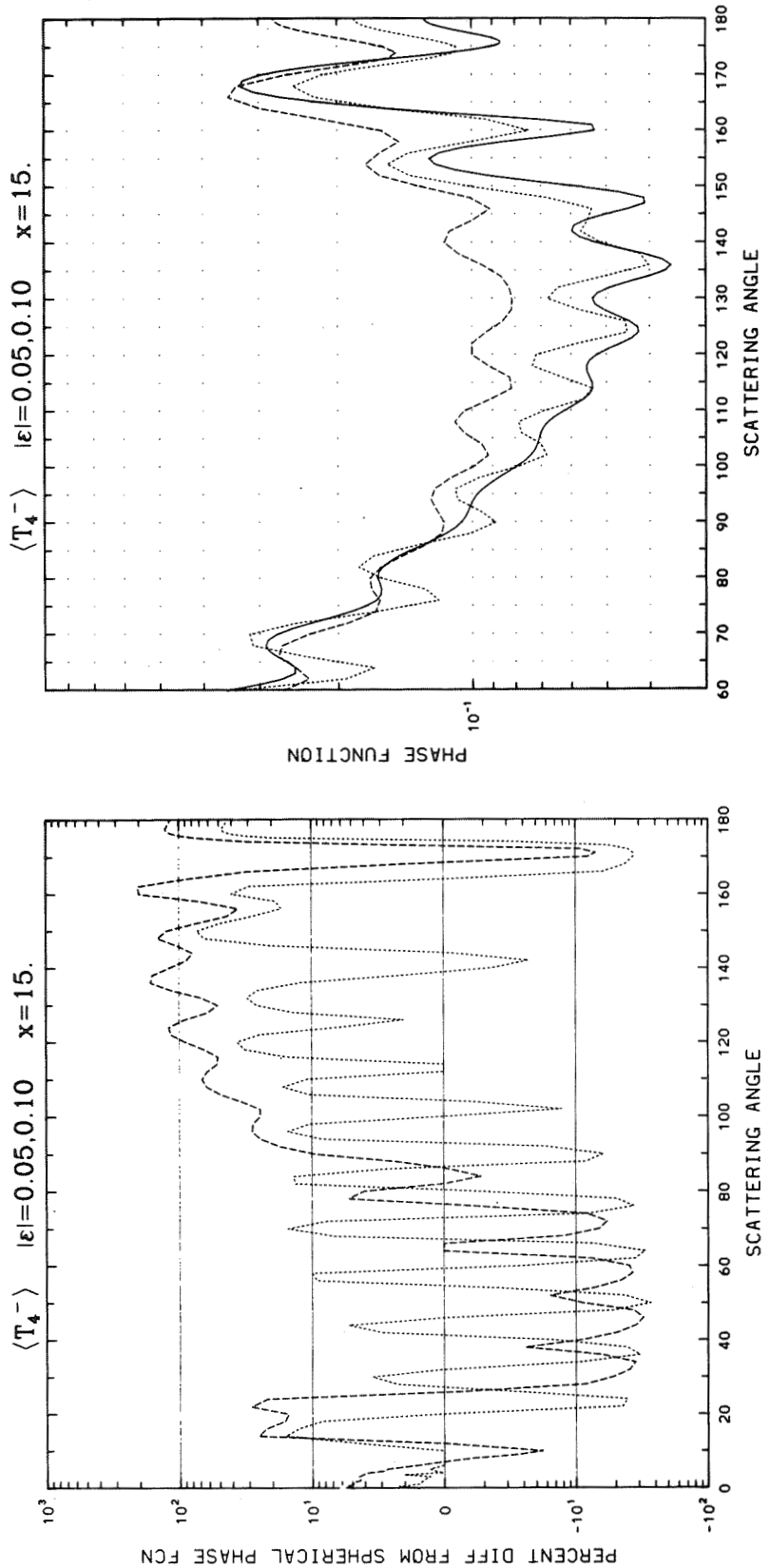

Appendix C (Continued)

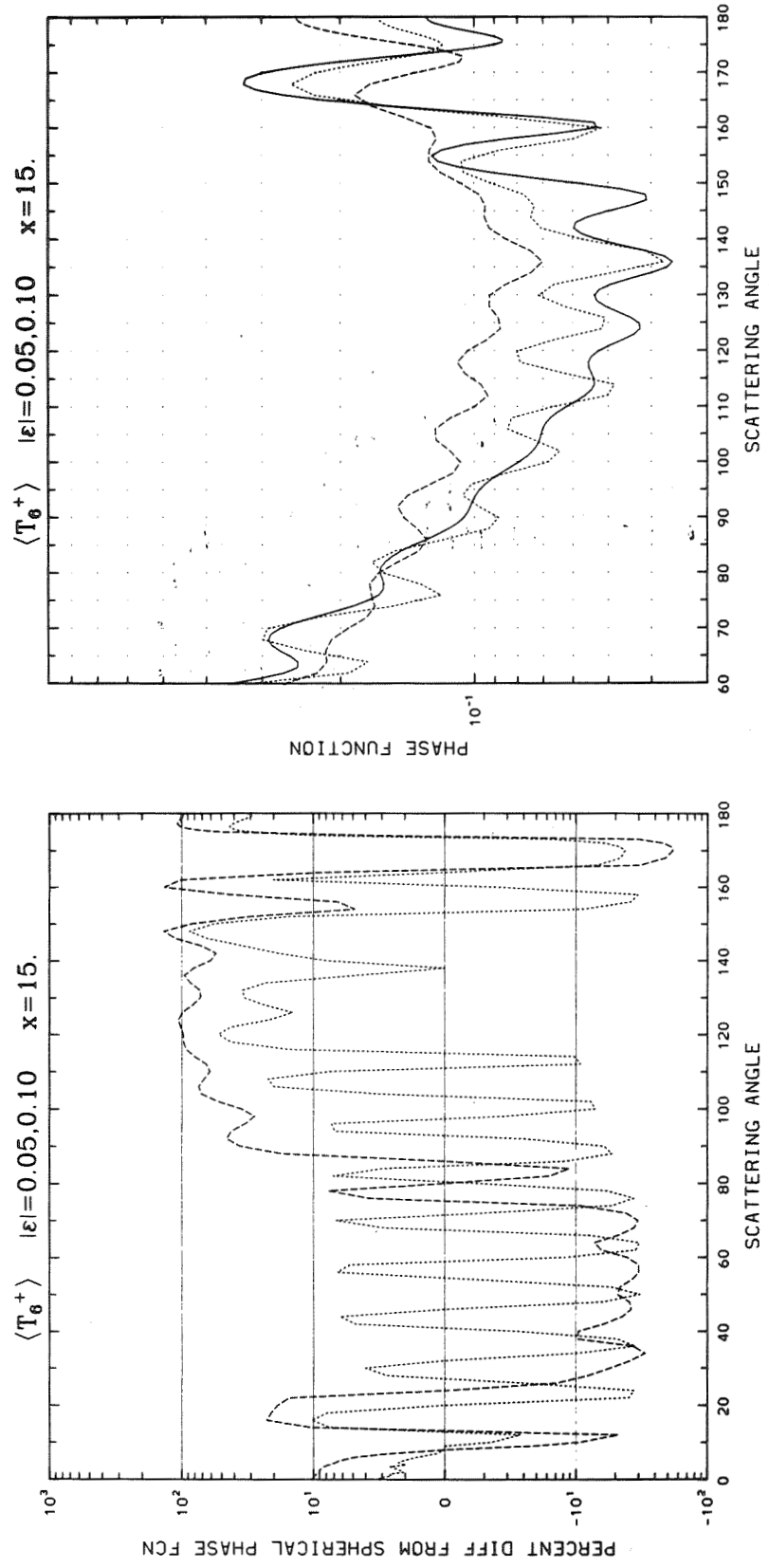

Appendix C (Continued)

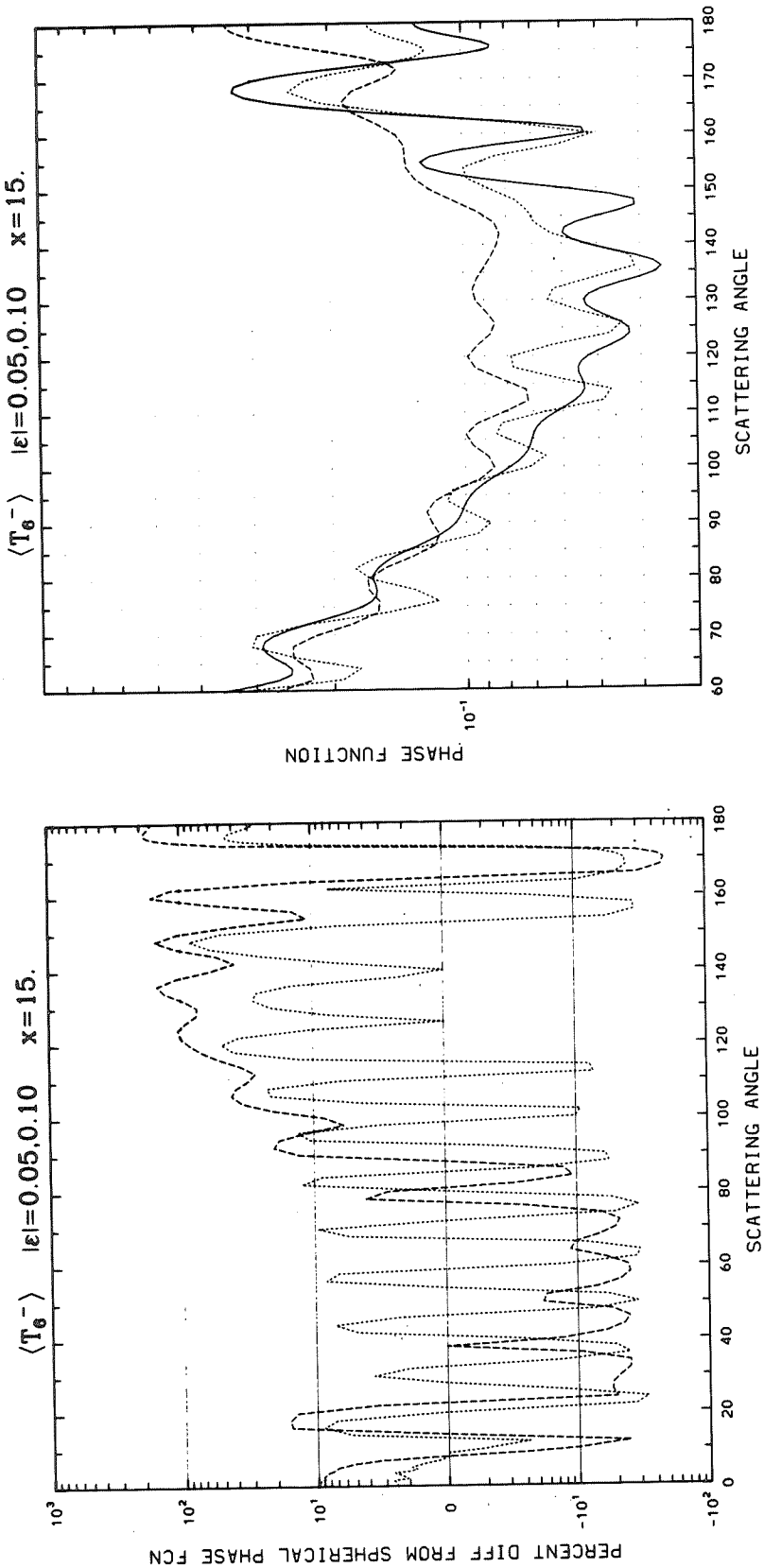

Appendix C (Continued)

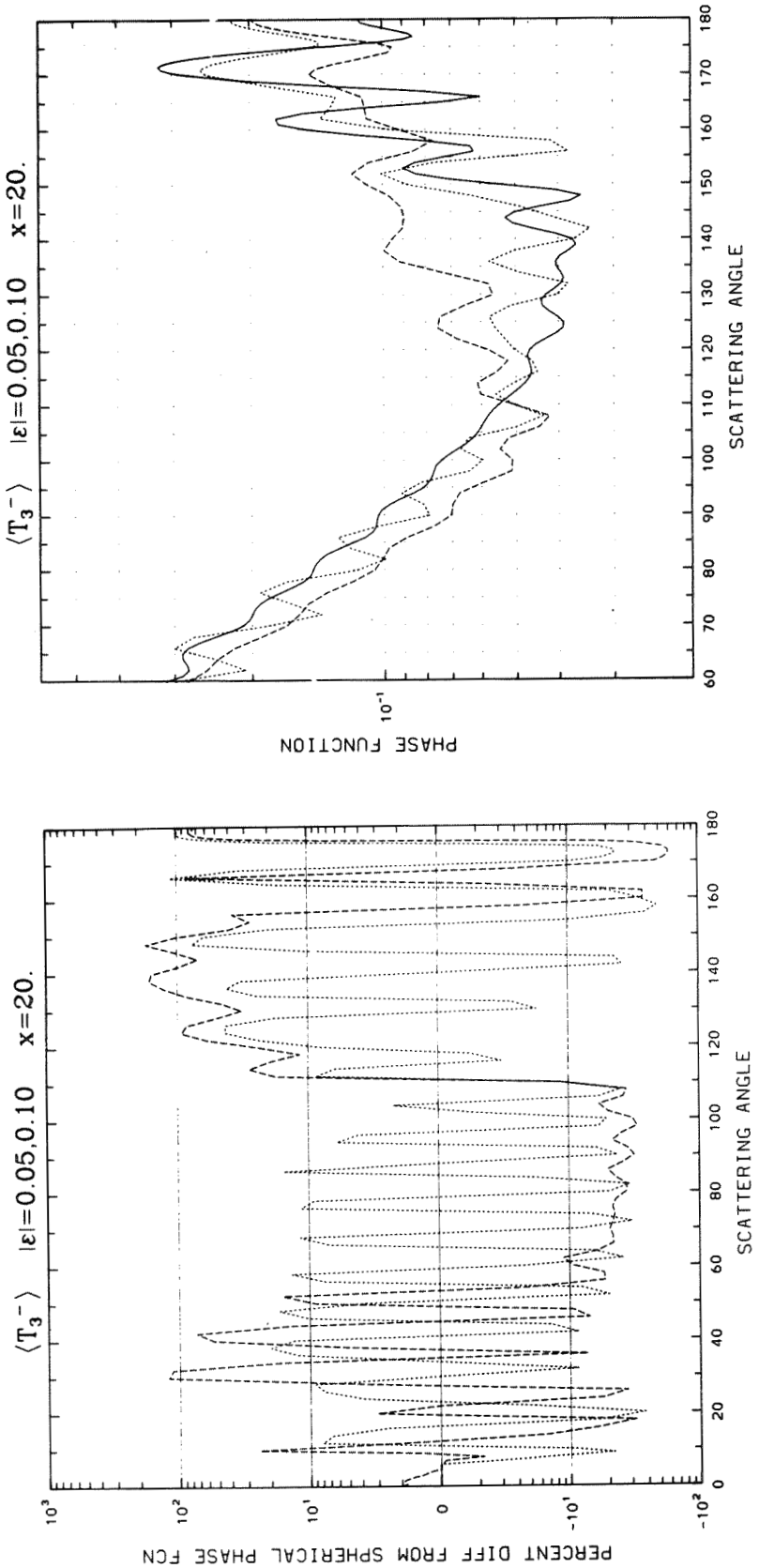

Appendix C (Continued)

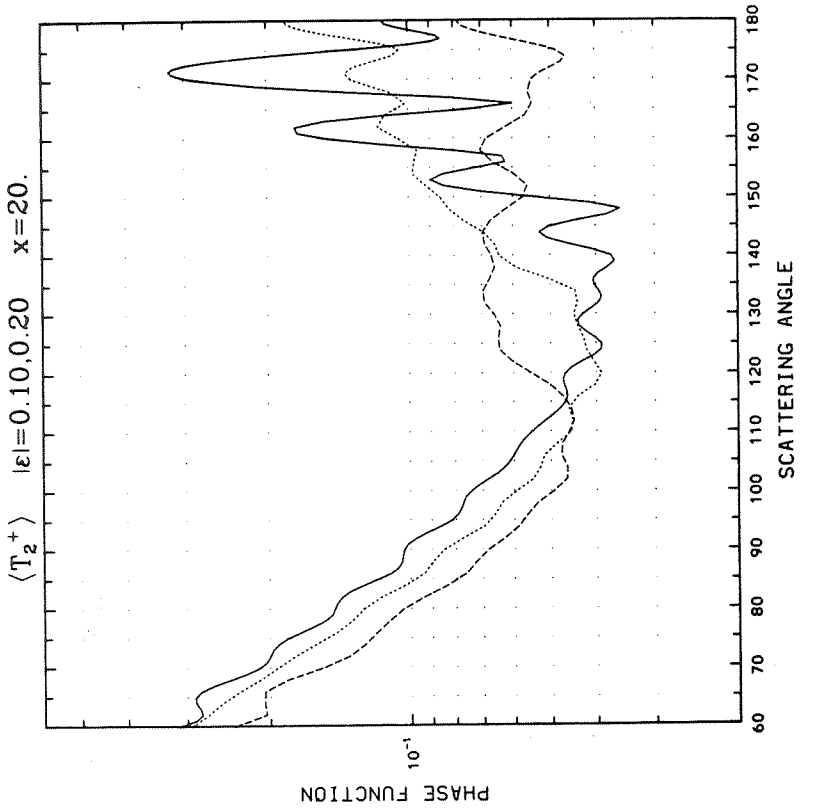

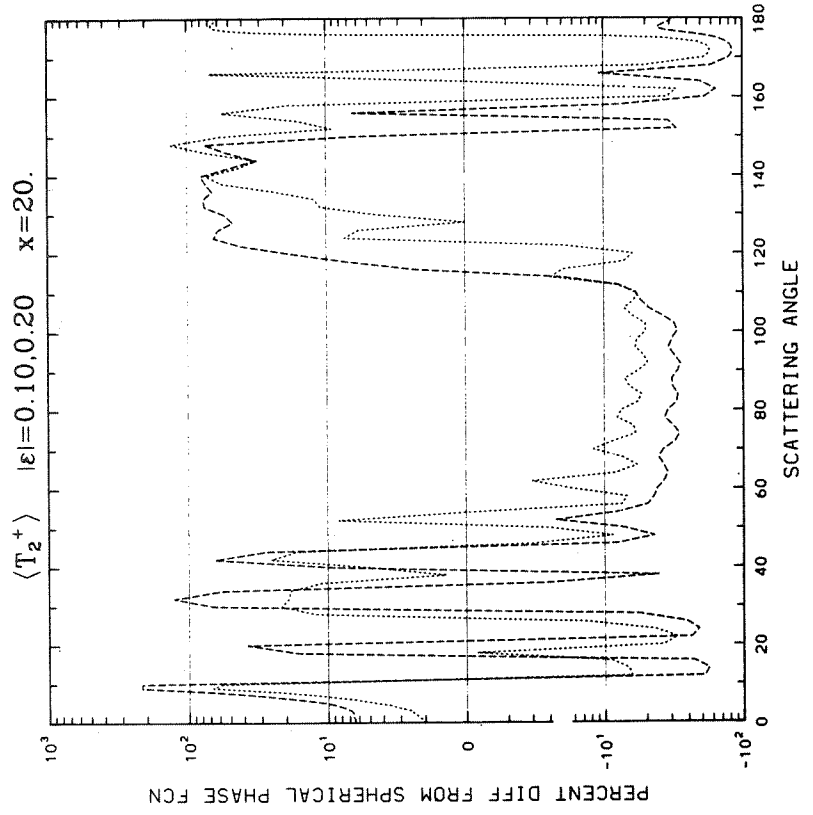

Appendix C (Continued)

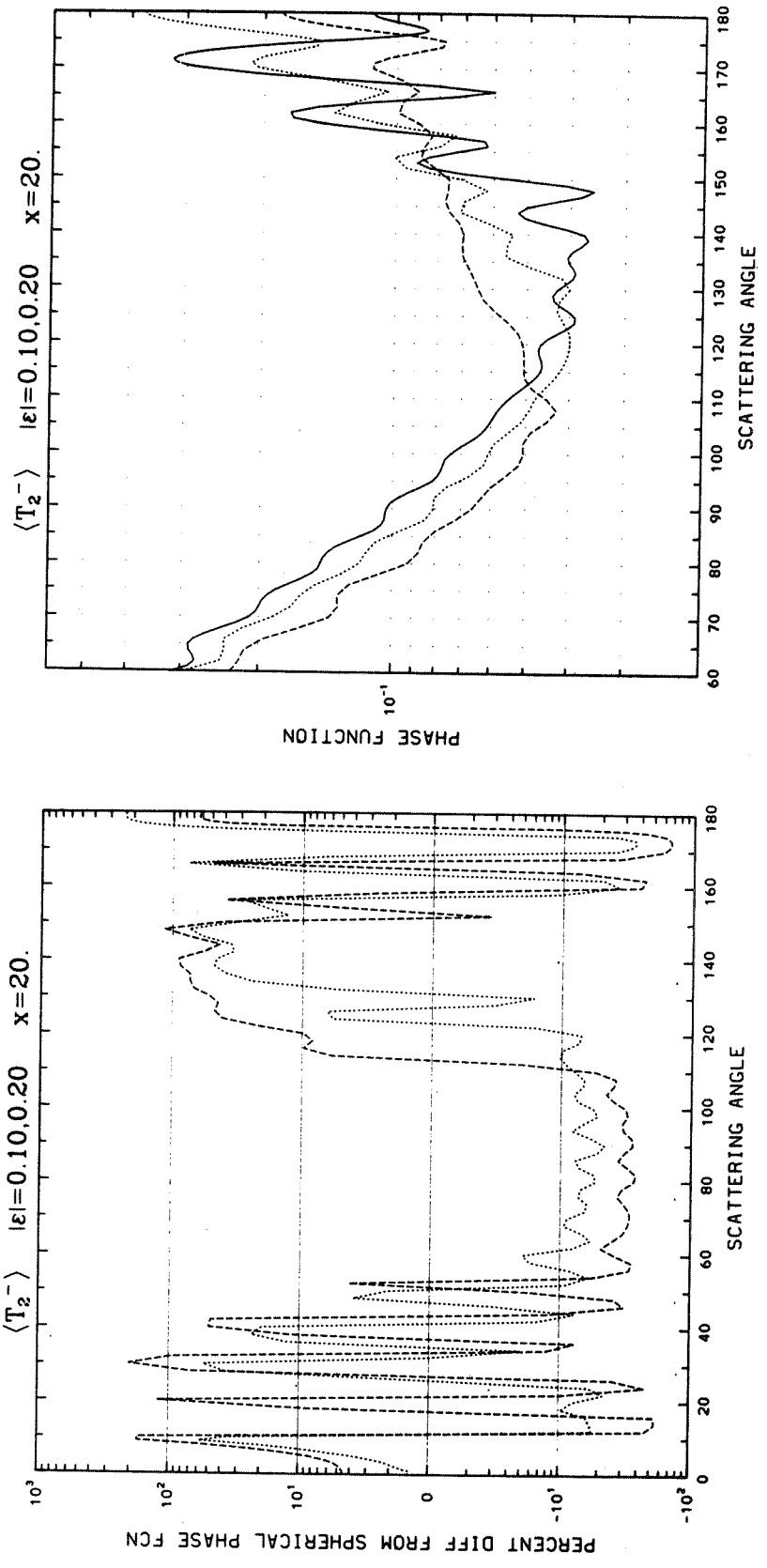

Appendix C (Continued)

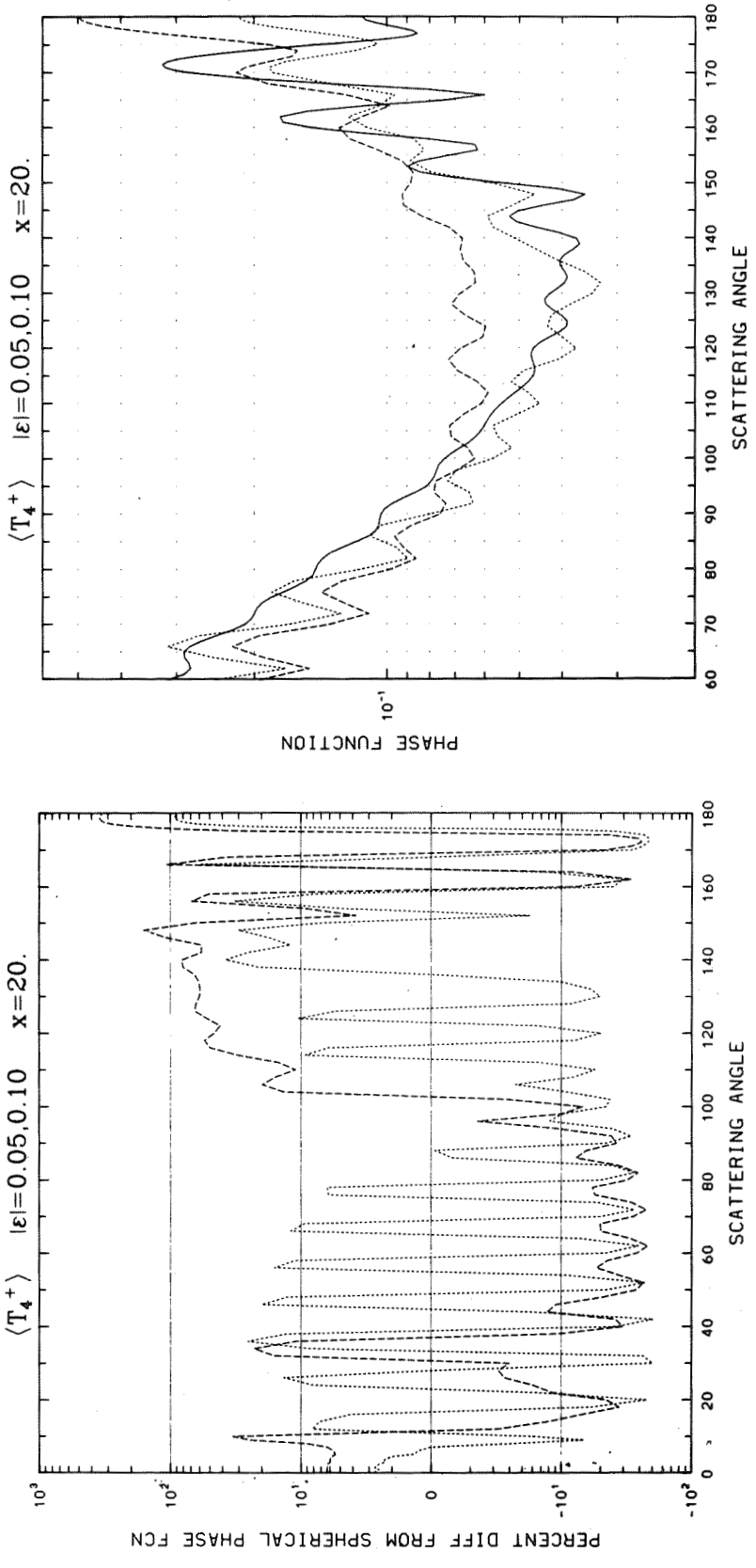

Appendix C (Continued)

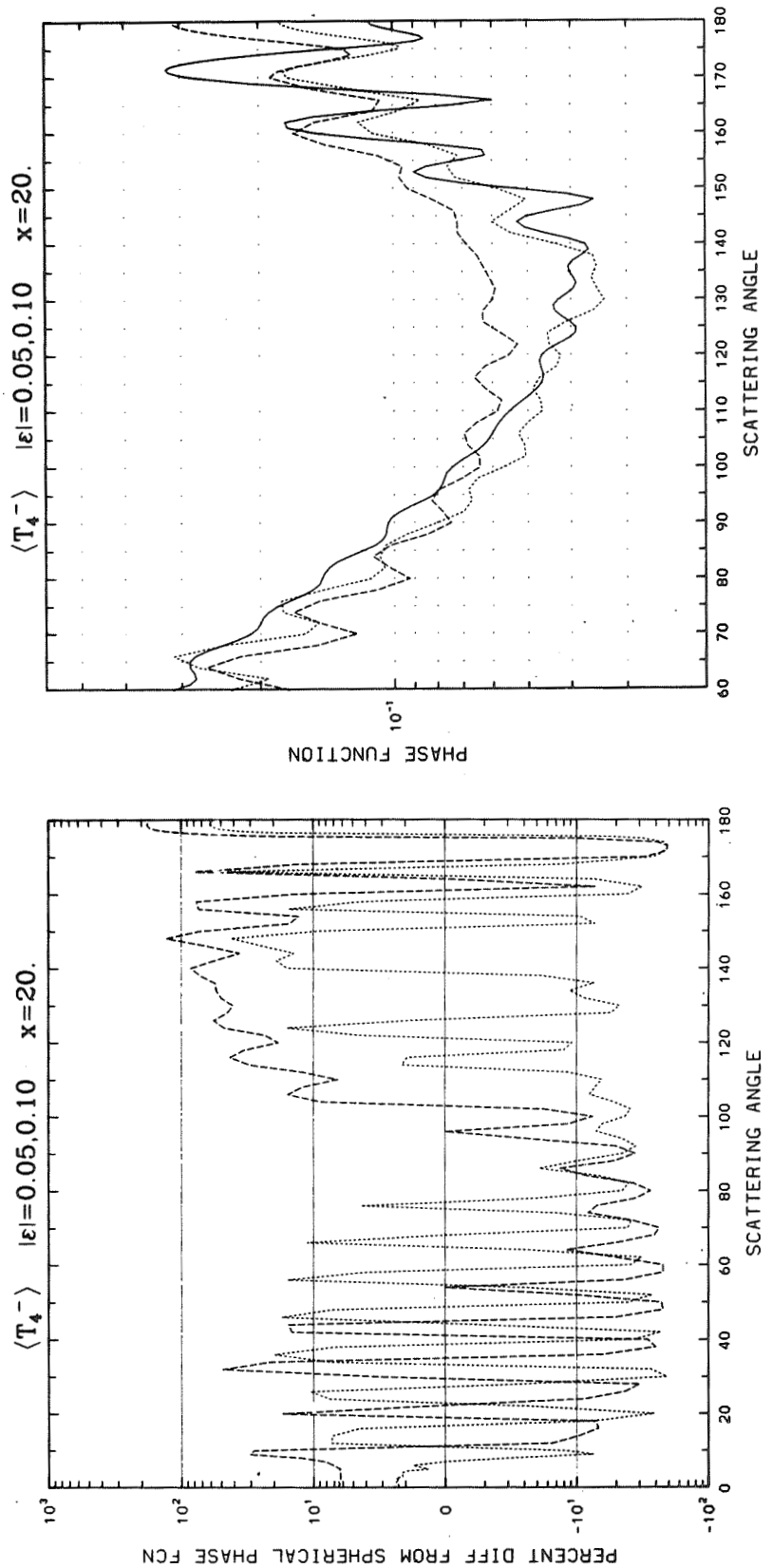

Appendix C (Continued)

APPENDIX D

Degree of polarization vs. scattering angle for randomly oriented Chebyshev particles T_3, T_2, T_4, T_6, and T_8; for various deformation parameters ϵ between -0.20 and 0.20 (as shown above each plot); and for size parameters x = 2,3,4,5,6,8,10,15, and 20. Solid line is for the $\Delta x = 0.1x$ size-averaged spherical result, interrupted lines are for non-sheres: dotted, dashed, and dot-dash lines refer to the various ϵ values shown, in increasing order (in general, the larger the value of $|\epsilon|$, the greater the general deviation from the spherical result). Not all particles are represented at larger values of x because of an inability to achieve satisfactory convergence of the EBCM.

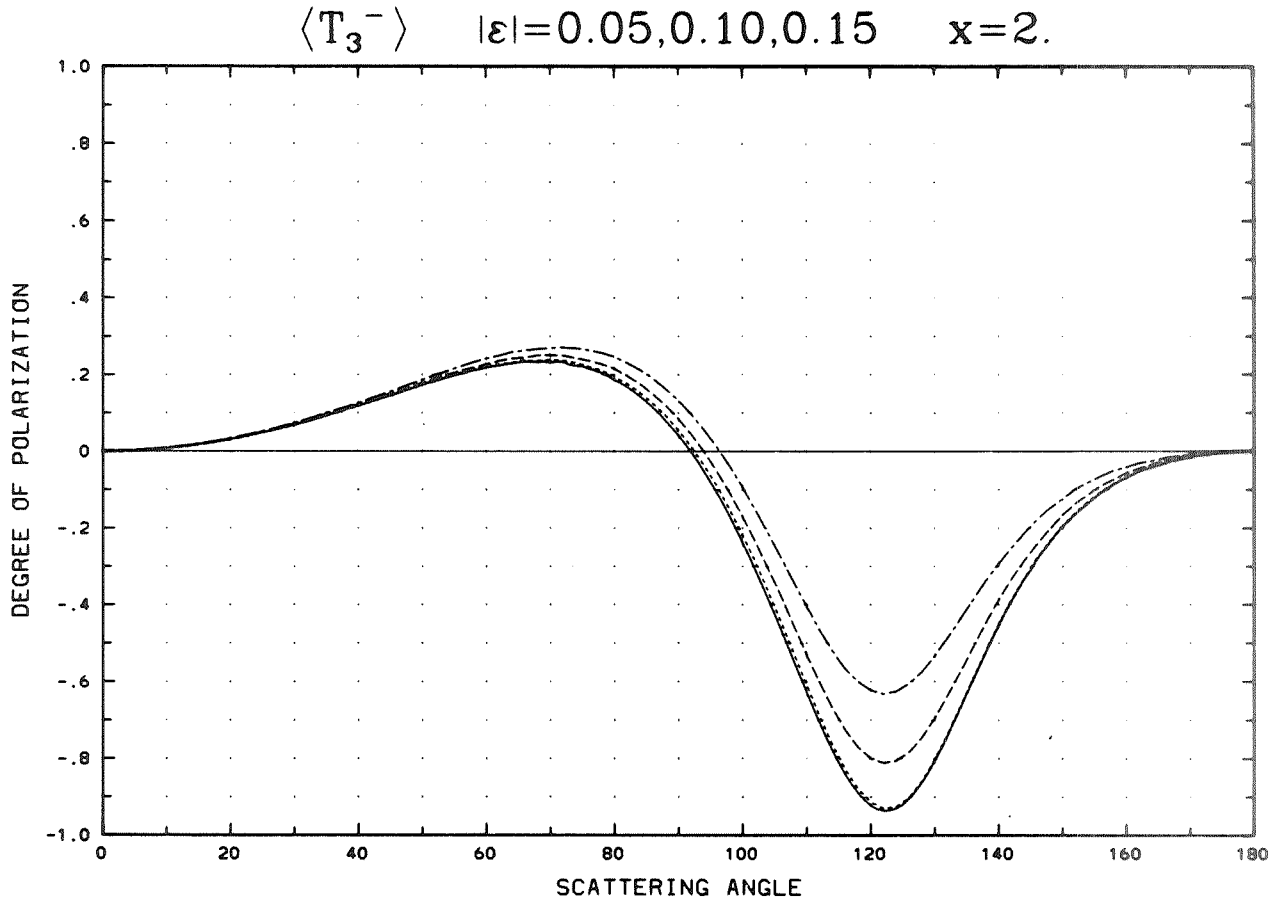

Appendix D. DEGREE OF POLARIZATION for Chebyshev particles in random orientation, vs. ANGLE

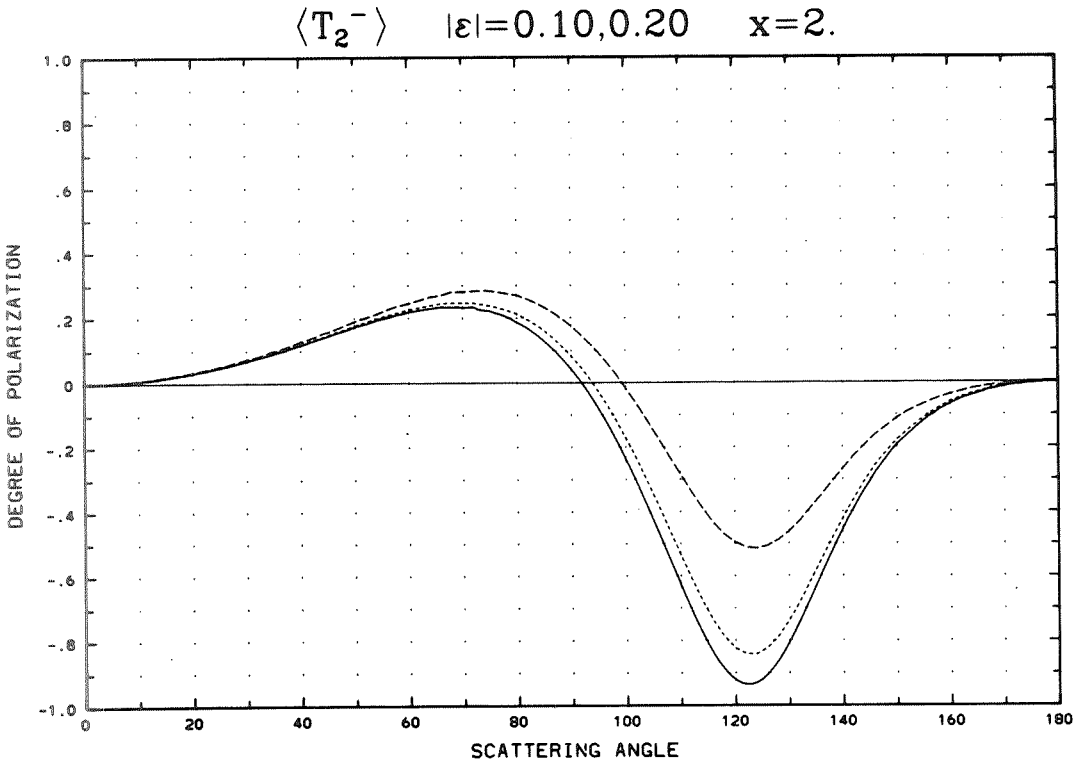

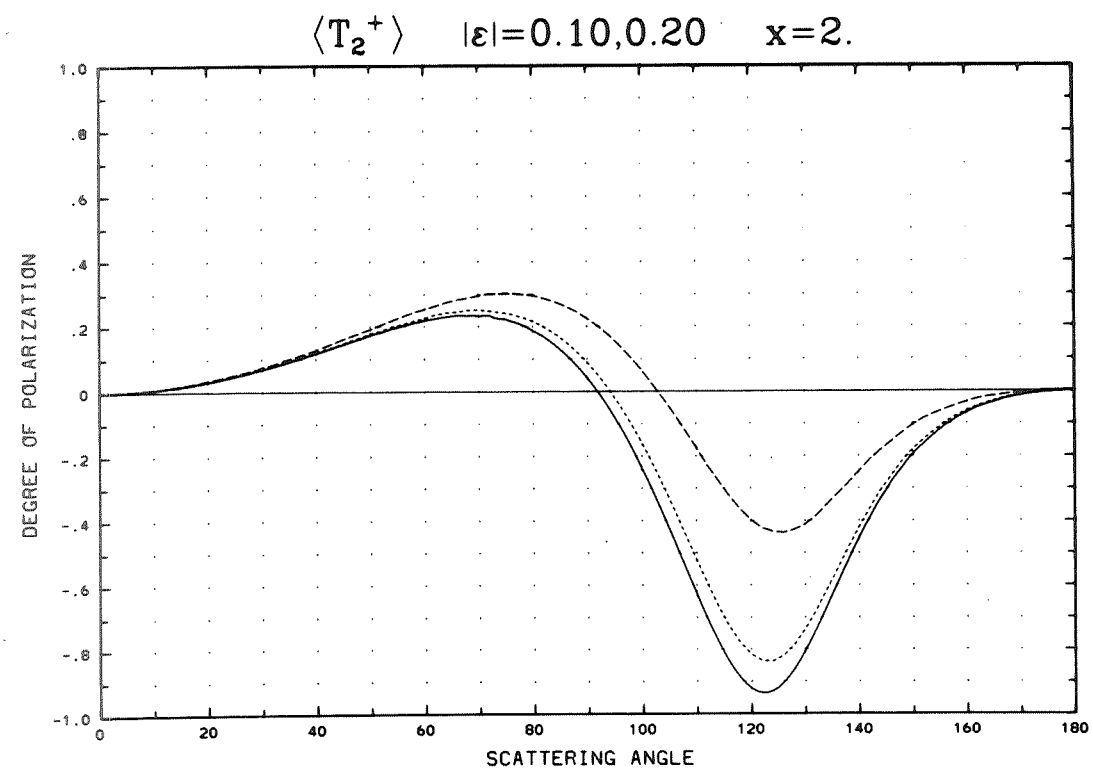

Appendix D (Continued)

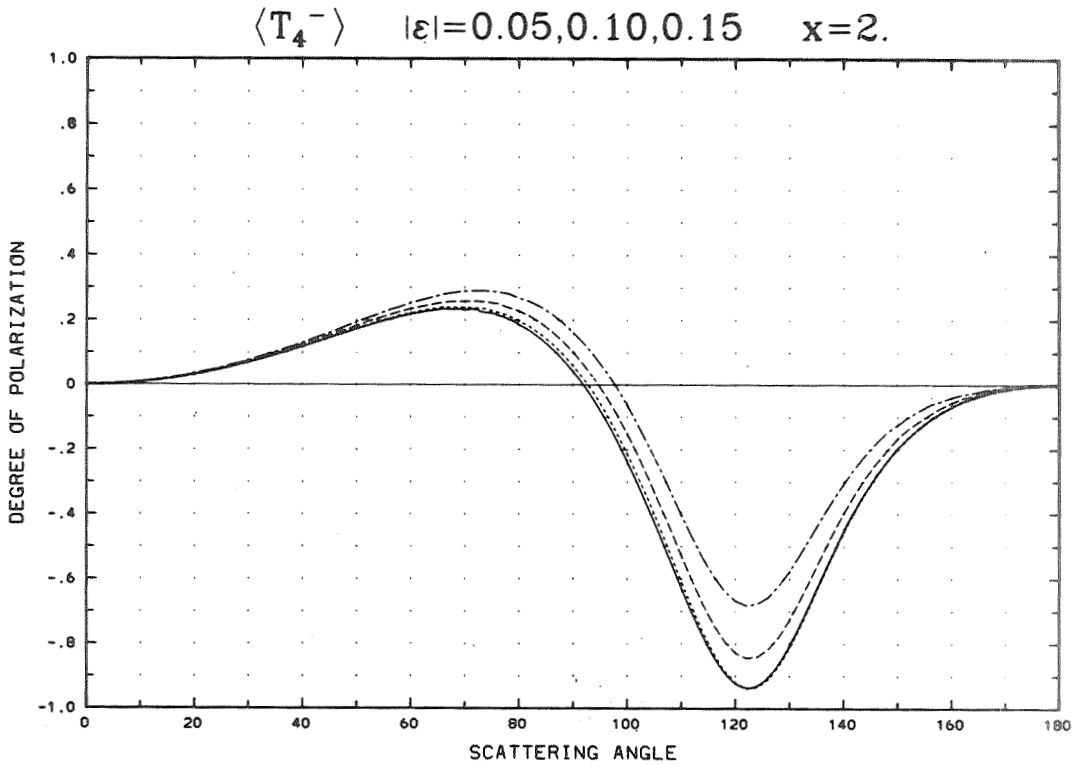

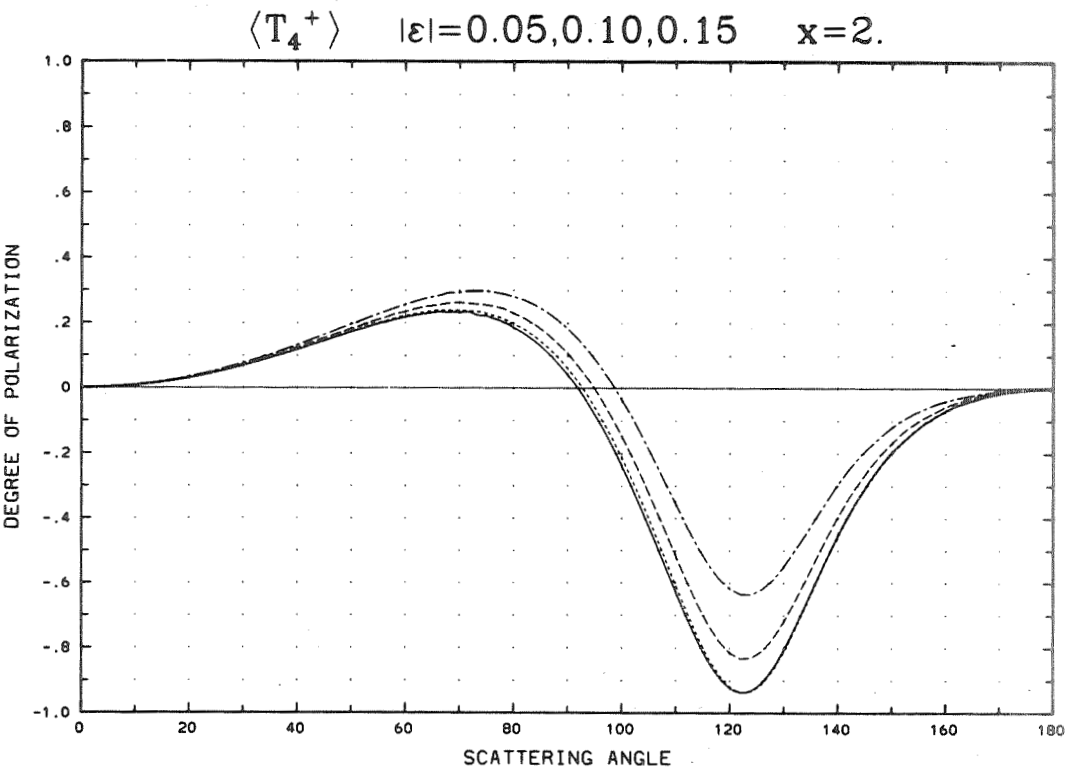

Appendix D (Continued)

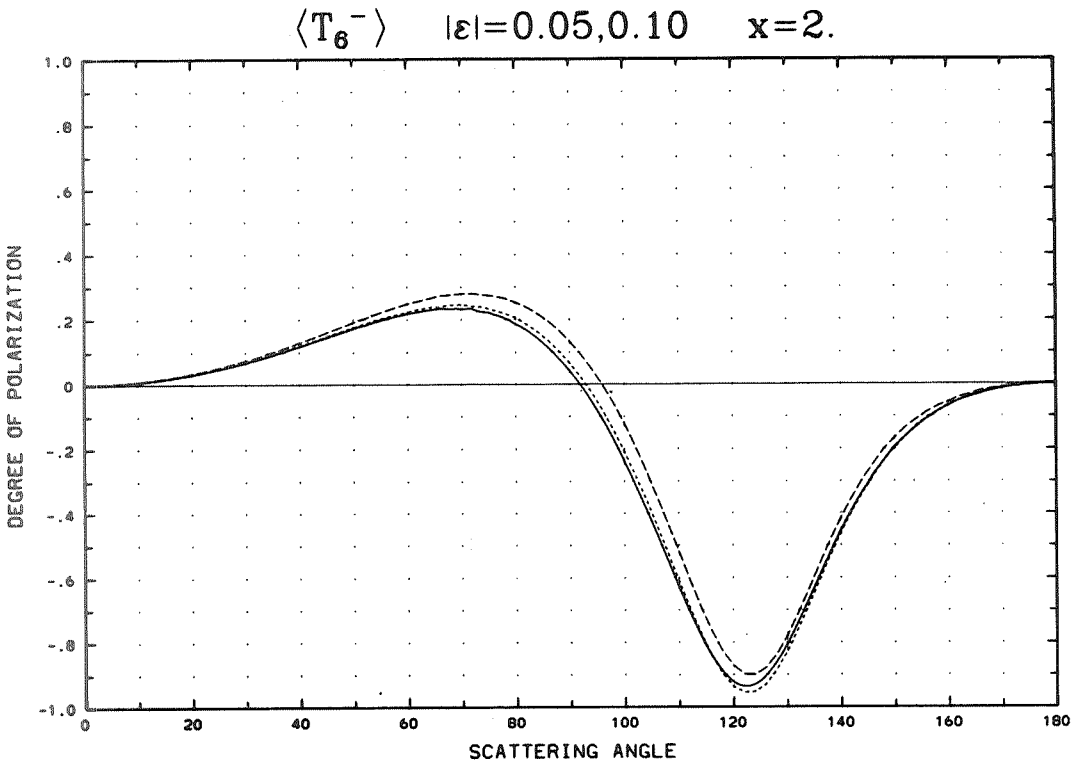

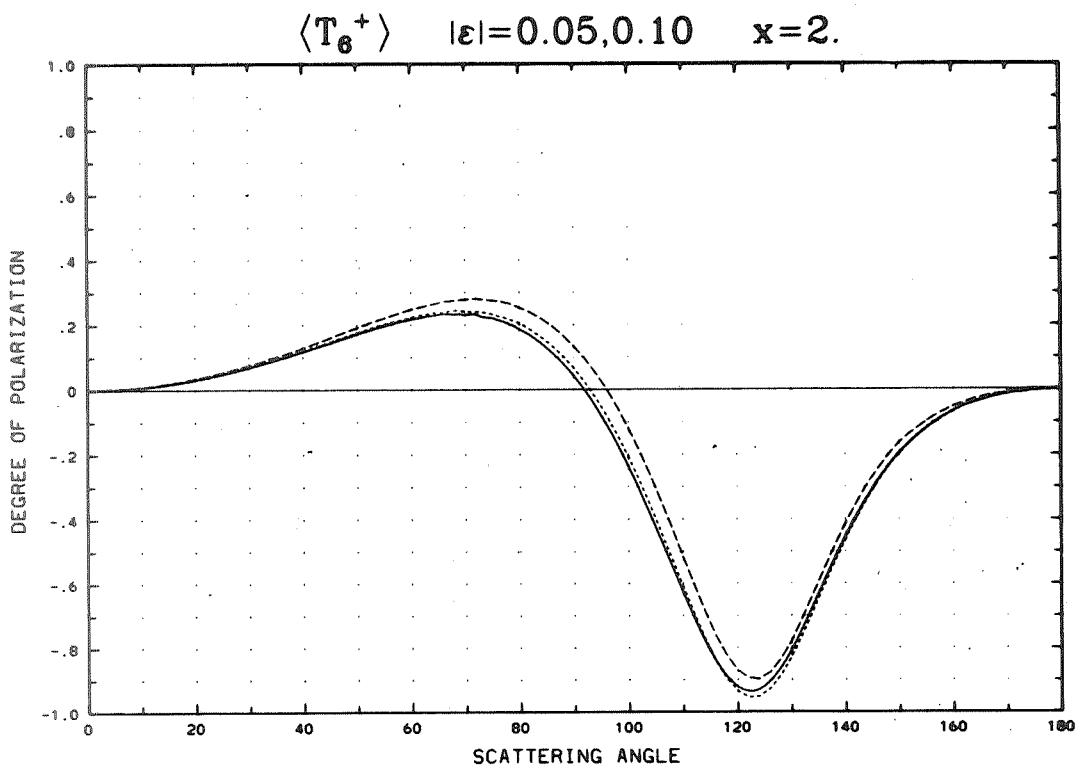

Appendix D (Continued)

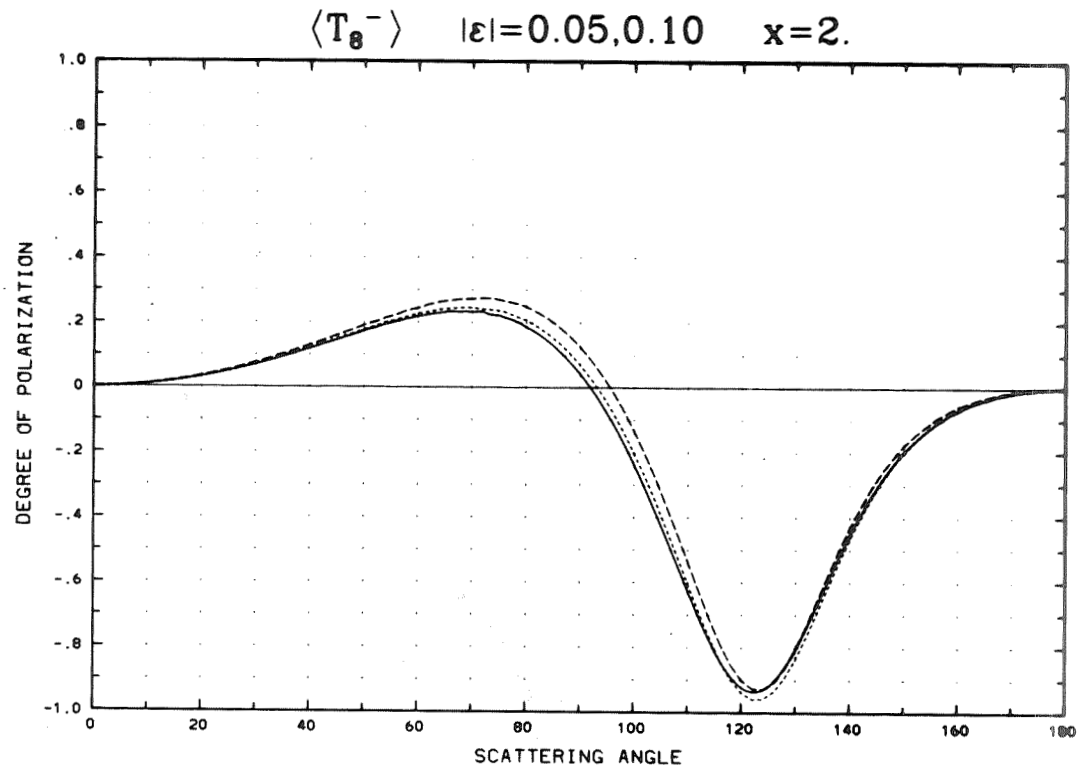

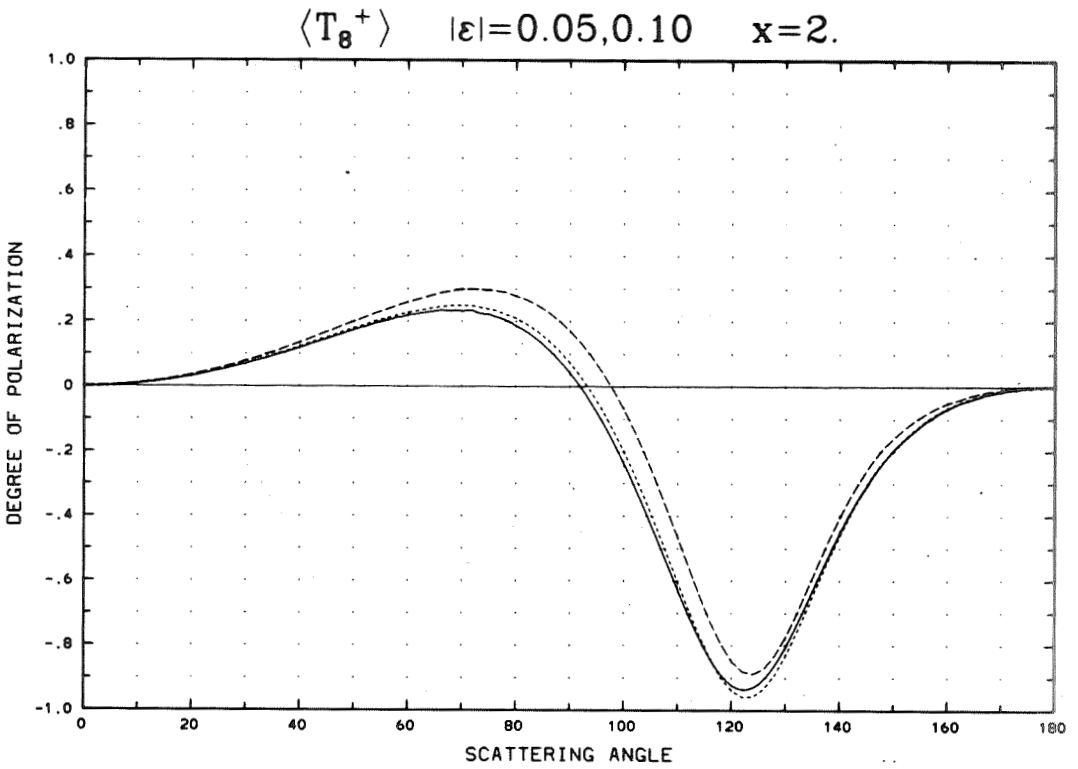

Appendix D (Continued)

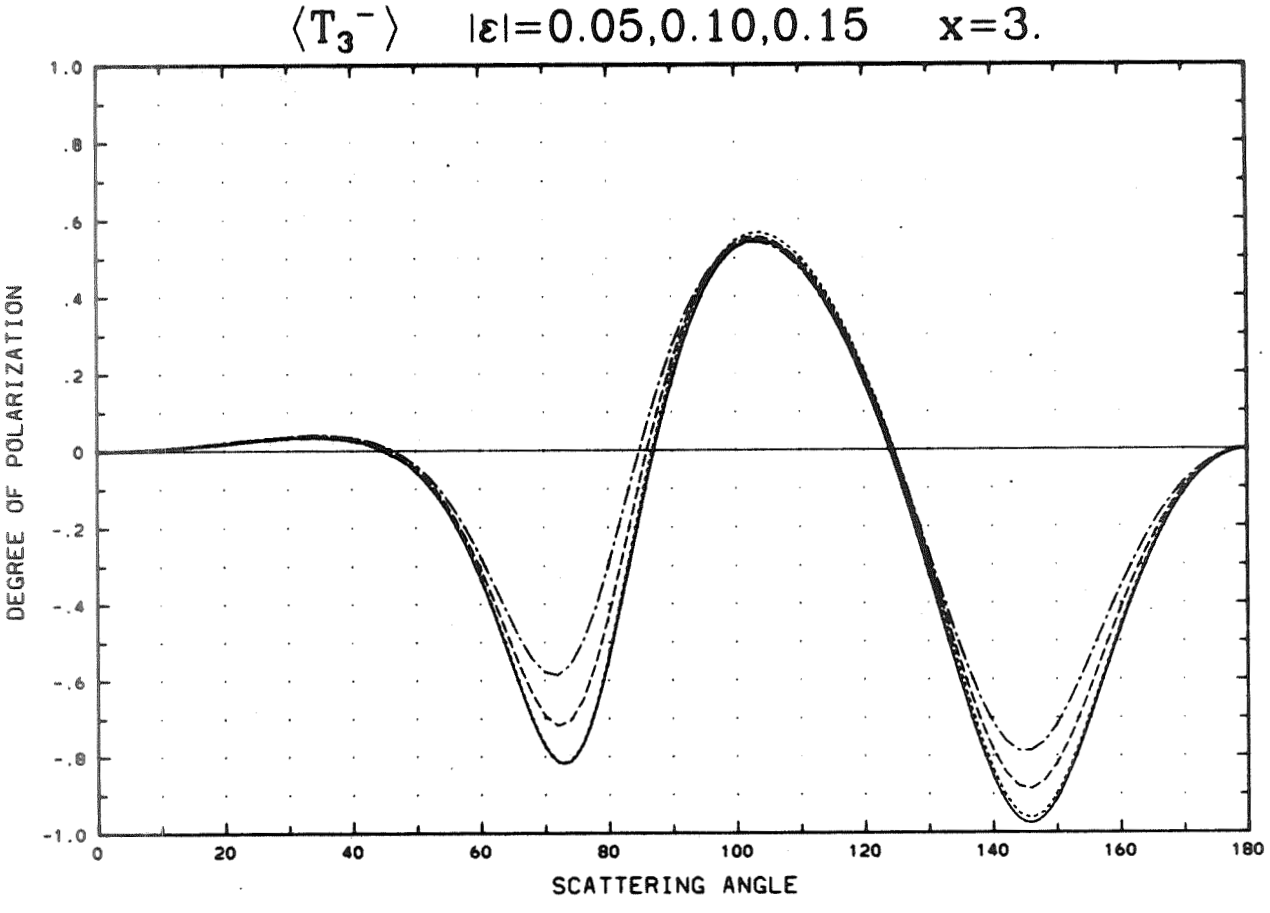

Appendix D (Continued)

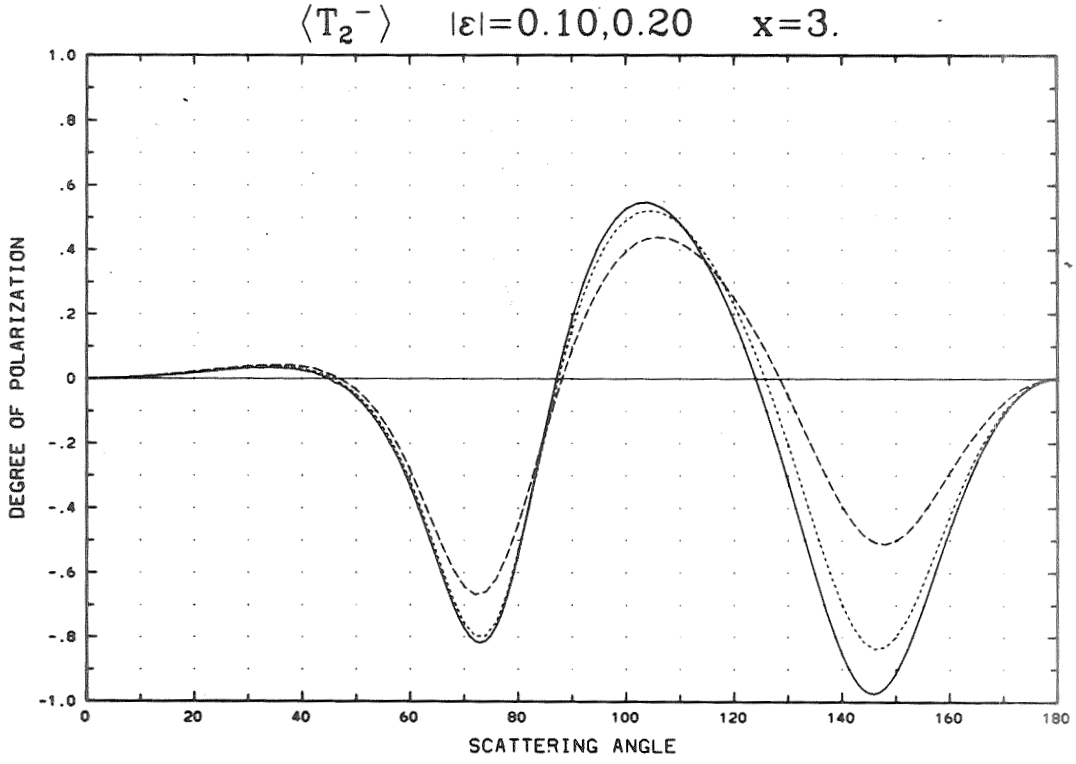

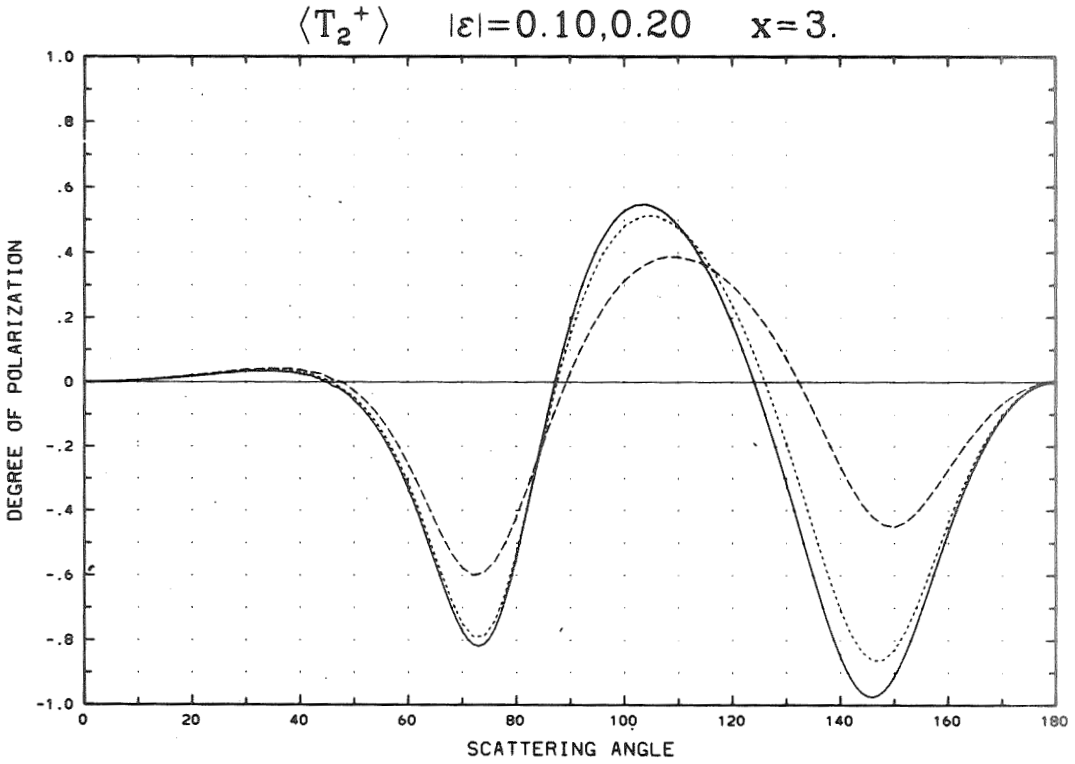

Appendix D (Continued)

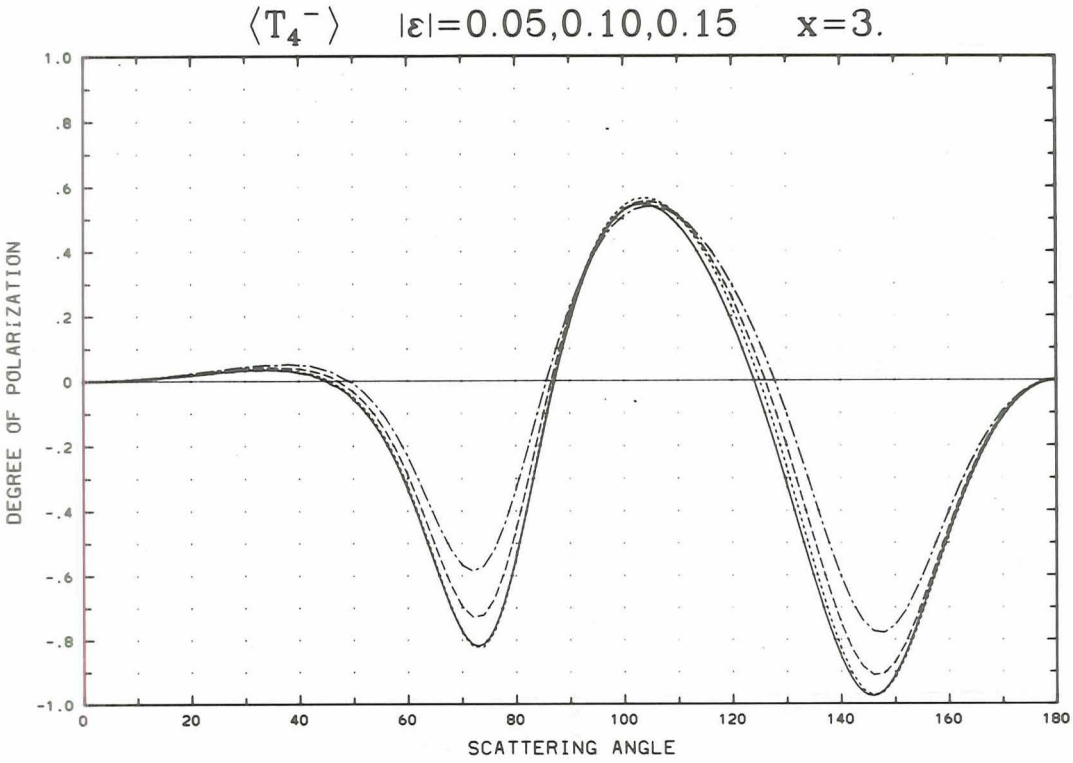

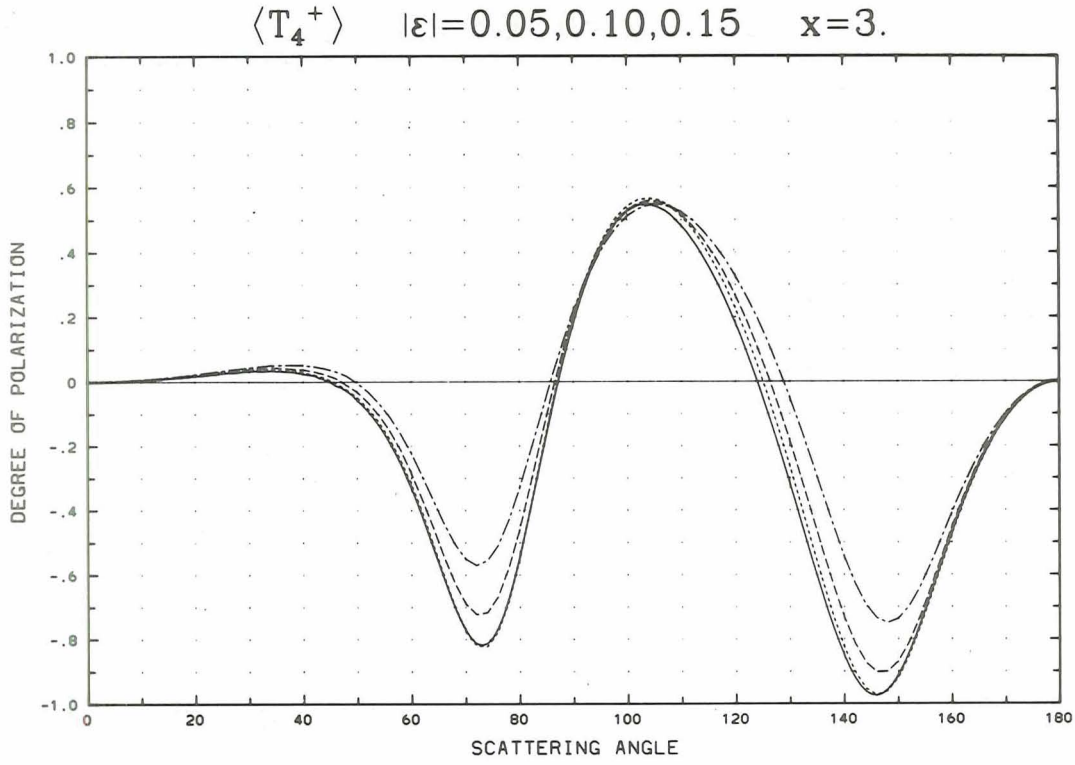

Appendix D (Continued)

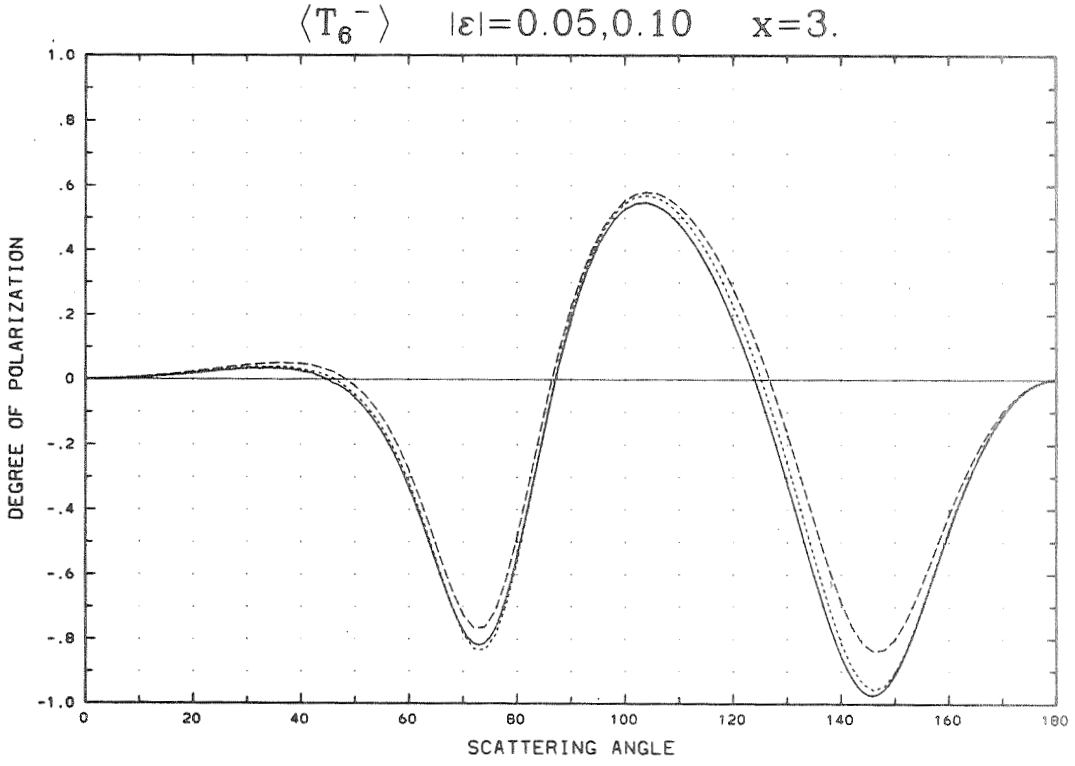

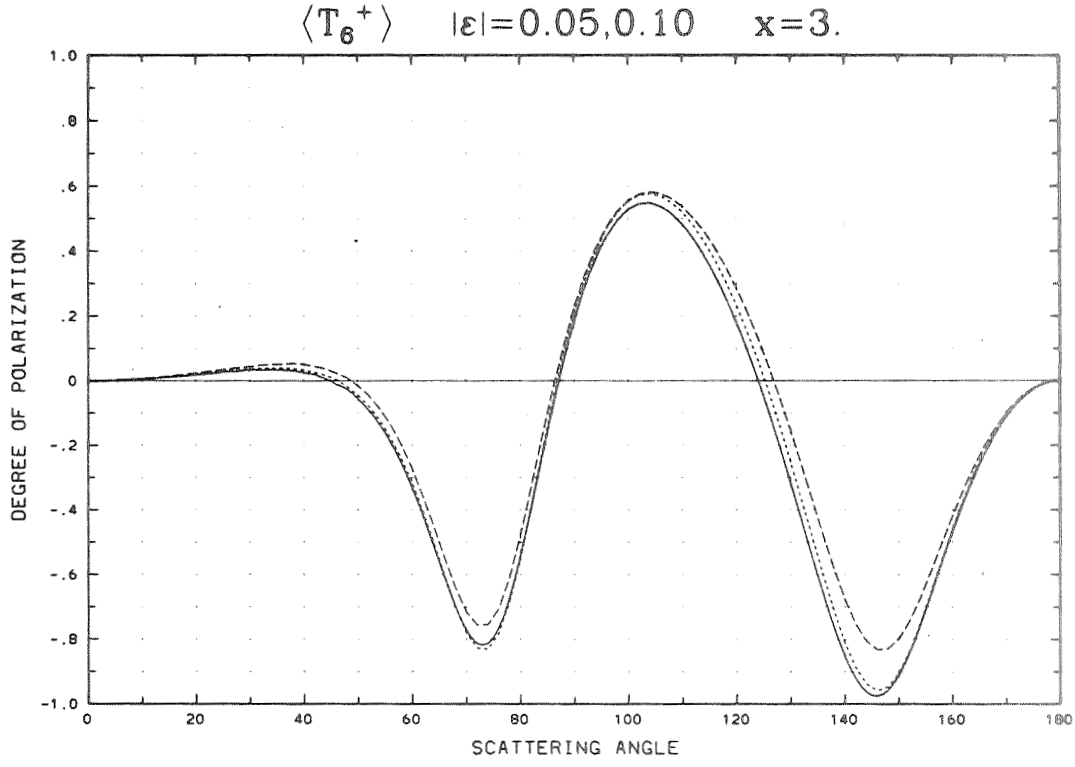

Appendix D (Continued)

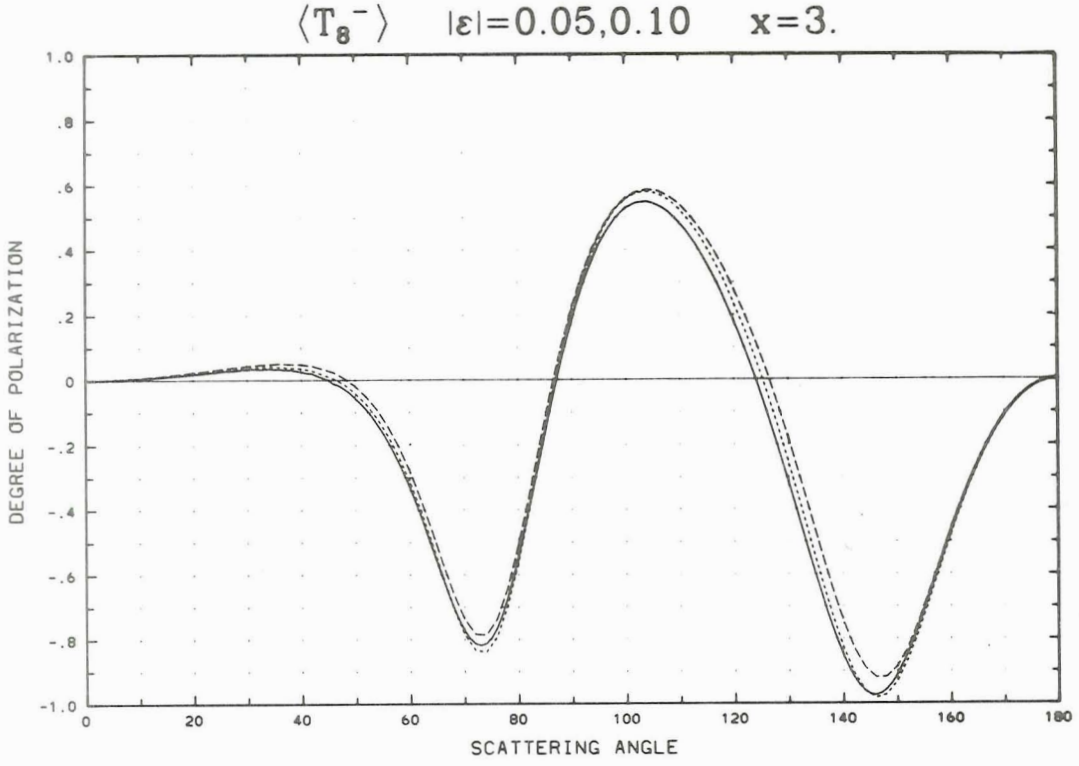

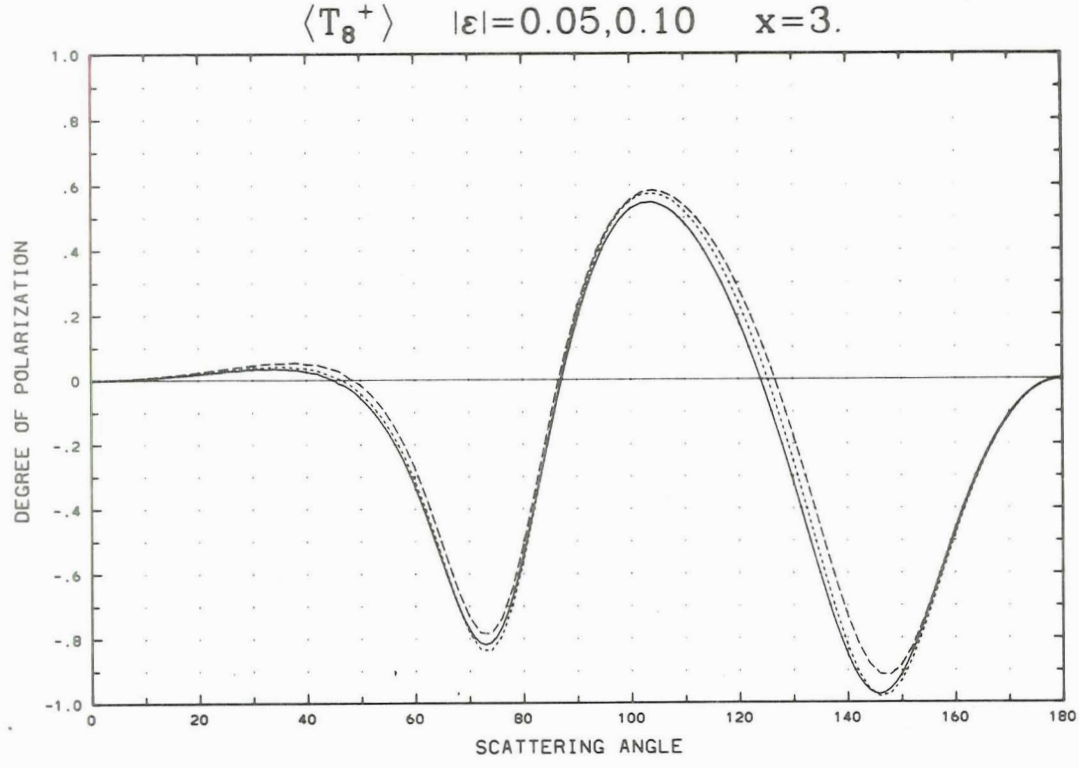

Appendix D (Continued)

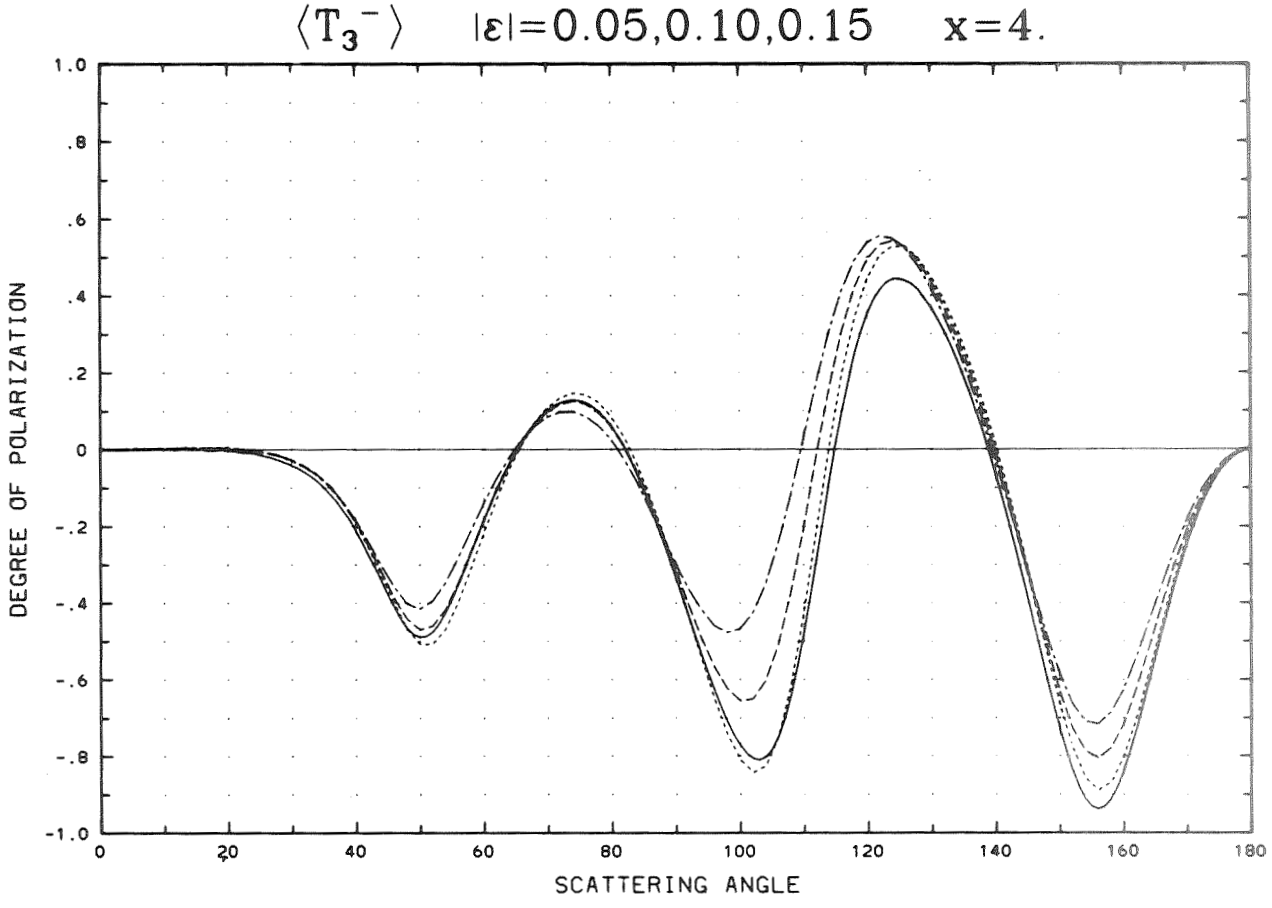

Appendix D (Continued)

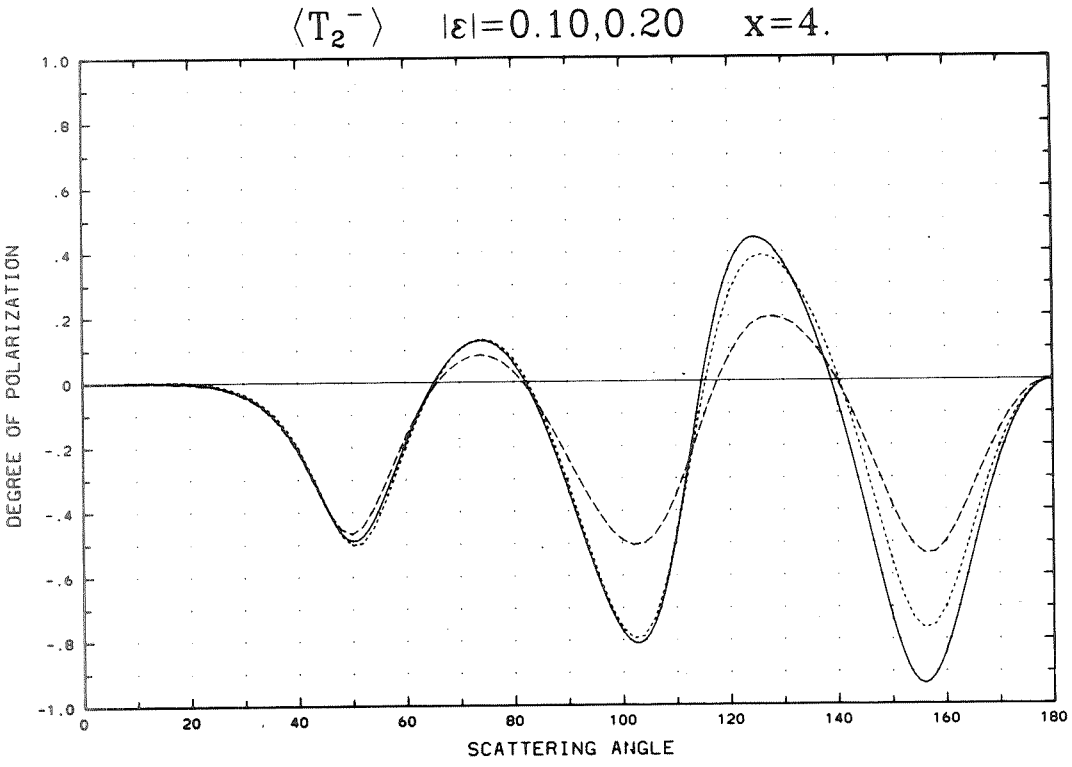

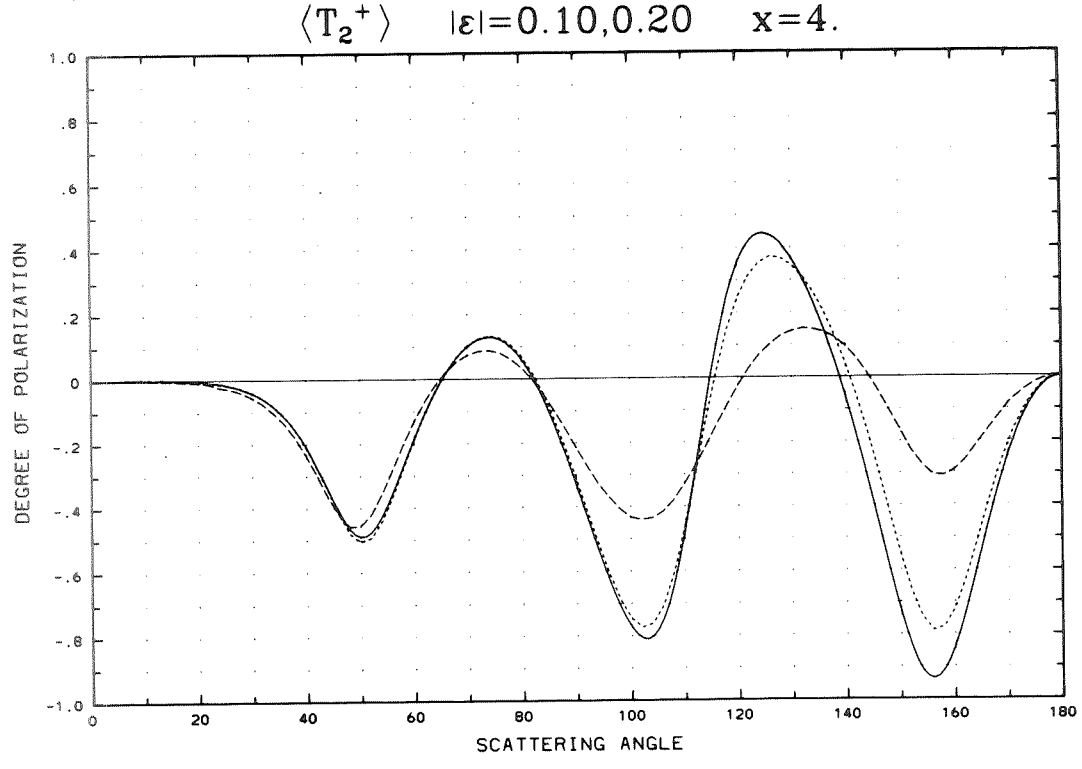

Appendix D (Continued)

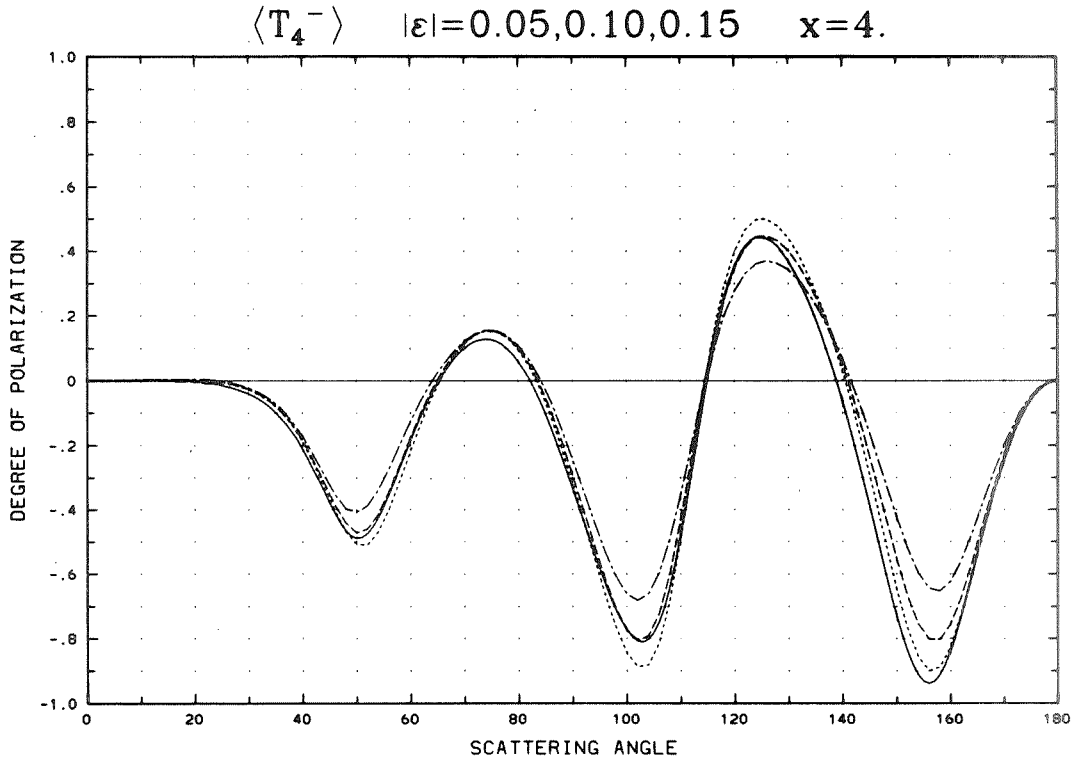

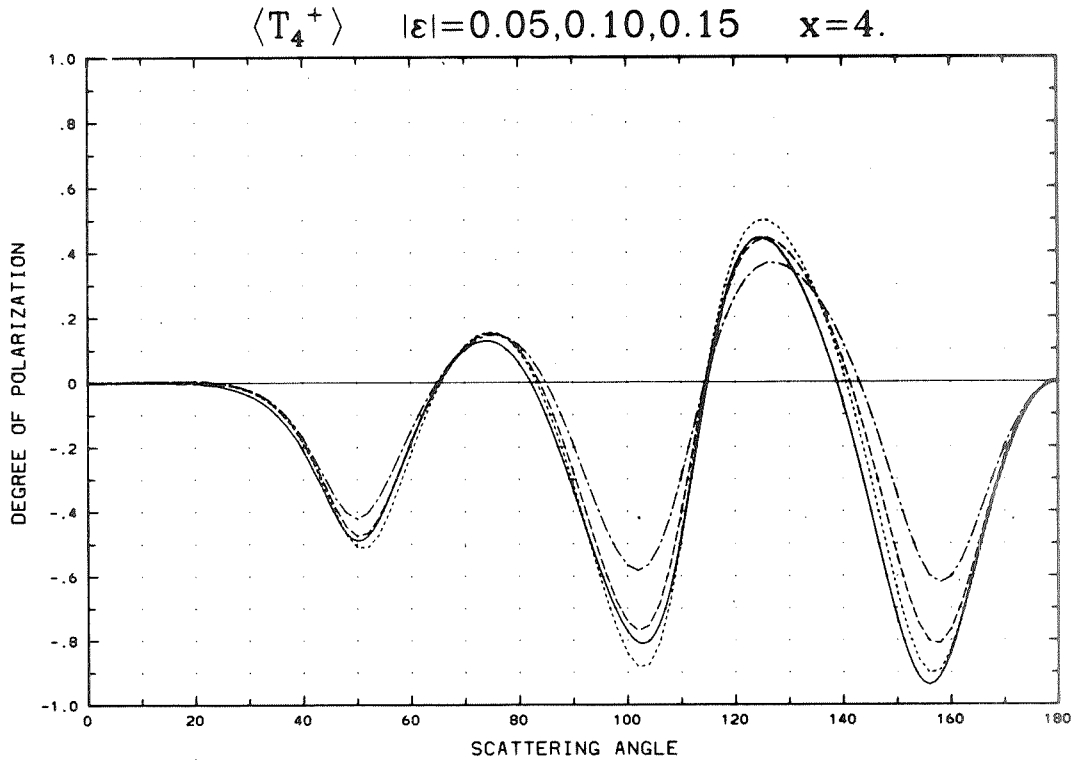

Appendix D (Continued)

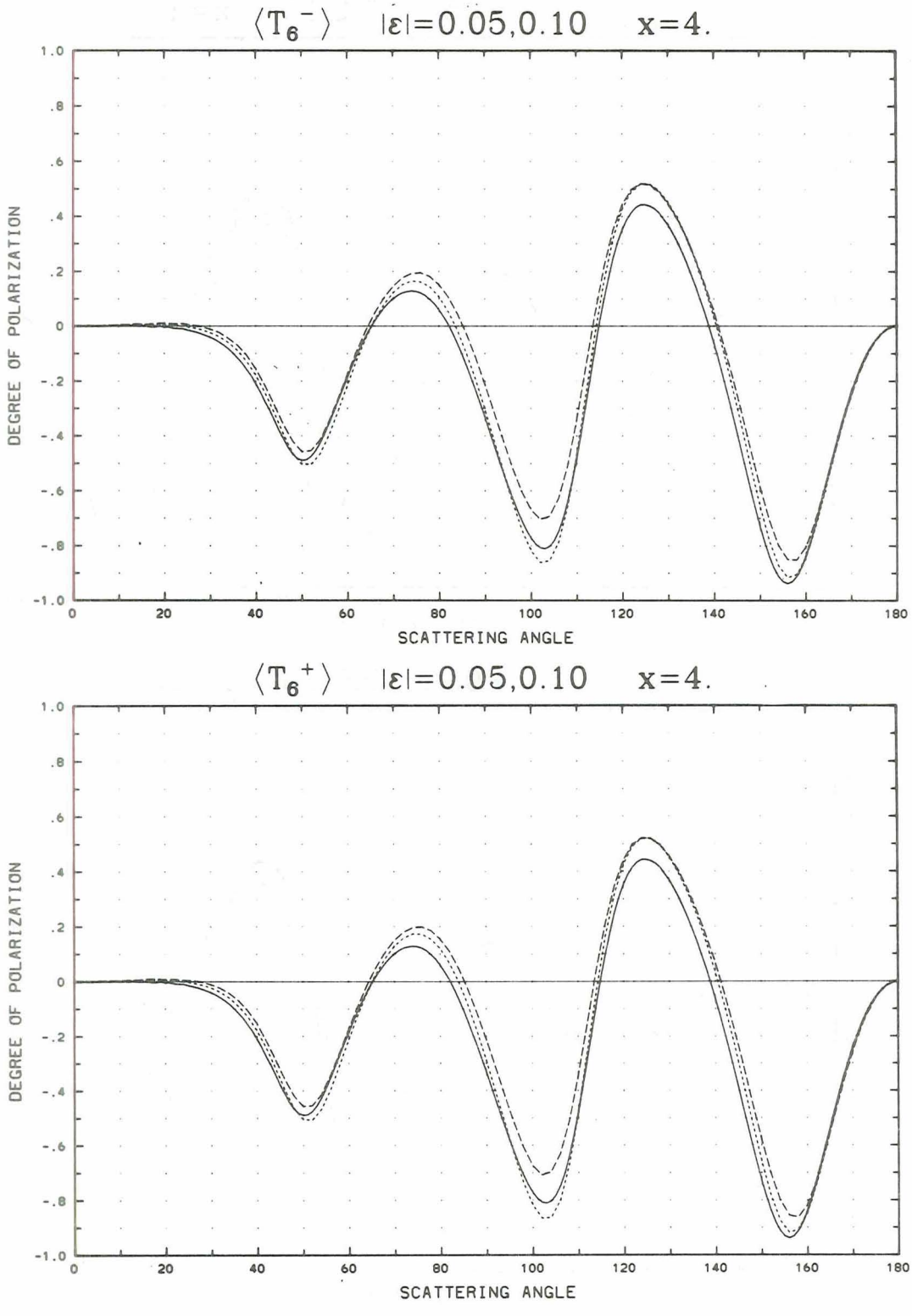

Appendix D (Continued)

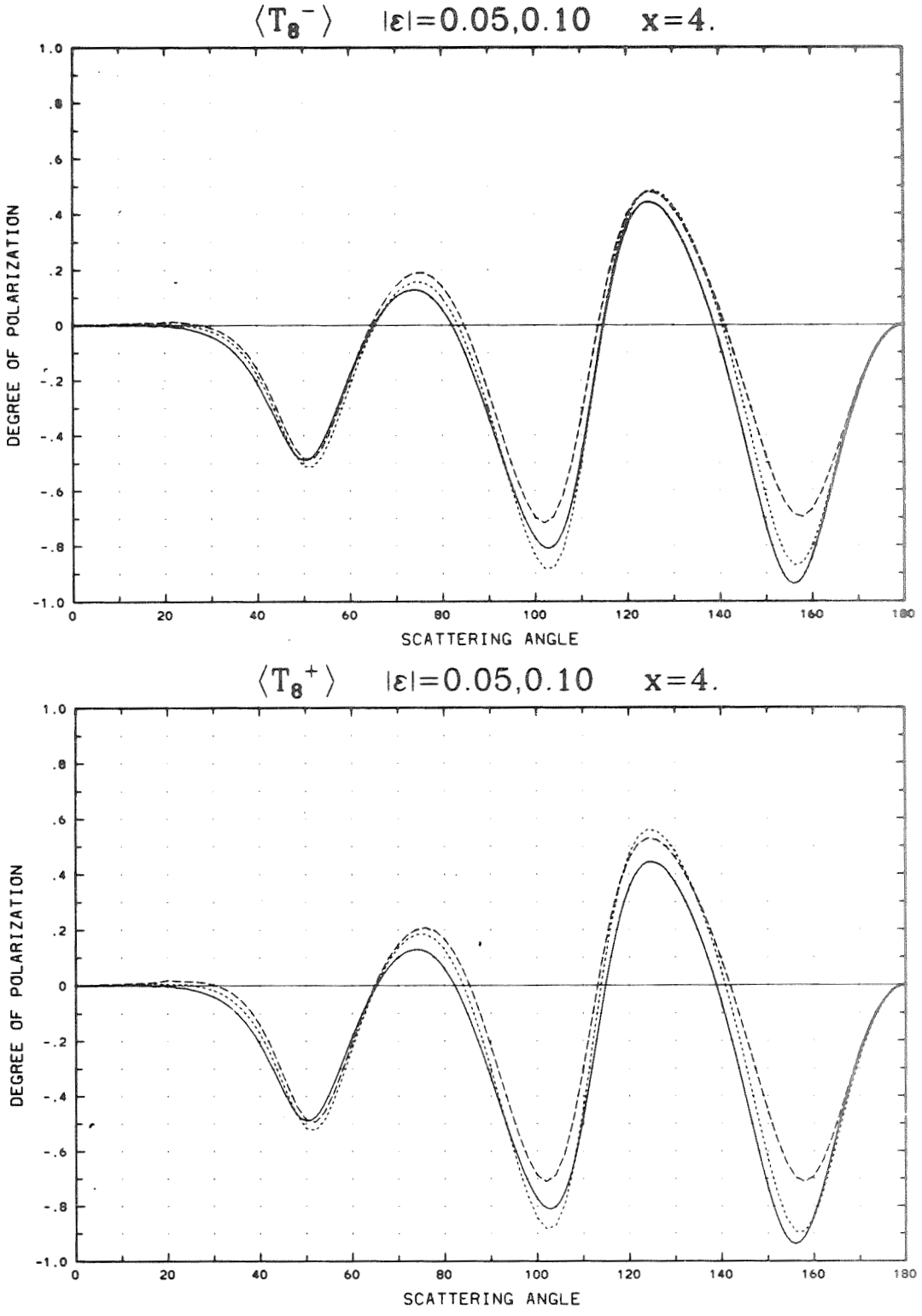

Appendix D (Continued)

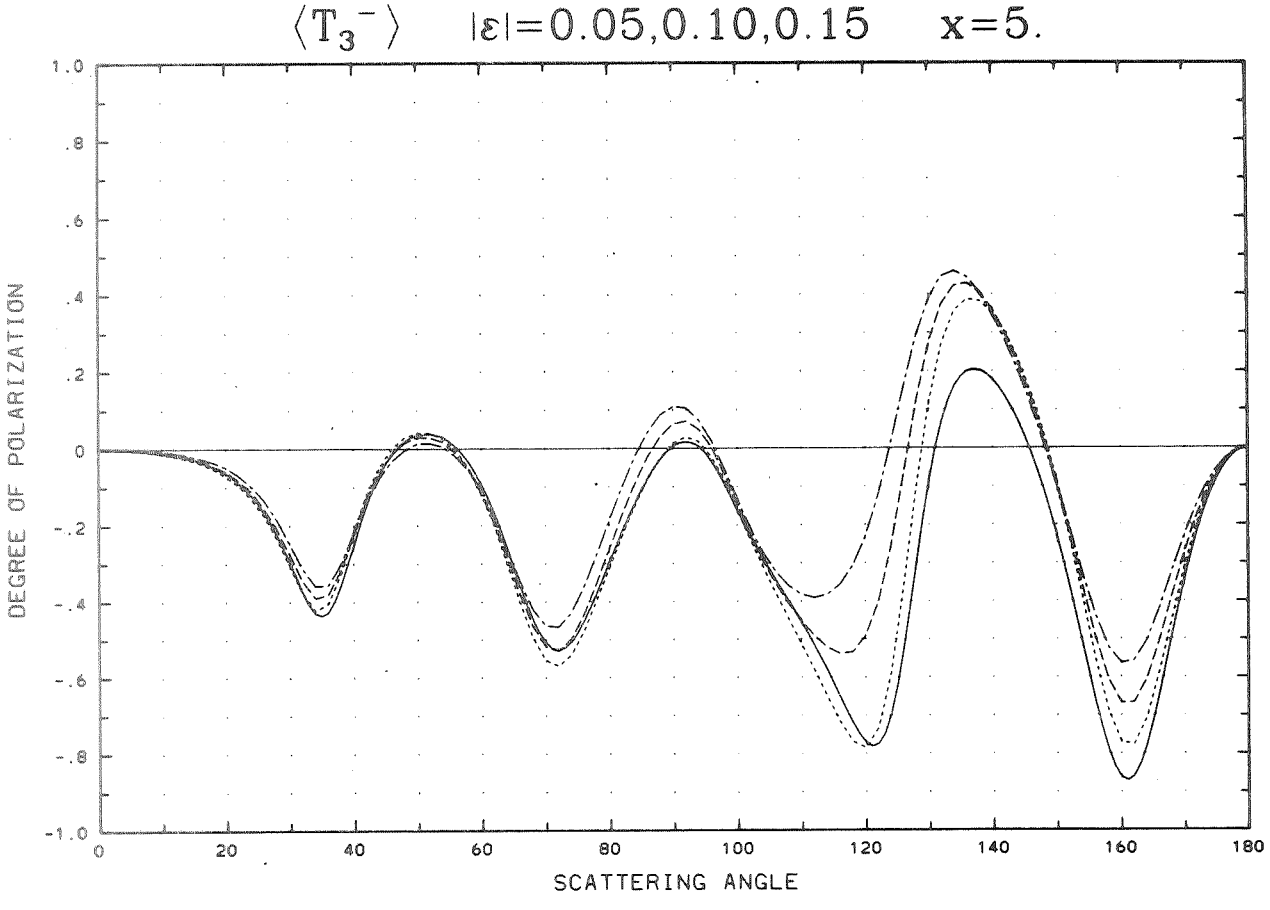

Appendix D (Continued)

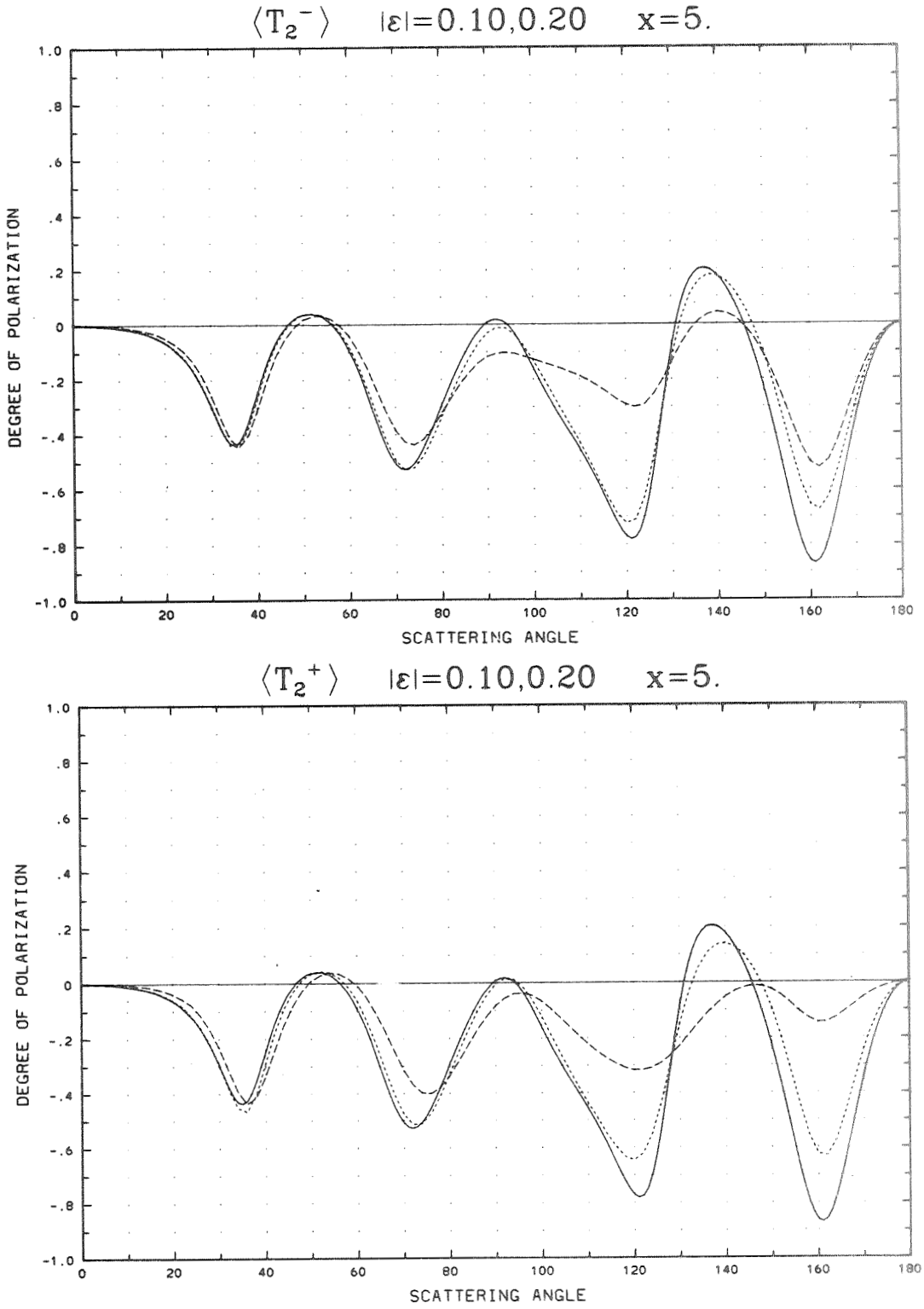

Appendix D (Continued)

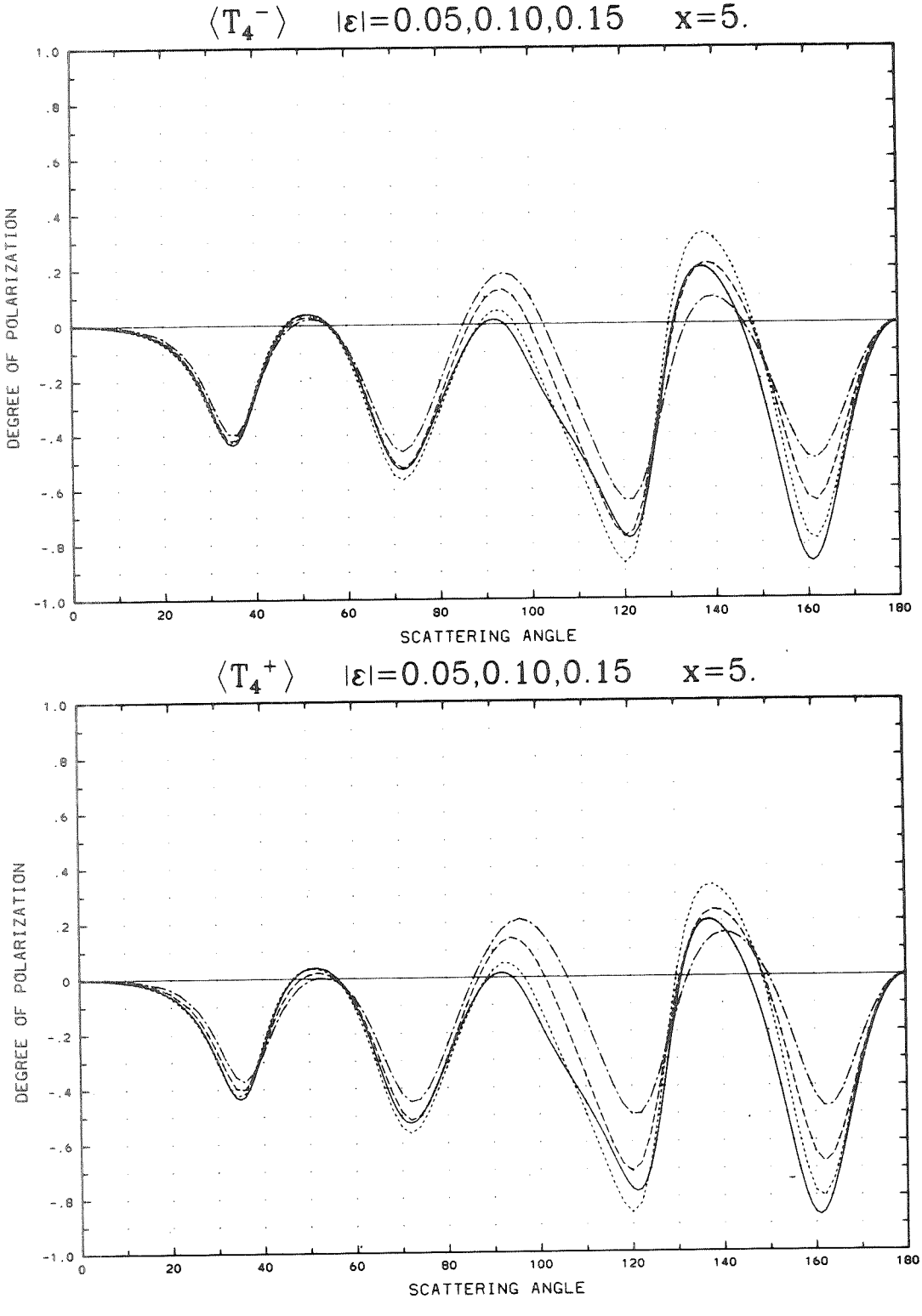

Appendix D (Continued)

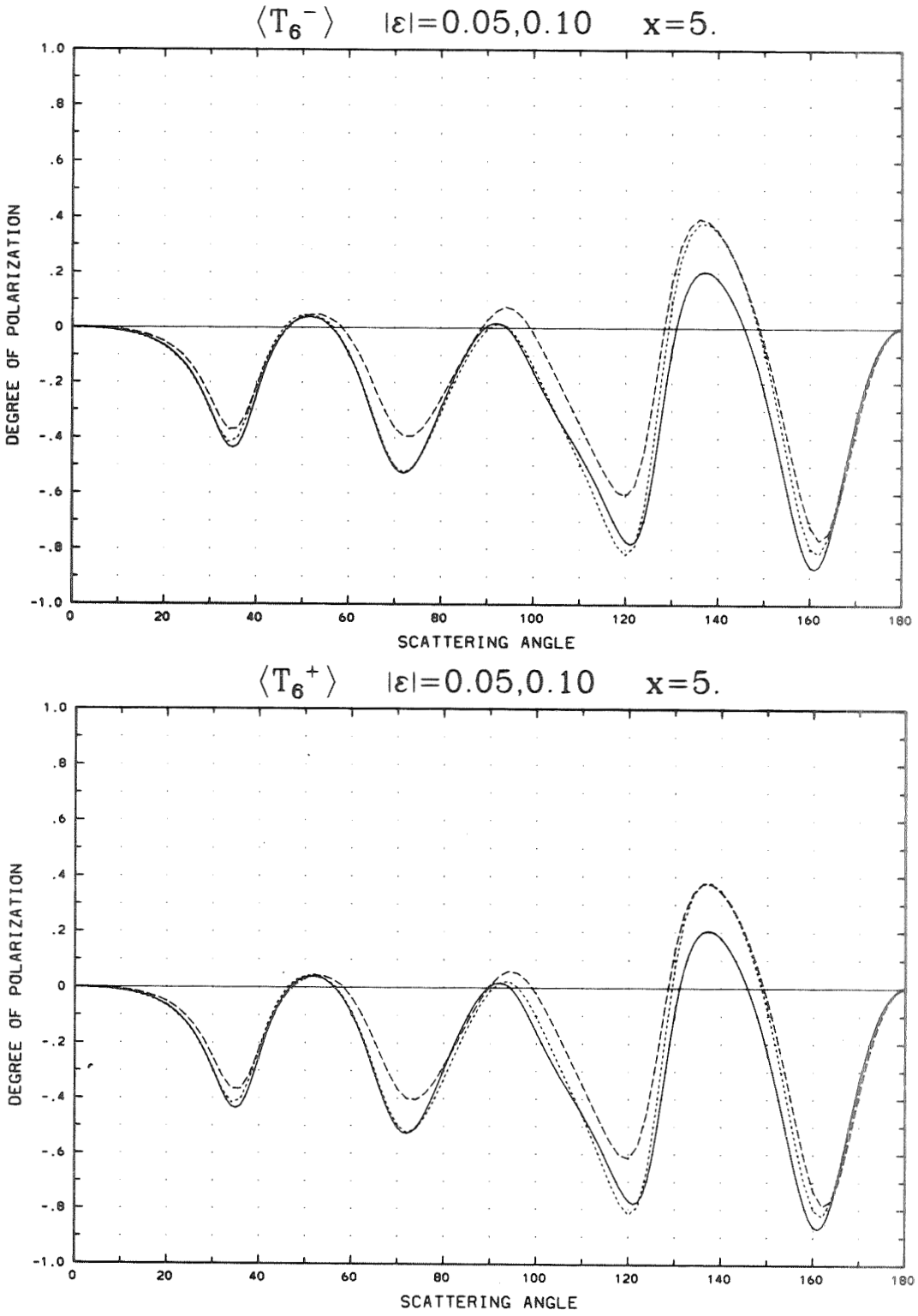

Appendix D (Continued)

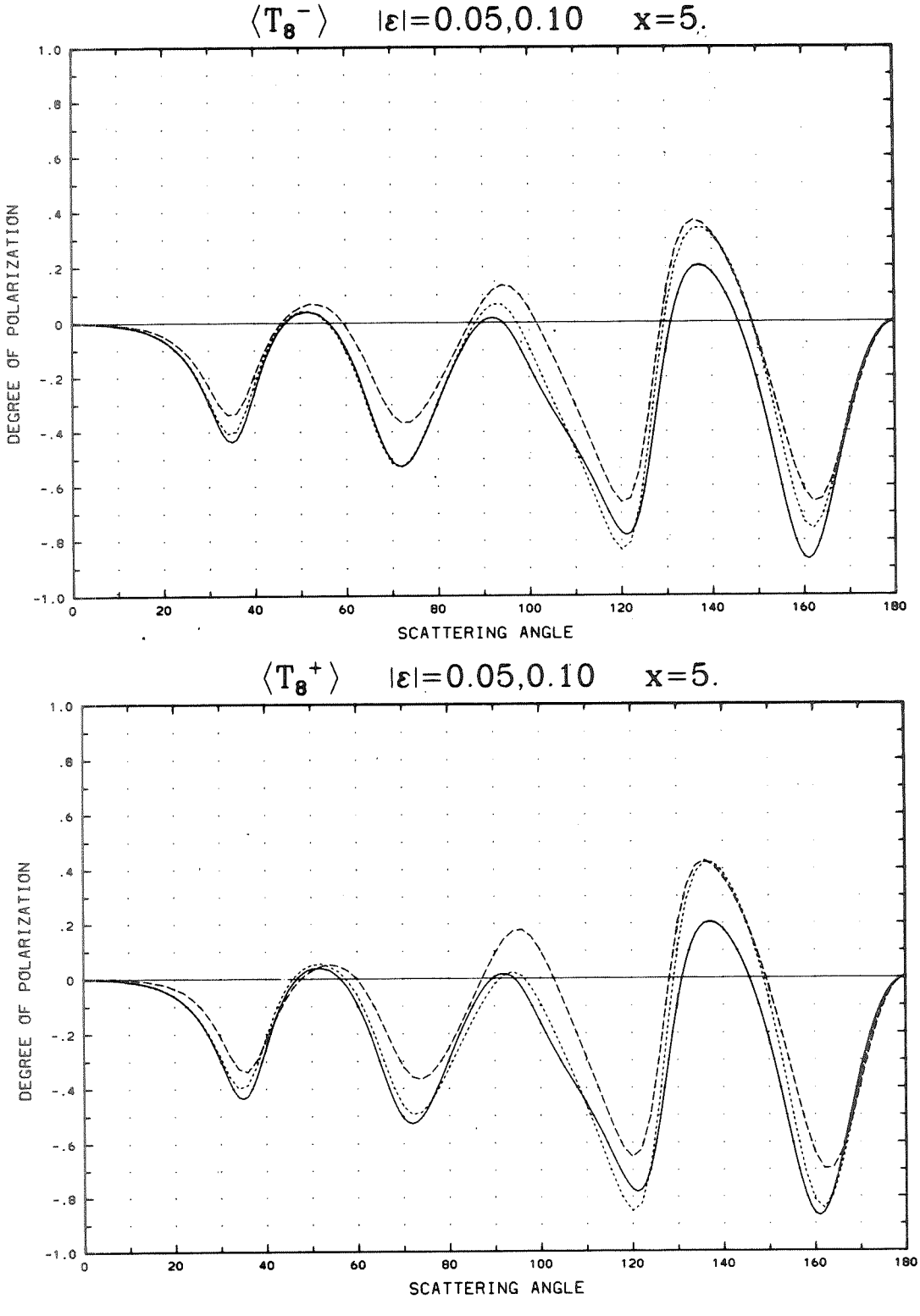

Appendix D (Continued)

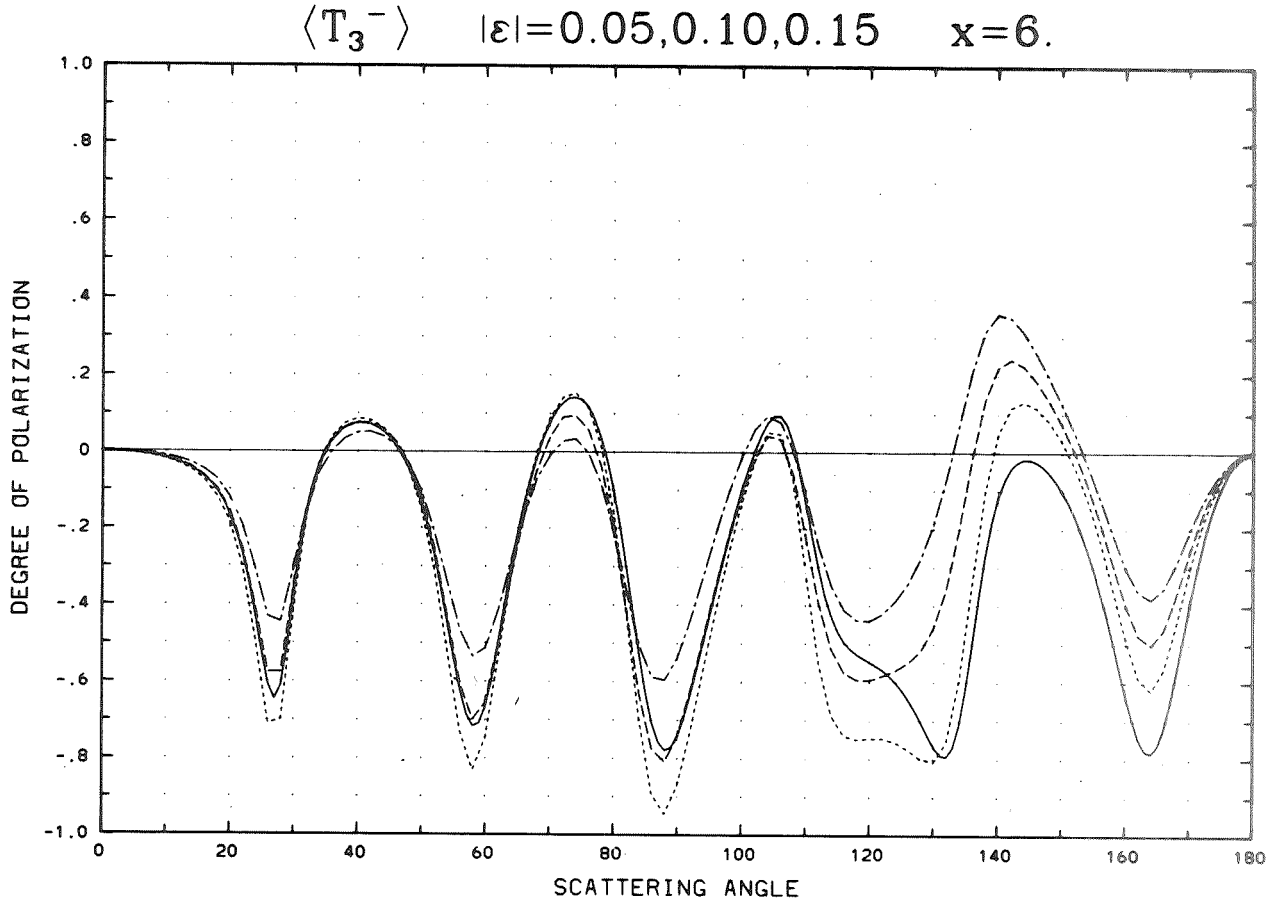

Appendix D (Continued)

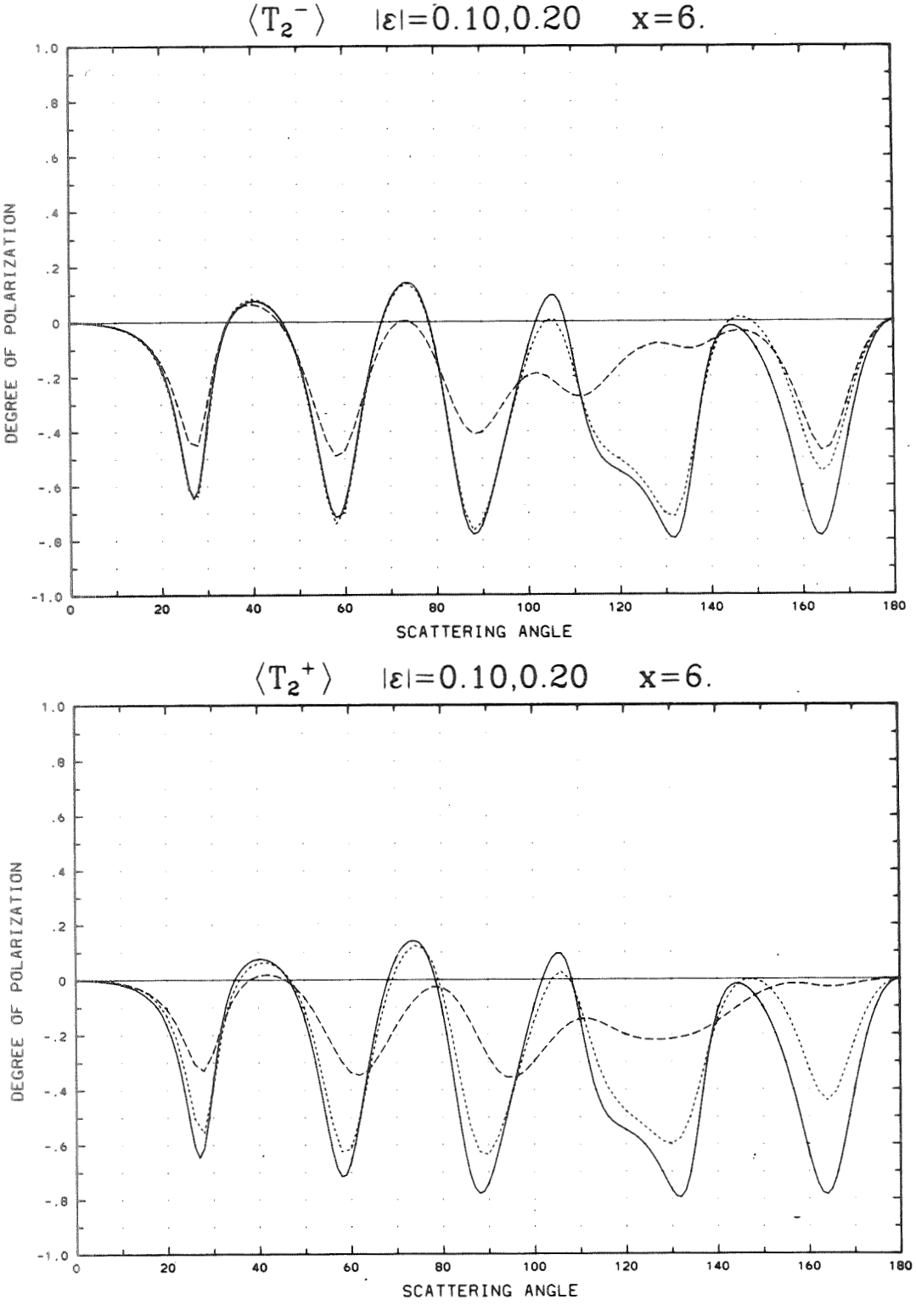

Appendix D (Continued)

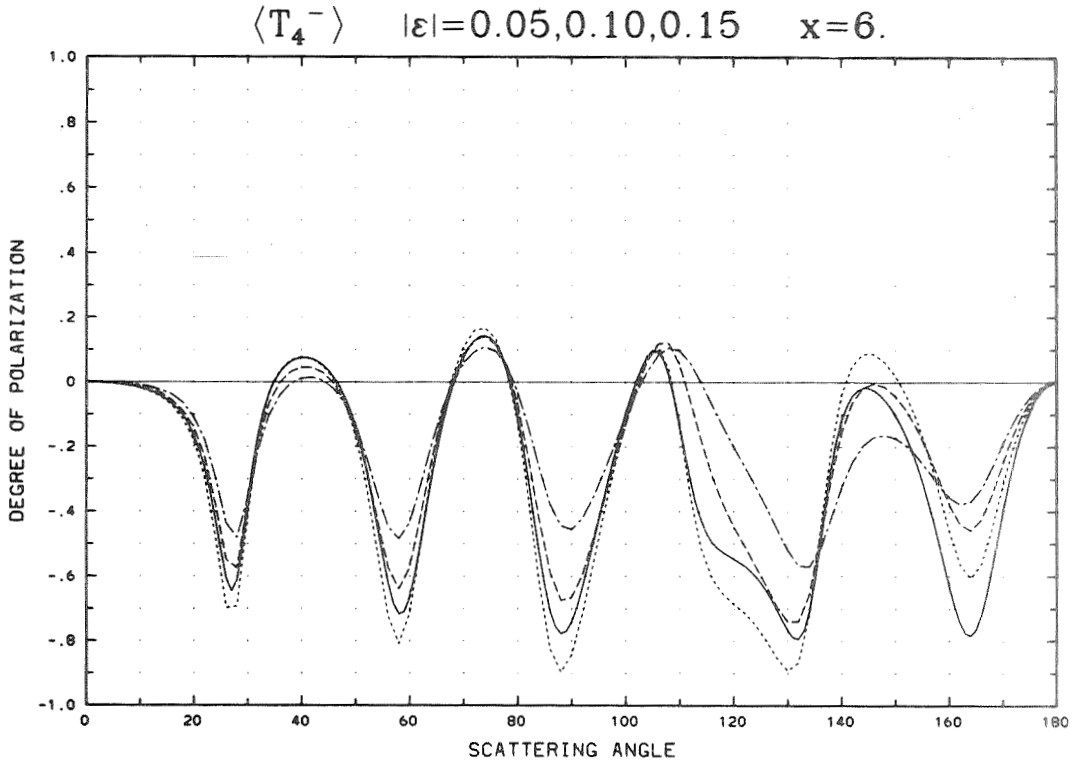

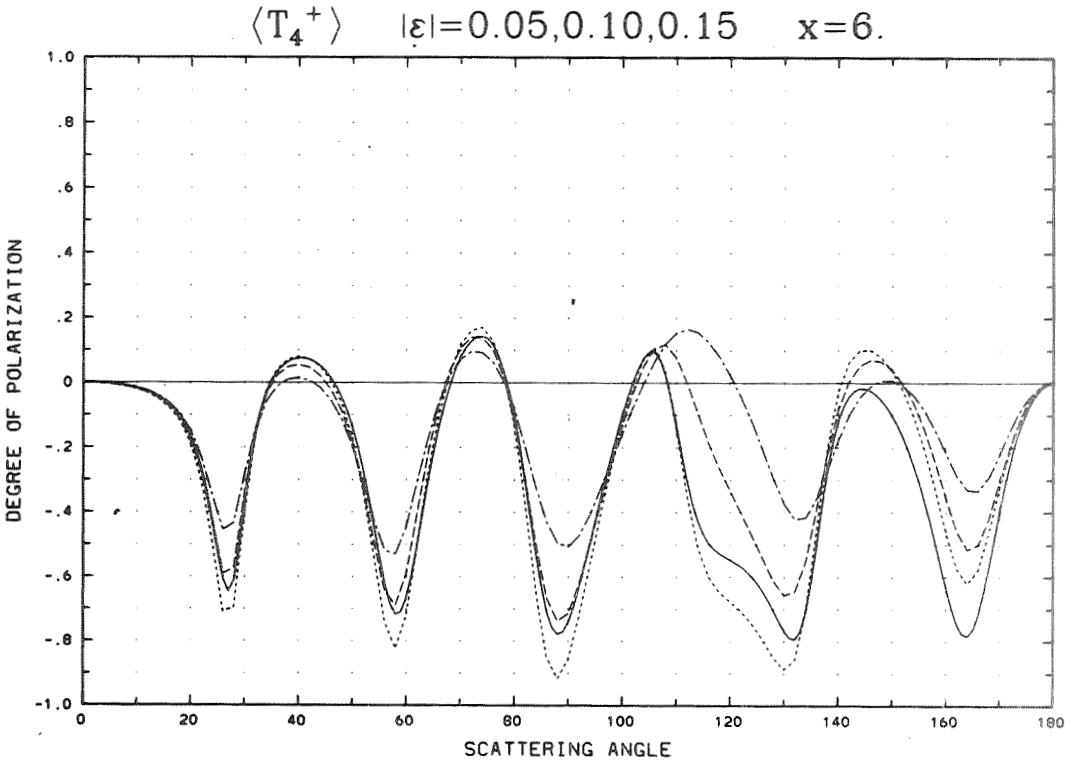

Appendix D (Continued)

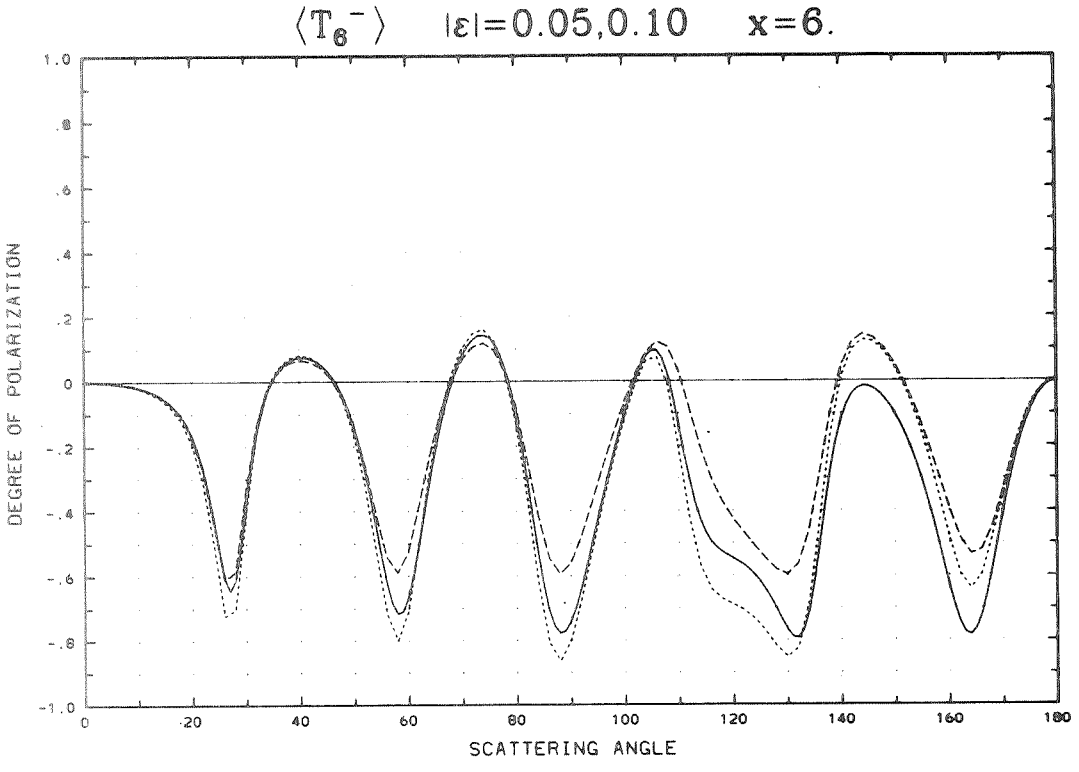

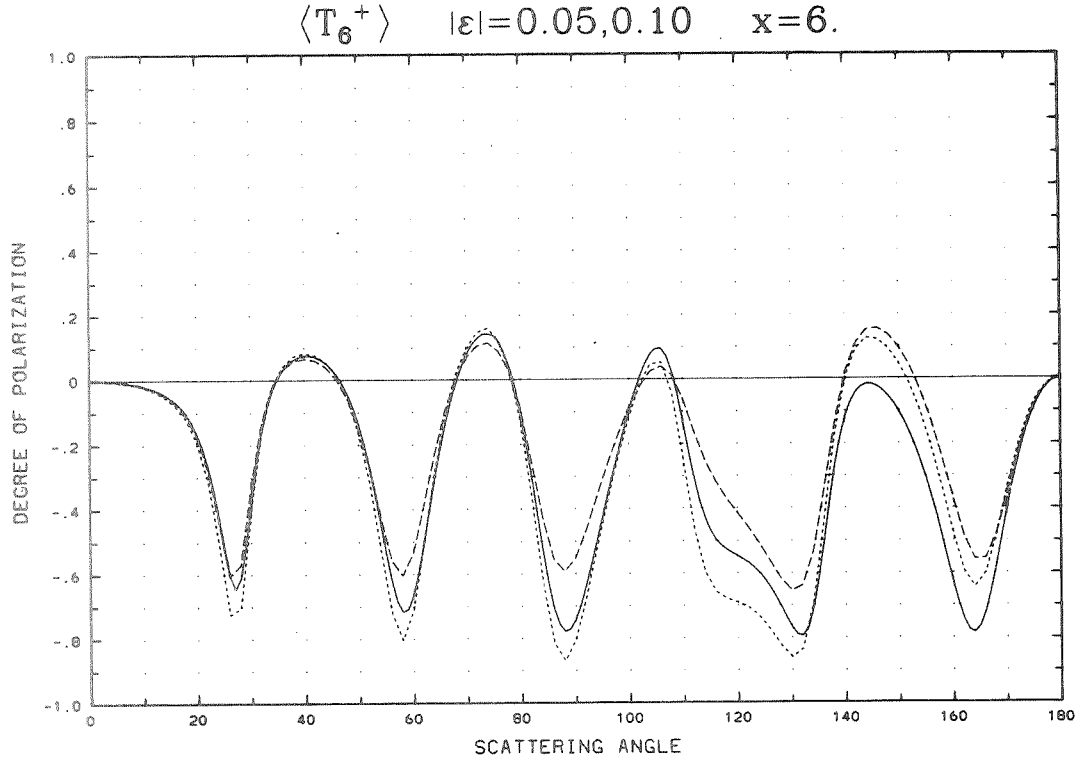

Appendix D (Continued)

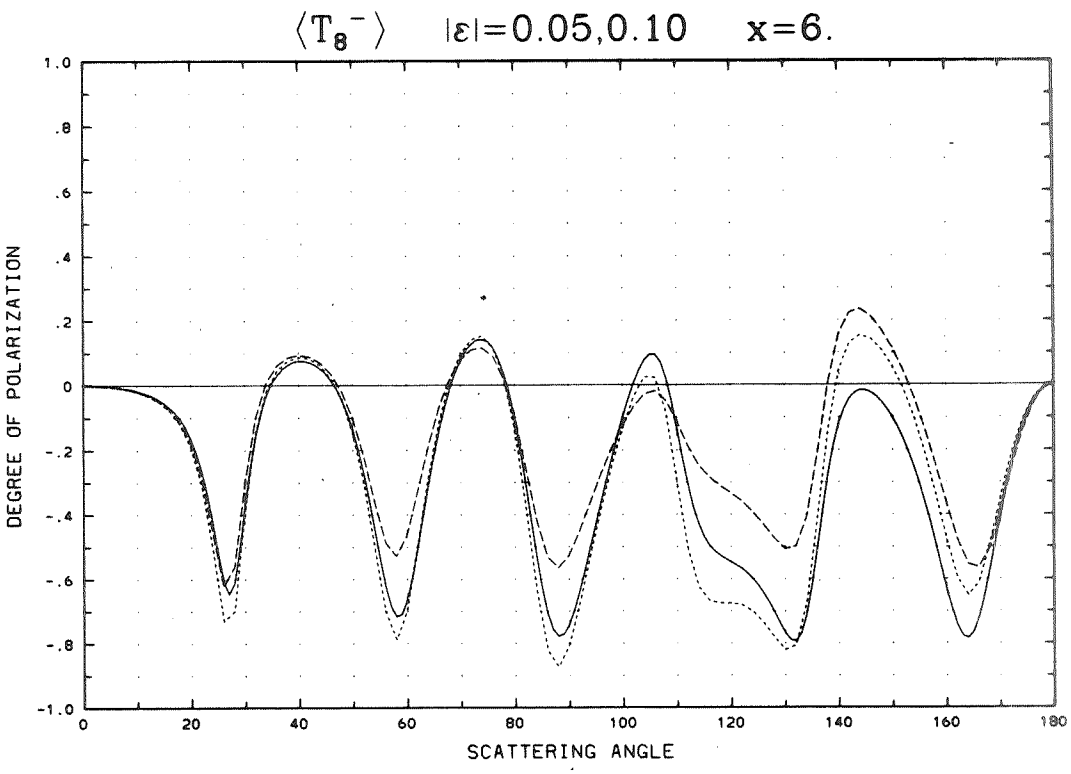

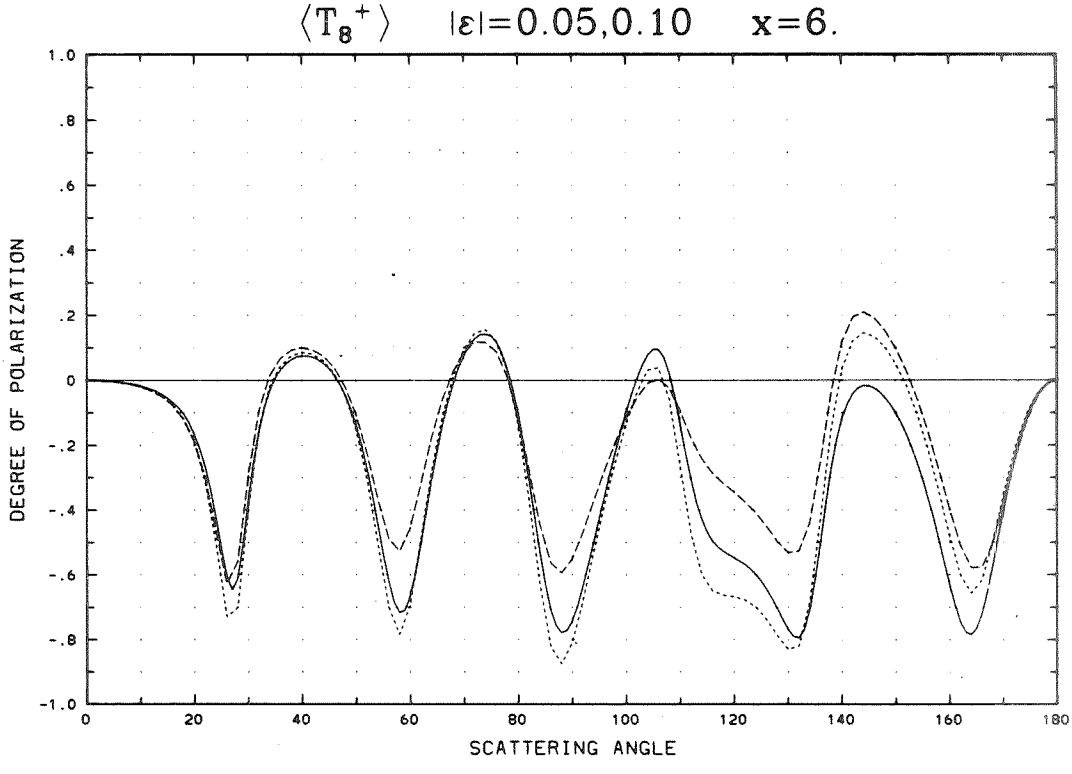

Appendix D (Continued)

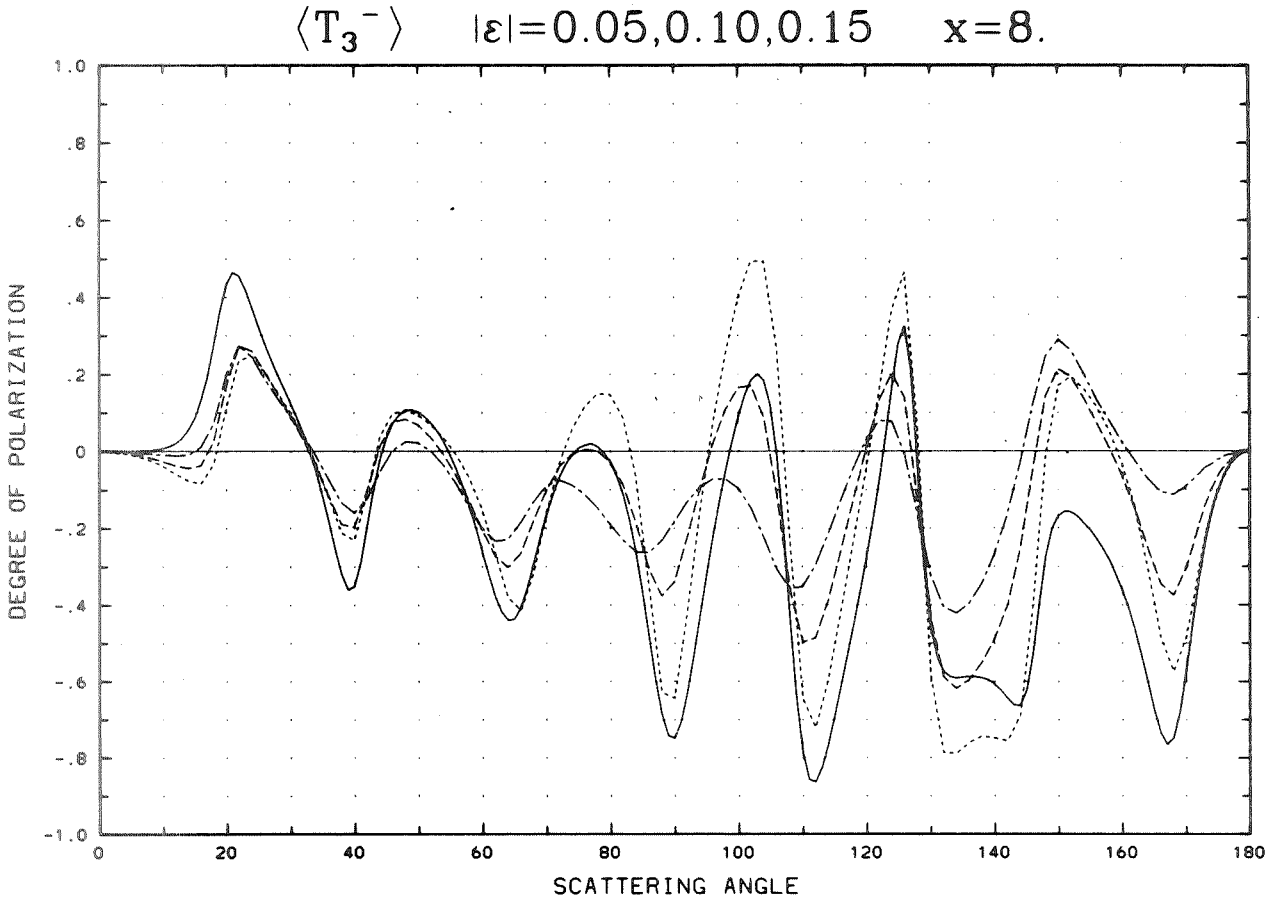

Appendix D (Continued)

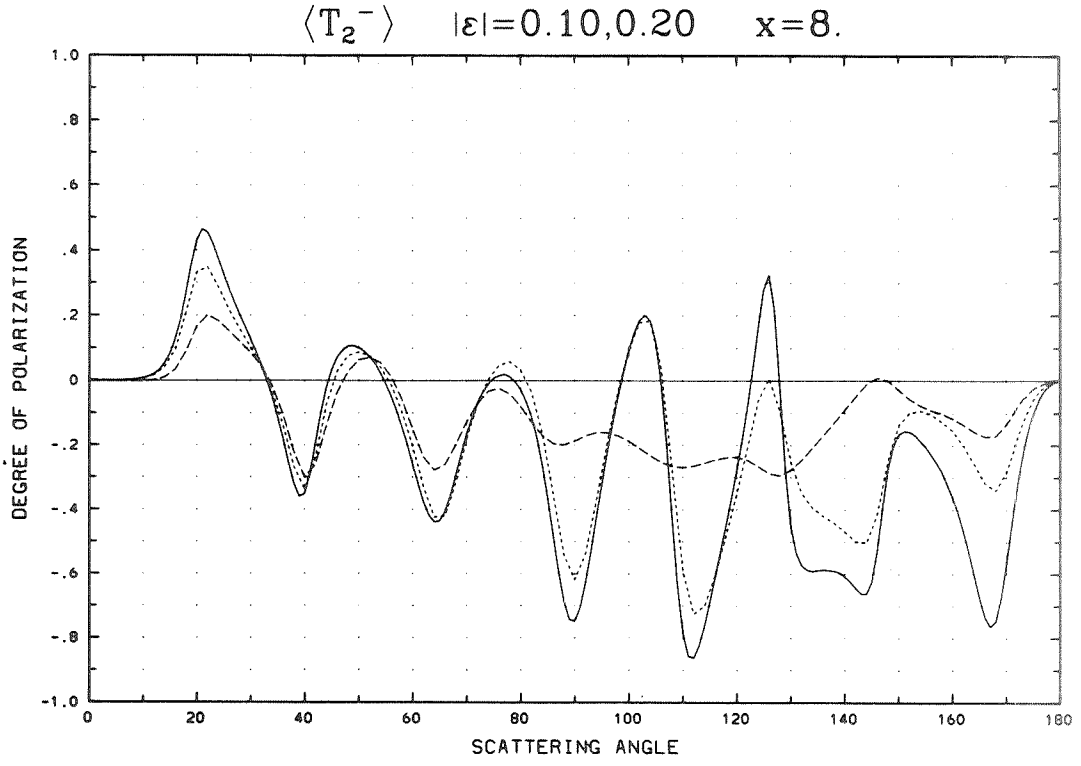

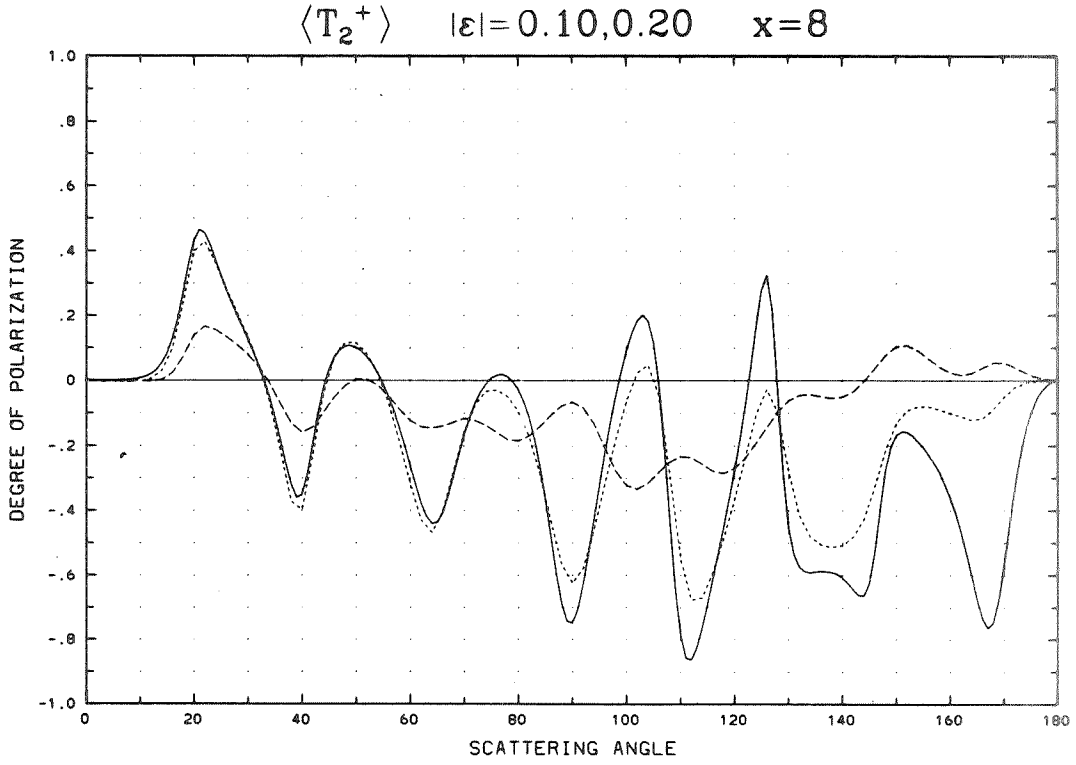

Appendix D (Continued)

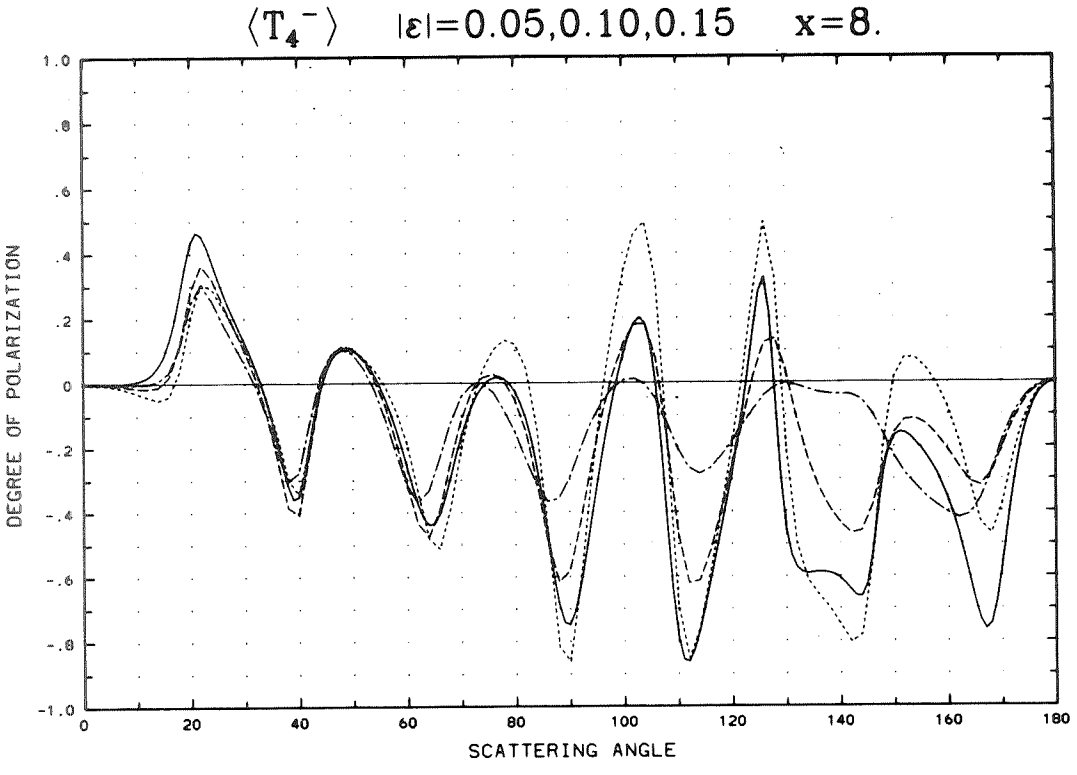

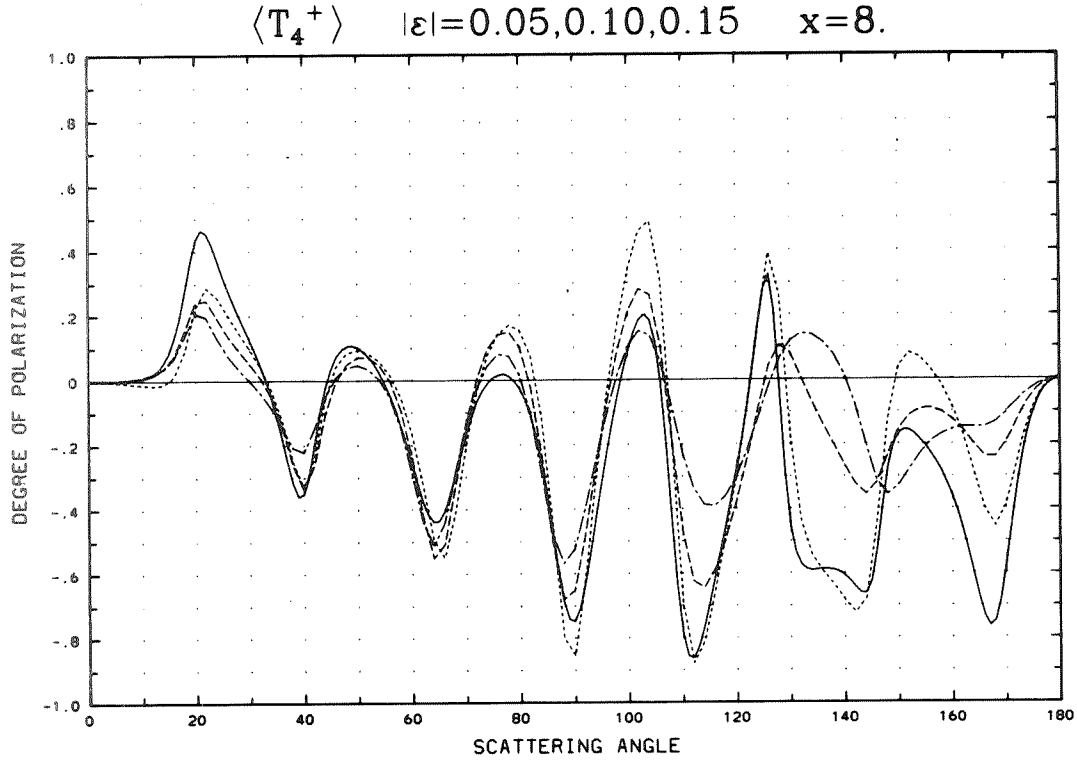

Appendix D (Continued)

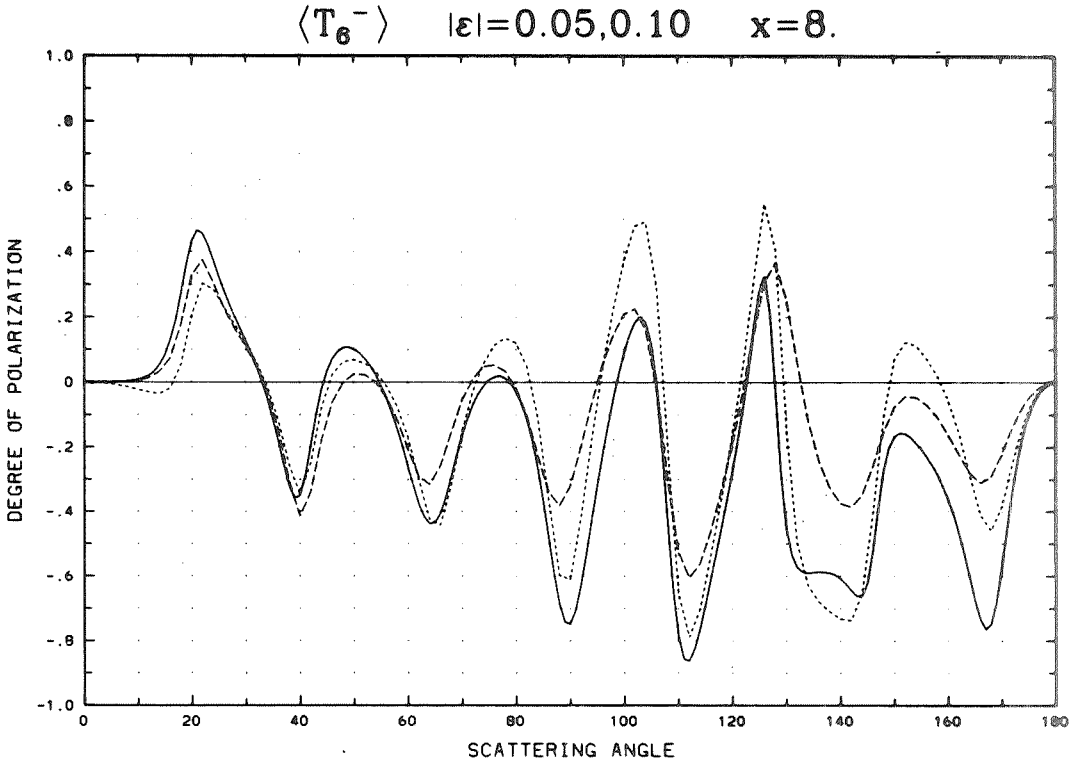

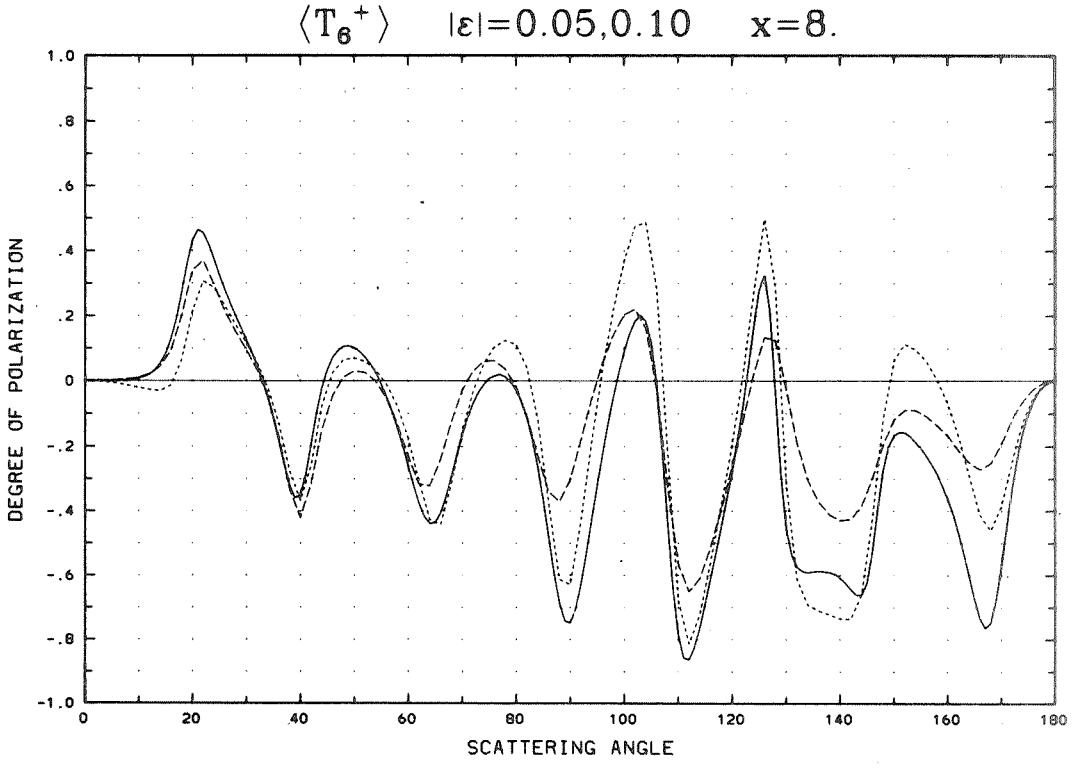

Appendix D (Continued)

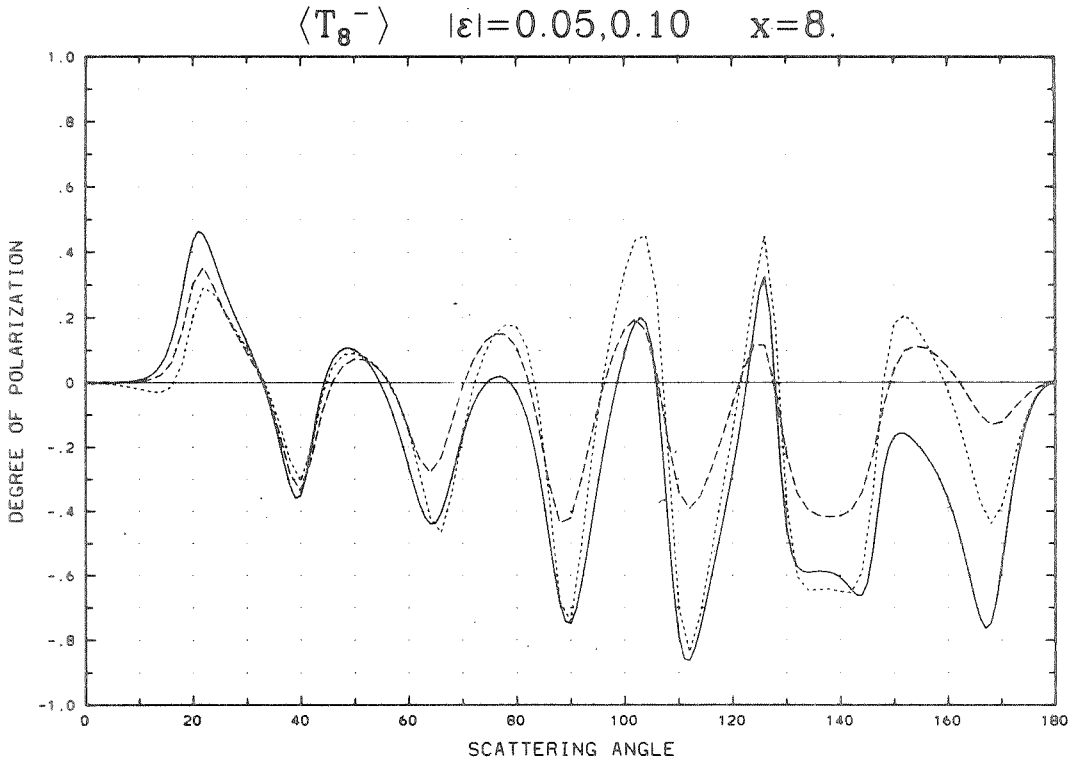

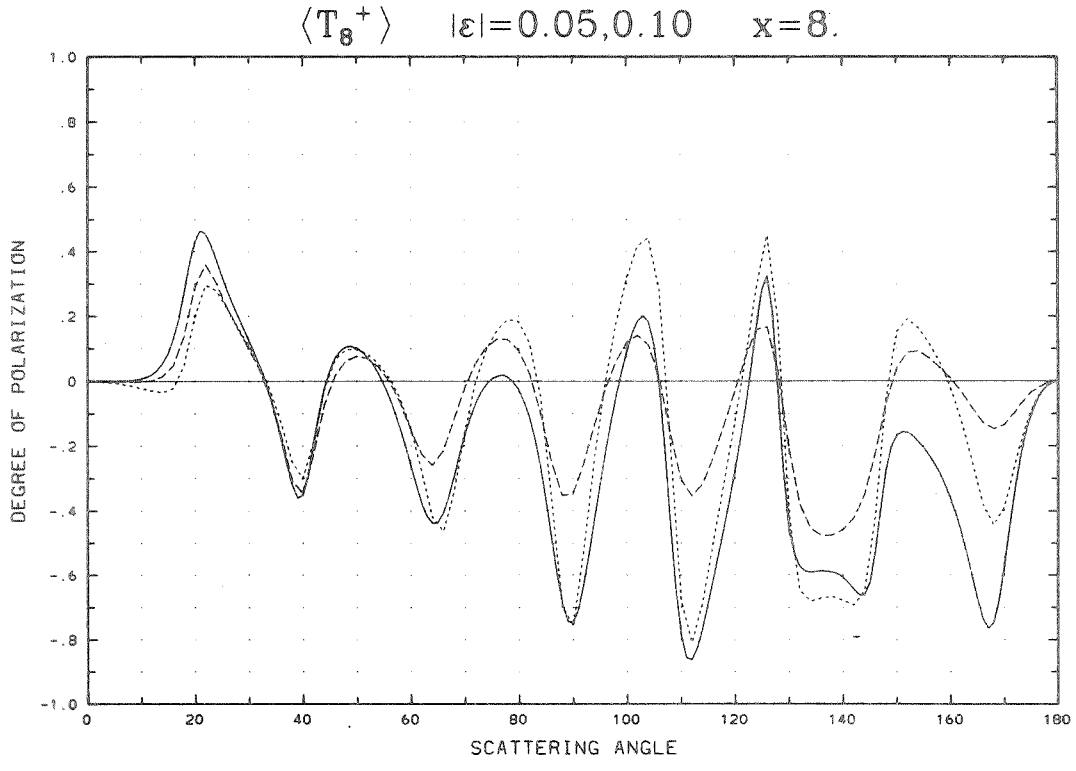

Appendix D (Continued)

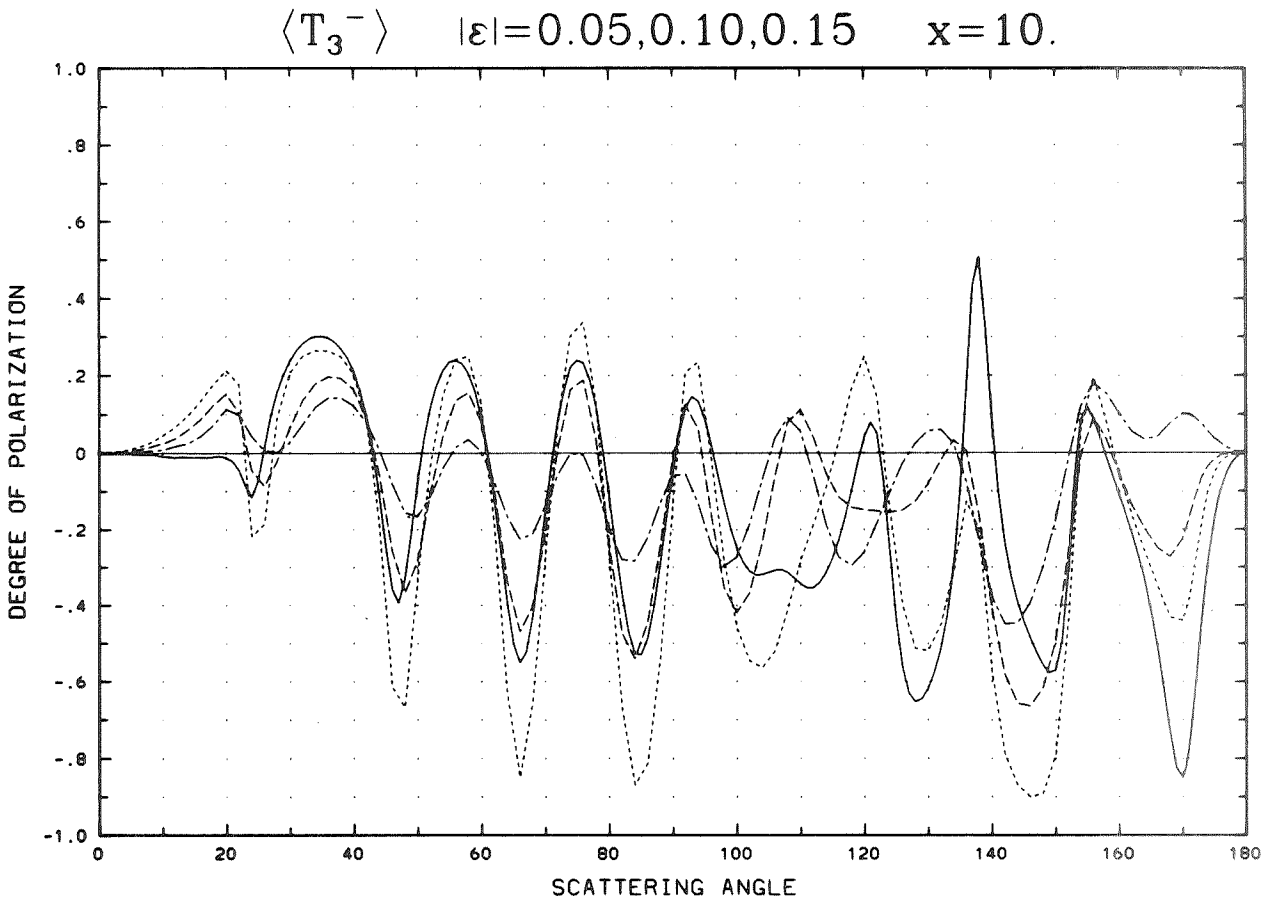

Appendix D (Continued)

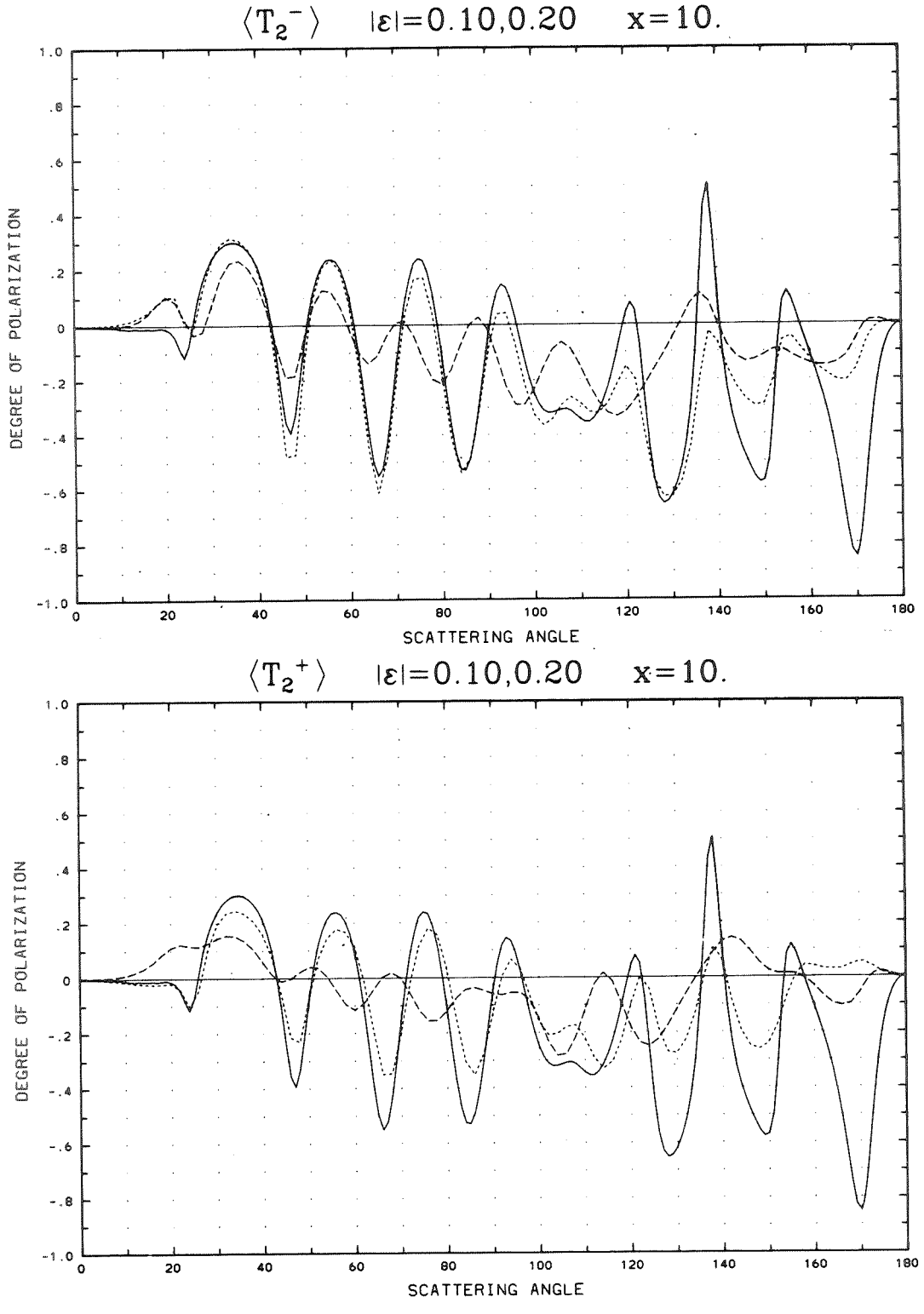

Appendix D (Continued)

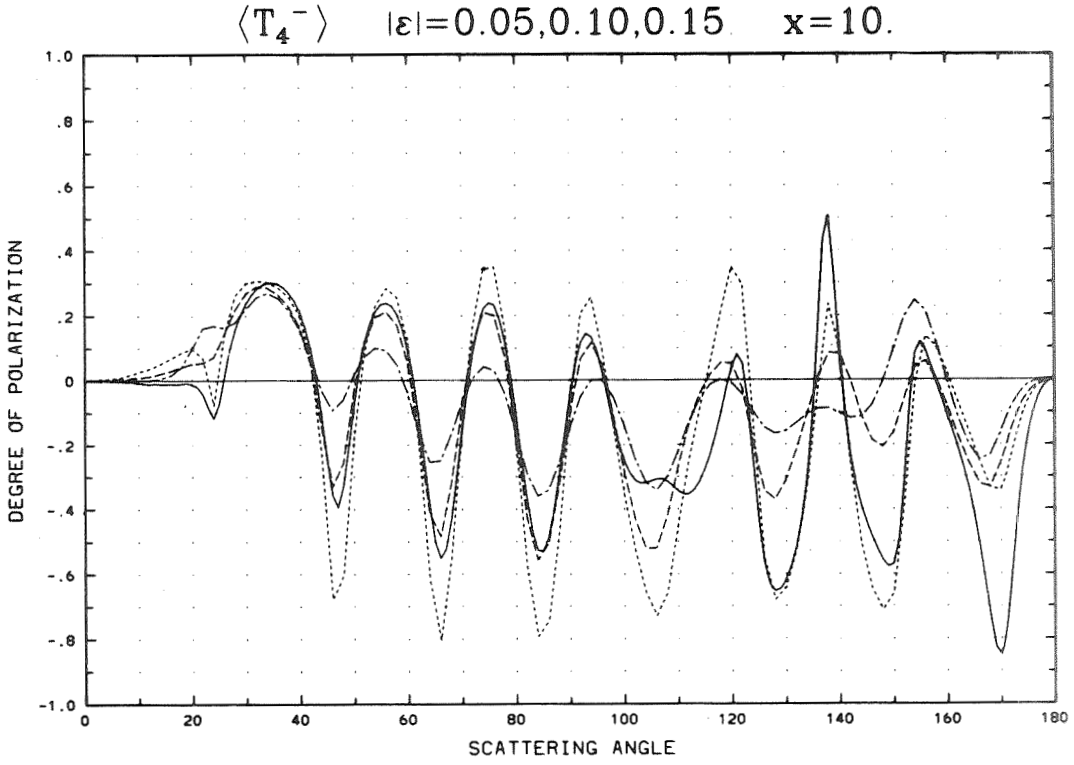

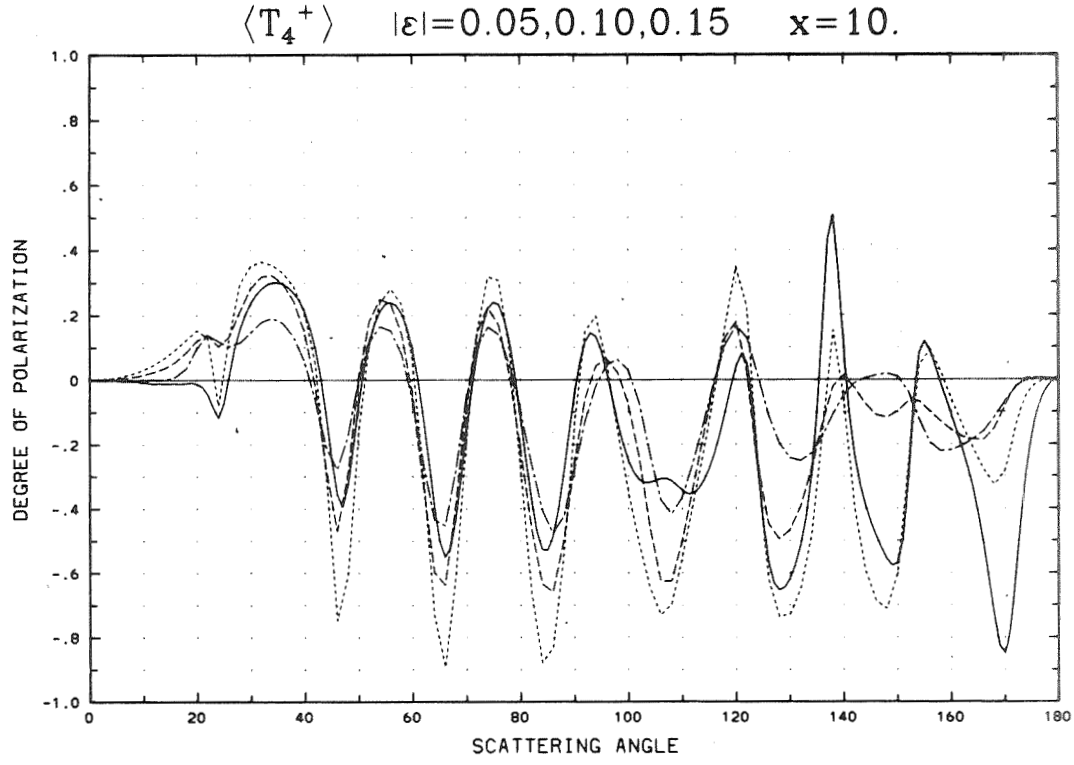

Appendix D (Continued)

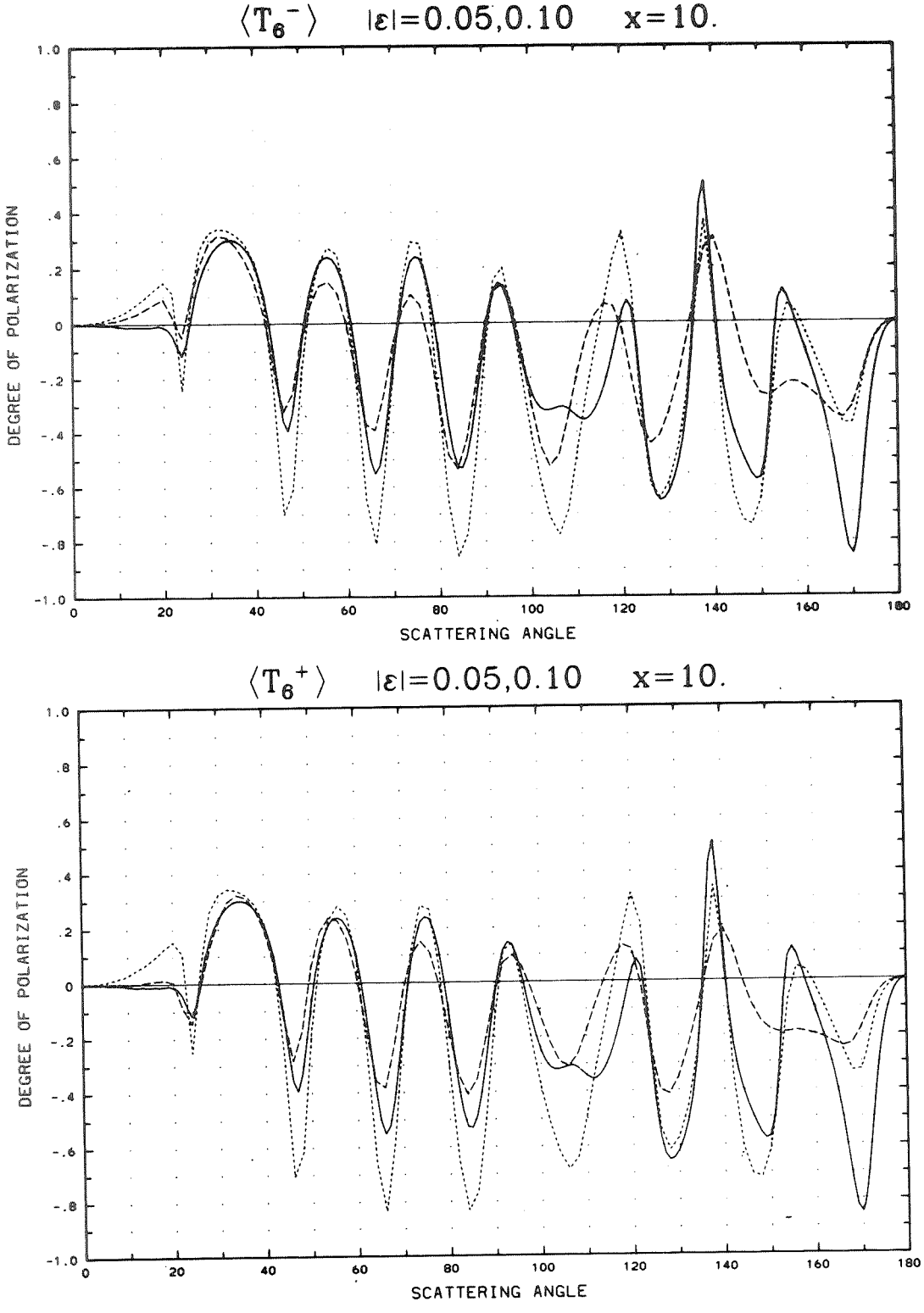

Appendix D (Continued)

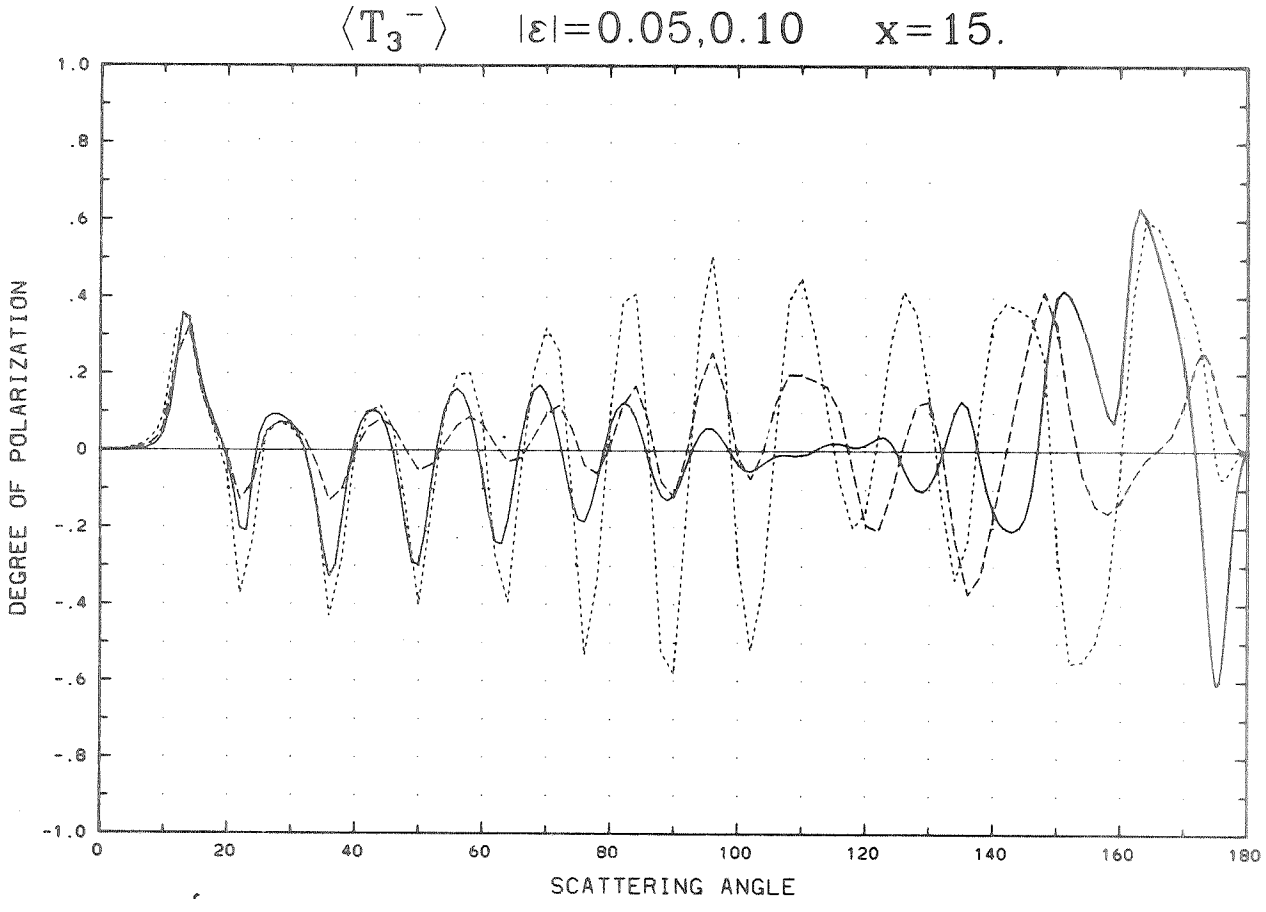

Appendix D (Continued)

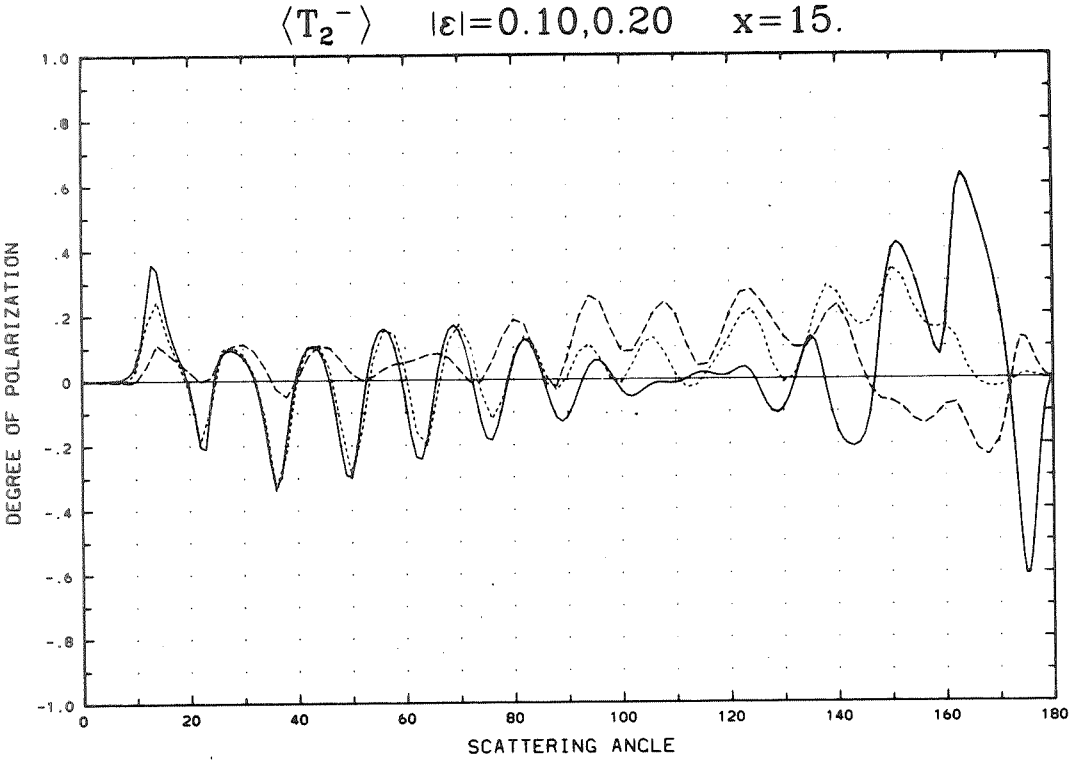

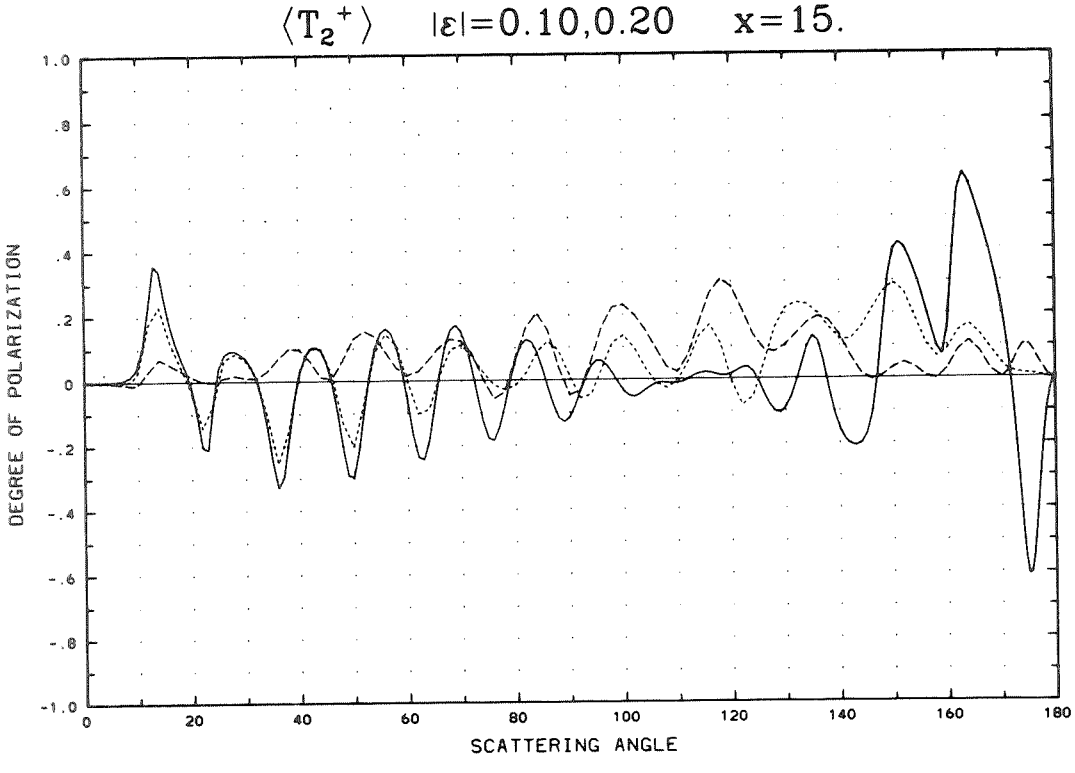

Appendix D (Continued)

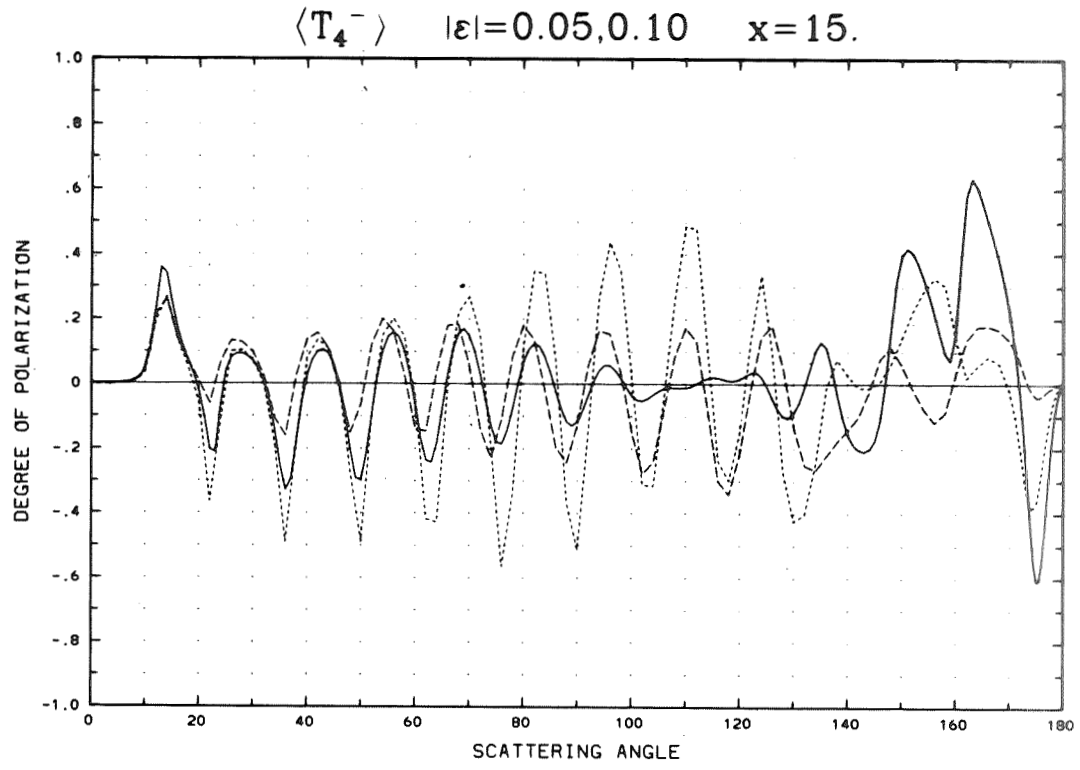

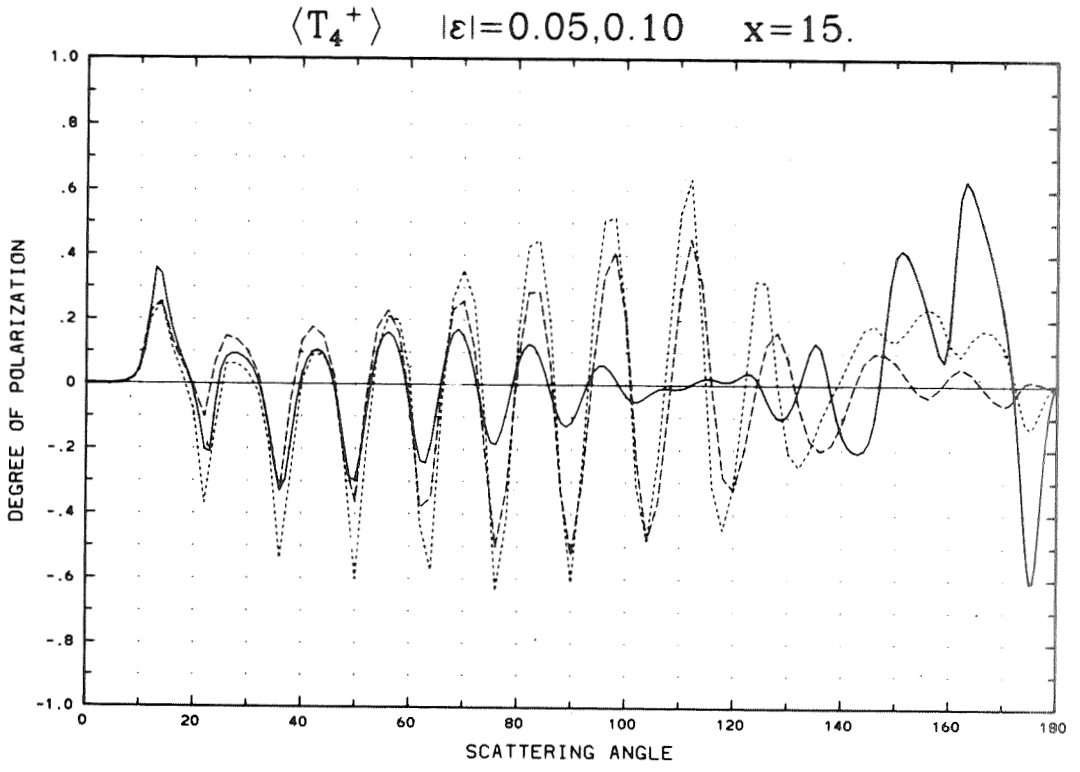

Appendix D (Continued)

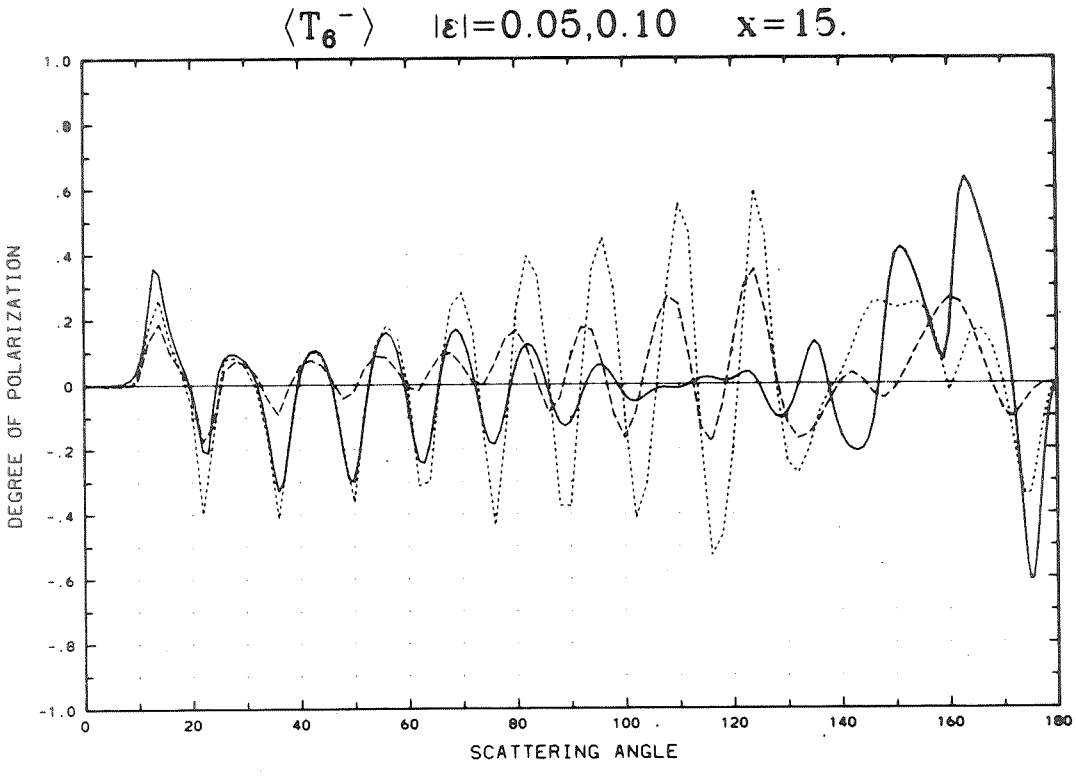

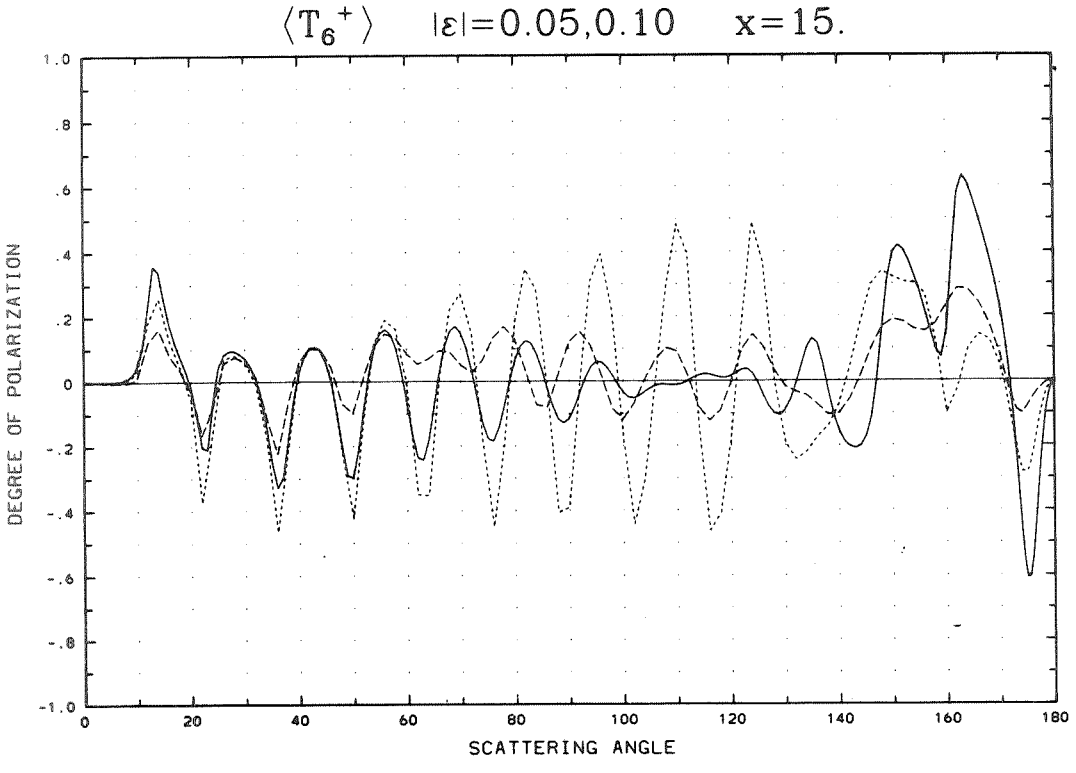

Appendix D (Continued)

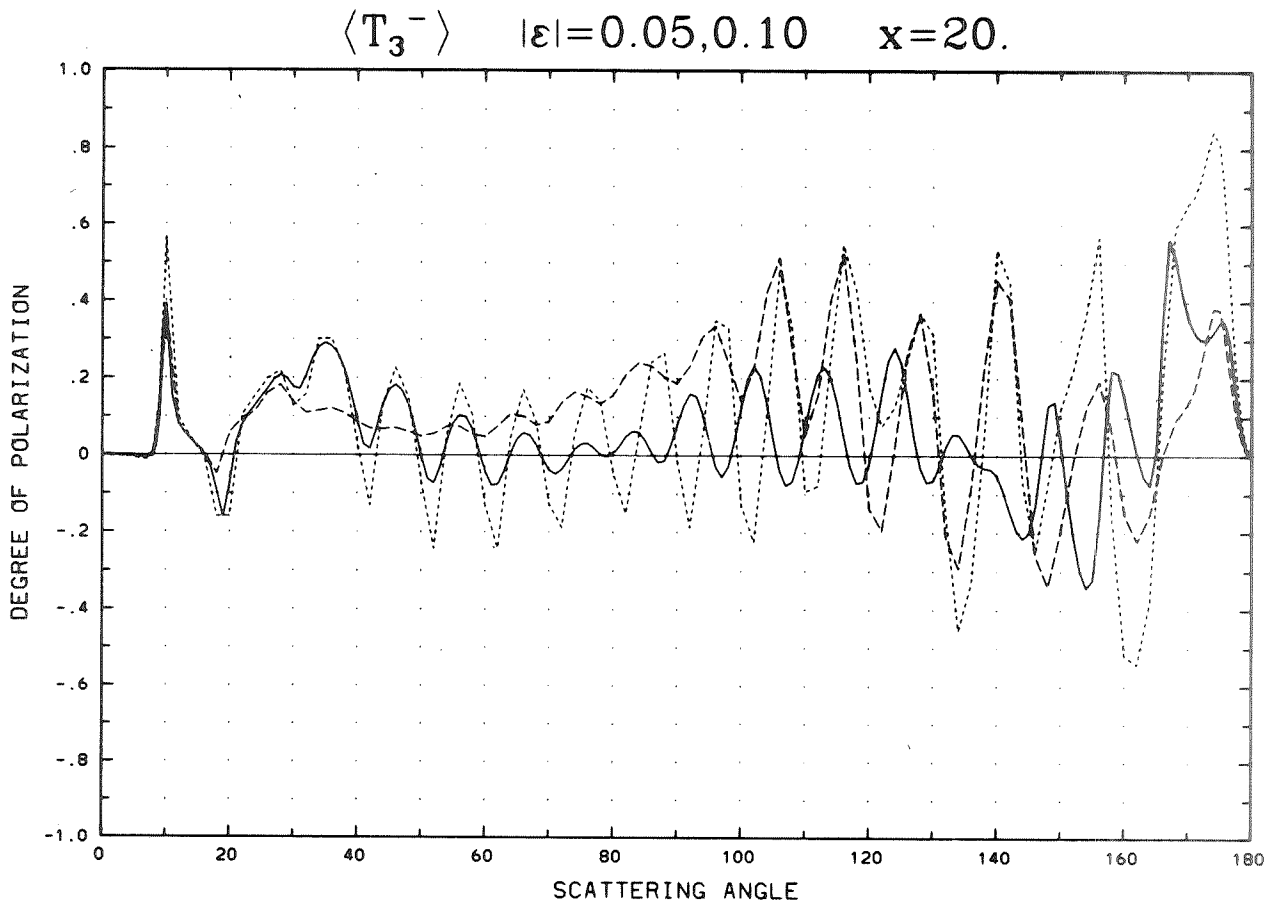

Appendix D (Continued)

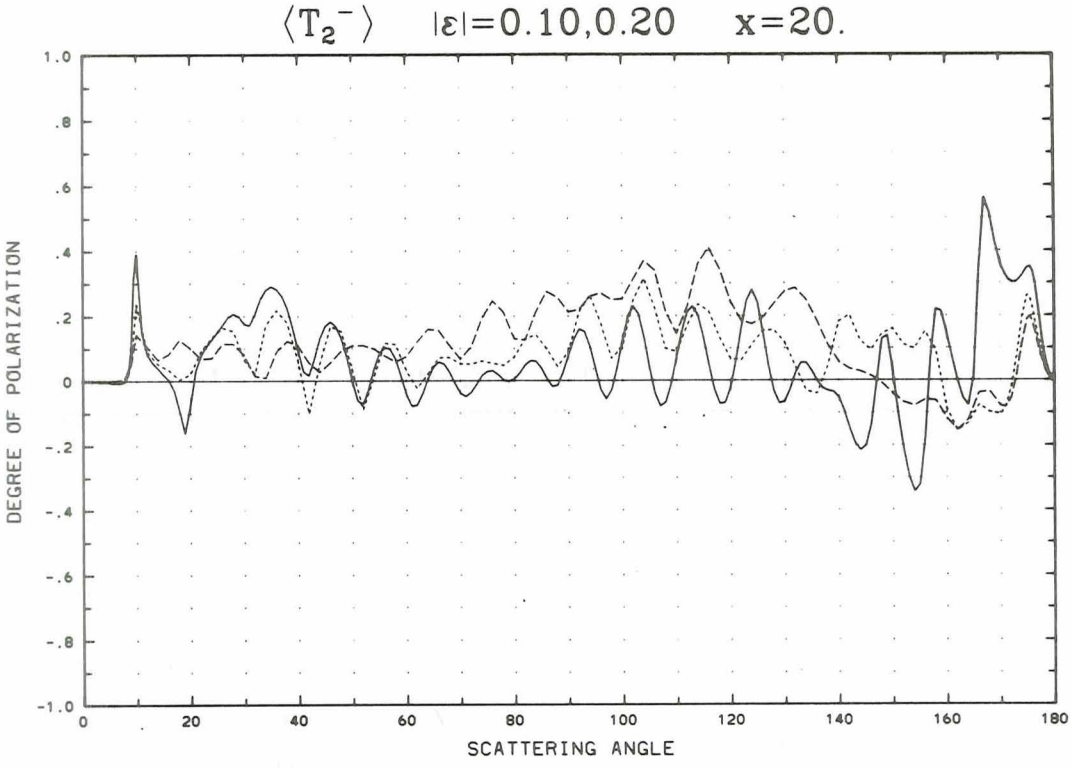

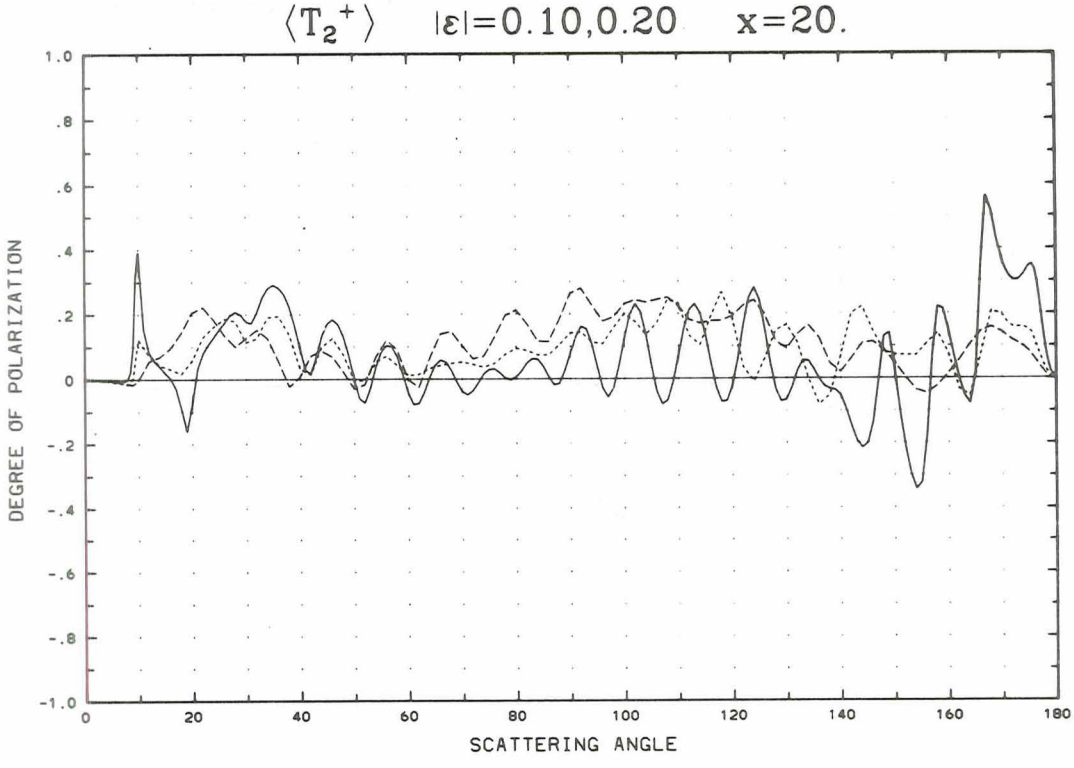

Appendix D (Continued)

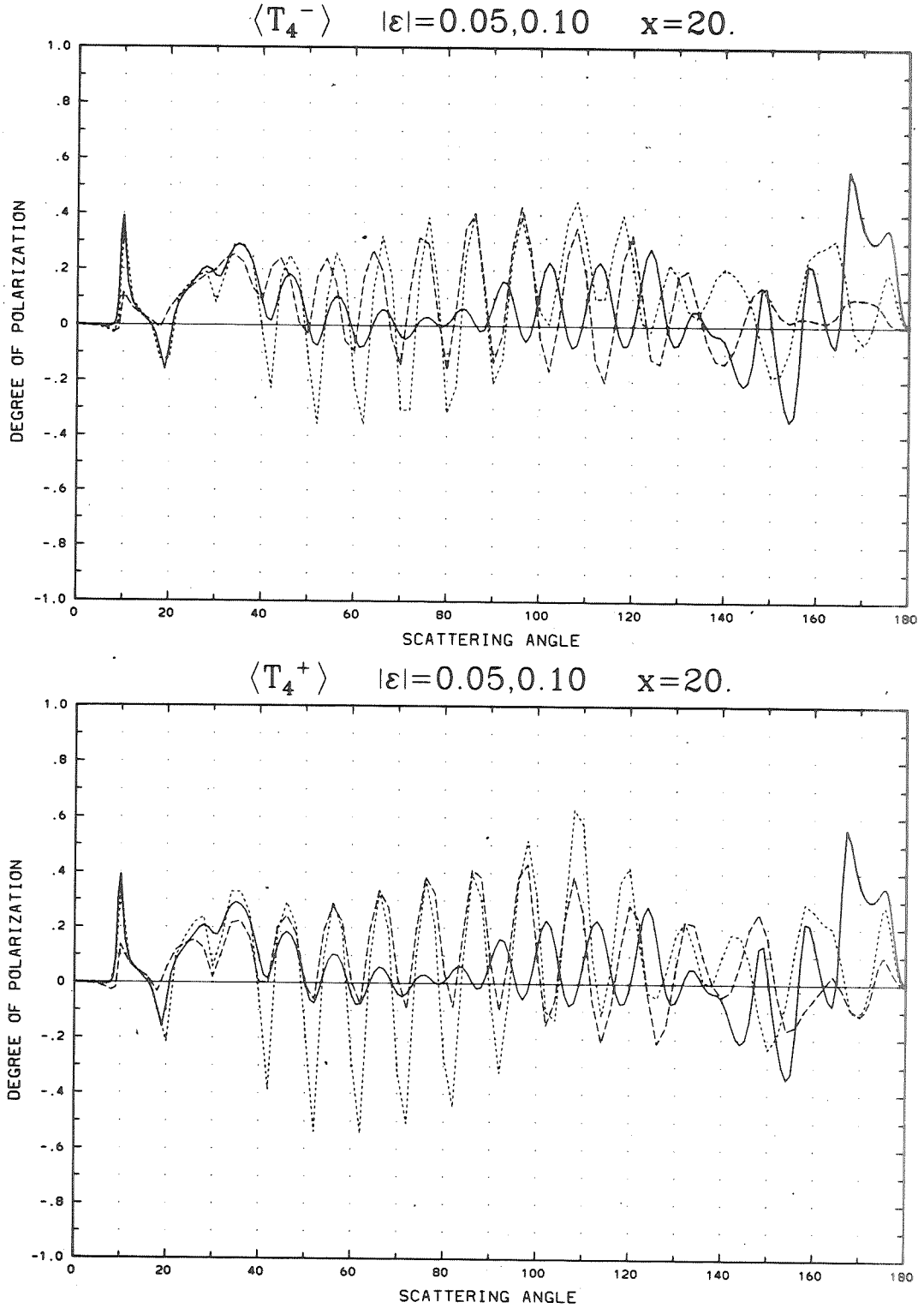

Appendix D (Continued)

BIBLIOGRAPHIC DATA SHEET

1. Report No.	2. Government Accession No.	3. Recipient's Catalog No.
NASA RP-1157		

4. Title and Subtitle	5. Report Date
Single Scattering From Nonspherical Chebyshev Particles: A Compendium of Calculations	January 1986
	6. Performing Organization Code 613
7. Author(s) Warren J. Wiscombe and Alberto Mugnai	8. Performing Organization Report No.
9. Performing Organization Name and Address NASA Goddard Space Flight Center Greenbelt, MD 20771	10. Work Unit No. 85B0264
	11. Contract or Grant No.
	13. Type of Report and Period Covered Reference Publication
12. Sponsoring Agency Name and Address National Aeronautics and Space Administration Washington, D.C. 20546	14. Sponsoring Agency Code

15. Supplementary Notes

Warren J. Wiscombe: Laboratory for Atmospheres, Goddard Space Flight Center, Greenbelt, Maryland.
Alberto Mugnai: Cooperative Institute for Research in the Atmosphere, Colorado State University, Fort Collins, Colorado, on leave from Istituto di Fisica dell'Atmosfera, Frascati, Italy.

16. Abstract

A large set of exact calculations of the scattering from a class of nonspherical particles known as 'Chebyshev particles' has been performed. Phase function and degree of polarization in random orientation, and parallel and perpendicular intensities in fixed orientations, are plotted for a variety of particle shapes and sizes. The intention is to furnish a data base against which both experimental data, and the predictions of approximate methods, can be tested. No analysis of the data is attempted here; that is reserved to a forthcoming journal article.

The calculations were performed with the widely-used Extended Boundary Condition Method. An extensive discussion of this method is given, including much material that is not easily available elsewhere (especially the analysis of its convergence properties). An extensive review is also given of all extant methods for nonspherical scattering calculations, as well as of the available pool of experimental data.

17. Key Words (Selected by Author(s))	18. Distribution Statement
Light Scattering Aerosol Scattering Atmospheric Radiation Nonspherical Scattering	Unclassified-Unlimited Subject Category 74

19. Security Classif. (of this report)	20. Security Classif. (of this page)	21. No. of Pages	22. Price
Unclassified	Unclassified	284	A13

For sale by the National Technical Information Service, Springfield, Virginia 22161 GSFC 25-44 (10/77)

☆U.S. GOVERNMENT PRINTING OFFICE:1985 -625-014/ 20020

5